AD787550

FLUIDIC

STATE-OF-THE-ART

SYMPOSIUM

1974

30 SEPTEMBER — OCTOBER

DDC
RECEIVED
OCT 23 1974
D

Reproduced by
NATIONAL TECHNICAL
INFORMATION SERVICE
U S Department of Commerce
Springfield VA 22151

VOLUME V

U.S. Army Materiel Command
Harry Diamond Laboratories
Washington, D.C.

DISTRIBUTION STATEMENT A
Approved for public release;
Distribution Unlimited

SECURITY CLASSIFICATION OF THIS PAGE *(When Data Entered)*

REPORT DOCUMENTATION PAGE

READ INSTRUCTIONS BEFORE COMPLETING FORM

1. REPORT NUMBER	2. GOVT ACCESSION NO. / 3. RECIPIENT'S CATALOG NUMBER
4. TITLE *(and Subtitle)*: Proceedings of the Fluidic State-of-the-Art Symposium, 30 Sep - 3 Oct 74, Vol. V	5. TYPE OF REPORT & PERIOD COVERED / 6. PERFORMING ORG. REPORT NUMBER
7. AUTHOR(s): Various	8. CONTRACT OR GRANT NUMBER(s): HDL Proj. No. 302531
9. PERFORMING ORGANIZATION NAME AND ADDRESS	10. PROGRAM ELEMENT, PROJECT, TASK AREA & WORK UNIT NUMBERS
11. CONTROLLING OFFICE NAME AND ADDRESS	12. REPORT DATE / 13. NUMBER OF PAGES: 518
14. MONITORING AGENCY NAME & ADDRESS *(if different from Controlling Office)*	15. SECURITY CLASS. *(of this report)*: Unclassified / 15a. DECLASSIFICATION/DOWNGRADING SCHEDULE

16. DISTRIBUTION STATEMENT *(of this Report)*

Unlimited

DISTRIBUTION STATEMENT A
Approved for public release;
Distribution Unlimited

17. DISTRIBUTION STATEMENT *(of the abstract entered in Block 20, if different from Report)*

18. SUPPLEMENTARY NOTES

19. KEY WORDS *(Continue on reverse side if necessary and identify by block number)*: Fluidics fabrication, fluidic products, fluidic industrial process applications, fluidic cooling controls, hydraulic control systems, fluidic fuel controls, fluidic ejection seat control, fluidic brake control, fluidic anti-skid systems, fluidic bag manufacturing control, fluidic military applications, fluidic oil-water separator, fluidic bistable actuator, fluidic missile control valve, flow control circuits.

20. ABSTRACT *(Continue on reverse side if necessary and identify by block number)*

This volume contains twenty-one papers for a total of 518 pages.

DD FORM 1 JAN 73 1473 EDITION OF 1 NOV 65 IS OBSOLETE

SECURITY CLASSIFICATION OF THIS PAGE *(When Data Entered)*

Block 19 con't:

fluidic programmer, underwater body control, fluidic motor repositioning, fluidic roll control.

Volume V

The Fabrication of Fluidics or the Search for Unconventional Practices
L. Cox, Harry Diamond Labs, Washington, D.C. 1

Epoxy Resin Casting of Planar Fluidic Components
K. Chithrabhann and N. Gopalakrishnan Unni, Space Science and Technology Center, India 9

Fluidic Products for the Individual
R. E. Bowles, Engineering Consultant, Silver Spring, Maryland . . 27

Aerospace Fluidics Applications and Circuit Manufacture
T. G. Sutton and W. J. Anderson, AiResearch Mfg. Co., Phoenix, Arizona 45

Some Industrial Process Applications of Fluidics
R. B. Adams, Moore Products Co. 91

Fluidics Controls Cooling of Diesel Locomotives
Robert B. Adams, Moore Products Co. 119

Application of Fluidic Concepts to Hydraulic Control Systems
R. H. Fashbaugh and E. Durlak, Naval Construction Battalion Center, Port Heuneme, California 135

Fluidic Fuel Controls -- A Narrated Bibliography
R. Woods, Harry Diamond Labs, Washington, D.C. 159

A Fluidic Control System for an Aircraft Ejection Seat
W. G. Beduhn, Systems and Research Center, Honeywell Inc., Minneapolis, Minnesota 173

A Fluidic Aircraft Brake Control System
H. H. Straub, Boeing Commercial Airplane Co., Seattle, Washington
P. M. Wagner, Air Force Flight Dynamics Lab,Ohio 203

Survey of Fluidic Anti-Skid Devices
S. Tenney, Harry Diamond Labs, Washington, D.C. 231

A Fluidically-Controlled Bag Manufacturing Machine for 105 mm Howitzer Propellant Charges
D. E. Scesney, Corning Glass Works, Corning, New York 241

Military Applications in Fluidics
R. Gottron and L. Cox, Harry Diamond Labs, Washington, D.C. 251

A Fluidic Oil-Water Separater
Dharam Pal, Naval Construction Battalion Center,
Port Hueneme, California 287

Design and Development of a Fluidic Bistable Actuator
J. C. Dunaway, U.S. Army Missile Command, Redstone Arsenal, Ala. . 323

Development of a Fluidic Missile Control Valve
Joe L. Byrd, U.S. Army Missile Command, Redstone Arsenal, Ala. . . 343

Flow Control Circuits for Toxic Fluids
J. R. Tippetts, University of Sheffield, United Kingdom
N. Syred, University of Sheffield, United Kingdom
J. Grant, Reactor Group, U.K.A.B.A., Risley, United Kingdom
R. E. Strong, Technical Services Department, British Nuclear
Fuels, Windscale 377

Development of a Miniature Fluidic Dual Channel Fluidic Programmer
T. S. Honda, General Electric Co., Schenectady, New York 425

Attitude Control System of the Underwater Body Using Liquid Fluidic Element
Y. Hara, T. Ogaya, and Y. Shimazaki, Mechanical Engineering
Lab of Japan 447

System Design for Fluidic Mortar Repositioning Control With Multiple Nonlinearities
C. N. Shen, Watervliet Arsenal, Watervliet, New York 465

Fluidic Emergency Roll Control
K. Haefner and T. S. Honda, General Electric Co., Schenactady,
New York 499

The Fabrication of Fluidics or The Search for Unconventional Practices

by
Lyndon S. Cox

INTRODUCTION

Over the 15 year history of fluidics, various methods have been used for the manufacture of fluid amplifiers and fluidic circuits. These have demonstrated varying degrees of success ranging from totally inadequate to highly successful, depending on both the manufacturing method and the application for which the product was being used. The purpose of this paper is to help the reader understand the relationship between the manufacturing processes and the successful manufacture of a product for a specific use. Some manufacturing methods failed when used simply because they were being used to produce the wrong kind of a product, and others succeeded because the product was suited to the process used with a given material and a given circuit design. These determine the degree of success. It is further necessary that unconventional practices, i.e. the special techniques that must be applied, be learned and utilized as necessary. One common difficulty appears in attempting to acquire unconventional knowledge. It is a human factor problem, in that the man or his organization realizes that his worth is in proportion to the exclusivity of his skills. Thus, the skilled technician who learns to successfully make fluidics does not always reveal his method, but keeps the unconventional practice as a trade secret. This fact has been recognized, and considerable effort has been spent in trying to professionally define the manufacturing processes for application to production rather than exclusively in the manufacture of research and development models.

Chronological exposition of the manufacture of fluidics would reveal many processes competing at all times with some being discarded and others being added. This would tend to confuse the reader; therefore, this history has been broken into six basic processes each of which will be covered in chronological detail and evaluated as to the use of the process.

THE FIRST PROCESS: CUTTING

As a simple examination of early fluid amplifiers will disclose, they were manufactured by cutting by bandsaws, by milling machines, by files and it's even said they were carved from soap and linoleum with penknives and carving tools. However, as fluidics emerged from the basement laboratory, into the scientific community, the need for precision to gain repeatability

brought the manufacture of fluidics to the machine shop, with the cutting tool being the end mill. In the early 1960's, the depth of fluidic channels, particularly power nozzles, was 4 or 5 times the width. This meant that side-cutting end mills larger than .030 in diameter were needed to provide the stiffness that was necessary to maintain dimensions and roughly perpendicular walls. It also meant that the walls were, of necessity, either straight or of constant radius because universal milling machines as well as calculations were suited to such shapes. Later, numerical control and optical tracers gave greater freedom in design.

Of course, the machinist was trained to remove burrs or sharp corners. The uncontrolled removal of sharp corners became a source of problems until recognized, and the removal of burrs on corners was controlled. If a passage narrower than .040 was required, it was made by machining two pieces and pinning them in place to provide a passage of the required width. It also meant that it was impossible to make even research models of very small amplifiers at that time. An advance came with the unconventional practice of using side cutting end mills as small as .004 in diameter in a pantograph or milling machine to cut even very elaborate patterns in miniature elements. This ability, and the fact that researchers stopped looking at nozzles that were more than twice as deep as they are wide, greatly facilitated manufacture of miniature amplifiers. Through this experience we learned that the shape of a corner affects the fluid flow in an amplifier - possibly as much as the location of the walls. Optical tracers have given greater freedom to design for milling, but corners must be avoided in the artwork. We also learned that machining soft metal would produce a large burr which is not tolerable unless the cover plate can conform to it and thereby eliminate leakage. In general, such conforming cover plates are not the case. The process of cutting, in particular through the use of end mills, is now sufficient for manufacture of research models. It is too slow and expensive for the economical quantity production of units, and the tolerances which can be held (dependent upon the operator) are in the region of .0001 to .0005 inch.

THE SECOND PROCESS: ETCHING

One of the first etching processes successfully used on fluid amplifiers was that using a photoceramic material. This material, while relatively thick, was initially transparent so that exposure could be made through the material and, as a result, deep channels could be readily formed. Corning has been producing commercially available fluidic components with this process for about 10 years. In recent years a thinner photoceramic material has become available which will allow us to have miniature fluidic amplifiers manufactured by this process. However, photoceramic is not useful in all applications of fluidics for in some cases it is too brittle. In these cases, manufacture from metal is much to be preferred. The first metal etching of fluidic amplifiers that the author is aware of was tried in a .030 inch sheet of copper and the results were so poor that pessimism

prevailed in the Government. Comercial vendors developed processes to provide metal-etched units, but the cost of purchasing these was often prohibitive. Etching in a photopolymer was also tried and it was found that nozzle widths less than .015 inch could not be reliably produced, and even in larger widths there was poor control of the wall geometry, channels being typically trapezoidal in cross-section.

Ultimately, after Air Force contracts with General Electric (1)* and Bendix (2) (5), Army Contracts with McDonnell-Douglas (3) and Orlando Fluidics (4), and in-house experiments at Picatinny Arsenal and the Missile Command at Redstone Arsenal, it was established that etching could be successfully done in thin metal foils typically between .002 and .005 inch thick with tolerances being held to at best 1/10 of the thickness of the foil. Through the examination of foils etched by the several contractors, it became apparent that it was also important that the etching fluid should attack the grains rather than attacking the grain boundaries (thereby allowing the grains to fall out of the polycrystalline structure). Such intergranular attack tends to continue after the etching process is nominally completed, thereby producing continuing changes in performance. Surprisingly, dip etching has produced results every bit as good and possibly superior to those produced by spray etching. The lack of a machining burr protruding above the surface of the foil means that sealing is much more readily accomplished by clamping and diffusion bonding. This fact, together with the ease of making parts with unusual curvature, accounts in large measure for the popularity of the metal etch process. Etching now allows manufacture of the smallext size amplifiers in corrosion resistant materials and, with diffusion bonding, virtually eliminates leakage problems. It is the process used in commercial manufacture of most jet deflection amplifiers. It is capable of holding tolerances of .0002 to .0005 inch.

It should be noted that a highly successful method of manufacturing pantograph templates for cutting fluidic amplifiers came from one of the least successful etching processes. This is the etching of a photopolymer having the brand name Templex, and often erroneously called Dycril.

THE THIRD PROCESS: CASTING

Among the first casting techniques employed for fluidics was the use of silicone rubber to provide a mold in which epoxy was cast to make the fluid amplifier. This was far superior in cost to machining because about a dozen epoxy amplifiers could be made from one silicone rubber mold before the catalyst in the epoxy distorted or cracked the silicone rubber. The success with the casting of epoxy led to the manufacture of metal dies for injection molding with several polymers. The relatively low cost of injection molded amplifiers meant that they could be discarded upon malfunction in dirty operating environments and that they were applicable to large quantity

*Numbers in parentheses refer to items in the annotated bibliography.

use. However, the bulkiness of the plastic amplifiers militated against complex circuits using them. Further, the variation in wall thickness that is typical of fluid amplifiers produced uneven shrinkage, leaving residual stresses which caused warpage of the plastic even after it was out of the mold for an extended period of time. This, and residual stresses from solvent welding or clamping of cover plates, sometimes led to cold flow of material - hence, long term changes in amplifier performance. Considerable effort was expended on finding an adhesive that could reliably hold plastic units together. One of the more successful efforts was that of Timothy Kilduff and Eleanor Horsey of HDL. (6)

Plastic is used today for molded amplifiers primarily in the impact modulator and turbulance amplifier units in which the configuration is less likely to cause warpage and soft gaskets can be used to accommodate that which occurs.

The casting of fluid amplifiers in metal has been done by Moore Products in their flowmeters and in their diverter valves. These typically have a nozzle one-quarter inch, or larger, and in this application they have been quite successful. Frankford Arsenal has investment cast some fluid amplifiers for HDL, but the investment casting process is not adequate to provide repeatable amplifiers in nozzle sizes of 20 mils and below. Interestingly enough, some very large flow diverters have been cast in concrete, and this apparently is satisfactory for very large sizes handling such things as sewage flow. Depending upon the casting process, tolerances of possibly less than .001 inch can be maintained immediately after molding. However, this degree of dimensional control cannot be maintained with mold erosion, shrinkage variations of different lots of material, and polymers exhibiting cold flow.

One novel approach, pioneered by Hellbaum, Philips, and Page of NASA Langley, was to cast a polymer around a wax pattern of the flow channels, and then remove the wax. This has been used to successfully manufacture amplifiers with nozzles of .040 inch.

THE FOURTH PROCESS: ELECTROFORMING

The Electroforming process, essentially heavy electroplating, has been used to manufacture numerous articles. It is normally done by electro-depositing metal on either a strippable or leachable pattern. For fluidics this requires that flow paths not be small or blind, because the leaching of the pattern cannot be assured in small places or in places where throughflow of the leaching fluid does not occur. Patterns which melt or evaporate are therefore more desirable. In this category one immediately thinks of the low shrinkage fusible alloys as materials to cast flow paths. However, these are not well-suited to electrodeposition because they have an adverse chemical effect on the plating bath and are hard to maintain free of oxide. The coating of wax patterns with graphite, electroless copper or electroless nickel was considered for a time. However, Honeywell, Inc., has now developed a low shrinkage conductive wax on which nickel can be electrodeposited. This process seems to be working quite well

in making acceptable circuits for helicopter stabilization. It is suited to relatively simple circuits which fit either a single plane configuration, or one in which all of the circuit components are in planes that are on sides of a manifold block. However, the process is unsuitable for circuits that require a large number of amplifiers which must be stacked for compactness. It is claimed that this process can maintain tolerances of .0001 inch.

THE FIFTH PROCESS: FORMING

Conventional practice would tell us that simple shapes and large tolerances (on items such as bolt heads) are suitable for forming processes such as cold heading. Complex shapes, having shallow open areas, are suitable for coining, but complex channel shapes with depth as great or greater than width are not suitable for cold forming.

Unconventional practice resulted when we started saying, "Perhaps if we refine a preform...". It was shown by Jack Dunn and John Burke at HDL that an investment-cast, aluminum preform could be refined by a coining process to produce repeatable fluid amplifiers. As previously implied, the amplifiers were not repeatable prior to this refinement. They also found that if a thick blank was used and a punch was imposed on the far side of the blank, the metal would flow around and conform to the punch having the flow channel configuration. Reproducibility of this was excellent. Thirty out of thirty were produced within .0001 inch of each other in nozzle width and with extremely consistent fluidic performance. As a production tool, it requires only that the tooling be polished into the right shape to provide channels giving the desired fluidic performance before production of repeatable fluid amplifiers can be accomplished.

THE LATEST PROCESS: STAMPING

Conventional practice tells us that any punch and die having long, narrow sections will deflect at some time during its operation, and the die set damaged on the next stroke. Further, there will be a burr that will rise above the surface of the sheet from metal flow in the clearance between the punch and the die. As previously stated, this burr will cause leakage problems. The unconventional practice came when someone said, "Don't let the punch enter the die, make the die with zero clearance, have punches supported within dies on both sides of the sheet of material and have the face of the punch stroke to flush with the top of the opposite die." This is done in the United States by a firm known as Connecticut Fine Blanking. HDL has received parts that have been manufactured by fine blanking dies, and presently a die is being produced to manufacture the laminar proportional amplifier. This process will be evaluated during 1974 and, if found satisfactory, it will give us a possibility of economically manufacturing fluid amplifiers in large quantities. One significant advantage over etching is the use of thicker sheets in order to avoid stacking several thin foils to make one amplifier; a tolerance of .0002 inch has been quoted.

THE PROBLEM AREA: QUALITY ASSURANCE

The current cost of fluid amplifiers is considerably in excess of the $1 to $10 unit cost of operating a low volume production process. This cost is largely the result of expensive quality control and quality assurance techniques. The dimensional and functional inspection of fluidic amplifiers has been, and still is, a major cost barrier for the technology and must be reduced to gain wider application. Several methods have been proposed. One technique is a test pattern in which lines are progressively etched out by undercutting of the photoresist. The final dimension is the photoresist channel width plus undercuts. Therefore, the dimensional control of the finished product is accomplished through observing etch-out of a test pattern. Lacking success in this endeavor, the manufacture by forming and stamping must be emphasized because they are highly repeatable processes requiring that only a small percentage of output be inspected.

SUMMARY

Succinctly stated, fabrication of fluidics has progressed from model making to production. There are presently six basic processes. Milling can provide almost any shape we wish to investigate; however, it is not suitable for manufacture of amplifiers in large numbers. Etching is suitable for the manufacture of moderately large numbers of laminae with tolerances of .0005 inch. Casting requires larger tolerances, often over .005 inch; however it is quite suited to very large amplifiers because it is much more economical in material and manufacturing costs. Electroforming has been demonstrated to be highly repeatable and suitable for at least limited production. Forming is a potential production process which has been shown feasible for close tolerance (.0001 inch) in which electroforming is now used; however it still remains to be proven economical. Stamping has a potential that is still to be measured, but which may allow us to economically produce quantities in the millions with tolerances of .0002 inch.

As previously stated, the process must be selected with care in terms of the materials that are to be used, and the accuracy which is required. Further, the unconventional practice must be applied if successful manufacture is to be the result. Fluidics are now available by etching in such metals as stainless steel, beryllium copper, aluminum and titanium. They are available in ceramics of the Corning variety. They are available by molding in polyvinyl chloride and in polysulfone. Amplifiers can be found cast in iron, steel and concrete. Electroforming is currently done only in nickel. Additional materials may become available as the processes of forming and stamping are developed. Existing processes in 1974 allow for the manufacture of fluid amplifiers at costs of from $1 to $10 per amplifier. The difference between this and the purchase price is largely the cost of quality assurance. The future of fluidics is to a large extent in the hands of the manufacturing processes, with the emphasis now shifted to quality assurance. Economical quality assurance methods are now being investigated to further reduce the cost of manufacturing fluid amplifiers.

ANNOTATED BIBLIOGRAPHY

1. Air Force Contract No. F33615-68-C-1700 with General Electric Specialty Fluids Operation was to perform pilot line production with unskilled personnel on fluidic systems made for jet engine service, (1200° F in air), missile service (600° F in air) and measurement of temperature to 3000° F. A wide variety of materials and processes were surveyed. Materials selected were stainless steel, aluminum, and silicon nitride. Assembly of silicon nitride was deemed impossible and dropped. No bonding of aluminum was done. Stainless steel bonding was achieved.

2. Air Force Contract No. F33615-71-C-1347 with Bendix was to photoetch and diffusion bond miniature fluid amplifiers into circuits in aluminum. This work is directly applicable if the specified process can be verified to be both satisfactory and repeatable in a pilot line. This verification is part of the present effort.

3. Army Contract No. DAAA21-73-C-0517 with McDonnel-Douglas Astronautics, Titusville, Florida, was for optimization of the process for etching titanium foils to produce fluidic amplifiers.

4. Army Contract No. DAAA21-73-C-0021 with Orlando Fluidics, Orlando, Florida, evaluated metal etch by several processes including their own.

5. Army Contract No. DAAA21-74-C-0316 with Bendix to photoetch miniature fluid amplifiers under production conditions for subsequent bonding to form circuits.

6. Kilduff, Timothy J.
   Horsey, Eleanor F.
   (USA) Dept. of the Army, Harry Diamond Laboratories
   Bonding of Fluid Amplifier Systems with A Dry- Film Adhesive

Fluidics Quarterly, Vol. 2, No. 1, 1970
This report describes an improved system for bonding and sealing fluid amplifiers. The principal feature of the new system is an experimental dry-film adhesive, which consists of a plastic support film 0.001 inch thick coated with a non-tacky epoxy resin adhesive about 0.002 inch thick. This film is die-cut to shape and cured in place between the amplifier halves. A secondary feature is an adhesive gasket of a commercial foamable epoxy resin designed to seal the connector tubes in place. Bonding and sealing are done simultaneously, which also represents an advance in the state of the art. Compared with older bonding procedures which gave about forty per cent rejects, the new method is less expensive and gave only six per cent rejects.

EPOXY RESIN CASTING OF PLANAR FLUIDIC COMPONENTS

K. Chithrabhanu
N. Gopalakrishnan Unni

SPACE SCIENCE AND TECHNOLOGY CENTRE
TRIVANDRUM
INDIA

Preceding page blank

INTRODUCTION

Fluidic devices, now being put to different applications, have no moving part which is an important advantage in building reliable systems.

The development of the technology depends very much upon the fabrication technique that will be adopted in the production of the components. Fluidic systems, in general are used for sophisticated applications where the requirements are rather exacting. This necessitates a high advancement in technology, which in turn will enable fluidic systems to cover more areas of applications. The components used are generally very small in size and minor changes in the vital dimensions can change their performance characteristics considerably.

There are many methods of fabrication that are generally used for making fluidic components. Rauch(1)* gives a very brief outline of many of the processes. Humphrey and Tarumoto (2) have discussed the manufacture of fluidic components in general, with greater details. Lundstrom (3) has discussed the relative merits and demerits of some of the methods of fabrication. A suitable process had to be selected from these and the technology of the chosen process had to be developed.

CHOICE OF A FABRICATION PROCESS

An ideal process for making fluidic components should yield a product that meets the standards and specifications laid down for any fluidic system. It may be further noted that the high cost of the fluidic devices has been a barrier to its widespread application. In this connection, the desirability of developing a manufacturing technique for producing components at a low cost is evident. As the fluidic components are put to a wide variety of applications, an ideal process for all the cases may not be practicable.

---

* Note: Underlined figures in brackets show references at the end.

The environmental conditions, and the stresses which these components have to withstand while operating, mainly decide the choice of the material. The universal properties required by these materials are dimensional stability, precision formability and sealability. The fluid dynamic phenomena utilised in the fluidic elements are very much sensitive to the slightest changes in channel shapes. For the miniaturisation of the components, the ability of the material to conform to the critical tolerance specifications also is to be considered. The sealing capability of the material is equally important, as leaks,if present will seriously arfect the performance in an adverse manner. Mcreover, in a circuit plane having several components, it is very difficult to locate leaks and they will affect the performance of the whole assembly.

Specific applications of the components may demand additional environment tolerance capability. They include chemical, thermal and moisture resistance. Certain other secondary requirements include colourability (where colours are used to identify different parts or merely for aesthetic reasons), surface finish, and opacity or transparency.

. For the fabrication of logic components (which operate at low pressures and might be needed in large numbers), the process should lend itself to the complex shapes and reproducibility within close limits of tolerance. The method selected should be capable of allowing for the miniaturisation of the components and integrated circuits. Further, it will always be an advantage if the laboratory fabrication method developed, can easily be transformed into an industrial manufacturing method. Over and above all these considerations, the investment cost involved will be an important factor in the selection of a fabrication process.

This broad range of requirements has led to the investigation of a number of fabrication techniques using several materials.

The process should be suitable for low as well as medium rate of production as our requirement will not be very large.

Materials that are more suitable for making fluidic elements may be broadly classified into ceramics, metals and plastics.

Ceramics are generally inorganic, non-metallic, materials which require exposure to high temperature during the manufacturing process. The three classes of ceramics include; glasses containing an oxide base which frequently is silica oxide, glass-ceramics, and ceramics such as carbides, nitrides and silicides which contain no glass. Ceramics are dimensionally more stable than both plastics and metals, and are resistant to high temperature, moisture and most of the chemicals. The major disadvantage is that they are brittle and hence require protection.

Metals have excellent mechanical, very good thermal and good chemical properties. When compared with ceramics and plastics, metals are stronger and heavier. They lie between ceramics and plastics when considering processability, elasticity, ductility, thermal expansion, hardness and resistance to moisture. But metals in general have very low resistance to corrosion. They are generally suitable for high stress fluidic system applications where severe environmental conditions may be encountered. Most commonly used metals are alloy steels, aluminium alloys, copper alloys, nickel and nickel alloys.

Plasticsinclude a large group of highly polymeric synthetic and organic compounds. In comparison with metals and ceramics, plastics are lighter and cheaper. They can be easily processed. Generally, they are not used for high stress applications and in high temperature environments. Many of the plastics have chemical and water absorption resistance.

Among the thermosetting plastics, epoxies have been found to be very much suited for casting fluidic components for logic circuits. The epoxies have high dimensional stability and moisture resistance.

Once the material selection is made, the choice of the method of fabrication is automatically narrowed down.

A comparison of different manufacturing methods for fluidic components has been made by Rauch (1) and Lundstrom (3). The tables given by them provide guidelines to evaluate the suitability of the various processes to meet our requirement. According to Rauch, photosensitive plastics and epoxy casting are the best two methods. But certain limitations follow the adoption of photosensitive plastic technique. Investment cost for equipment and special photopolymers required are high. Also, they are not available indigenously. The aspect ratio obtainable by this method is limited to 3, which again depends upon the thickness of the available photo-polymer sheets. The photopolymers are sensitive to moisture and some chemicals, and for operation, their maximum temperature is limited to 200°F.

The comparison made by Lundstrom gives a different picture when considering the smallest channel width, surface finish, investment cost etc. It can be seen that the epoxy resin casting method is far better than the photosensitive plastic. Engraving and epoxy casting are the only methods which do not demand a high investment cost and in the method adopted by the authors, these two are combined as can be seen later. The simplicity of the method and the low investment cost required have been the main deciding factors in selecting the epoxy resin casting method.

EPOXY RESIN CASTING METHOD

The method of epoxy casting had earlier been used by Marsh and Hobbs (4), Brown (5) and also by Hellbaum, Phillips and Page (6) with variation in the actual procedure involved.

Marsh and Hobbs had used silicone rubber moulds made from an adjustable master unit. Different amplifier

plates were cast in epoxy resins using the rubber moulds. The method was used for the development of fluidic components. Each component plate was tested using a single interchangable cover plate. Or, in otherwords, they did not attempt the casting of an integral top cover.

Brown made use of 'Dycril' plastic to make masters using photoetching technique. A silicone rubber negative was made from the 'Dycril' master and this negative was used for casting the amplifier plates. Later, a top cover was cast on the amplifier plate using epoxy resin.

Hellbaum, Phillips and Page also start the technique with the photo etching of 'Dycril'. A negative of the circuit is etched on the 'Dycril' plate. Water soluble wax is injected at a temperature of 65.5° C and under a pressure of approximately 300 psi on the negative kept in vacuum (1 mm of Hg absolute) to get the soluble wax laminate. Molten pattern wax is again injected under pressure (pressure of 100 to 500 psi and temp 65.5 to 82.2°C) on to the soluble wax laminate kept in vacuum (1mm of Hg). This results in a composite laminate consisting of pattern wax core in the channels embedded is soluble wax. The water soluble wax is then washed away in hydrochloric acid solution resulting in the pattern wax core. Epoxy resin is poured around the core and is cured in place. The pattern wax core is melted away and the component is cleaned in kerosene at 100°C.

The last two references mentioned above use the method of photo etching of 'Dycril' as the first stage. The technique of photo etching is quite complicated and has many limitations (2,3) regarding

smallest channel size, aspect ratio, dimensional stability etc. The procedure followed by Hellbaum is more complex than that given by Brown for casting the final unit from the master.

In many cases, the details given by the authors are too little to be of any practical use to the user. In view of the procedure adopted by others, it was felt desirable to have a simpler method of epoxy casting for making integral units using a permanent engraved metal master instead of the photo-etched ones.

From the various combinations of resins and hardeners available commercially, a two component casting system, consisting of Araldite D(CY 230) and Hardener HY 951 which has definite advantages, was selected.

The curing of the component after casting need not be under pressure or at elevated temperatures. The shrinkage of the resin during curing is negligibly small. Further, it is not necessary to heat either the resin or the hardener for making the resin mix.

A master component is used for making a negative die which in turn is later used for casting the positive (component plates) by pouring the resin mix into it.

The master (Fig.1) is made by engraving the component silhouette in an aluminium alloy plate using a precision pantograph engraving machine in the conventional way. The template for engraving is 6 to 8 times the original size and is made of thin perspex sheet of approximately 3 mm thickness. It is inspected using a profile projector before it is used as a template for engraving the amplifier.

Any conventional material like metals, plastics, wood, etc. can be used for making the mould box. Acrylic perspex is found to be well suited. The inside of the mould box is given a slight taper to facilitate the easy removal of the castings.

A mould release agent is applied on the mould surface as well as on the master to prevent the resin mix from adhering to the surfaces while setting. There are many mould release agents commercially available (which are generally silicone fluids of special formulae) and most of them are quite good for the purpose. Assembled mould ready for casting the negative die is shown in Fig.2.

Resin and the hardener are mixed in the correct ratio (10:1 by weight) for preparing the resin mix. Care should be taken to remove all the air bubbles that are trapped in the resin while mixing. All the air bubbles should be removed before the resin starts setting. The pot life of the resin hardener mix is 1 to 1½ hours at 20°C. The polymerisation reaction that takes place is exothermic in nature. Fillers if added (eg. talc, graphite, chalk flour etc.) will reduce the heat developed during the curing process and will also reduce the shrinkage. Pigments may be added to the resin to get any desired colour.

The resin mix prepared as mentioned above is poured along the sides of the mould in a thin stream (Fig.3) to avoid trapping of air bubbles. A vacuum chamber may be used to facilitate the removal of air bubbles.

The resin mix in the mould will set at room temperature within 24 hours. However, the curing time can be reduced very much (to the order of 5-10 minutes) if the castings are cured at higher temperatures (a maximum up to 130°C); prolonged curing time or higher curing temperature gives slightly better thermal stability. The negative die is taken out of the mould after curing (Fig. 4).

The casting procedure for the negative die and the component plate are identical except in that the assembled moulds are different. The mould assembled with

negative die (Fig.5) is used for casting the component plate as shown in Fig.6. Figure 7 shows the component plate cast in epoxy resin.

The component (a bistable amplifier) cast as described above is to be fitted with a top cover. This top cover, called the cover plate carries the tube fittings at the supply, control and output ports. Reliable working of fluidic components can be ensured only by providing perfect sealing all along the periphery of the component silhouette. Inter channel leakage will alter the flow conditions and will adversely affect the performance of the component. Leakage of fluid from the components is accompanied by undesirable power loss and probable malfunctioning of the system. In a circuit plane having several components, it is difficult to locate any leakage which may cause unpredictable and undesirable interaction of the components.

CHOICE OF THE SEALING METHOD

An ideal method of fixing the cover plate on to the component plate would be to use an adhesive, as discussed by Brown (5). But, a serious problem will follow if the adhesive is applied directly on the component plate of the element as the adhesive has a tendency to squeeze into the power and control nozzles and other channels and alter their geometry, if not result in partial blockage. Even the thinnest layer that can be applied (which requires a very high surface finish and flatness of the two parts to be mated) exhibits a tendency to squeeze into the channels.

The authors have tried the method of fixing cover plate using screws. The method may not ensure perfect sealing as it will not provide uniform pressure on the cover plate (because the number and locations of the screws are limited by the small size of the logic components). Using a gasket in between the plates will ensure the sealing at the expense of slight alteration in the channel shapes, as these gaskets (which are gererally elastomers) will partly be pressed into the channels as the screws are tightened and alter their geometry. Gaskets obstruct visibility and hence prevent visual inspection of the channels of transparent components after assembly. Using an adhesive

coated film to fix the cover plate has been suggested by Kilduff and Horsey (7) as a solution to the sealing problem. This method uses a thin supporting film with an adhesive coating on both the sides. This film is kept in between the cover and component plates and is cured in place to make a perfect bond. At room temperature, the film should be nontacky and inactive. A suitable bonding film is not readily available in the market and its development needs separate attention and hence was not attempted.

In the method adopted by the authors, the channels of the components are filled with paraffin wax and then the top cover is cast. The wax is later removed from the channels after the cover plate is cast, and the component is ready for use.

CASTING THE COVER PLATE

This method when adopted for epoxy cast fluidic components will result in a homogeneous integrated component with cover plate permanently bonded to the component plate. The sealing capacity of the joint is limited only by the strength of the resin. The same resin mix and mould used for casting the component plate are used for casting the cover plate also.

Once the component plate is ready (Fig.7), its surface is finished smooth and flat. Holes are drilled for fixing the tube fittings at the supply, control and output ports.

These holes will provide outlets for the molten wax, when it is to be removed from the channels after casting the top cover. The component plate is cleaned thoroughly and is ready for pouring the wax.

Paraffin wax used for filling the channels must be very pure, without any dirt or other contaminants. It is heated to a temperature of 10 to 12°C above its melting point before pouring. Refined wax having higher setting point in the range 60 to 62°C has been found suitable for filling the channels. Utmost care should be taken when the wax is poured over the component plate. The modification of molten wax should be slow and uniform to obtain a smooth surface after finishing it flat.

Sufficient thickness is built up on the top surface of the component to ensure that the channels will be filled up even after the top surface is finished flat.

The wax, after complete solidification, is finished flat on the surface with a straight edge. The wax present on the surface, should be removed very carefully using a clean soft cloth dipped in a suitable solvent. Care should be taken to see that wax filled in the channels is not disolved away.

SOLVENT FOR PARAFFIN WAX

A number of organic solvents were tested for selecting a suitable solvent for dissolving paraffin wax; viz.

1) Acetone (2) Benzene (3) Carbon tetra Chloride.
4) Chloroform (5) Trichloro ethylene & (6) Xylene.

From experience the authors have found Xylene to be the most satisfactory one, among the six solvents tested. It is a clear, colourless liquid with less volatility. Solubility of paraffin wax in Xylene is very high, and it can be increased by warming Xylene slightly in an oven. Once the top surface is finished flat as described earlier, the component plate is ready for casting the cover plate. Care should be taken to see that the surface surrounding the channels (component silhouette) is completely free of wax. The resin mix is poured into the mould to make a cover plate.

During curing a lot of heat is developed and utmost care is to be taken to see that the temperature does not rise enough (40°C)to melt the wax. This can be done by keeping it partly immersed in cold water.

Demoulding is done after a curing period of 24 hours at ambient temperature. Before heating the component for melting away the wax, all the drilled holes on the component plate (at the supply, control and output ports) are cleared to provide way for melting wax to come out.

The component is heated in an oven to a temperature of approximately 70°C to remove the wax from the channels.

Molten wax will come out through the connecting ports. This process alone will not remove all the wax from the channels. The thin layer of wax left in the channels can finally be removed by cleaning the components in Xylene using an ultrasonic cleaner for 2 or 3 minutes. After removing the wax from the channels, tube fittings are provided at the connecting ports to make the component ready for testing. Bistable amplifiers with cast cover plate are shown in Fig.8.

CONCLUSION

The epoxy casting method, as mentioned earlier has been used by others for casting fluidic components mainly for the development purposes. Marsh and Hobbs (4) used an interchangable cover plate, and casting a cover plate integral with the component plate was not attempted. Brown as well as Hellbaum, Phillips and Page have used 'Dycril' for making the master. The limitations of using this photo etching technique has been listed by Brown himself (5). It has been mentioned that the important dimensions are consistently larger and under cutting is 'general'. The smallest channel dimension also cannot be less than 0.5 mm (0.02 in) and the channel length should be kept a minimum. This might create problems in miniaturisation and channel design of integrated circuits. The author also mentions about the "ship's prow" effect that can occur at sharp edges like splitters etc. due to the under cutting (3 to 4°) involved. 'Dycril' cannot be used as a permanent master due to its water absorption properties. It also has the limitation in the maximum value of aspect ratio obtainable with the photo etching technique. As mentioned earlier, the procedure adopted by Hellbaum, Phillips and Page is more laborious with the injection of molten soluble wax as well as pattern wax under vacuum at high pressure(upto 500 psi).

Considering these points and also the fact that 'Dycril' is not available indigenously, alternatives for making masters were sought and the authors found the engraving of the master as a promising alternative. The method of pantograph milling gives a master with dimensional stability and good accuracy. Channels with a width of 0.5 mm have been machined on aluminium alloy plates without much problems. This master can be used for almost an unlimited number of castings.

The engraved master does not necessarily require casting of flexible rubber negatives as used by Brown, since

there is no under cutting in the master like the etched ones.

Casting of the cover plate over the component plate is essentially the same in principle though the actual procedure adopted might vary. The advantage of the procedure adopted by the authors is that the investment cost involved is negligible and the whole procedure is less complex and can be best adopted for R&D work in the field. The amplifiers cast in epoxy resin using the method developed are being used in various circuit applications. With proper standardisation and a certain amount of mechanisation, the method seems to be highly promising for mass production as well.

-oo 0 oo- -oo 0 oo-

REFERENCES

1. "Fluid Amplifier state of the Art", Vol.1 Research and Development-Fluid Amplifiers and Logic. NASA Contractor Report NASA CR-101. Prepared by General Electric Company October 1, 1964.

2. Humphrey, E.F. and Tarumoto, D.H., Ed. "Fluidics". Published by Fluid Amplifier Associates, Ann Arbour, Michigan, Jan. 1968.

3. Lundstrom "An investigation of Fluidic Element Fabrication Techniques, Specially Chemical milling of Stainless Steel", Paper D2, Fourth Cranfield Fluidics Conference Comentry, 17-20 March, 1970.

4. Marsh, David S., and Hobbs, Edward S., "Use of Epoxy Castings for fluid amplifiers design HDL Report TR-1102, AD 401319 Feb. 1963.

5. Brown, C.C., "Design and Manufacture of Pure Fluid elements" Paper F4, 2nd cranfield fluidics Conference Cambridge, 3-5 Jan., 1967.

6. Hellbaum, R.F., Phillips, A.R. and Page A.D., "Monolithic Precision Casting Technique" ASME Paper 70-Flcs-8 June 1970.

7. Kilduff T.J., and Horsey E.F., "Bonding of Fluid Amplifier systems with a Dry-Film Adhesive" Fluidics Quarterly, Vol.II No.1, Fluid Amplifier Associates, Ann Arbor, Michigan, 1970.



Fig. 1. Master Component in Aluminium Alloy



Fig. 2. Mould assembled for casting
the negative die



Fig. 3. Pouring the resin over the master for casting the negative die



Fig. 4. Negative die



Fig. 5. Mould ready for casting the component plate



Fig. 6. Pouring the resin to cast the component plate



Fig. 7. Fluidic component plate cast in epoxy resin

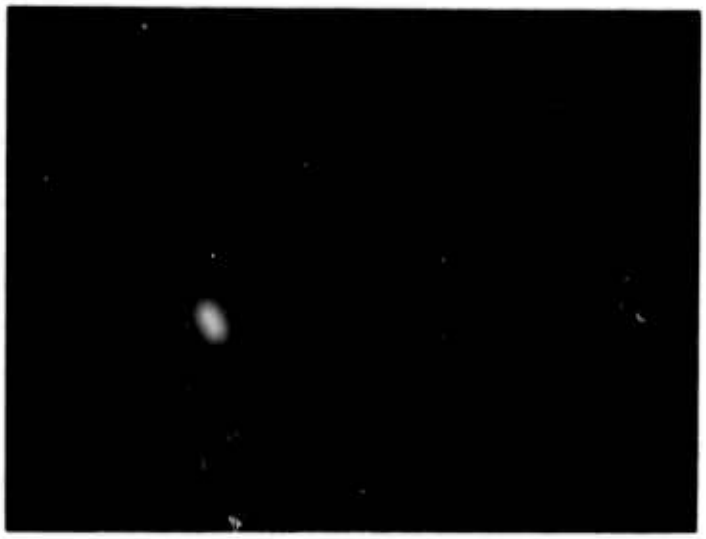


Fig. 8. Fluidic components with cast cover plate



DR. R. E. BOWLES ENGINEERING CONSULTANT
REGISTERED PROFESSIONAL ENGINEER
2105 SONDRA COURT
SILVER SPRING, MD. 20904
PHONE (301)-421-1099

FLUIDIC PRODUCTS FOR THE INDIVIDUAL

Almost everyone at this conference is technically oriented. Each of you is interested in how Fluidic Devices work and how they can solve problems in the area of your technology. It is easy to overlook the fact that each of you is also an individual person.

Not only do you work, you also eat, sleep, get sick, get well and have fun. Please listen to this presentation as a person because I am going to talk about Fluidic Products that you, the person, can use. I will briefly cover products from a number of companies. There are other interesting products on the way to market which I could not get permission to describe at this time.

In 1962 Moore Products Co made a small plastic diverter valve model shown in Fig 1a. Fig 1b shows the interior flow pattern of this device but with a fixed divider. This toy-demonstrator was used to introduce their work in "Solid State Pneumatic and Hydraulic Devices". The unit has a soft rubber sealing washer so that it can be pressed against the sink faucet to provide a water supply. It demonstrates both digital and analog operation of a boundary layer or wall interaction unit. A number of these units were given to potential customers. They are still being sold by Edmond Scientific through their catalog. Fifty Thousand of these toy-demonstrators have been built so far.

In the 1963-1964 period, a California firm produced another toy-demonstrator. I am sorry but I do not recall the firm's name. I would appreciate it if someone could identify it for me. This unit was a wooden model of a bistable flip-flop. It had a transparent cover plate and used burning incense as a power supply and flow tracer combined. The controls permitted demonstration of the bistable memory and switching capabilities of the wall interaction flueric amplifier. As with the Moore Products device this toy-demonstrator provided both fun and education. I do not have figures as to how many were sold.

The first Fluidic Product for the Individual that performed a necessary as well as a useful function was the Breathing Assistor. This device provides us with the opportunity to track a product through several stages of evolution.

Starting with a bistable flip-flop and a conventional mask, Ray Warren of the Harry Diamond Laboratories assembled a device which helped the individual breathe. Further work at HDL resulted in the configuration shown in Fig 2. Subsequently Bowles Fluidics Corp, Retec and Senko Medical of Japan developed units. The Senko unit was very simple and was used during operations. About 1000 were built and were supplanted by the BFC unit. The BFC unit was developed cooperatively with MSA. It is an IPPB, Intermittant Positive Pressure Breathing Assistor. In this therapeutic unit the patient creates a slight negative pressure to start the inhalation. The unit then drives air (mixed with medication from a nebulizer) into the patients lungs until a preset positive pressure level is reached. At that point the unit switches to the exhale mode. The downstream vent allows an

expiration pause at ambient pressure at the end of exhalation. The patient must try to inhale creating the slight negative pressure to start the next cycle. This unit shown in Fig 3 is in use and being sold both domestically and overseas.

The next generation of the IPPB at MSA is shown in Fig 4. The fluidic unit has been relocated at a greater distance from the patient. The compressor operating pressure has been increased and flow to the fluidic unit decreased. A bypass valve has been added. Goals of the modifications were:

1. Reduce sound level at the patient due to the compressor (low frequency) and the fluidic unit (high frequency).
2. Soften the dynamic response to conform to other IPPB units (this was a change for marketing and not for clinical reasons).
3. Reduce exhalation resistance (this was a change for marketing, i.e. for customer appeal and not for clinical reasons).
4. Reduce compressor air temperature rise at the patient (this was a change for marketing purposes).
5. Improve nebulizer performance via higher supply air pressure.

Note that there is no significant change in the fluidic control. These are changes in Product System to help its marketability. MSA sells a variety of Breathing Equipment. They state that the Fluidic IPPB has an outstanding field history of reliability. Only ruined elements come back, elements which have been grossly abused.

These Breathing Assistors are designed, built and sold to individuals just like you and me. As a matter of fact, I was astounded several years ago when my Doctor prescribed one for me. When I asked if I really needed it he stated that my alternative was to have a lung operation. Needless to say, I consider that the $150.00 I spent was a good investment as it solved my medical problem within three weeks in a painless and economical fashion.

Other Fluidic Breathing Equipment on the market includes Respirators by Ohio Medical and Monahan and large PBA units such as one from MSA. These use Corning Glass Fluidic elements or integrated circuitry to achieve reliable control.

In 1968 the Sherman Manufacturing Co introduced a Fluidic Lawn Sprinkler. This impulse type sprinkler uses a fluidic oscillator to digitally traverse the desired arc. A sliding member reverses the direction of traverse at each extreme position. The oscillator discharge waters the grass. This was the first Fluidic Product to be mass produced in large quantities and is shown in Fig 5.

Another serious product for indivicuals was the "Yacht Thruster" (a Fluidic Bow Thruster). This is a large diverter valve for seawater, Fig 6. Water flow is supplied by a Berkley Jet Pump. Atmospheric air is used as a control for the liquid flow. Purpose of the unit is to permit precision turning and translation of Yachts and Houseboats without the need for forward motion. This is particularly valuable during docking and undocking operations, traversing locks, etc. The capability is especially useful for power boats or houseboats having large sail area exposed to the wind. The systems work quite well. Problems and major cost items are not the Fluidics or the sea water pump or diverter valve controls. The problems are related to getting power from the engine to the sea water pump. Small boat power plants come in many varieties. They are almost allways installed using a shoehorn with little or no room left for the auxiliary power takeoff equipment. Each engine is a special problem the first time it is encountered.

Two thirds of the installations will require Engineering Design even if the engine is one previously encountered. The most profitable way to sell this Fluidic device is to sell only the Diverter Valve with controls and its matched sea water pump. Such a course leaves the power take-off and hydraulic power transmission system in the hands of the boat builder or owner. A boat builder can handle it with his in-house Engineering staff. Most boat owners can't and would end up paying far more than they anticipate for these engineering services which must be amortized over their single boat. The Yacht Thruster is a luxury item. The disappearance of the houseboat market and curtailment of the power boat market due to the energy crisis will limit the number of Yacht Thrusters put into service. Sales are concentrating on Boat Building Companies such as Burgher as the contact point with the new boat owner.

It is apparent that it is easier to make a profit on large quantity items where R&D costs can be distributed as a small unit price increment. The simpler the unit the better. Many times multiple uses or applications of the fundamental unit can provide several products from the same R&D base. One example is found in oscillation of a flow pattern. This is easy to accomplish by Fluidics. It has led to a number of Products for the Individual. I could not get permission to describe all of them to you. However, the following examples demonstrate the general path of such developments.

The Power Jet shown in Fig. 7 was a flop. It was however the forerunner of a group of successful products. The Power Jet was a simple oscillator having two discharge nozzles. Flow was digitally cycled between these two nozzles and provided discrete slugs of water. The initial models performed well as cleaning aides and provided impact cleaning action. Two reference points in the artwork were used to establish a reference distance parallel to the y axis. This reference was rigidly controlled in each step from original to production hardware. Unfortunately each step between the initial model and the production hardware introduced an assymetric distortion. Thus all y dimensions in the final hardware were true but all x dimensions were in error by a fixed percentage. The production unit flow channels were distorted from the desired shape and it did not do a good job of cleaning. The inventory was ultimately salvaged by sale to a European firm for use as high pressure pulsing massage nozzles in Sauna baths.

The Power Jet was an educational experience. The pulsing jets of water felt good when directed against the body. Thus the logical path was towards a massage shower. As insurance that the shower stay sold it was decided to provide the user with an option in his shower. The option was achieved by an internal valve which permitted the shower to be used either in the massage mode or in a spray mode. The spray mode turned out to be another winner. Wall attachment was used in the shower comb which formed the spray to provide individual jets which stayed coherent, had an excellent impact pattern coverage and didn't seem to spatter on impact. This AQUA-MASSAGE shower is a successful product for the individual. Fig. 8 shows the spray mode of operation. Figure 9 shows the Massage Mode capturing one slug of water as it impacts (and splashes) while a second slug of water is in flight towards but has not yet reached the target.

Another outgrowth of the Power Jet is the AQUA-SWIRL, a hydro massage unit for use in the bath tub. This unit operates fully submerged and is shown in Fig. 10. It was introduced at the beginning of 1974.

A further outgrowth of the Power Jet is a low cost clothes washer. This unit is shown in Fig. 11a. It clips on the side of any bucket as shown in Fig. 11b. A detergent such as Wo‡lite or Salvo is placed in the bucket with the clothes which are to be washed. Water flows through the Fluidic Oscillator and agitates the clothes+detergent as shown in Fig 11c. Small bubbles which are introduced help to float the dirt (even such heavy items as metal chips) to the surface. Surface water overflows the bucket rim into the sink or bathtub in which the bucket has been placed. After the detergent has been fully dissolved the unit continues to operate as a rinsing action. The clothes do not tangle or pebble. Action is gentle enough for the most delicate fabrics. Yet there is good cleaning action and the rinsing is excellent with a reasonable use of water. This product was introduced in the Spring of 1974.

With the success of the AQUA-MASSAGE shower, a second type of Massage shower was developed. This one, the AQUA-VIBRATOR, cyclicly issued a conical spray pattern and then a central concentrated stream of water. The sensation is quite different from that of the AQUA-MASSAGE. So is the effect. If you hold your hand in the AQUA-VIBRATOR spray massage pattern it will change color and become quite red. On removal from the spray pattern your hand will tingle. It appears that the local blood circulation has been improved, both as to flow rate and volume of blood in the local area. Fig. 12 shows the pulsing action of the conical spray pattern. The wave front of particles approaching the target is nearly a step input. Both types of showers are being tested by the Vererans Administration for potential therapeutic uses.

My last example of Fluidic Products for the Individual is also water actuated. The water pic is the most frequently mentioned potential fluidic application in the consumer area. A number of groups are (or have been) working on the fluidic water pic in a variety of configurations and capabilities. The water pic concept is to provide a jet of sequential pulses directed at the teeth and gums. A related product is the oral irrigator which uses a steady jet rather than an interupted jet. A new Fluidic Product for 1974 is an oscillating oral irrigator. In this product a small fluidic oscillator is located at the discharge end of the irrigator nozzle. Such a nozzle is shown in Fig. 13a. This causes the steady water jet to sweep back and forth as shown in Fig. 13b, a high speed photograph of an earlier model. In use the oscillator discharge is held within an inch or so of the teeth and gums. The Dentists appear to be divided roughly into two camps. One group thinks that a pulsing jet of water is God's gift to good dental hygine. The second group thinks that such high pressure pusing jets are bad for the user and cause gum separation from the teeth. The latter group appear to feel that this new oscillating oral irrigator is the optimum solution offering the advantages desired without the concurrant disadvantages of pulsing jets. As of the date this paper is being submitted the clinical tests are yet to be completed. It is however anticipated that this product will be on the market in 1974. Fig. 13c shows the complete product as it looks installed in a bathroom sink.

It is my hope that the above will serve to acquaint you with some of the possibilities, pitfalls and successes of this product area. I have described a number of Fluidic Products which have been aimed at you as an individual. I

sincerely believe that they are but forerunners of many such Fluidic Products. Products which will find their way into your everyday lives. It should be noted however that except for the two demonstrator examples each of these products exists not because it is Fluidic but because it meets a need. Each incorporates our technology because FLUIDICS offers a simple and outstandingly reliable solution to the product need. In each case Fluidics has provided a new and useful control dimension. There are many opportunities for you to contribute Fluidic Products for the Individual. Why don't you give it a try?

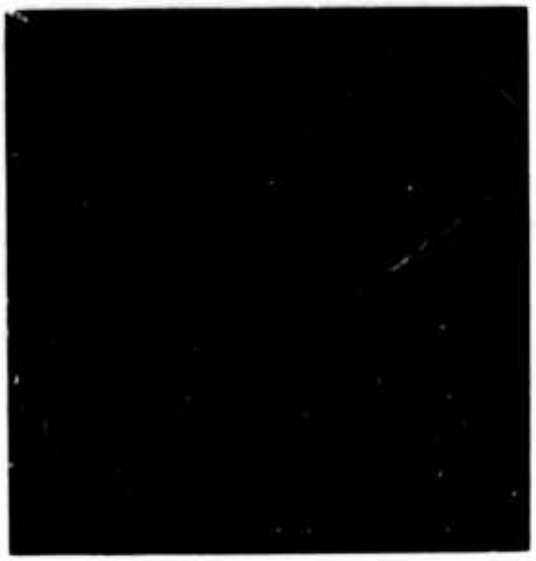


FIG. 1a
MOORE PRODUCTS DEMONSTRATOR

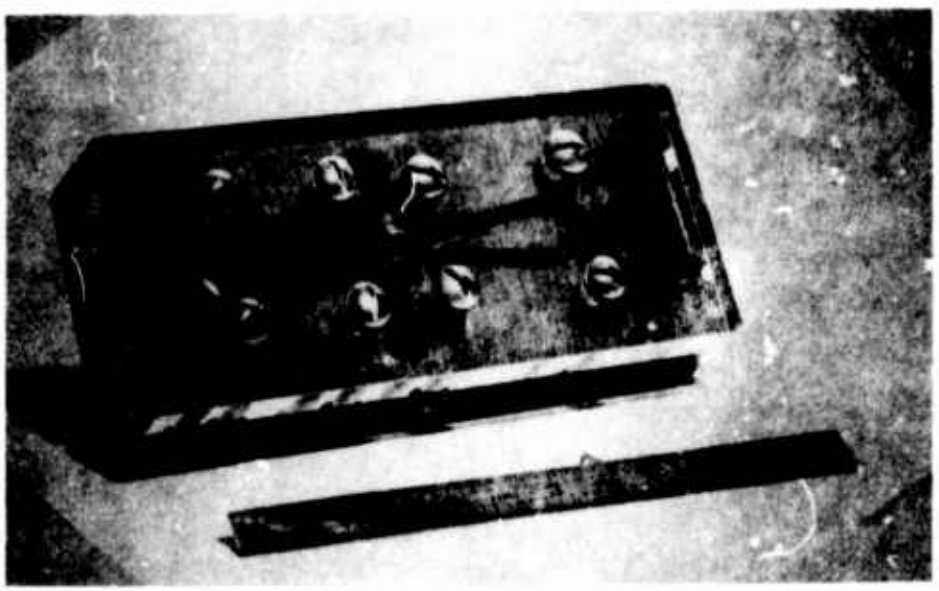


FIG. 1b
FLOW CHANNELS OF THE MOORE PRODUCTS DEMONSTRATOR

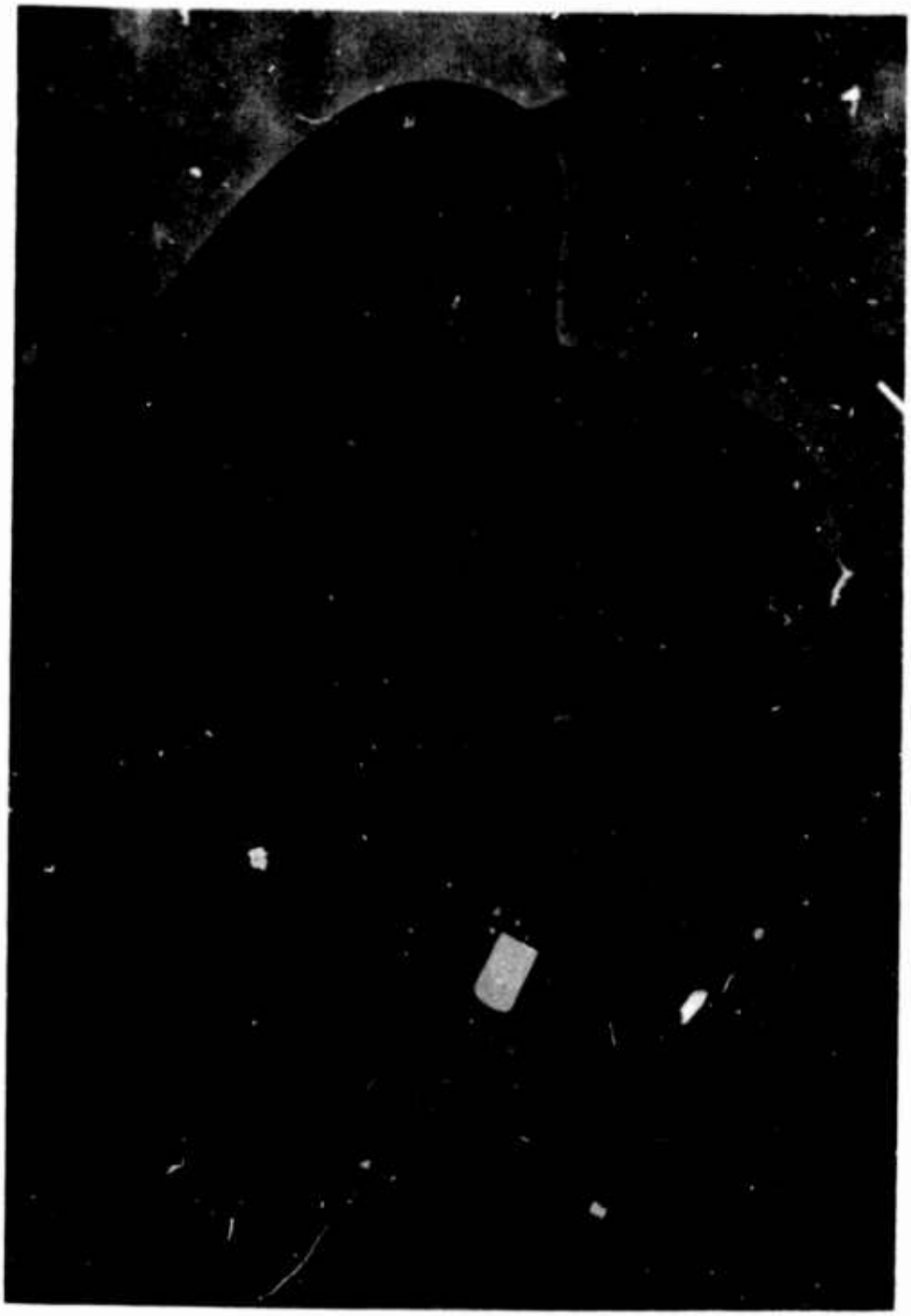


FIG. 2
HARRY DIAMOND LABORATORIES EMERGENCY RESPIRATOR

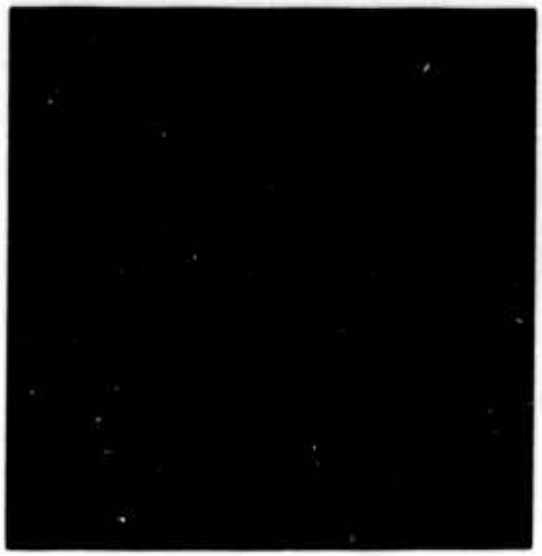


FIG. 3a
BOWLES FLUIDICS CORP I.P.P.B.

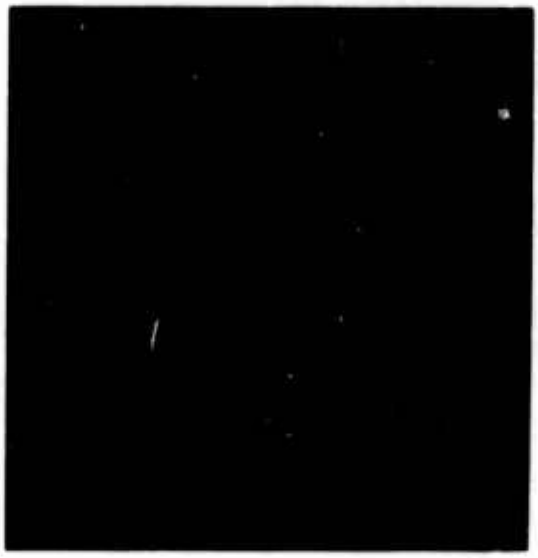
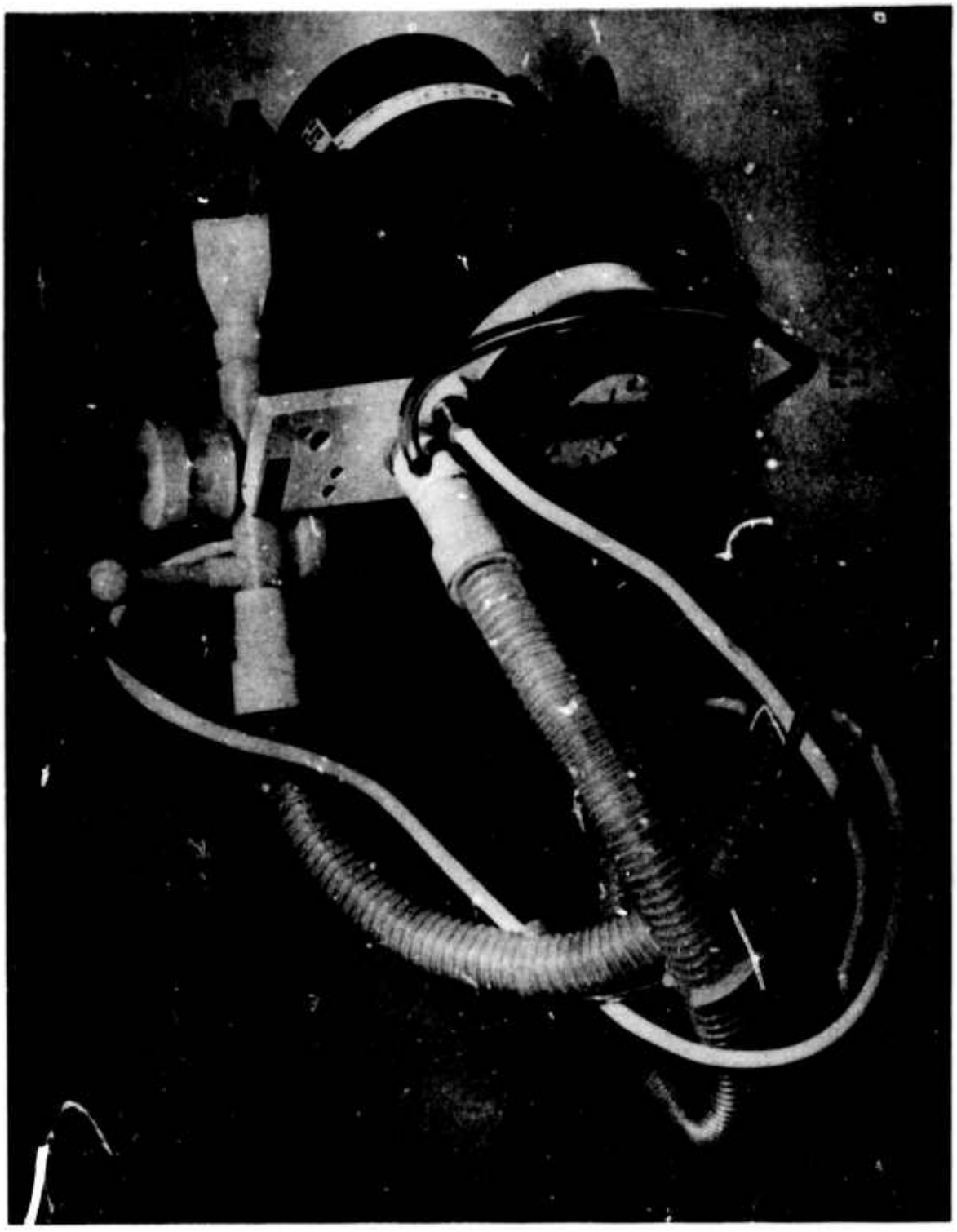


FIG. 3b
BOWLES FLUIDICS CORP I.P.P.B.



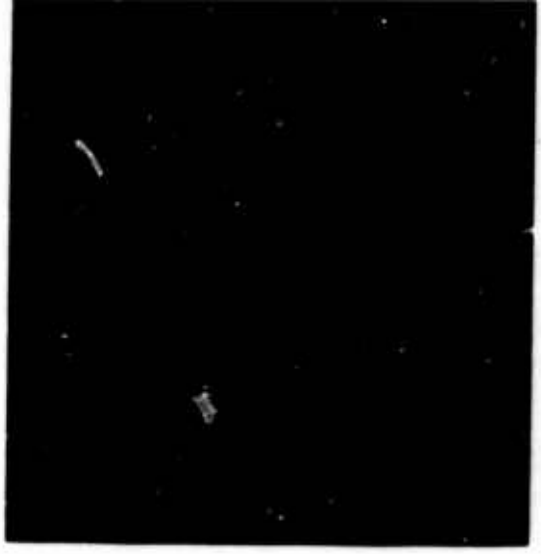


FIG. 5
SHERMAN MFG. LAWN SPRINKLER

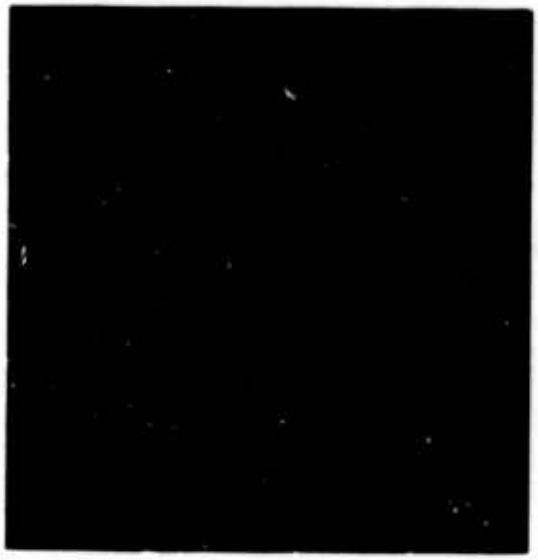


FIG. 7
BFC POWER JET



FIG. 6



FIG. 8
THE "AQUA-MASSAGE" IN THE SPRAY MODE

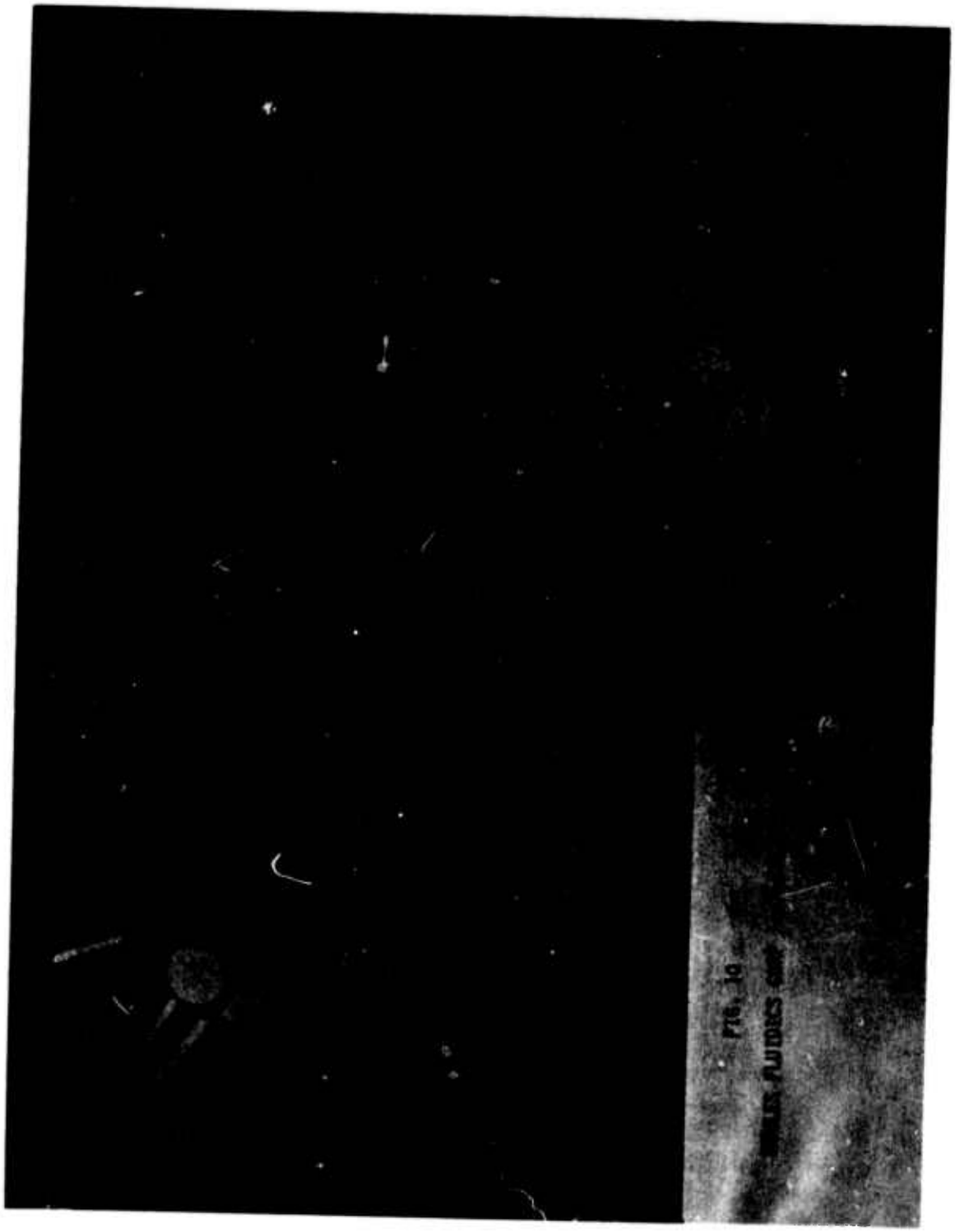
A DIFFERENT "FEELING" SHOWER. SIXTY COHERENT STREAMS OF WATER ARE FORMED INTO THREE CONCENTRIC RINGS FOR FULL COVERAGE. FLUIDIC ENGINEERING HAS ACHIEVED A LAMINAR FLOW SO THAT THE WATER "STREAMS" CARESSINGLY OVER THE BODY.



FIG. 9

THE "AQUA-MASSAGE" IN THE MASSAGE MODE

ALTERNATING JETS OF WATER RYTHMICALLY DRUM AGAINST THE BODY LIKE THE PROBING FINGERS OF YOUR OWN PERSONAL MASSEUR. IN THE UNRETOUCHED PHOTO ABOVE, NOTE HOW ONE PULSE OF WATER HAS STRUCK WHILE THE NEXT IS ON THE WAY. AT 25 PSI DEADHEADED PRESSURE (NORMALLY AVAILABLE) THE "AQUA-MASSAGE" PROVIDES 480 PULSES PER MINUTE.


FIG. 10

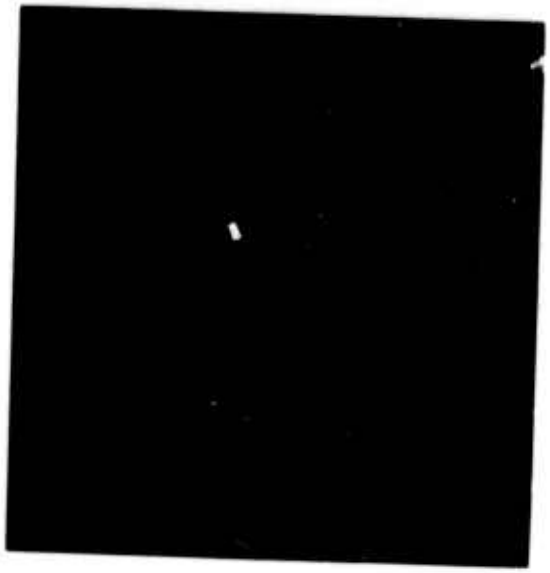


FIG. 11a
BFC AQUA-WASHER

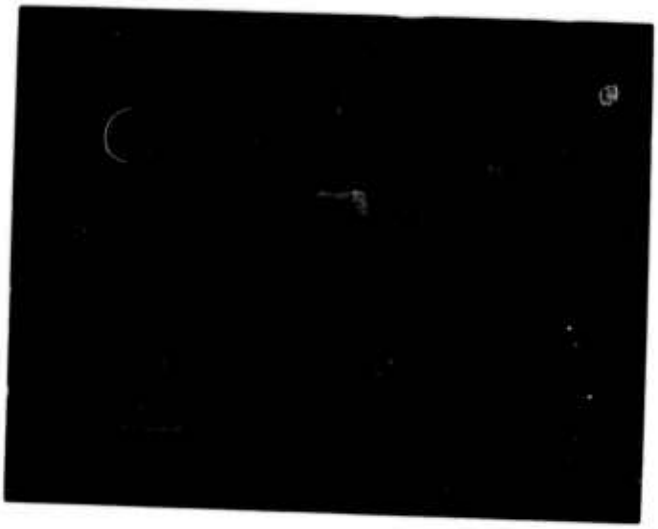


FIG. 11b BFC AQUA-WASHER WITH BUCKET

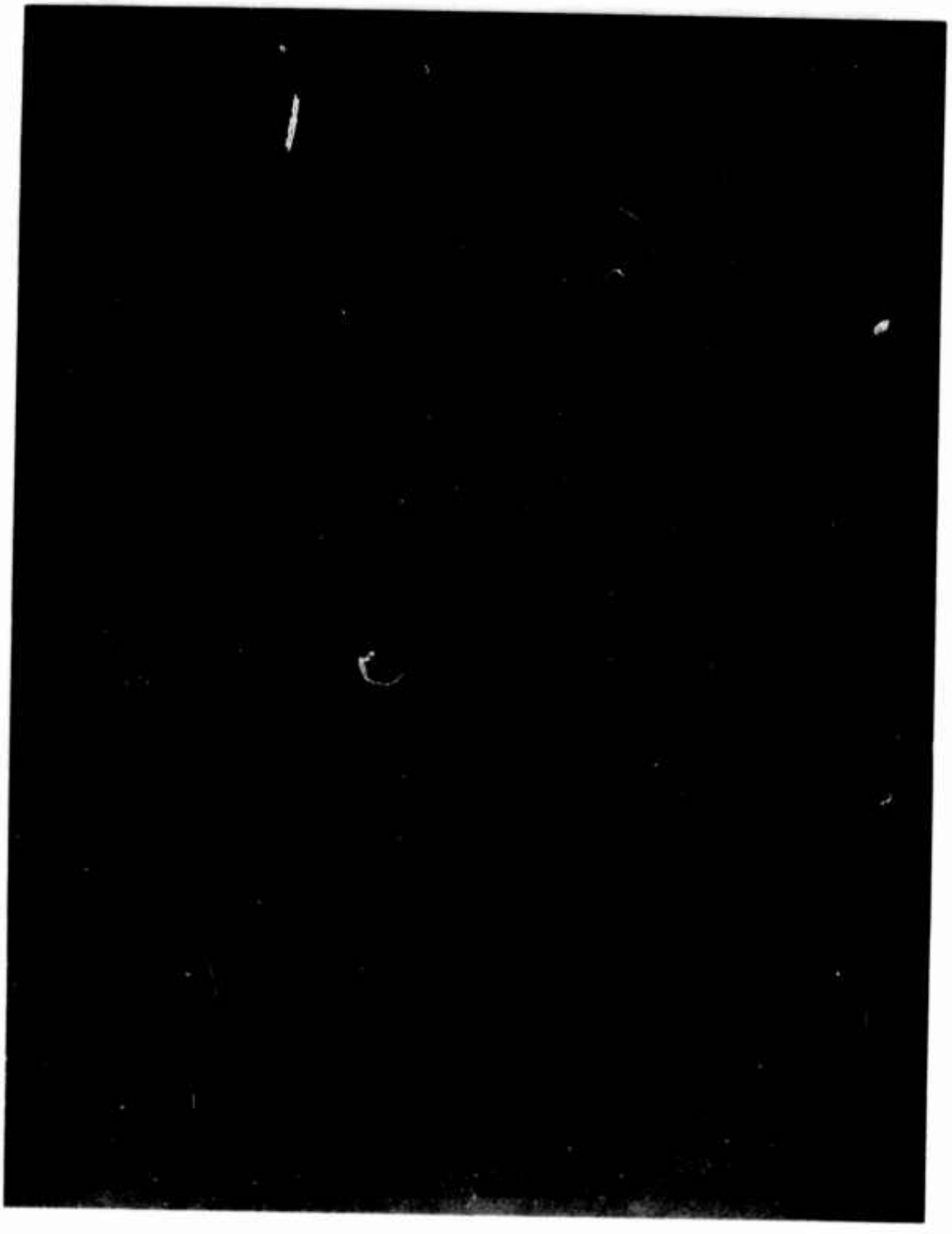




FIG. 12
BFC AQUA-VIBRATOR SHOWER

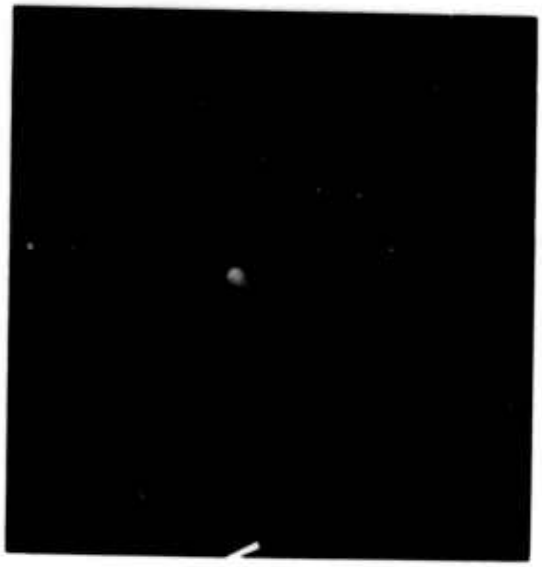


FIG. 13a
BFC AQUA-IRRIGATOR NOZZLE

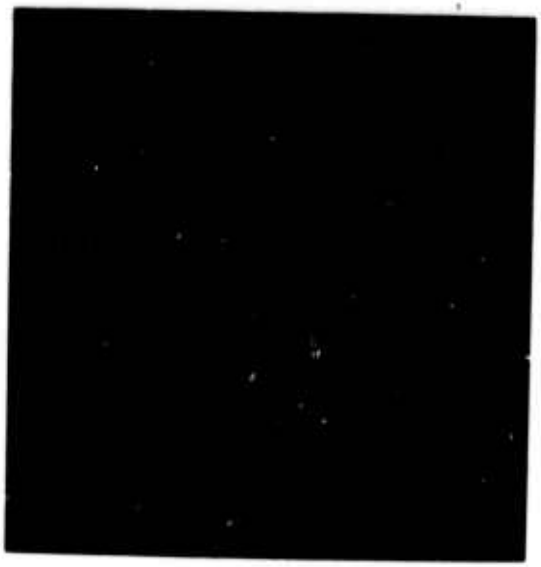


FIG. 13b
SWEEPING ACTION OF AQUA-IRRIGATOR

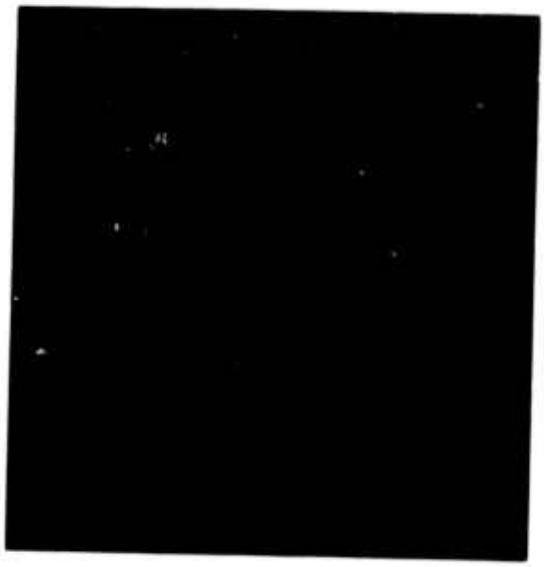


FIG. 13c
AQUA-IRRIGATOR INSTALLATION

AEROSPACE FLUIDICS
APPLICATIONS AND CIRCUIT MANUFACTURE

T. G. SUTTON, SR. DEVELOPMENT ENGINEER
FLUIDIC SYSTEMS
AIRESEARCH MANUFACTURING COMPANY
A DIVISION OF THE GARRETT CORPORATION
PHOENIX, ARIZONA

W. J. ANDERSON, METHODS ENGINEER
AIRESEARCH MANUFACTURING COMPANY
A DIVISION OF THE GARRETT CORPORATION
PHOENIX, ARIZONA

Preceding page blank

ABSTRACT

The application of fluidics to the solution of aerospace control problems began at AiResearch in 1964. Several development programs have resulted in production applications related to the major AiResearch product lines which include gas turbines, propulsion engines, air motors, and environmental control systems. Early in these development programs, it was realized that the manufacture of monolithic flueric circuits would be necessary for aerospace use of this new technology. Research and investigation of production processes resulted in the use of photo-chemical machining and assisted diffusion bonding for manufacture of production and development fluidic circuitry. The use of these processes has led to the successful application of fluidics to aerospace products.

TABLE OF CONTENTS

	PAGE
ABSTRACT	46
INTRODUCTION AND SUMMARY	49
APPLICATIONS	50
REQUIREMENTS FOR FLUIDIC CIRCUIT CONSTRUCTION	68
FUTURE FLUIDIC CONTROL APPLICATIONS	68
MANUFACTURING OF FLUIDIC CIRCUITS	70
FLUIDIC CIRCUIT MANUFACTURING PROCESS	74
CONCLUDING REMARKS	80

LIST OF FIGURES

FIGURE	DESCRIPTION	PAGE
1	LOAD CONTROL SYSTEM	51
2	FLUIDIC TEMPERATURE SENSOR INSTALLATION ON AN AIRESEARCH 95-2 APU, FLUIDIC TEMPERATURE SENSOR DEVELOPMENT PROGRAM	52
3	AIRESEARCH TSE231 ENGINE OVERSPEED CONTROL	54
4	OVERSPEED FUEL SHUTOFF VALVE ON AIRESEARCH TSE231 ENGINE	55
5	FUEL CONTROL OF AIRESEARCH GAS TURBINE APU	57
6	BREADBOARD FUEL CONTROL OF AIRESEARCH GAS TURBINE APU	58
7	BLOCK DIAGRAM OF TURBOJET CONTROL SYSTEM	59
8	INSTALLATION OF FLUIDIC FUEL CONTROL IN ETJ-331	61
9	BLOCK DIAGRAM OF SURGE VALVE ON NORTH AMERICAN ROCKWELL B-1 AIRPLANE	62

TABLE OF CONTENTS (CONCLUDED)

FIGURE	DESCRIPTION	PAGE
10	B-1 APU SURGE VALVE	63
11	THRUST REVERSER SPEED AND TORQUE CONTROL OF GENERAL ELECTRIC CF6 ENGINE	65
12	FLUIDIC CIRCUIT FOR CF6 THRUST REVERSER DRIVE UNIT	66
13	PRESSURE REGULATING VALVE OF LOCKHEED S-3A AIRCRAFT	67
14	FLUIDIC ENVIRONMENTAL CONTROL SYSTEM LOGIC DIAGRAM	71
15	ELECTRO-HYDROFLUIDIC TRANSDUCER	72
16	STEPS IN PHOTOCHEMICAL MILLING OF FLUERIC CIRCUITS MADE BY AIRESEARCH-PHOENIX	75
17	ETCHING PROCESS AND ARTWORK ALLOWANCE	77
18	QUARTZ LAMP FURNACE USED FOR BONDING FLUIDIC CIRCUITS	79

LIST OF TABLES

TABLE	DESCRIPTION	PAGE
1	SUMMARY OF OPERATING CONDITIONS IN AEROSPACE FLUIDIC APPLICATIONS	69
2	SUMMARY OF FLUIDIC ELEMENT MANUFACTURING PROCESSES	73

LIST OF ATTACHMENTS

APPENDIX 1 FLUIDIC CIRCUIT DIAGRAMS

AEROSPACE FLUIDICS
APPLICATIONS AND CIRCUIT MANUFACTURE

T. G. SUTTON
W. J. ANDERSON

INTRODUCTION AND SUMMARY

The purpose of this paper is to outline the development and production applications of fluidics as related to AiResearch aerospace product lines and to describe the manufacturing process used for these applications.

Fluidics technology as it is known today started in the late 1950's and was widely publicized in the early 1960's. Initially, fluidics was considered as being applicable to most control systems in production at that time. This concept was soon shown to be untrue in the aerospace field as production applications did not materialize as expected. However, industrial applications flourished for many reasons, among which were reliability of the components, flexibility in control system packaging, and availability of components with which to make these systems.

Aerospace requirements differ from industrial requirements mainly in that each application tends to pose unique package and environmental conditions on the system. This has presented designers with a continuous problem, not only in how to make a part work but also how to make it fit in the available space. This is further accentuated in fluidics by the variation of flow in small passages with temperature and pressure level changes, thereby causing mismatching of amplifiers and resistance or capacitance networks. These basic phenomena impose severe problems during flueric* circuit development unless the breadboard circuits and components are practically identical with those which are considered ready for production.

Fluidic circuits also are akin to electronics in many respects and, as such, perform complex functions requiring large numbers of components and connecting paths. To overcome these obstacles, it was necessary that a manufacturing

* Fluerics: The area within the field of fluidics in which fluid components and systems perform control functions without the use of mechanical parts.

technique which would satisfy both development and production be found. After considerable research into the manufacturing processes in use in development and production stages, the photo-chemical milling process employed in the electronics industry was shown to provide a good solution to the unique problems of fluerics. The process enables parts to be obtained rapidly at minimal cost for development and is readily adaptable to aerospace-type production. Initial testing of circuits made from the laminations produced by the process may be accomplished by simply clamping the parts together; final checks may be made with the parts bonded together. Although bonding was not originally considered a major problem, the small leakage rates acceptable within flueric circuits soon showed that bonding was essential for high reliability. This again led to a continuation of the manufacturing research program and to the decision to use an assisted diffusion bonding process.

APPLICATIONS

AiResearch Manufacturing Company of Arizona has three main product lines, namely: propulsion engines, gas turbines, and pneumatic systems including air motors. Fluidics technology has been applied to all of these product lines by incorporating temperature sensors, speed sensors, pressure sensors, and their associated computational circuitry into various components. Some of these applications are described in the material that follows.

A. Auxiliary Power Unit (APU) Bleed Air Load Control

A test program to demonstrate the capabilities of fluidics was begun at AiResearch in 1967. This program was aimed at solving some reliability problems associated with the bi-metal thermostat used in an APU load control system. This bi-metal thermostat sensed exhaust gas temperature and modulated a valve to control the engine bleed air load to limit temperature. The replacement sensor consisted of a flueric temperature-sensitive oscillator, a frequency converter, and a gain block. Supply pressure was obtained from the engine compressor plenum via a 150-micron wash filter and a 40-micron inline filter. A simple pneumatic pressure regulator held the pressure to the flueric circuits at 20 ±1.5 psig over the control range. The output of the fluidic gain block drove the butterfly valve actuator directly. Figure 1 shows a block diagram of the control system and Figure 2 shows a photograph of a sensor installation.

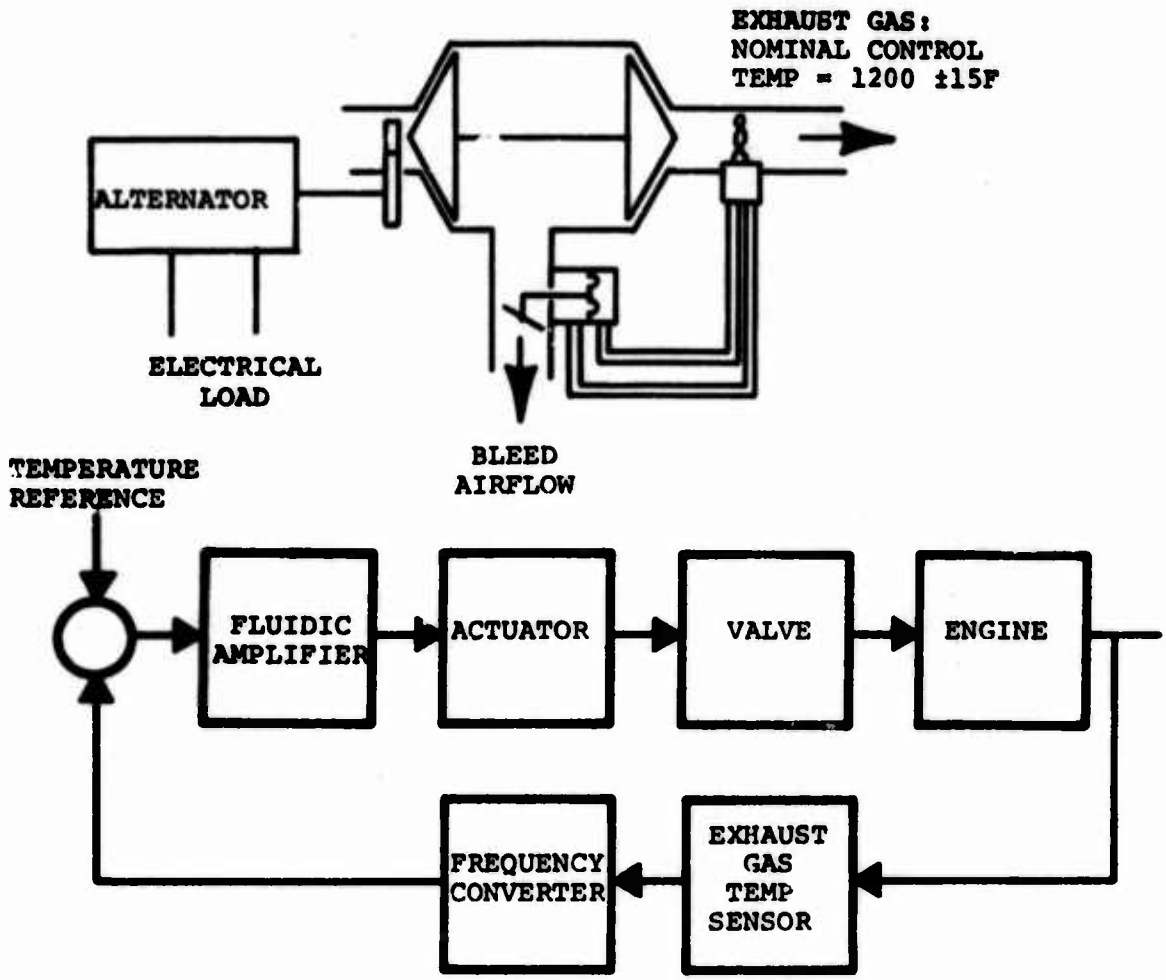


FIGURE 1

LOAD CONTROL SYSTEM

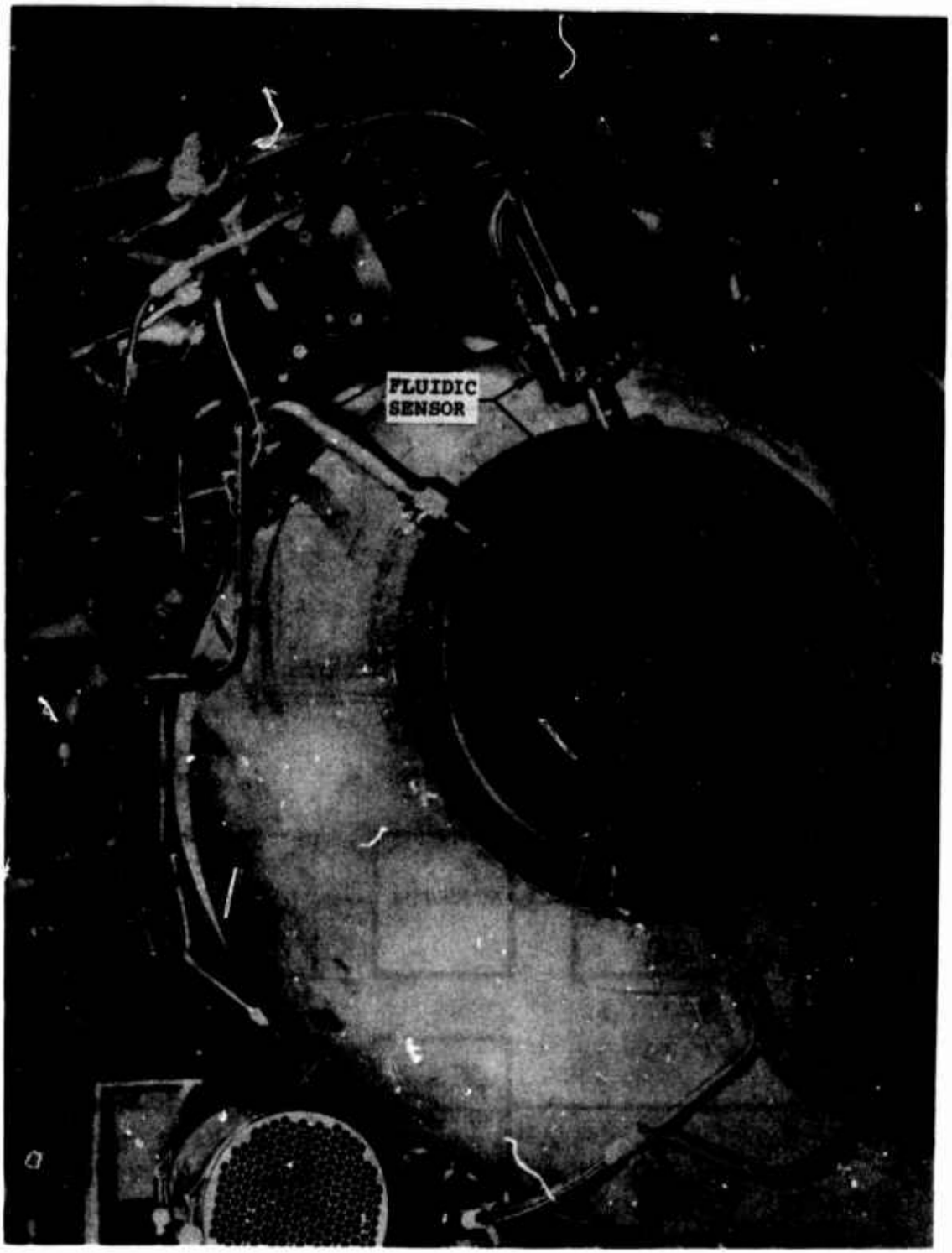


FIGURE 2

FLUIDIC TEMPERATURE SENSOR INSTALLATION
ON AN AIRESEARCH 95-2 APU
FLUIDIC TEMPERATURE SENSOR
DEVELOPMENT PROGRAM

Testing of the system was accomplished over a two-year period with the cooperation of several airlines and the Air Force Aero Propulsion Laboratory. Both ground and airborne equipment were involved. A total of 780 hours and 3400 cycles of operation were accumulated on ground equipment and 90 hours of operation on airborne equipment. No flueric failures occurred although filters were plugged and two mechanical problems were encountered.

This program showed the capability of flueric temperature sensors while operating on gas turbine engines and provided a small amount of background and experience in the operation of fluerics in the field.

B. Free Turbine Overspeed Fuel Shutoff

Free turbine engines, either for primary or secondary power, must meet an F.A.A. requirement that calls for protection against free turbine overspeed and possible wheel burst. Either a containment shield must be provided for the turbine wheel or a secondary backup control must be used to prevent the overspeed condition. The AiResearch TSE231 engine is a 450 shp free turbine machine. Overspeed protection by the use of a secondary overspeed fuel shutoff valve was chosen based on the tradeoff of size and weight against containment capability. The overspeed-sensing device was required to operate on the turbine wheel in an 800F ambient which made fluidics the ideal candidate for the control.

A block diagram of the fluidic system is shown in Figure 3 and a photograph is shown in Figure 4. The flueric control module consists of a frequency converter that uses a frequency input generated by a lobe on the free turbine hub which interrupts a nozzle and receiver as it rotates. The output of the converter is compared to a dual set point reference to enable ground checkout and normal operation. A final bi-stable output is achieved using amplifiers with regenerative feedback. This on-off pneumatic signal drives a diaphragm-operated sear pin to allow closure of the spring-operated fuel shutoff valve located between the main fuel control and the combustor nozzles. Manual override of the fuel shutoff valve is available in the event of inadvertent failure of the control.

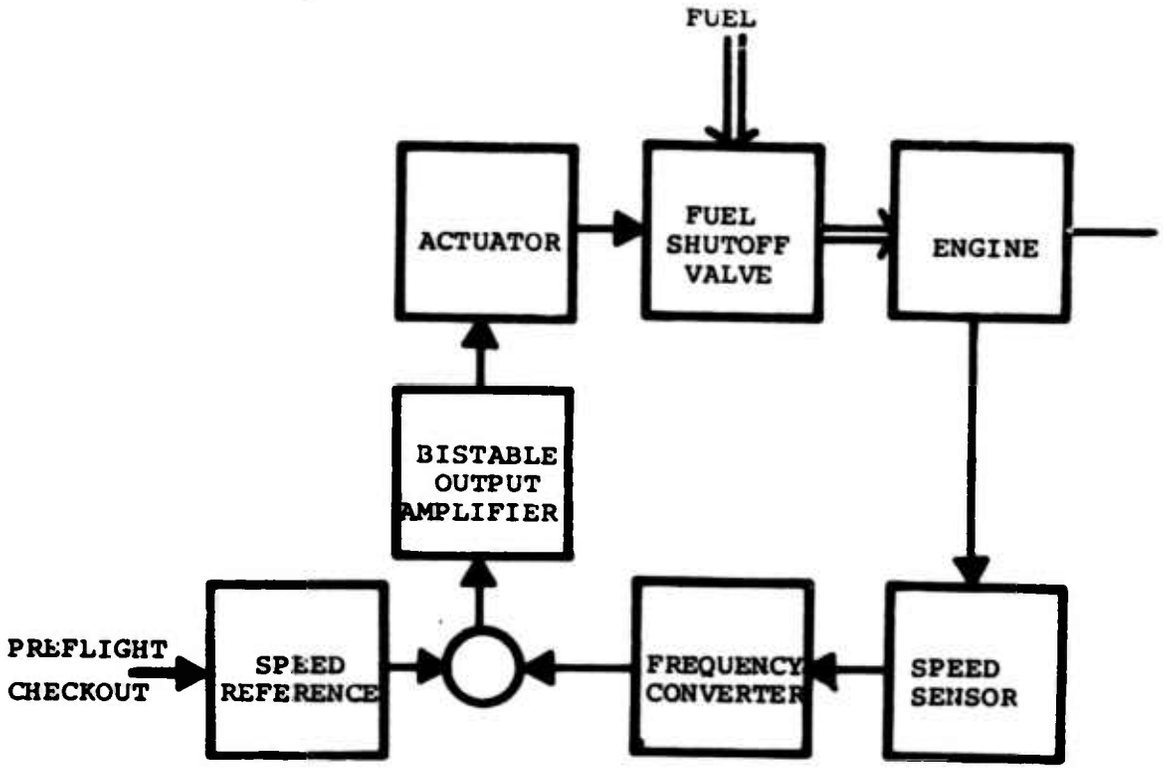
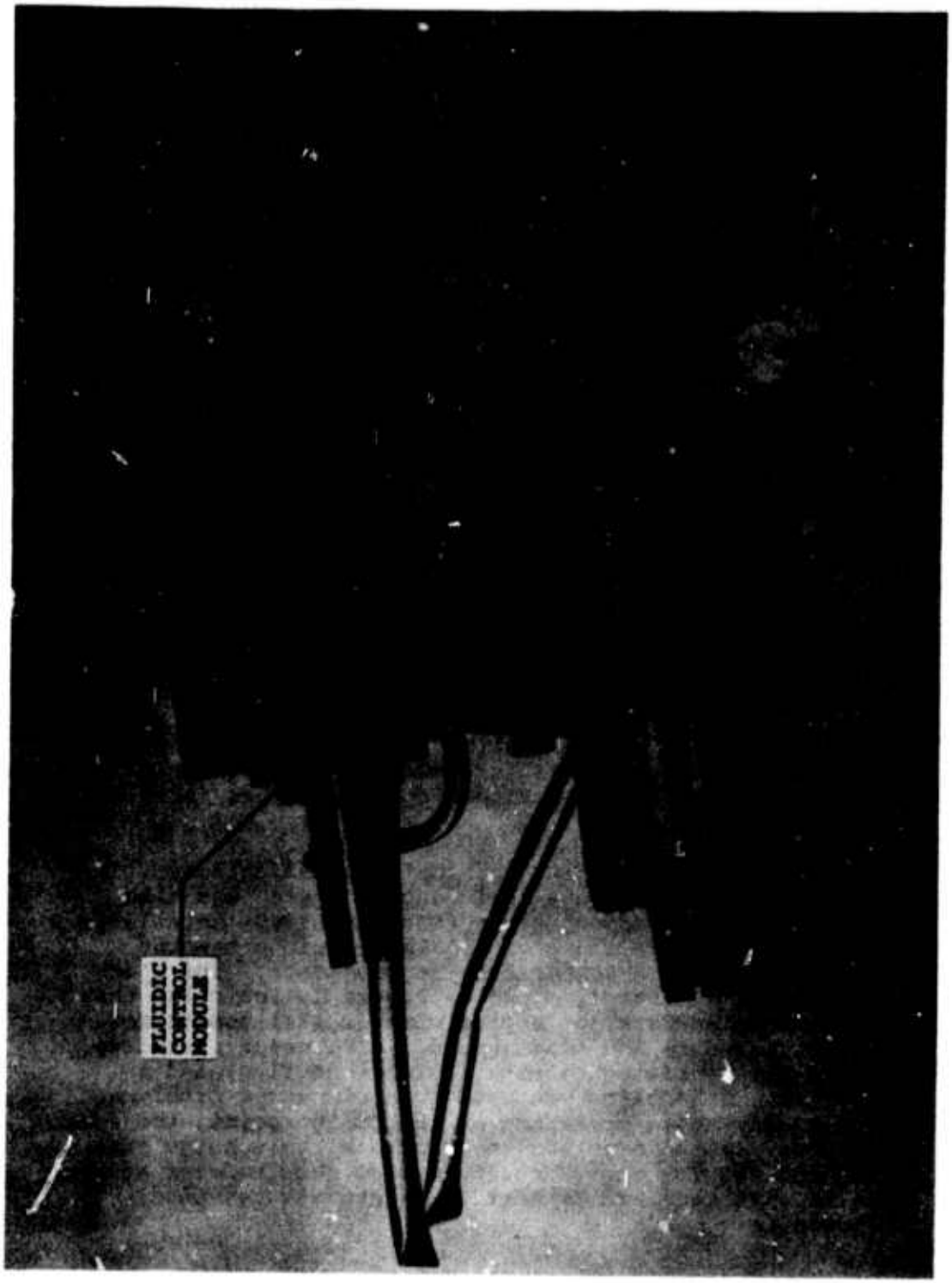


FIGURE 3

AIRESEARCH TSE231 ENGINE
OVERSPEED CONTROL



OVERSPEED FUEL SHUTOFF VALVE ON
AIRESEARCH TSE231 ENGINE

FIGURE 4

C. Auxiliary Power Unit Fuel Control

Since its inception in the late 1950's, fluidics has often been considered as a solution to many of the problems associated with fuel controls, particularly those related to cost and reliability. When a small, 50-horsepower, low-cost APU was under development, fluidics was chosen for the fuel control system.

The control was designed to perform the following functions: (a) provide fuel flow at a rate to prevent surge during acceleration, (b) limit droop of speed during steady-state operation, and (c) prevent engine damage by conditions which could cause overspeed or overtemperature. A block diagram of the control is shown on Figure 5 and a photograph of the breadboard control is shown on Figure 6. The flueric control block contains a frequency converter, "least wins" logic, and output amplification stages which provide the compressor discharge scaling and limit functions in addition to the overall signal scaling.

D. Turbojet Fuel Control

This turbojet engine application for fluidics is typical of the requirements for low cost and high reliability. The engine was designed for expendable (single mission) missile use.

In addition to meeting the cost and reliability requirements, the complete fuel control system was also constrained by the added feature that required installation of the system inside the engine. This again presented unique packaging and temperature requirements. The block diagram for the control, shown by Figure 7, indicates that the sensed parameters for engine control were compressor discharge pressure and shaft speed. Compressor discharge pressure was scheduled to obtain light-off flow, and acceleration scheduling was used to avoid surge problems. During steady-state operation at the design point, the speed signal was used to override the compressor discharge pressure signal and thereby reduce the fuel flow required for acceleration to that required to meet the steady-state speed requirements.

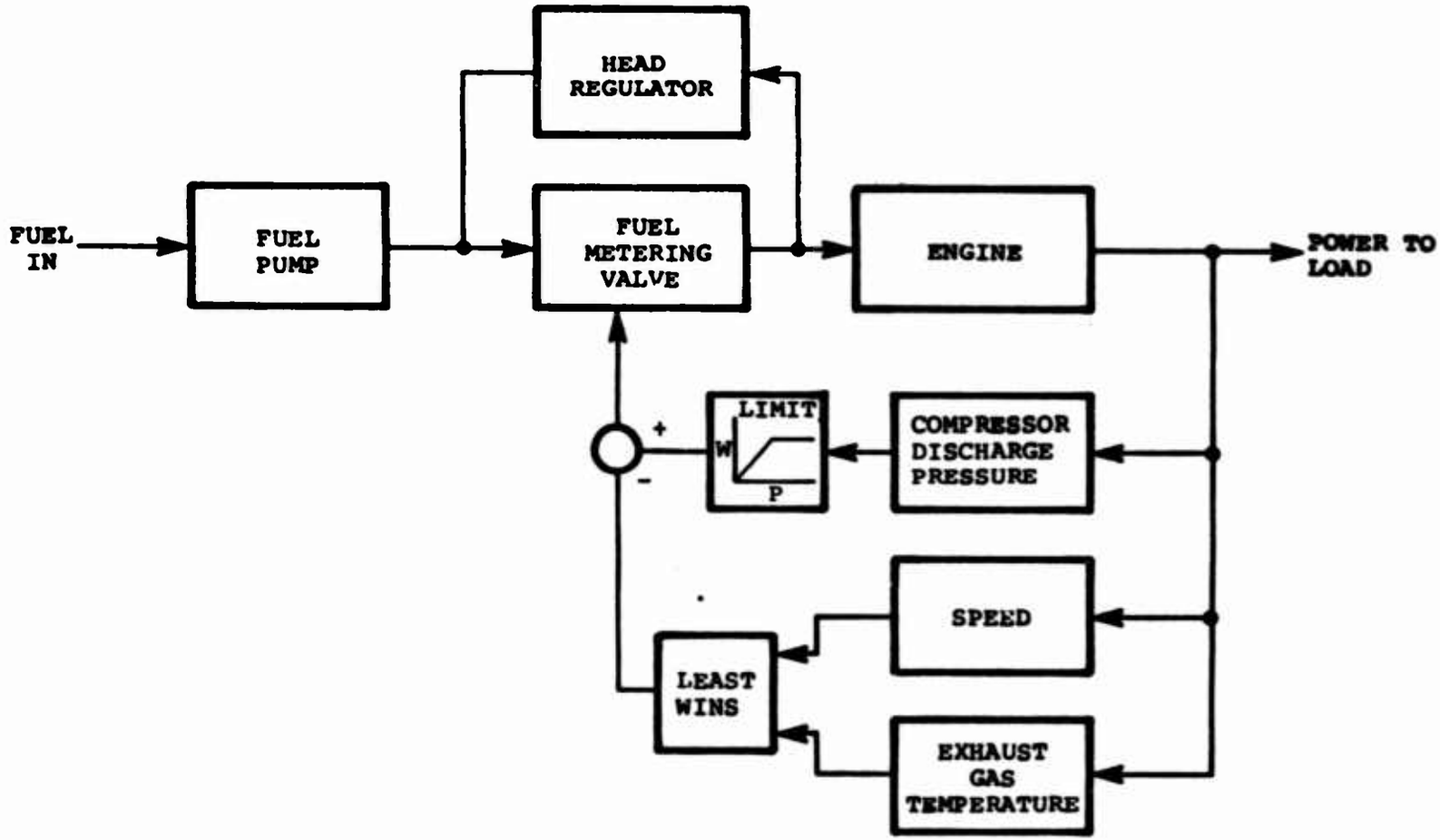


FIGURE 5

FUEL CONTROL OF
AIRESEARCH GAS TURBINE APU



BREADBOARD FUEL CONTROL OF
AIRESEARCH GAS TURBINE APU

FIGURE 6

W_f = METERED FUEL TO ENGINE
P_{CD} = COMPRESSOR DISCHARGE PRESSURE
N = ENGINE ROTOR SPEED
X = METERING VALVE POSITION
ΔP_G = POSITION SENSOR OUTPUT PRESSURE
P_F = ORIFICED COMPRESSOR DISCHARGE PRESSURE
P_E = SPEED SENSOR OUTPUT PRESSURE
ΔP_K = METERING VALVE ACTUATION PRESSURE

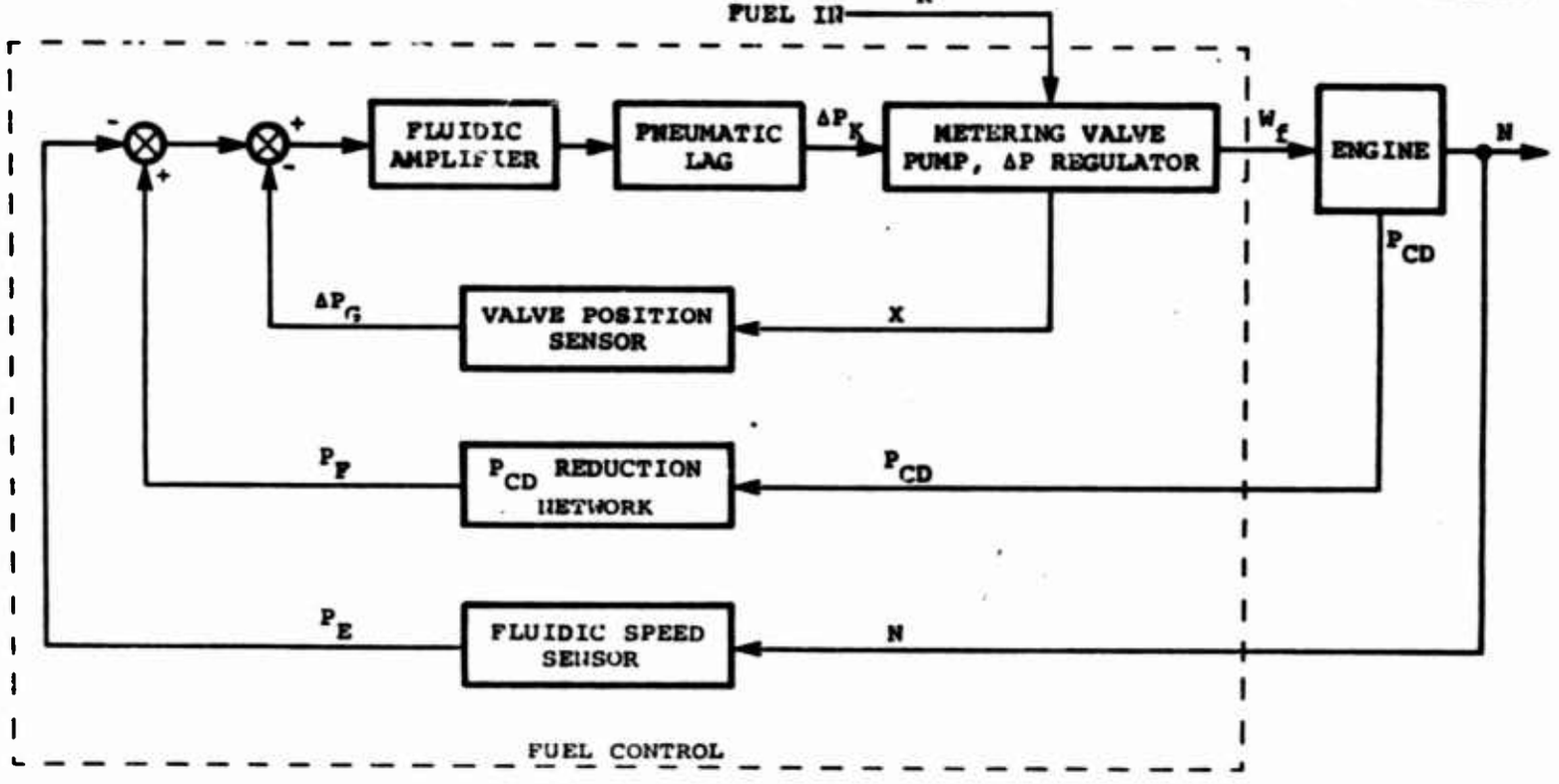


FIGURE 7

BLOCK DIAGRAM OF TURBOJET CONTROL SYSTEM

The compressor discharge pressure was scheduled by a flueric pressure reduction circuit and the speed signal, generated by a nozzle-receiver-interrupter assembly mounted on the fuel pump shaft, was converted to a pressure by a flueric frequency-to-analog converter. These circuits and the flueric output amplifiers are shown in Figure 8 as mounted on the engine. This figure also shows the location of the hydraulic portion of the control consisting of a high-speed vane pump, delta pressure head regulator, and the metering valve whose diaphragm actuator was modulated by the flueric circuit output. As previously mentioned, this installation presented problems of packaging, installation, and performance under a hostile environment which few technologies could solve. Ambient temperatures ranged from minus 65F to 500F and ambient pressures ranged from 6 psia to 20 psia. Control accuracies over the range had to be maintained at three percent during acceleration and two percent under steady-state operating conditions. Actual engine tests with many engines over a period of a year showed that the requirement for three percent accuracy was met by the control and that, after the first major temperature transients had occurred, a control accuracy of one percent was achieved.

E. APU Surge Control Valve

A large number of gas turbines used for auxiliary power are designed with oversize compressor sections so that compressed air may be extracted for many uses. The auxiliary power unit for the North American Rockwell B-1 engine is such a machine. During the start and acceleration sequence or under any transient condition when bleed air is not extracted, the backpressure on the compressor may cause surge. To avoid this, a scheduled amount of air must be bled from the compressor plenum. AiResearch chose a fluidic controller to operate a mechanical valve to meet the requirements. The controller schedules the bleed flow for the engine as a function of a demanded electrical signal received from the main fuel control. Figure 9 shows a block diagram and Figure 10 presents a photograph of the valve. This approach has resulted in a valve which has performed throughout engine testing without malfunction or change and which meets all the predicted performance requirements under temperature, vibration, and altitude conditions.

INSTALLATION OF FLUIDIC
FUEL CONTROL IN ETJ-331

PHOTO NO. P-43611-1

FIGURE 8

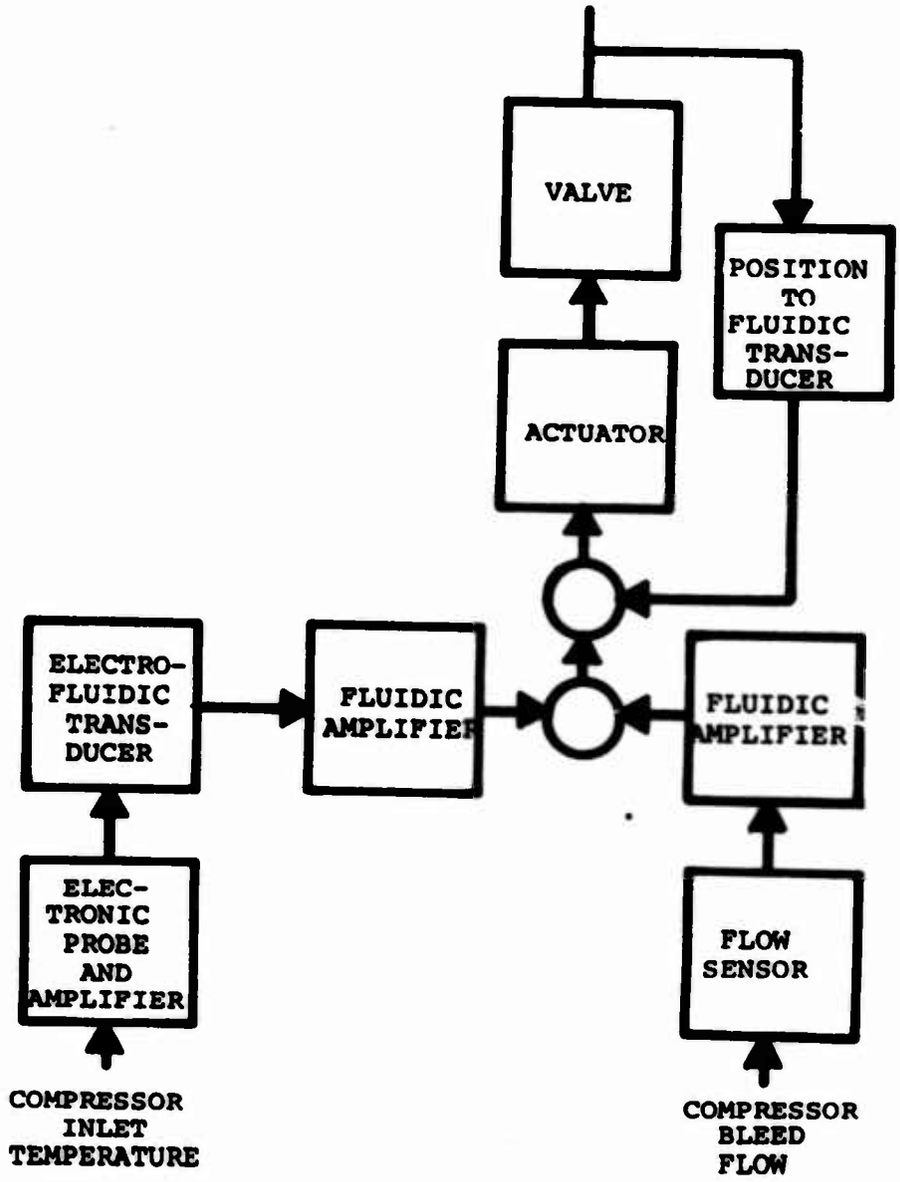


FIGURE 9

BLOCK DIAGRAM OF SURGE VALVE ON
NORTH AMERICAN ROCKWELL B-1 AIRPLANE

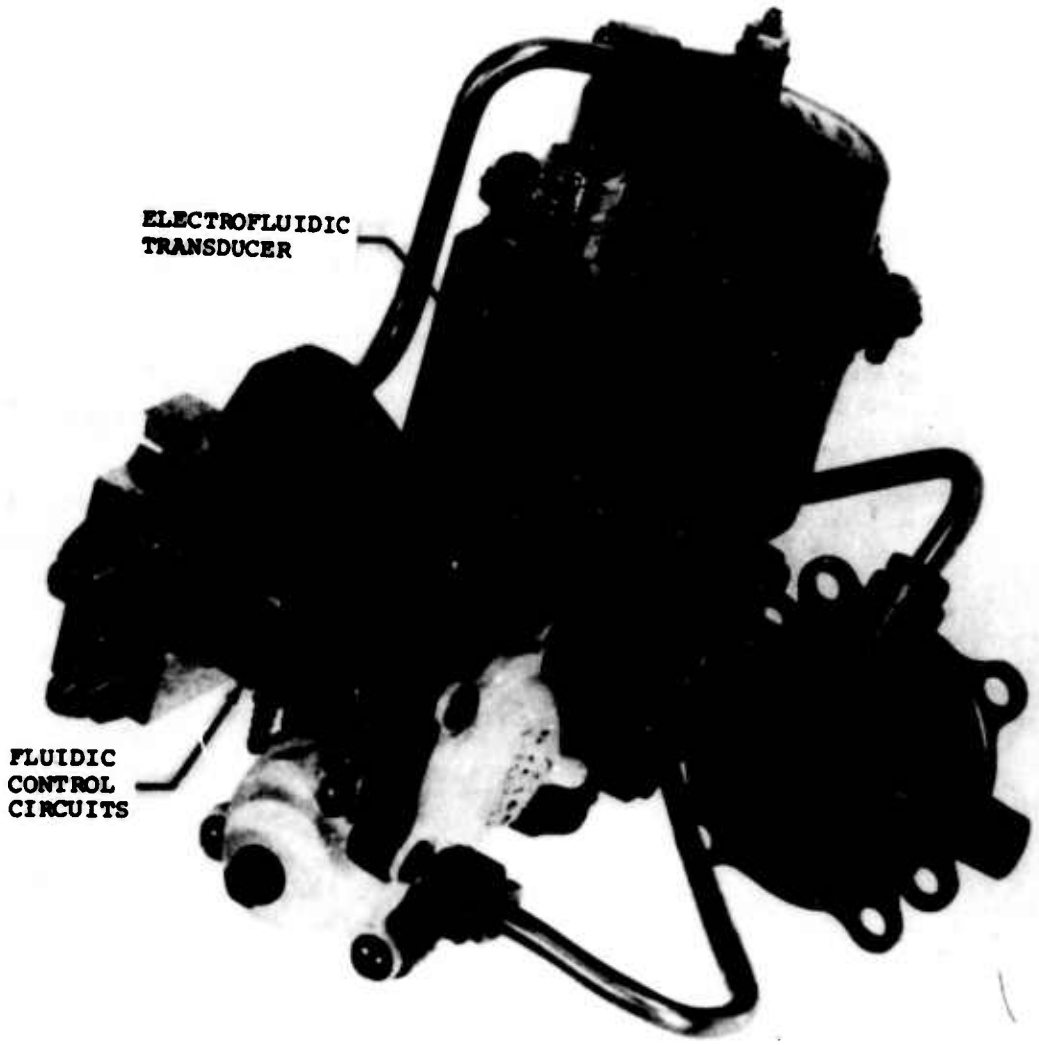


PHOTO NO. P-45807-2

FIGURE 10

APU SURGE CONTROL VALVE ON THE
NORTH AMERICAN ROCKWELL B-1 AIRCRAFT

F. Thrust Reverser Actuator Controls

In recent years, commercial aircraft have turned to pneumatic actuators for operation of their thrust reverser mechanisms. The thrust reversers for the General Electric CF-6 engine (used on the DC-10 and A300 airplanes) and the Rolls-Royce Olympus engine (used on the Concorde SST airplane) have such rotary gear motor actuators. These actuators are equipped with fluidic speed controls. In terms of production, these represent the highest quantity production rate for aerospace fluidics with over 600 systems already delivered.

The Concorde/Olympus system operates not only during thrust reversal but also during transonic flight to optimize the exit nozzle area and during takeoff to minimize noise. The gear motor actuator contains the now familiar nozzle-receiver interrupter pulse generator. A fluidic frequency-to-pressure converter provides the control signal to limit the speed of operation of the gear motor. This control is unique in that it operates over an altitude range from sea level to over 80,000 feet.

The CF-6 thrust reverser system was the first production aerospace fluidic application. This again is a speed control system; however, in addition, the system must perform a torque-limiting function at the ends of the stroke. To meet performance requirements (under both steady-state and transient conditions), this system also uses an operational amplifier with a lead-lag characteristic. A block diagram is shown in Figure 11. Figure 12 shows the fluidic circuit.

G. Pressure Regulator for Lockheed S-3A

The avionics bays on the Lockheed S-3A airplane are cooled either from the aircraft environmental control system or by ram air. When ram air is used, the large butterfly valve shown in Figure 13 is opened and the flow rate into the avionics bay is controlled by the fluidic module. This module consists of a simple gain block which maintains the butterfly valve opening such that a constant pressure drop of 7 in. H_2O is held between the inlet to the bay and the bay itself.

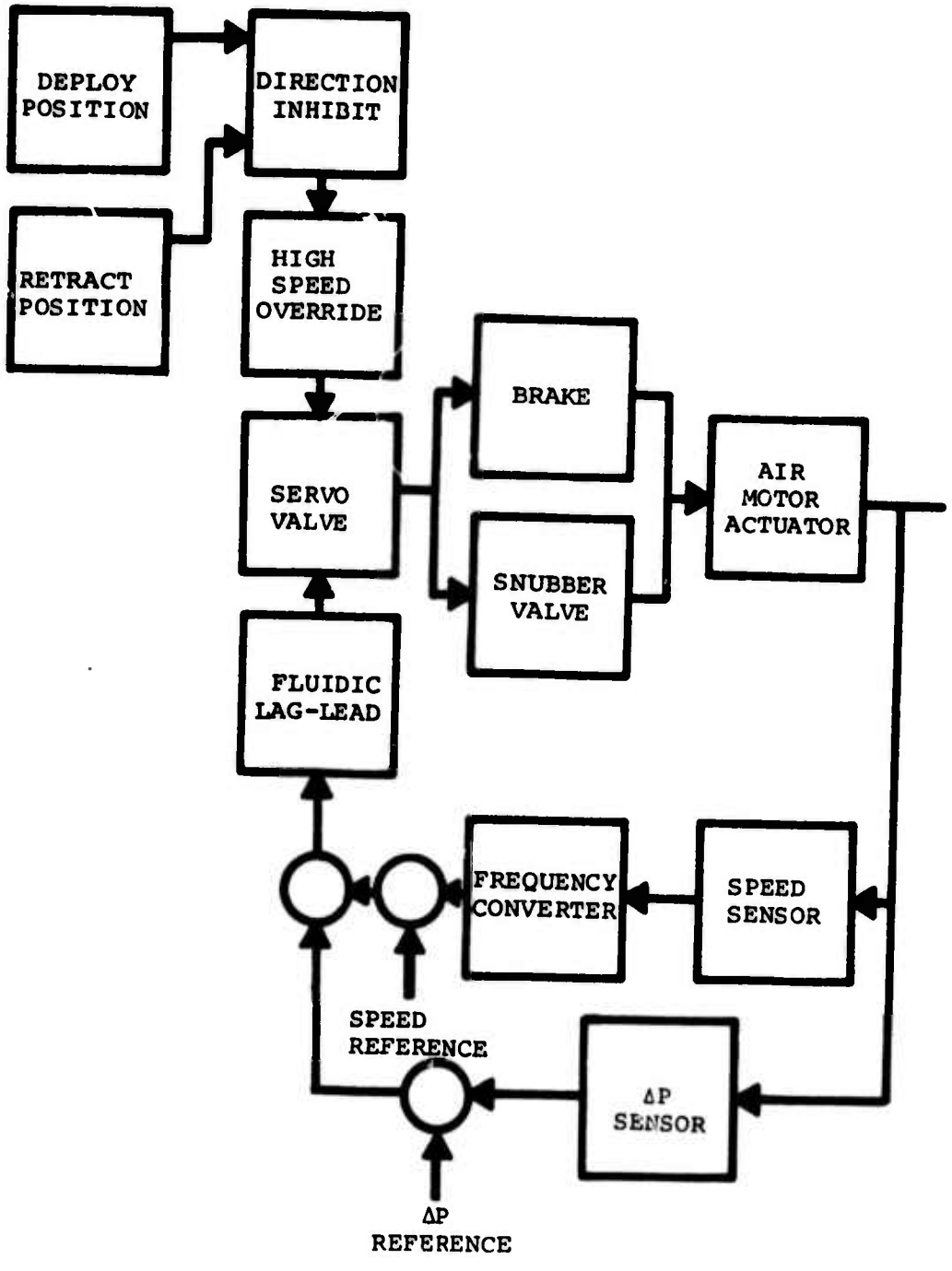


FIGURE 11

THRUST REVERSER SPEED AND TORQUE CONTROL
OF GENERAL ELECTRIC CF6 ENGINE



FIGURE 12

FLUIDIC CIRCUIT FOR CF-6
THRUST REVERSER DRIVE UNIT

PHOTO NO. P-40263-1

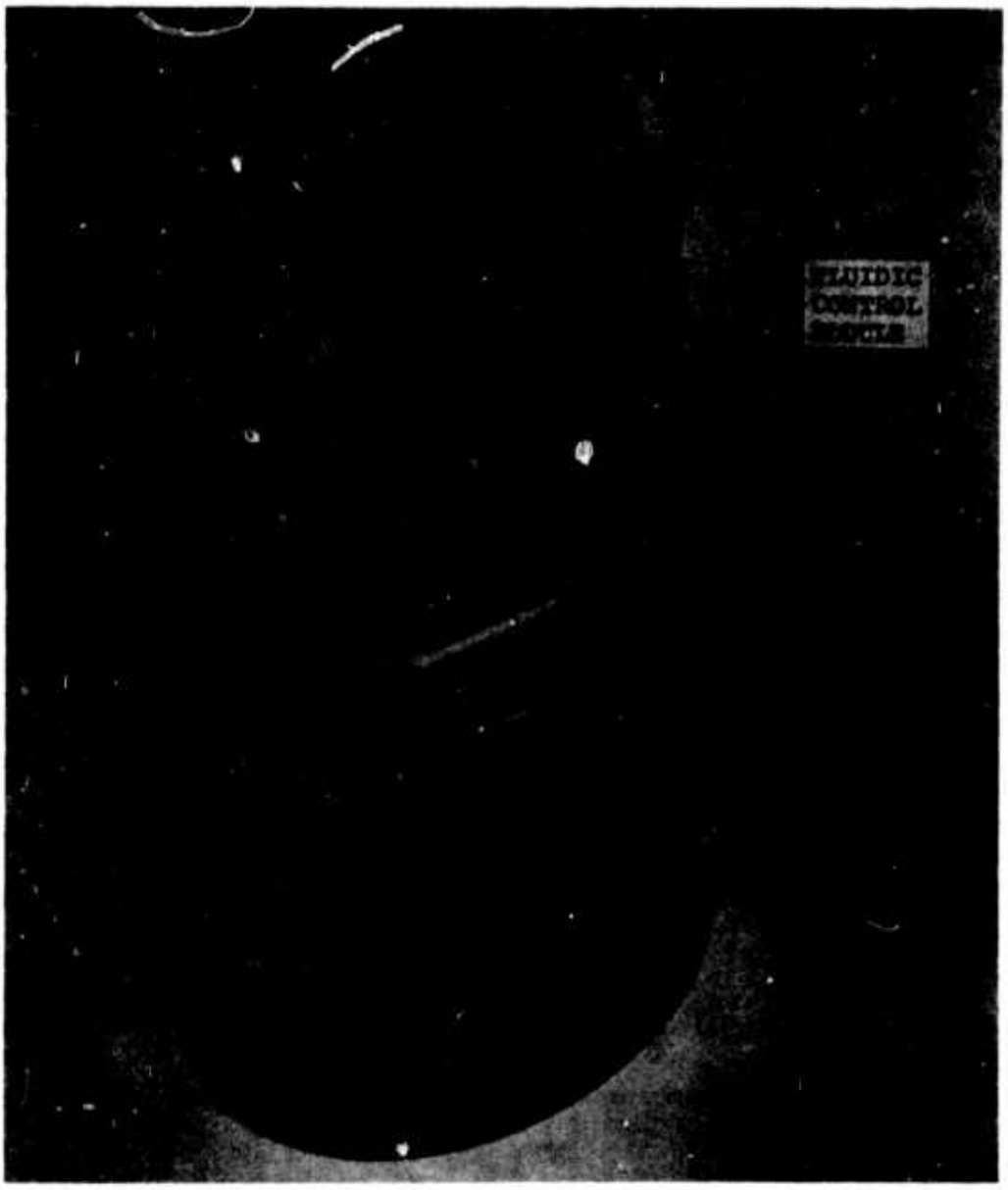


FIGURE 13

PRESSURE REGULATING VALVE OF
LOCKHEED S-3A AIRCRAFT
(AIRESEARCH PART 898524-1-1)

REQUIREMENTS FOR FLUIDIC CIRCUIT CONSTRUCTION

The aerospace fluidic applications described above show that fluidics technology has been used successfully under severe conditions. To recap these applications and their requirements, the tabulation shown in Table 1 is presented.

Table 1 shows that fluidics must operate over a temperature range of minus 65F to 600F and over an altitude range from sea level to 80,000 feet. The fluidics circuitry must be manufactured in a manner to prevent leakage which would affect performance while operating under these conditions.

One additional requirement which is not apparent from the preceding discussion of applications is related to the basic phenomena of fluidics, namely fluid flow. When designing any breadboard circuitry, it is easy to fall into the trap of forgetting the effects of temperature and pressure level on the flow in the circuits. To maintain accuracy, appropriate compensation must be provided for these phenomena. The exact value of the compensation may also vary with package design. For example, capillary flow may be required to obtain a given flow characteristic. If the capillary line used has bends, introduced for packaging, the value of the flow for a given pressure will change; therefore, the characteristic of the circuit is dependent upon the packaging used. This shows that breadboard, development, and production hardware must be as similar as possible to achieve accurate circuitry characteristics and timely fabrication of production hardware.

FUTURE FLUIDIC CONTROL APPLICATIONS

The applications of fluidics at AiResearch to date has been aimed at controls which are presently in production or are being considered for possible immediate production. A second development phase has now started which is directed primarily towards future production use of fluidics. These first applications were the stepping stones towards the use of fluidics as a prime control technology or as a supporting technology for use in hybrid systems containing electronics and mechanical parts.

TABLE 1

SUMMARY OF OPERATING CONDITIONS IN AEROSPACE FLUIDIC APPLICATIONS

	AMBIENT CONDITIONS		BLEED AIR SUPPLY	
	Temperature Degrees F	Altitude Feet	Temperature Degrees F	Pressure psig
EGT Sensors	-65 to +600	10,000	450	50
Turbine Overspeed (Sensor location: 800F)	-65 to +350	20,000	450	80
APU Fuel Control	-65 to +350	10,000	400	50
Thrust Engine Fuel Control	-65 to +500	20,000	550	90
APU Surge Valve	-65 to +300	25,000	400	65
Concorde Thrust Reverser	-65 to +600	80,000	500	35
CF-6 Thrust Reverser	-40 to +350	45,000	600	70
Lockheed S-3A Pressure Regulator	-65 to +160	5,000	350	20

Fluidics technology is now being applied to more advanced systems. Interface devices involving fluidic circuitry have been produced that are suitable for use in converting electrical, mechanical, hydraulic, or pneumatic input signals to either pneumatic or hydraulic outputs. An example of the complexity of fluidic systems which may be reasonably achieved at this time is shown by the diagram in Figure 14 which depicts an environmental control system for the cabin of a fighter aircraft. As shown on the figure, this system involves temperature, pressure, speed, and mass flow controls. Other systems of equal complexity which will soon enter the development and production phases are missile and helicopter flight control and actuation systems. Many of these applications require the use of the previously mentioned interface devices. Figure 15 shows a typical electro-hydrofluidic transducer.

MANUFACTURING OF FLUIDIC CIRCUITS

AiResearch has been active in fluidics for approximately nine years. Soon after the first programs were initiated, it became apparent that there was no available manufacturing process suitable for these research programs or for anticipated production programs. A major portion of the fluidics effort was therefore diverted to this manufacturing area. The initial thrust of the manufacturing effort involved investigation of die stamping, machining, electro-forming, photo-chemical milling, ceramic casting, and plastics. Early development hardware was made using the Dycril photo-sensitive plastic process; however, this was only a stop-gap measure to enable component designs to be tested. In 1967, the photo-chemical milling or photo-etching method was selected as the manufacturing method to be used. Table 2 lists the advantages and disadvantages of each of the processes investigated.

Photo-chemical milling offered a rapid means of obtaining parts for development; tooling was cheap and accuracy requirements could be met. In addition, development and production parts could be made from the same tooling. This eliminated the problems associated with transferring breadboard circuitry into production circuits, and reduced development cost and risk.

SYSTEM BLOCK DIAGRAM

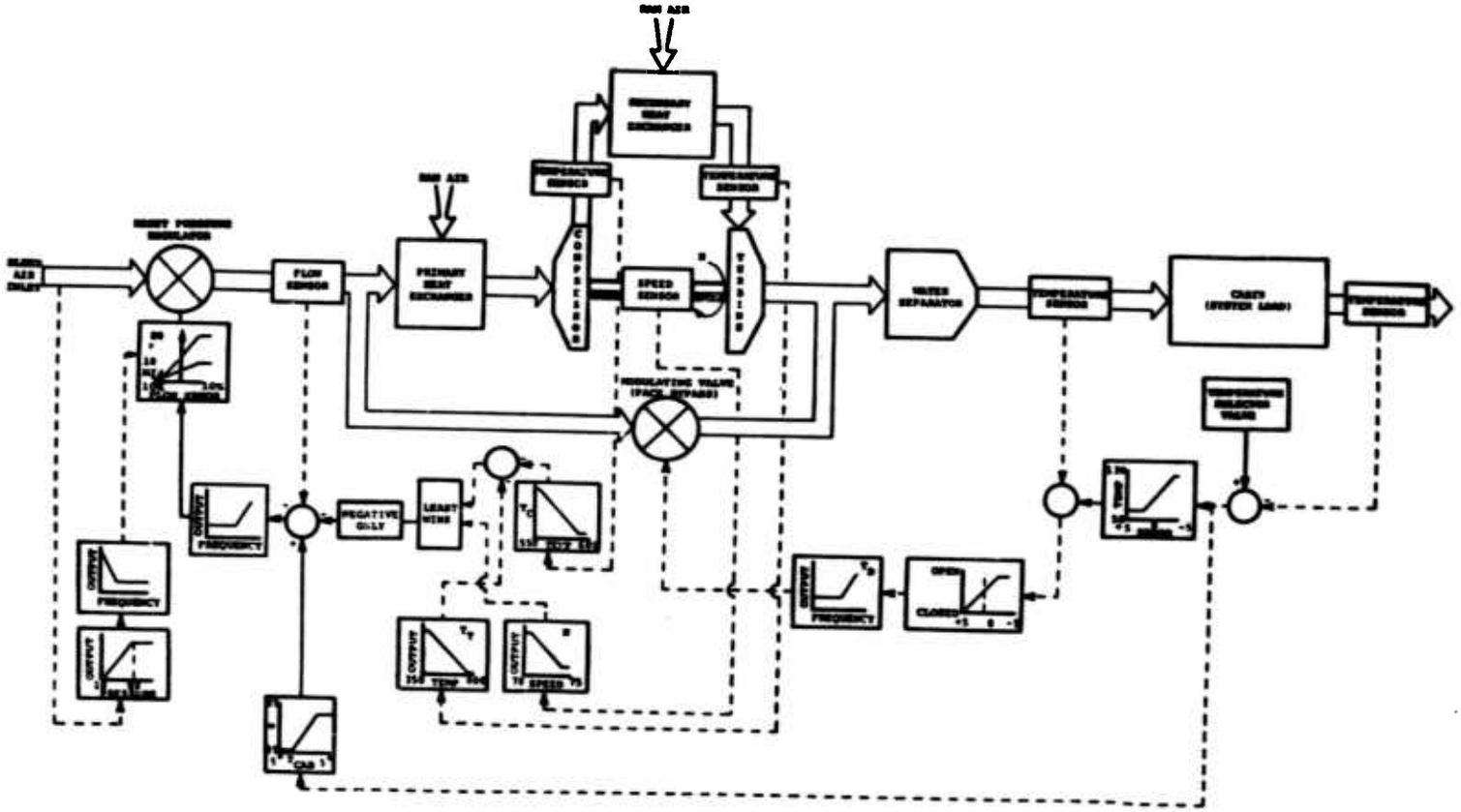


FIGURE 14

FLUIDIC ENVIRONMENTAL CONTROL SYSTEM 710390-1
LOGIC DIAGRAM



DEVELOPMENT UNIT OF
ELECTRO/HYDRAULIC FLUIDIC TRANSDUCER
(SHOWING PARTIALLY DISASSEMBLED UNIT)
FIGURE 15

TABLE 2

SUMMARY OF FLUIDIC ELEMENT MANUFACTURING PROCESSES

1. PHOTOSENSITIVE GLASS
   - Low Cost - Good Accuracy
   - Unsatisfactory for Development
   - Difficult to handle in Aerospace Applications
2. SLIP CAST AND PRESSED CERAMICS
   - Low Cost - Satisfactory Accuracy
   - High Tooling Cost
   - More suited to high quantity, simple component production
3. INJECTION AND TRANSFER MOLDED PLASTICS
   - Low Cost - Poor Accuracy
   - Materials not suitable for most applications
   - High Tooling Cost
4. PHOTO-PLASTIC
   - High Cost - Satisfactory Accuracy
   - Material Affected by Humidity
   - Short Term Development Use Only
5. DIE-STAMPING
   - Low Cost - Accuracy Unsatisfactory
   - High Tool Cost - Short Life
   - Suitable for High Production of Non-Critical Parts
6. ELECTRO-FORMING
   - Medium Cost - Good Accuracy
   - Poor Range of Materials
   - Packaging Difficult
   - High Tooling Cost
7. PHOTO-ETCHING
   - Low Cost - Good Accuracy
   - Wide Range of Material
   - Low Tooling Cost - Short Turn-Around Time
   - Good Packaging Capability

After the process for manufacture of basic components was selected, the next major hurdle became that of leakage and repeatability. To overcome these problems, the individual laminations were sealed after being stacked into the desired circuits. Many sealing techniques, ranging from gluing to diffusion bonding, were investigated. At first, it appeared that pure diffusion bonding could be employed. However, the requirements for cleanliness of components before bonding were more stringent than desired and there was a problem of component distortion under the temperatures and pressures that are associated with pure diffusion bonding. Therefore, an interface material with a lower temperature melting point, which would diffuse into the two adjoining surfaces with lower bonding temperature and also a lower pressure or clamping force, appeared to offer the best solution. This process is known as the assisted diffusion bonding process.

FLUIDIC CIRCUIT MANUFACTURING PROCESS

As previously discussed, photo-chemical milling and assisted diffusion bonding were selected as the methods to be used to manufacture fluidic circuitry. Other steps such as inspection and test of the individual parts and bonded circuits complete the manufacturing process. Figure 16 shows the flow chart describing the process steps as performed at AiResearch on a production basis.

The first step in photo processing is the preparation of the master art work of the fluidic element. This is an accurate representation that is made up to 20 times the actual size of the part using a stable base, strippable film. This master art work is reduced photographically to a working size negative, which is inspected for accuracy to within 0.0005-inch and designated as the master profile for this part.

Multiple images of this master are reproduced on two registered, back-to-back, 0.007-inch thick Mylar films by a step and repeat photographic process. This multi-image step and repeat tooling permits the simultaneous chemical milling of many parts per sheet. Typically, a 12 x 18 inch step and repeat tool contains from 16 to 240 reproductions, dependent upon the size of the part. Photo processing of the metal sheet material consists of the following steps:

1. Cutting the sheets to size from raw stock
2. Cleaning and coating the sheet with photo resist material

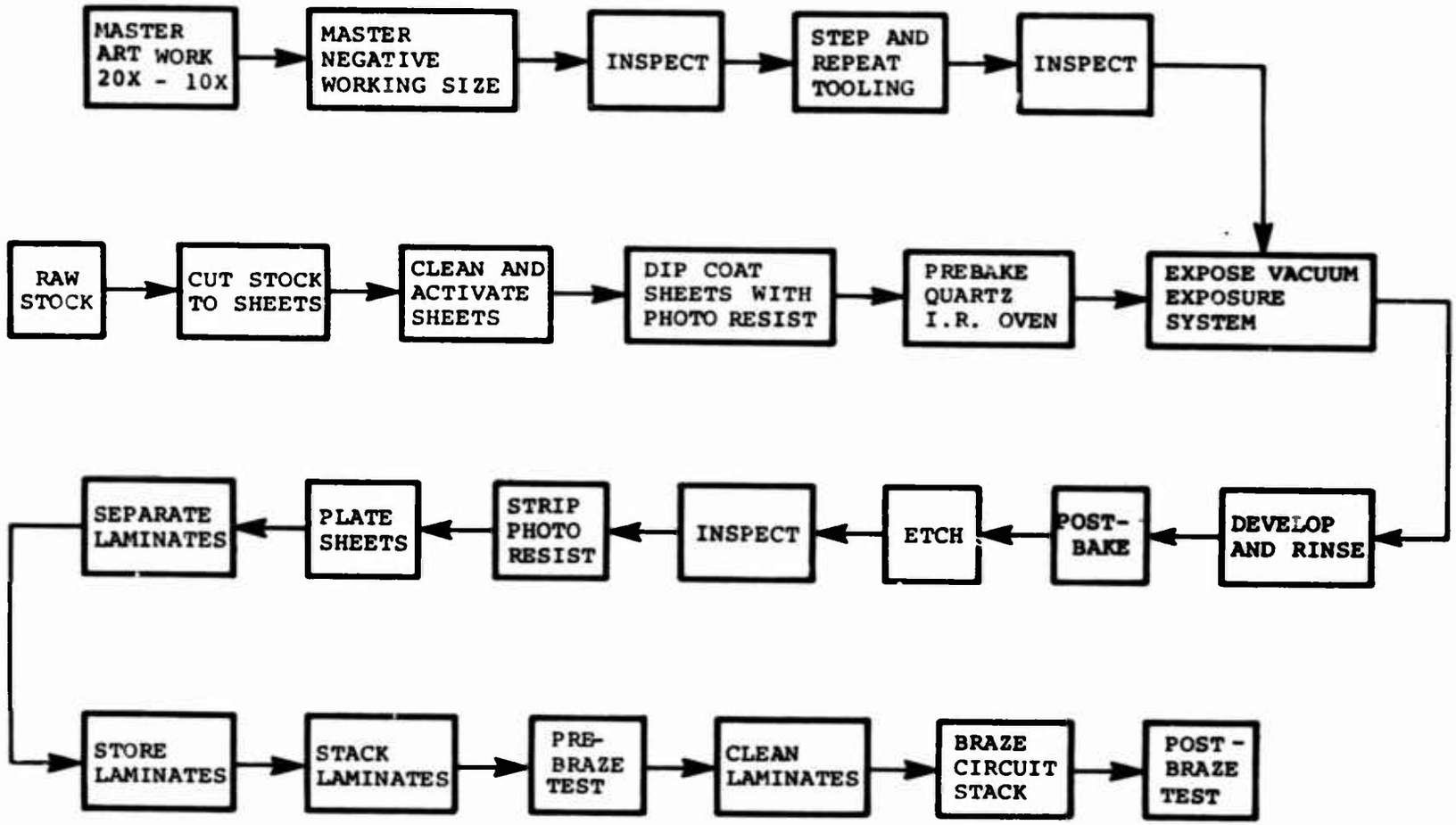


FIGURE 16

STEPS IN PHOTOCHEMICAL MILLING
OF FLUERIC CIRCUITS MADE
BY AIRESEARCH-PHOENIX

3. Drying the photo resist material

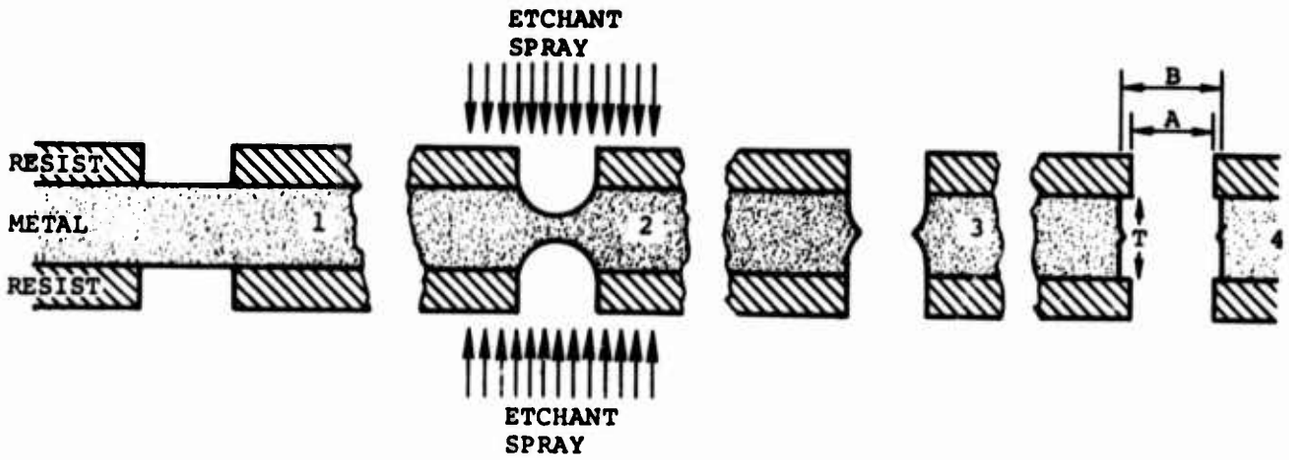
4. Exposing the images on the sheet using the step and repeat tooling

5. Developing and baking the finished sheet.

The materials presently used are SAE 347, 304L, and 440C corrosion resistant steels, various aluminum alloys, and Waspalloy, with thickness ranging from 0.002 inch to 0.062 inch. The photo-resist coatings used to date have all been of the negative type (i.e., when exposed to an ultraviolet light source, the part exposed remains and that not exposed is removable with solvent which is termed development of the resist).

The image of the part is thereby printed on the metal in the form of bare metal and metal protected by the resist film. The material is then etched by spraying the surface from both sides with a 46 degree Baumé solution of ferric chloride. This attacks the bare metal by chemical action along the material grain boundaries. As etching progresses, the wall of the material which is being formed by the depth of cut is also attacked which leads to an enlargment of the width of the slot being cut. An allowance for this "over-etch" must be made in the design stages. Figure 17 shows the etching action and typical allowances made for slots. As can be seen, the etching allowance is varied according to material, material thickness, and the width of slot being etched.

The etched or chemically milled sheet is then inspected. This was found to be an extremely difficult task since parts vary in profile and size, material, and thickness in practically every conceivable combination. Profile checking with projection equipment was found to be too expensive and impractical for quantity production. A simple go-no-go procedure was required. To accomplish this, one feature of the part, usually a round hole, is designated as the gauge hole and this is checked with a plug-gauge. In the design of the artwork, allowances are made for varying etching rates to ensure that this gauge hole etch is typical of the part etching and over-etch. In addition, a spot visual check on a sheet of parts is used to ensure the condition of the etched walls of the part. This simple technique has proven to be acceptable for production quantities presently being produced. Larger quantity production would require an automated test; however, the same go-no-go procedure could be used.



FOR "B" DIMENSION OF 0.020-INCH ON 0.020-INCH THICK MATERIAL, DRAW "A" LINE AT 60 PERCENT OF WIDTH, OR 0.012-INCH ON ARTWORK.

EXAMPLES:

"A" 0.020-INCH IN 300 SERIES STAINLESS STEEL

THICKNESS OF MATERIAL INCH	"B" DIMENSION INCH
0.002	0.022
0.005	0.024
0.010	0.026
0.020	0.030

FIGURE 17

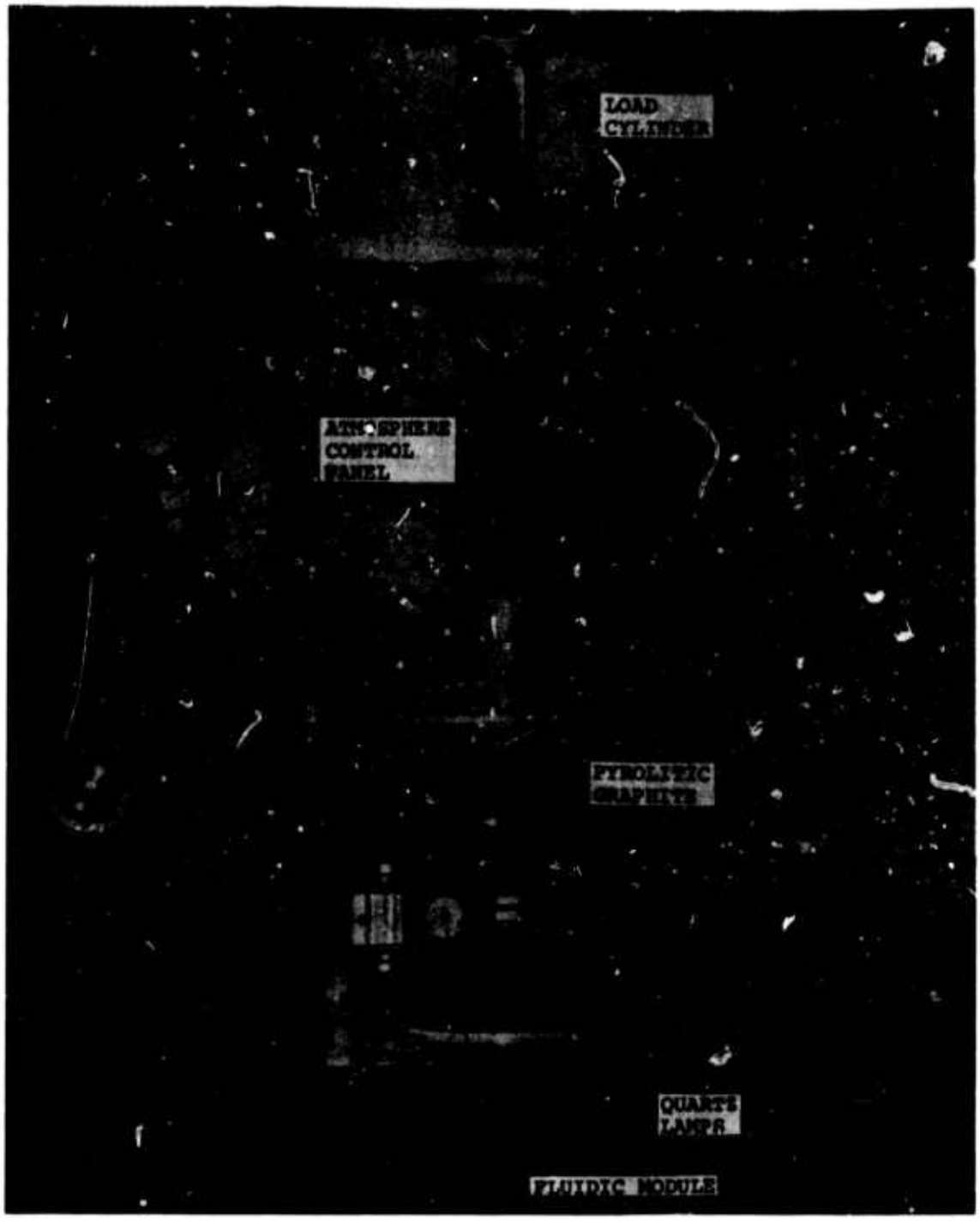
ETCHING PROCESS AND
ARTWORK ALLOWANCE

After inspection, the photo-resist is removed by a chemical stripper which softens the resist and allows it to be rinsed off of the surface of the metal. The cleaned metal is then plated with various combinations of metals to obtain the desired bonding temperature for the complete flueric circuit. Electro-plating of these combinations of materials is usually used. The plating thickness is maintained such that the material practically diffuses into the surface during heating. A small amount of residual material, however, remains which fills small voids along the mating joint where insufficient clamping forces exist for complete bonding to occur. Control of this plating thickness is important since an excess of plating will plug passages in the circuit; too little plating will result in an inadequate bond. Control of the thickness is maintained by use of a Beta-ray, back-scatter technique wherein a radioactive source is aimed at the material and the radioactive particles reflected are counted. The angle of reflection and count represents the plating thickness.

The plated parts are removed from the sheet and then stacked vertically in the required combination to form the fluidic circuit. This circuit is then clamped to a test fixture and subjected to performance tests to ensure that the assembly is correct and that the desired performance will be obtained when the assembly is bonded.

The bonding operation is preceded by cleaning the laminations and machined parts which form the assembly. This cleaning consists of ultrasonic degreasing in triethane, followed by an acid rinse to remove any buildup of salts which form on the surface of the plating during storage.

The bonding operation itself is conducted in an inert atmosphere. Initially, a conventional vacuum heat treating furnace was used. However, cycle times due to furnace thermal capacity were excessive and this led to the use of a quartz lamp furnace. With this furnace, the cycle time of five hours was reduced to 30 minutes. Figure 18 shows the furnace with a CF6 thrust reverser circuit installed ready for bonding. When closed, the furnace is airtight and may be purged with an inert gas mixture. The load cylinder applies a precise bond via springs to four parts on the circuit which is thermally insulated from its surrounding by pyrolitic graphite. The quartz lamps apply a localized heat input only to the central area of the furnace. The required heating time of five minutes is so short that only the part to be bonded placed in line with the lamp is heated. This means that the cooling cycle for the furnace is short, thereby increasing production rates over conventional furnaces.



QUARTZ LAMP FURNACE USED FOR
BONDING FLUIDIC CIRCUITS

FIGURE 18

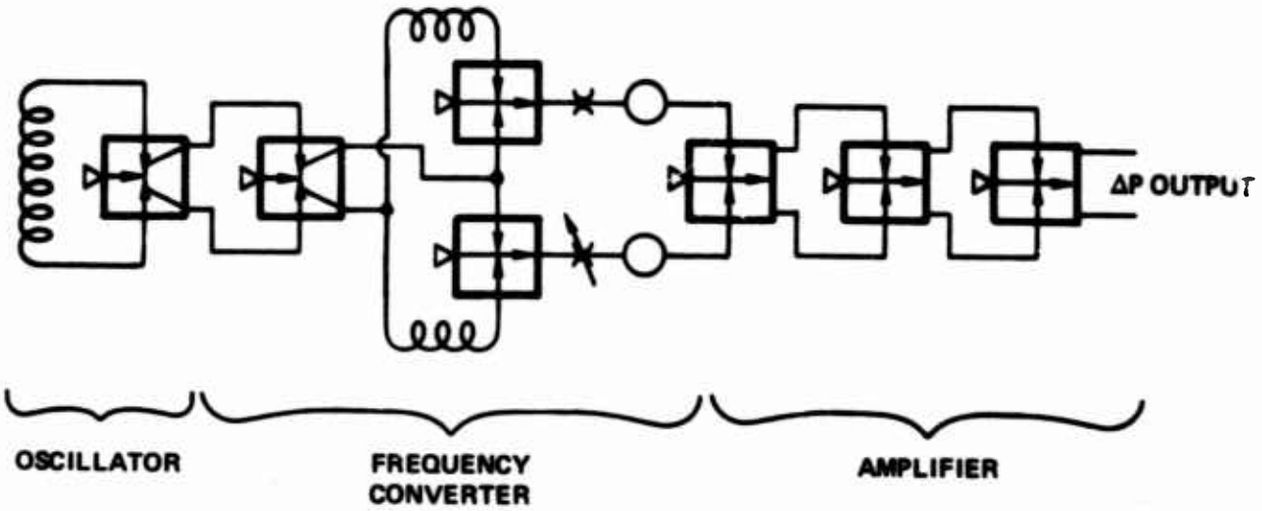
On removal from the furnace, the circuit is pressurized to check for leakage and then assembled with the necessary mechanical components for functional test and delivery.

CONCLUDING REMARKS

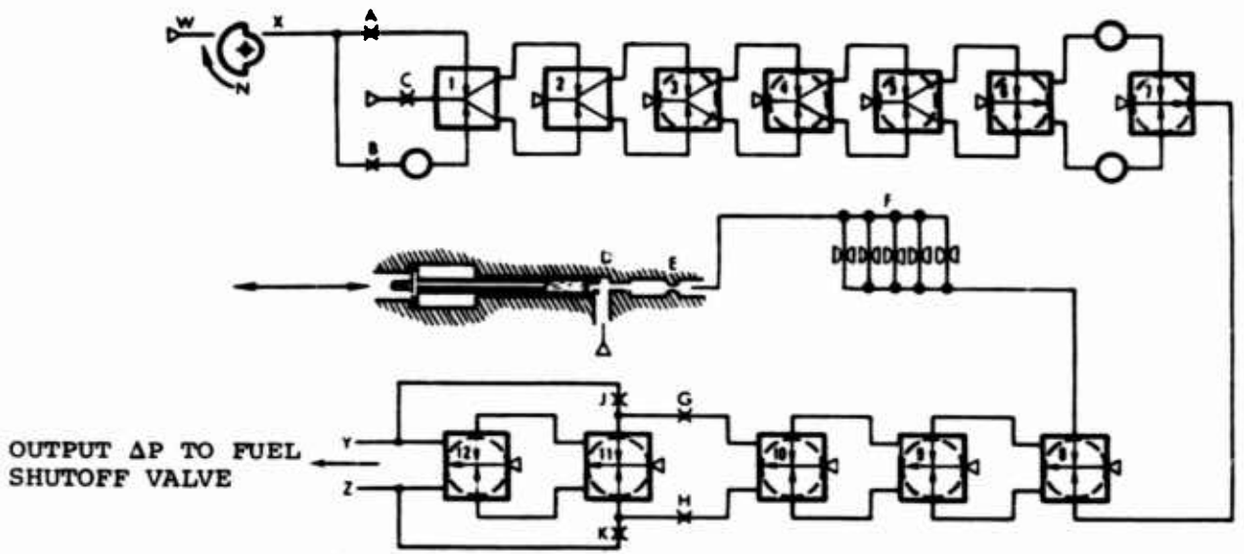
A few applications of fluidics have now been in production for aerospace applications for a number of years. These systems have proven that use of fluidics for aerospace applications is a good, reliable choice where other technologies have trouble in meeting reliability, cost, and environmental tolerances. The unique package and development requirements of fluidics have led to the photo-chemical milling and activated diffusion bonding processes as acceptable production techniques. There is a need for continued development in this area to improve inspection methods and to generate the procedures for large-scale production which is anticipated to occur within the next two to five years. During this period, it is expected that fluidics will be applied to gas turbine accessories and to most aircraft pneumatic or hydraulic systems such as environmental controls and braking systems. In addition, fluidics technology is showing great promise for use in missile directional control and stability systems.

APPENDIX 1

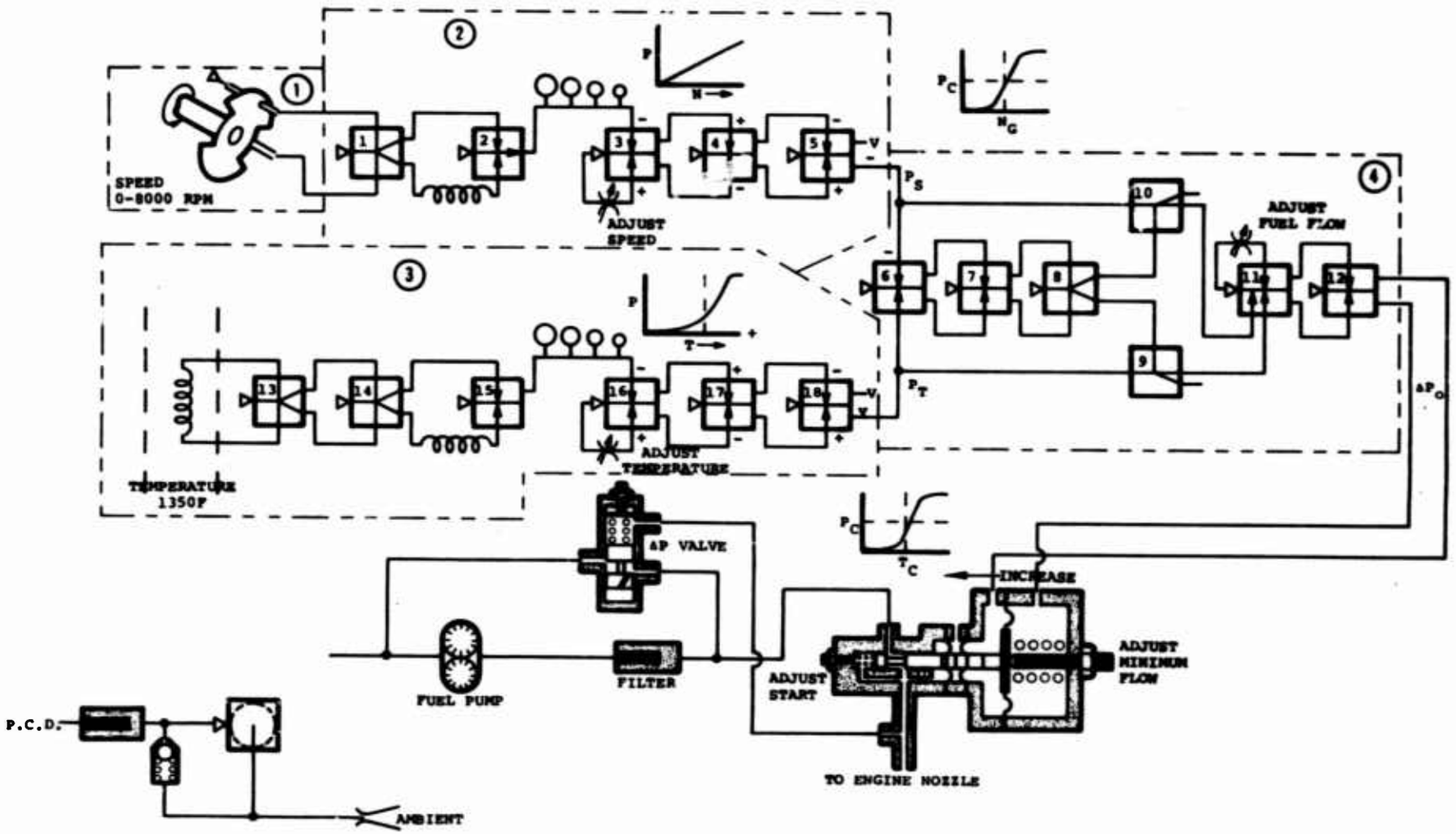
FLUIDIC CIRCUIT DIAGRAMS



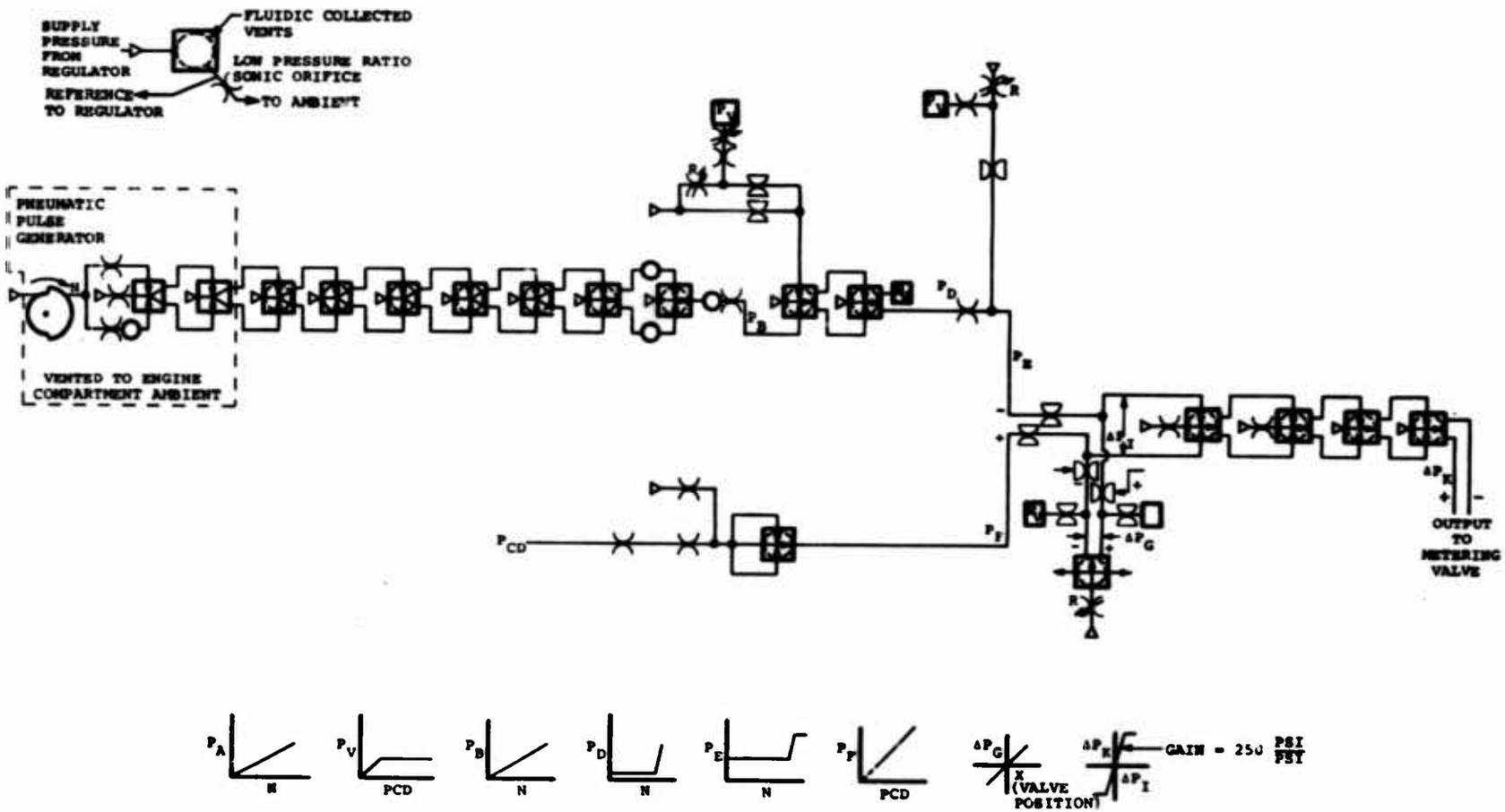
1. SCHEMATIC DIAGRAM OF FLUIDIC TEMPERATURE SENSOR



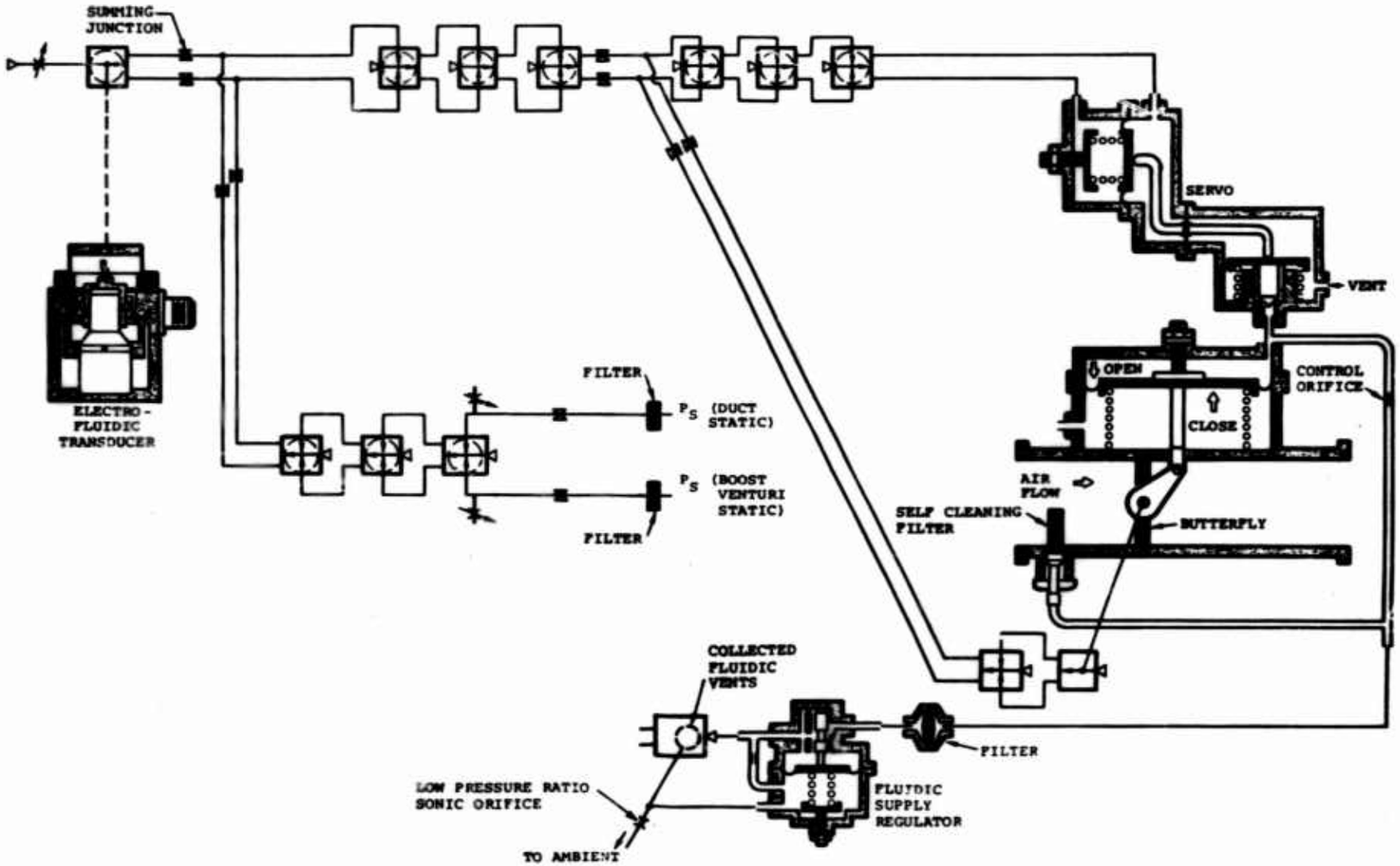
2. SCHEMATIC DIAGRAM OF OVERSPEED FUEL SHUTOFF VALVE ON TSE231 ENGINE



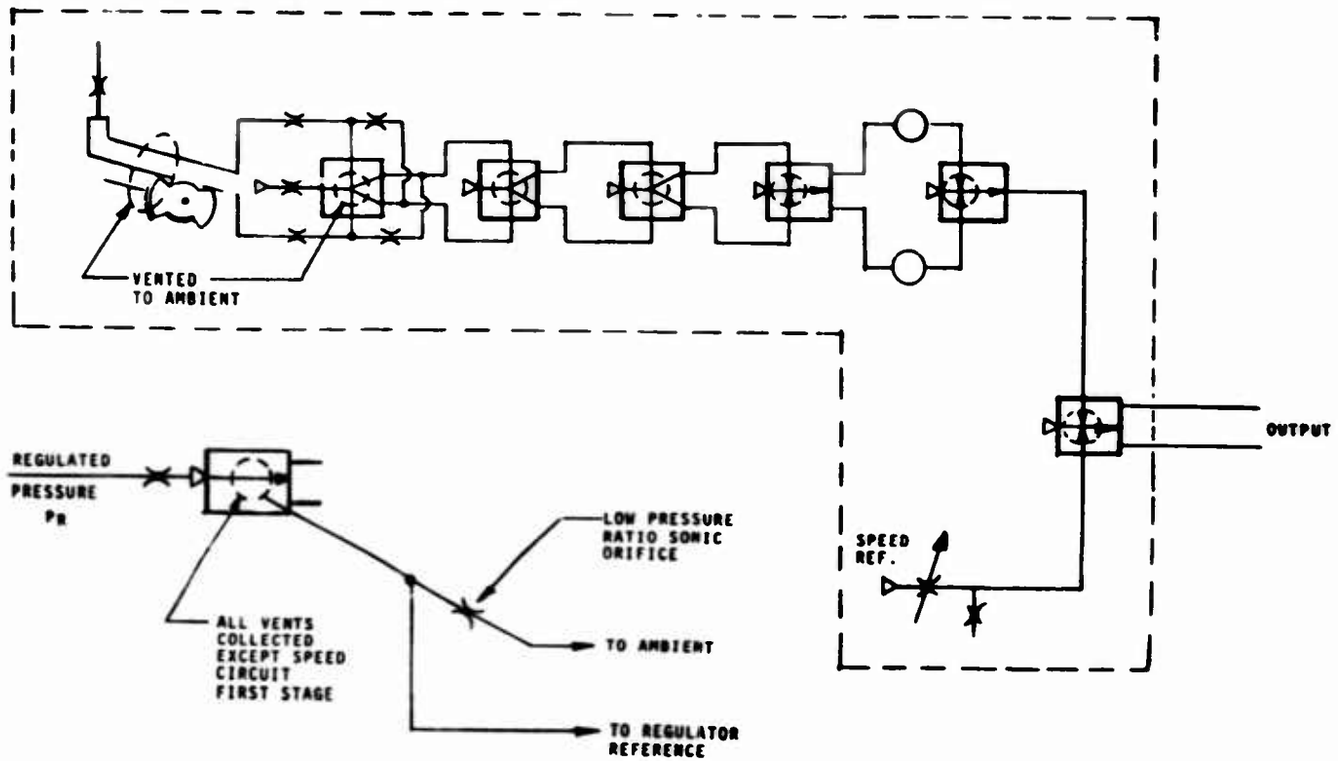
3. CONTROL SYSTEM OF AIRESEARCH GAS TURBINE APU



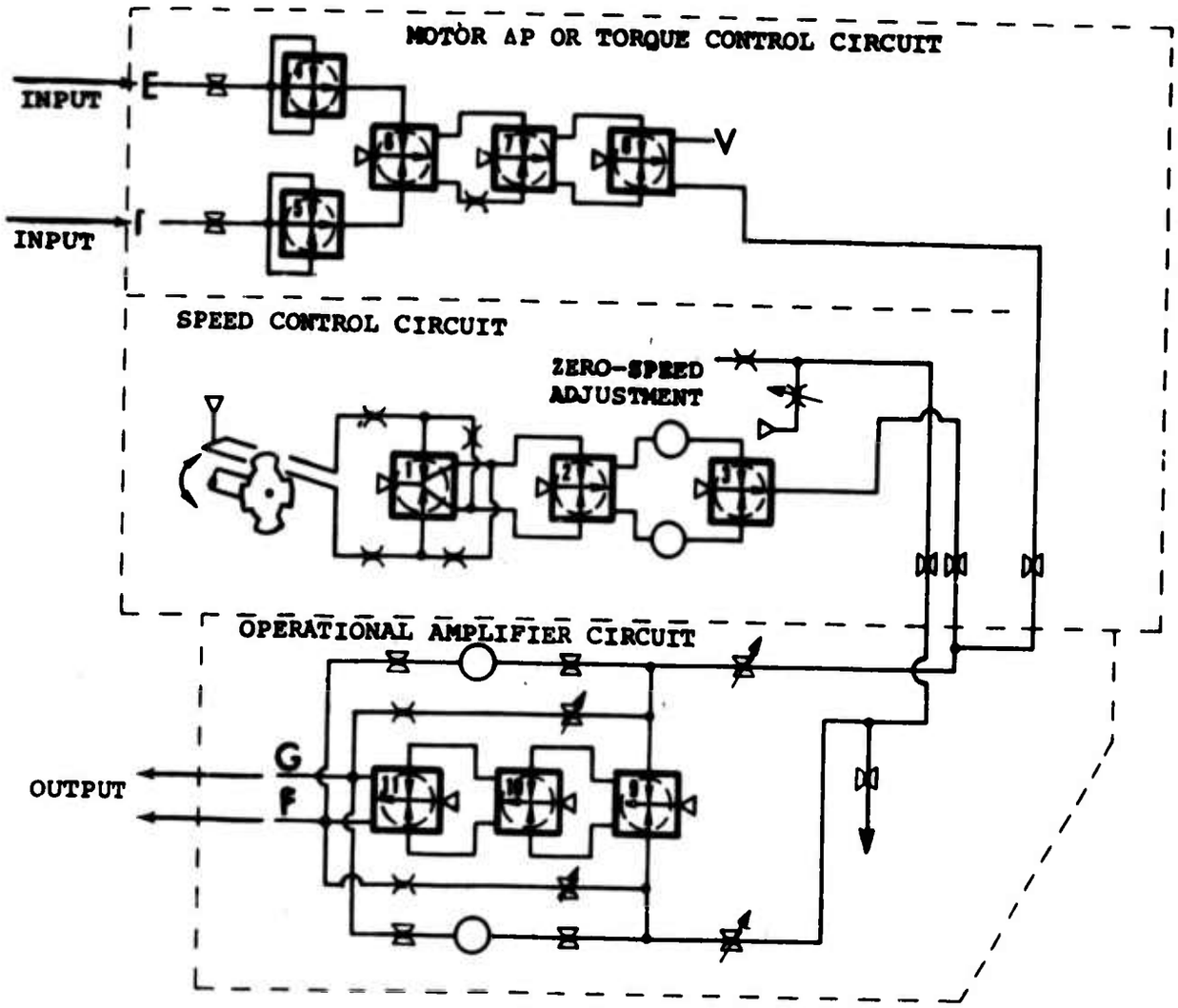
4. FLUIDIC CIRCUIT SCHEMATIC OF ENGINE FUEL CONTROL



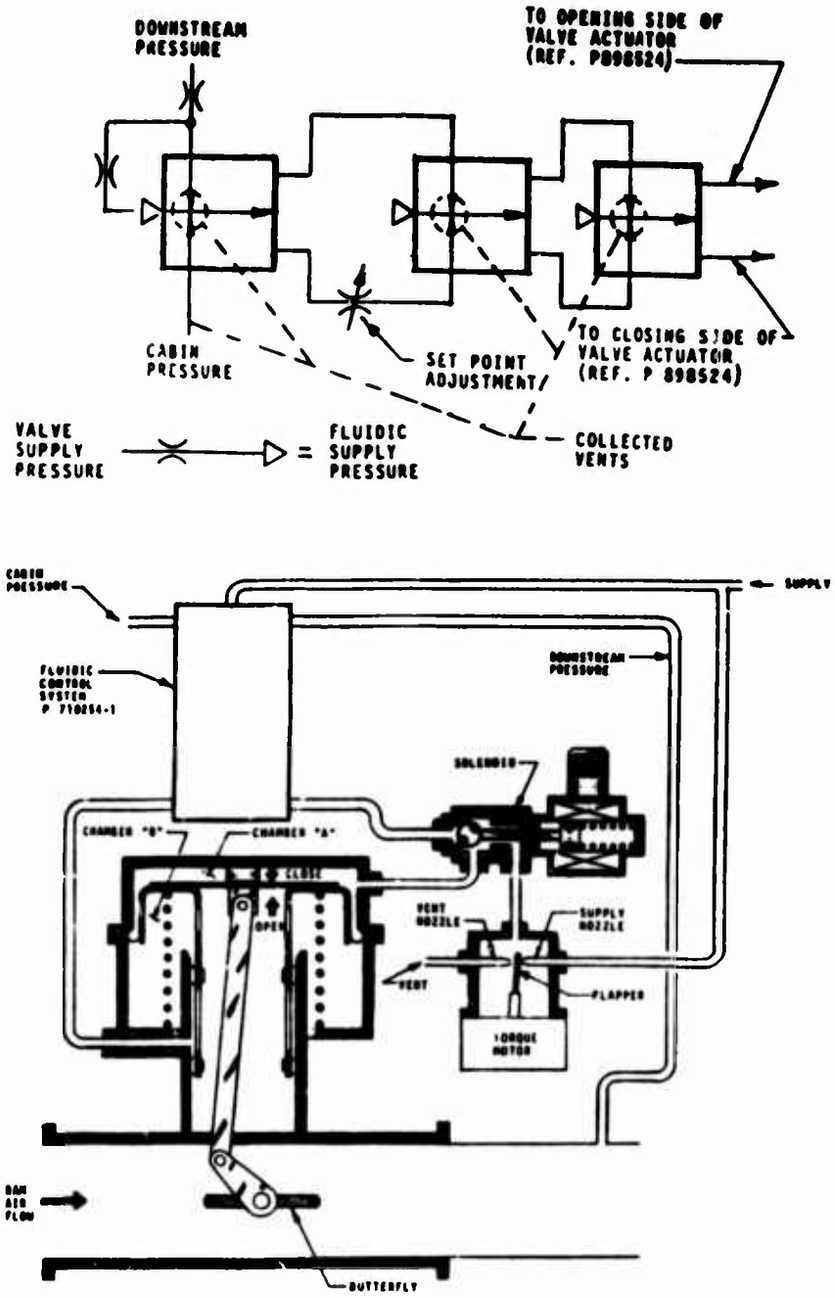
5. APU SURGE CONTROL VALVE ON NORTH AMERICAN ROCKWELL B-1 AIRCRAFT



6. FLUIDIC SPEED CONTROL SYSTEM ON THRUST REVERSER AND NOZZLE CONTROL OF CONCORDE SST AIRCRAFT



7. SCHEMATIC DIAGRAM OF FLUIDIC CONTROL SYSTEM ON CF6 THRUST REVERSER ACTUATOR



8. FLUIDIC CIRCUIT AND SCHEMATIC DIAGRAM OF LOCKHEED S-3A PRESSURE REGULATING VALVE (AIRESEARCH PART 898524-1-1)

SOME INDUSTRIAL PROCESS APPLICATIONS

OF

FLUIDICS

by

Robert B. Adams
Moore Products Company
Spring House, PA

Prepared for
The Harry Diamond Laboratories
Fluidic State-of-the-Art
Symposium
30 Sept - 04 Oct 74

Preceding page blank

SOME INDUSTRIAL PROCESS APPLICATIONS OF FLUIDICS

Many successful industrial applications of fluidics have been made over the last decade to a wide variety of industrial process control problems. As is typical with any new technology, fluidics has often been given its "first chance" where "all else has failed". Experiences gained under these hardships demonstrate that fluidics, properly applied, provides benefits due to elimination of moving parts. These are:

1. Higher reliability and less maintenance.
2. Longer operating life.
3. Ability to withstand adverse conditions such as formation of deposits, corrosion, abrasion, etc.
4. Better accuracy.
5. Lower cost.
6. Faster speed of response.

No-moving-part fluidics are not limited to tiny gas breathing logic devices. The Coanda effect has been used to make large liquid diverting valves that are stocked in pipe sizes through four inches. Other valves, custom tailored to specific applications, have been made for gases as well as liquids. One gas valve was large enough to permit a man to walk through it. Large scale fluidics has also proven useful for measuring volume flow rate with a combination of advantages not previously available.

An example of large fluidic diverting valves is shown in Figure 1. These are liquid diverting valves in two of the stock sizes, one-half inch and four inch, for flow rates ranging from 1/2 to over 1000 gpm. These valves have a single control port which makes them useful for the control of liquid level. When a gaseous fluid is admitted to the control port, the liquid flowing through the valve is diverted to an outlet for filling a vessel (Figure 2). However, when the level rises to admit liquid at the control port, flow is automatically diverted to the outlet by-passing the vessel (Figure 3). Neither auxiliary power nor moving parts are required for this completely fluidic level control.

The first of these valves was installed at a West Virginia Paper and Pulp Company plant early in 1964, and is still in operation today (Figure 4). The valve controls level in a white water (paper stock with a 1/2% consistency) chest by adding waste condensate water whenever the chest level is low. The only maintenance required has been an infrequent cleaning of the control tube to remove pulp deposit.

Several hundred fluidic level controls have since been put into service. Three applications in particular illustrate their ability to cope with difficult fluid conditions such as abrasion, corrosion and deposit forming tendencies.

Extremely abrasive conditions are present in a proprietary glass industry application for control of a pumice slurry. Typically, dilute pumice slurry flows through the valve and is diverted to a

RBA:mcd

vessel, containing a concentrated pumice slurry, when level is low. The fluidic valves have proven to require less maintenance and last longer than the mechanical valves they replaced.

In the area of corrosive applications, fluidic valves have been successfully employed to maintain level in electroplating tanks (Figure 5). Water is circulated through the valve from a reservoir. When the electroplating solution level falls, due to evaporation, water is diverted into the plating tank. As the level rises to cover the control tube, the plating solution must not be drawn into the fluidic valve since dilution might result. Dilution is prevented by making the elevation of the control tube greater than the suction lift at the control tube. Service has proven to be trouble-free.

Figure 6 shows a fluidic valve in a hardness sampling system, replacing a conventional solenoid which had stopped functioning within a week of installation because of internally formed deposits. Water passing through the sampling leg is diverted down a drain if the hardness is greater than 1200 ppm. Make up water with hardness of 200 ppm is then added to reduce system hardness. When the hardness falls below 1200 ppm, the fluidic valve diverts the sampled water back into the system. The solenoid at the fluidic valve control port handles atmospheric air and, therefore, is not affected by the hardness. The fluidic valve has been in service for six years without requiring maintenance.

In another application involving a potentially troublesome fluid, a tristable diverting valve, at a Beckly, West Virginia, sewage disposal station, has been connected since 1965 to deliver sewage pumped at 900 gpm from a tank to two filtration beds (Figures 7 and 8). The valve has two manually operated control ports. Normally both are open so that the sewage is divided evenly between both beds. When it is necessary to temporarily take one bed out of service, closure of one of the control ports will deliver all sewage to the other bed.

The application of custom designed fluidic valves to the Diesel locomotive cooling system has been made the subject of a separate paper "Fluidics Controls Cooling of Diesel Locomotives".* However, another interesting railroad application of large fluidic valves occurs on tank cars for transporting cement in bulk (Figure 9). The cars, manufactured by the General American Transportation Company, are unloaded at their destination by blowing air into the tank through a fluidic diverting valve (Figure 10). The valve, a two-stage self-oscillating diverter, alternates between delivering air to the underside of either half of the tank. The alternate bursts of air, through internal air slides, agitate and fluidize the cement to flow toward the tank discharge from where it is pneumatically conveyed through a four inch line to a storage silo.

The importance of the fluidic valve lies in the fact that it has proved impossible to unload the tank completely without them. The rapid switching action and maintenance-free life cannot be duplicated by any

*Paper to be offered for Harry Diamond Laboratories State-of-the-Art Symposium on Fluidics, September 30 to October 3, 1974.

RBA:mcd

mechanical valve. A recent check with personnel of the Lehigh Portland Cement Company, unloading operators of these cars since 1966, revealed that the fluidic valves have continued to satisfactorily perform their function of completely unloading the cars.

Figure 11 shows the operation of the oscillating valve. Pressure picked up from the main stream in the interaction chamber is fed back to the pilot control ports to produce the oscillation. The feedback acts to divert the pilot stream which, in turn, diverts the main stream to the other sidewall of the interaction chamber. The new position of the main stream establishes feedback to the other pilot control port, thus setting up a train of events which return the main stream to its original position. The feedback on each side is delayed by volume chambers to establish the frequency of oscillation at approximately 15 cpm.

Oscillation is maintained at any outlet loading. This result is achieved by taking the feedback from the interaction chamber which is separated from the outlets by the interaction chamber discharge. Oscillation occurs with outlet conditions ranging from no loading to complete blocking of one outlet.

Flow capacity may reach 1000 CFM at 50 psig tank pressure. The pilot flow capacity is only 2% of the main valve capacity and power gain per stage is the order of 100. Maximum energy recovery at the main valve outlet is 55%. The energy losses imposed on the system by the fluidic valve are not significant, because the pressure drop across the valve is a small fraction of the pressure required for pneumatic conveying through the discharge line.

Another example of oscillating service is a large duct size valve with 1300 CFM capacity at 36 inch H_2O drop for manipulating sheet stock during a manufacturing operation. The air blast blows the sheet back and forth at the rate of 1 CPS. Assuming that a mechanical valve of that capacity could be found to act at the required frequency, it would soon beat itself to pieces. The fluidic valve, presently in service for over two years, could continue for an infinite number of cycles since there is no wear and tear from repeated operation.

Considering all the fluidically based measurement techniques of which the writer is aware, the fluidic flow meter is the only large scale Coanda device. This liquid meter, Figure 12, is a fluidic oscillator whose frequency is proportional to volume flow rate. Figure 13 illustrates the action that takes place during one-half cycle of oscillation.

The meter body is installed in the process pipe to receive the full flow. The stream passing through the meter is attracted to one of the interaction chamber sidewalls. Starting with the stream completely attached to the upper wall, impact occurs at the upper receiver as the stream bends to pass through the discharge. The impact develops a small flow at the upper control port, deflecting the stream toward the lower wall. The stream travels down the lower wall at a speed related to its average velocity. When it reaches the lower receiver, feedback develops a small flow at the lower control port, returning the stream toward the upper wall.

RBA:mcd

The oscillation is sensed by a self-heated temperature sensitive element. The element is sheathed in stainless steel and operated in a constant temperature anemometer bridge for fast response to changes occurring in one of the feedback passages. As fluid pulses past the sensor once each cycle, the anemometer bridge voltage automatically pulses to maintain the element at constant temperature with respect to the fluid.

The voltage pulses may be used for totalizing fluid volume or developing an analog signal proportional to volume flow rate. The converter of Figure 14, located in a control room up to 1000 feet from the meter body, shapes the sensor voltage pulses into square waves. The square wave is further conditioned into two pulses each with constant volts-seconds area, which are filtered to provide a 4 to 20 ma current regulated output proportional to frequency (volume flow rate). If desired, the pulses may be multiplied and divided by a totalizer scaler (Figure 15) to provide a pulse output to a counter for indicating volume in gallons or other engineering units.

Calibration data taken with a one inch meter and three fluids of different densities is shown in Figure 16. The data demonstrates that (1) frequency is linear with volume flow rate and (2) calibration is the same for all fluids. The slope of the calibration curve is the meter factor in pulses per unit volume (usually taken as gallons for liquid measurements).

At some low flow, viscosity effects become important, the Coanda effect weakens, and the meter ceases to function. Operation, although possible below a pipe Reynolds number of 3000, may not be reliable. Prior to that point there is some change in meter calibration factor which is too small to be seen in Figure 16. Figure 17, plotting meter factor versus pipe Reynolds number, more clearly shows how meter calibration factor (slope of Figure 16) is affected by kinematic viscosity at low Reynolds numbers in a one inch meter.

At present, this meter is manufactured in pipe sizes from one inch through four inches for full scale flow ranges from 16 to 900 gpm. The more significant pluses are: linear calibration; no moving parts; elimination of impulse lines external to process pipe, resulting in simpler and less costly installation and elimination of errors; no effect on calibration from over-pressure, shock, vibration or field temperature change; elimination of field zeroing; wide rangeability; does not require conductive fluid.

In another application, a fluidic pressure comparator is a good illustration of performance improvement and cost reduction obtained by replacing moving parts with fluidics. The comparator is a small component of a control station (Figure 18), a number of which are typically located on a control room panel (Figure 19). The panel provides a central location from which to monitor and control an industrial process. Each control station provides a means by which control of a process variable can be instantly changed between automatic and manual modes. Manual control is required to start up a

RBA:mcd

process and in case of an emergency.

In panic situations, a control room operator must quickly take over and manually control the process. If the manual output to the control valve is different than the automatic control output, switching to manual will "bump" the process, further aggravating the emergency.

The bump can automatically be prevented by synchronizing the manual output, when in the automatic mode, with automatic output. The synchronizing is accomplished by the relay of Figure 20. The relay output (manual output) is made to follow relay input (automatic control output) when the control station is in automatic mode. This is done by the action of the fluidic pressure comparator (deviation controller) on the turbine wheel. A decrease in relay input diverts the fluidic output to move the turbine wheel in a direction to relax spring compression and reduce relay output. When relay output again matches input, the fluidic deviation controller stops the turbine wheel. When the control station is changed to manual operation of the process, air to the fluidic deviation controller is terminated, allowing relay output to be further changed manually (at the upper adjustment).

Reliable operation of the deviation controller is crucial to "bumpless" operation. Originally, a deviation controller design using moving parts was developed for this job. The manufacturing cost required to meet the precise performance requirements proved greater than anticipated. A fluidic design was undertaken which resulted in substantially reduced manufacturing cost, greater sensitivity, and more power to the turbine.

A differential change as little as 0.1 inch H_2O (less than one part in 3000 of the 3-15 psi pressure range) can reverse the motion of the wheel. Experience with over 10,000 comparators, thus far sold, has been satisfactory.

The future will bring many new and interesting applications of fluidics.

RBA:mcd
4/10/74

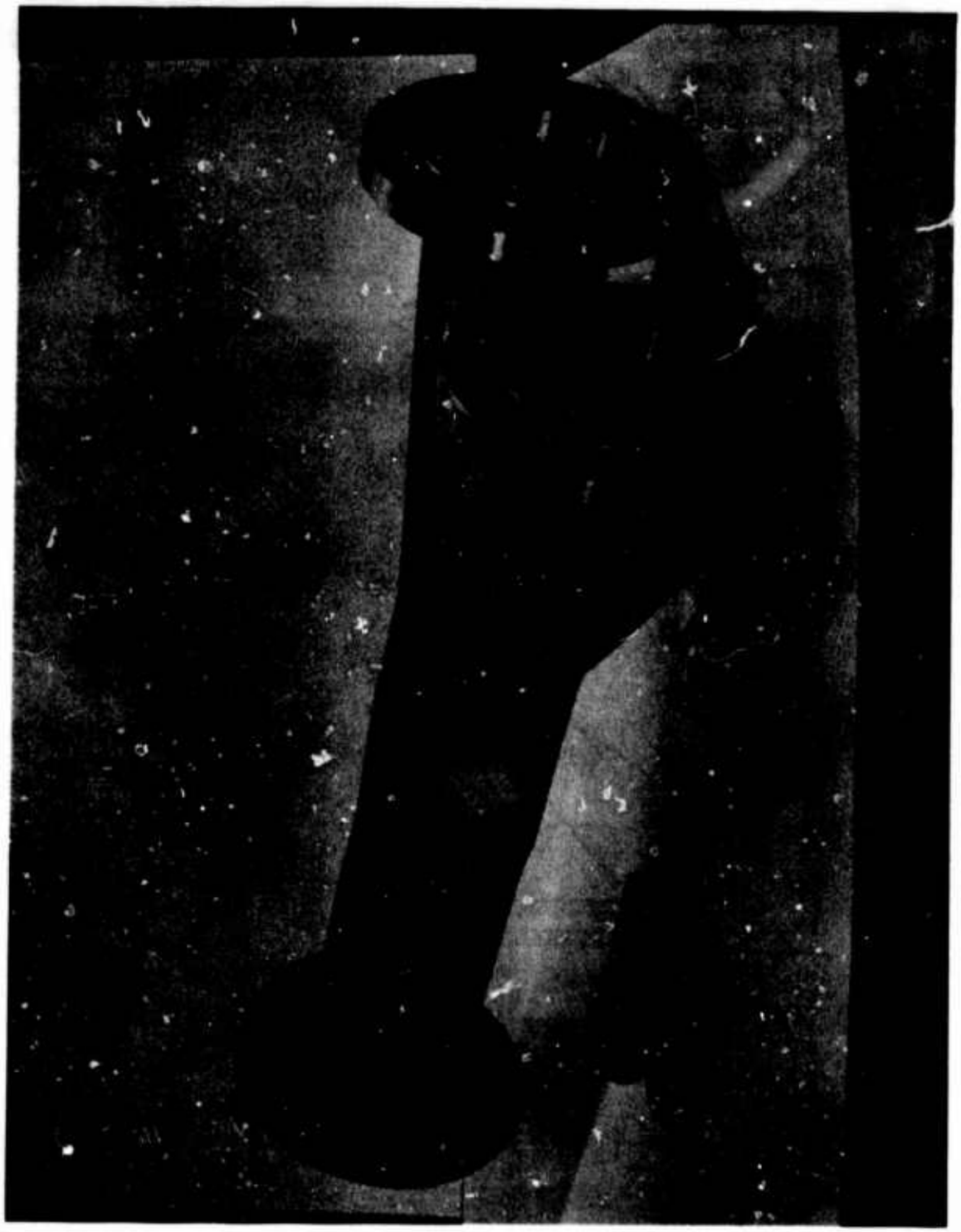


FIG.1 ½ AND 4 INCH LEVEL CONTROL VALVES

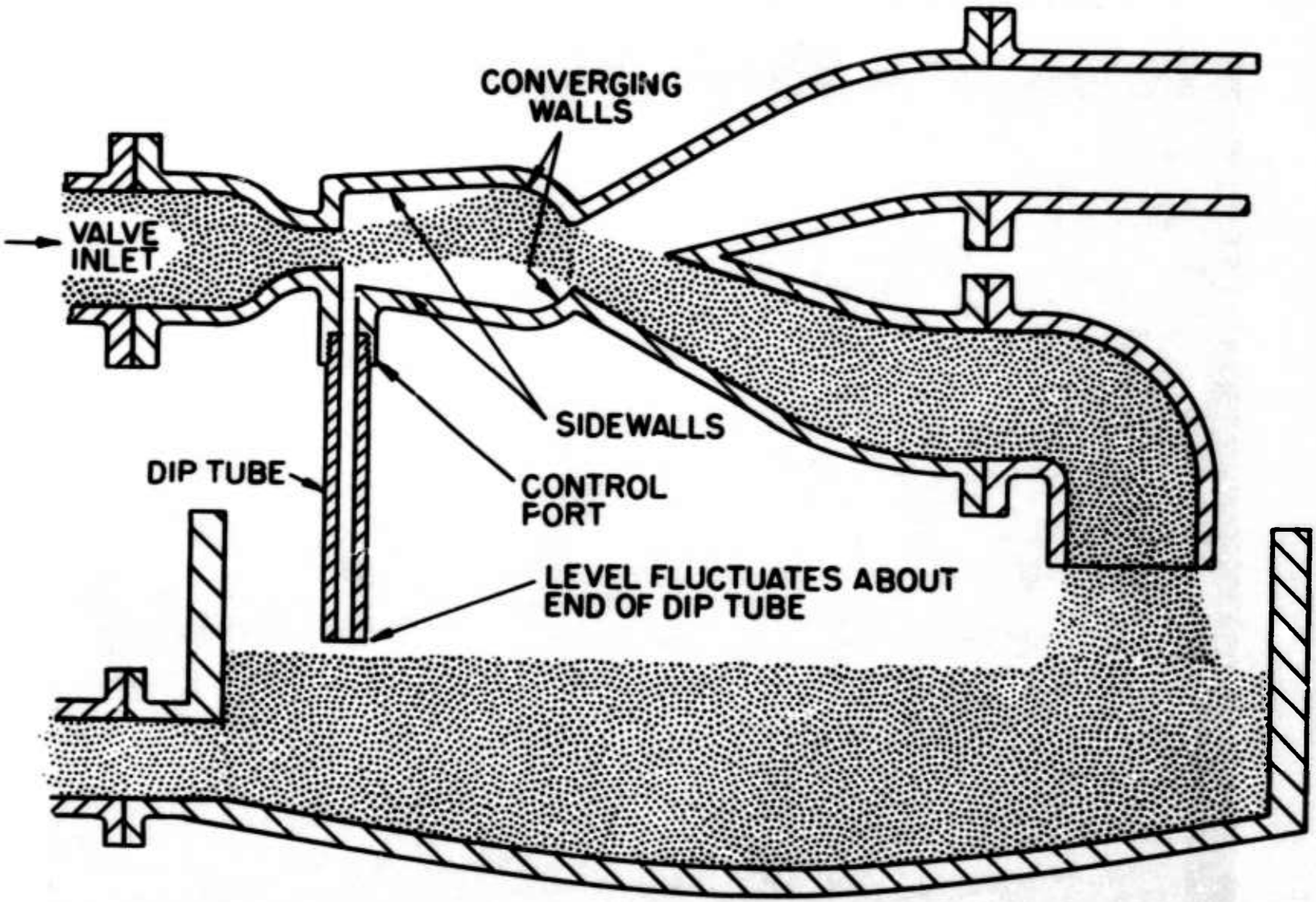


FIG.2 VALVE DIVERTS TO VESSEL WHEN LEVEL IS 'LOW'

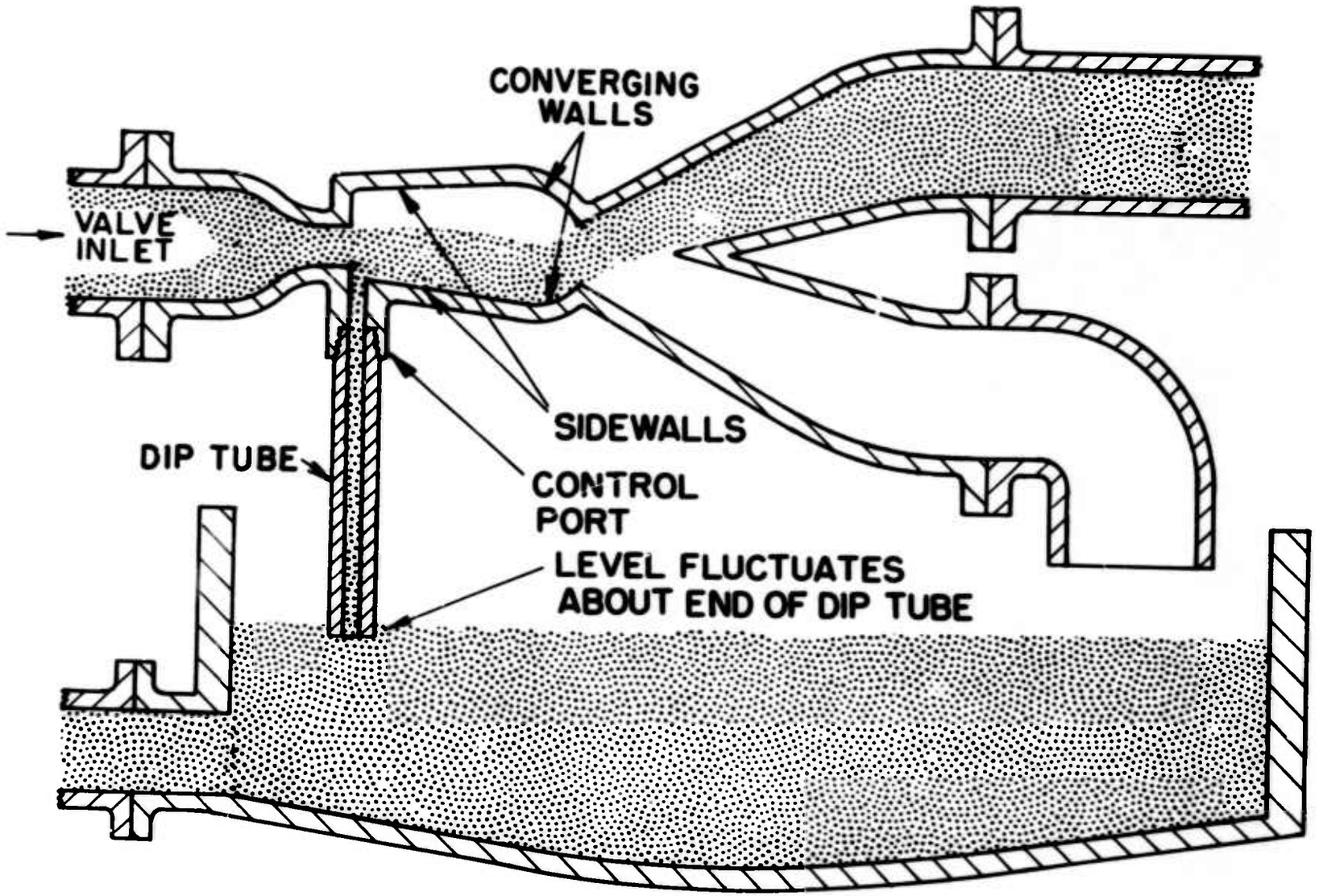


FIG.3 VALVE BYPASSES VESSEL WHEN LEVEL IS 'HIGH'

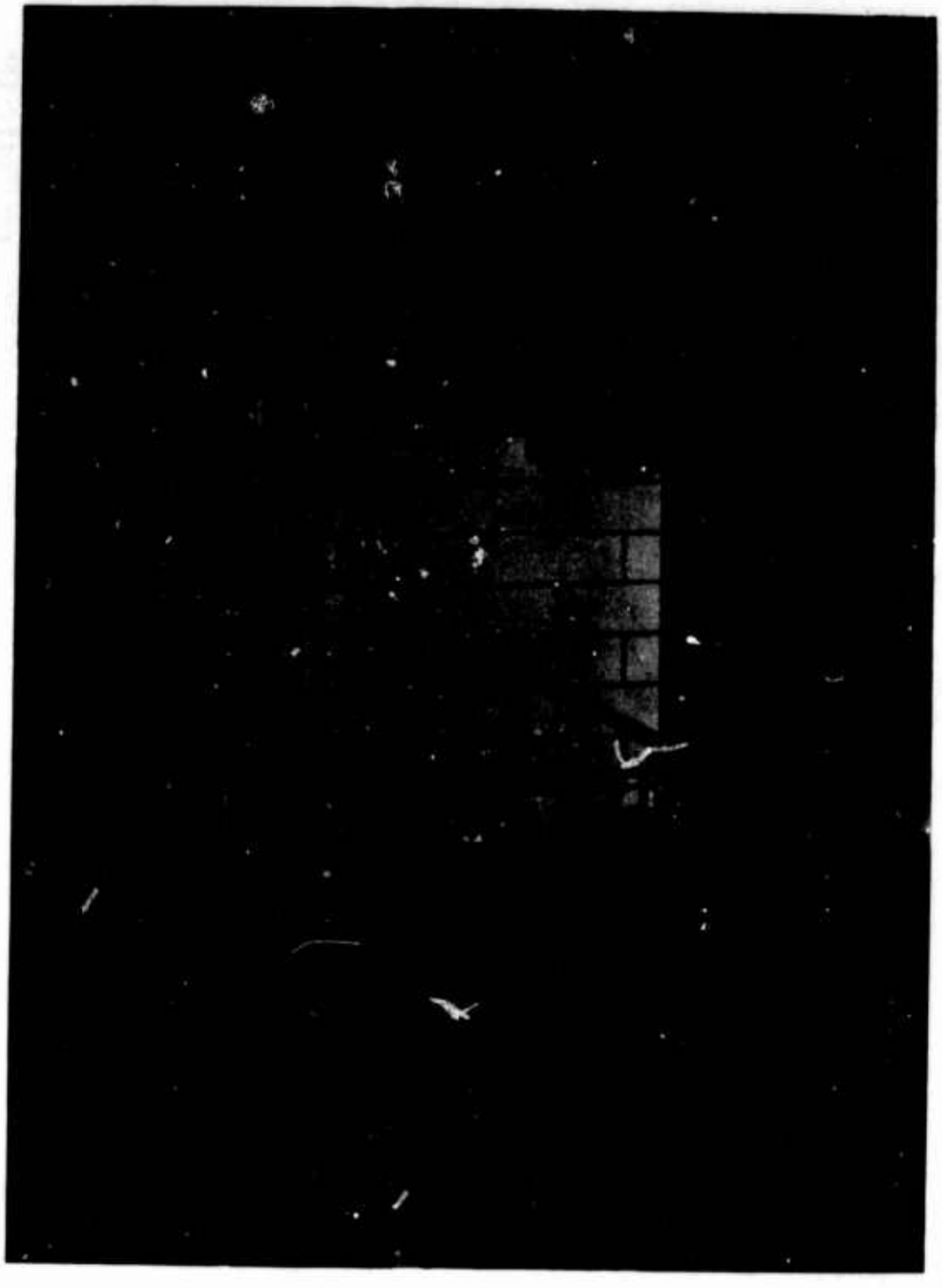


FIG.4 VALVE CONTROLLING WHITE WATER LEVEL IN PAPER PLANT



FIG.5 FLUIDIC VALVE MAINTAINS ELECTROPLATING TANK LEVEL

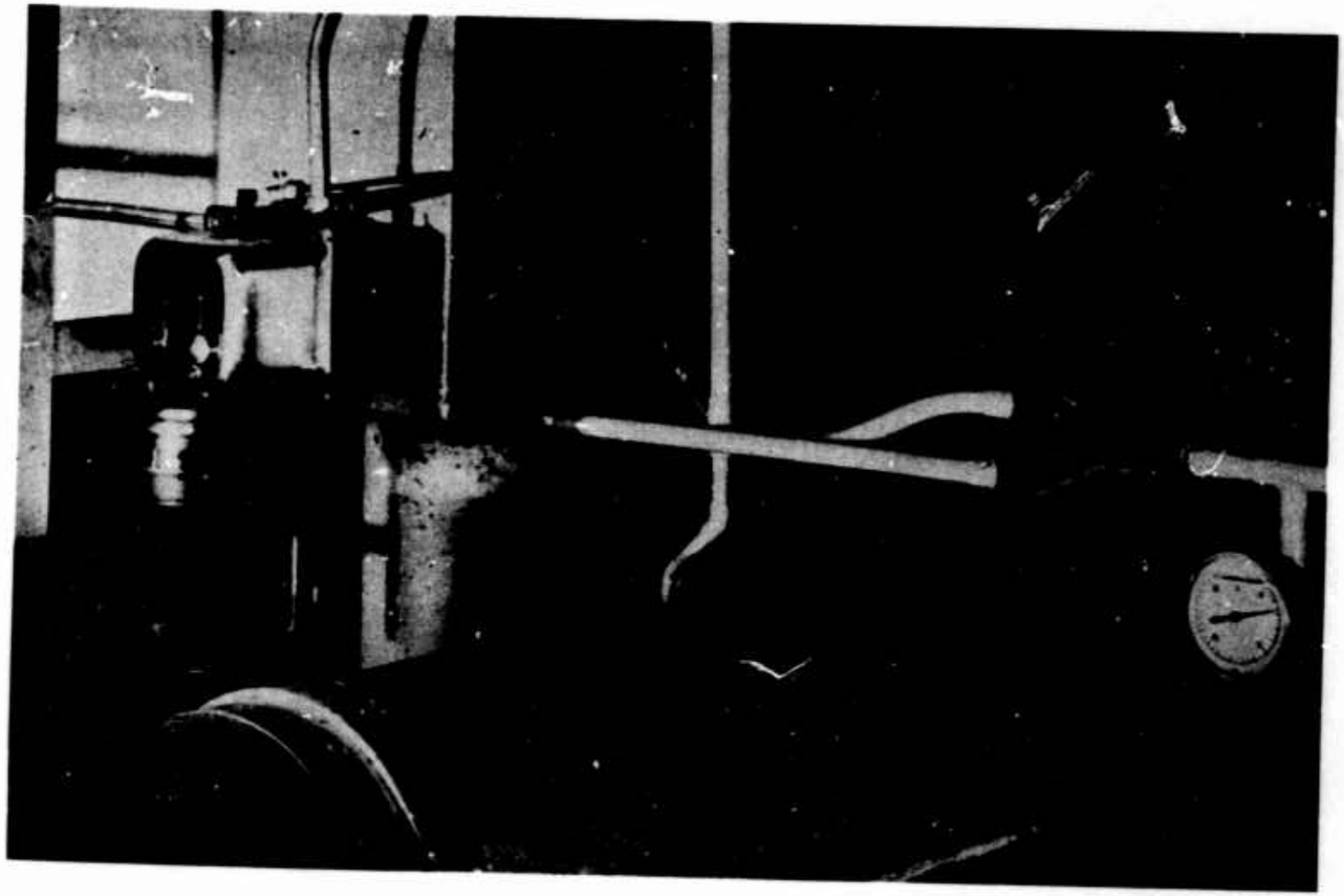


FIG.6A HARDNESS CONTROL SYSTEM SCHEMATIC

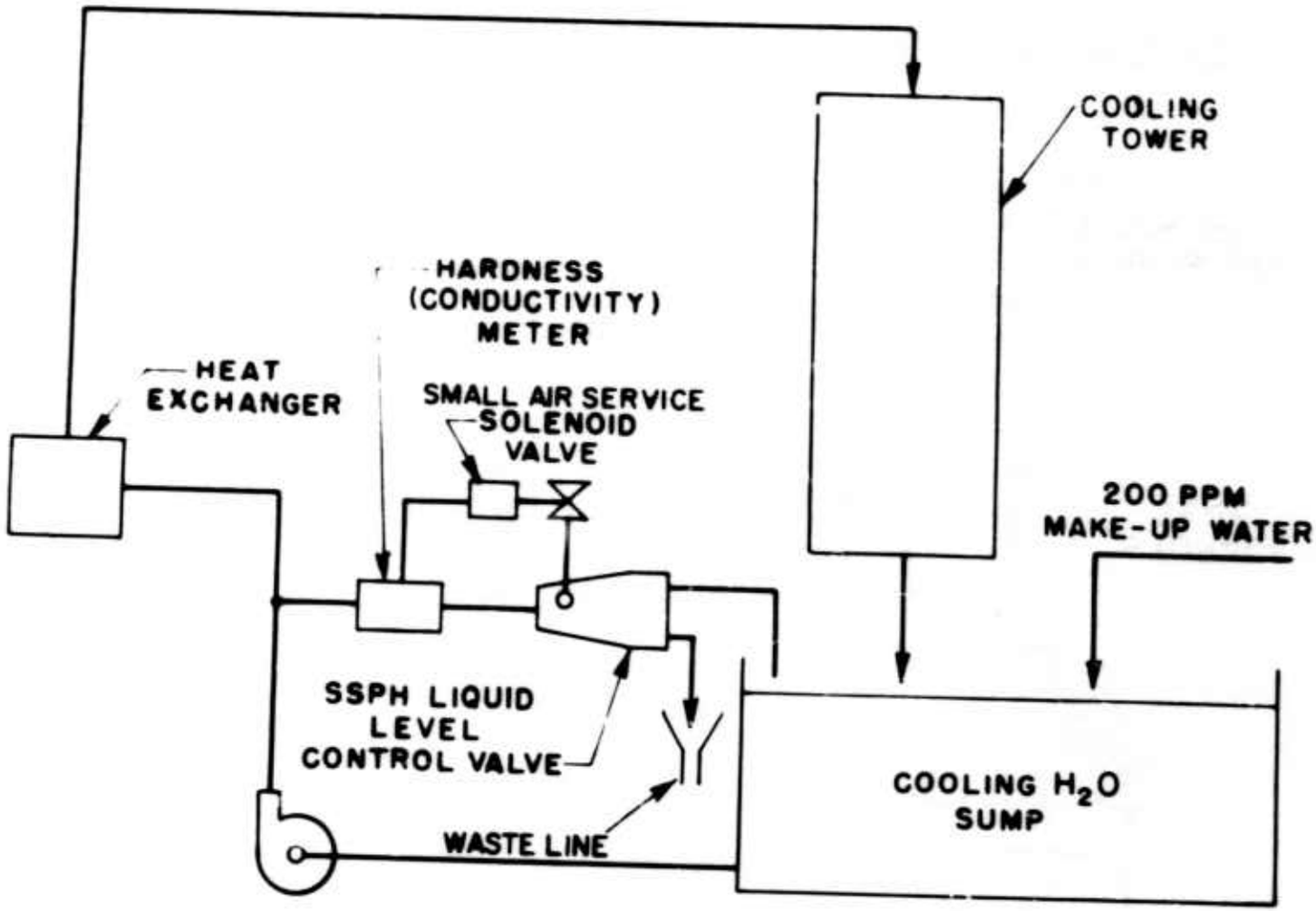


FIG.6B FLUIDIC VALVE INSTALLATION IN HARDNESS CONTROL SYSTEM

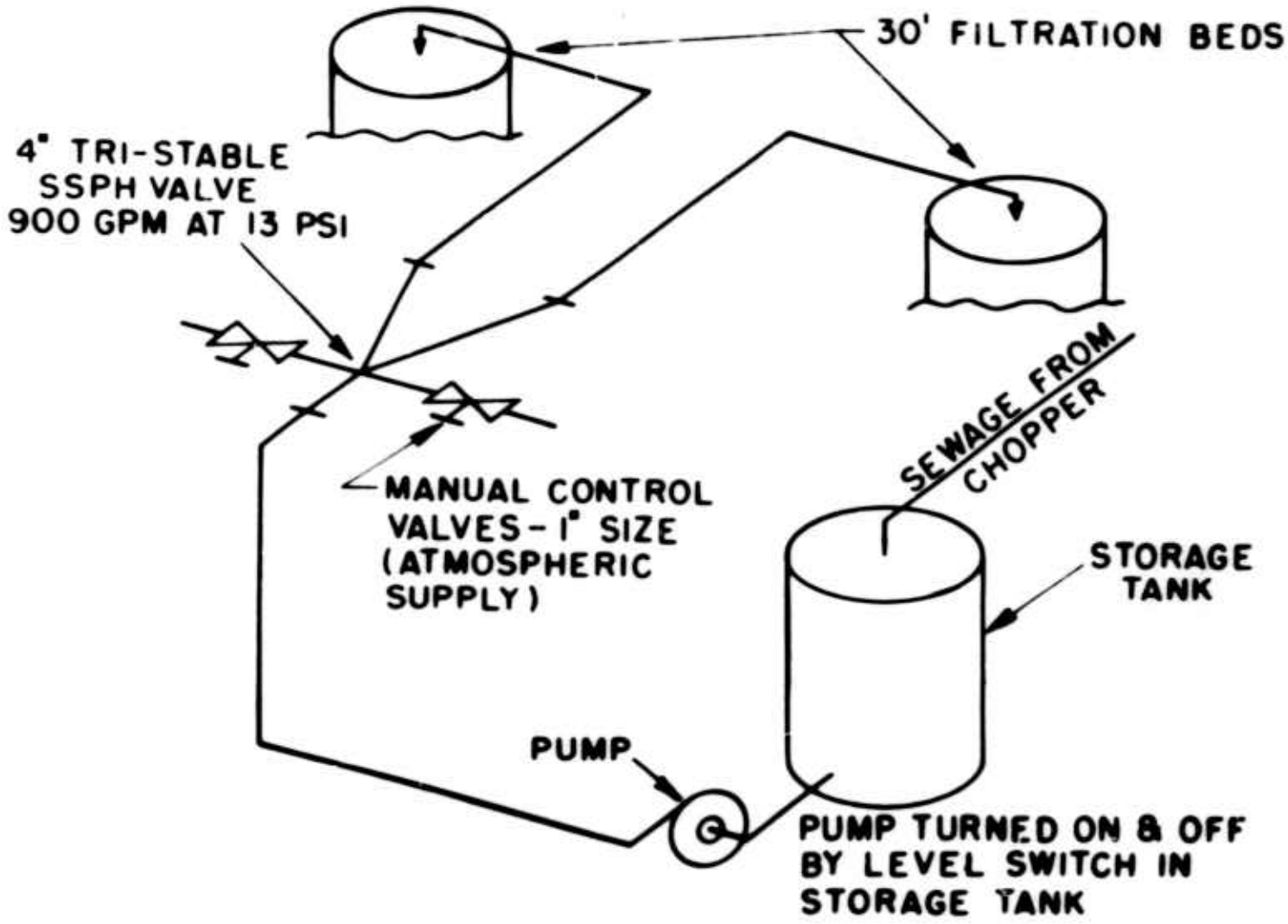


FIG.7 SEWAGE DISPOSAL STATION SCHEMATIC

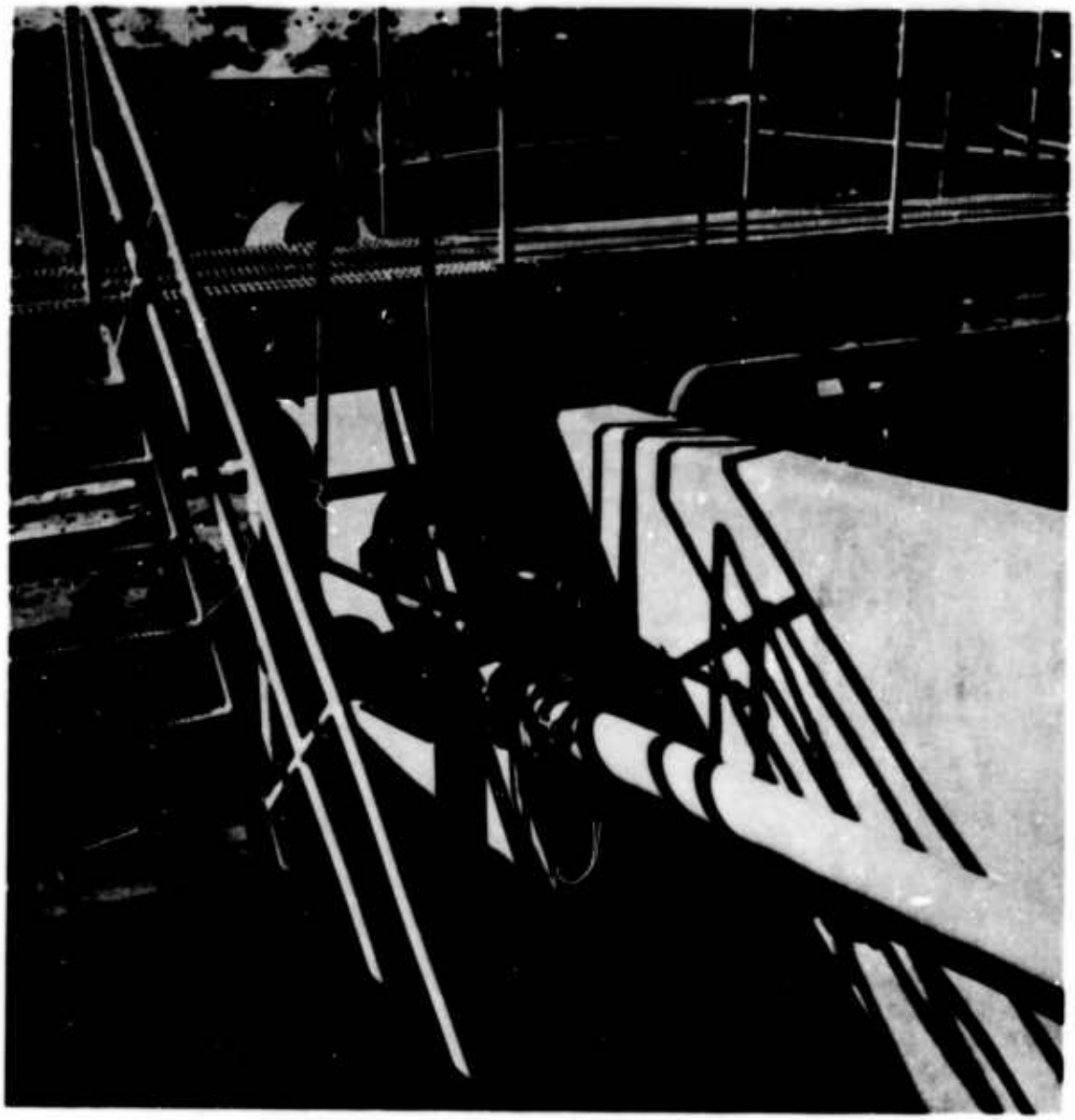


FIG.8 TRI-STABLE VALVE INSTALLATION AT SEWAGE DISPOSAL STATION

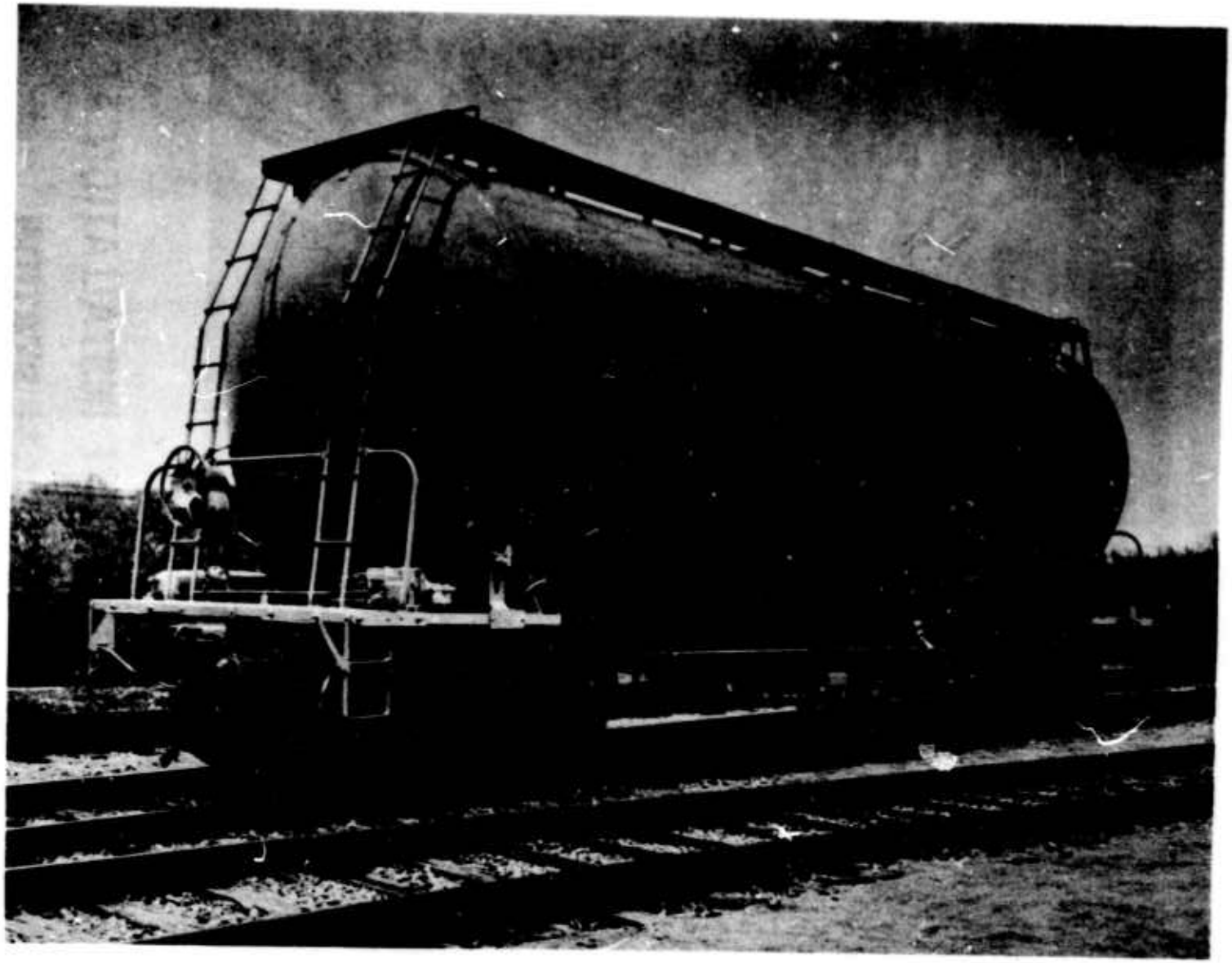


FIG.9 TANK CAR FOR BULK CEMENT

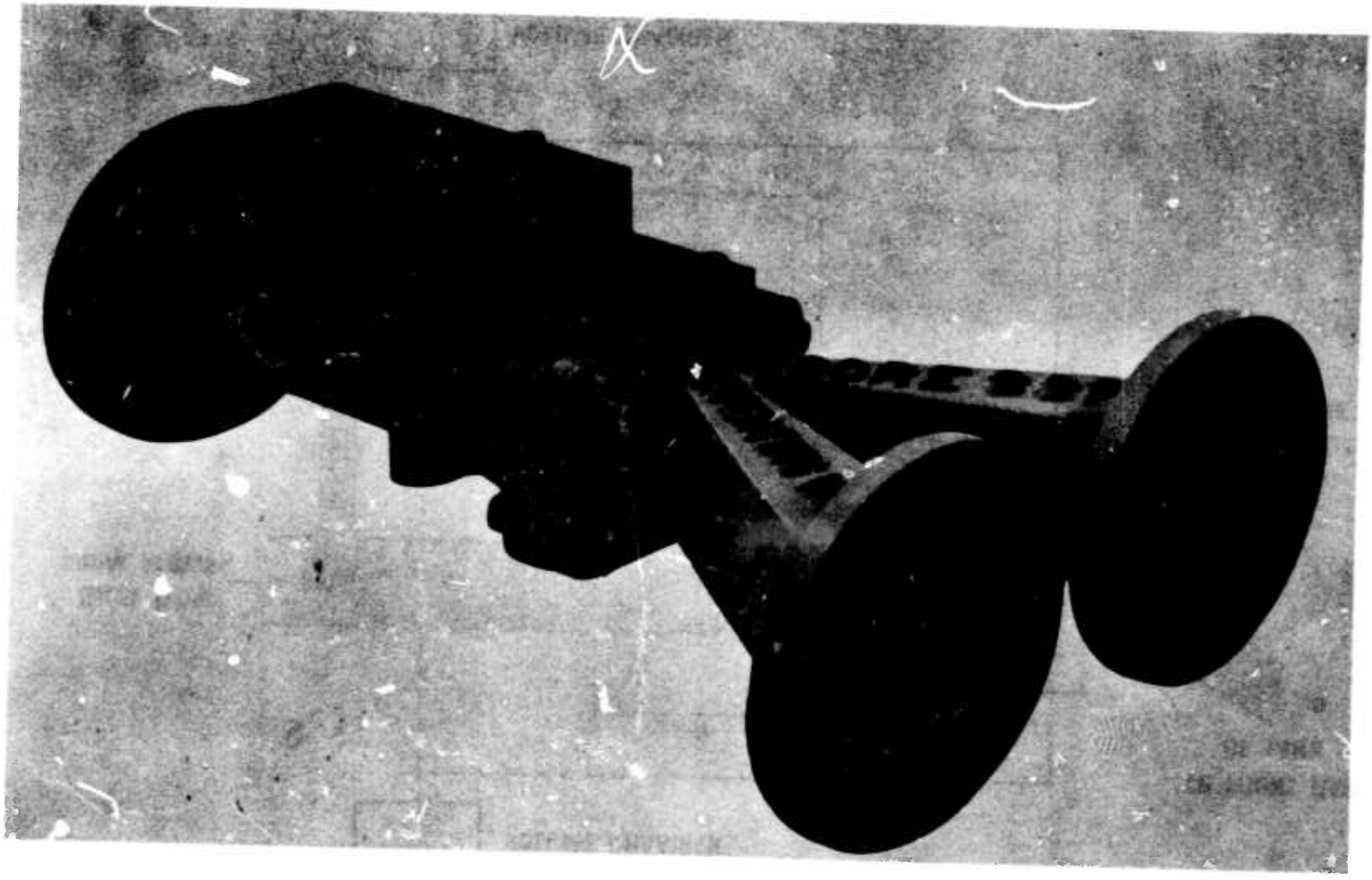


FIG.10 STAGED OSCILLATING VALVE FOR CEMENT CAR

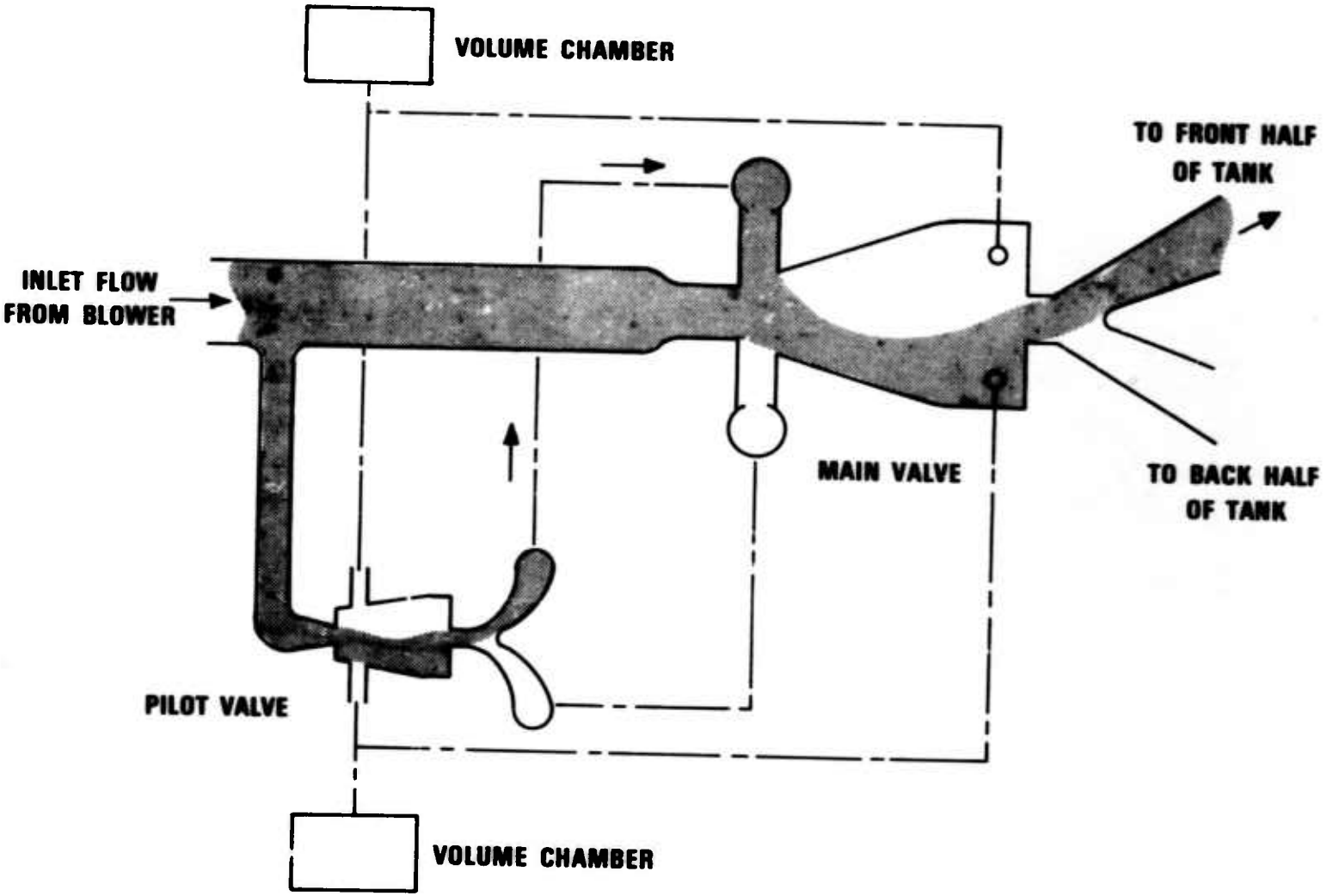


FIG.11 SCHEMATIC OF FLUIDIC OSCILLATOR CIRCUIT

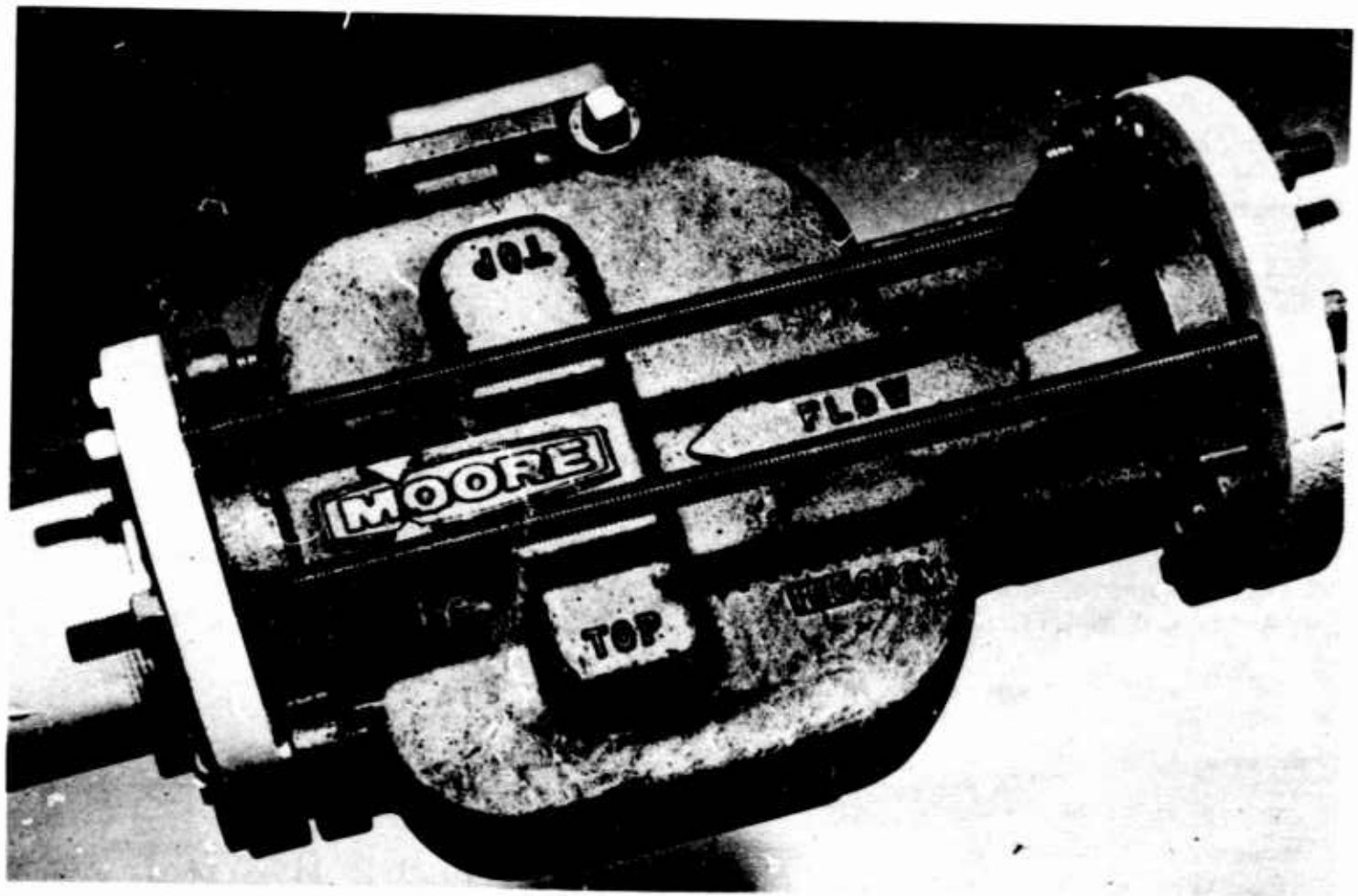
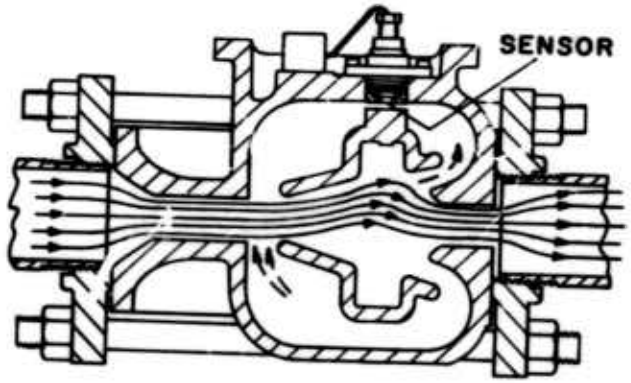
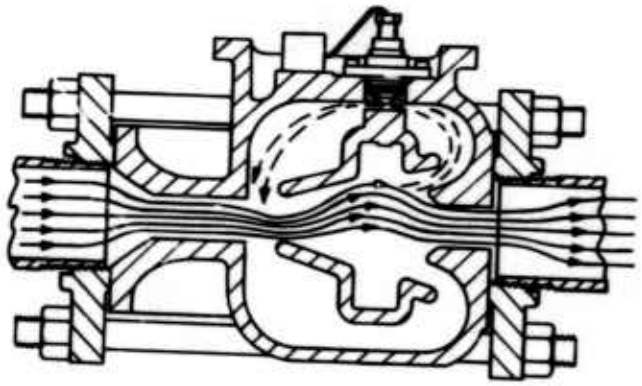


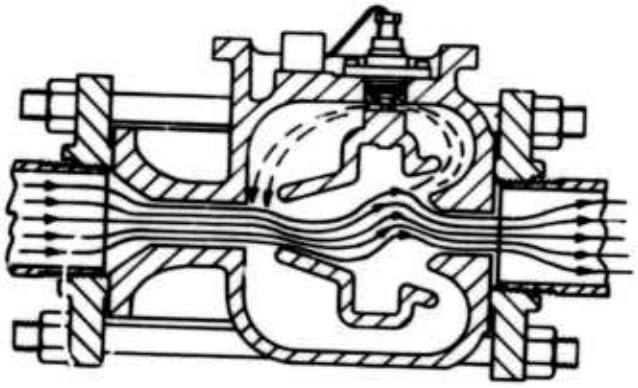
FIG.12 4 INCH FLUIDIC FLOWMETER



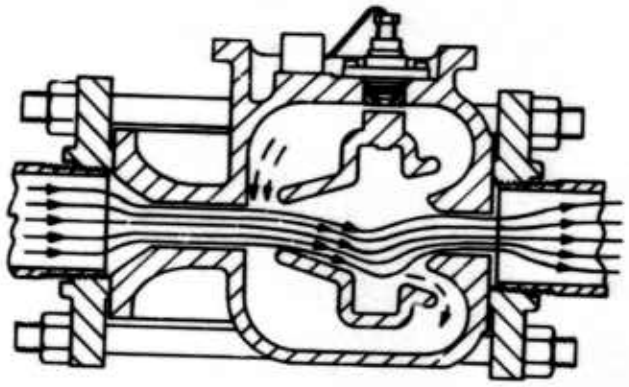
A. MAIN STREAM ATTACHED TO UPPER WALL; UPPER FEEDBACK PASSAGE FLOW INCREASING FROM ZERO ; LOWER FEEDBACK PASSAGE FLOW DECREASING



B. MAIN STREAM DEFLECTED TOWARD LOWER WALL BY UPPER FEEDBACK FLOW; LOWER FEEDBACK FLOW STOPPED



C. MAIN STREAM PROCEEDS DOWN LOWER WALL TOWARD RECEIVER OF LOWER FEEDBACK PASSAGE



D. MAIN STREAM COMPLETELY ATTACHED TO LOWER WALL FORCING FLOW IN LOWER FEEDBACK PASSAGE TO BEGIN

FIG.13

SCHEMATIC DEPICTING FLUIDIC FLOWMETER OSCILLATION (HALF-CYCLE)

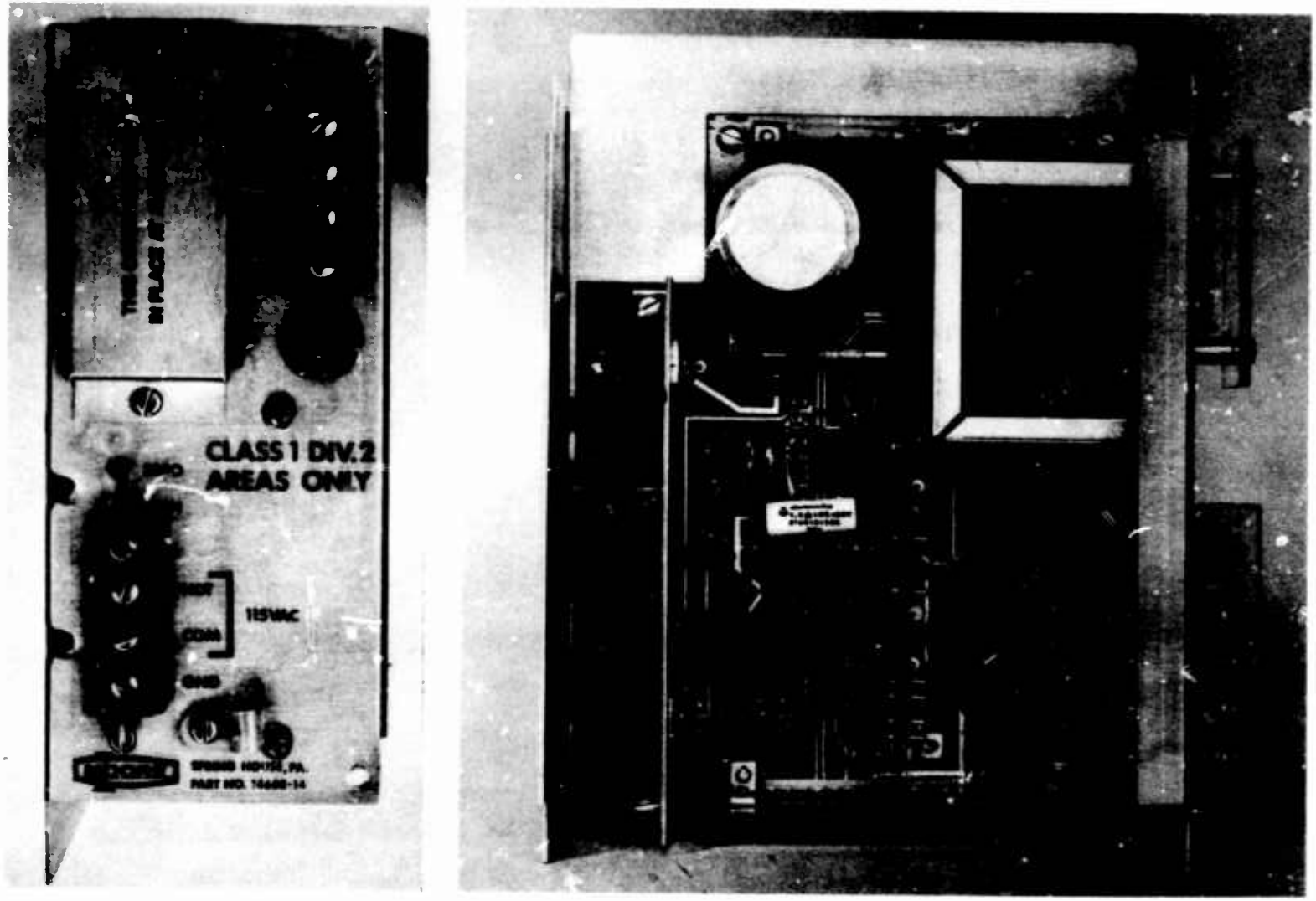


FIG.14 CONVERTER CHASSIS

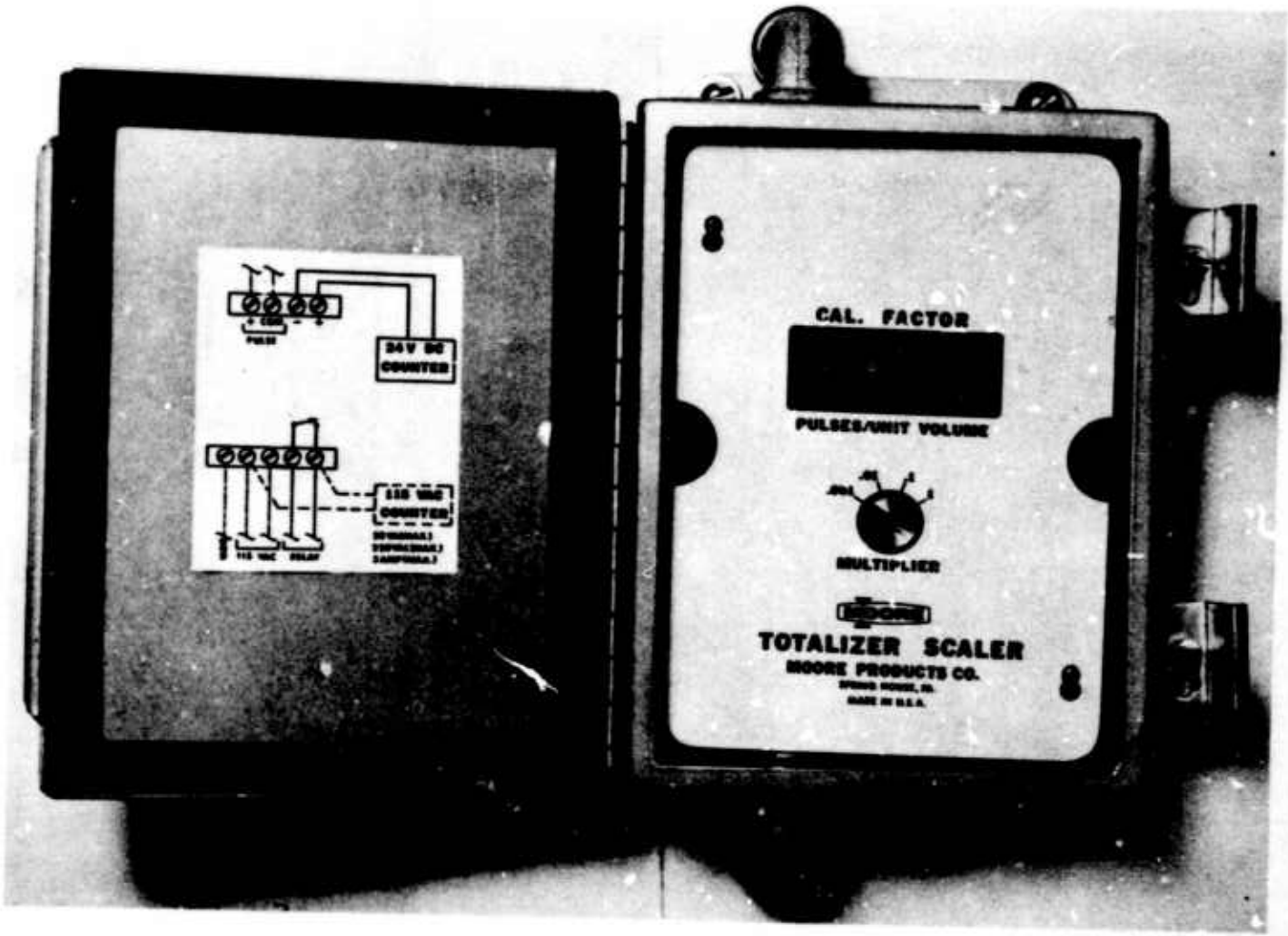


FIG.15 TOTALIZER SCALER

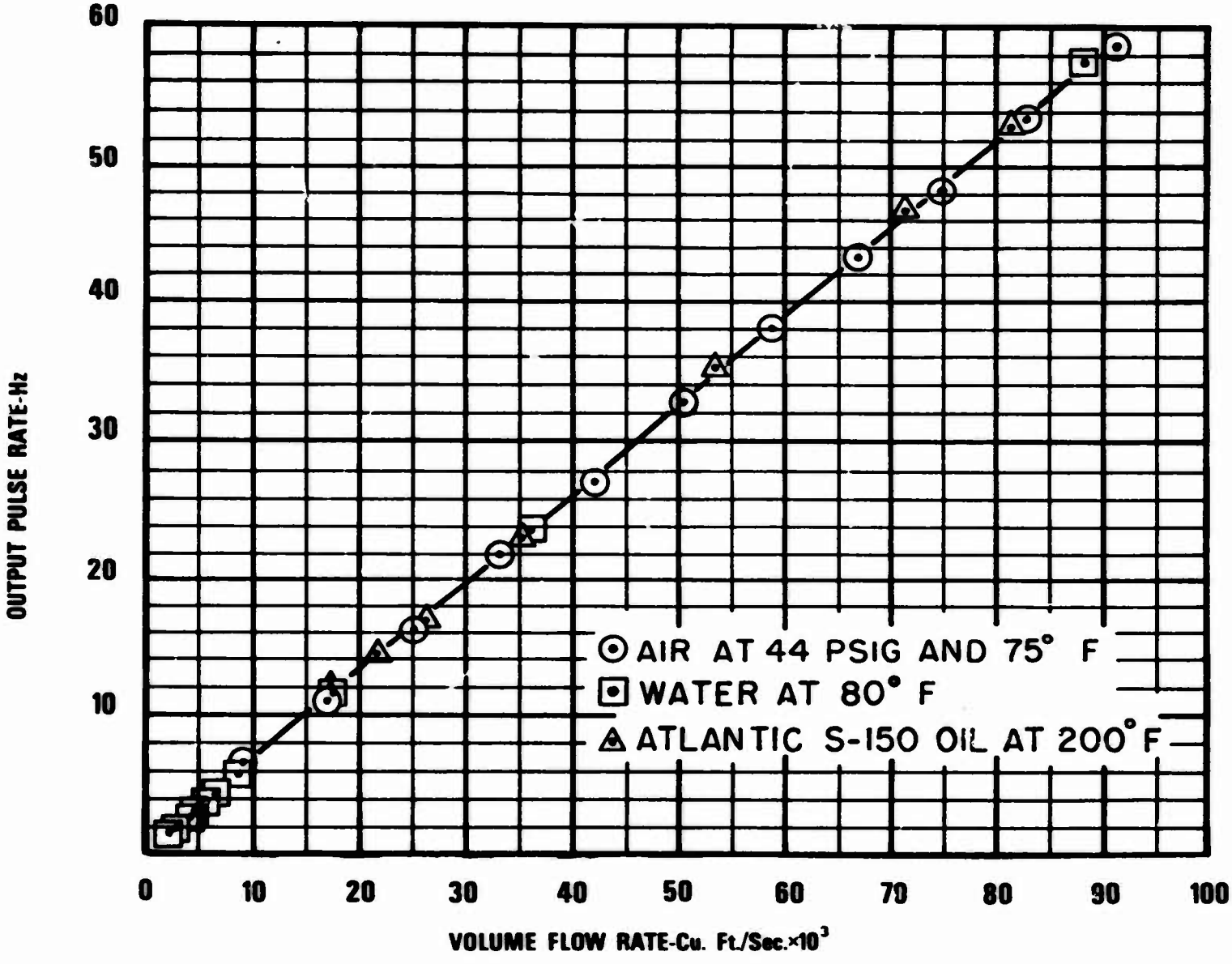


FIG.16 FLUIDIC FLOWMETER CALIBRATION DATA

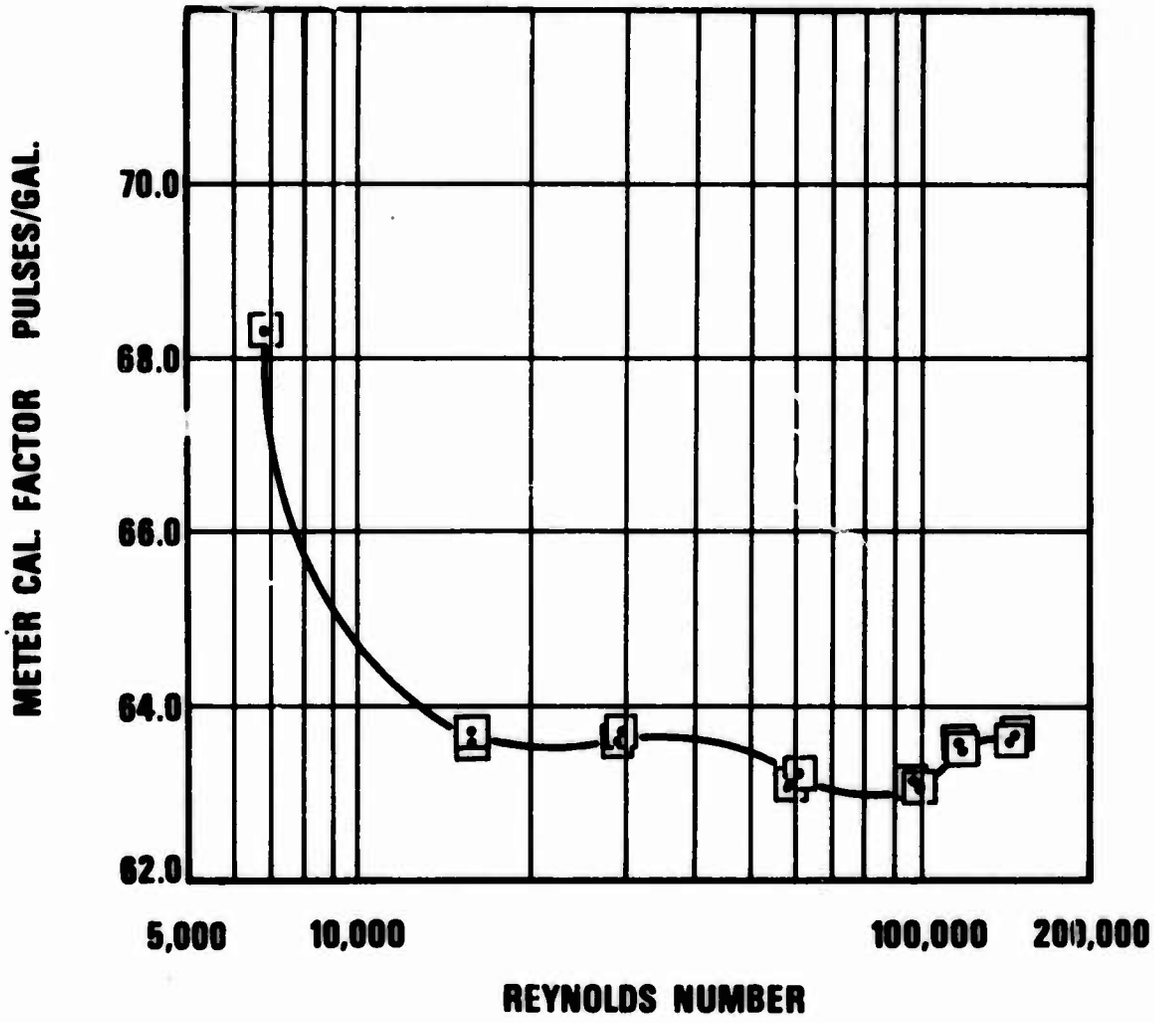


FIG.17 REYNOLDS NUMBER EFFECT ON FLUIDIC FLOWMETER CALIBRATION

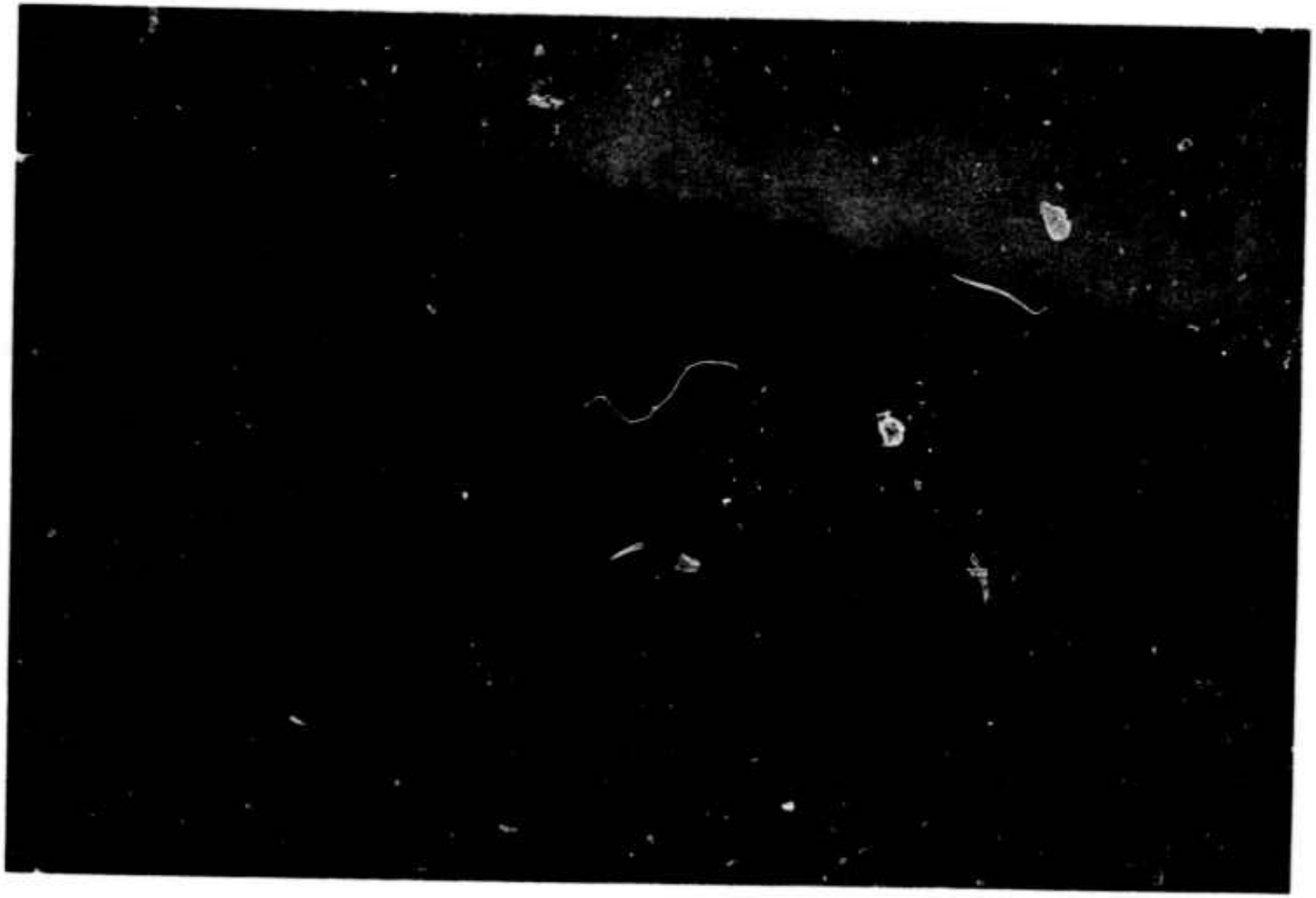


FIG.18 CONTROL STATION FOR INDUSTRIAL PROCESS CONTROL LOOP

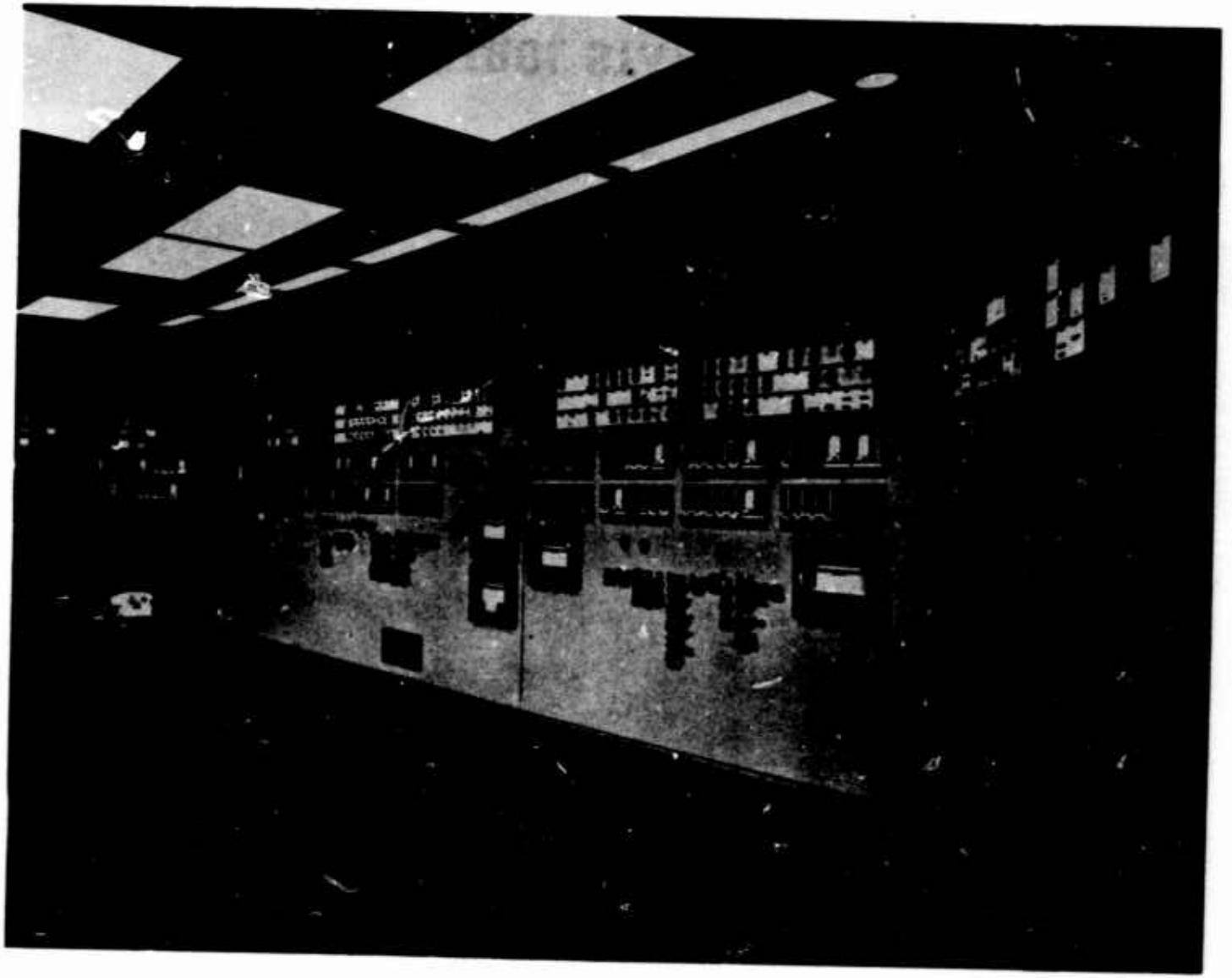
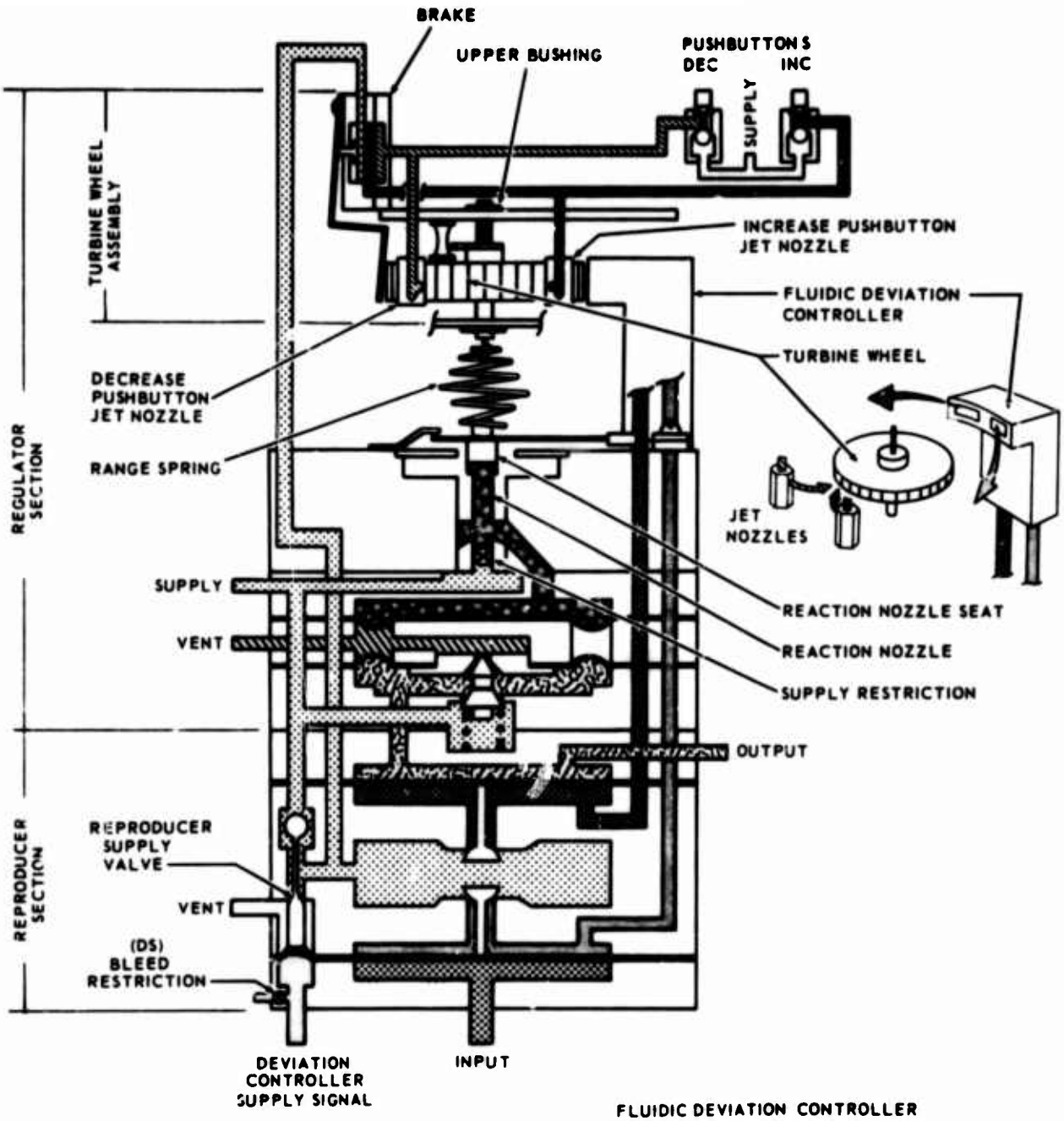


FIG.19 INDUSTRIAL PROCESS CONTROL PANEL



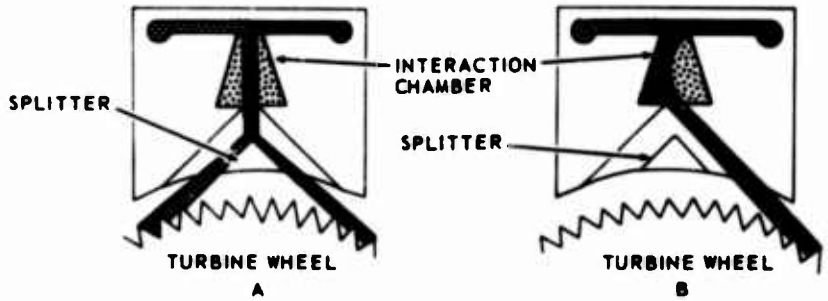


FIG.20 CONTROL STATION RELAY DESCRIPTION

FLUIDICS CONTROLS COOLING

OF

DIESEL LOCOMOTIVES

by

Robert B. Adams

Moore Products Co.

Prepared for
The Harry Diamond Laboratories
Fluidic State-of-th-Art
Symposium
30 Sept. - 04 Oct. 74

Preceding page blank

FLUIDICS CONTROLS COOLING OF DIESEL LOCOMOTIVES

A fluidic system for controlling Diesel engine water temperature has been standard equipment on General Electric domestic locomotives since the end of 1971. Fluidically speaking, highlights of this application are:

1. Large fluidic valves (Figure 1) divert water to the radiators for cooling. These valves have the capacity to handle up to 1000 gpm of cooling water.

2. The fluidic system increases the locomotive cooling capacity because the fluidic diverters have less pressure loss than the mechanical valves they replaced. Naturally, the use of fluidics resulted in the almost complete elimination of moving parts in the cooling system control.

3. Fluidic pilots (Figure 2) work to prevent radiator freeze-up by temporarily overriding the temperature control.

4. The fluidic pilots automatically change the characteristic of the fluidic diverting valves from analog to digital.

The locomotive cooling system (Figure 3) pumps water from the tank through the engine and on to a pair of fluidic diverting valves. Each valve is connected to a bank of radiators. Water is diverted to the first bank of radiators when cooling is required and, if necessary, also to the second bank. Under some cold weather conditions, cooling is not required and both valves divert all flow directly to the water tank, thus bypassing the radiators.

The General Electric locomotive has a dry radiator system. A vent from the radiator to the top of the water tank allows water to drain from the radiator when all flow is bypassed to the tank. This must be done because any water left in the radiator would quickly freeze in winter. The dry radiator system eliminates the need for fan and air shutter controls to vary the cooling rate and does not require anti-freeze.

The fluidic valves should be of the analog type, rather than bistable to reduce thermal cycling of the radiators. Bistable, or "on-off" control can only deliver full engine water flow to the radiator when cooling is required. This maximum cooling rate, too great for most operating conditions, would force engine water temperature to fall below the control level. Bistable control would thus continuously subject parts of the radiator to alternate periods of hot and cold. The resulting cycles of thermal expansion would serve to decrease radiator life expectancy. Analog control minimizes thermal cycling by providing flow to the radiator in just the amount necessary to maintain a stable temperature.

RBA:mcd

However, since a small initial flow would quickly freeze under winter conditions, the valve performance must be tailored to delay analog operation until the required flow rate to the radiator is large enough to prevent freezing. Therefore, control is bistable between zero and a flow rate which will not freeze in the radiator. Beyond this minimum allowable flow rate, the valve proportions flow to the radiator with temperature to minimize cycling. The fluidic valve, therefore, combines bistable and analog action into its operation.

Figure 4 shows performance of fluidic valves for avoiding freezing and minimizing cycling. Part (a) plots water flow to the radiators versus water temperature at maximum engine speed. Part (b) repeats this curve at engine idle.

Follow the curve of Figure 4, part (a), in the direction of increasing temperature. At T_1, a flow of 300 to 400 gpm, Q_1, is suddenly delivered by the first valve to the first radiator bank. At T_2, the flow to the first bank has increased to its maximum, Q_2 (i.e. the first valve diverts all flow that it receives from the engine to the first radiator bank). Also, at T_2, the second valve suddenly diverts a flow of 300 to 400 gpm to the second bank of radiators, increasing the total flow to the radiators to Q_3. Between T_2 and $T_{max.}$ the flow to the second bank increases proportionally with temperature to the point where all flow from the engine is diverted to the two radiator banks.

For decreasing temperature from $T_{max.}$, the flow to the second bank decreases and at T_2 the flow to the first bank also starts to decrease. At T_3, the flow to the second bank is reduced to the minimum allowable to prevent freezing and the second valve abruptly diverts the flow remaining in the second bank to the water tank. At T_4, the flow in the first bank has fallen to Q_4, the point where it must be diverted abruptly to the water tank to avoid freezing.

The curve for part (b) of Figure 4, shows much smaller switch-up flow Q_1' and maximum flow, $Q_{max.}'$, to the radiator because of the lower engine speed. However, the switch down flow level, Q_4', must be the same as that for maximum throttle, Q_4, in order to avoid freezing.

The fluidic system for one bank of radiators is shown schematically in Figure 5, the diverting valve is controlled by a thermostatic pilot valve (Figure 6). Less than 5% of the water leaving the engine passes through the thermostatic pilot and is apportioned between the hot and cold control ports of both fluidic valves. The pilot is actuated by a wax filled element (power pill) that expands with engine water temperature. Expansion of the element rotates the beam assembly to increase flow through the hot control port and decrease flow through the cold control port.

The fluidic valve acts as an analog diverter when water is supplied to the minimum flow control port. Upon temperature increase, flow from the thermostat to the hot control port increases and proportionally

RBA:mcd

deflects the stream in the interaction chamber toward the lower sidewall. A proportional increase in flow to the radiator now occurs because, at the discharge, the stream is deflected upward toward the radiator outlet. A pressure equalizing chamber located between the discharge and the receivers prevents "lock-on" of the stream to either of the discharge sidewalls.

However, when air, instead of water, is aspirated through the minimum flow control port, the stream discharging from the interaction chamber "locks-on" to the lower discharge wall. This action, overriding control by the thermostatic pilot, sends all water directly to the tank.

Starting with cold water, Figure 7, the thermostatic pilot sends all control flow to the fluidic diverting valve through the cold water port. The fluidic valve now diverts fully to the water tank. The radiators and the fluidic pilot valve are filled with air. Air is continuously aspirated into the minimum flow control port from the top of the tank.

As the water first heats, the fluidic valve, although directed by the thermostat to send water to the radiator, cannot do so. Air present at the minimum flow control port locks all flow directly to the tank. However, the water level in the outlet to the radiator rises proportionally with temperature (Figure 8). The rising water level reaches the fluidic pilot through the radiator outlet at temperature T_1 (Figure 4a). Water, as it fills the fluidic pilot is aspirated into the minimum flow control port and unlocks the stream from the lower discharge wall. Water now flows partially into the radiator outlet as directed by the thermostat (Figure 9).

Suppose now that cooling by the radiator reduces the water temperature. Radiator flow is automatically reduced by the thermostat action proportionally with temperature until T_4. The fluidic pilot continuously receives a small flow of water from the radiator outlet. One outlet of the fluidic pilot is connected to the minimum flow control port of the fluidic valve. The pilot continuously diverts water to the minimum flow control port when radiator back-pressure is great enough to force a continuous escape of water through the pilot valve control tube. However, when the radiator flow is no longer sufficient to force water to bleed from the control tube, the pilot diverts to the vent outlet (Figure 10). Air, now enters the minimum flow control port, and immediately reduces flow to the radiator from Q_4 to zero (Figures 4a and 7).

The minimum flow allowed to remain in the radiator is controlled by the fluidic pilot's measurement of radiator back-pressure, which is an indication of flow. Therefore, this "switch down" point is completely independent of engine speed as is required to minimize cycling.

Fluidic bi-stable diverting valves were first tried on two General Electric locomotives delivered to the Penn Central in 1967. Their success led to a development contract for a fluidic cooling control

RBA:mcd

system. The new system was first installed on five General Electric U36B (Figure 11) and nineteen U23C locomotives delivered to the Seaboard and Penn Central Railroads in 1970. After 1971, all General Electric domestic Diesel electrics were equipped with the fluidic system, whose installation is illustrated in Figure 12.

The system first diverts water to the radiators at a water temperature of approximately 192°F. The maximum flow, about 1000 gpm at full throttle, is delivered to the radiators at 198°F. The pressure drop across the fluidic system, including losses in the radiator, is 17 psi at maximum flow. The minimum flow allowed in one radiator bank is controlled at approximately 100 gpm.

The fluidic cooling system does not require auxiliary power as all energy for control is taken directly from the water. The fluidic system, in addition to increasing cooling capacity, has contributed to greater reliability and a reduction in maintenance of General Electric Locomotives.

RBA:mcd

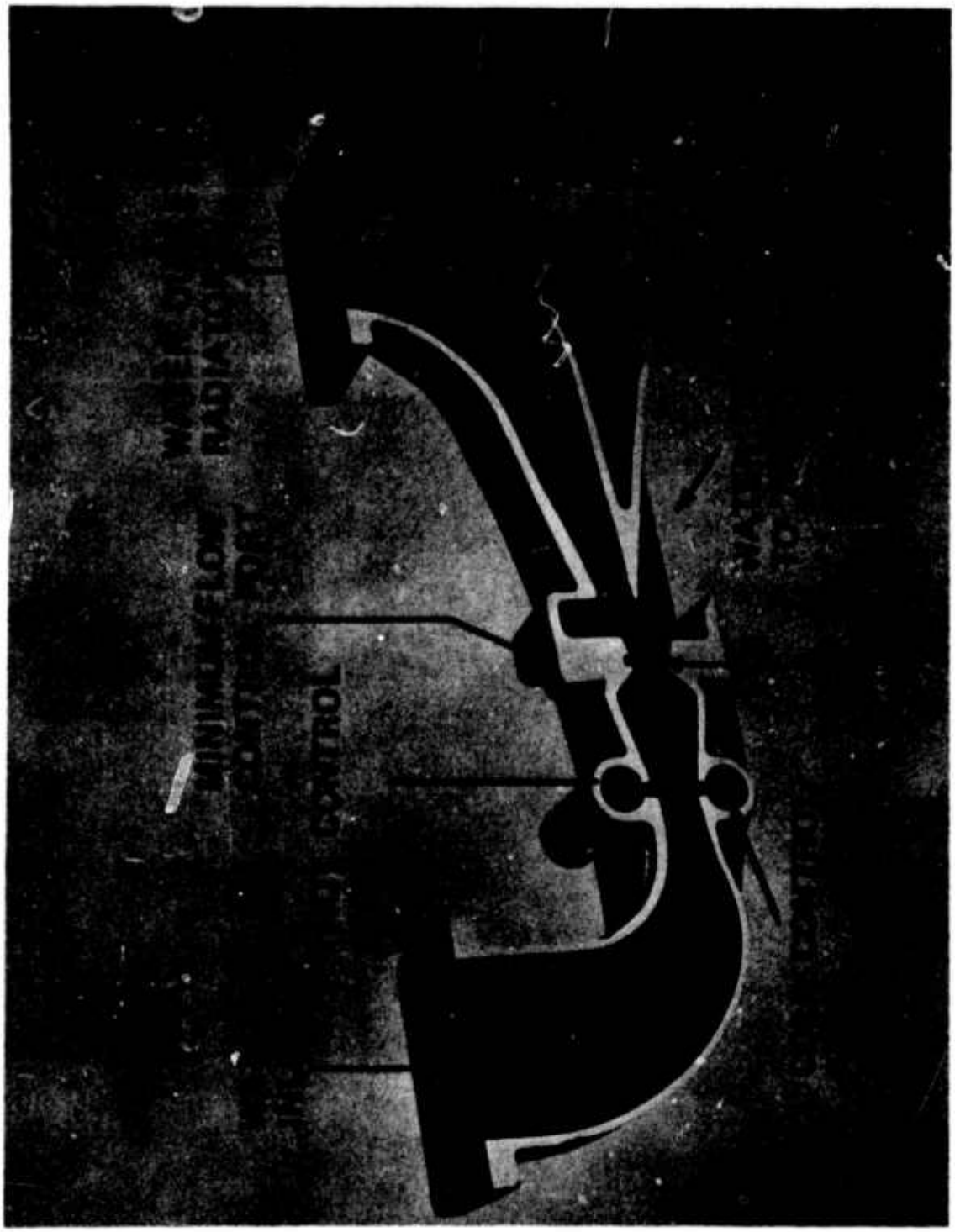


FIG.1 FLUIDIC DIVERTING VALVE

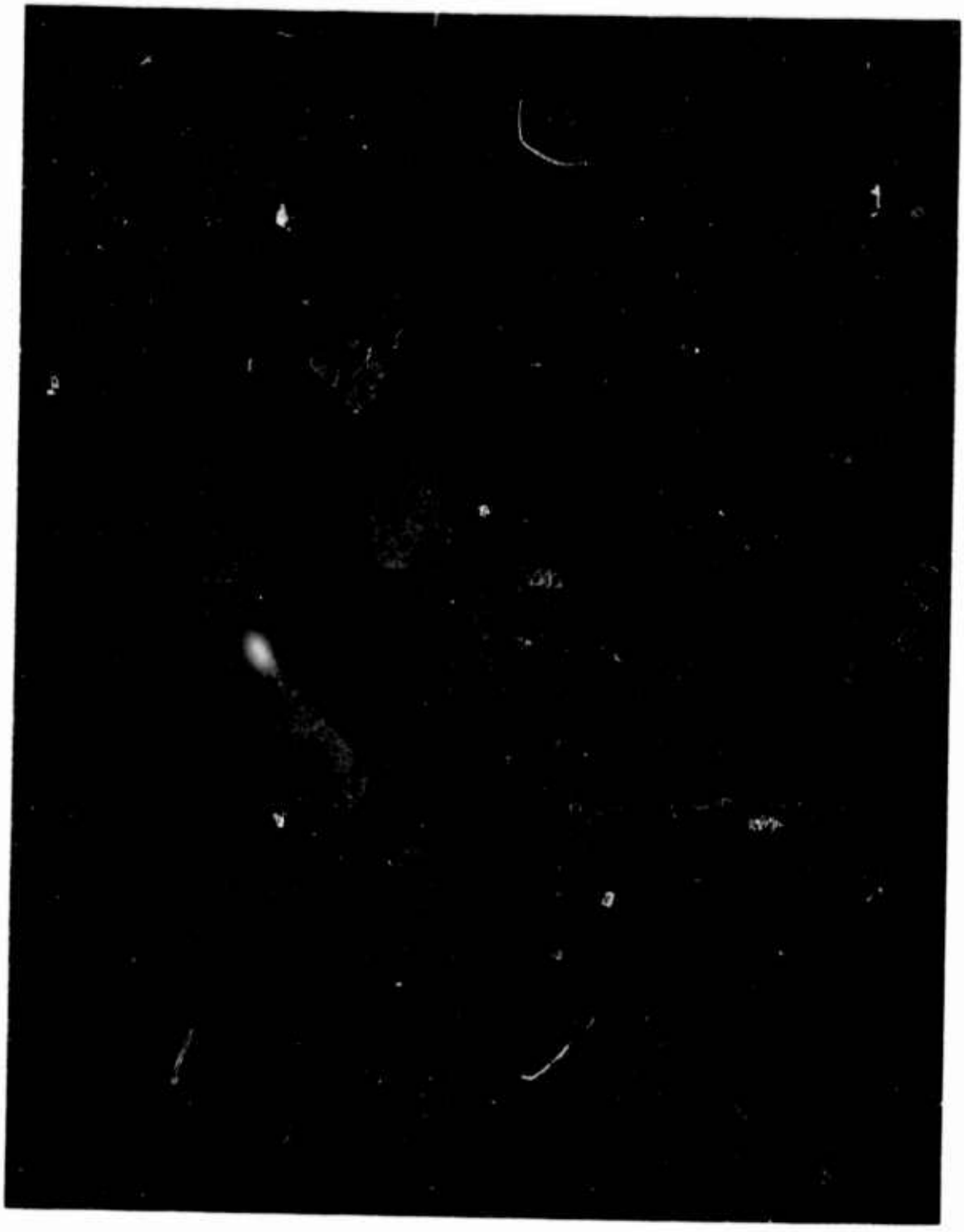


FIG.2 FLUIDIC PILOT

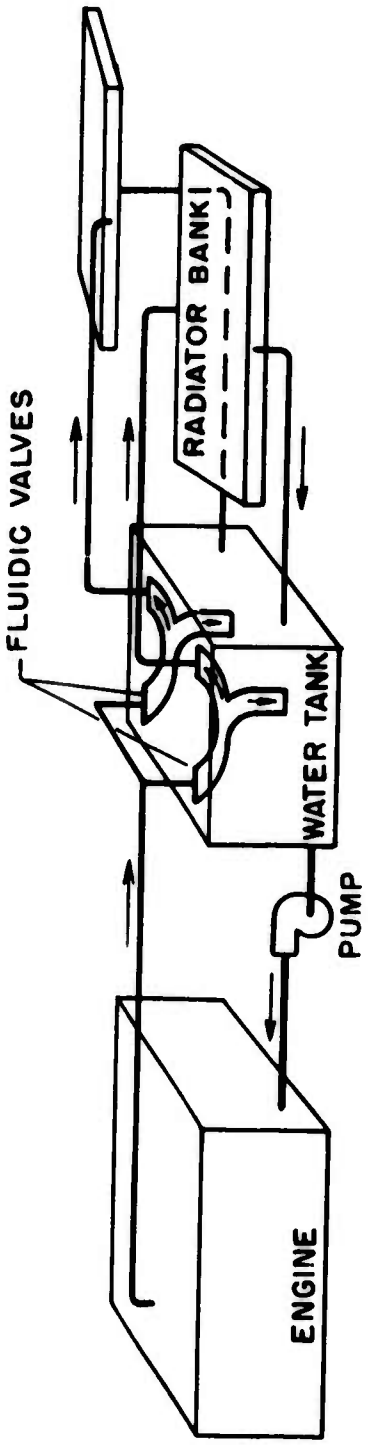


FIGURE 3. COOLING SYSTEM ARRANGEMENT

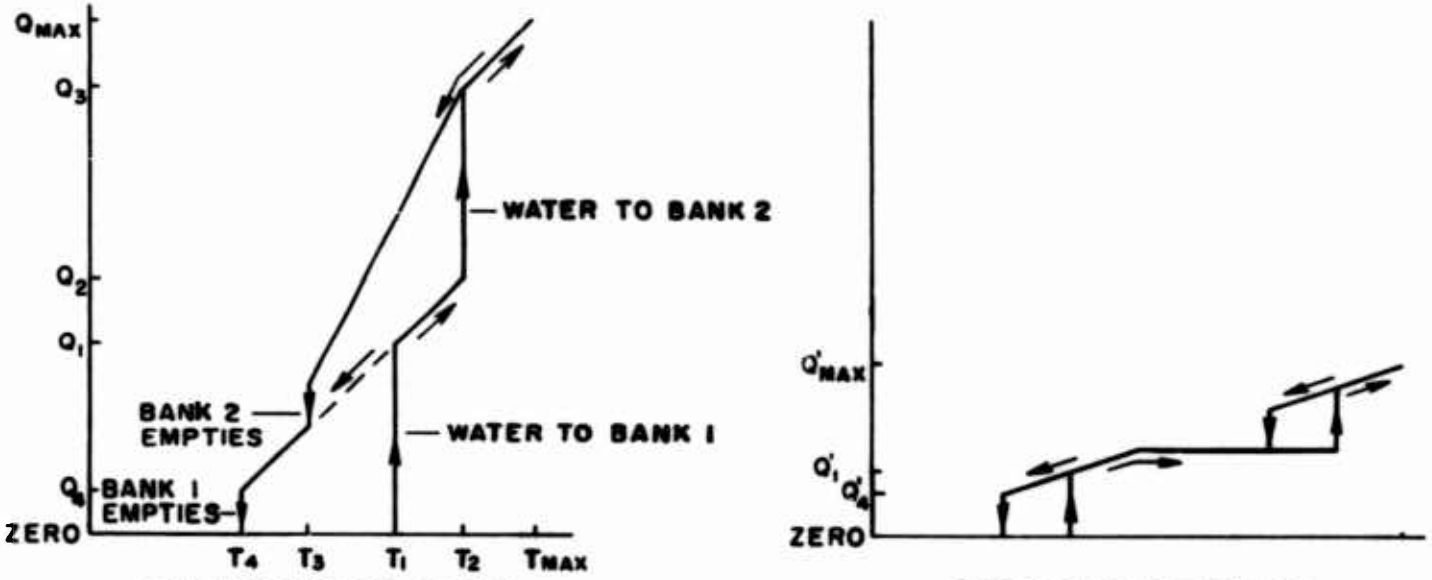
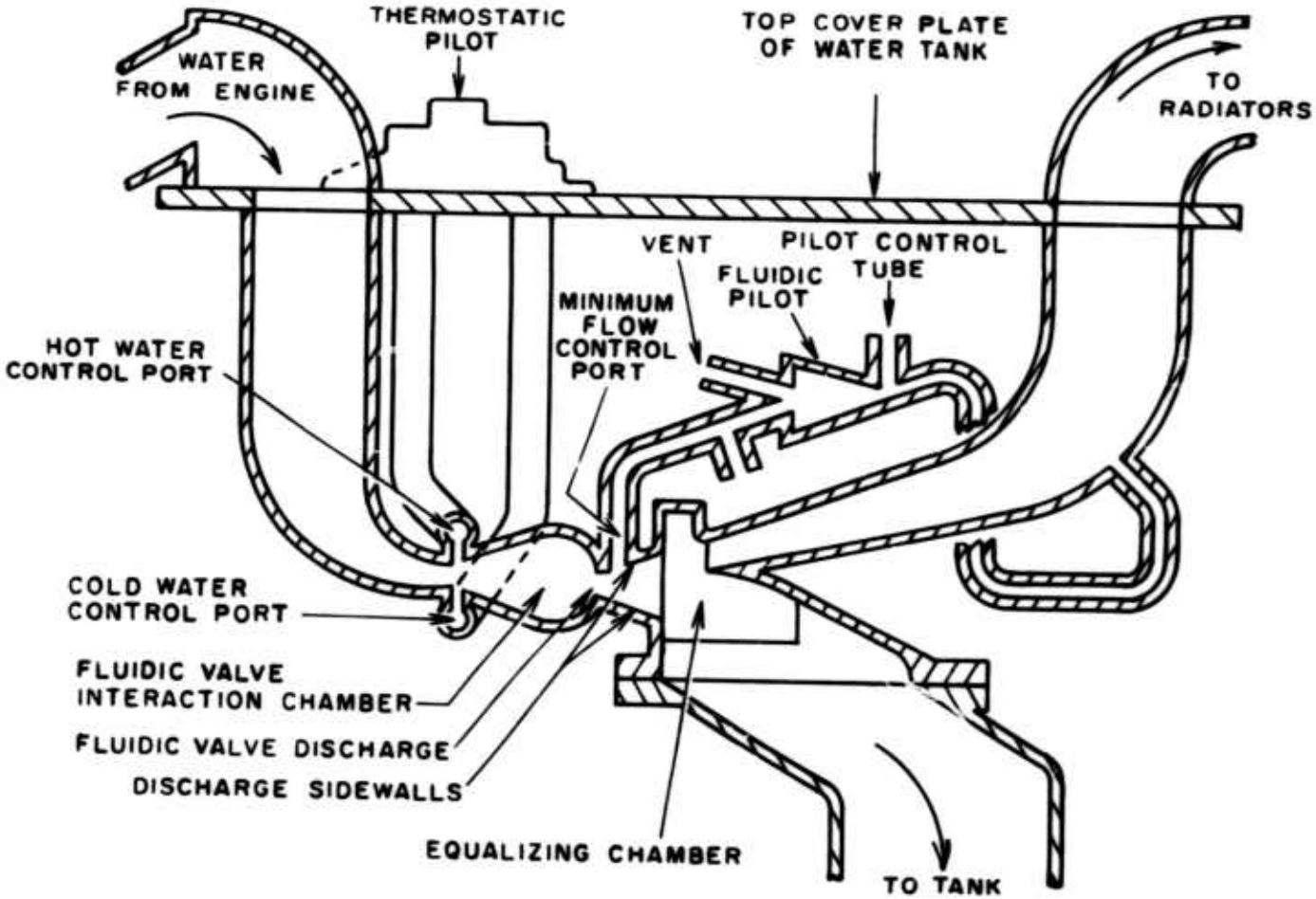
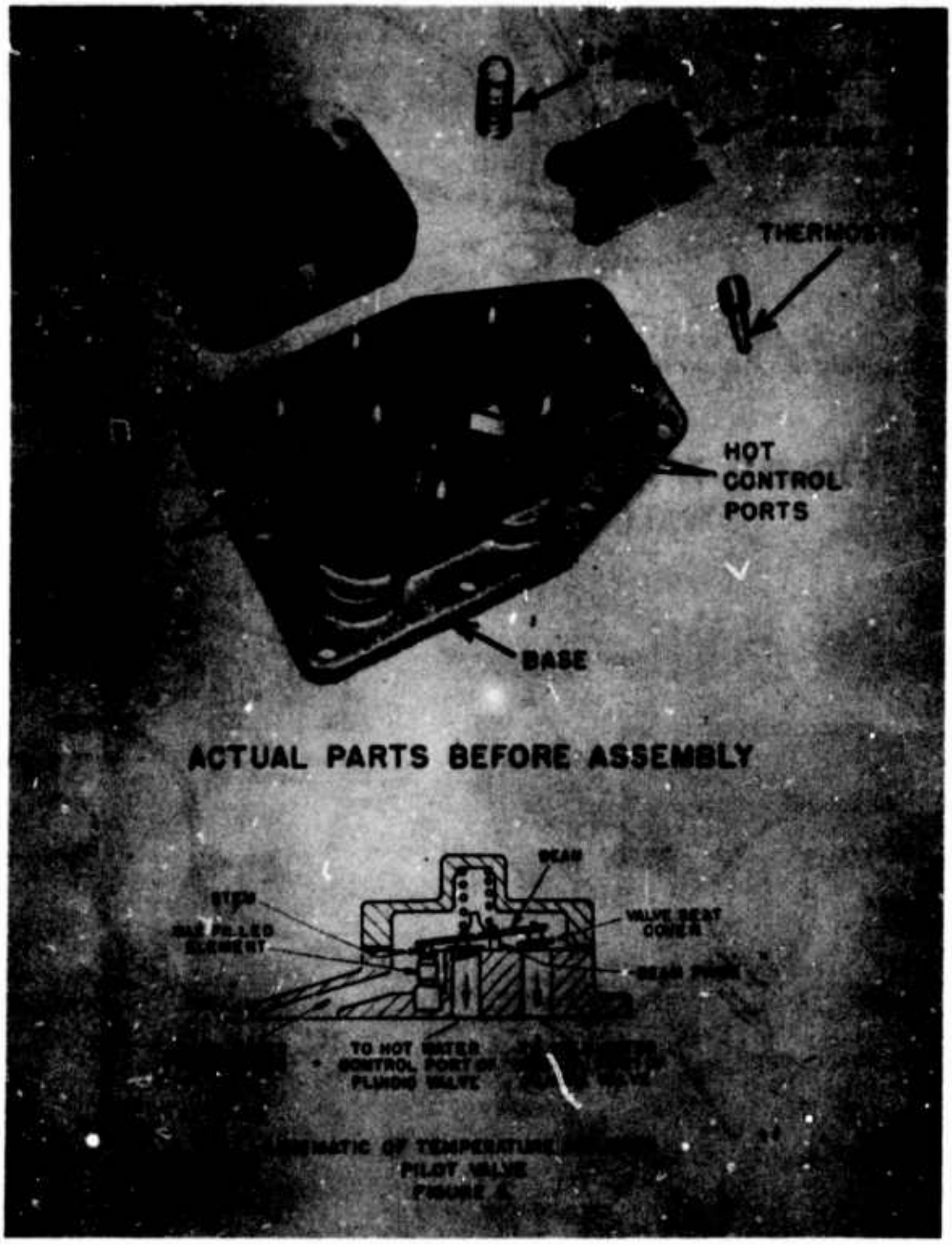


FIGURE 4. DESIRED RADIATOR FLOW VS TEMPERATURE



FLUIDIC CONTROL SYSTEM
SCHEMATIC FOR ONE RADIATOR BANK
FIGURE 5.


THERMOSTAT
HOT
CONTROL
PORTS
BASE
ACTUAL PARTS BEFORE ASSEMBLY
BEAM
VALVE SEAT
COVER
TO HOT WATER
CONTROL PORT OF
PILOT VALVE

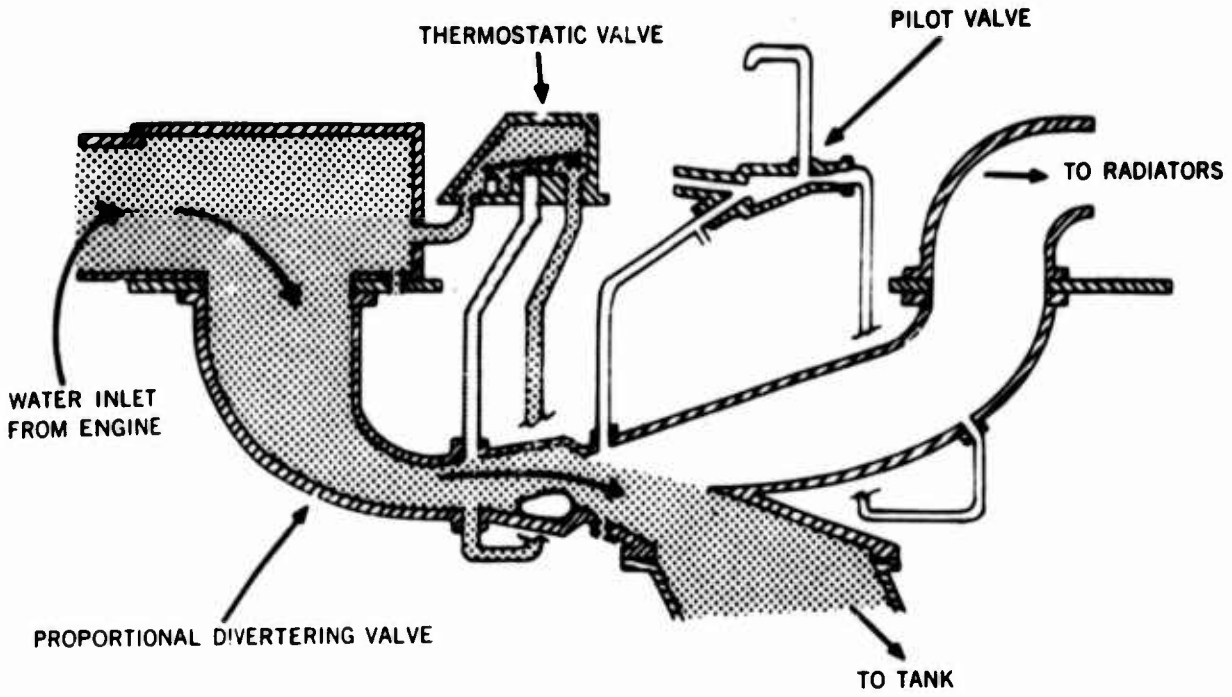


FIGURE 7. WATER FLOW, LOW COOLING WATER TEMPERATURE

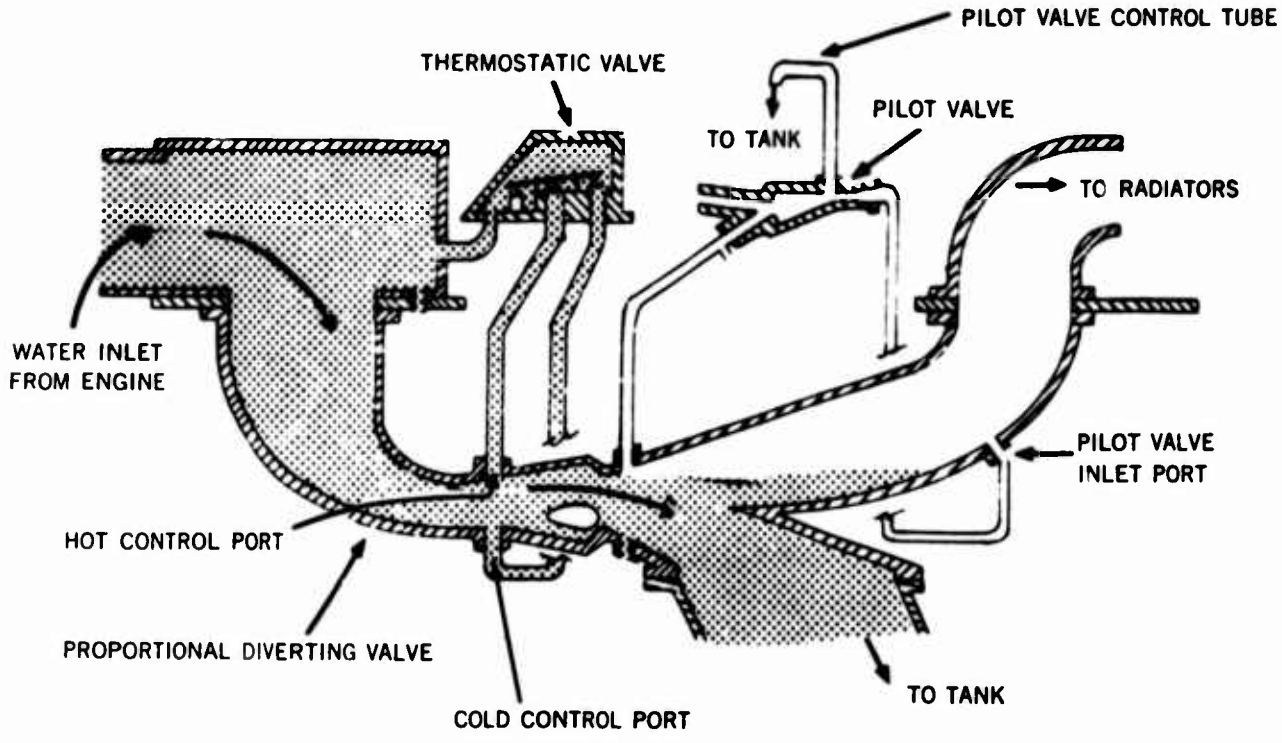


FIGURE 8. WATER FLOW, COOLING WATER TEMPERATURE RISING

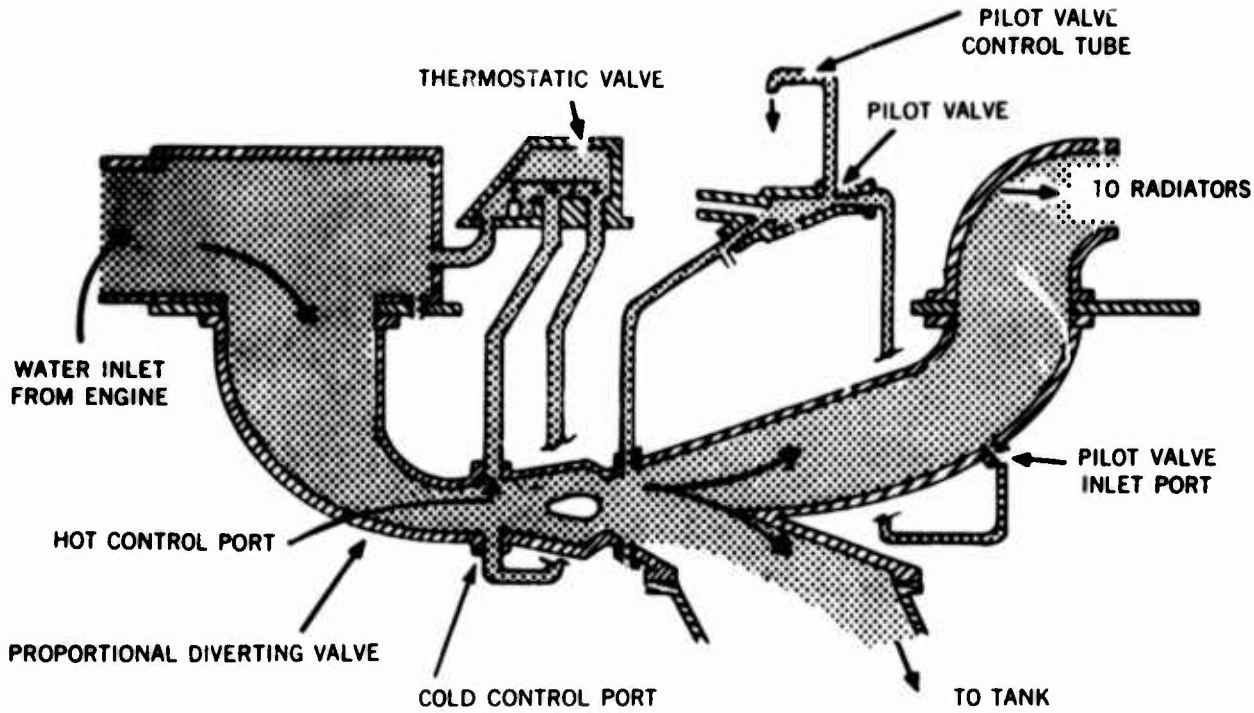


FIGURE 9. WATER FLOW, COOLING WATER AT "SWITCH-UP" TEMPERATURE

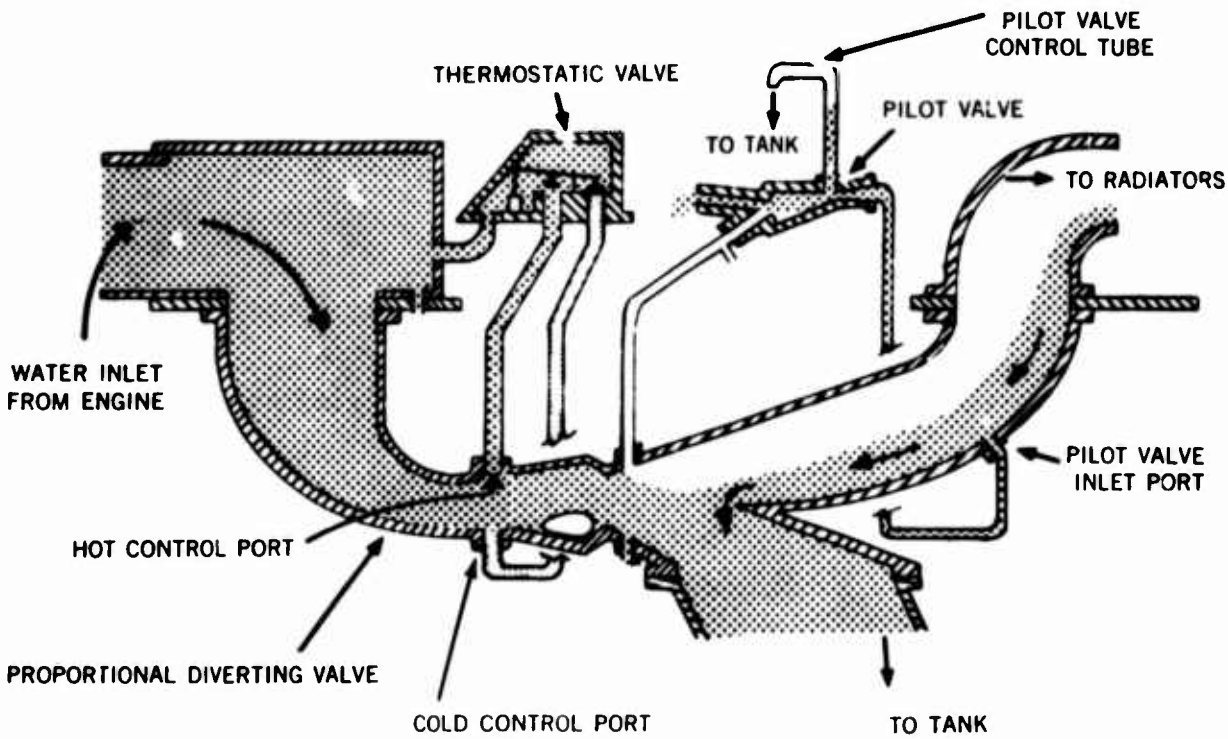


FIGURE 10. WATER FLOW, COOLING WATER AT "SWITCH-DOWN TEMPERATURE

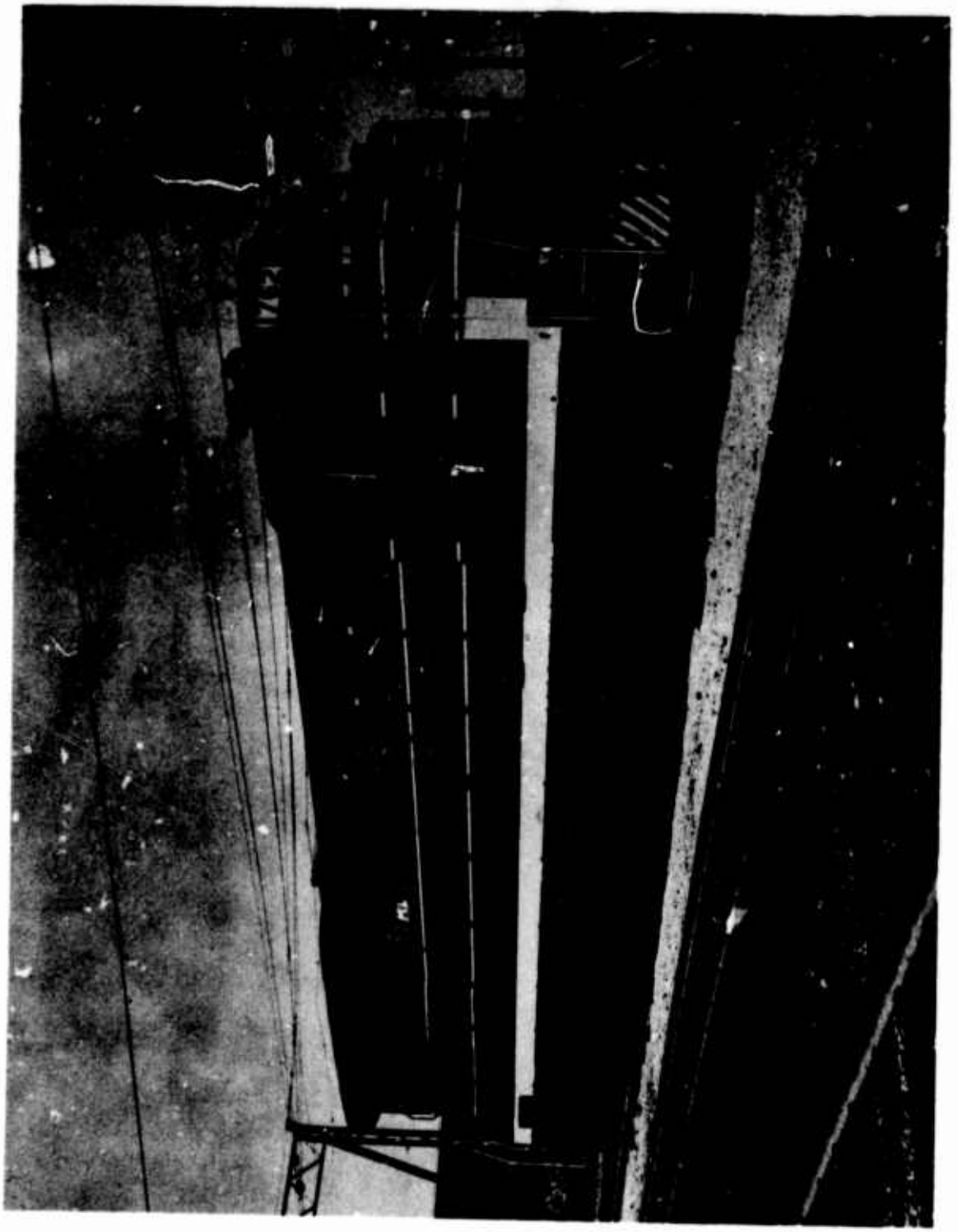


FIG.11 GENERAL ELECTRIC U36B LOCOMOTIVE

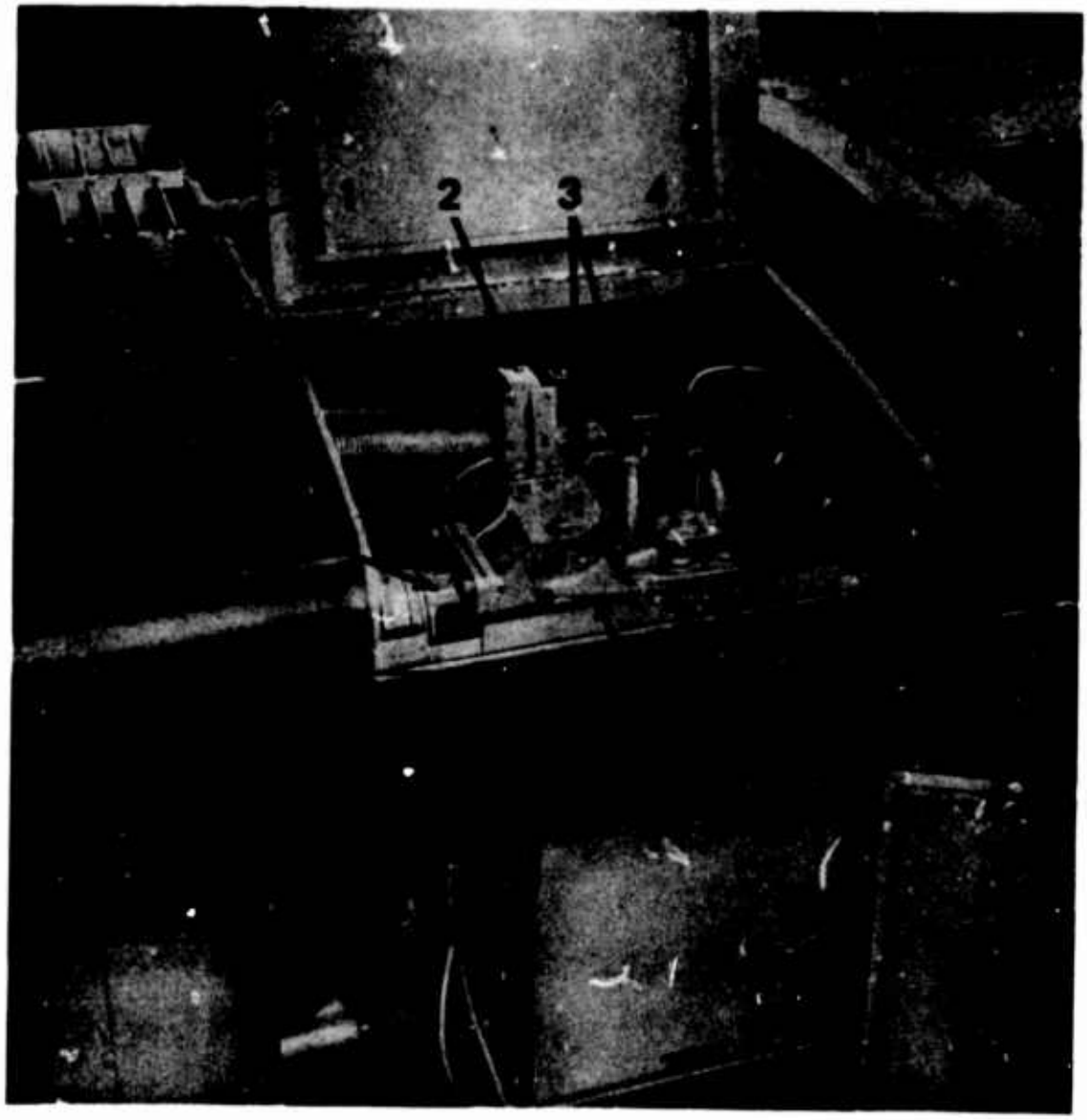


FIG.12 COOLING SYSTEM COMPONENT INSTALLATION

APPLICATION OF FLUIDIC CONCEPTS TO HYDRAULIC CONTROL SYSTEMS

By

R. H. Fashbaugh and E. R. Durlak
Research Mechanical Engineer and Mechanical Engineer
Civil Engineering Laboratory
Naval Construction Battalion Center
Port Hueneme, California 93043

ABSTRACT

This is the first of a two part test program to determine the feasibility of using fluidic concepts to develop a fluidic control unit that will detect and correct angular variations in position such as those experienced by a bulldozer blade during operation. The hydraulic proximity sensor is a key component in the control unit.

Experimental test results are presented showing the evaluation of a fluidic proximity sensor using hydraulic oil as the working fluid. The sensor was designed by scaling a pneumatic proximity sensor using a constant value of Reynolds number as the scaling parameter. Test results show that the hydraulic proximity sensor will detect the distance of an object from the sensor by relating that distance to a pressure signal. The performance characteristics of the hydraulic sensor correlated well with those of the pneumatic sensor. The sensor jet force variation with distance was also determined.

Preceding page blank

INTRODUCTION

The purpose of this work unit was to develop a hydraulic control system using fluidic components as the control elements. The use of fluidic concepts in place of electro-hydraulic or electro-pneumatic systems offers advantages of fewer moving parts, improved reliability, and the capability to withstand severe vibration. Fluidic controls are not affected by electromagnetic fields, electrical discharges, and most corrosive environments typically encountered. Although control systems perform many functions on Navy construction equipment, there is a need for a control system that would automatically detect and control angular motions, such as those experienced by a bulldozer blade. During operation the bulldozer blade is subjected to the variations in terrain that cause lifting or rotating of the blade. For finish grading operations it takes a skilled operator to maintain the bulldozer blade in the proper position to make a smooth horizontal cut. An automated system incorporated on the vehicle to perform this task would reduce the operator skill required and would provide a more consistent and accurate grading operation.

An automatic control system would require a means to detect deviations of the blade from a horizontal position and a device to translate this information to pressure pulses that would use conventional hydraulic actuators to correct the deviation.

The means to detect blade motion is provided by a specially designed, highly damped inverted or unstable pendulum unit that has been designed and constructed (Figure 1a). This unit works on the pendulum principle in that a weight or a rotating rod displaces with changes in the gravity vector and senses changes in rotation from the vertical. An experimental unit will be ready for testing after some minor modifications have been performed. The operation of the pendulum unit (see Figure 1a) will be reported in detail at a later date subsequent to the completion of its test program.

The sensor that translates the position of the pendulum to a pressure signal in the unit described above is a hydraulic fluidic sensor designed similarly to an existing pneumatic fluidic proximity sensor. This sensor has been designed, built, and tested, the results of which are presented in this report. The test results show that the sensor is capable of detecting the position of a solid object and translating this data to a change in pressure that can be converted to motion through hydraulic actuators. Two of these sensors are required in the pendulum control unit to detect the position of the pendulum control rod. As the pendulum rod rotates, due to the rotating bulldozer blade for example, the sensors will provide a differential pressure signal output which is used in correcting the angular motion through use of hydraulic actuators.

Future plans are to test the hydraulic sensor and pendulum unit together to determine the dynamic response characteristics of the system.

DESIGN ANALYSIS OF HYDRAULIC PROXIMITY SENSOR

To design a proximity sensor that is compatible with existing construction equipment, it is necessary to select hydraulic oil, MIL-H-5606, as the design working fluid. Proximity sensors using pneumatics, typically air, are readily available as off-the-shelf items. Similar sensors using hydraulic fluid are not available.

The most feasible approach seemed to be to modify an existing pneumatic sensor so that it would operate with hydraulic oil as the working fluid. As explained in References 1 and 2, the most important parameter to consider is the Reynolds number based on the sensor outlet nozzle flow. To operate at an equivalent Reynolds number, a system with higher density fluid (hydraulic oil) must operate at higher supply pressures than a system with a lower density fluid (air). For example, a given nozzle size in a system using oil operating at 375 psig and 120°F will yield the same flow Reynolds number when air at 1 psig and 70°F is used as the fluid. A comparison of power consumption and gain characteristics of a fluidic proportional amplifier, from Reference 1, for oil and air for equivalent Reynolds numbers shows the feasibility of using the Reynolds number criterion for proximity sensor scaling.

To accomplish the modification of an existing pneumatic proximity sensor for oil operation it was necessary to first provide a mathematical model of the pneumatic sensor. Figure 1b shows a sketch of the sensor. The principle of operation explained in simple terms is that the closer the object is to the sensor, the more restricted the sensor flow becomes, which results in an increase in the output pressure. The sensing pressure, P_c, varies with S, the distance from the sensor to the object. The sensor operation was calculated using the simplified model shown in Figure 2.

Using the model and the relationships for isentropic compressible flow, a series of flow conditions were calculated. From the data supplied for the pneumatic sensor, it was possible to calculate an effective area for A_1. Then, typically, the sensing pressure, P_c, and the supply pressure, P_s, were chosen, and a corresponding sensor flow, Q_s, was calculated. Once the sensor flow was known, the effective exit area could be calculated. The gap, S, (Figure 1) was then related to the calculated exit area using a cylindrical area at the exit.

$$A_{calc} = A_2 = \pi d S$$

or

$$S = \frac{A_{calc}}{\pi d} \qquad (1)$$

where d = exit diameter

S = sensing gap

A_{calc} = calculated exit area

Figure 3a, taken from the data procedures of Reference 3, shows the relationship of the sensing gap, S, to the ratio P_c/P_s for the pneumatic proximity sensor. The performance originally predicted by the mathematical model did not correlate well with this data. It was decided that the flow characteristics at the exit area were not known in sufficient detail to assume a simplified cylindrical exit area as πdS. Therefore, a factor k was introduced into Equation 1 to account approximately for two-dimensional flow effects that cannot be determined; the value of this factor was determined from experimental data. Equation 1 then becomes,

$$S = \frac{A_{calc}}{\pi d k} \qquad (2)$$

Using Equation 2 and known values of S, P_c, P_s from Figure 3a and the calculated area, A_{calc}, a value of k equal to 0.122 was determined. Using this value of k and the calculated exit areas, the sensing gaps, S, were computed using the mathematical model. The results are shown in Figure 3b. The mathematical model predictions correlate well with the actual performance. A further refinement of the model allows the use of a variable k as a function of the Reynolds number of the flow (Figure 3c). This gives a little better agreement at the higher sensing gaps, although this is of minimal importance since operation at the higher gaps is not anticipated. The dependence of k on Reynolds number also indicated that operation below a Reynolds number of about 800 was not advisable due to the undetermined behavior of the value of k below this value. Once a working mathematical model for the pneumatic sensor was developed, the next step was to convert the equations to hydraulic oil as the working fluid, keeping the Reynolds number the same for each flow medium.

A series of different flow conditions were computed for the hydraulic oil case allowing the Reynolds number, sensor exit diameter, sensing gap, and operating pressures to vary. Then, a set of operating pressures was selected with the value of k specified to be 0.122, and the minimum value of Reynolds number to be equal to 850. From this, the sensor exit diameter and the sensor flow were computed. The calculated physical size of the sensor with hydraulic oil as the working fluid was found to be very close to the actual size of the pneumatic sensor. Therefore, other than increasing the body length to accommodate the bulky hydraulic fittings, a new sensor was fabricated with the same dimensions and tolerances as the pneumatic sensor. This was a reasonable choice, considering all factors, based on the model predictions and the operating limits that much of the available test equipment imposed.

Two sensors were fabricated and prepared for test and evaluation. A photograph of the experimental sensor is shown in Figure 4.

TEST AND EVALUATION OF HYDRAULIC PROXIMITY SENSOR

The testing consisted of an evaluation of the hydraulic proximity sensor unit shown in Figure 4.

Test Set-Up

The hydraulic proximity sensor was installed in a specially designed test fixture, Figure 5. As shown, the sensor was installed in one arm of the fixture, and the other arm was hinged so that it could be moved to vary the distance between the sensor and the fixed arm. This simulated an impingement of the fluid from the sensor against a flat plate. A calibration plate was attached to the fixed arm so that the distance between the sensor and the fixed arm could be measured. Hydraulic oil at high pressure was ducted to the sensor through the flexible tubing. The entire fixture was submerged in a tank, Figure 6, to capture the return hydraulic oil from the sensor. A small pump was used to return the hydraulic oil to the hydraulic pumping unit. A schematic of the test set-up of Figure 6 is shown in Figure 7.

Two sensors, designated sensor A and sensor B, were fabricated. These sensors are as identical as practical machining tolerances would allow. Each sensor was tested individually in the test fixture of Figure 5.

The test procedure was designed to test each sensor at supply pressures of 300, 500, 750, and 1000 psig. At each of these pressure settings, the sensor output pressure was measured at various gap settings between the sensor and the movable aluminum arm. This gap, called the sensing gap, was varied from about 0.015 inch to 0.115 inch.

Also, at selected supply pressures and gap settings, the sensor flow and impingement force were determined. Since the sensor impingement force was small, it was necessary to remount the sensor midway on the fixed arm to get accurate measurements. In effect, this reduced the lever arm distance between the sensor location and the measurement location, thus allowing a larger force to be measured at the end of the movable arm than if the sensor had been in its original position. The sensor impingement force was the only measurement that required relocation of the sensor.

Test Results

The tabulated results of the testing are presented in Tables 1 and 2 (see Figure 7 for measurement locations). It should be noted that because of the moment arm effects, the force measurements given in Table 2 are half the total force of the sensor jet. As a special

case, sensor B was tested with a 3/8-inch shoulder attached to the movable arm directly below the sensor unit. This simulates more closely the configuration of the presently designed pendulum control unit into which the sensor will be installed. This test was made to see what effect the shoulder would have on the sensor performance. The design could be modified to remove the shoulder, if necessary, but at least for the initial evaluation it will be present in the control unit. The results of this test are given in Table 3.

The primary function of the sensor is to develop a sensing pressure (P_c in Figures 2 and 7) that is a function of the sensing gap. When used in the control unit, the sensors will provide a differential pressure that will be used as inputs to the control systems of the construction equipment (i.e., bulldozer, grader, etc.). For purposes of evaluation it is convenient to compare the ratio of sensing pressure to supply pressure, P_c/P_s, to the sensing gap, S. Figure 8 shows a comparison of the characteristic curve for a pneumatic sensor and the data for the hydraulic sensor that was designed using a Reynolds number correlation and tested as described above. The results of the sensor testing are given in Figures 9a and 9b for sensor A and B, respectively. Only the operating pressures of 500 psig and 750 psig are presented. The other data points are tabulated in Tables 1 and 2. The original design calculations indicated an operating range in this region of supply pressure would be optimum. These data indicate a good correlation with the pneumatic data and show that the sensor is capable of good sensitivity (characterized by the slope of the curve) in sensing pressure, P_c, as a function of the sensing gap, S. Due to variations in machining tolerances, each sensor has its characteristic flow pattern, but the overall performance shown in Figures 9a and 9b is quite similar. One potential area of concern is the flow condition with the 3/8-inch shoulder attached (Figure 9b). The response is somewhat flattened and shifted. It may be necessary to modify the pendulum control unit to remove the shoulder if this should prove to be a problem.

The mathematical model indicates that the hydraulic sensor should be sized about the same as the pneumatic sensor. Figure 8 shows the performance of both sensors. The flow response of each sensor has about the same characteristic curve, but the hydraulic sensor is slightly more sensitive to sensing gap and its performance curve is shifted towards smaller sensing gaps. This is probably due to the value of k, the exit flow coefficient, that was selected. The value of k was determined by forcing the mathematical model to fit the pneumatic data. The extension of this value to the hydraulic oil regime is obviously subjected to some uncertainty. However, since k is used here as a design tool, it has served this function well as illustrated by Figure 8. Also it should be noted that although the P_c/P_s ratios are about the same, the sensor using hydraulic oil operates at pressures about 20 times that of the pneumatic sensor.

Figures 9a and 9b indicate that an approximate sensing gap of 0.055 inch to 0.075 inch yields about a 40 to 60 psig differential sensing pressure for a supply pressure in the 500 to 750 psig range.

This is an adequate pressure differential to control a servo unit that would in turn provide hydraulic pressure input to a control system of construction equipment.

In the control unit that the sensor will be installed, the pendulum system is used to provide gravity or angular motion detection and proper system damping characteristics. The proper functioning of this unit is dependent on each sensor developing a jet impingement force as it senses the gap between it and the ''object.'' In the test fixture of Figure 5 the ''object'' is the movable arm, but in the control unit design this is replaced with one of the movable parts of the pendulum. The force developed (see Table 2) on the movable arm (or pendulum) is shown in Figures 10a and 10b. Essentially this force is that of a jet force impingement on a flat plate. The nondimensional term, F/P_sA, is used in Figures 10a and 10b where (after the method in Reference 4) F equals force of impingement at sensor, P_s equals supply pressure, and A equals effective area of sensor exit. The area term, A, was calculated by assuming that $F/P_sA = 1$ at $S = 0$. That is, at zero sensing gap there is zero flow, and the force is pressure times area. Since both force and pressure are measured, the area can be calculated. Calculating the area in this manner was used in lieu of measuring the area since accurate measurements were not feasible. The effective exit area of sensor A and sensor B was calculated to be 0.0031 $in.^2$ and 0.0037 $in.^2$, respectively. These values will be useful in refining calculations of other operating characteristics of the system. As given in Table 2, each sensor is capable of producing about 0.4 to 3.0 pounds of force depending on the gap and pressure settings. A design value of about 1.0 pound was used in the control unit; therefore, the sensor designs tested adequately meet the desired requirements.

The flowrate of each sensor was measured at a gap setting of about 0.062 inch at each supply pressure. As shown in Table 1, the flow varied from 1.16 to 3.05 gpm.

CONCLUSIONS

The results of tests show that a proximity sensor using hydraulic oil as the working fluid can be adequately designed based on pneumatic sensor data. The performance characteristics of the hydraulic sensor tested were similar to those of a comparable pneumatic sensor. The flow characteristics and jet impingement force of the hydraulic sensor have been determined by test to be adequate for use in the control unit for which it was designed. The use of Reynolds number scaling, based on exit nozzle flow, has been shown to be adequate for the dynamic similitude parameter in the design of a hydraulic proximity sensor when utilizing pneumatic sensor data.

PLANS AND RECOMMENDATIONS

The proximity sensor that has been tested was designed as a component of a control unit for detecting angular movement with respect to the vertical. This control unit has been designed and fabricated. Further tests of the experimental control unit are planned to determine its performance characteristics. If the test results show the performance to be as predicted, it will be recommended that the program be continued and the unit installed and tested on a road grader control system.

REFERENCES

1. ''Hydraulic Fluidics,'' Kelley, L. R., and Boothe, W. A. ASME Paper 68-WAIFE-26, 1968.

2. NCEL, Technical Note N-1255: Application of Fluidic Concepts to Hydraulic Control Systems, by E. R. Durlak and R. H. Fashbaugh, Dec 1972.

3. ''Fluidic Components and Control Systems,'' Fluidonics, division of Imperial-Eastman Corp., catalog of product information.

4. ''Advances in Fluidics,'' Publication of ASME, New York, NY 10017, 1967, pp. 120-121.

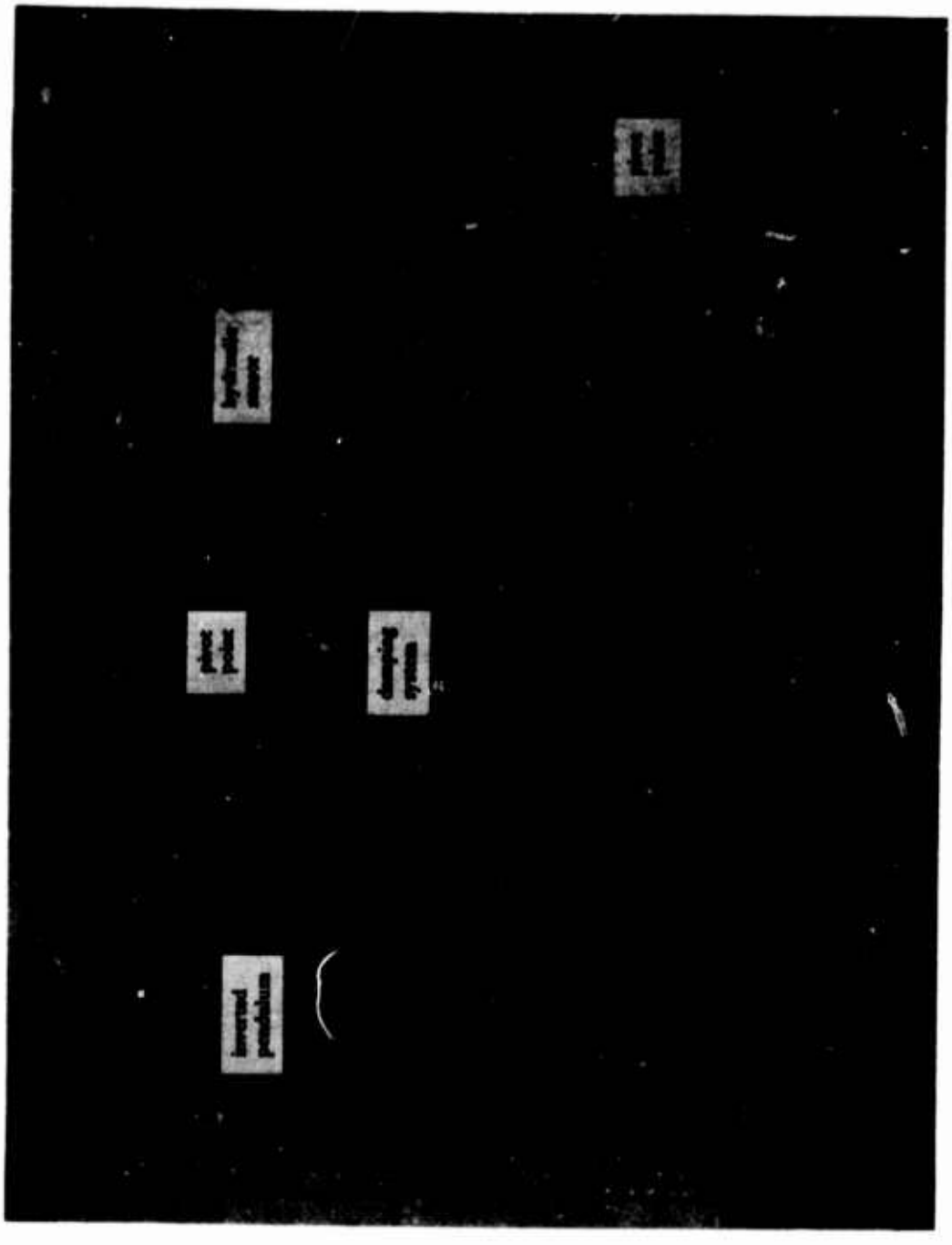


Figure 1a. Highly damped pendulum control unit.

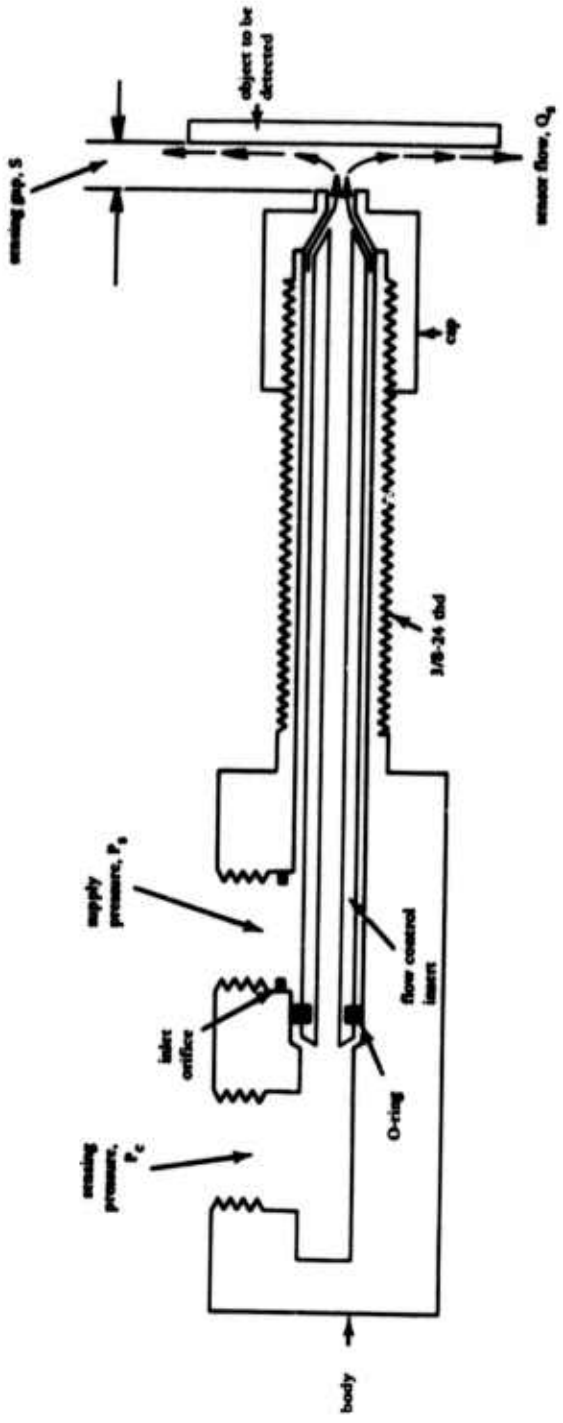
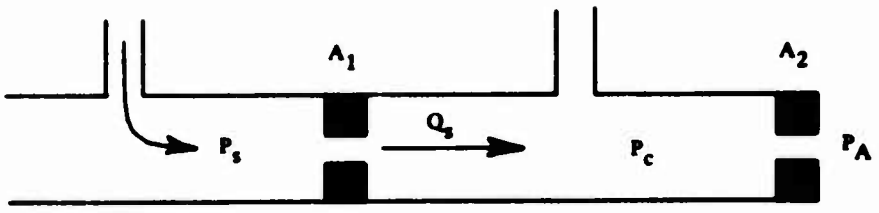


Figure 1b. Sketch of proximity sensor.



P_A = ambient pressure
Q_s = sensing flow
P_s = supply pressure
P_c = sensing or output pressure
A_1 = inlet orifice area
A_2 = exit orifice area

Figure 2. Mathematical model for pneumatic proximity sensor.

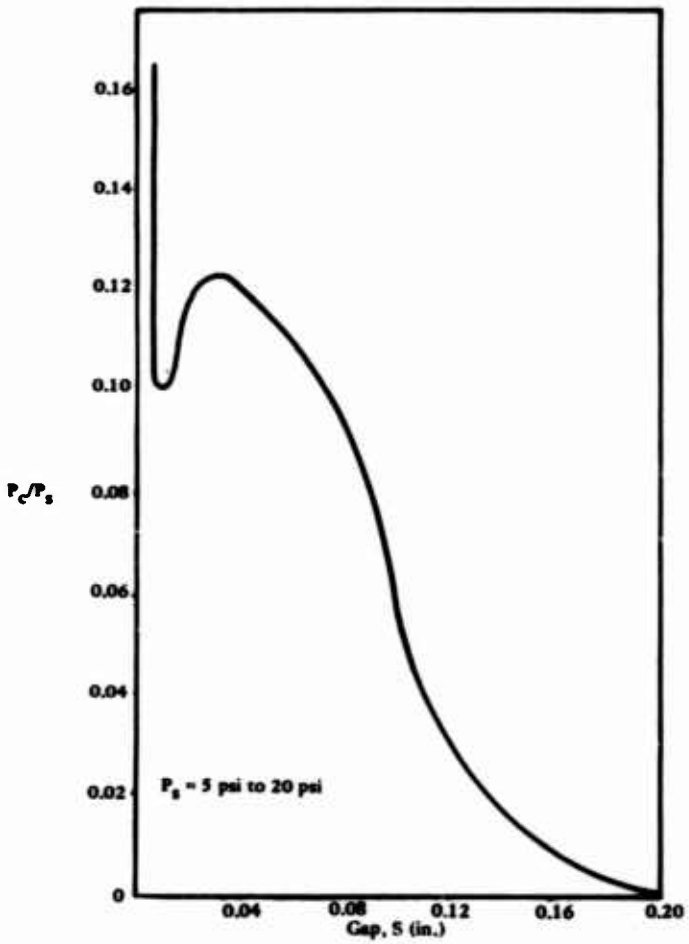


Figure 3a. Sensing gap versus P_c/P_s for pneumatic proximity sensor.

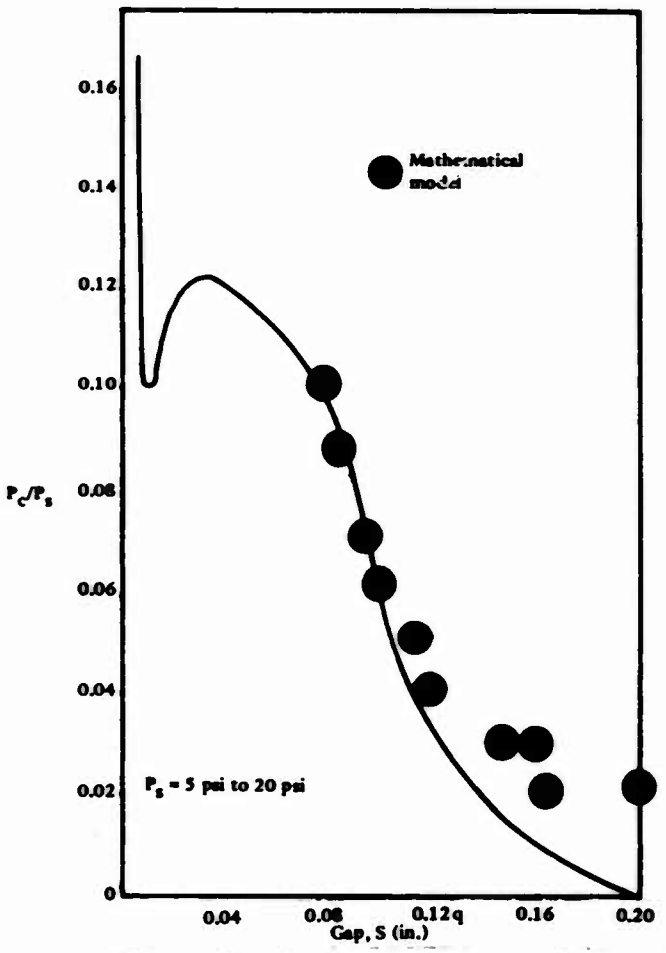


Figure 3b. Sensing gap versus P_c/P_s for pneumatic sensor and mathematical model results.

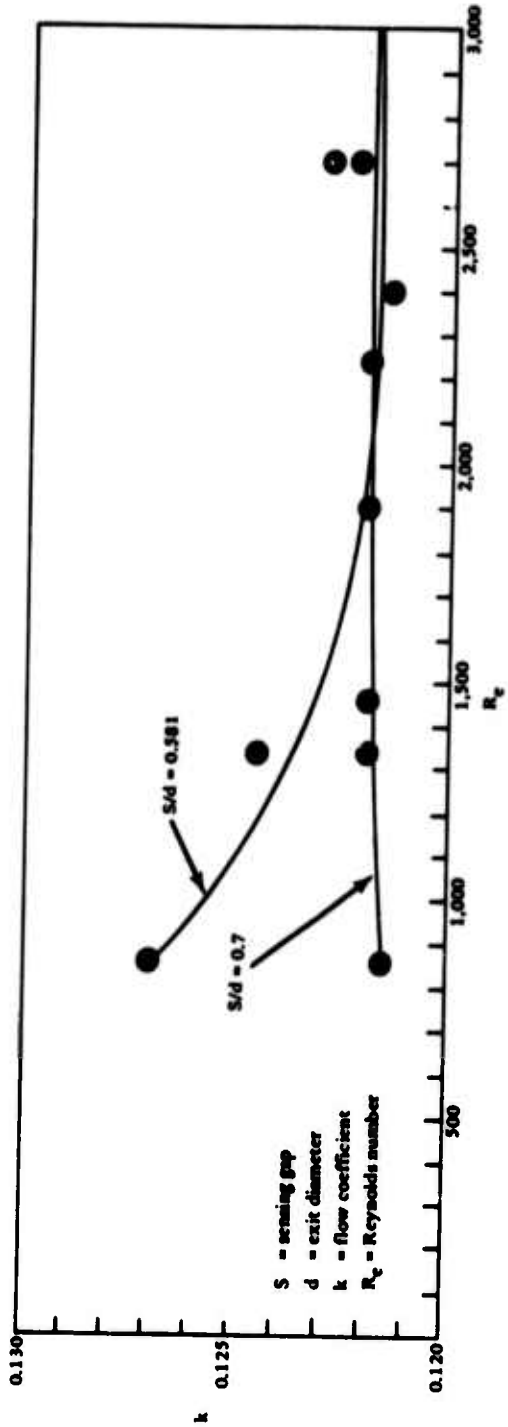


Figure 3c. Exit flow coefficient versus Reynolds number.



Figure 4. Experimental hydraulic proximity sensor.



Figure 5. Sensor test fixture.



Figure 6. Experimental test set-up.

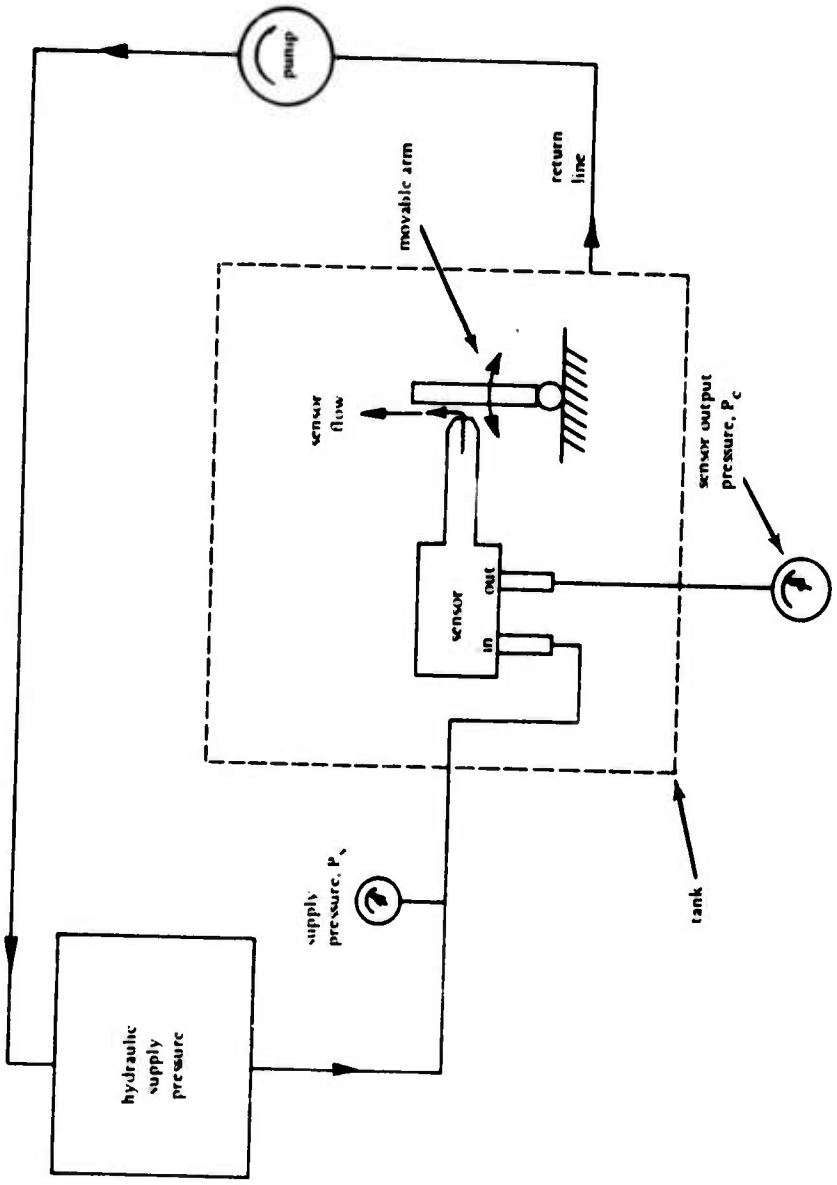


Figure 7. Schematic of test set-up.

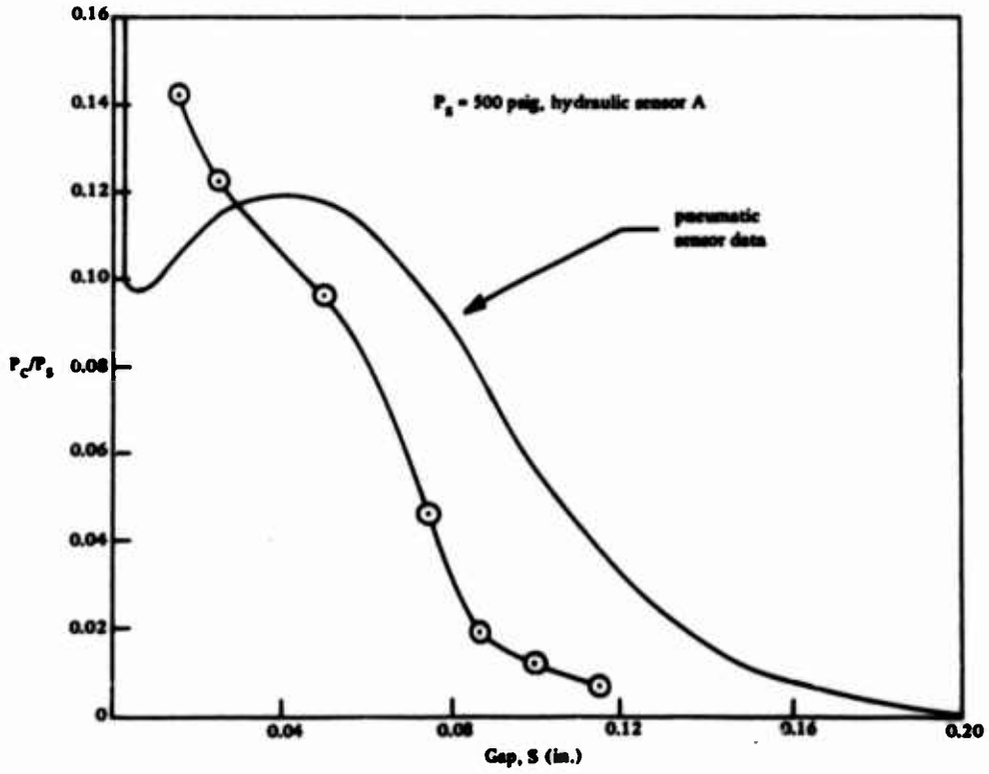


Figure 8. Comparison of pneumatic sensor and hydraulic sensor.

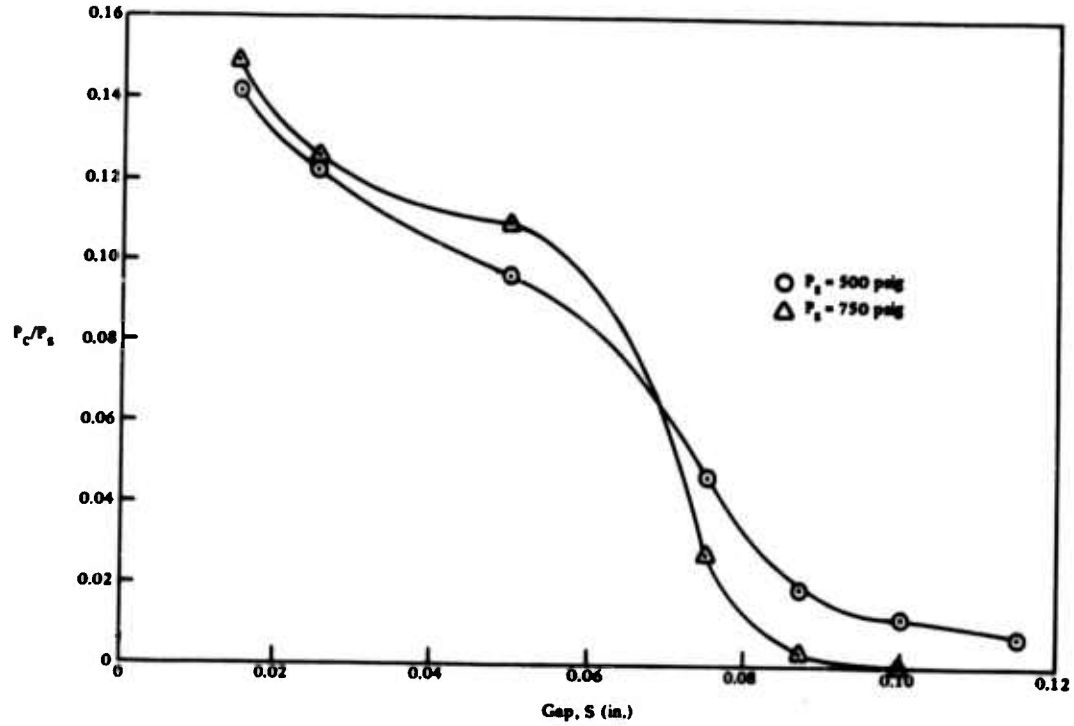


Figure 9a. Characteristics of sensor A.

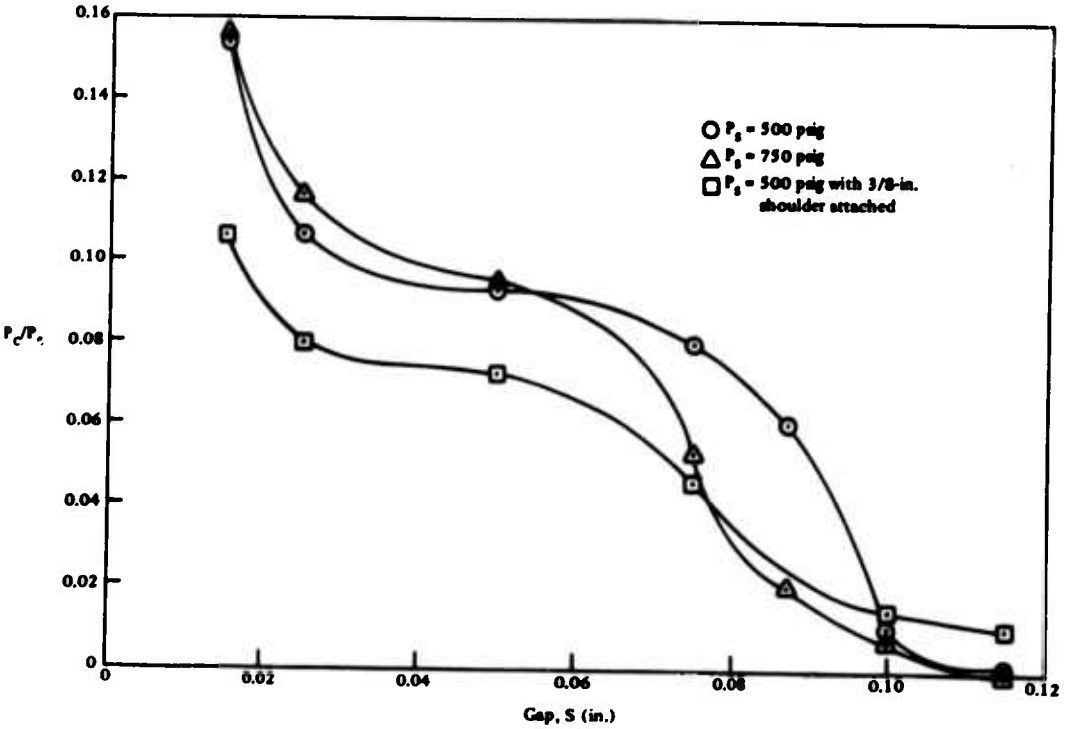


Figure 9b. Characteristics of sensor B.

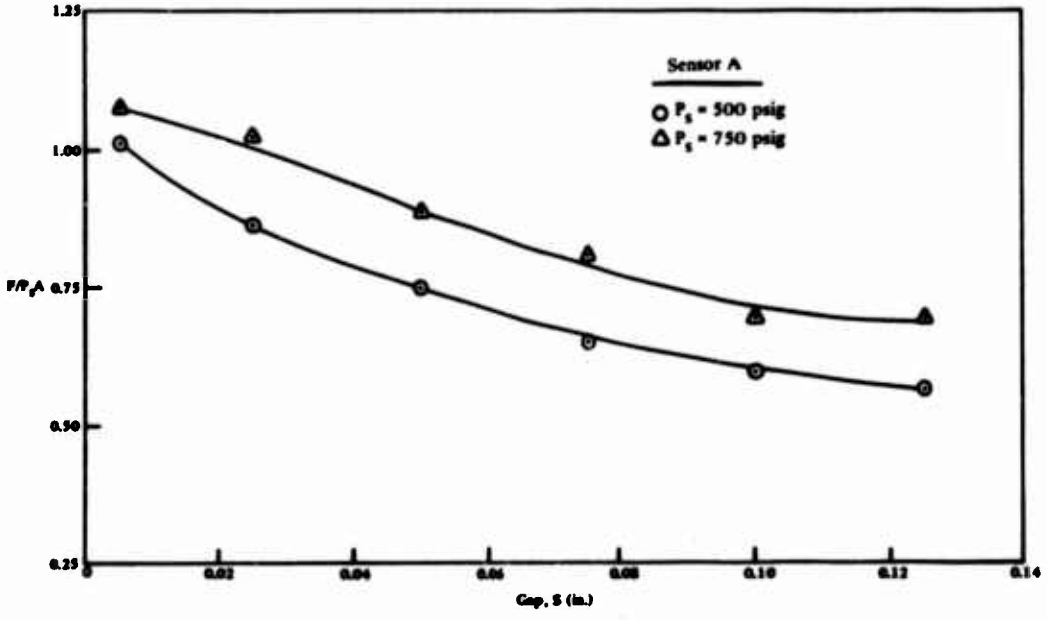


Figure 10a. Sensor gap versus normalized sensor force.

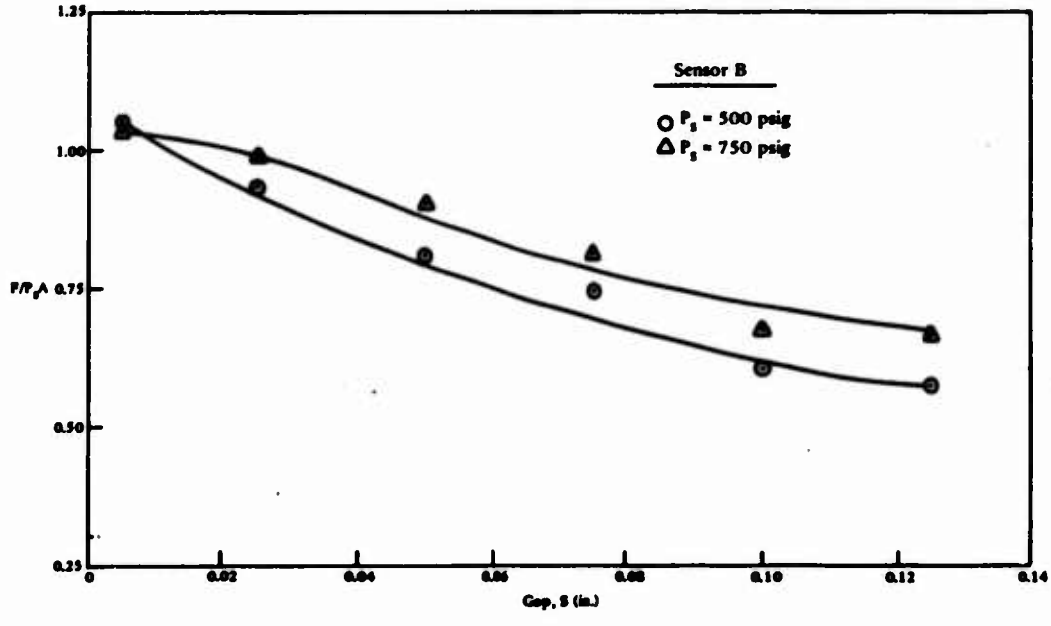


Figure 10b. Sensor gap versus normalized sensor force.

Table 1. Pressure and Flowrate Measurements

Sensing Gap, S (in.)	Supply Pressure, P_s (psig)	Sensing Pressure, P_c (psig)		P_c/P_s Ratio		Flowrate* (gpm)	
		Sensor A	Sensor B	Sensor A	Sensor B	Sensor A	Sensor B
0.015	300	34	37	.113	.123		
	500	71	77	.142	.154		
	750	112	117	.149	.156		
	1000	150	138	.150	.138		
0.025	300	32	30	.107	.100		
	500	61.5	53	.123	.106		
	750	94	87	.125	.116		
	1000	125	87	.125	.087		
0.050	300	34	30	.113	.100		
	500	48	46.5	.096	.093		
	750	82	71	.109	.095		
	1000	96	50	.096	.050		
0.062	300	**	**	**	**	1.17	1.17
	500	**	**	**	**	1.79	1.99
	750	**	**	**	**	2.46	2.17
	1000	80	**	.080	**	2.58	3.05
0.075	300	12	24	.040	.080		
	500	23	40	.046	.080		
	750	20	40	.027	.053		
	1000	56	28	.056	.028		
0.087	300	5	12	.017	.040		
	500	9.5	30	.019	.060		
	750	2	15	.003	.020		
	1000	22	5	.022	.005		
0.100	300	2	2	.007	.007		
	500	6	5	.012	.010		
	750	0	5	.000	.007		
	1000	10	4	.010	.004		

continued

Table 1. Continued

Sensing Gap, S (in.)	Supply Pressure, P_s (psig)	Sensing Pressure, P_c (psig)		P_c/P_s Ratio		Flowrate* (gpm)	
		Sensor A	Sensor B	Sensor A	Sensor B	Sensor A	Sensor B
0.115	300	0	0	.000	.000		
	500	3.5	0	.007	.000		
	750	0	0	.000	.000		
	1000	5	2	.005	.002		

* Flowrate measured at 0.062-in. gap only.
** Not measured.

Table 2. Force Measurements

Sensing Gap, S (in.)	Supply Pressure, P_s (psig)	Force* (lb)	
		Sensor A	Sensor B
0.005	300	0.38	0.44
	500	0.78	0.98
	750	1.25	1.50
0.025	300	0.31	0.37
	500	0.67	0.86
	750	1.19	1.37
0.050	300	0.25	0.34
	500	0.58	0.75
	750	1.06	1.25
0.075	300	0.22	0.31
	500	0.50	0.69
	750	0.94	1.13
0.100	300	0.22	0.25
	500	0.46	0.56
	750	0.81	0.94
0.125	300	0.19	0.23
	500	0.44	0.53
	750	0.81	0.91

* Force as measured at end of movable arm in Figure 5. Sensor jet force is double the measured values shown.

Table 3. Pressure and Flowrate Measurements With 3/8-In. Shoulder Attached

Sensing Gap (in.)	Sensing Pressure, P_c (psig)	P_c/P_s Ratio	Flowrate (gpm)
0.015	53	0.106	2.17
0.025	40	0.080	
0.050	36	0.072	
0.075	23	0.046	
0.100	7	0.014	
0.115	5	0.010	

FLUIDIC FUEL CONTROLS — A NARRATED BIBLIOGRAPHY

by

ROBERT L. WOODS*

ABSTRACT:

Fluidics offers a natural technology for sensing, computing, and controlling fuel and airflows to combustion engines. This paper lists and classifies a bibliography representative of the trends, progress, and state-of-the-art of fluidic engine controls for spark-ignition internal-combustion and gas-turbine engines. A new concept for digital fluidic fuel management is outlined.

Prepared for the
Harry Diamond Laboratories
Fluidic State-of-the-Art
Symposium
30 Sep - 4 Oct 74

*Fluidic Systems Research Branch
Harry Diamond Laboratories

Preceding page blank

1. INTRODUCTION

In most engines, the fuel flow and air flow must be coordinated and controlled. It is very logical to accomplish the sensing, computation, and control of fluid variables with fluid signals, and thereby avoid the interfaces with other technologies. Literature related to fluidic fuel controls for both piston and gas-turbine engines is reviewed.

This paper is divided into two major sections: fuel controls for spark-ignition internal-combustion piston engines (diesel engines presumably have not received much attention), and gas-turbine fuel controls including the required sensors. Also this paper describes a new concept for control of a constant mass air-fuel ratio for spark-ignition internal-combustion piston engines.

2. PISTON ENGINE FUEL CONTROLS

There have been many investigations of fluidic fuel control for automotive applications. Most of this work has not appeared in the open literature; however, by searching the patent literature and conversing with individuals from various industrial firms, one can form a picture as to the direction and progress of fluidic fuel control.

Fluidic fuel control ranges from what might be termed carburetor enhancement through complete pulse-width modulated all-flueric systems. These systems can generally be classified into the following four categories, according to fluidic complexity.

2.1 Carburetor Enhancement Devices

Fluid amplifiers may be used to improve the carburetor operation by linearizing or enhancing weak venturi signals [1-6]. The resulting devices still rely upon aspiration of fuel by the venturi vacuum; they cannot have an arbitrary point of fuel injection and, thus, cannot be classified as fuel-injection devices.

2.2 Continuous Fuel-Injection Systems

The systems described in references [7-18] fall into the category of fuel-injection systems since the location and number of injection points are not fixed as in carburetion systems. They are, however, quite similar to the carburetor, in that venturi vacuum (and manifold vacuum) determines the amount of fuel to be delivered in a continuous manner.

One of the first reported "fluidic carburetors" was that of Binder [8]. This concept utilizes a fuel-powered fluid amplifier deflected by the venturi-vacuum signal to modulate the amount of fuel delivered to the engine. Subsequently, fluidic fuel system designers considered such

things as power enrichment due to manifold vacuum [12, 13], acceleration enrichment [10,12,13], idle circuits [10,13], and other system requirements.

One problem common to these systems is the required venturi vacuum-to-gasoline signal interface. Reference [19] is one possible solution to this problem; in some systems, fuel is drawn from the amplifier control ports into the venturi as metered fuel [12].

The fuel-injection systems described above were operated with fuel-powered fluidics. The main problems experienced were: vaporization of fuel having high velocity in the power jets of amplifiers, noise, and inadequate scheduling accuracy. To obtain the desired air-fuel schedule, the fluid amplifier must have a square root single-sided transfer characteristic that results in a slight leaning of the fuel-air mixture (lower output) in the mid-range region. This function is difficult to obtain fluidically.

Several investigations have taken the pneumatically-controlled fuel valve approach [20-27] that allows the sensing and computation to be done by pneumatic fluidics with a mechanical interface to fuel control. Many of these systems include compensation for varying ambient conditions.

A few papers discuss feasibility and bench studies of other continuous fuel-injection systems [28-30].

In a different approach to fuel management, the density of the actual air-fuel mixture is measured fluidically, and the fuel flow is controlled in a closed loop to maintain the desired air-fuel ratio [31].

A new approach to fuel injection that utilizes an oscillating air flowmeter and constant pulse width fuel injection is outlined in section 2.5 of this paper. This system can easily be compensated to deliver a constant mass air-fuel ratio in an extremely simple control system.

2.3 Pulsed Fuel-Injection Systems

In continuous fuel-injection systems, the air consumption varies over a range of about 10 to 1; the air flow pressure signal (venturi vacuum) varies as the square of the air consumption and thus extends over a range of 100 to 1, which is pushing the dynamic range for fluidic amplifiers under turbulent flow conditions. Furthermore, since the fuel delivery signal must vary over a similarly large pressure range, the spray characteristics of the fuel nozzle cannot be maintained for optimum atomization.

A pulsed fuel-injection systems offers some relief from these problems. In a pulse-width modulation system, the pulse frequency is directly proportional to the engine speed and the pulse width (at constant pressure) is modulated to vary the fuel consumption. In this manner, the pulse width need only be controlled over a range of 3 to 1; however, an additional variable, speed, must be sensed. Since fuel can be injected at

high pressures for short durations, fine atomization can be maintained. On the other hand, the short-duration pulse widths (below 1 ms) push the response limits of most fluidic amplifiers. Pulse-height or combination width-height systems have not had as much attention as pulse-width modulation.

Some pulsed fuel-injection systems use pneumatic fluidic computation with mechanical fuel injectors [32-35], and others use flueric fuel injection with a no-moving part interface between the pneumatic and gasoline signals [36-41]. Other work is continuing on similar systems [42].

2.4 Air-Modulation Fuel-Injection Systems

The air-modulation fuel system differs from all other fuel management systems for spark-ignition engines [43-45]. In the air-modulation system, the driver controls the fuel consumption directly, and the control system adjusts the air consumption in a prescheduled closed-loop system. This system has several inherent features that make the system functional but simple. Also, the fluidic scheduling of air-fuel ratio is simple with the air-modulation approach, whereas it is generally very difficult with fuel-modulation.

2.5 DIGITAL FUEL INJECTION

In fuel management systems, it is often desirable to maintain a constant mass air-fuel ratio. This is difficult since the basic measurement of air flow generally is on a volumetric basis, which must then be compensated for air-density variations due to barometeric pressure and ambient temperature.

A recent development describes a flow sensor that can be inherently compensated to measure mass air flow [46]. This flowmeter is an adaptation of the well-known principle of the "von Karman vortex" oscillations due to flow past a bluff body. The frequency of oscillation, f, is usually directly proportional to volume flow rate, Q, but, by varying the bluff body dimension, d, in inverse proportion to the gas density, ρ, the flowmeter can be made to measure mass air flow, A, directly.

$$f = \frac{Q}{d} \quad \rho Q = A$$

Since the flowmeter produces a frequency proportional to mass airflow, it is desirable to deliver a constant mass, C, of fuel for each cycle of the air flowmeter.

$$C = \frac{\text{mass of fuel}}{\text{cycle of oscillation}} .$$

Thus, for each pulse from the air flowmeter, a fixed mass of fuel is injected into the engine; furthermore, the fuel mass flow rate, F, is given by the product of the mass per cycle and the cycles per second.

$$F = Cf.$$

Since the flowmeter frequency, f, is directly proportional to air flow, the fuel injected is directly proportional to the airflow thereby maintaining a constant mass air-fuel ratio to the engine.

$$F \sim CA, \text{ or}$$

$$A/F = \text{constant}.$$

If it were desirable to schedule the air-fuel ratio as a function of engine loading, it would be a simple matter to vary the fuel injected per cycle (pulse width) to modify the air-fuel ratio.

This approach is a fuel-modulation of fuel-metering system and is applicable to either liquid fuels (such as gasoline) or to gaseous fuels (such as natural gas, butane or propane, or hydrogen). The advantage of such a system is positive fuel metering with utter simplicity and no moving parts.

The implementation of the fuel metering system can be explained by visualizing a positive displacement pistion pump that is driven by the amplified air-flowmeter oscillations, and delivers a constant volume of fuel per cycle of oscillation (the density of liquid fuel is relative independent of temperature so that mass compensation would not be required of a constant volume injection). The piston could have adjustable or variable limits of travel to adjust the air-fuel ratio. If a gaseous fuel were used, these limits, or the volume per cycle, could be varied in accordance with the gas density.

The moving piston pump could be objectionable for reliability reasons and could be replaced by a monostable fluid amplifier operating on pressurized fuel. The monostable amplifier produces a pulse of constant duration and height when pulsed by the amplified signal from the air flowmeter, as shown by figure 1. The pulse width is determined by a delay in the feedback circuit of the monostable amplifier, and the pulse height (fuel flow) is determined by the supply pressure to the amplifier. Together, the pulse width and height determine the fuel injected per cycle of oscillation from the flowmeter.

It is possible to utilize pressurized fuel to power the entire fluidic circuit. This system could be extremely simple, offering a new approach to fluidic fuel controls. The main application for this system is envisioned to be for piston engines; however, the system could be used in the control of any combustion process in which air and fuel flows must be coordinated.

2.6 Miscellaneous Applications

There has been other work related to overall fuel management utilizing fluidics. Such applications include flow control of the intake air in response to air temperature [47], "float bowl" replacement [48], and aspirators to relieve any vent back pressure in fuel fluidic circuitry [49,50].

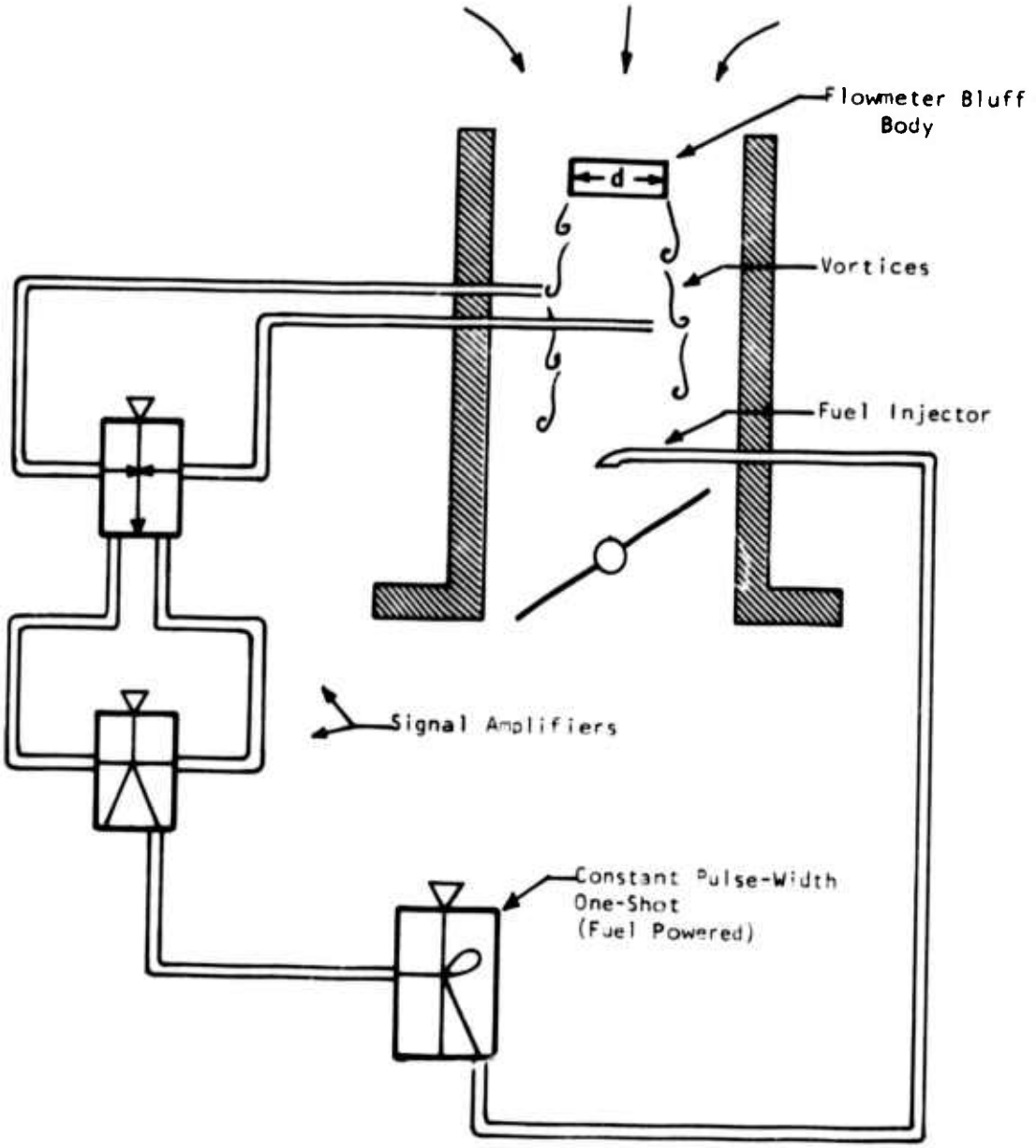


Figure 1. Digital Fluidic Fuel-Injection System

2.7 Summary on Piston Engine Control

There was an initial "boom" on fluidic carburetors in 1965 since they appeared promising with respect to cost and reliability; however, before a model could be put into production, the emissions concern developed. Fluidics did not show as much promise for the precise fuel controls required to meet the emissions standards and has consequently suffered. Today the emphasis is shifting back to fuel economy with low emissions; and, with the improved state-of-the-art in fluidic control technology, a fluidic fuel control system appears to have a future in the automobile.

3. GAS TURBINE FUEL CONTROLS

Turbine fuel controls offer another natural application for fluidics, with the hope of low cost and high reliability. Almost every major turbine control industry has investigated the feasibility of fluidics.

3.1 Fuel-Control Systems

Several companies have built complete control systems requiring temperature, speed, pressure ratio, or surge sensing with fluidic computation and control actuation [51-58]. These systems have dramatically demonstrated the feasibility of fluidic controls.

3.2 Temperature Sensors

One of the first fluidic sensors proposed for turbine-engine controls was the fluidic oscillator temperature sensor which has received much attention [59-69]. The resistive bridge temperature sensor also shows promise [62, 66, 70, 71]. Fluidic devices were proposed because although turbine inlet temperature is probably the most critical parameter in a turbine engine, conventional sensors have difficulty in measuring the extreme temperatures with high response and reliability.

There are two basic types of fluidic oscillator temperature sensors: through flow and heat transfer. The through-flow oscillator has various configurations but is powered with fluid of the temperature to be measured (such as turbine inlet). These oscillators have good time response but are exposed to the contamination present in the gas. This contamination can change the properties of the gas as well as cause reliability problems. Heat-transfer oscillators are powered by pressure from the filtered compressor discharge; thus, they are not as exposed to contamination, but they do not have fast time response necessary for preventing surge and flame out. These devices are better suited to exhaust gas temperature measurements.

3.3 Speed Sensors

Turbine shaft speed sensing [72-74] has also received attention by several researchers in addition to those concerned with complete engine controls. Engine speed is probably the second most critical parameter in turbine control. Turbine overspeed must be carefully avoided, thereby requiring an accurate, high-response speed measurement. A common approach is the chopper-wheel frequency-to-analog conversion.

3.4 Pressure Ratio Sensors

In some engines the pressure ratio is an important control parameter. There are several approaches to this measurement: straight computation by division [66], pressure ratio sensitive oscillator [66,75], specially designed nozzle-receiver arrangement [76], pulse-width modulation [77], and digital computation [66].

3.5 Miscellaneous Applications

Other literature references fluidic sensors or control devices for gas-turbine engines. Control systems feasibility [78] as well as complete systems requirements such as startup [79] have been considered. A device that measures Mach number has also been documented [80]. Inlet guide vane control using a pressure ratio measurement has been successfully tested [81]. Fabrication techniques have been developed and have proved to be applicable to fluidic circuits in the harsh turbine environment [82]. Consideration has been given to vortex fuel control devices in the burner [83]. The Mobility Equipment Research and Development Center (MERDC), Ft. Belovir, has investigated fluidic controls for Rankine cycle generator [84], and is presently developing fluidic fuel controls for a small gas-turbine engine under contract.

3.6 Summary on Gas-Turbine Control

The first investigations of fluidic turbine controls were applied to high-performance engines in competition with established control technologies and did not live up to expectations. A more logical approach is being followed which begins with the development of less critical controls for small engines such as APU and electric generator applications, then progresses to automotive sized engines, and finally to high-performance aircraft engines.

4. CONCLUSIONS

Fluidics has proved to be a feasible approach to fuel controls. It is felt that the state-of-the-art needs only a few more improvements before fluidic fuel controls for piston and gas-turbine engines will be a competing technology.

5. REFERENCES

CARBURETOR ENHANCEMENT DEVICES

1. York, J. B., "Fluid Controlled Carburetor," US Patent 3,656,736, assigned to General Motors Corp., 18 Apr 72.

2. York, J. B., "Fuel System," US Patent 3,386,710, assigned to General Motors Corp., 04 Jun 68.

3. Wyczalek, F. A. "Fuel System," US Patent 3,388,898, assigned to General Motors Corp., 18 Jun 68.

4. Marks, C., "Fluid Amplifier Arrangement and Fuel System Incorporating Same," US Patent 3,406,951, assigned to General Motors Corp., 22 Oct 68.

5. Drayer, W. L., "Metering Means," US Patent 3,477,699, assigned to General Motors Corp., 11 Nov 69.

6. Drayer, W. L., "Fuel System and Method of Operation," US Patent 3,386,709, assigned to General Motors Corp., 04 Jun 68.

CONTINUOUS FUEL-INJECTION SYSTEMS

7. Weissler, P., "Amazing New Miniature Carburetor," Mechanics Illustrated, pp. 62, Jan 68.

8. Binder, A. M., "Throttle in Only Moving Part in a Low-Cost Fluidic Carburetor," SAE Journal, Vol. 75, No. 8, pp. 36, (Aug 68).

9. Binder, A. M., "Fuel Induction Device," US Patent 3,389,894, 25 Jun 68.

10. Nardi, G., "Experimental Research on a Carburetor with a Fluidic Injection Device," (In Italian), Associazione Technica dell'Automobile, Vol. 21, No. 5, pp. 265 (May 1968).

11. Nardi. G., "Carburetor System Having a Fluidic Proportional Amplifier," US Patent 3,679,185, assigned to Compagnia Italiana Westinghouse Freni E Segnali., 15 Jul 72.

12. L. Taplin, Bendix Corp., personal communication, Sep 71.

13. T. Moran, Ford Motor Company, personal communication, Oct 72.

14. Sulich, J. S., "Fuel System," US Patent 3,574,346, assigned to the Bendix Corp., 13 Apr 71.

15. Arikawa, T., "Carburetor with Fluid Elements," US Patent 3,556,488, assigned to Aisan Kogyo Co., Japan, 19 Jan 71.

16. Arikawa, T., "Carburetor with Fluid Amplifying Elements," US Patent 3,570,823, assigned to Aisan Kogyo Co., Japan, 16 Mar 71.

17. Ishida, T., "Carburetor Utilizing Fluidics," US Patent 3,690,625, assigned to Mikuni Kogyo Company, 12 Sep 72.

18. Lazar, J. M., "Fluidic Carburetor," US Patent 3,655,170. assigned to ACF Industries, 11 Apr 72.

19. Woods, R. L., "A Flueric Gas-to-Liquid Interface Amplifier," Trans. of ASME, J. of Dynamic Systems, Measurement, and Control, Jun 73.

20. York, J. B., "Fuel System," US Patent 3,302,935, assigned to General Motors Corp., 07 Feb 67.

21. A. Otte, Honeywell Corp., personal communication, October 1972.

22. Casey, E. H. and Bickhaus, J. T., "Fluidic Controlled Carburetor," US Patent 3,652,065, assigned to ACF Industries, 28 Mar 72.

23. Lazar, J. M., "Control Apparatus," US Patent 3,577,964, assigned to Honeywell, 11 May 71.

24. Lazar, J. M., "Control Apparatus," US Patent 3,548,794, assigned to Honeywell, 22 Dec 70.

25. Lazar, J. M., "Fluidic Fuel Control System," US Patent 3,463,176, assigned to Honeywell Inc., 26 Aug 69.

26. Weissler, P., "Corning's Fluidic Carburetor," Science and Mechanics, pp 55, Feb 70.

27. Howland, G. R., "Fluidic Fuel Injection System for Combustion Engine," US Patent 3,548,795, assigned to the Bendix Corp., 22 Dec 70.

28. Orner, P. A. and Shimrony, Y. "Fluidic Fuel Injection Control System," Paper No. 69-548 presented at the ISA Annual Conference, Oct 69.

29. Erickson, H. I. and Wilson, J. N., "Feasibility Study of Fluidic Fuel-Injection System," Paper No. 69-WA/Flcs-11, presented at the ASME Winter Annual Meeting, Nov 69.

30. Gau, L. P., "Automobile Applications of Fluidics," Fluidics Quarterly, Vol. 3, No. 2, pp 9 (Apr 71).

31. H. Lake, General Electric Company, personal communication, Jan 72.

PULSED FUEL-INJECTION SYSTEMS

32. R. Husted, Automatic Switch Company, personal communication, Oct 72.

33. Sulich, J. S., "Fluidic Fuel-Injection with Bistable Valve," US Patent 3,587,543, assigned to the Bendix Corp., 28 Jun 71.

34. Lazar, J. M., "Fuel Injection Apparatus," US Patent 3,672,339, assigned to Honeywell Inc., 27 Jun 72.

35. Matsui, K. and Tusbouchi, H., "Fluidic Control System of Fuel Injection Device for Internal Combustion Engine," US Patent 3,690,306, assigned to Nippondenso Kabushiki Kaisha, 12 Sep 72.

36. Tuzson, J. L.., "Fuel System," US Patent 3,556,063, assigned to Borg-Warner Corp., 19 Jan 71.

37. Tuzson, J. L., "High-Gain Monostable Fluidic Switching Device," US Patent 3,586,024, assigned to Borg-Warner Corp., 22 Jun 71.

38. Tuzson, J. L., "Fuel System," US Patent 3,687,121, assigned to Borg-Warner Corp., 29 Aug 72.

39. Ishida, T., "Fluidic Fuel-Injection System," Paper 327 presented at 2nd International JSME Symposium on Fluid Machinery and Fluidics, Tokyo, Sep 72.

40. Yazawa, H., "FFIS..A Unique-System from Japan," Automotive Industries, 1972.

41. Matsui, K., "Gas Controlled Liquid Proportioning Fluidic Device," US Patent 3,718,151, assigned to Toyota, 27 Feb 73.

42. R. Bowles, Bowles Fluidics Corp., personal communication, Apr 73.

AIR-MODULATION FUEL-INJECTION SYSTEMS

43. Woods, Robert L., "A Study of Optimum Engine Scheduling and Its Application to Fluidic Fuel-Injection," HDL-TR-72-31, Dept of the Army, Harry Diamond Laboratories, Wash., DC 20438 (1972).

44. Woods, Robert L., "A Fluidic Fuel-Injection System Utilizing Air Modulation," Paper 73-WA/Flcs-3 presented at the 1973 ASME Winter Annual Meeting, Nov 73.

45. Woods, Robert L., "Fluidic Fuel Injection Device Having Air Modulation," US Patent 3,771,504, assigned to US Army, 13 Nov 73.

DIGITAL FLUIDIC FUEL INJECTION

46. Frederick, G. L., AiResearch Co., personal communication, Apr 74.

MISCELLANEOUS APPLICATIONS

47. Low, G. M. and Mangion, C., "System for Preconditioning a Combustible Vapor, " US Patent 3,640,256, 08 Feb 72.

48. Hanaoka, M., "Liquid Level Controlling Apparatus, US Patent 3,702,122, 07 Nov 72.

49. Sulich, J. S., "Fluidic Fuel Metering System," US Patent 3,698,413, 17 Oct 72.

50. Sulich, J. S., "Fluidic Fuel Metering System," US Patent 3,628,774, 21 Dec 71.

GAS TURBINE CONTROL SYSTEMS

51. Rose, R. K., and Phipps, W. L., "Fluidic Control of a J79 Turbojet Engine," ASME Paper No. 67-WA/FE-33, Nov 67.

52. Taplin, L. B. et al, "Pneumatic Engine Fuel Control System," US Patent 3,392,739, assigned to the Bendix Corp., 16 Jul 68.

53. Bentz, C. E., "Introduction to Turbine Engine Controls Session," Fluidics Quarterly, Vol. IV, No. 2, pp 47-48, Apr 72.

54. Kunkle, C. B. and Webb, W. L., "Fluidics--A Potential Technology for Aircraft Engine Control," Fluidics Quarterly, Vol. IV, No. 2, pp 49-58, Apr 72.

55. Small, L. L., "Turbine Engine Sensors for High Temperature Applications," Fluidics Quarterly, Vol. IV, No. 2, pp 59-68, Apr 72.

56. Wetzel, A. J., Arnett, S. E., and High, R., "A Fluidic Sensor for Closed Loop Engine Acceleration Control," Fluidics Quarterly, Vol. IV, No. 2, pp 68-79, Apr 72.

57. Schaffer, D. J. and Sutton, T. G., "Production Aerospace Fluidic Applications," Fluidics Quarterly, Vol. IV, No. 2, pp 80-89, Apr 72.

58. Sutton, T. G., and Frederick, G. L., "Application of Fluidics to Small Gas Turbine Engine Fuel Controls," Presented at the Fluid Power Controls and Systems Conference, May 1973.

TEMPERATURE SENSORS

59. Gottron, R. N. and Gaylord, W., "A Temperature Control System Using Flueric Components," 3rd HDL Fluid Amplification Symposium, Vol. III, pp 244-265, Oct 65.

60. Kelley, L. R., "A Fluidic Temperature Control Using Frequency Modulation and Phase Discrimination," Proc. of the JACC, pp 123-131, Aug 66.

61. Halbach, C. R., et al, "A Pressure Insensitive Fluidic Temperature Sensor," Advances in Fluidics, pp 289-312, ASME, May 1967.

62. Kirshner, J. M., "Fluid Thermometry," IEEE Transactions of Industrial Electronics & Control Instrumentation, Vol. IECI-16, No. 1, Jul 69.

63. Black, J. I., "Feasibility Study of Fluidic Turbine Temperature Sensors in Gas Turbine Engines," ASME Paper 69-GT-70, Mar 69.

64. Gottron, R. N. and Gaylord, W., "Pneumatic Thermometer," US Patent 3,706,227, 19 Dec 72.

65. Carter, Vondell, "Flueric Temperature Sensor," US Patent 3,667,297, 06 Jun 72.

66. Bland, M. P., "Fluidic Sensors for Measuring Engine Pressure Ratio and Turbine Inlet Temperature," Paper L4, Fourth Cranfield Fluidics Conference, Coventry, England, Mar 70.

67. McMillan, J. G. and Pamperin, R. H., "Application of Fluidic Sensors for Measurement of Turbine Inlet Temperature," SAE Paper No. 720158, Jan 72.

68. Anon., "Honeywell's New Fluidic Turbine Inlet Temperature Sensor," Honeywell Technical Brochure, Jan 72.

69. Anon., "Pneumatic Heat Sensors Beat the Hottest Heat," Product Engineering, pp 106, Oct 69.

70. Anon., "Temperature Sensor Goes Wireless," Control Engineering, Dec 69.

71. Frederick, G. L., "Temperature Compensating Circuit," US Patent 3,707,440, assigned to the Garrett Corp., 26 Dec 72.

SPEED SENSORS

72. Boothe, W. A., "Feasibility Study of a Fluid Amplifier Steam Turbine Speed Control," HDL Fluid Amplifier Symposium Vol. 2, 1964.

73. Kast, H. B. and Uheling, D. E., "Fluidic Overspeed Sensor for a Power Turbine," ASME Paper No. 69-GT-17, Mar 69.

74. Williams, J. E., "Power Control Apparatus for an Engine," US Patent 3,552,365, 05 Jan 71.

PRESSURE RATIO SENSORS

75. Johnson, J. L., "Absolute Pressure Ratio Sensed by Fluidics," Space and Aeronautics, pp. 120-126, Dec 66.

76. Rimmer, R., "A Fluidic Pressure Ratio Sensor for Gas Turbine Engine Control," IFAC Symposium on Fluidics, paper C3, 1968.

77. Davies, G. E. and Wilson, C. G. S., "Fluidic Apparatus, More Particularly for the determination of Pressure Ratios," US Patent 3,722,521, assigned to Plessey, 17 Mar 73.

MISCELLANEOUS APPLICATIONS

78. Gerg, D. F., et al, "Fluidics has a Future in Jet Engine Control," Control Engineering, Vol. 13, No. 7, Jul 66.

79. Morton, R. C., et al, "Engine Start-up Sequence Control Apparatus," US Patent 3,478,731, 18 Nov 69.

80. Anon., "Fluidic Sensors Read Mach Number Directly," Product Engineering, pp 89-90, 01 Dec 69.

81. Davies, G. E., "A Fluidic Method of Inlet Guide Vane Control for Jet Engines," Automatica, Vol. 6, pp 527-534, 1970.

82. Love, K. L. and Shinn, J. N., "Fabrication Techniques for Fluidic Propulsion-Engine Controls," ASME Paper No. 70-Flcs-7, Jun 70.

83. Wilcox, R. L. and Shodowen, J. H., "A Fluidic Fuel Control Valve for Turbine Engines," ASME Paper No. 71-GT-44, Mar 71.

84. Haefner, K. B. and Ringwall, C. G., "Investigation of Fluidic Controls for Closed Rankine Cycle Power Plants," AD 881-980, prepared for US Army MERDC, Ft. Belvoir, by General Electric Co., Schenectady, New York, Dec 70.

A FLUIDIC CONTROL SYSTEM FOR AN AIRCRAFT EJECTION SEAT

W. G. Beduhn

Systems and Research Center
Minneapolis, Minnesota

31 January 1974

A FLUIDIC CONTROL SYSTEM FOR AN AIRCRAFT EJECTION SEAT

W.G. Beduhn

Systems and Research Center
Minneapolis, Minnesota

ABSTRACT

Active stabilization of an aircraft ejection seat during the motor burn portion of the egress has been demonstrated using a fluidic control system. The output of the control system generated control moment by deflecting motor thrust vector with 33 gpm of Freon 113 at ± 800 psid being supplied to motor nozzle secondary injection ports. Including the secondary injection fluid amplifier, the system consisted of a vortex rate sensor, a five-stage amplifier cascade, and a 5000 psi blow down power supply. The control system limited the man/seat pitch rotation to less than 5 degrees on a flight demonstration.

A FLUIDIC CONTROL SYSTEM FOR AN AIRCRAFT EJECTION SEAT

W. G. Beduhn

Systems and Research Center
Minneapolis, Minnesota

INTRODUCTION AND SUMMARY

Man/seat pitch stability is a problem in all current operational escape systems since the ejection seat is basically aerodynamically unstable. This system instability may be magnified during the early phase of ejection by the moments produced by the rocket thrust line and the aerodynamic center of pressure misalignments with the man/seat system center of gravity.

This paper describes the design and flight evaluation of a fluidic ejection seat pitch stabilization system. The system was developed by Honeywell Inc. and flight tested at NATF, Lakehurst, New Jersey, under Naval Air Development Center contract number N00156-71-C-0226. On the zero altitude, zero airspeed flight test, the fluidic control system completely stabilized a 2-deg equivalent cg rocket motor thrust line pitch offset on a Navy Maximum Performance Ejection Seat (MPES).

PERFORMANCE REQUIREMENTS

The ejection seat stabilization system must be capable of producing pitch control moments that will maintain a preferred seat attitude. Moments that tend to alter attitude stem from two sources: 1) aerodynamic forces, and 2) misalignment of the sustainer motor thrust line with respect to the ejection seat/man center of gravity. Aerodynamic moments for a typical ejection seat geometry were calculated in References 1 and 2. As shown in Figure 1, the aerodynamic moment is predominantly negative (tends to pitch the seat forward) and may be as high as 2500 foot-pounds at an aircraft velocity of 600 knots. In addition to the aerodynamic moment, variations in the man/seat center of gravity on the order of ± 1 inch will result in moments of ± 400 foot-pounds with a main rocket thrust of 4800 pounds.

High-frequency response is a performance requirement of the control system. Response is important due to the large angular acceleration of the seat. For example, with a total moment on the seat of 1500 foot-pounds, a typical man-seat will accelerate at 4800 deg/sec^2. The response time of the system must be less than $8.0 \cdot 10^{-3}$ sec in order to limit pitch axis rotation to 10 degrees. System threshold should be less than 25 deg/sec equivalent. input rate.

SYSTEMS DESCRIPTION

The block diagram of the control system is shown in Figure 2. A schematic of the mechanized concept is shown in Figure 3. A fluidic vortex rate sensor senses the man/seat pitch rate and provides a pressure signal proportional to that rate to a fluidic amplifier cascade. This cascade amplifies the rate sensor signal -- both pressure and flow amplification. The final stage of the cascade supplies a high-energy liquid jet stream into secondary injection ports in the pitch plane side walls of the ejection seat rocket motor nozzle. This jet stream deflects the rocket motor thrust vector, thereby producing a control moment. This control technique is called liquid secondary injection thrust vector control (TVC-SI). The control system is supplied with 2000 psi liquid Freon 113 at 40 gpm for 0.4 sec from the designed self-contained power supply.

COMPONENT DESIGN

Design of the various components of the control system depends on the amount of flow required for delivery to secondary injection ports for the desired control moment. The design for the liquid IVC-SI, therefore, had to be completed prior to designing the fluidic hardware for the control system. After required injectant flow rates were determined, designs for the amplifier cascade, the vortex rate sensor and the power supply system could be finalized.

Secondary Injection System Design

For a given conical rocket motor nozzle, the amount of TVC angle - ϕ - is mainly a function of the magnitude of the secondary injectant flow rate; $\dot{m}_1$, for the optimum design case. Figure 4 shows the TVC angle expected for various secondary injection mass ratios, $\dot{m}_1 I_{sp}/T$

Where $\dot{m}_1$ = Secondary injection flow rate - lbs/sec

I_{sp} = Propellant specific impulse - sec

T = Axial thrust - lb

The overall program objective was to prove feasibility of the fluidic control system concept. Therefore, a simple brute force design technique was used to obtain control moments. The design ultimately selected resulted from a brief literature survey on liquid secondary injection (References 3, 4, 5, 6). Significant details of the selected design are as follows:

- Injection liquid, Freon 113 - This Freon was used as the working media for the fluidic circuitry.

- Injection pressure, ~ 800 psi - This pressure represents the recovery pressure from the secondary injection fluid amplifier supplied with 2000 psia.

- Injection location, 0.42 - This is defined as the ratio of the throat distance to injection location divided by the throat distance to the nozzle exit.

- Injection ports, multiple ports with parallel centerlines - Three ports (diameter 0.147 inches) were used.

- Injection flow ratio $\frac{\dot{m}_1 I_{sp}}{T}$, 0.5 - This is equal to 33 gpm flow rate delivered by the secondary injection fluid amplifier. A TVC angle of ±5.4 degrees is estimated using this flow ratio.

Figures 5 and 6 show details of the injection port design.

Amplifier Cascade Design

The basic requirement was to design a fluidic amplifier cascade driven by a vortex rate sensor and to supply liquid into the nozzle side walls of an ejection seat rocket motor. The bistable cascade output should produce about 33 gpm at the highest possible pressure for injection into the nozzle and should switch at an input pressure equivalent to 25 deg/sec rate. In addition, the total cascade flow rate should be kept to a minimum to minimize the size of required support equipment. Response of the cascade should be 0.005 sec.

A convex-walled bistable amplifier design similar to that found in the literature (Reference 7) was used as a basis for the ejection seat amplifier design. The closed interaction region design was selected for reasons of good pressure recovery and maximum delivery of liquid to the secondary injection ports. Sizing of the power port (with aspect ratio = 3) for the final amplifier was calculated using the following equation:

$$W = \left(\frac{1}{3} \frac{Q}{\sqrt{\frac{2p}{\rho}}} \right)^{1/2}$$

where

W = power nozzle width - in.

Q = power nozzle flow rate - in^3/sec

p = supply pressure - lb/in^2 -2000 psi, the rocket motor chamber pressure was selected as the supply pressure

ρ = Freon 113 density - $lb\ sec^2/in^4$

$\therefore$ W = 0.088 in.

Remaining amplifiers of the cascade were then designed based on the size and supply pressure of the final stage. A typical pressure gain for a bistable amplifier is 1/15 p supply (control Δp required to switch power flow), and a typical flow gain is 5.

Figure 7 shows the amplifier cascade circuit designed for the ejection seat control system. It uses one proportional amplifier for impedance matching the vortex rate sensor and four bistable amplifiers for main signal amplification.

The amplifiers are stepped up in size and pressure to a final amplifier power port size of 0.088 in. x 0.260 in. and a pressure of 2000 psi. Because the vortex rate sensor requires a back pressure of 100 psi (to minimize cavitation problems) which results in a sensor pickoff level of about 120 psi, the first three stages of amplification are required to be open-type to allow interaction impedance matching. These early-stage, open-type amplifiers cause only a small percentage increase in the overall system flow rate requirements which are estimated at 40 gpm.

Vortex Rate Sensor Design

Various designs for the vortex rate sensor were reviewed. For reasons of simplicity, size, weight, and required time response, a single-sink, high Reynolds number sensor was selected. This sensor has a sink diameter of 0.100 in., a coupling diameter of 1.500 in., a flow rate of 2.5 gpm, a response time of 0.005 sec and a sink Reynolds number of 238,000. Figure 8 shows the vortex rate sensor as installed in the final hardware. The pickoff for the vortex rate sensor uses a 0.008-in. thick stainless steel blade across the pickoff ports. This blade is used as a streamline element which detects any induced swirl in the exit flow. The amount of the induced swirl is proportional to the sensor turning rate about its axis.

This pickoff also incorporates an external null adjust capability. This null adjust device consists of a movable blade located in the vortex sensing

chamber near the coupling element rings. When the blade is externally rotated, it produces a swirl in the sensing chamber which nulls out any net unwanted signals as read by the pickoff ports.

The vortex rate sensor coupling elements consist of two 0.014-in.-thick stainless steel rings. Each of these rings has 90 small airfoil-shaped flow passages to rate couple the input flow. When the coupling element is assembled in the unit, the net flow spacing is about 0.015 in.

Deadended scale factor of the vortex rate sensor is calculated using

$$\left(\frac{\Delta P}{\omega}\right)_{D.E.} = \frac{4.5 \times 10^{-5}\, \eta \cdot C_{n\alpha} \cdot Q_T\, \rho}{4\pi R_i} \left(\frac{R_o}{R_i}\right)^2 \qquad \text{(Reference 8)}$$

$\eta \cdot C_{n\alpha} \cong 4.5$ for this application (an efficiency term)

$$\left(\frac{\Delta P}{\omega}\right)_{D.E.} = 0.12 \text{ psi/deg/sec}$$

ΔP = Rate sensor output differential pressure in psi

ω = Input rotational rate in deg/sec

D.E. = Dead ended - output blocked

Q_T = Total rate sensor flow in^3/sec

ρ = Liquid density in $\frac{lb\ sec^2}{in^4}$

R_o = Outer coupling radius in inches

R_i = Sink radius in inches

Power Supply System Design

A schematic of the power system designed to supply Freon 113 to the control system at a flow rate of 40 gpm is shown in Figure 9. A 160 in^3 4500 psi lanyard valve-activated air pressure vessel was used as the basic pressure source for the system. This pressure source drove Freon 113 out of a 60 in^3 piston accumulator through the 40 gpm flow control valve and into the control system. Equivalent fluidic resistance of the control system was designed such that the input 40 gpm flow rate resulted in a 2000 psi pressure drop. Total operating time was designed to be 0.4 sec. (This is adequate time in that a typical rocket motor burns 0.5 sec with the man/seat being on the aircraft rails for a duration of 0.150 sec, leaving about 0.350 sec of required control.)

BENCH EVALUATION

After the fluidic control system was developed and laboratory tested at Honeywell Inc., Minneapolis, it was installed on a dynamic bench test stand at the Naval Weapons Center, China Lake, California, for development tests with a rocket motor. Figure 10 shows a photograph of the complete

control system mounted on brackets to mate with the rocket motor test stand. Two successful thrust-vectored motor tests were conducted.

During laboratory development testing, it had become apparent that secondary injection amplifier performance was not optimum. The output flow split was five to one. Pre-rocket motor bench test checkouts revealed a further reduction in the injection amplifier performance - down to two and one half to one output flow split. This was due to a change in the injection port plumbing. Optimum components were not considered mandatory to prove concept feasibility.

The first dynamic bench test, with a secondary injection output ratio of 2.5 to 1, demonstrated an effective control system TVC angle of ±2.35 degrees. On the second dynamic bench test a mechanical plug was installed into one injection port to simulate an ideal secondary injection amplifier, i.e., infinite output flow ratio. This test was conducted to determine maximum TVC angle obtainable from the given geometry and design. The test resulted in a maximum TVC angle of ± 5.8 degrees for the given design. This TVC angle resulted to a control moment of ± 710 foot-pounds. It is felt that, with proper redesign, this magnitude of TVC angle is readily attainable in a system configuration.

FLIGHT EVALUATION

The control system was installed on a Navy MPES seat for the flight demonstration. The man/seat and the control system were completely instrumented. Electronic rate gyros and accelerometers were installed in the chest cavity of the dummy to record the motion of the man/seat. Trip wires on the seat guide rails were incorporated to record seat position versus time. The flight test was recorded by camera coverage - both real time and 400 frames per second. Rocket motor chamber pressure, fluidic supply pressure, secondary injection output amplifier pressure, and control system pitch rate were recorded.

Figure 11 is a photograph of the complete man/seat ready for flight demonstration. The feasibility control system was mounted around the sides of the seat. No attempt was made to minimize system size or weight.

Table I gives a numerical summary of the flight test conducted on 28 February 1973 at Lakehurst, New Jersey. Figure 12 is an oscillograph recording of pertinent instrumentation test results. Figure 13 is a photographic sequence of the man/seat during the motor burn portion of the test.

Flight Test Summary

- During active control, the pitch rate of the man/seat was continuously held near zero degrees per second. The control system completely corrected for the 2-degree pitch forward cg motor thrust line input misalignment.

- The 8.5-g seat acceleration did not affect performance of the control system.

- The control system changed direction of the rocket motor exhaust vector a total of 10 times during the 0.4-second control portion of the flight.

- After control burnout, the man/seat began rotating in pitch due to the 2-degree equivalent pitch forward input. (The rocket motor burned longer than expected, which resulted in the fluidic control system exhausting its secondary injectant prior to motor burnout.) It attained a pitch rate of about 5 deg/sec by motor burnout.

CONCLUSIONS

Feasibility of the concept of using fluidics to stabilize an ejection seat during the rocket motor burn portion of the ejection has been demonstrated. This concept shows promise of attaining the requirements of high reliability, minimum maintenance and long shelf life.

More development work is required to reduce the size and weight of the system and to increase its control moment capability. It is projected that this liquid secondary injection design concept can be reduced to less than 15 pounds total weight and provide up to plus or minus 6 degrees equivalent control. (Calculations show that this amount of control would stabilize an ejection seat through 450 KIAS with proper system biasing. For ejections above 450 KIAS, the system would provide its maximum control authority, resulting in some expected small man/seat rotational rate.)

REFERENCES

1. Bailey, R.G., and J.B. Starr, "Feasibility Study for the Propulsion Phase of a Fluidic Control System for an Aircraft Ejection Seat," Honeywell Inc., Final Report 12122-FR1 on Naval Weapons Center Contract No. N60530-68-C-1039, March 1969.

2. Rupert, J.G., "Feasibility Study for the Sensing and Amplification Phase of a Fluidic Control System for an Aircraft Ejection Seat," Honeywell Inc., Final Report 12178-FR1 on Naval Air Development Center Contract No. N00156-69-C-2023, December 1969.

3. Green, C.J., and F. McCullough, Jr., "Liquid Injection Thrust Vector Control," AIAA, pp. 573-578, 1963.

4. Kirkup, R.P., "Secondary Injection for Thrust Vector Control," Report No. M-1129-r AiResearch Manufacturing Division.

5. Kock, W.G., "Design Concepts for Liquid Injection Thrust Vector Control," Parts 1 and 2, Hydraulics and Pneumatics, September 1965.

6. Newton, J.F., Jr. and F.W. Spaid, "Interaction of Secondary Injectants and Rocket Exhaust for Thrust Vector Control," ARS Journal, August 1962.

7. Sarpkaya, T., "The Performance Characteristics of Geometrically Similar Bistable Amplifiers," Paper No. 68-WA/FE-18, ASME, December 1968.

8. "Vortex Rate Sensor Theory," Honeywell Internal Document, SRM-77, Honeywell Systems and Research Center, July, 1968.

REFERENCES

1. Bailey, R.G., and J.B. Starr, "Feasibility Study for the Propulsion Phase of a Fluidic Control System for an Aircraft Ejection Seat," Honeywell Inc., Final Report 12122-FR1 on Naval Weapons Center Contract No. N60530-68-C-1039, March 1969.

2. Rupert, J.G., "Feasibility Study for the Sensing and Amplification Phase of a Fluidic Control System for an Aircraft Ejection Seat," Honeywell Inc., Final Report 12178-FR1 on Naval Air Development Center Contract No. N00156-69-C-2023, December 1969.

3. Green, C.J., and F. McCullough, Jr., "Liquid Injection Thrust Vector Control," AIAA, pp. 573-578, 1963.

4. Kirkup, R.P., "Secondary Injection for Thrust Vector Control," Report No. M-1129-r AiResearch Manufacturing Division.

5. Kock, W.G., "Design Concepts for Liquid Injection Thrust Vector Control," Parts 1 and 2, Hydraulics and Pneumatics, September 1965.

6. Newton, J.F., Jr. and F.W. Spaid, "Interaction of Secondary Injectants and Rocket Exhaust for Thrust Vector Control," ARS Journal, August 1962.

7. Sarpkaya, T., "The Performance Characteristics of Geometrically Similar Bistable Amplifiers," Paper No. 68-WA/FE-18, ASME, December 1968.

8. "Vortex Rate Sensor Theory," Honeywell Internal Document, SRM-77, Honeywell Systems and Research Center, July, 1968.

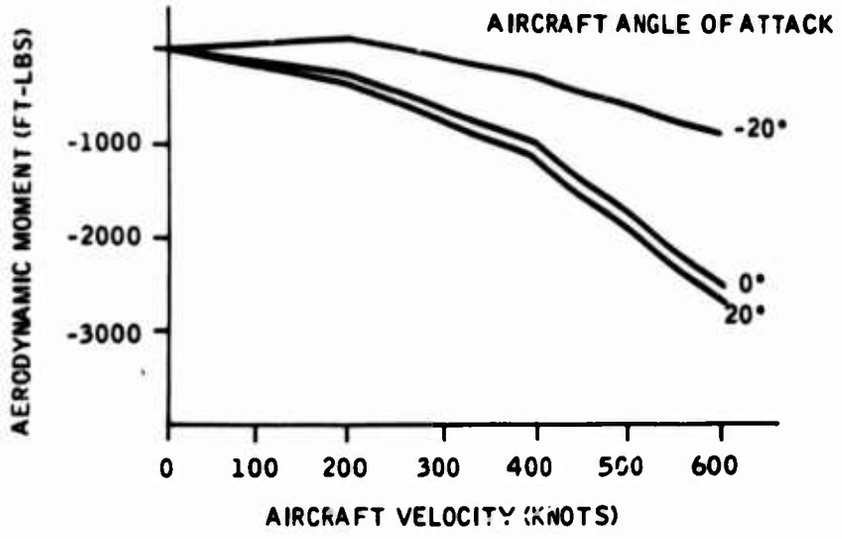


Figure 1. Maximum Aerodynamic Moments

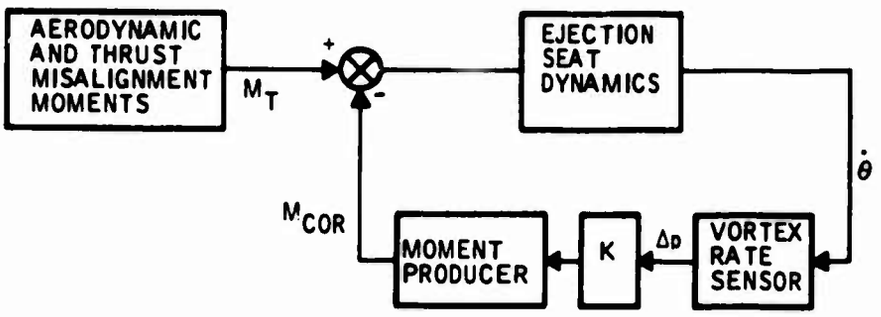


Figure 2. Block Diagram of Ejection Seat Control System

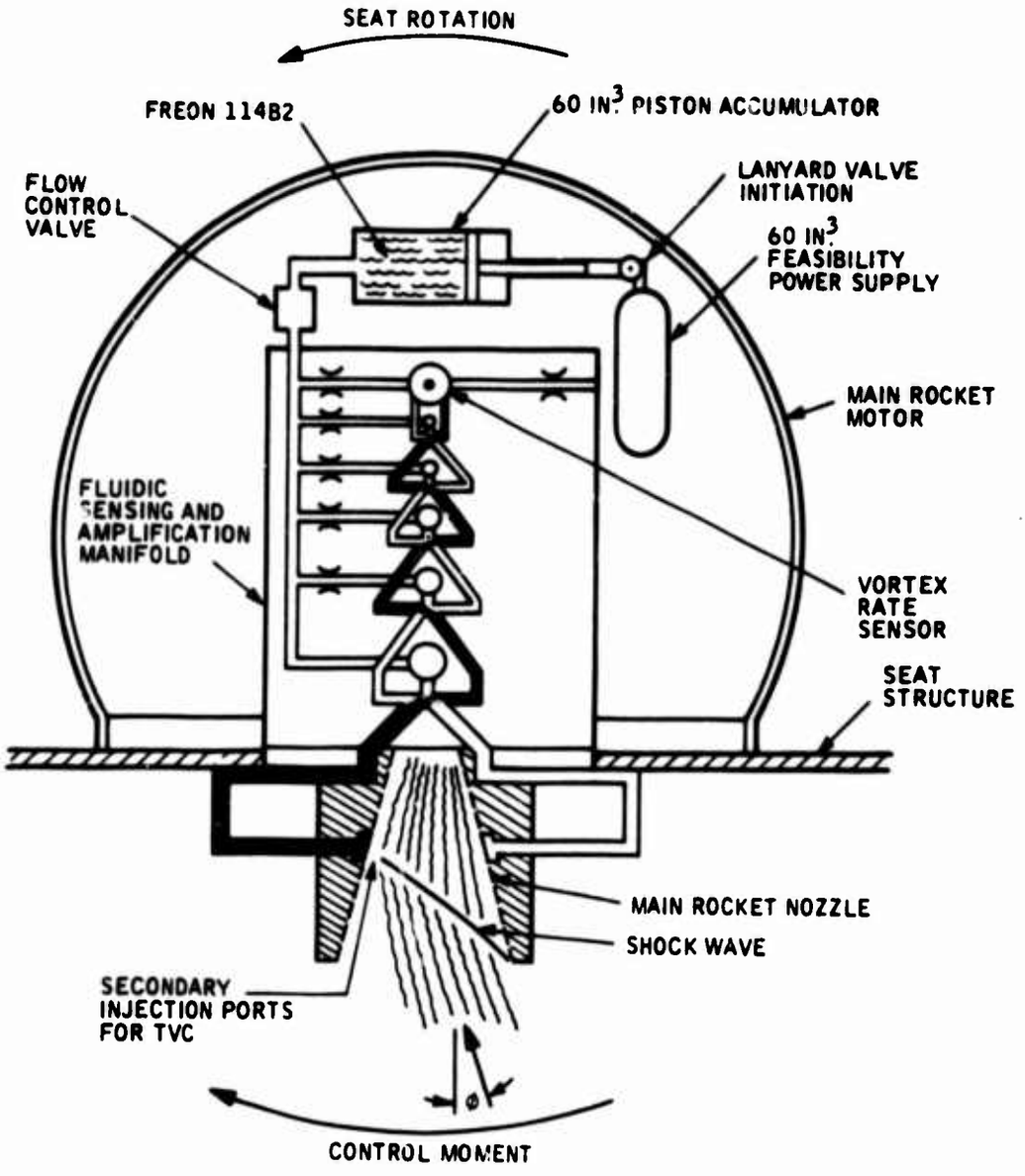


Figure 3. Schematic of Fluidic Control System

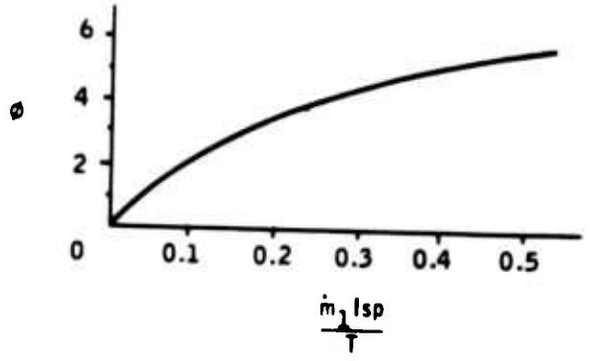


Figure 4. Expected TVC versus Secondary Mass Ratio

Reproduced from best available copy.

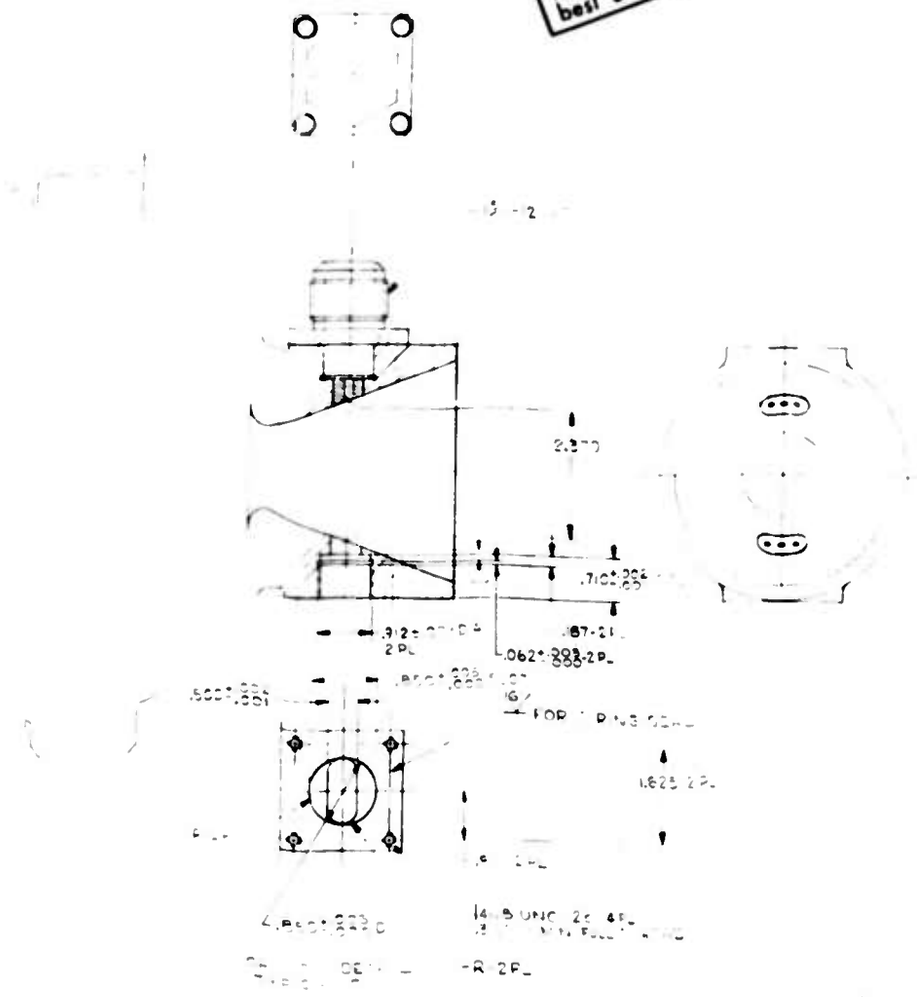


Figure 5. Secondary Injection Nozzle Sidewall Port Display

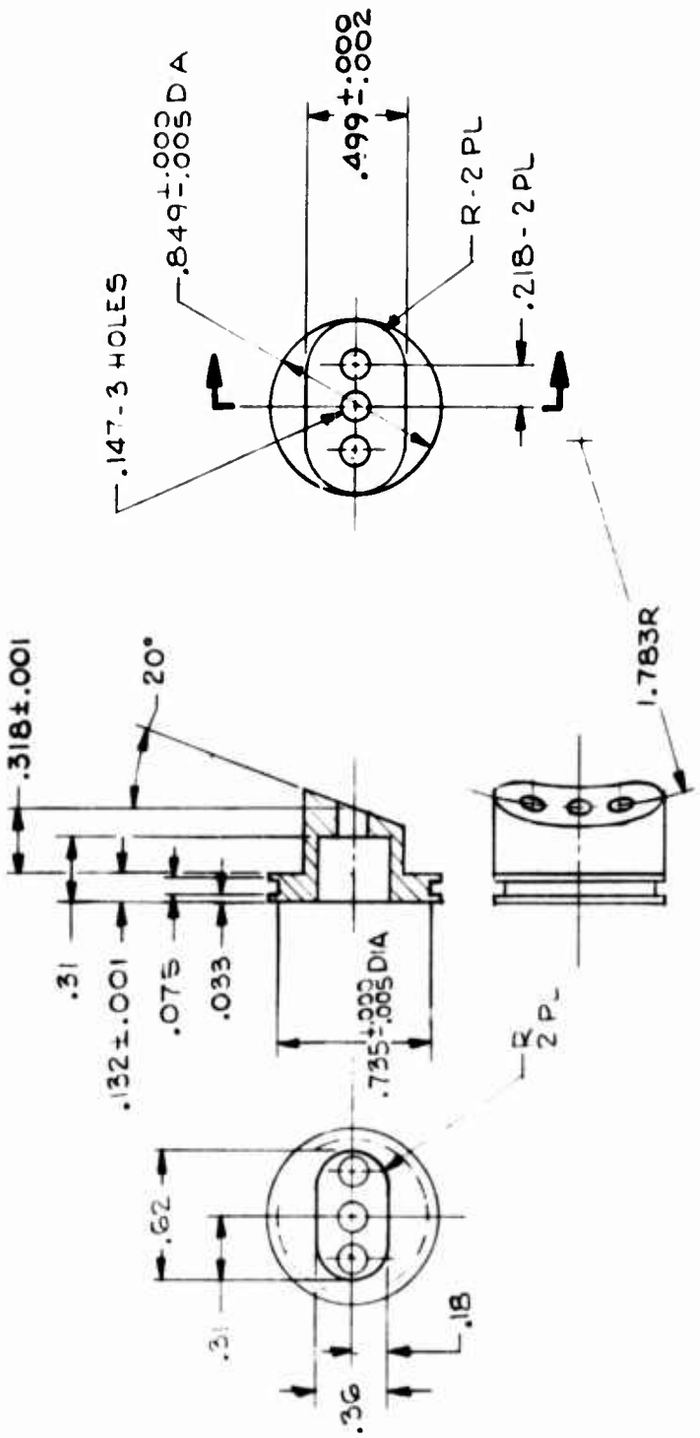
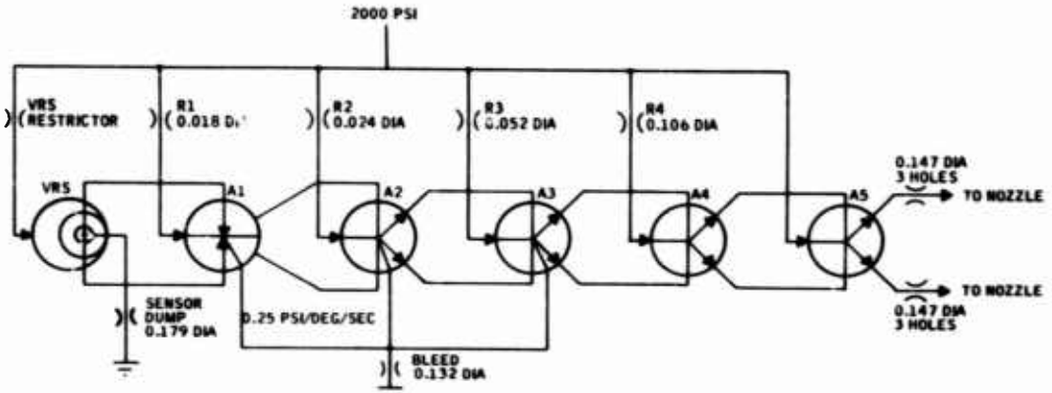


Figure 6. Secondary Injection Orifice



COMPONENT TYPE	R.S VORTEX R.S.	NO. 1 PROP AMP	NO. 2 BISTABLE	NO. 3 BISTABLE	NO. 4 BISTABLE	NO. 5 BISTABLE
POWER PORT (W AND H) IN	.10 SINK DIA	.025 x .025	.025 x .050	.025 x .100	.050 x .125	.088 x .260
CONTROL PORT (W AND H) IN	.050 x .025	.037 x .025	.025 x .050	.025 x .100	.050 x .125	.088 x .260
SUPPLY PRESS (PSI)	900	390	450	800	1100	2000
REF PRESS (PSI)	100	90	90	90	NONE	NONE

Figure 7. Amplifier Cascade Circuit

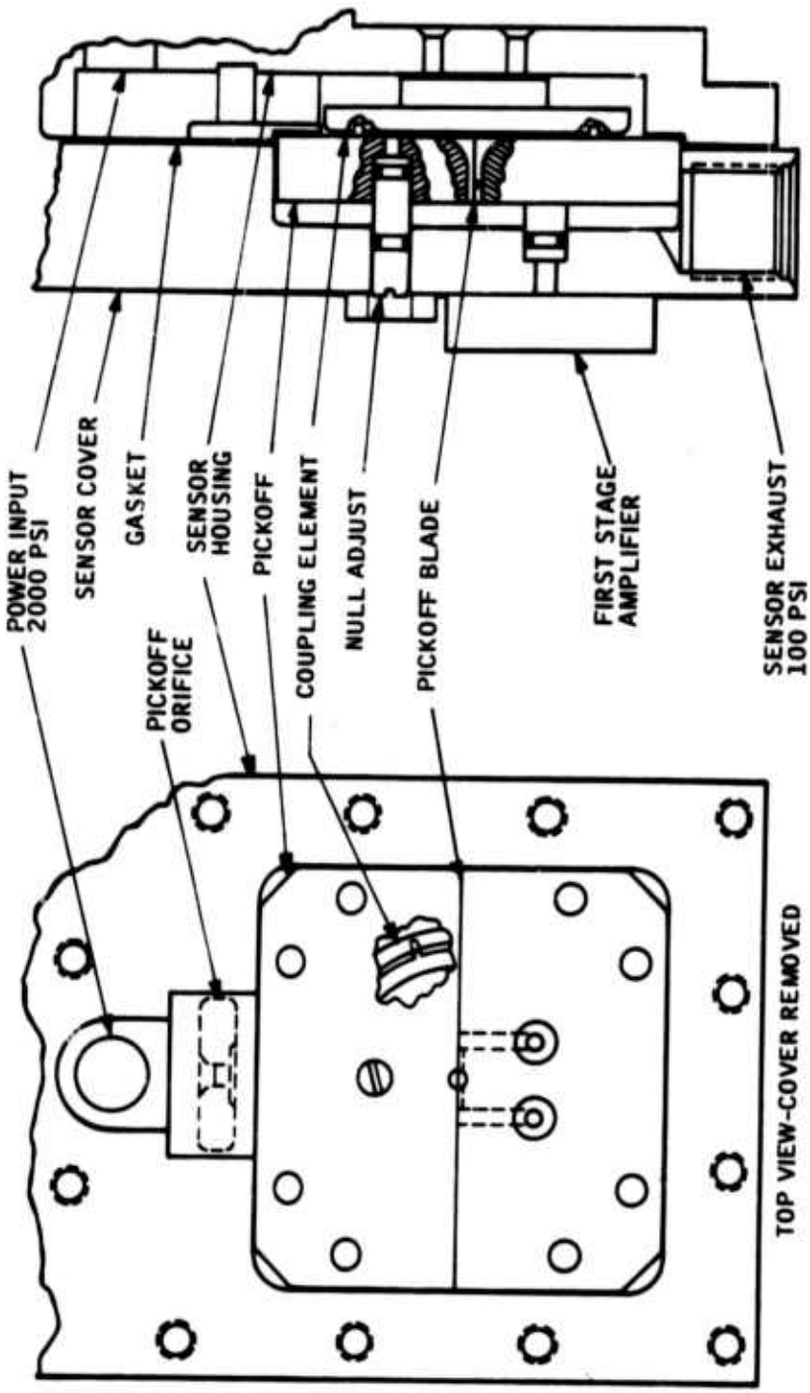


Figure 8. Ejection Seat Rate Sensor

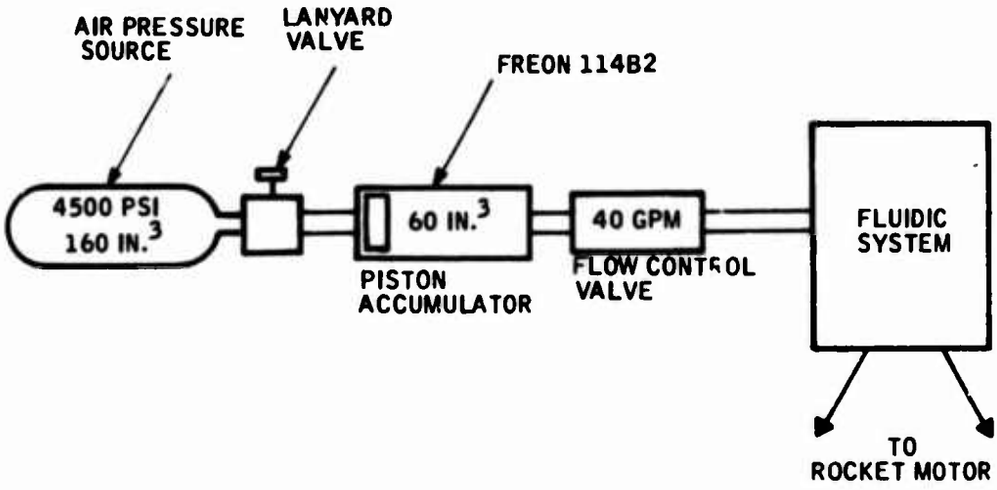


Figure 9. Ejection Seat Control System Power Supply

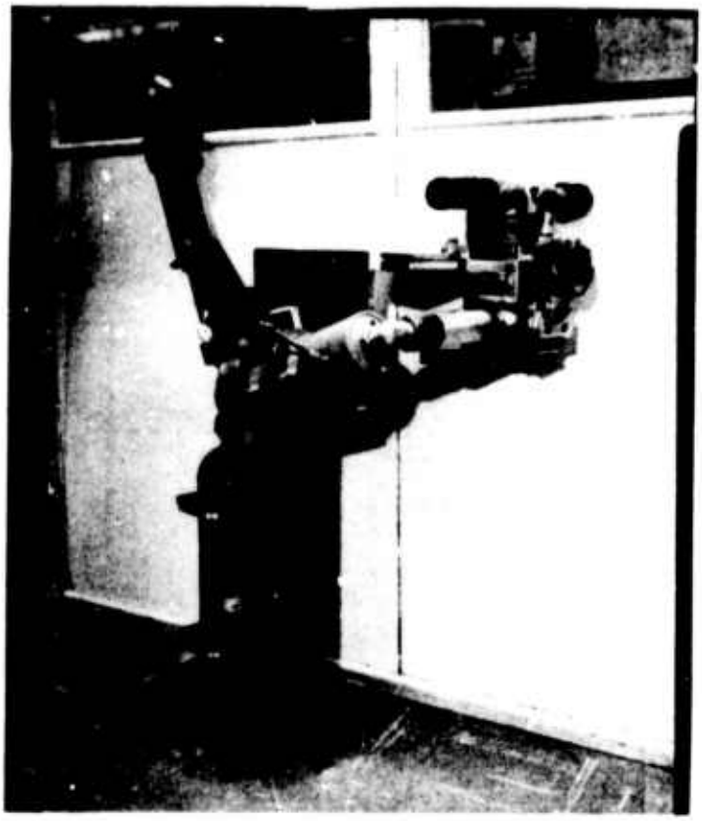


Figure 10. Control System Hardware Mounted on Bench Test Brackets



Figure 11. Complete Man/Seat Mounted on Flat Bed on Track 5

Table I. 0/0 Ejection Test - Fluidic Stabilization System Conducted 28 February 1973 at NATF, Lakehurst, N.J.

Item	Quantity
MPES seat ejectable weight	232 lb
Dummy weight	142 lb
Total ejectable weight	374 lb
CG/rocket thrust offset (forward pitch)	2° (3/8 inch)
Maximum rocket pressure	1434 psi
Rocket burn time	0.75 second
Maximum seat acceleration	8.5 g
Rocket rate of buildup (from vertical dummy acceleration trace)	502 g/second
Seat first motion (1/16") from time 0	0.054 second
Actuation of fluidics from time 0	0.107 second
Duration of fluidics secondary injection	0.42 second
Fluidics system switched back and forth	10 times
Pitch rate at fluidics burnout	0 deg/second
Pitch rate induced from time fluidics burned out to burnout of rocket	55 deg/second
Total MPES ejected height	200 ft

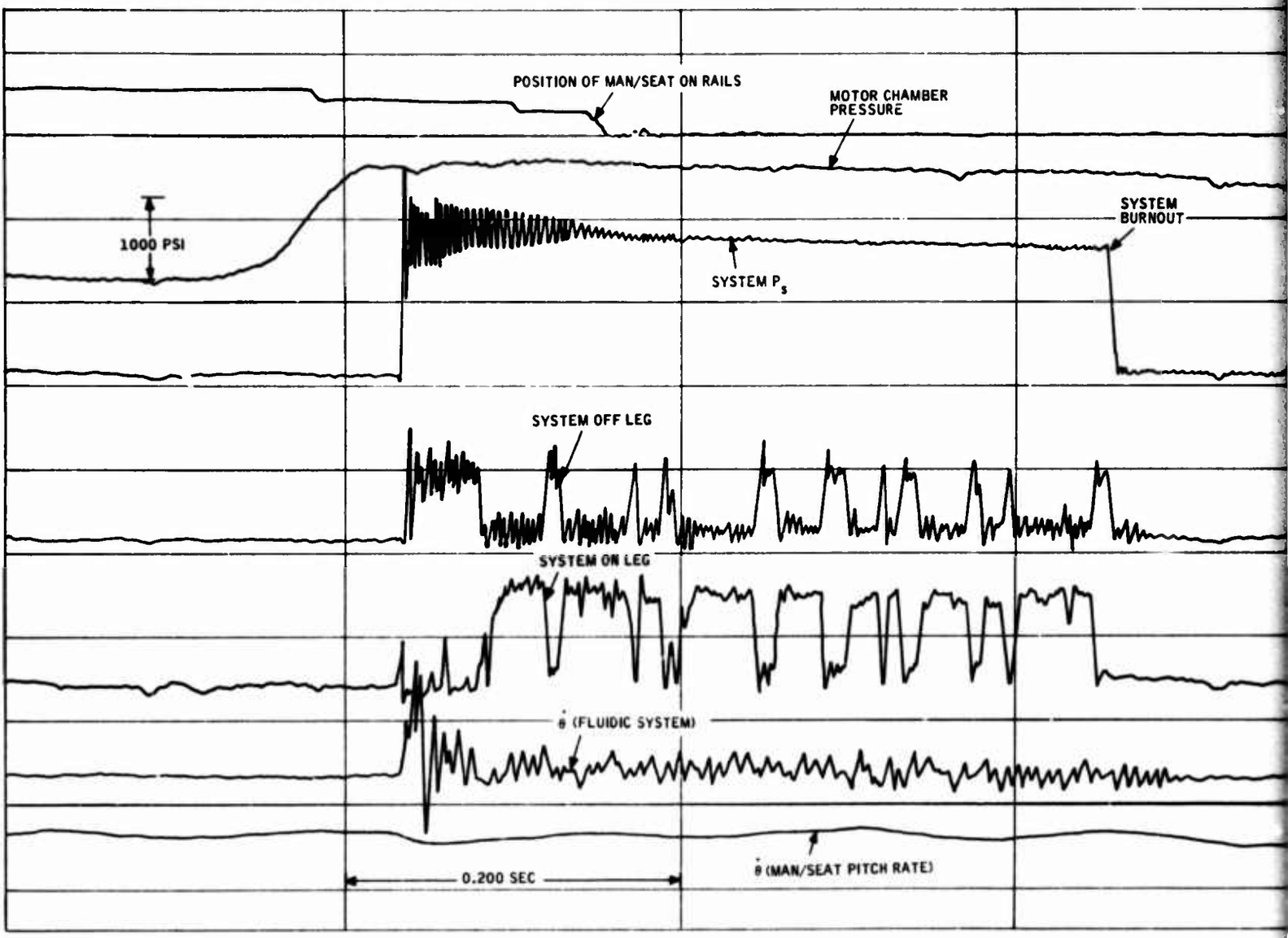
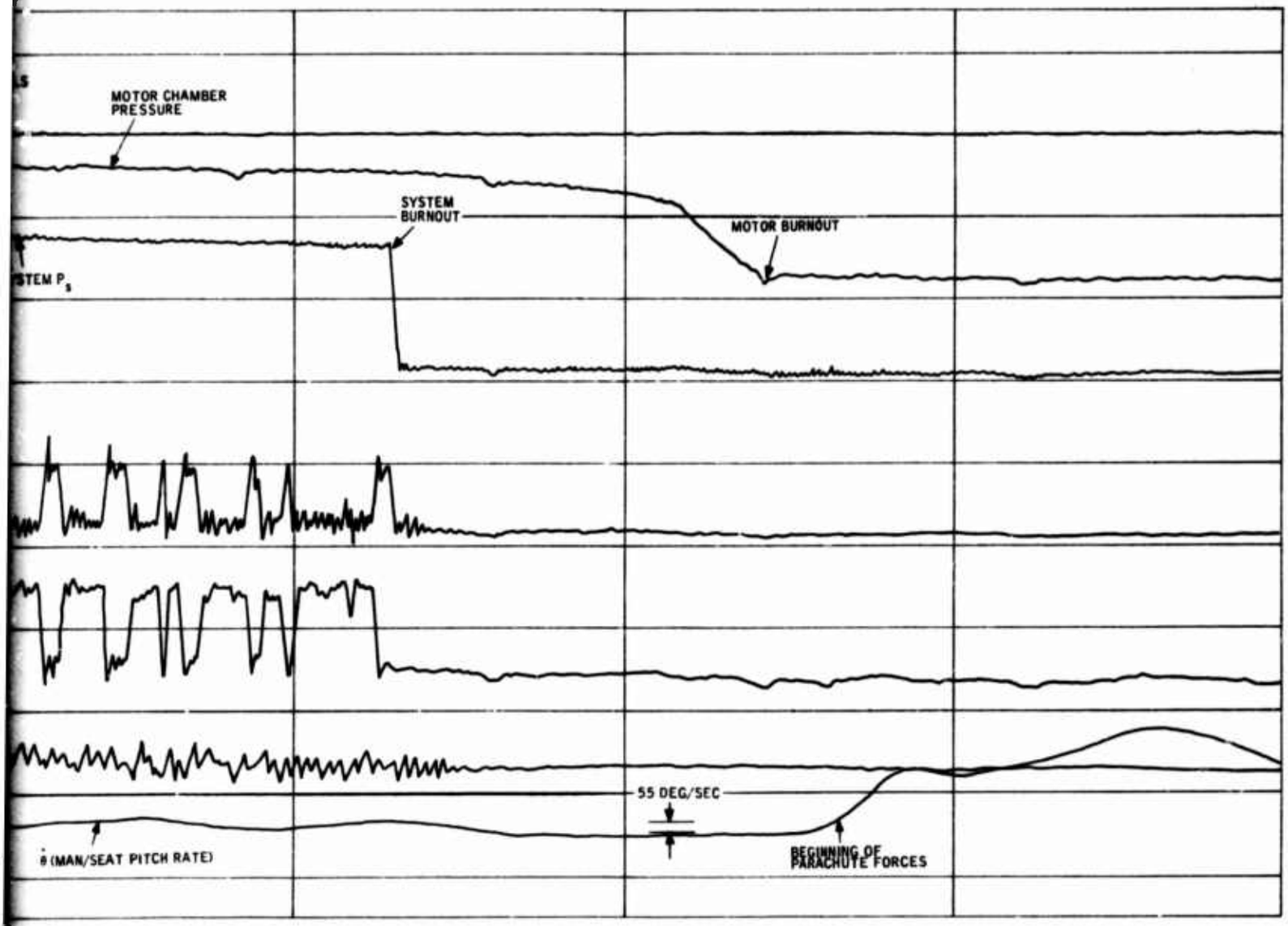
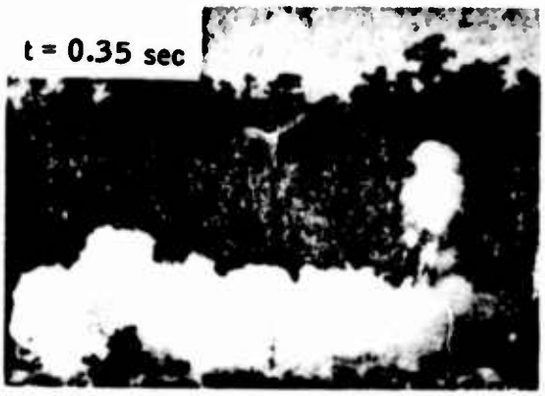
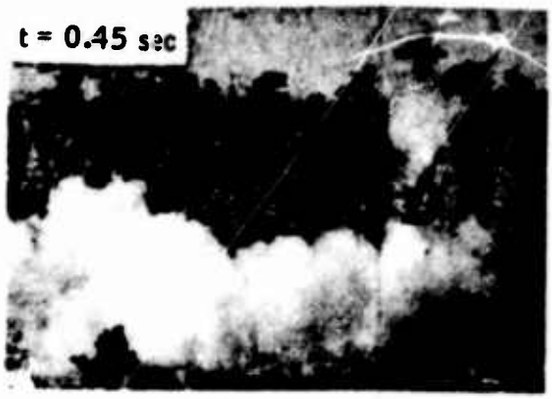


Figure 12. Oscillograph of Controlled Flight Demonstrat

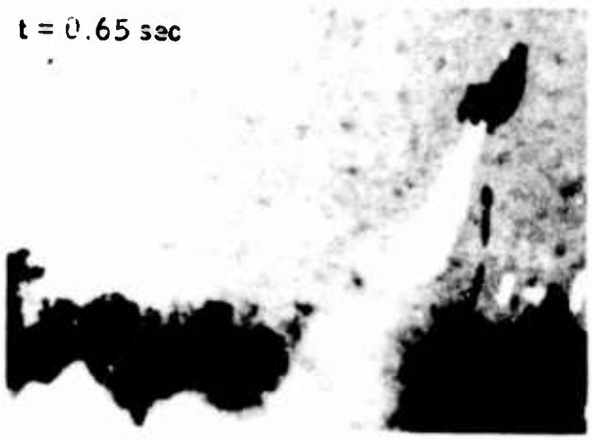


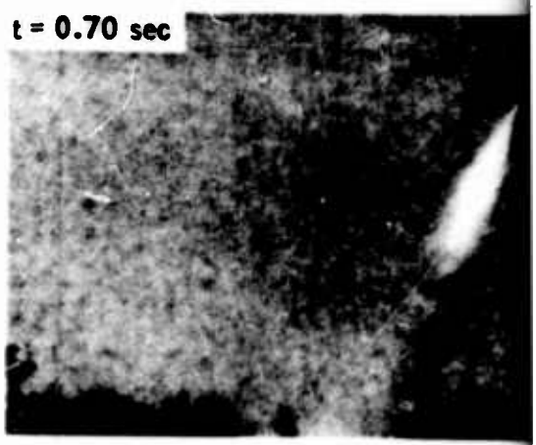
2. Oscillograph of Controlled Flight Demonstration

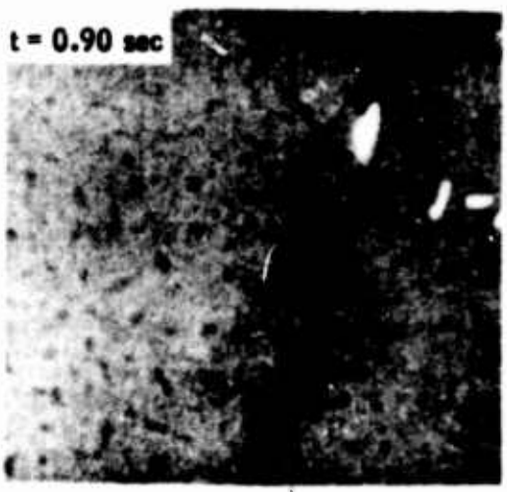

t = 0.35 sec

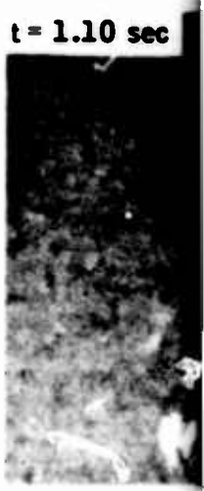

t = 0.45 sec


t = 0.55 sec

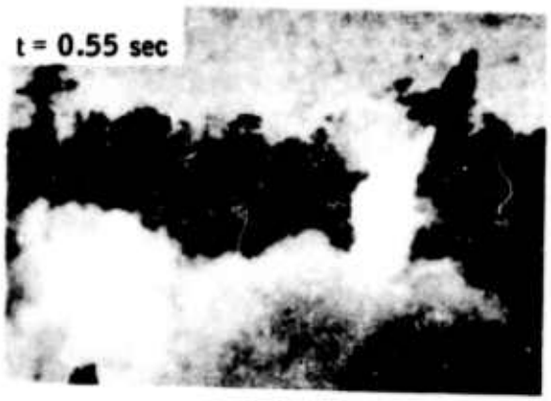

t = 0.65 sec

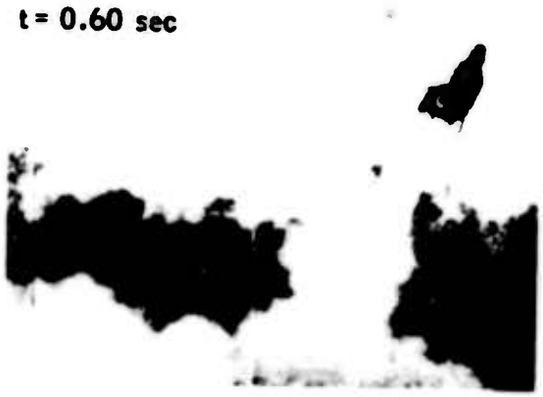

t = 0.70 sec


t = 0.90 sec

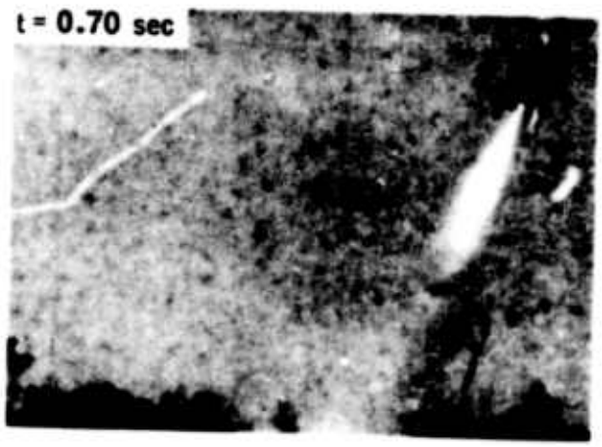

t = 1.10 sec











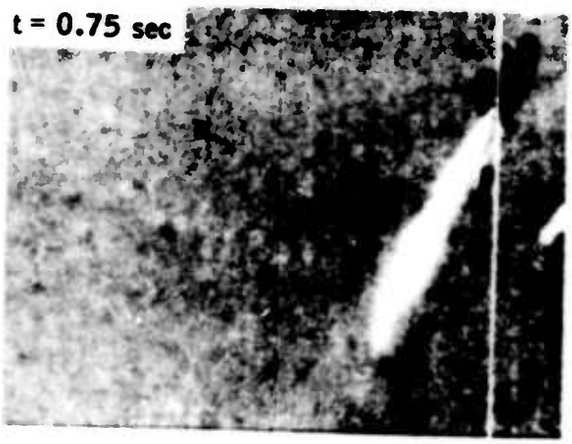






Figure 13. Ejection Sequence

A FLUIDIC AIRCRAFT BRAKE CONTROL SYSTEM

H. H. Straub, Boeing Commercial Airplane Company

P. M. Wagner, Air Force Flight Dynamics Laboratory

ABSTRACT

The high temperature capability, insensitivity to vibration, and high reliability offered by fluidics are attractive to aircraft brake control systems which will operate in an increasingly hostile environment as carbon brake applications become more widely accepted.

A concept study indicating the feasibility of a pneumatic fluidic brake control system with antiskid and automatic brake mode of operation is described. Evaluation of commercial fluidic elements, approaches to fluidic analog circuit design, and operation of a breadboard brake control system are presented. Performance results on the Boeing antiskid simulator, followed by a full-scale test at the Wright-Patterson Air Force Base Landing Gear Test Facility, are discussed.

INTRODUCTION

Similar to their counterparts on automobiles and trucks, brakes of modern aircraft have excessive torque capability under adverse conditions such as wet and icy runways and light loads. Due to the large size of today's jet transports and the resulting multiple wheel landing gear configuration the pilot does not have control over each individual wheel and can, therefore, lock the wheels due to the large forces available from the hydraulic brake actuation system. This would result in considerably longer braking distances, blown tires and loss in lateral ground control. To insure safe and economic aircraft stopping, numerous antiskid systems have been developed which control the braking force to a level which does not result in wheel lockup, regardless of how hard the pilot attempts to brake the aircraft. In addition, more advanced antiskid systems try to extract the maximum available retardation force from the tire-runway interface.

DESCRIPTION

Conventional antiskid systems (Figure 1) consist of a wheel speed sensor, a control box, and an interface valve to control hydraulic pressure in the brake. The wheel speed sensor is usually located in the axle and consists of an AC generator with a frequency output dependent on the number of exciter teeth and the wheel speed. This signal is converted to an equivalent DC signal which is proportional to wheel speed. Operation of a typical control box is based on the computed deceleration of the wheel, which increases rapidly as a wheel skid is approached. As wheel speed decreases markely below synchronous velocity, the friction between tire and runway drops as shown in Figure 2. This figure represents the typical tire dynamic response on dry runways. As brake pressure is applied, the tire slip increases and initially results in increased available friction coefficient. Beyond some

value thermodynamic effects reduce friction. The control circuit senses the incipient skid and issues a signal to decrease brake pressure. The wheel spins up to near synchronous velocity and brake pressure is gradually increased until the next incipient skid is sensed. The control box is located in the wheel well or electronics bay of the aircraft,while the brake pressure control valve is frequently mounted in the vicinity of gear-wing/body attachment point.

Due to recent growth in aircraft takeoff weight and speed, the brake energy absorption capability had to be continuously increased. This has led to the development of more efficient heat absorbing material such as structural carbon which can withstand temperatures far in excess of the more conventional steel heat sink. However, the full advantage of hotter brake stacks can only be realized if the brake structure, the surrounding wheel, the axle and other components in the vicinity of the brake can withstand the harsher thermal environment. Here pneumatic-fluidics offers a solution to the potential design problems of the wheel speed sensor. Because fluidics can operate in an environment of wide temperature variations, vibration, and shock, the attractive possibility of mounting the whole antiskid system inside the axle as an integrated package cannot be overlooked. While the need for such a system on a production aircraft may still be some time away, a spin-off application to truck, bus, and railroad airbrake control systems could be more imminent because compressed air systems are already incorporated into these vehicles.

The basic concept of the pneumatic-fluidic antiskid system is similar to that of the electric counterpart, consisting of a wheel speed sensor, computation circuit, and an interface valve between low pressure pneumatics and high pressure hydraulics. In lieu of a new control concept development, the existing Boeing Closed Loop System was chosen as baseline. This system was originally developed for the Boeing 737 aircraft. More advanced versions of a similar concept are now operating on the Lockheed L-1011 and Douglas DC-10. The Boeing Closed Loop System uses the wheel speed signal to operate through two parallel paths (Figure 3) to control brake pressure. In the major loop wheel deceleration is computed with a differentiator and modulates brake pressure through a time constant circuit. If an incipient skid exceeds the authority of this path the skid detector is switched on, dumping brake pressure and resetting the integrator to a lower commanded pressure. For the implementation of the fluidic circuit (Figure 4) it was desired to let the pilot select aircraft stopping performance by way of a selector switch setting the reference deceleration. When this reference is less than the peak deceleration available from the runway-tire interface, the aircraft stops without brake pressure cycling. With the exception of brake initiation, such a stop duplicates the behavior of an automatic braking system. If the reference exceeds the available level, incipient skids are sensed and the system operates in the normal antiskid mode of operation. Also a second order lead from converted wheel speed to valve signal was added to damp strut oscillations.

FLUIDIC ANTISKID SIMULATION

Prior to the design and procurement of hardware for the breadboard system, the fluidic antiskid system concept was simulated on the Boeing analog-hard-

ware brake control simulator. This setup (Figure 5) consists of the aircraft brake hydraulic hardware to duplicate the response of brake pressure to antiskid valve signal. A real time analog simulation incorporating all parameters of major influence to airplane stopping uses brake pressure to compute wheel speed. The latter signal is then fed to the antiskid system which controls brake pressure. In simulating the fluidic antiskid system, special emphasis was placed on the wheel speed sensor, integrator time constant, and AC-DC converter. The lack of effective fluidic diodes somewhat complicated the task. Some preliminary hardware tests indicated that the repsonse of typical fluidic components is approximately ten times faster than that of a typical electric-hydraulic antiskid valve. Hence dynamic effects of fluid amplifiers were not a factor in the circuit design. Similarly, hardware tests indicated that the capacitive lag caused by line volumes could be effectively decreased by stacking more laminates on a fluid amplifier. The results of the computer study indicated that a fluidic antiskid system would be feasible and could result in stopping efficiencies in excess of 80 percent.

HARDWARE DEVELOPMENT

Development of the breadboard hardware was first initiated for the wheel speed sensor and antiskid valve because these components interface with the rest of the brake control system and were not commercially available in their entirety. This approach left the fluidic circuit to bridge the gap later and provided more freedom over the choice of dynamic and static gain in the circuit.

The wheel speed sensor (Figure 6) consists of 50 evenly spaced teeth on a 5-inch diameter which alternately interrupt two air jets in the open duck bill sensing head. The teeth are 1/16" thick and move through a 3/16" gap, thus allowing up to 1/16" of misalignment or eccentricity in either direction without affecting sensor performance. Nozzles and receivers are both 1/16" diameter and thereby reduce the risk of contamination through dirt particles entrained from ambient air. The air pulses are fed directly into a General Electric AC-DC converter (MC12B) resulting in performance as shown in Figure 7. The dynamic performance is primarily affected by switching delays and the output filter in the converter. The sensor was designed to operate at a frequency up to 1000 Hz. However, tests indicated that it could operate up to 1500 Hz with some sacrifice in linearity.

A DC wheel speed sensor relying on the principle of the vortex rate sensor was also designed and evaluated. Due to the low output and poor signal to noise ratio, however, this approach was abandoned.

An existing electro-hydraulic brake pressure control valve was modified to accept low pressure pneumatic signals. The valve, shown schematically on Figure 8, is a two-stage device. A differential pressure across the main spool is developed by deflection of the flapper of the first stage. The spool moves until the unbalance in force is equalled by the change in delivered pressure and bias spring force. Normally, the first stage flapper motion is controlled by an electric coil placed around the cross bar of the flapper. With the coils removed, two instrument bellows can work in push-

push action against the crossbar. The selection of the bellows was partially dictated by envelope constraints posed by the physical location of first stage relative to the valve body (Figure 9). Other requirements were low stiffness, large effective area, and small internal volume all of which led to a compromise selection. The bellows were sealed with a disk on one end and a threaded fitting on the other. The fitting was extended into the bellows to reduce the internal air volume and to serve as a compression travel limit. Static tests (Figure 10) on the assembled valve indicate that a differential pressure of 4.1 paid across the bellows is required to reach hydraulic reservoir pressure in the brake. This pressure differential can be delivered by a proportional fluid amplifier with 10 psig supply. Dynamic tests (Figure 10) on the valve, including the effect of a short piece of hydraulic hose and the brake fluid volume, show good response to 12 Hz, which is also typical for an electrically driven antiskid valve.

With the successful hardware implementation of wheel speed sensor and antiskid valve, the development effort was then concentrated on breadboarding the fluidic circuit. Components were purchased from General Electric, Fluidics Operation and included several summing, digital and three stage amplifiers and one operational amplifier. Also, laminates for a single stage proportional amplifier (TR-1608) were borrowed from Harry Diamond Labs., Washington, D.C.

In the planning stage of the program it was recognized that not enough component performance data was available to allow immediate design of the circuit. Hence, a thorough performance evaluation of each component was carried out, to establish the following operating characteristics.

- Supply flow
- Input impedance
- Output impedance
- Gain
- Noise
- Response
- Null sensitivity to supply pressure and temperature variation.

While this is a time consuming task, the data is required before a circuit can be successfully breadboarded. Data which generally was taken with X-Y plotter and the oscilloscope would be too voluminous for a detailed review here. However, it should be mentioned that, with few exceptions, all components performed admirably well. Input impedance ranged from 18,000 to 210,000 sec/in^2. Output impedance which is generally an indication of the component output power capability ranged from 10,000 to 70,000 sec/in^2 under blocked load conditions. Response of all components, with exception of the operational amplifier was flat beyond 60Hz. Signal to noise ratio at a bandpass of 100 Hz ranged from 100 to 200. Finally output null sensitivity to changes in supply pressure were less than 0.16 psid over a range from 2 to

10 psi supply. The effect of raising supply air temperature from 70°F to 150°F was immeasurably low. A closer examination of the fluidic circuit concept discussed earlier will show that basically three lead functions and one lag function with summing at the proper locations were required to implement the breadboard circuit.

The lead circuit can be built by subtracting the steady state output of a passive lag from a pressure ratio circuit with a proportional amplifier as shown on Figure 11. External restrictors, R_E, were made by flattening short sections of brass tubing. Measurements indicated that above a pressure drop of 0.5 psi, the resistance value was relatively linear. Fixed air volumes served as capacitors as expressed by

$$C = \frac{V}{KRT} \ (in^2)$$

where

V = volume (in^3)

K = specific heat ratio

R = gas constant ($in/^oR$)

T = absolute temperature (^oR)

For air at room temperature

$$C \ (in^2) = 2.1 \times 10^{-6} V \ (in^3)$$

The lag circuit can be breadboarded as shown on Figure 12. Because a relatively long time constant of 5 seconds was required, the bootstrap configuration with a finite feedback resistance, R_F, value was used. This reduced the volume of the capacitor from a nominal 32 in. to 4 in^3. The only drawback to this approach is that due to the resulting difference equation, small restrictor nonlinearities and amplifier gain variations render a direct mathematical circuit component selection ineffective. Consequently the lag circuit was designed by test.

With the use of a simplified braking simulation (Figure 13) the circuit was developed in a closed loop manner. The output pressure differential of the circuit was measured and converted to simulated brake pressure. The computed wheel speed was converted to a pneumatic signal by use of a small electric motor driving the actual wheel sensor when fast response was not required. By substituting a torque motor-flapper valve arrangement the rapidly decreasing speed of a wheel approaching lockup could be simulated. Sequentially the modulator, skid detector, and second order lead path were added to the circuit and the effect of each addition tested.

The effectiveness of this real time simulation approach in breadboarding and quickly evaluating the fluidic antiskid circuit cannot be overemphasized. The progress of the breadboard development was quickly assessed by running the simulation with the circuit over a wide range of conditions. Also the need for a costly and time consuming circuit sensitivity study was avoided.

A transfer function representation of the final circuit is shown on Figure 14. This diagram also depicts the concept used in the development of the antiskid circuit. The chain consisting of differentiator, summer, and integrator make up the major loop controlling brake pressure. Skid detector and second order lead act as transient control inputs and must be fast in response.

Typical performance traces using actual brake hydraulics hardware, the fluidic breadboard, and simulated wheel and dynamometer inertia are shown on Figure 15. In a typcial cycle after a skid, brake torque gradually increases until the wheel speed starts dropping rapidly. At this point the skid detector fires, quickly reducing brake torque and resetting the integrator. As the ground force brings the wheel speed back to near synchronous, the skid detector switches off and brake pressure and torque is reapplied until the next incipient skid is sensed.

Due to the fast response required in the antiskid system, the fore and aft motion of an oscillating gear is measured by the wheel speed sensor. With improper circuit design this could cause system instability and structural damage. In giving an indication of the rate of change of wheel deceleration the double lead proved to be effective in damping a strut represented by a simple second order simulation as shown on Figure 16. However, it could not effectively add damping to a strut simulated by a more conservative fourth order system which included the effect of axle windup. This was due to the inherent noise and lower than desired gain of the fluidic implementation of the double lead.

A circuit diagram of the breadboard is shown on Figure 17. Peripheral equipment such as pressure regulator, air filter, pneumatic hoses, selector switch, orifices, trim valves, and solenoids were supplied by Norgen Fluidics and Clippard Instrument Lab. Manifold supply pressure was regulated to 10 psig. No special attempt was made to optimize supply pressure to the fluidic components relative to flow consumption as long as individual component tests indicated satisfactory performance at that level. Total air consumption of the circuit and sensor is approximately 4.0 SCFM.

DYNAMOMETER TEST

The fluidic antiskid system was tested on the 84 inch dynamometer in the Landing Gear Test Facility of the Air Force Flight Dynamics Laboratory. To demonstrate the capability of the system with an operating brake and wheel, the fluidic panels, Figure 18, were placed in close proximity to the wheel and tire to keep pneumatic transmission lines from wheel speed sensor to circuit as short as possible. The antiskid valve was located approximately 18 inches below the fluidic panels. Installation of the sensor and converter is shown in Figure 19. To avoid contamination by dirt and dust particles generated by the brake a cover was placed around the pneumatic sensor and fluidic panels for the duration of the test. After some initial tuning of the skid detector threshold and deceleration command the fluidic system operated very well. The tests demonstrated quite readily that deceleration could be varied by the setting of the command level and that the

circuit would sense an incipient skid and release the brake pressure. Typical test traces are shown in Figure 20 and are similar in appearance as those obtained on the simulator (Figure 15).

CONCLUSIONS

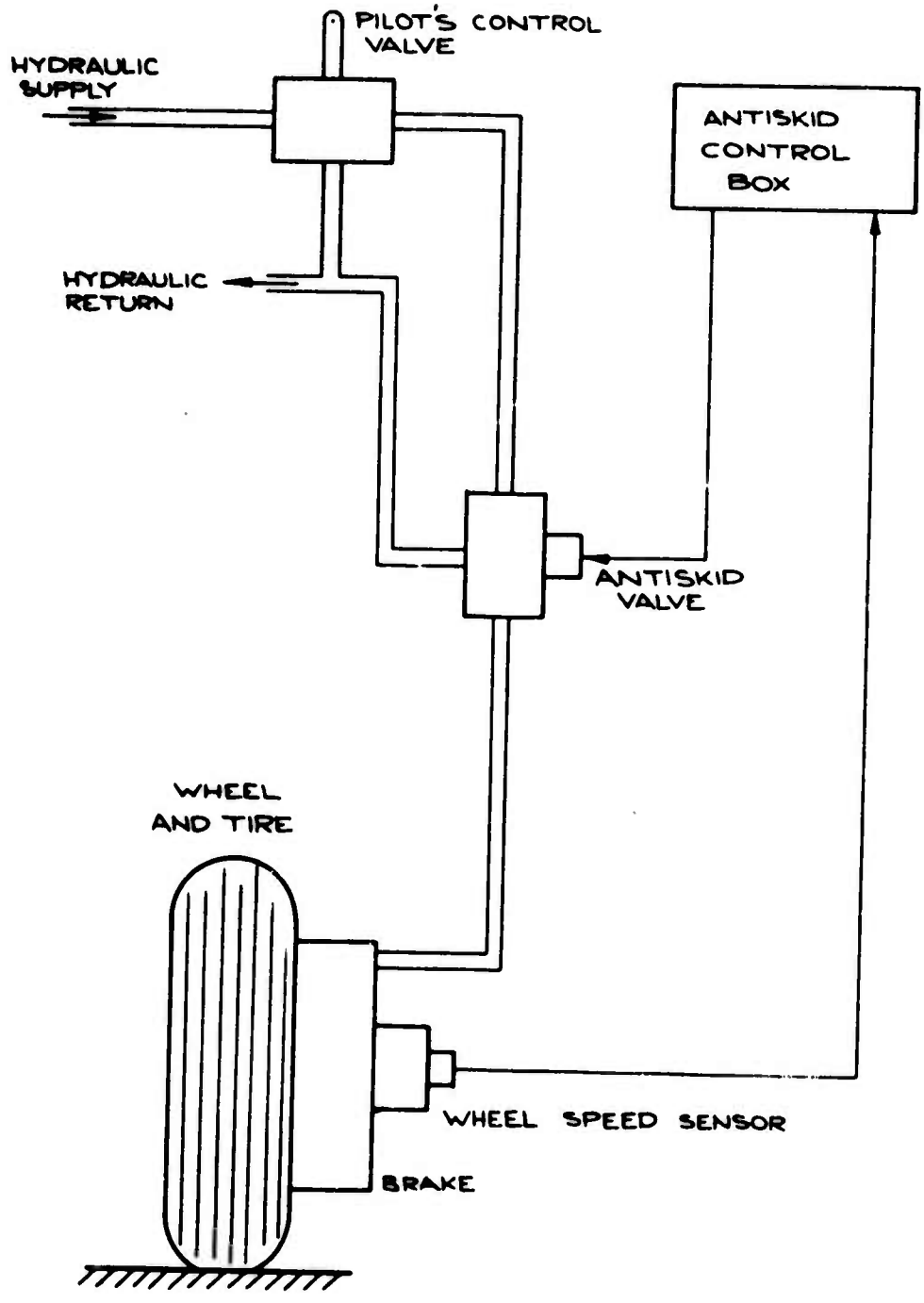
Using an existing antiskid circuit concept an analog-hardware study indicated that a pneumatic fluidic system would be feasible. Commercially available fluidic components were procured and evaluated. Then a breadboard antiskid system consisting of an AC wheel speed sensor, a computing circuit, and a modified brake pressure control valve was developed. No technical problems were encountered in converting the imulated fluidic concept into breadboard hardware. A simulated braking process was used to evaluate the performance of the system during the hardware development effort, thereby providing some freedom over the implementation of the fluidic circuit.

Evaluation tests on the Boeing antiskid simulator and the 84" dynamometer of the Air Force Flight Dynamics Laboratory demonstrated that the fluidic system could maintain control over the wheel speed by sensing incipient skids, and modulate brake pressure accordingly. The deceleration rate could be set with a selector switch. As long as the pneumatic fluidic system is placed in the vicinity of the brake, it can respond at the speed required for antiskid operation.

Although the breadboard circuit was developed with the Boeing 737 (T43-A) as baseline aircraft it is anticipated that with some minor tuning, the antiskid circuit could provide effective brake control for other aircraft applications. Also potential derivatives of this application to truck, bus and railroad air brake systems should be thoroughly evaluated.

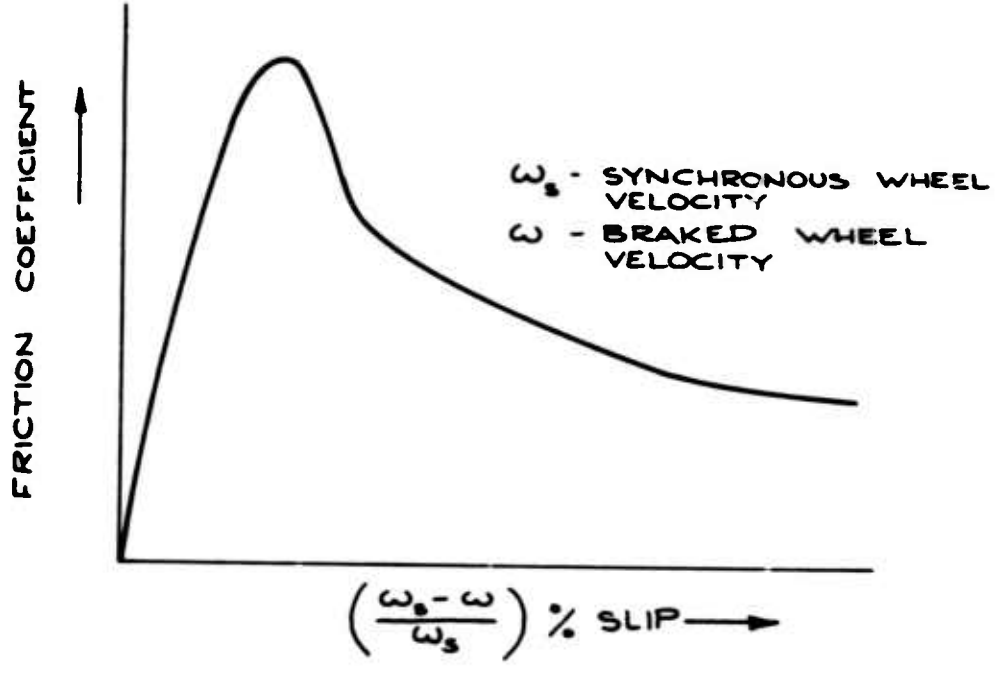
ACKNOWLEDGEMENTS

The development of the fluidic antiskid system was funded through contract F33615-73-C-3017 "Antiskid Performance - System Compatibility and Improvements as Applicable to Military Aircraft," issued by the Air Force Flight Dynamics Laboratory. The technical contributions of Mr. J. Anselmi and Mr. R. Yurczyk in testing the system on the Boeing antiskid simulator and the 84" dynamometer at AFFDL are recognized and greatly appreciated.



ANTISKID HARDWARE SCHEMATIC

FIGURE 1



TIRE FRICTION - SLIP CURVE
FIGURE 2

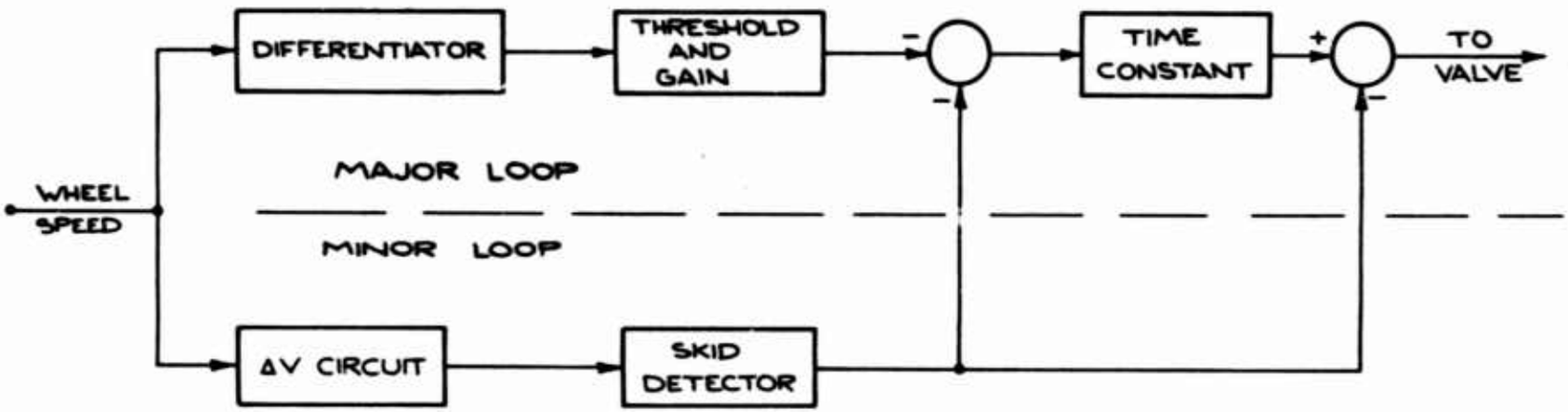
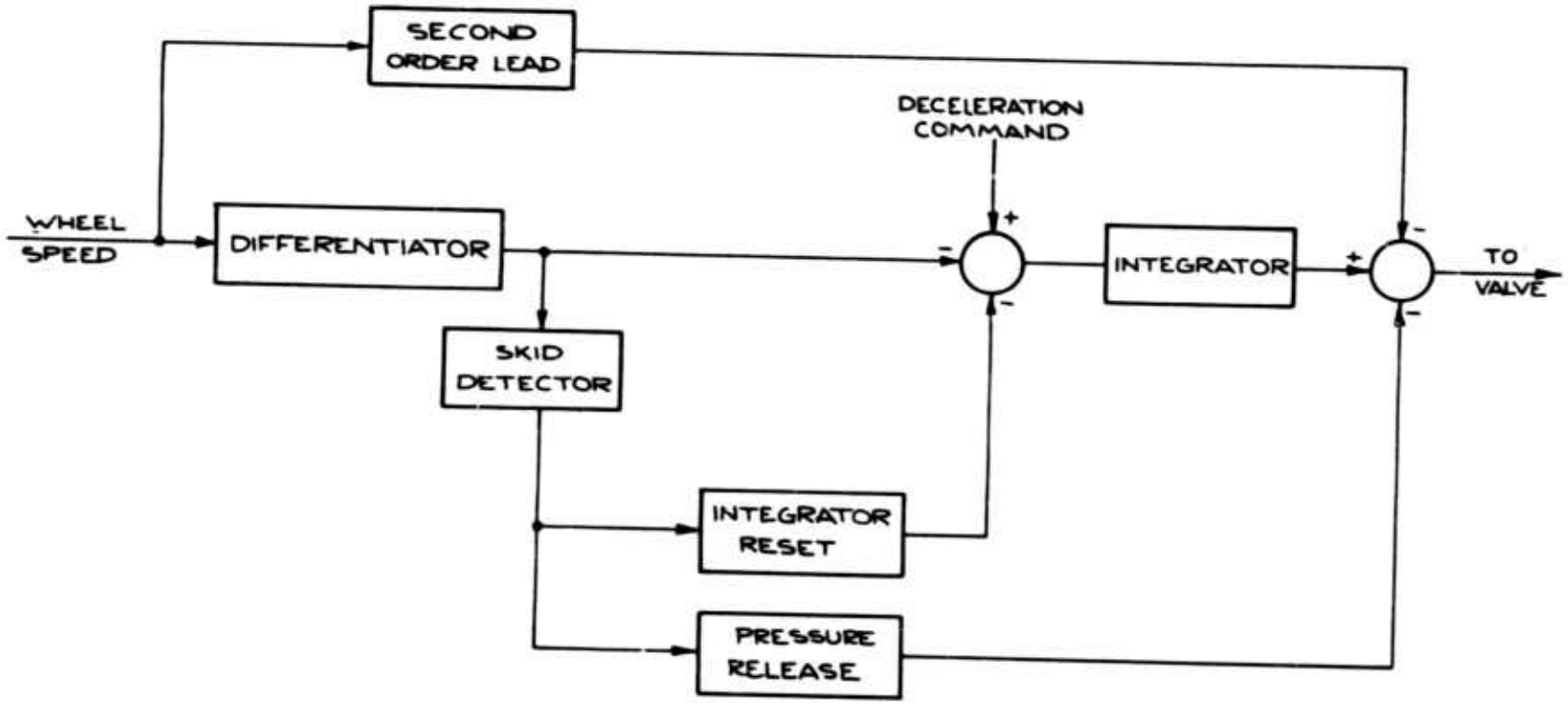
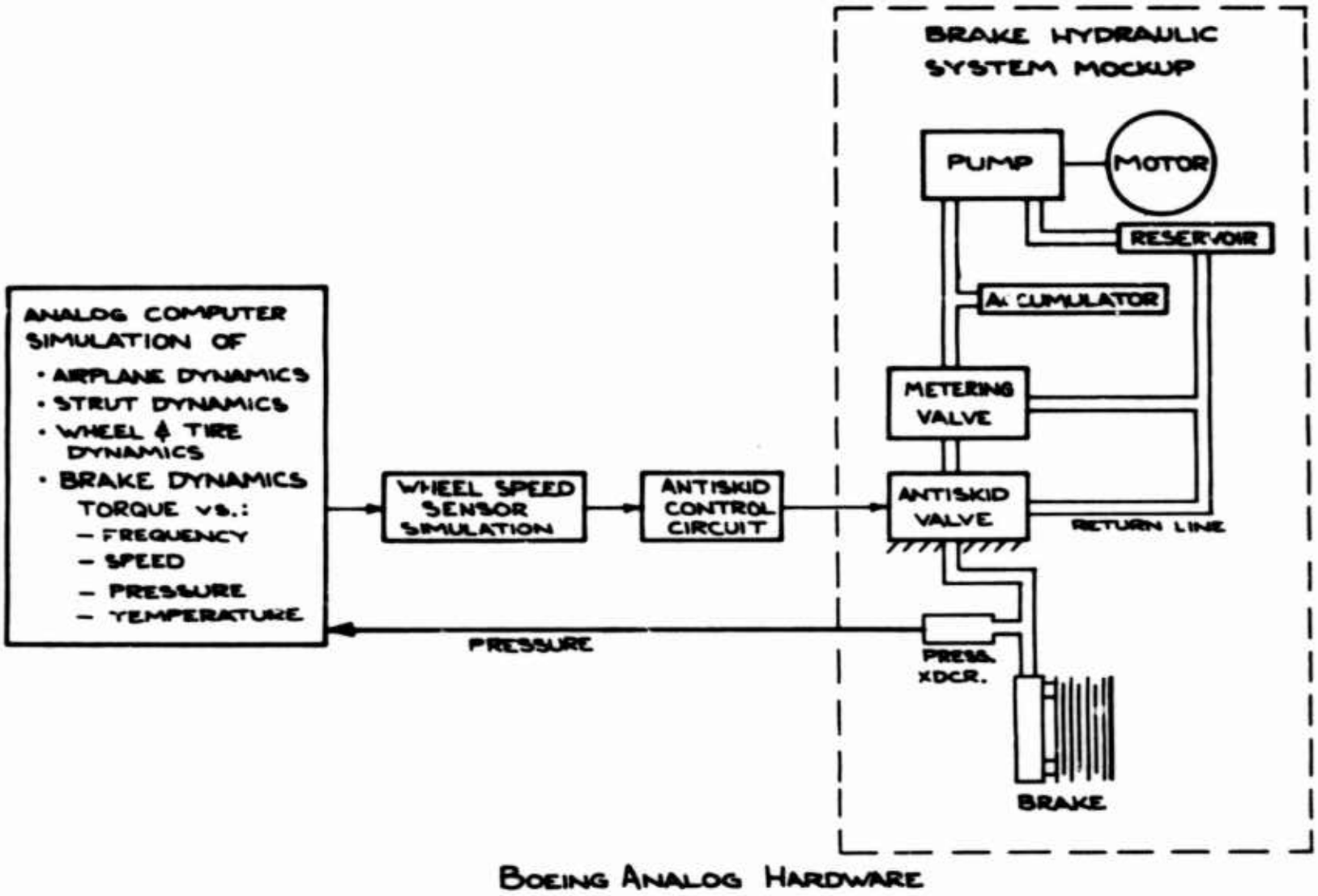


FIGURE 3 BOEING CLOSED LOOP SKID CONTROL CONCEPT



FLUIDIC CIRCUIT CONCEPT
FIGURE 4



BRAKE CONTROL SIMULATOR SCHEMATIC
FIGURE 5

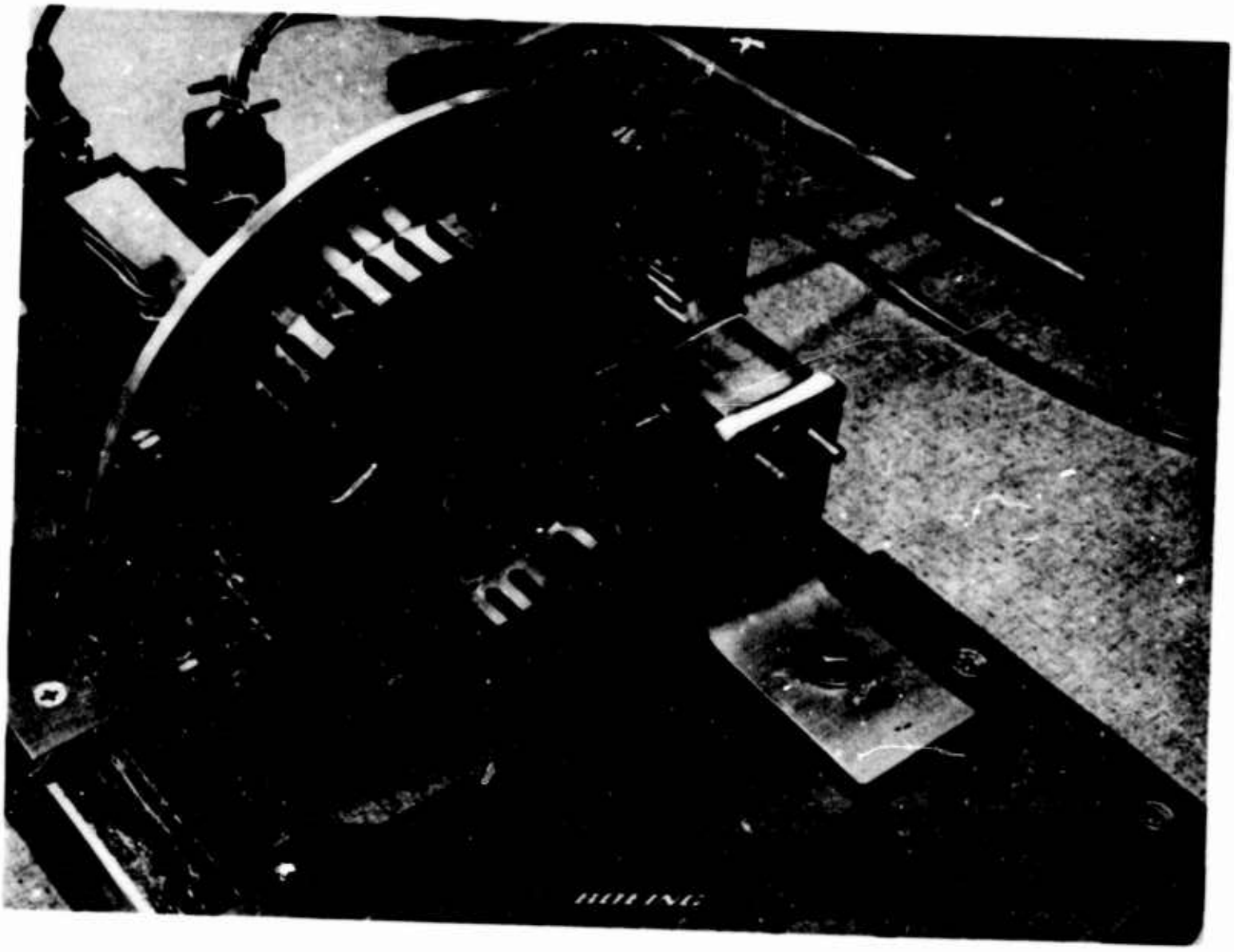
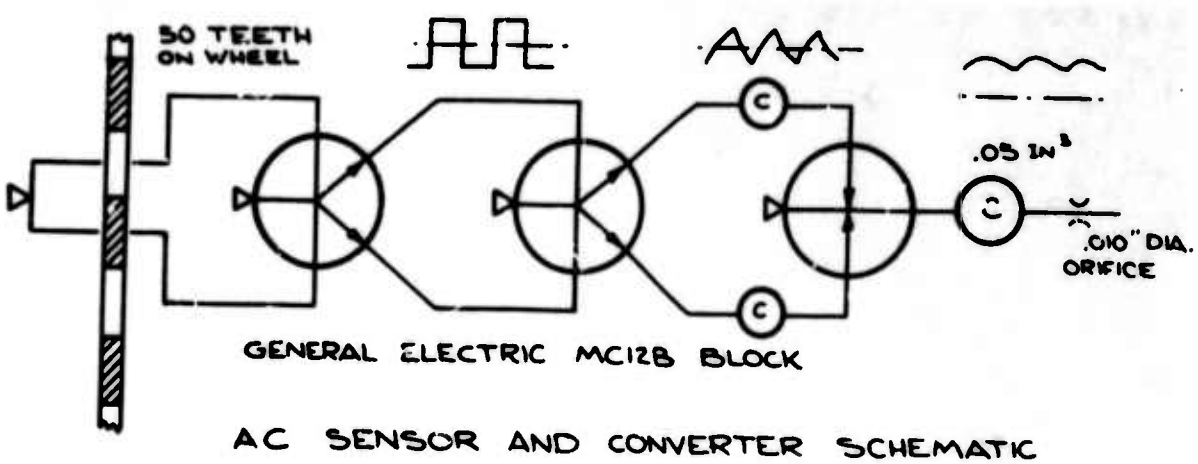
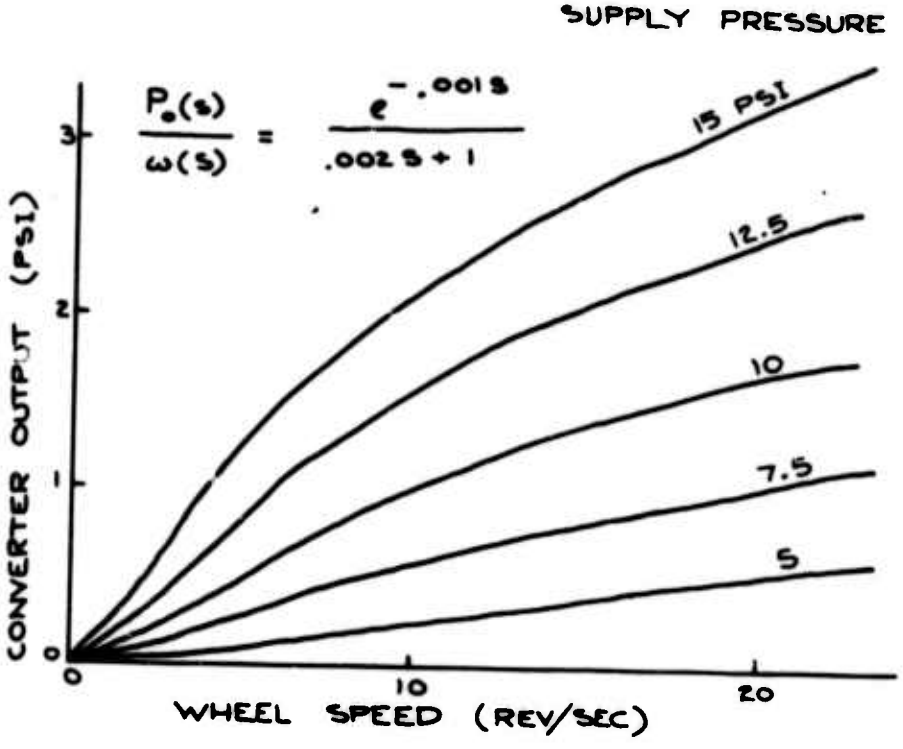


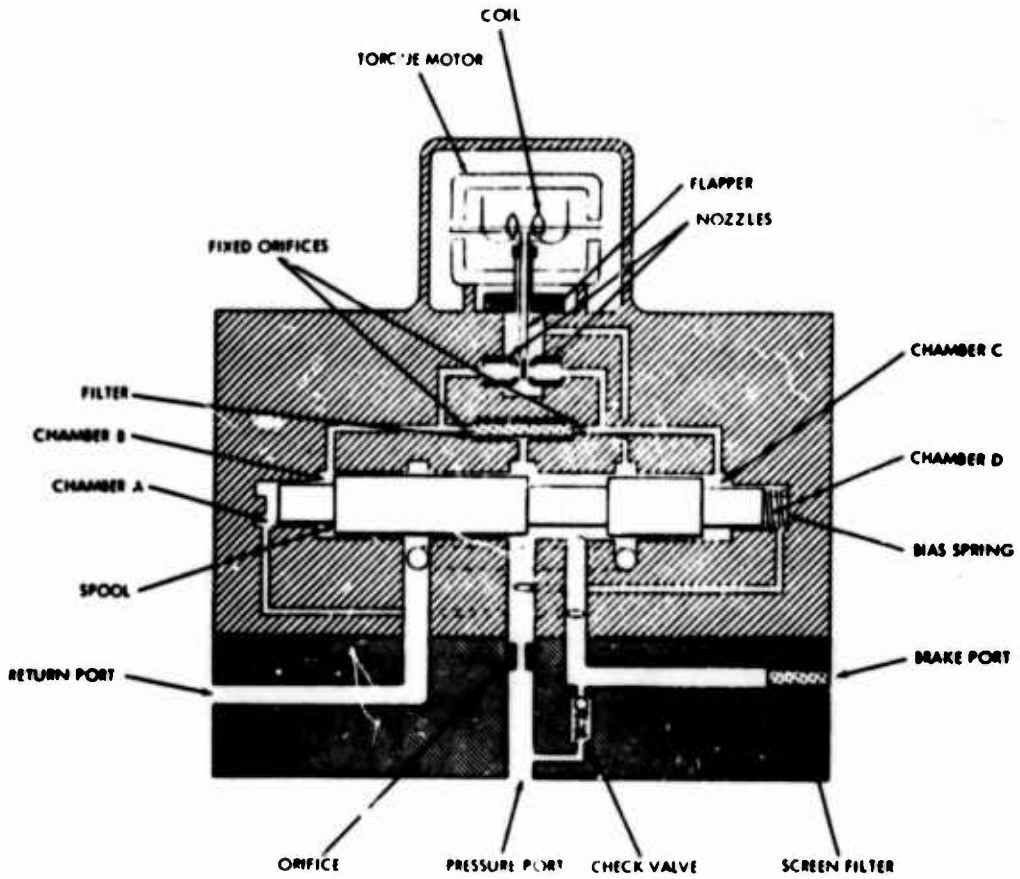
FIGURE 6 FLUIDIC WHEEL SPEED SENSOR



AC SENSOR AND CONVERTER SCHEMATIC



AC WHEEL SPEED SENSOR PERFORMANCE
FIGURE 7



67QS136A

Skid Control Valve Unit Schematic

FIGURE 8

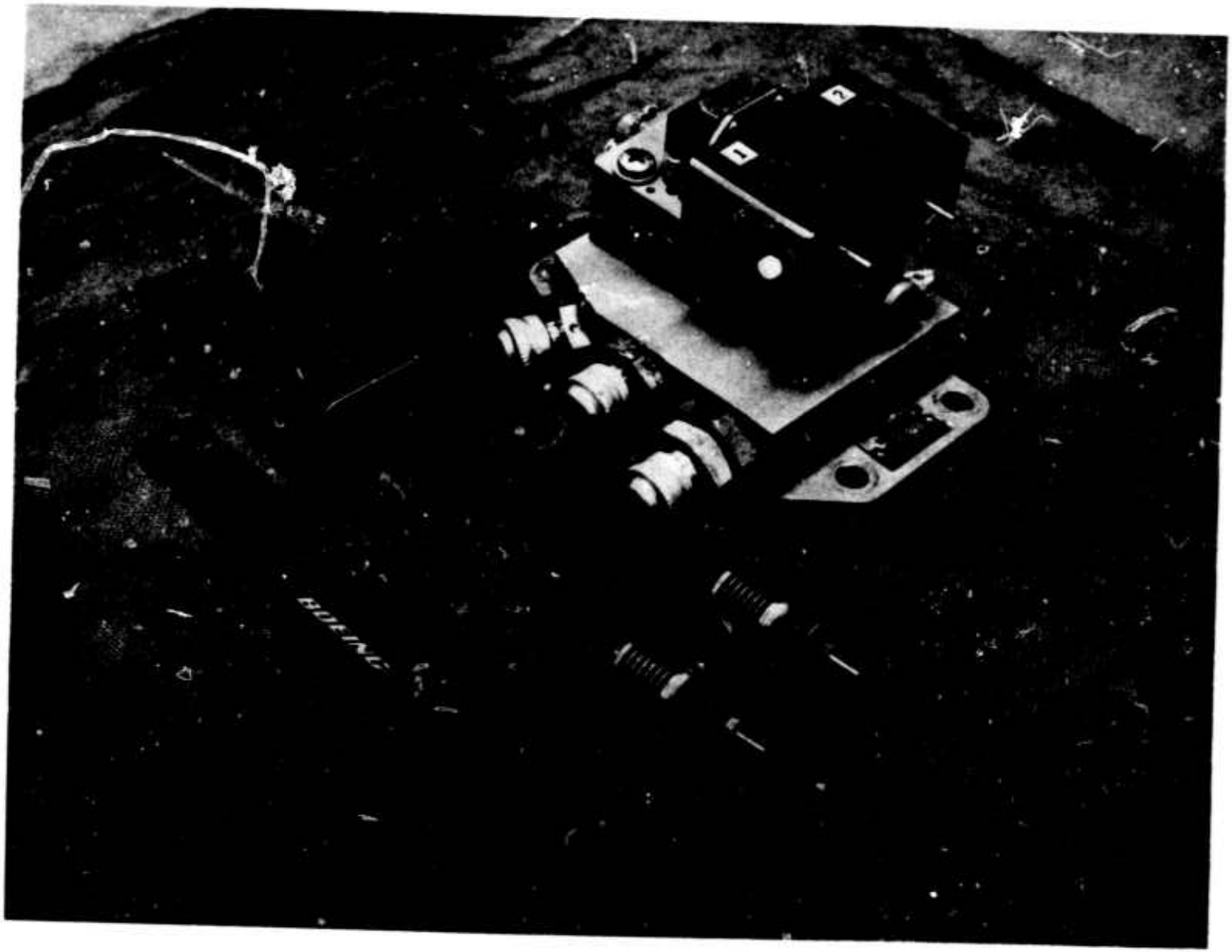
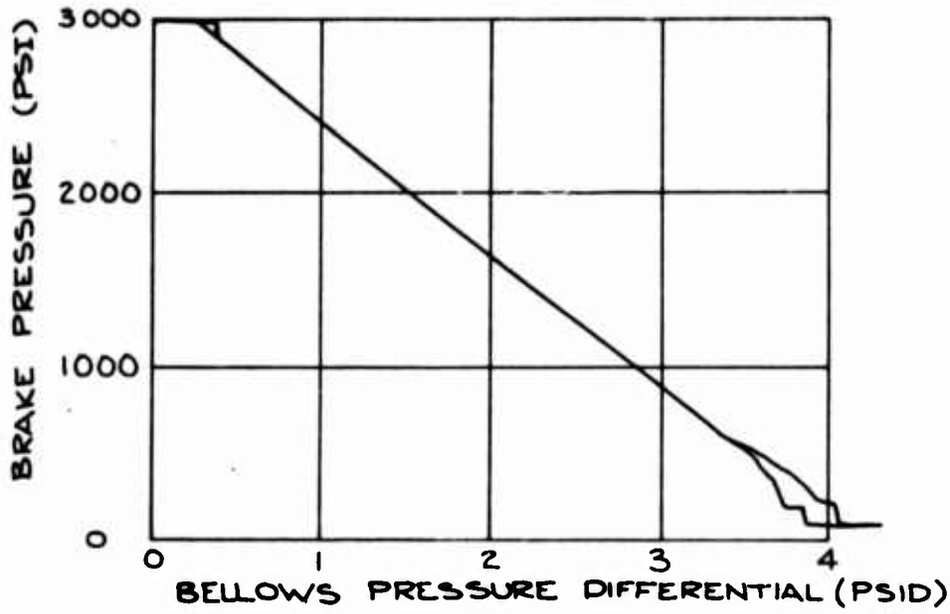
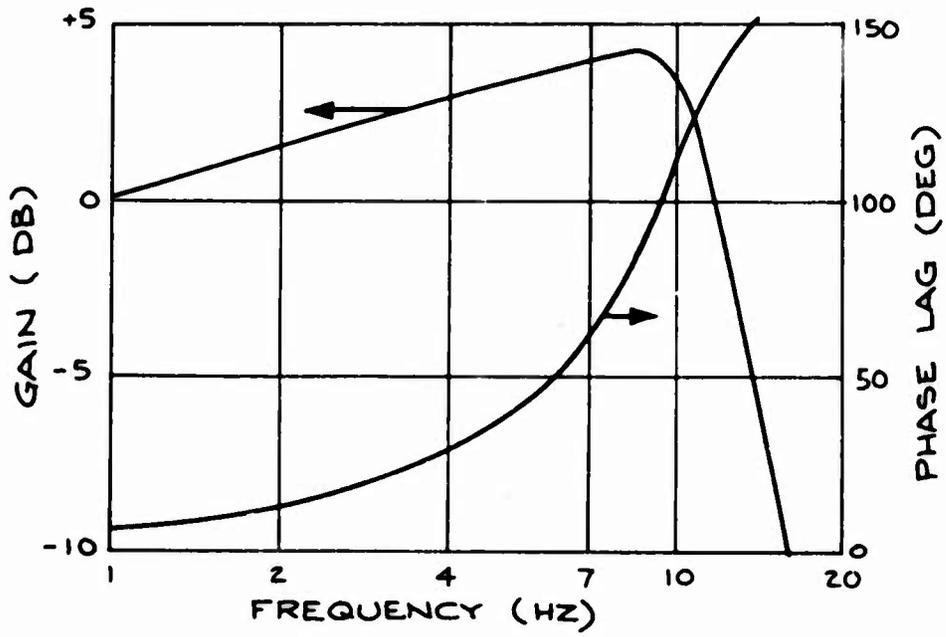


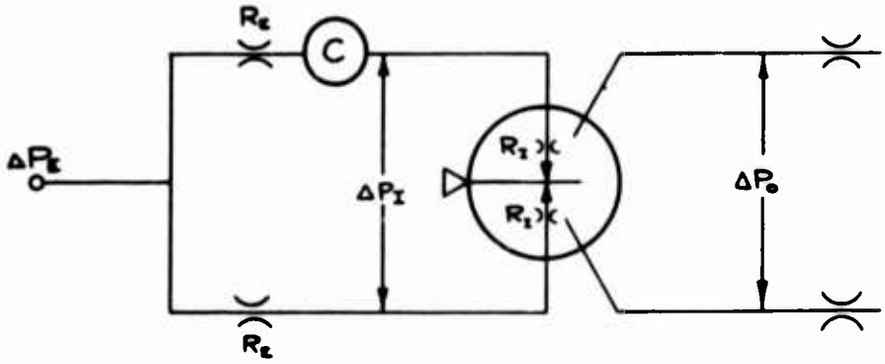
FIGURE 9 MODIFIED ANTISKID VALVE



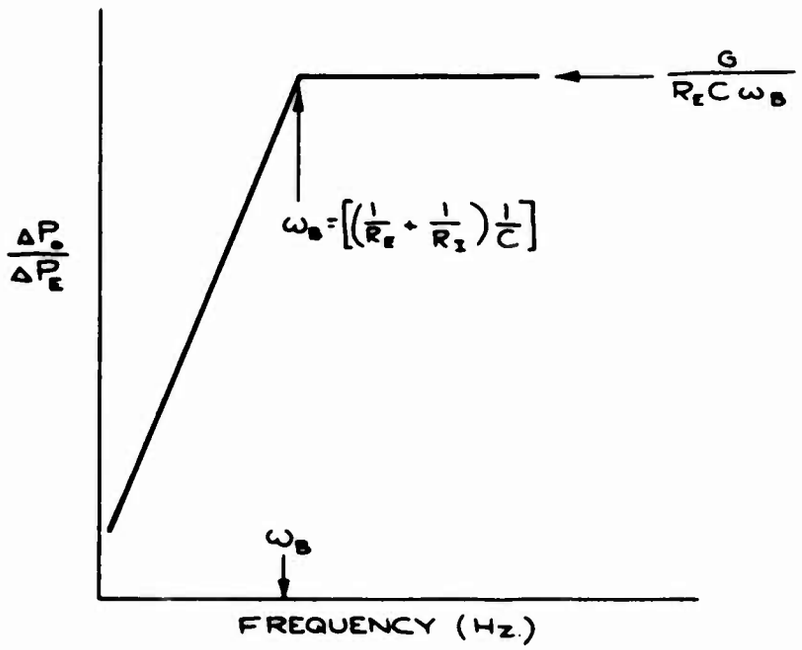


ANTISKID VALVE PERFORMANCE

FIGURE 10

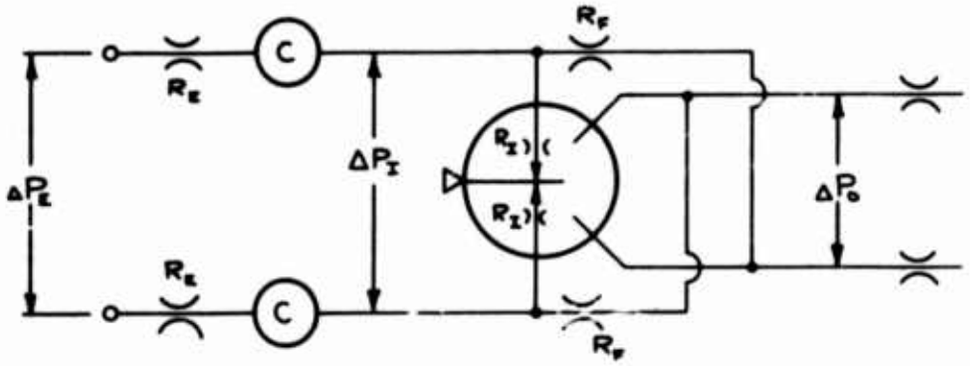


$$G = \frac{\Delta P_o}{\Delta P_I}$$

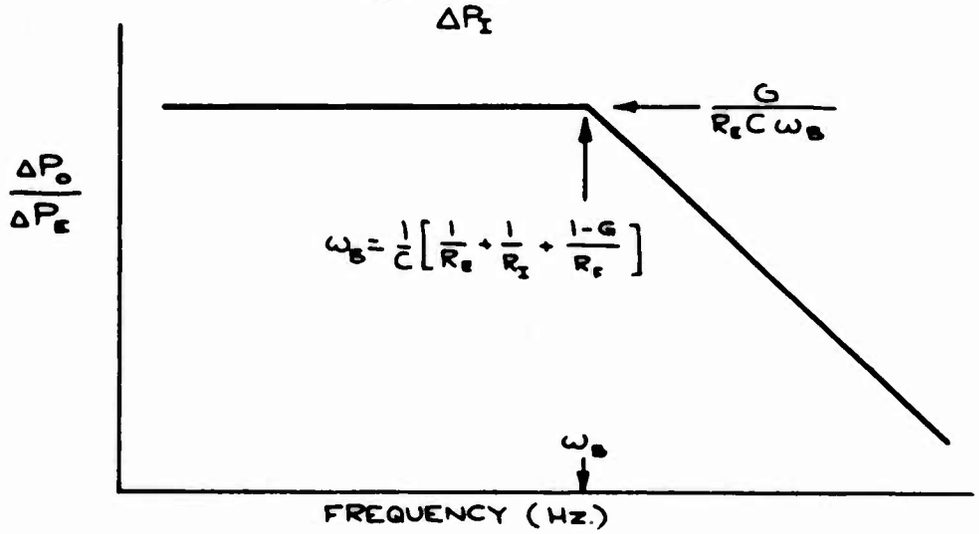


FLUIDIC LEAD CIRCUIT

FIGURE 11

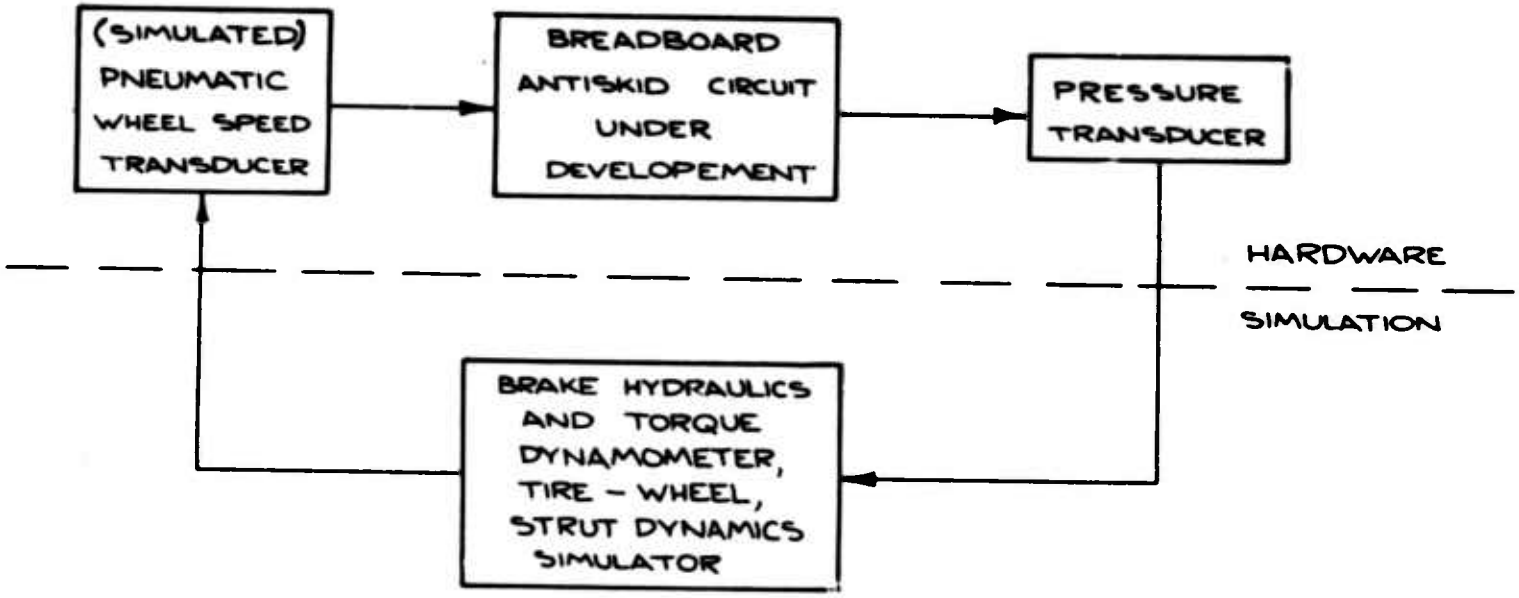


$$G = \frac{\Delta P_O}{\Delta P_I}$$



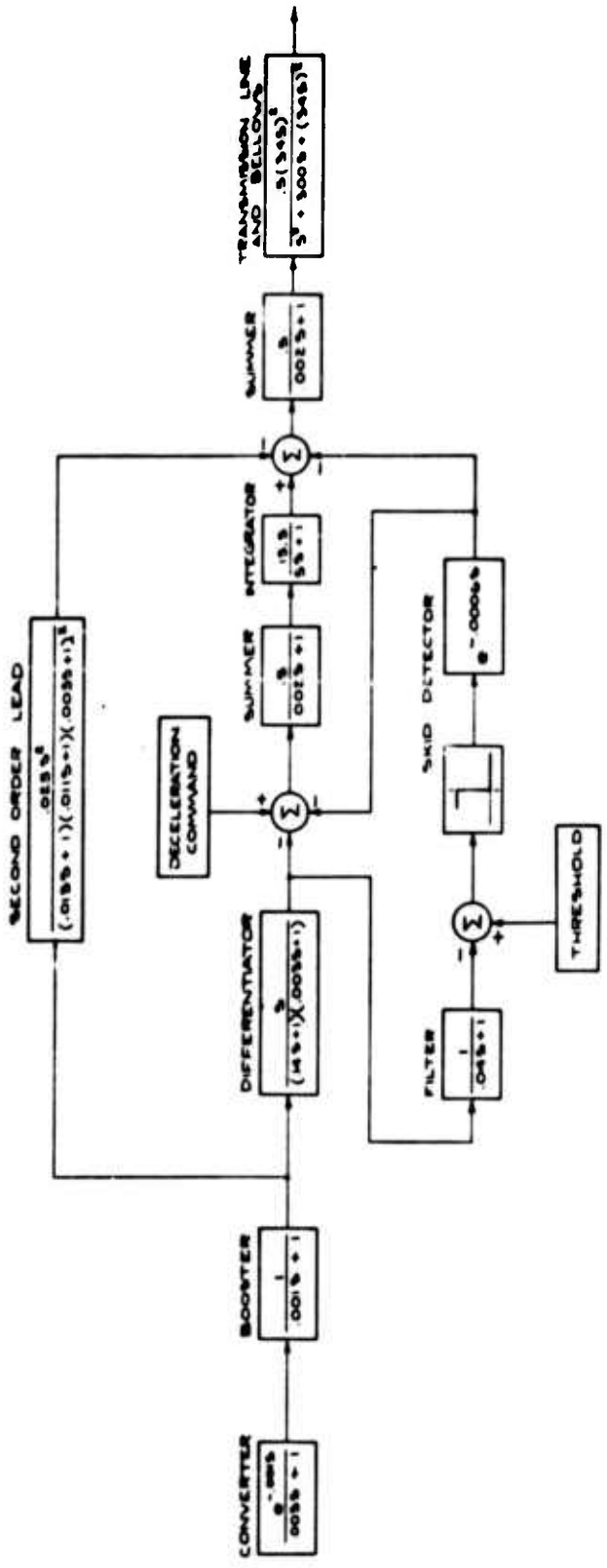
FLUIDIC LAG CIRCUIT

FIGURE 12



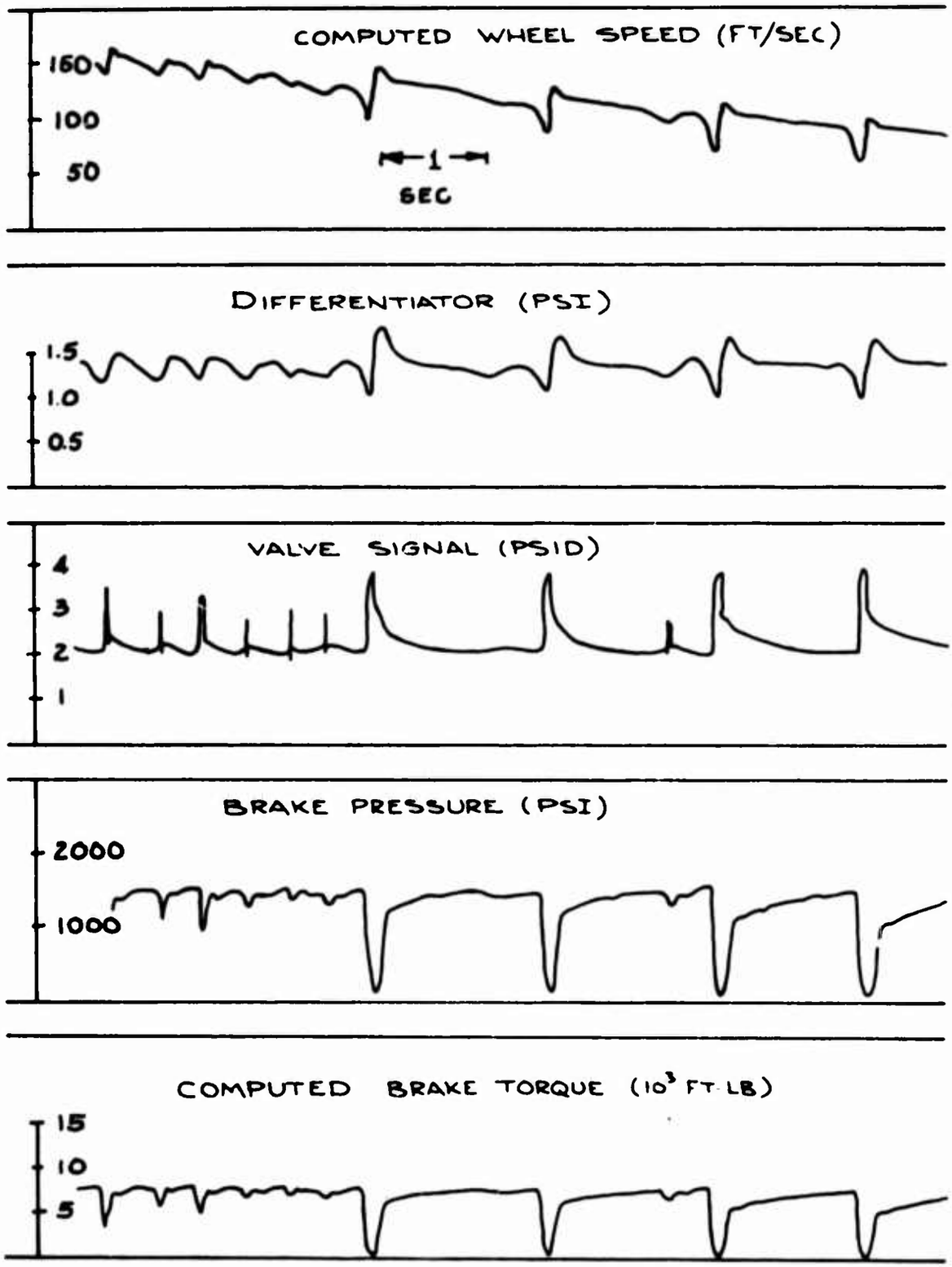
BREADBOARD DEVELOPMENT APPROACH

FIGURE 13

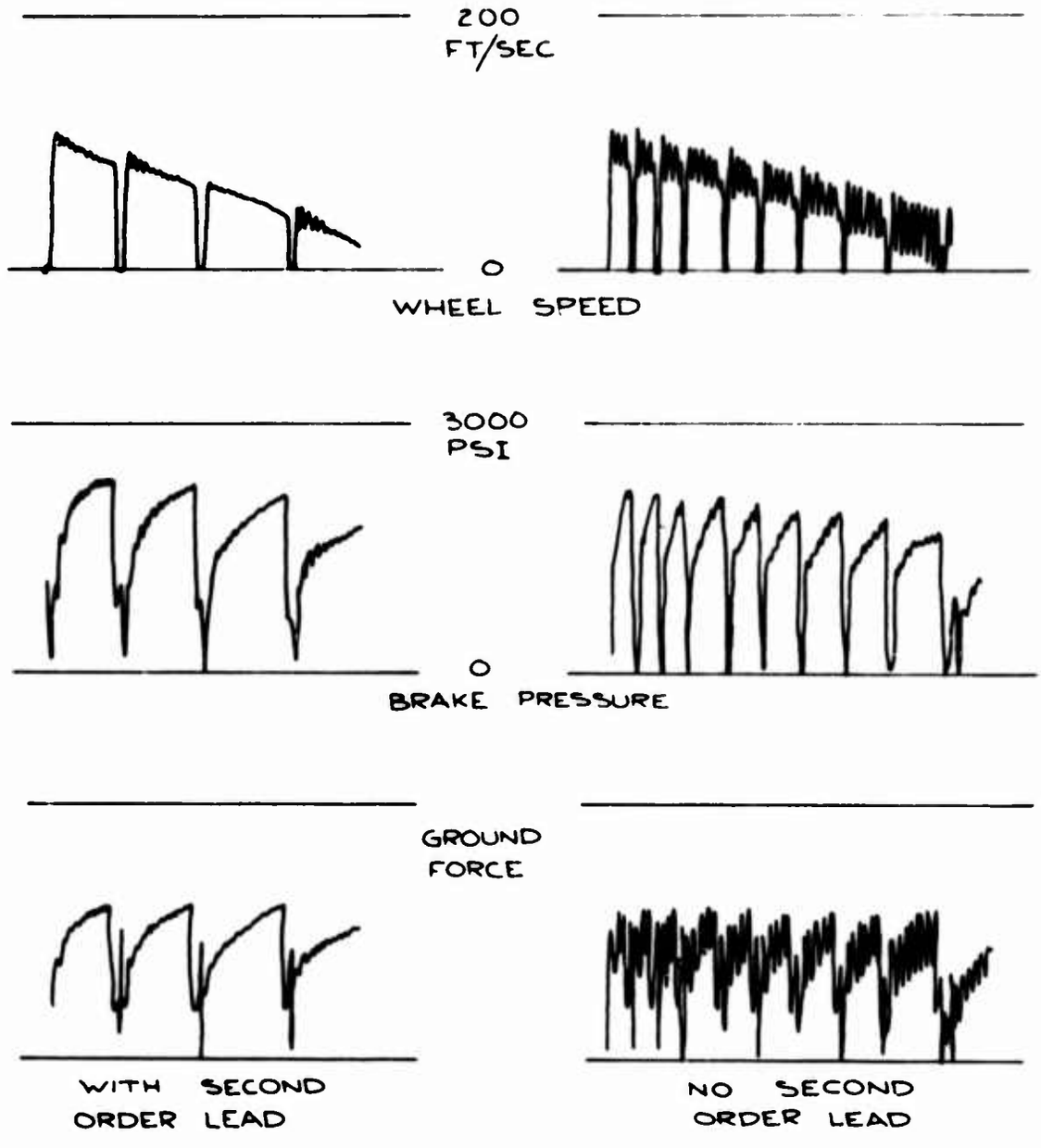


TRANSFER FUNCTION DIAGRAM

FIGURE 14

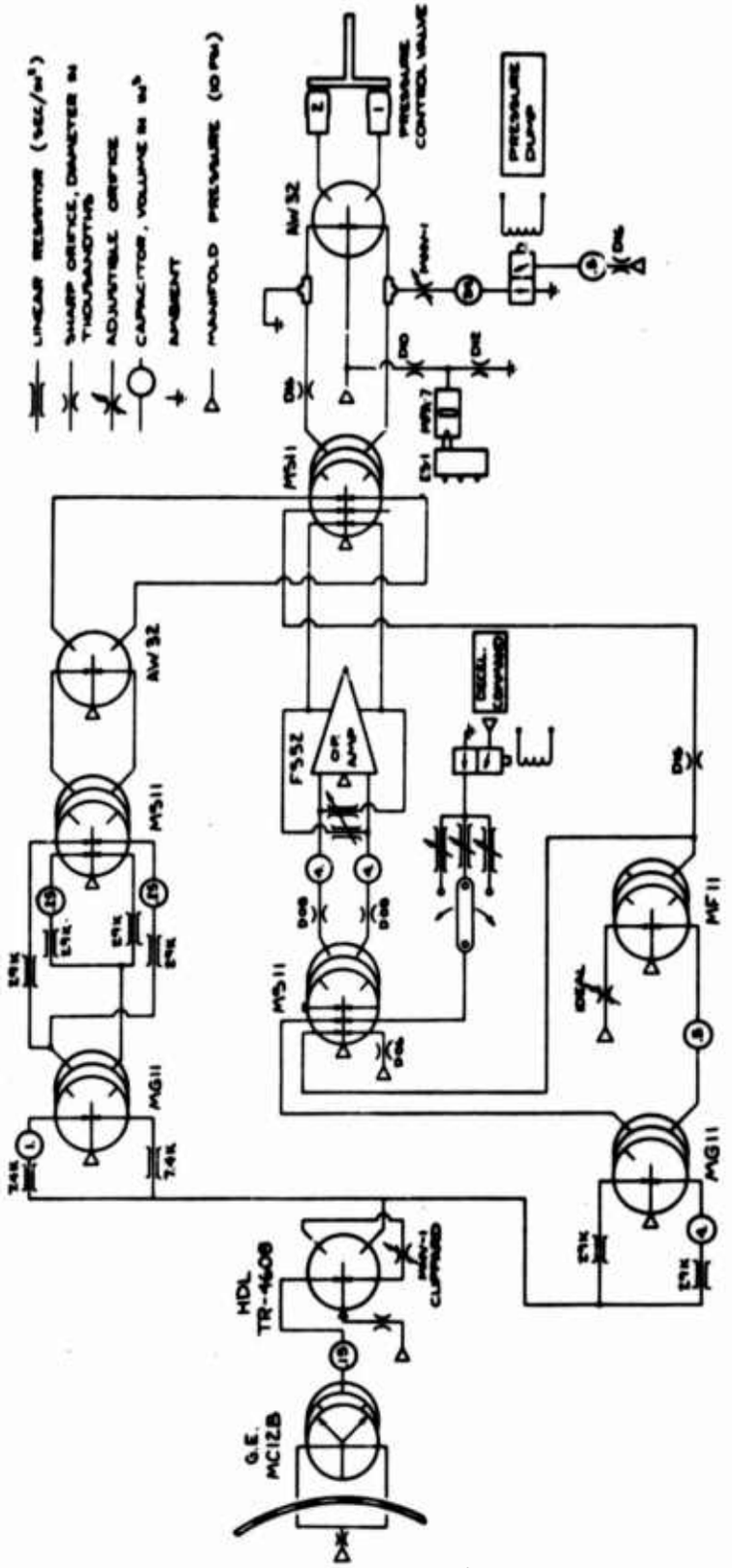


DYNAMOMETER SIMULATION
FIGURE 15



STABILITY TEST
WITH SIMPLE STRUT SIMULATION

FIGURE 16



FLUIDIC ANTISKID CIRCUIT

FIGURE 17

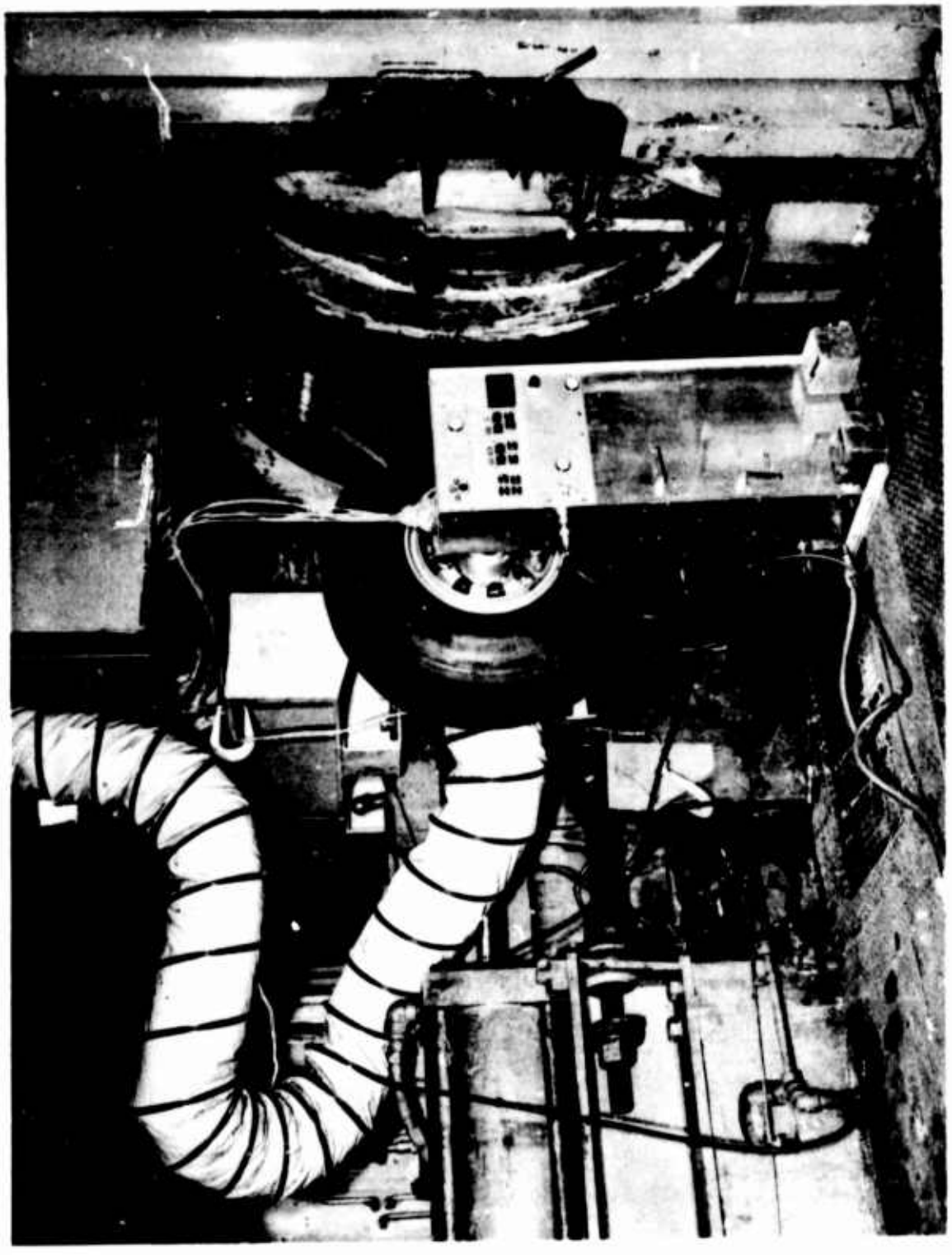


FIGURE 18 DYNAMOMETER TEST HARDWARE

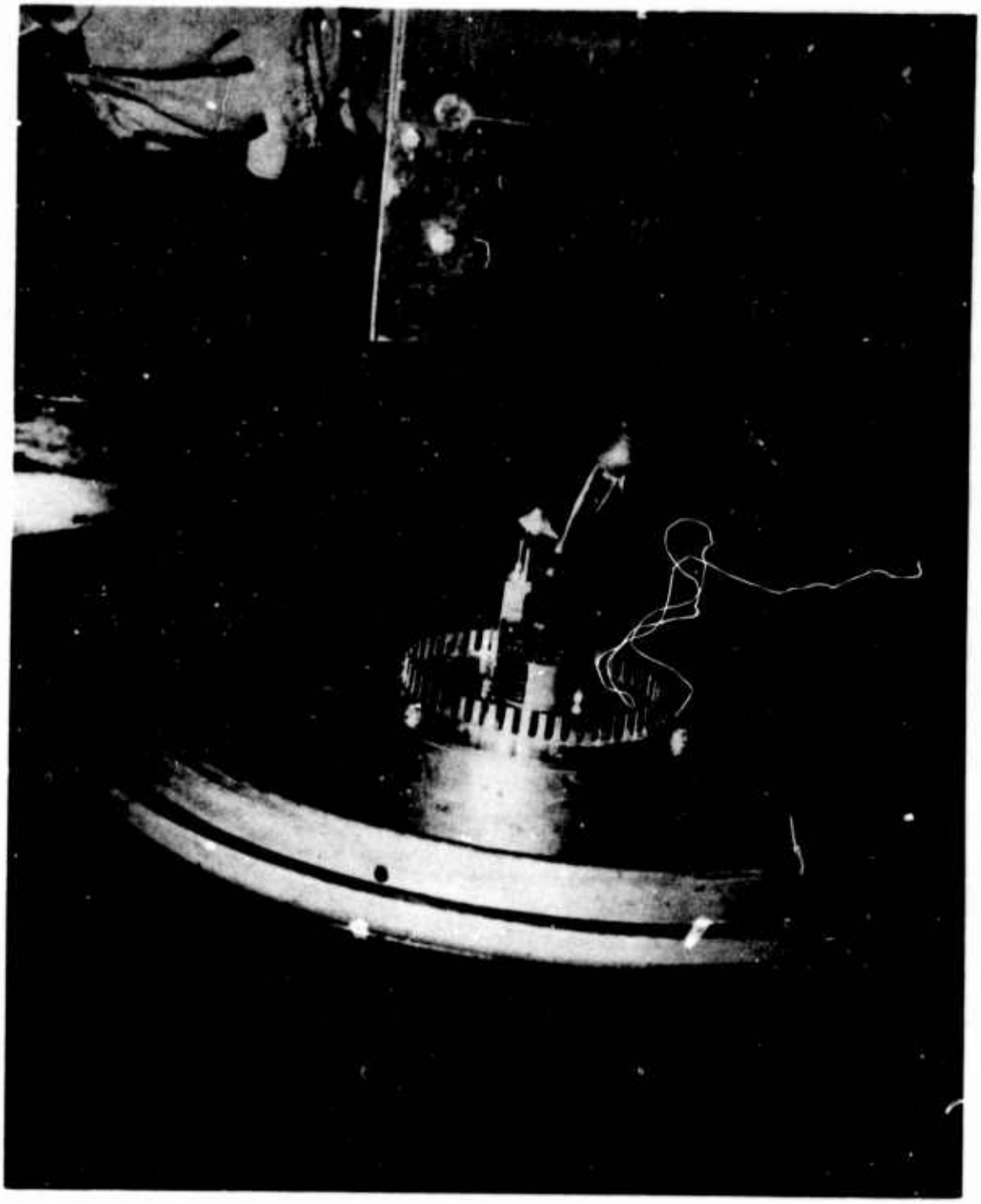
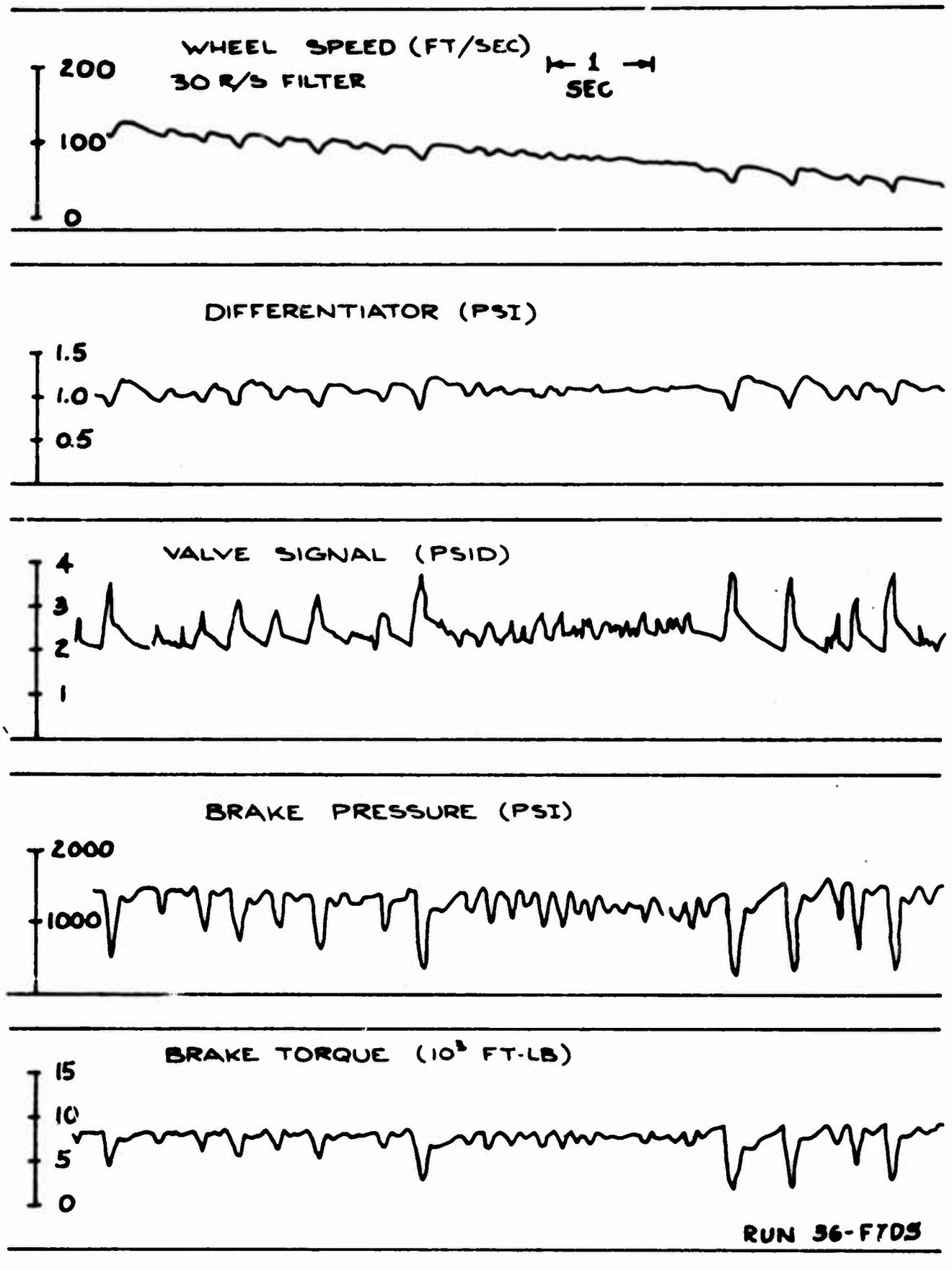


FIGURE 19 WHEEL SPEED SENSOR INSTALLATION



DYNAMOMETER TEST

FIGURE 20

SURVEY OF FLUIDIC ANTI-SKID SYSTEMS

by

Stephen M. Tenney
Harry Diamond Laboratories

ABSTRACT:

A survey has been conducted of the state-of-the-art of fluidic anti-skid systems. The results compiled indicate the fluidic approach to be feasible for essentially every mode of travel that involves the braking of wheels. Approaches to the development of fluidic anti-skid systems that have been considered are acceleration-control and slip-control, and a combination of the two is included. This paper lists the manufacturers known to be involved in this development, and summarizes the approaches and results attained.

The comments on the various systems reported herein have been summarized from the referenced reports or from personal communication with the system designer, and do not necessarily reflect the position of the Harry Diamond Laboratories.

Preceding page blank

1. INTRODUCTION

In virtually every mode of travel that involves the braking of wheels, the capability must exist for the vehicle to be be decelerated smoothly and without loss of control. This is especially important in emergency situations or when the road surface is not conducive to achieving the ideal maximum vehicle deceleration. In such conditions, the operator is required to control the brakes so that wheel lockup does not occur and also to keep the vehicle in a stable attitude such that vehicle control is not lost. In order to accomplish this the operator must be able to sense wheel lockup and release the brake pressure accordingly. He must also sense and correct for vehicular rotation. The changes in vehicular stability are not always easily sensed and corrected in time. In the case of a panic or emergency stop or in the case of large vehicles (trucks, aircraft) where the operator cannot sense that wheels have locked, an automatic control system is needed. Thus, the operator would have complete control for normal stops, and could stop at the maximum allowable rate of vehicle deceleration in an emergency situation. The system must also automatically adapt to variations in the frictional coefficient (μ) between the wheels and the road surface and the condition of tires and brakes in order to stop the vehicle in the minimum time and distance.

Since braking systems normally utilize fluid power, fluidic circuitry may provide an advantageous approach to the problem. This paper is therefore concerned with a survey of the state-of-the-art in fluidic anti-skid systems in order to point out the practicality of these systems.

2. DISCUSSION

Two basic approaches to the problem of anti-skid systems are wheel acceleration-control and slip-control. In acceleration-control systems, wheel deceleration is computed and compared with some maximum allowable value. If this value is exceeded at one of the wheels, the braking pressure to that wheel is removed until its deceleration rate is below the maximum value. The brakes are then reapplied. In slip-control systems, individual wheel speed is compared with a computed average of all wheel speeds and the braking pressure is released when a certain difference between the two is detected. The brakes are then reapplied when this difference is decreased to an acceptable value.

Under any given set of conditions the stopping distance will be minimized if the value of μ is at a maximum. Figure 1 shows, that in order to get maximum frictional coefficient (μ), the control system must allow some wheel slippage. The control system must therefore be designed to seek this maximum value of μ regardless of the conditions present at the wheels. The work documented in this field is summarized in table 1.

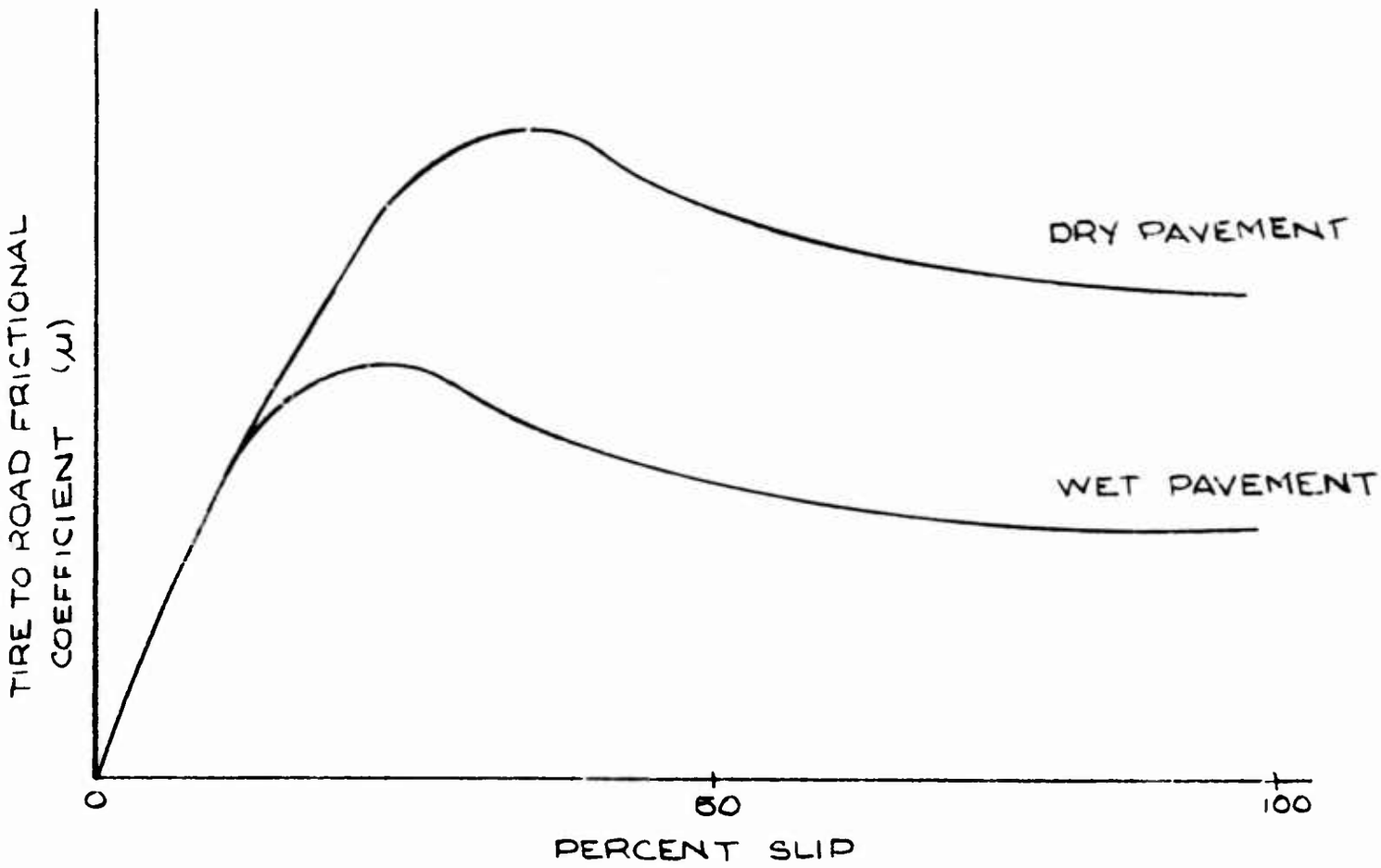


FIG. 1 SLIP VERSUS FRICTIONAL COEFFICIENT (μ)

TABLE 1 -- SUMMARY OF ANTI-SKID SYSTEMS

INVESTIGATOR	WHEEL SPEED SENSOR	TYPE CIRCUIT	BRAKE-PRESS. REGULATION	MATH OR COMP. ANAL.	NOTES*
BENDIX	Electro-Mag. Pulsed.	NOT FLUIDIC, electronic, accel. control. Slip control not feasible in their opinion.	Power brake units, Solenoids not fast enough.	Yes	Represents electronic approach. Hardware tested.
GRUMMAN	D.C. tach drives torque motor flapper.	Electronic-Fluidic Hybrid. Accel.-slip control	Valve	Yes	Recommends feasibility, no hardware.
OKLA. STATE UNIV FOR G. D.	Vortex Rate Sensor.	Fluidic Accel. control, diode-time delay differentiator drives Schmitt trigger.	Relay	Yes	Analysis only.
GENERAL ELECTRIC #1	No Hardware	No Hardware	No Hardware	Computer Analysis to check sensitive parameters.	Preliminary study to convince of feasibility. Curves show success. No specific circuit components suggested but would be fluidic.
BOEING	Interruptible Jet. Frequency to Analog converter.	Fluidic Two parallel paths acceleration & slip control. Pneumatic circuit drives hydraulic control valve.	Electro-hydraulic control valve modified for low press. pneumatic signal. Bellows Repl. Coil.	Yes Circuit transfer function.	Vortex rate sensor too noisy-low signal. Air cons. 4.0scfm. No Tech Problems, Hardware tested.
GENERAL DYNAMICS #1	Air bearing pressure drop due to shaft rot.	Fluidic Bang-bang. Rate of change of wheel speed switches Schmitt trig. at threshold, oscillates at slip. All fluidic-pneumatic.	All Pneumatic.	None	Worked extremely well. Needs to be adapted to hydraulics.
#2	later tried pulsed & Frequency to Analog converter.	Hunts for optimum s. All fluidic-pneumatic. Completely adaptive.	Pneumatic Proportional Valve.	None	Only slight improvement. Does not justify cost.
POLITECNICO	Toothed disc. & back press. switch drive pneu. step motors which drive planet. gear. No slip-gear stationary.	Fluidic-Mechanical Slip-control. Digital Second circuit monitors speed & dir. of rot. of planet. gear.	Valve	None	Hardware tested. Air Consumption, 1.5 LPS (3.17Gscfm)
GENERAL ELECTRIC #2	Electronic	Electronic	Electro.-Hydr. Transd. Interface Elec. with Brakes.	None	Torque Motor-Jet Deflection controlled by elec.
GENERAL ELECTRIC #3	Interruptible Jet. Pneumatic.	Indicates selected speed pts. to traction windings. Frequency to Analog converter. Average speed compared to individual. Wheel slip drops sand on tracks.	Tranction Motor Windings.	None	Met all requirements but temp. sens. All pneu.- for locomotives.

*NOTES-Abbreviated reported conclusion or from personal communication with the investigator.

3. FEASIBILITY STUDIES

The electronic approach by Bendix [1] is considered here because the systems analysis approach is useful in its overall view of the problem. The computer simulation discussed by Bendix is helpful, since the basic circuit functions are similar in an electronic or fluidic circuit. Bendix has made some design decisions that are very pertinent and should be considered by the fluidic designer. Points raised by Bendix include the advantage of vacuum power-brake units over solenoids as the brake modulators due to the improved response. The best and most versatile system is that which controls all wheels individually; such a feature would allow the shortest possible stopping distance while maintaining "steerability." Other circuitry and wheel speed selection schemes are also discussed here. Contrary to the Bendix report, a slip-control circuit is considered less difficult than was indicated. Other work included here demonstrates that slip-control may be effectively accomplished.

A study was conducted by Grumman Aerospace Corporation [2] to investigate advantages of a fluidic anti-skid system and to suggest an actual circuit. Although no hardware was tested, feasibility of the concept of employing a combination of acceleration and slip-control is indicated. The major difference is that this concept uses a speed sensor consisting of an electronic tachometer to drive a torque motor flapper valve. Differentiation is accomplished fluidically while wheel speed is monitored for slip. A valuable concept suggested is the comparison of average wheel speed to each individual wheel speed. If the speed is different by a certain percent, the brake pressure is released. This should prevent wheel lockup.

A computer study done for General Dynamics by Oklahoma State University [3] suggests a system that uses an acceleration-control approach and a vortex rate sensor wheel speed sensor. Although no hardware was tested, the computer analysis indicates the system to be very promising.

General Electric has also modeled a fluidic anti-skid system for computer analysis [4]. This system was applicable to trucks. No technical problems were encountered, and the circuit is believed to be easily implemented.

4. DEVELOPED SYSTEMS

Of all the fluidic anti-skid systems investigated, the types of circuits are evenly distributed among acceleration-control, slip-control, and a combination of the two. There is generally no preference for one solution over another. Considering all the work done in this respect, it appears that Boeing [5] has the most developed system. Their system is a combination acceleration and slip-control system that also combines pneumatics and hydraulics. Speed is sensed through an interruptible pneumatic jet, chopper wheel, and a frequency to analog converter. The system uses a differentiating-type circuit that also monitors wheel slip. The actual brake modulation is accomplished through the use of a control valve that allows the low-pressure pneumatics to control the high-pressure

hydraulics. Since the system was designed for aircraft, air and hydraulic power supplies are available. Computer analysis, as well as actual testing, shows this system to be very practical.

Of the other work considered, the system developed by General Dynamics/Ft. Worth [6-8] appears to have been the one most thoroughly investigated, and it is all fluidic (pneumatic). This development has undergone extensive testing but has not been put into production. Two circuits have been built and tested; one is a bang-bang type (brakes oscillate at slip) and the other is adaptive. In either case, the hydrostatic pressure difference created by shaft rotation in an air bearing is used as a speed sensor.

The first system senses the rate of change of wheel speed by differentiation and modulates brake pressure when wheel deceleration exceeds a desired value. When any given wheel exceeds this value, the system releases the brake pressure to that wheel and immediately reapplies it, setting up an oscillation in the brakes. This concept was adapted from the electronic anti-skid system General Dynamics had in use. The fluidic system worked extremely well.

The second system investigated by General Dynamics is adaptive and has the most advanced circuitry of any of the anti-skid systems discussed in this paper. The system controls the brake pressure while hunting for the maximum value of the frictional coefficient (μ). It was felt, however, that the extra cost of the adaptive system makes it too expensive, considering the slight improvement realized over the bang-bang system.

Although both systems performed well, they still need adaptation to hydraulics in order to be utilized further in aircraft applications. The previously mentioned computer study conducted by Oklahoma State University analyses the General Dynamics system although it uses a different wheel speed sensor.

Although the majority of the systems discussed so far have been for application to aircraft, automotive applications are equally important. The only system we have found that is intended specifically for automotive use is that of Politecnico of Turin, Italy [9]. This system is also a very different approach from the others. The basic approach is that of slip-control but the system can best be described as fluidic-mechanical. It is the only entirely digital circuit of those surveyed. A pulsed speed signal (back-pressure switch chopper) is used to drive pneumatic stepping motors that drive a planetary gear. In a condition of no slip the planetary gear is still; when slip occurs the gear rotates. A second speed sensing circuit is required to monitor the planetary gear for sufficient speed and direction of rotation. In so doing, the second circuit determines the allowable slip and which brakes require modulation. Test results show that the system functions satisfactorily at an air consumption of 1.5 liters/sec (3.178 scfm).

General Electric (G.E.) has done a considerable amount of work in the area of anti-skid systems [4]. In addition to the previously discussed computer analysis for feasibility investigation in which no insurmountable problems were discovered, a transducer developed by G.E. would interface electronic circuitry with the hydraulic brakes. This is actually a torque motor. The most extensive work done by G.E. is in the area of locomotive anti-skid. In this case, pneumatic (interruptible jet chopper) speed sensors are used to sense speed points to control the traction windings of the locomotive. Threshold of the speed points are measured by using frequency-to-analog converters. The speeds are averaged to sense slip. Also, wheel slip in this case causes sand to be dropped on the tracks. A completed demonstrator showed feasibility and satisfied all functional requirements. This all-pneumatic circuit was found to be temperature sensitive and therefore requires further development.

5. CONCLUSIONS AND RECOMMENDATIONS

Sufficient work has been done to show that fluidic anti-skid systems are producible systems, not only for aircraft and locomotive but for automotive application as well. The technology of fluidics has thus been shown to be adaptable to the problem of brake control. It is significant that most of the work presented in this paper was done a few years ago. With improvements in the state-of-the-art, fluidic anti-skid systems should pose almost no problems in implementation today.

Given a federal requirement for anti-skid systems on trucks, there is a need for these devices. Since pneumatic power is available on trucks, use of fluidic anti-skid systems can be considered a desirable approach. Considering the environment that any anti-skid system will be exposed to and the dependence of human life on its operation, the design of such a system must be very thorough. The proven reliability and immunity to shock and vibration of fluidic circuitry makes their use advantageous for anti-skid systems.

6. LITERATURE CITED

1. Hickner, G. B., "Systems Approach to Adaptive Braking Design," Bendix Technical Journal, Vol. 2, No. 3, Autumn 1969, pp 1-14.

2. Brenner, W., Conway, T., and Cycon, M., Jr., "Fluidic Applications to Naval Aircraft," Prepared for Naval Air Systems Command under Contract N62269-71-C-0417 by Grumman Aerospace Corporation, June 1972.

3. Lewellen, M., Hullender, D., and Orloski, E., "General Dynamics' Fluidic Anti-Skid Braking System," School of Mechanical Engineering, Oklahoma State University Research Report, 15 May 1967.

4. Stern, H., General Electric Company, personal communications, 5 Dec 73.

5. Straub, H. H. and Wagner, P. M., "A Fluidic Brake Control System," to be published in the HDL Symposium Proceedings, Sept 1974.

6. Rowell, W. M., Jr., General Dynamics/Fort Worth Division, personal communication, 26 Mar 1974.

7. Rowell, W. M., Jr. and Bose, R. E., "Fluidic Skid Control System," Internal Research Report No. ERR-FW-631, General Dynamics/Fort Worth Division, 13 Dec 1967.

8. Rowell, W. M., Jr. and Bose, R. E., "Fluidic Systems Development: 1969-1970," Internal Research Report No. ERR-FW-1022, General Dynamics/Fort Worth Division, 21 Aug 1970.

9. Romiti, A. and Belforte, G., "Fluidic-Pneumatic Anti-Skid System for Cars," 2nd IFAC Symposium on Fluidics, paper E7, Prague, Czechoslovakia, 1971.

ACKNOWLEDGEMENTS

The author wishes to express his thanks to the following individuals: H. Stern of General Electric Company, W. M. Rowell, Jr. of General Dynamics/ Ft. Worth, and A. Seleno of Bendix Corporation for compiling the results of the work done by their respective companies.

Also, the author acknowledges the assistance of Dr. Robert L. Woods, HDL Staff member, for suggesting the topic of this paper, for gathering the reports presented, and for giving his general encouragement.

A FLUIDICALLY CONTROLLED BAG MANUFACTURING MACHINE FOR 105 MM HOWITZER PROPELLANT CHARGES

David E. Scesney
Equipment Engineer
Corning Glass Works
Corning, New York

Preceding page blank

1. Introduction

One phase of the modernization program at the Indiana Army Ammunition Plant is to automate the production of cloth bags used for the 105 MM Howitzer propellant charge. The bags are 4-1/2" wide by 5-1/2", 10" or 13" in length, with a bottom closure seam sewn at an 8^{o} angle. To insure compatibility with subsequent automated loading and weighing equipment the bag length must be held within $\pm$ 1/8" while the width must be held within $\pm$ 1/16". It is required that each bag be marked to identify the type and size of bag produced. For optimum utilization of equipment when the bag sewing machine is integrated into a total loading system the production rate is required to be 50 bags per minute of the 5-1/2" long bag. The bags are made from 9" wide resin impregnated rayon cloth wound on a 35 pound roll.

The Bag Manufacturing Machine designed for this program utilizes 100% digital fluidic logic control. Fluidic elements used are standard, off-the-shelf components fabricated using photo etched glass ceramic techniques. There are approximately 130 discrete fluidic elements mounted on glass ceramic interconnection manifolds. These manifolds are contained in two control enclosures which maintain a slight positive internal pressure to prevent atmospheric contaminants from entering the logic elements. (Figure 1) The Bag Manufacturing Machine has a self-contained filtration-regulator system to provide 80 psi air to the pneumatic machine actuation cylinders and 5 psi air to the fluidic logic circuits. Filtration of particles to 0.5 micron enables the machine to operate directly from 100 psi shop air. Air consumption is approximately 35 scfm.

The interface between the fluidic control signal and the high pressure pneumatics are diaphragm

poppet valves mounted on a common supply manifold. A pressure to electric switch is interlocked with the electric motor circuit to turn it off if air pressure is lost or on operator command.

2. Why Fluidics

There are several reasons why fluidics were chosen for this system and why they offer advantages over other methods.

Fluidic controls have been used in the garment industry with favorable results for many years. It provides a reliable method for non-contact sensing of fabrics through low pressure interruptible air jet sensors on a variety of garment manufacturing machines. These machines usually require simple machine control in the millisecond speed range with more complex logic functions added on as in the case of the Bag Manufacturing Machine. These functions are easily and flexibly implemented with fluidics. Since these machines are mostly pneumatically actuated, fluidics allows the use of simple, reliable interfaces between control and machine.

The explosion proof qualities of fluidics are not a requirement here since the Bag Manufacturing Machines are to be used in an inert area.

As of this writing two machines of a total of 35 have been built and delivered to the customer. The first of these has undergone preproduction testing consisting of 30 days operation at 8 hours per day with no fluidic failures. This is part of a continuing testing program with more data to be added as subsequent machines begin to accumulate running time.

3. Machine Description

The following is a brief description of the machine. Basically the Bag Manufacturing Machine takes cloth

from a 9" wide roll of material, folds it in half and sews the folded edges together to form a continuous tube. It then cuts the tube to the proper length and sews across one end to form the bag bottom.

Returning to the front of the machine for a more detailed description, a continuously turning rubber roller pulls cloth from the material roll and supplies it on demand to the folder. (Figure 2) The folder is adjustable in two directions to provide exact edge match and proper positioning of the seam from the folded edge. A belt system pulls the folded cloth under the straight sewing machine and feeds it continuously into an accumulator. (Figure 3)

The accumulator provides a buffer between the continuously running straight sew and the stop and go movement through the bag length cutter position. The cloth tube is pulled from the accumulator to the desired bag length by two rubber rollers driven through a clutch/brake system. When the cloth stops to be cut it is simultaneously printed.

The cut bag is then transferred sideways at an 8° angle by the cross sew belt system (Figure 4). The cross sew sewing machine operated intermittently through a clutch/brake system as bags are supplied to it from the cutter position.

4. Machine Control

Five sensors provide for control of machine functions and sequencing. These sensors are of the interruptible air jet type. They, along with several operator controls, are interfaced with the machine through the logic circuitry. In the manual mode of operation, the circuits associated with several of these sensors are inhibited to allow the operator to run each section of the machine independently.

The five sensors are:

A. Accumulator empty and accumulator full - sense the position of the accumulator roller and, through time delays, cause the roller to oscillate about the midpoint of its travel.

B. Bag length - A moveable sensor that determines bag length. When interrupted, the brake, cloth cutter and printer are actuated.

C. Bag transfer - determines when a bag has cleared the cloth cutter so more cloth can be brought out to be cut to length and also sets the space between bags moving in the cross sew belts. The upper half or transmitter can be seen in Figure 5 while the receiver is visible through the slot in the table.

D. Thread chain cut - activates the thread chain cutter knife to cut the thread between bags moving in the cross sew belts.

These sensors are operated at a reduced pressure of 1-2 psi where cloth deflection by the air jet is a problem. A typical sensor circuit is shown in Figure 6.

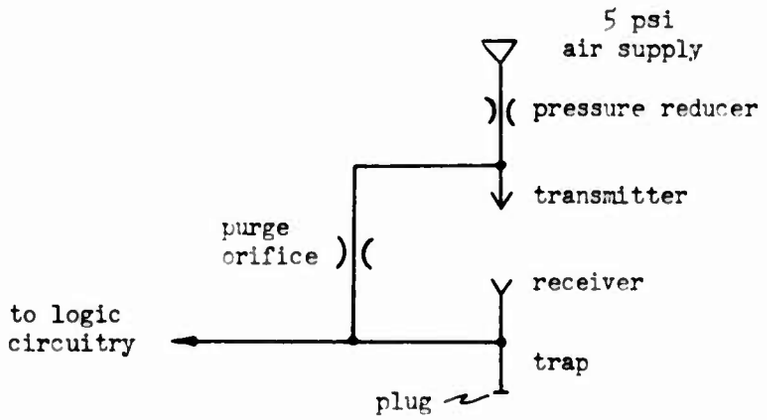


Figure 6 Interruptible Jet Sensor Circuit

The major contaminant on the Bag Manufacturing Machine is lint. As long as the sensor is interrupted by cloth or a machine member, the purge air tends to prevent lint and particles from entering the receiver port. The trap shown in Figure 6 is used on interruptible jet sensors with a straight through configuration to catch some of the heavier dust and lint particles which may enter the receiver when the sensor becomes uninterrupted.

5. Control Features

The Bag Manufacturing Machine has been designed to prevent defective bags from appearing at the output of the machine. This is done through automatic detection and removal devices so that there is minimum disruption of the flow of acceptable bags at the output. The reject conditions are caused by defects in the cloth supply or thread, machine malfunctions or misadjustments and the exhaustion of cloth and thread supply. These conditions and corrective measures taken are described in the following paragraphs.

The cloth roll contains splices in its length that are not acceptable in a finished bag. Normally the roll lasts for approximately 2-3 hours of running. If the thread breaks due to knots or if it runs out, bags would be produced with missing stitches. Folder misadjustment or drastic variations in cloth width will result in a mismatch of the folded edge with an open seam in the worst case. Finally the bag length could exceed the maximum length specified.

The sensors used to detect the above conditions utilize both interruptible air jets and back pressure sensing. Automatic removal of defective bags is accomplished through a high pressure air jet, tied in to the logic circuitry, that blows bags off after they have been cut by the cloth tube cutter. If the machine must stop for operator attention, a fluidic visual indicator turns red indicating the corrective action required such as cloth roll empty, thread break, etc.

The cloth roll empty and thread break sensors cause the machine to stop. Empty cloth roll is detected by an interruptible air jet while the thread break sensor uses back pressure sensing. The thread, normally under tension, holds up a wire loop. When the thread breaks the tension is released allowing the wire loop to drop and close off a back pressure sensing port.

A folded edge mismatch will widen the cloth tube, interrupting an air jet sensor. This activates a pneumatic device to cut a notch in the edge of the cloth. The notch is then detected by a second interruptible air jet sensor near the cloth tube cutter. Through a two-stage shift register, clocked by the cutter operation, the next two bags are blown off the machine.

Cloth splices are detected just ahead of the cloth tube cutter by the sensor shown in Figure 7. A thickness of 10 thousandths or greater over normal cloth thickness passing under the roller wheel will raise the lever arm approximately 50 thousandths off of a back pressure sensing port. This activates the reject blow off circuitry to remove the next two bags to insure that the bag containing the splice is ejected.

Over length bags are detected by an interruptible air jet sensor. When interrupted it activates the reject blow off circuitry to remove one bag from the machine.

6. Conclusion

Fluidics is now beyond the laboratory stage and is used in many applications ranging from simple sensing and gaging functions to sophisticated automated systems controls.

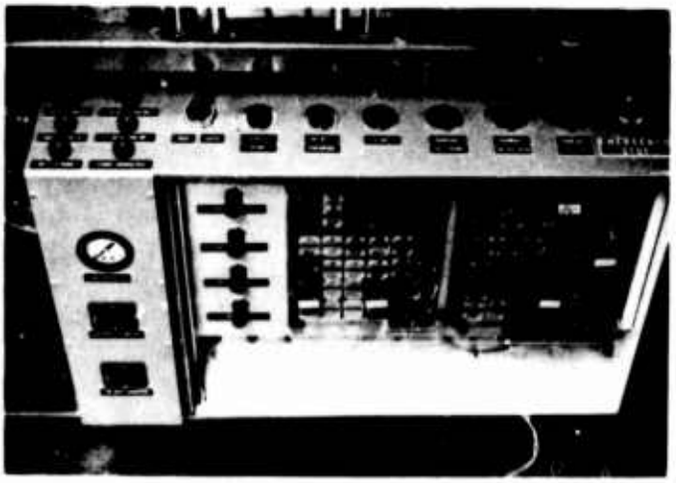


Figure 1. Fluidic Control Enclosure



Figure 2. Folder



Figure 3. Accumulator

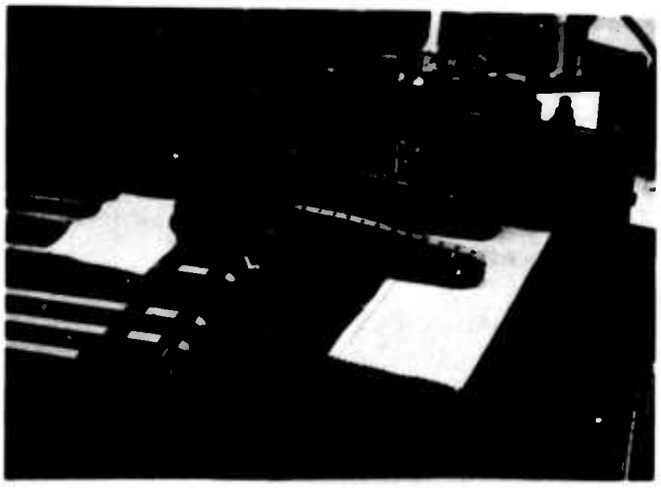


Figure 4. Cross Sew

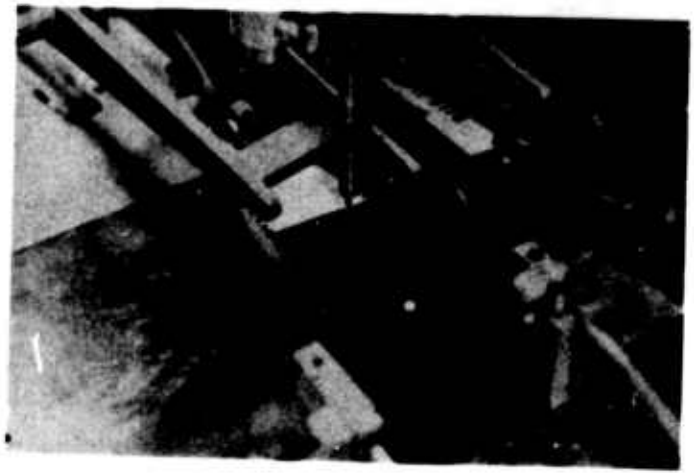


Figure 5. Bag Transfer Sensor



Figure 7. Splice Detector

MILITARY APPLICATIONS IN FLUIDICS

By

R. N. GOTTRON

L. S. COX

HARRY DIAMOND LABORATORIES

Washington, D. C. 20438

ABSTRACT

US Army programs in fluidics are discussed with brief descriptions of current system applications along with present government efforts in fabrication and reliability.

MILITARY APPLICATIONS IN FLUIDICS

R. N. Gottron

L. S. Cox

1. INTRODUCTION

Numerous fluidic systems are being developed for the military covering the gamut from high-performance weapon system controls to munition production line controls. Five USAMC commodity commands and several Army laboratories are engaged in these efforts with the Navy, Air Force, and other government agencies.

The technical problems involved in military applications differ from those encountered in commercial usage in system size and operating temperatures and pressures. Military systems generally must be light- and must consume very little power. Consequently, the military has concentrated on developing miniature components and on the consequent problems of fabrication and power supply contamination. These problems have been solved to the extent that widespread application of the technology to military systems now appears possible. A previous study describes numerous potential military applications (ref. 1) that might make advantageous use of currently available fluidics technology. The same study lists many other potential applications that would require only minor advances in the technology. Some current and recently completed contractual efforts (table I) indicate the extent of current military and NASA interest when one realizes that the contracts are generally directed toward hardware development.

2. ARMY FLUIDIC FUNDING

The trend of Army expenditures in the field of fluidics from its inception in the late 1950's to 1973 is shown in figure 1. There are two periods during which expenditures increased significantly. The first was after the initial conception of fluidics when Army expenditures increased to slightly over 2.5 million dollars in fiscal year 1962. Expenditures then leveled off and even decreased slightly in the mid-1960's as people realized that fluidics was an easy concept to understand but indeed very difficult to apply. Hence, a considerable amount of the effort from 1962 to 1968 involved the establishment of a broad research base. The second significant increase in expenditures occurred from 1970 to 1973. This increase can be attributed to system applications going beyond exploratory development and into advanced and engineering development. Table II itemizes the estimated Army program for fiscal year 1973. The funds for exploratory development are divided into two categories; one, for funds that flow through the Harry Diamond Laboratories as lead laboratory to the various commodity

commands, and the other for additional funds that the various commodity commands use to support the technology. The total funding in table II is greater than figure 1 since the contractual efforts include ancillary equipment and other non-fluidic expenditures.

3. ARMY APPLICATIONS

The Army, as previously mentioned, is undertaking a wide variety of fluidic projects, and the various organizations are making presentations at this symposium. Thus, a few of these projects are described here briefly, primarily to illustrate the variety and extent of the Army fluidics program.

3.1 Mortar Repositioning (Watervliet Arsenal)

The mission of Watervliet Arsenal is tube weapons including guns, mortars, and recoilless rifles. In particular, Watervliet has developed a mortar with a fluidic system to reset the azimuth and elevation after each shot. This eliminates variations in aim that heretofore have limited the accuracy and/or rate of fire and prevented the use of the mortar for point as opposed to area targets. This concept of repositioning the tube can be applied to any tube weapon for which an attitude reference can be maintained.

U. S. mortars have always used the tube resting on the baseplate with an adjustable bipod to form a tripod for positioning. The soil under the baseplate compresses, rebounds, and flows on absorbing recoil energy. The baseplate therefore shifts from shot to shot, which shifts the aim, unless the gunner adjusts the bipod. In the mortar repositioning system, the attitude reference is maintained on a tripod which does not include the baseplate. Angular position comparators based upon a cam (attached to the tube) rotating in a sleeve (attached to the tripod) with back pressure sensors are used to detect differences between the elevation and azimuth of the mortar and reference. These signals, when amplified by interface valves, drive actuators that reposition the mortar tube until the differences are reduced to the sensor/logic threshold level. The power supply can be stored gas or propellant gases tapped from the mortar tube.

A 60-mm mortar with a working model of this system has been fired successfully. The automatic repositioning was performed in approximately 1 to 2 sec, depending on the displacement due to the shot; whereas, a highly trained gunner takes at least seven sec. Test firings of the prototype system using the 60-mm mortar demonstrated repositioning accuracy of 1.5 mils in azimuth and $\pm$ 3 mils in elevation (ref. 2). The Benet Laboratory is presently integrating the system for use with an 81-mm mortar so that the tubing shown in figure 2 is eiliminated.

3.2 Fluidic Generator (HDL):

A device that converts pneumatic energy into a significant amount of electrical energy is being investigated at Harry Diamond Laboratories (HDL) for possible use in fuzing systems. The device, called a fluidic generator (ref. 3), introduces a new fuzing principle, a new power supply, and a new safing and arming signature. These innovations promise improvements in safety and reliability, especially for systems with no spin and only small setback forces, such as mortar shells and rockets.

The generator (fig. 3), when used as a power supply in a projectile or missile, obtains its driving energy from ram air through an opening in the nose of the shell. The air, after passing through an annular nozzle, generates acoustic energy via an oscillating jet impinging on a resonating cavity. The acoustic energy drives a metal diaphragm at resonance. A reed attached to the diaphragm is driven to modulate magnetic flux in a coil. This generates an emf in the coil. The output voltage, depending on its use and the velocity of the air, is then rectified, regulated, or amplified before utilization in a fuze. The generator can be operated in the subsonic and supersonic flow regimes and can produce up to 6 W of electrical power. The generator's function is not restricted to use as a power source. A linear relationship between output voltage and velocity can be achieved. Integration of the output voltage provides a measurement of distance traveled by a round or an aircraft. Thus the use of complex timing systems can be eliminated.

Increased safety in armament systems aboard aircraft can be achieved by adding a fluidic generator to the present system. By utilizing the aircraft velocity to provide ram-air pressure, it is possible to obtain electrical energy to fire the armament but only when a prescribed minimum air velocity has been achieved. The firing circuit remains inactive whenever the aircraft is on the ground. Only after the aircraft is airborne and reaches a specified minimum velocity will the system become active and generate the energy required to fire the weapon. This concept was employed in developing the fluidic generator for the Navy's SUU dispenser system (fig. 4). The SUU system is now undergoing fleet evaluation.

The fluidic generator was also developed to meet the requirements of a fluidic-electronic-mechanical point-detonating fuze (fig. 5). In this application, the fluidic generator provided an arming signature (ram air pressure), and the power to initiate the explosive actuators in the safety and arming mechanism rotor assembly. Also, it provided a fuze backup function, as interruption of airflow at impact triggers a function-on-generator-stop circuit thereby setting off the electric detonators. This circuit is primarily intended to destroy the round if the fuze fails to function at impact.

Another type of generator was developed for the Advanced Beehive fuze. This generator (fig. 6) is much smaller than others since the connecting rod and reed mechanisms were eliminated by using the diaphragm to modulate the magnetic field. Although smaller and more rugged, it produces only about 20 percent of the power obtainable from the larger reed-type devices.

3.3 Gas Turbine Control (TACOM)

The US Army Tank-Automotive Command (TACOM) has been investigating fluidic control techniques for the automotive gas turbine 1500-horsepower engine (AGT 1500). The first effort was an investigation to demonstrate feasibility of fluidic temperature sensing and control of stator vanes to increase engine economy. The AGT 1500 engine (fig. 7) has stator vanes presently prescheduled to hold the turbine inlet temperature (T_5) constant. The hydromechanical control system degraded with time and computed T_5 from other variables. TACOM instituted work to fluidically measure T_5 directly for feedback control of the stator vanes. Fluidics was chosen for this task since T_5 was greater than 2000°F, and electronic control was not desirable because of electromagnetic interference.

The fluidic sensor was a jet-edge resonator oscillator that was inserted at T_5, and the hot gas passed directly through the sensor, which reduced response time and size over what could be obtained by removing the sensor to the end of a bleed intake. The sensor and the beat detection fluidic control system (fig. 8) used off-the-shelf components in the feasibility study.

Laboratory and engine tests were conducted on the fluidic temperature sensor. Laboratory tests of the fluidic temperature control loop were successful up to the maximum temperature capability (1000°F) of the test facility. The sensor performed satisfactorily in the AGT 1500 engine for several hours, but scaling caused the sensor to fail. The sensor material could not withstand the high temperatures in the turbine, and a change in material is necessary if this approach is to be pursued.

3.4 Plant Modernization

Several years ago, the Army initiated projects to modernize their munition production lines, and the use of fluidics in sensing and control in munition production lines is now widespread. Numerous articles and papers describing some of these applications appear in the literature (ref. 4, 5, and 6). Some of the more interesting sensing capabilities developed at the Harry Diamond Laboratories (HDL) are as follows:

The Army had a problem in determining if the required number of holes had been drilled in a mortar tail cone. The usual procedure was

to visually count the 25 holes, but this was subject to human error. Figure 9 shows a fluidic sensing system that was developed at HDL to count these holes; an operator merely feeds tail cones to the machine, and the inspection is automatic. The sensing head is a modified impact modulator. The fluidic system consists of a series of threshold level detectors, sequencing circuits, and reject indicators.

A fluidic primer-height sensor was developed for use with an artillery-shell primer remover and replacer machine at Tooele Army Depot (ref. 7). The system (fig. 10) can reliably detect 0.001-in. variations in the height of an artillery shell primer and demonstrates the relative effectiveness and simplicity of utilizing fluidics for this inspection. The detection system eliminated the requirement for an operator to inspect each shell visually after a primer had been inserted, which made full machine automation possible and took the operator out of the hazardous area.

Another interesting development is the fluidic strain gage (ref. 8) for use in munition production; electronic strain gages are undesirable because of the danger of initiating explosions. The fluidic gage (fig. 11) uses the same principle of operation as its electronic counterpart; namely, the resistance changes with a change in length. In the fluidic strain gage, the channels can be small slots milled into the structural member or a tube welded on the member. Laboratory tests have shown that the fluidic gage sensitivity is about the same as the electronic gage. A fluidic gaging system is now being developed for munition production line applications.

3.5 Stability Augmentation System (AAMR&D LAB)

The Eustis Directorate of the U. S. Army Air Mobility Research and Development Laboratory at Fort Eustis, Virginia became interested in fluidics in the mid 1960's. Most of their work to date has been directed toward development of a hydrofluidic stability augmentation system (SAS) and autopilot development for helicopters. The purpose of these systems is to assist the helicopter pilot in maintaining an exact heading by minimizing wind gust effects and other external disturbances.

Before the Eustis Directorate became interested, very little work had been done on liquid-powered fluidic systems. Thus, a considerable amount of time was required on component and system development. Emphasis was placed on component characteristics leading to fluidic systems for which there were known requirements. Thus, component development led to a single-axis yaw damper for stabilizing a UH-1C test helicopter in 1968. A flight test of approximately ten hours demonstrated the feasibility of employing fluidics for helicopter stabilization. In addition to work on this system, the Eustis Directorate conducted a

small hydrofluidic reliability program at approximately the same time. The results of this program predicted an 83,000-hr mean time between failures. This was a reliability figure an order of magnitude larger than that of equivalent systems using other technologies and undoubtedly generated considerable interest in employing fluidics in aviation systems.

The second flight test conducted by Eustis was that of a three-axis SAS. Flight hardware was fabricated, installed and evaluated in 1970. Sixty hours of flight tests were conducted, and a summary of pilot comments are as follows (ref 9):

(1) The helicopter could be flown with more precision with the fluidic system engaged.
(2) The helicopter could cruise at a higher speed.
(3) The fluid SAS decoupled external cross coupling distrubances.
(4) The fluidic SAS stabilized the helicopter as well as or better than the present system.

Flight tests were also conducted on a two-axis hydrofluidic system installed in the OH-58 helicopter (Jet Ranger). The two-axis system was developed to meet an Army need to stabilize yaw and roll. Results of the flight tests showed that the handling ability of the OH-58 was definitely improved, and the dutch roll on the OH-58 was eliminated. The system (fig 12) senses and compensates for aircraft disturbances, but the pilot still has complete authority over the system at all times.

Recent tests, completed in late 1973 and early 1974, include those of the two-axis OH-58 SAS, a three-axis SAS for Sikorski's CH-54 Flying Crane, and a fluidic auto-pilot for the UH-1M. The UH-1M auto-pilot, shown in figure 13, was designed for stability augmentation from zero to maximum cruise speed, attitude-hold from 50 knots to maximum speed, and altitude-hold from 0 to 6,000 ft. (ref. 9). Initial test results on the auto-pilot have been impressive.

Current programs include a joint Army/Navy effort to determine reliability and maintainability data from flight tests. Twelve two-axis systems will be installed in OH-58 helicopters, and 14 yaw systems will be installed and flight tested on the Navy's TH-57 helicopter. Flight tests will be conducted for a one-year period in active squadrons.

The most advanced application of a fluidic SAS is the three-axis system in one version of the UTTAS helicopter program. The system is currently under development and will be ready for flight tests in the near future.

3.6 Missile Control (MICOM)

The US Army Missile Command has been developing fluidic directional control systems. These include systems for both the missile guidance

(identifying the correct missile attitude) and the missile position control (applying force to control missile attitude).

The directional control anti-tank missile uses electrical signals to operate an interface device that controls reaction jets through a fluidic diverter. The control signal alters the duty cycle of rapid pulses to change the net average steering thrust.

The directional control system demonstrated on Honest John (fig. 14) is a complete fluidic attitude control. The pneumatic output of an attitude gyro is processed fluidically to control actuators for jet vanes. This system has successfully reduced errors due to tipoff and low level wind.

Additional work is being done to utilize a gas bleed directly from the rocket motor to provide steering forces through secondary injection into the rocket nozzle. This concept has been tested in static firings on Little John motors.

3.7 Missile Safing and Arming System (Picatinny Arsenal)

The Picatinny Arsenal (PA) fluidic program was initiated in the early 1960's. Most of the PA effort has been directed toward missile safing and arming (S & A) systems. This program was instituted and continued due to the inherent nuclear hardness of fluidic systems.

The initial PA effort was directed toward developing critical components that could be utilized in an S & A system. A potential missile S & A was hypothesized, and hardware using available technology was developed, tested, and analyzed. Problem areas were then well-defined, and effort was directed toward research and development of components that could be utilized in a specific S & A. System integration followed when components were sufficiently developed.

This approach has continued at PA, with emphasis shifting to integrated systems. However, PA has continued to develop components that would enhance system performance. Recent emphasis has been on sensors, transducers, interface devices, power supplies, and fabrication techniques.

Sensor effort has been directed toward accelerometers and spin sensors, with emphasis in the past year on accelerometers. The G-Sensor, shown in figure 15, has been in existence for several years. Vibrating string and digital accelerometers are currently being evaluated.

PA initiated the development of the Flueric Explosive Initiator (FEI). The device, shown in figure 16, has a number of military uses. The principal use of the device at PA is as an initiator in the fluidic

S & A. In this configuration, the FEI is used to initiate an explosive cutter valve.

PA is developing a compact, one-shot fluidic power source for a missile S & A system. The present S & A system uses a cold gas supply that, depending on the application, could be as large or larger than the remaining fluidic system. PA showed that a subliming solid would be the most efficient source of fluidic power, and a low level effort concerned with the various problems encountered in obtaining a controlled amount of clean gas from this source is continuing. PA has also developed a hydrazine power supply and is currently testing it to determine its suitability. Although the hydrazine supply is not as efficient as the subliming solid, it is much lighter and smaller than the cold gas source.

Several years ago, the Air Force sponsored work on fluidic fabrication techniques. PA has continued this effort with emphasis on metal etching and diffusion bonding. This effort is associated with a fluidic missile S&A system, and consequently, the components are small to reduce power consumption. PA has developed techniques for making miniature components both on contract and in house, and currently is applying these techniques to manufacture hardware on a pilot production line.

3.8 Weapon Stabilization (Rock Island Arsenal):

Rodman Laboratories at Rock Island Arsenal (RIA) became interested in fluidics in the late 1960's. There are presently three programs at the laboratories, two in fluidic control of aircraft armament and the other in ground-vehicle turret control. These projects involve stabilization of turrets and attenuation of recoil.

RIA is using the XM28 system to demonstrate fluidic aircraft turret stabilization. The initial effort demonstrated accuracies of 5 to 10 mils. The present program is to develop flight hardware for a two-axis system integrated into the XM28 for helicopter ground firing tests and flight tests.

High impulse weapons require a reduction in the high peak recoil forces that severely decrease gunner accuracy, and the second fluidic program attempts to reduce the effect in aircraft by averaging the peak impulses. Present efforts involve development of critical components with emphasis on low initial cost and high reliability.

Fluidic technology is being considered for turret stabilization on armored vehicles. The essential objective is to increase the effectiveness of the firing from vehicles on the move.

A short range, hybrid program utilizes the vortex rate sensor in place of conventional gyroscopes, and is expected to provide the transition to a more comprehensive fluidics system. In this first program, a two-axis fluidic vortex rate sensing package with transducers for electronic output has been built and integrated into an existing M60A1 add on stabilization (AOS) system. The present M60A1 AOS has a mechanical gyro and a solid-state, electronic signal conditioning package. The fluidic sensor package is a direct replacement for the gyros and has an output that is compatible with the electronic system. The M60A1 used to test the system is currently undergoing evaluation in the field, and this test should show how the vortex rate sensor compares with the existing sensor.

The long range objective is to show the feasibility of an all-fluidic, two-axis system. The elevation axis has been constructed and is presently under evaluation while the azimuth axis is under development. When completed, both axes will be integrated and mounted on the MICV-65 Cupola. Testing on the MICV-65 Cupola will show feasibility of firing on the move.

4. RELIABILITY

Several years ago, the Government Fluidics Coordination Group (GFCG) organized a Reliability Committee to obtain data on fluidic reliability. Under funding from all three services, the committee initiated contractual efforts. Table III lists the current efforts. The first two efforts were started in 1972 and the last four in 1973.

The preliminary results of the Real-Time Reliability Study were reported at the ASME 1972 Winter Annual Meeting (ref. 10). The system under evaluation was the fluidic thrust reverser control unit for the CF-6 engine on the DC-10 aircraft (fig. 17). At that time it was reported that 118,000 hours elapsed between failures. It was then stated that the newness of the technology should be taken into account, and a much larger time between failures should be expected as the system matures. A recent revision (February 1974) shows a time between failures of over 425,000 hours (ref. 11). Included in the recent report are data on fluidic applications in the Navy S-3A aircraft and the Concorde. Obviously, the greatest accumulation of data is on the DC-10 application. All of these applications use compressor bleed air to power the fluidic systems.

The above reliability data are presented to suggest that, once fluidics has been utilized in an industry such as aerospace, it is accepted as a viable, competing technology to be seriously considered. It is interesting to note that practically every new aircraft engine, including the English engine in the L-1011 aircraft, has used one or more fluidic systems for control purposes.

5. FABRICATION

Fabrication of fluidic systems has been and is a major concern of the government and emphasis in the military is placed on low cost, small size, completely integrated packaging. The techniques receiving the most attention are electroforming and metal etching/diffusion bonding. Electroforming is being utilized for hydraulic fluidic systems; whereas, metal etching/ diffusion bonding is being employed in gas-powered systems.

The Eustis Directorate initiated a manufacturing technology program in 1973 to study the reproducibility of electroforming SAS's. This study should result in low-cost, repeatable helicopter stabilization systems.

A program was initiated in FY 74 on metal etching and diffusion bonding of titanium. The objective of this joint HDL-PA effort is to develop a pilot production line over a two-year time frame. The first year study will transfer the laboratory-developed process to a manufacturing line, including such necessary developments as low-cost visual inspection techniques.

6. CONCLUSIONS

The military is actively involved in applying fluidics in weaponry, and a number of systems are being developed under Army funding. There also is considerable and significant effort under Navy, Air Force, and NASA direction.

The aerospace industry has accepted fluidics as a competing technology based on present use in a number of different applications. As in the aerospace industry, once fluidic control systems are employed by the military, the technology will be accepted as competitive.

The hydrofluidic stabilization of helicopters is the most advanced fluidic Army application. Field tests have demonstrated its suitability, and the UTTAS will have one of its two models equipped with a three-axis fluidic SAS. Not far behind the SAS development cycle are fluidic systems for fuzing, missile control, weapon stabilization, and engine control. Due to the emphasis of the military on low initial cost, high reliability, and maintainability, emphasis on fluidics in weaponry should continue to increase.

References

1. "A Forecast of Applications of Fluidics," Cox, L.S. & J. W. Joyce, Jr., HDL TR-1568, Jan. 1972

2. "Design of Automatic Repositioning Mortar System," Woods, G. W. and W. H. Ziegler, TR WVT-7235, Watervliet Arsenal, July 1972.

3. "The Fluidic Generator: A New Electrical Power Source," Campagnuolo, C. J., and R. N. Gottron, Proceedings, 24th Annual Power Sources Symposium, May 1970.

4. "Fluidics in Ordnance," Smith, R. K., Ordnance, March-April 1972.

5. "MUCOM Centers Developing Practical Applications for Fluidics," Staley, C. H., and A. E. Schmidlin, Army Research and Development, Jan-Feb. 1972.

6. "Fluidics Pick Off Weight Information," Balmer, T., Design News, Sept. 1972.

7. "A Fluidic Primer Height Sensor," Funke, M.F., HDL-TM-72-38, Feb. 1973.

8. "Fluidic Strain Gauge Concepts, "Drzewiecki, T.M., HDL-TR-1575, Dec. 1971.

9. "Army Helicopter Fluidics Control Systems," Smith, Robert P., ASME Winter Annual Meeting, Nov. 1973.

10. "Reliability of Aerospace Fluidic Controls," Mix, J. M., Fluidics Quarterly, Vol. 5, No. 1, Jan. 73.

11. "Reliability Data for Fluidic Systems," Engineering Report, Airesearch Corp., Feb. 1974.

TITLE	SPONSOR	CONTRACTOR	AMOUNT	DATE
Research and Development of the Fluidic Control System	Naval Air Eng. Center	Honeywell	$ 43,612	14 June 71
Fabrication of Fluidic Pulse Duration Modulator	MICOM	General Electric	27,170	8 July 71
Engineering Support for Flight Test of OH-58A Hydrofluidic Yaw SAS	AAMR&D Lab	Honeywell	37,164	19 July 71
Fluidic Free Flight Sensor	Eglin AFB	Honeywell	42,000	17 Sept 71
Feasibility of Adapting Pneumatic Match to Ram Air Fuzing	Picatinny Arsenal	Kearfott	39,970	22 Oct 71
R & D for Fluidic Control Sub-System for AGT-1500 Gas Turbine Program	TACOM	Lycoming	58,000	7 Dec 71
Advance Hydrofluidic Stabilization System	AAMR&D Lab	Honeywell	387,720	9 Dec 71
Hydrofluidic Servoactuator	AAMR&D Lab	Honeywell	34,600	9 Dec 71
Vortex Rate Sensor-Controller Unit	Rock Island	Honeywell	48,250	16 Dec 71
Development of a Three-Axis Fluidic Airspeed Sensor	NASA	Bowles	40,067	30 Dec 71
Design, Develop and fabricate a Flueric Laminar Rate Sensor	NAVAIR	General Electric	35,072	29 Feb 72
Real Time Reliability	HDL	AiResearch	17,000	10 Mar 72
Hydrofluidic SAS Suitability Demonstration	AAMR&D Lab	Honeywell	88,882	11 Apr 72
Development of Critical Components for an Advanced Fluidic Stable Platform	NAVAIR	Martin Marietta	45,000	13 Apr 72

TABLE I

TITLE	SPONSOR	CONTRACTOR	AMOUNT	DATE
R & D Program to Design, Fabricate and Evaluate a Laminar Fluidic Missile Control System	NAVAIR	General Electric	49,588	16 May 72
Development of a Digital Fluidic Accelerometer	Picatinny Arsenal	AVCO	25,574	31 May 72
Development of an all-Fluidic Cold Power Source	Picatinny Arsenal	Chandler Evans	58,363	5 Jun 72
Fluidic Programmers	Picatinny Arsenal	General Electric	36,500	15 Jun 72
Fluid Proportional Thruster	NASA	General Electric	98,024	28 Jun 72
Two-Axis Fluidic Inertial Damper System	Rock Island	Honeywell	97,726	28 Jun 72
Three-Axis Hydrofluidic SAS System	HDL	Sikorsky	90,561	11 Jul 73
Fluidic Second Generation Programmer	Picatinny Arsenal	General Electric	33,078	13 Jul 72
Test Program for Fluidic Reliability	HDL	McDonnell Douglas	26,880	14 Jul 72
OH-58 Yaw SAS Flight Test Program	AAMR&D Lab	Honeywell	46,595	17 Jul 72
Analysis of a Resonance Tube	Picatinny Arsenal	Kearfott	39,500	21 Jul 72
Hydrofluidic Yaw Axis SAS	Wright-Patterson	Honeywell	105,500	8 Dec 72
Design, Fabricate and Test a Breadboard Model of a Pneumatic Power Supply	NAVAIR	AiResearch	38,500	16 Feb 73
Exploratory Development for Fluidic Missile Autopilot	NAVAIR	General Electric	50,000	16 Feb 73
Evaluate Use of Gas Turbine Engine Compressor Bleed	NADC	AiResearch	31,000	22 Feb 73

TABLE I (con't)

TITLE	SPONSOR	CONTRACTOR	AMOUNT	DATE
R & D Program for Test and Evaluation of a Laminar Flueric Angular Rate Sensor	NAVAIR	McDonnell Douglas	39,699	22 Feb 73
Fabricate and Test a Single Degree of Freedom Fluidic Inertial Gyro	NAVAIR	Martin Marietta	68,689	21 Mar 73
Develop Fluidically Controlled Cargo Hook	AAMR&D Lab	Sikorsky	98,800	12 Apr 73
Development of Photochemically Etched Diffusion-Bonded Aluminum Fluidic Circuits	Picatinny Arsenal	Bendix	90,116	2 May 73
Hydrofluidic Yaw Stability Augmentation System	AAMR&D Lab	Honeywell	773,600	2 May 73
Roll Axis Hydrofluidic SAS Development	AAMR&D Lab	Honeywell	89,560	2 May 73
Fluidic Rate Sensing Package	HDL	AiResearch	17,000	10 Mar 72
Experimental Classification of Fluidic Power Supplies	HDL	McDonnell Douglas	53,767	6 Jun 73
Development of a Laminar Rate Sensing Roll Control System	MICOM	General Electric	34,877	8 Jun 73
Development of Dual Channel Fluidic Programmer	Picatinny Arsenal	General Electric	50,953	23 Jul 73
Development of Insensitive Fluid Logic Circuitry	Picatinny Arsenal	Lintec	38,393	23 Jul 73
Warm Gas Pneumatic Actuator	NOTS	AiResearch	44,505	23 Aug 73

TABLE I (con't)

TITLE	SPONSOR	CONTRACTOR	AMOUNT	DATE
Study to Design, Fabricate, Test and Deliver a Breadboard Model of a Hydrofluidic Servovalve	AAMR&D Lab	Honeywell	47,300	23 Aug 73
Analyze and Define a Hydrofluidic Fly-By-Tube Flight Control System	NAVAIR	Honeywell	26,206	24 Aug 73
Fluidic Thermal Controls	Wright-Patterson	AiResearch	150,354	3 Dec 73
Fluidic Thermal Controls	Wright-Patterson	Hamilton-Standard	84,644	7 Dec 73
Producibility Study of Photo-Chemical Etching Processes	Picatinny Arsenal	Bendix	95,000	Mar 74

TABLE I (con't)

TABLE II

FLUIDICS

ESTIMATED ARMY EFFORT (FY 73)

6.1	$ 1,000 K
6.2 (LEAD LAB)	1250 K
6.2 (OTHER)	1,000 K
6.3	1,500 K
6.4	500 K
6.7	500 K
TOTAL	$ 5.75 M

TABLE III

FLUIDIC RELIABILITY STUDIES

1. Contamination Study (McDonnell Douglas)	79.5 K
2. Real-Time Reliability Data (AiResearch)	16.6 K
3. Cyclone Separator (McDonnell Douglas)	36.7 K
4. Classification Of Military Power Supplies (McDonnell Douglas)	56.0 K
5. One Shot Reliability (Singer)	43.8 K
6. Study Of Comressor Bleed Power Supply (AiResearch)	31.0 K

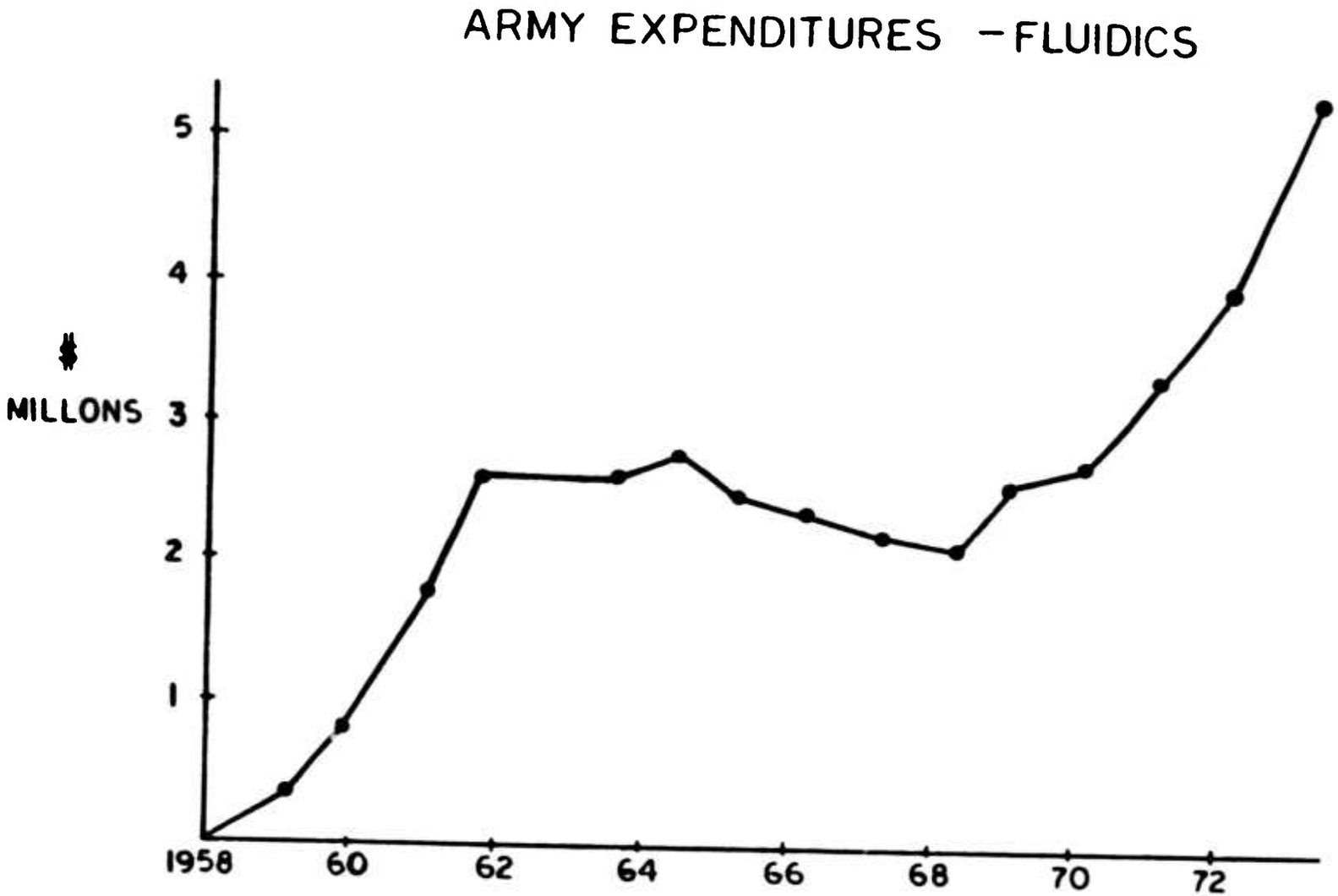

ARMY EXPENDITURES - FLUIDICS
$
MILLONS
5
4
3
2
1
1958
60
62
64
66
68
70
72

Figure 1

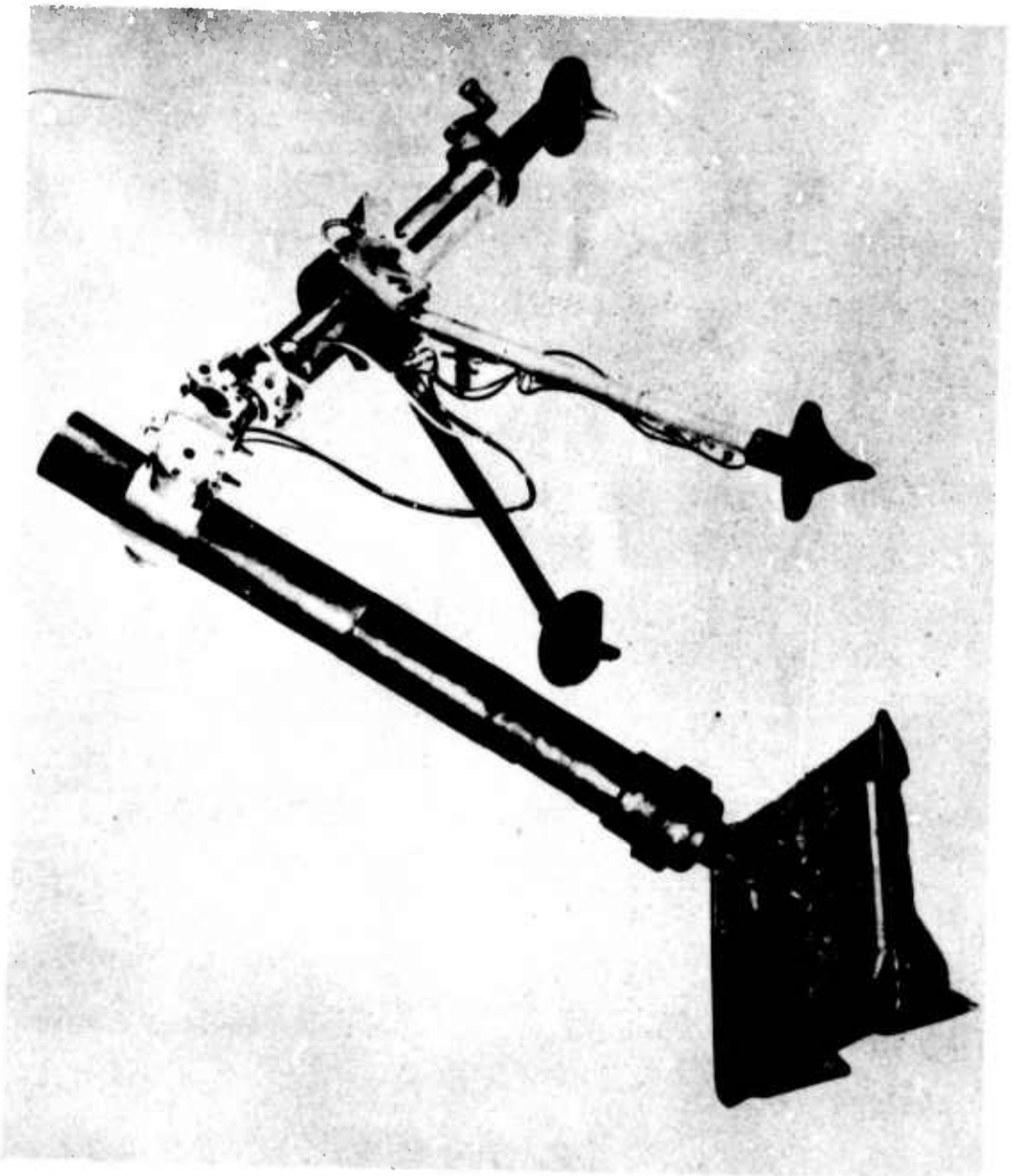


Figure 2. Breadboard of mortar repositioning

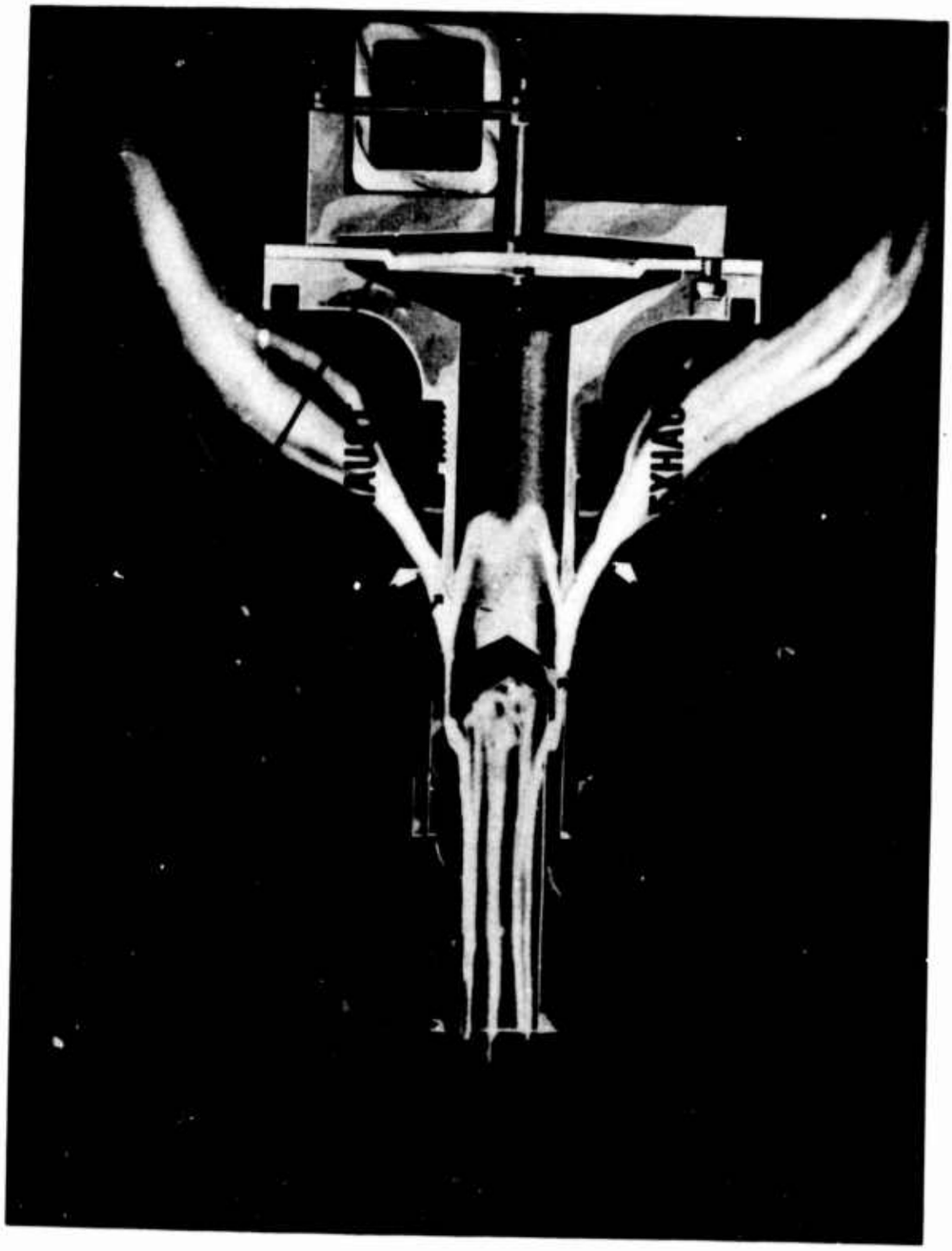


Figure 3: Fluidic generator

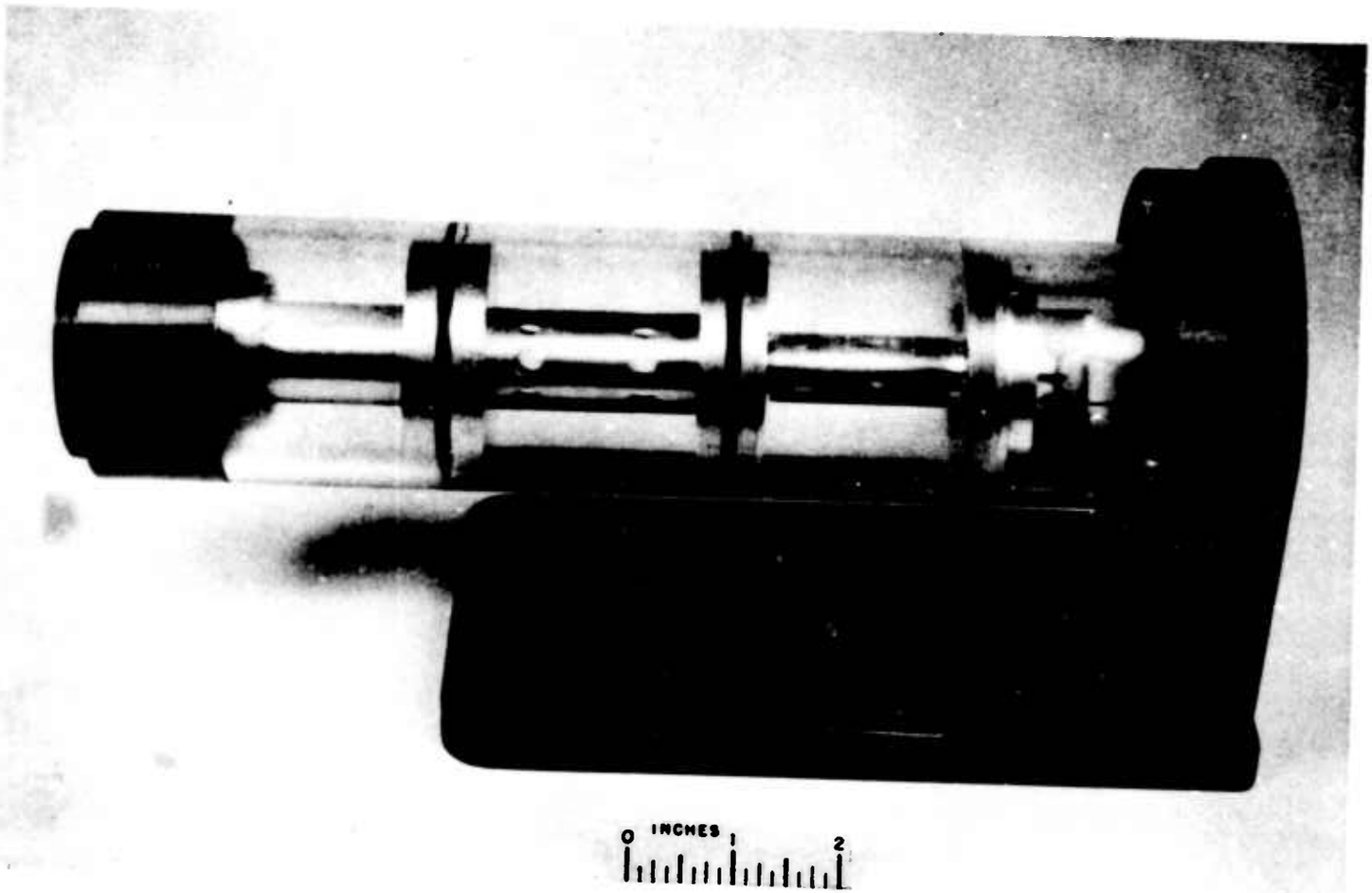


Figure 4. Fluidic generator for SUU Dispenser

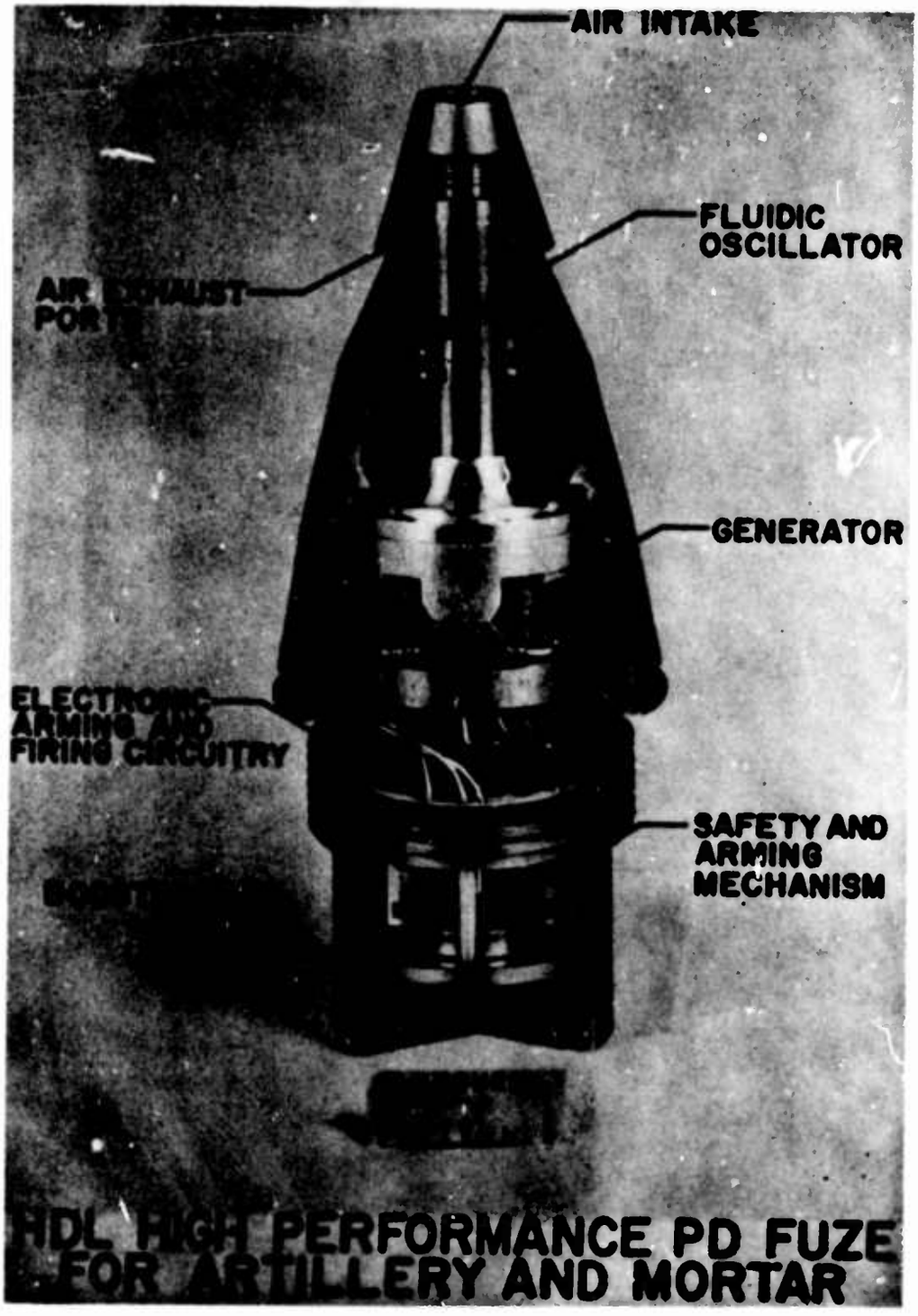

AIR INTAKE
FLUIDIC OSCILLATOR
GENERATOR
SAFETY AND ARMING MECHANISM
HDL HIGH PERFORMANCE PD FUZE FOR ARTILLERY AND MORTAR

Figure 5

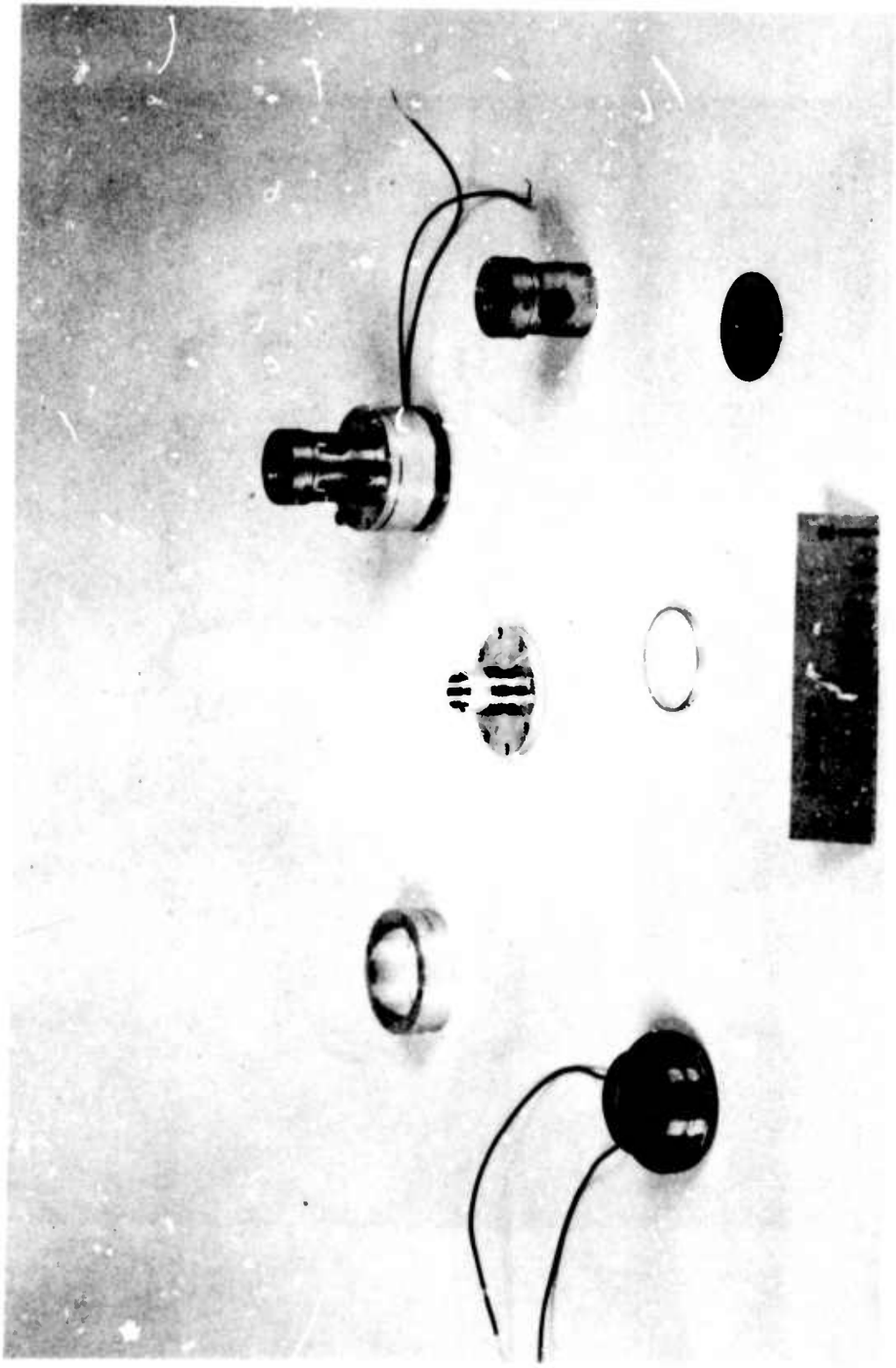


Figure 6. Fluidic generator for Advanced Beehive

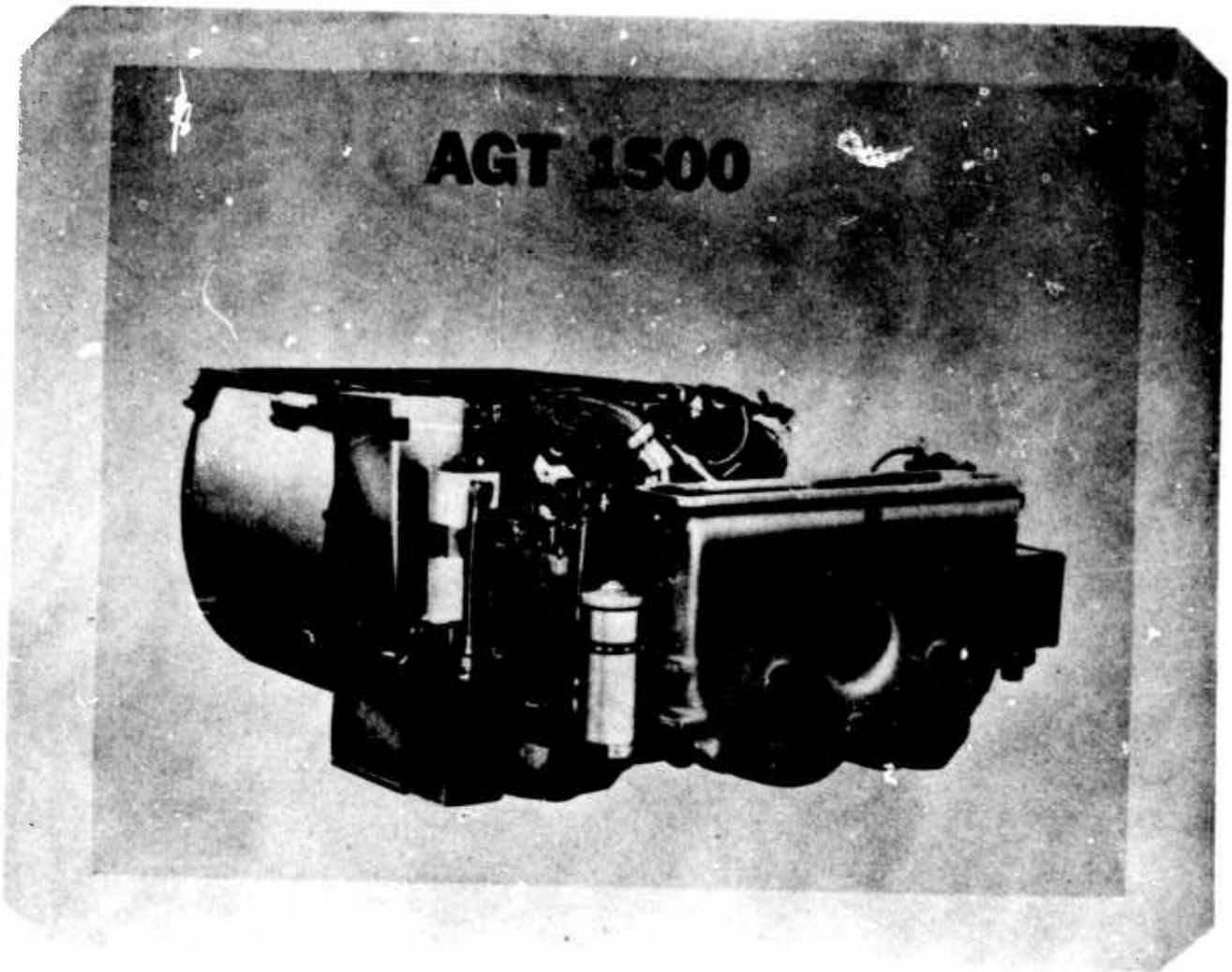


Figure 7. Automotive gas turbine, 1500 horsepower

BEAT DETECTION CIRCUIT

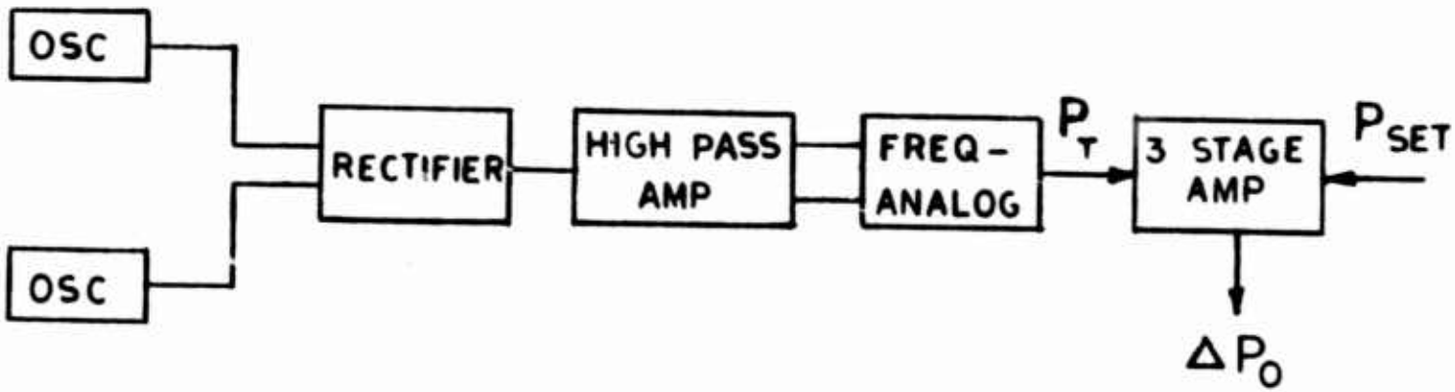


Figure 8

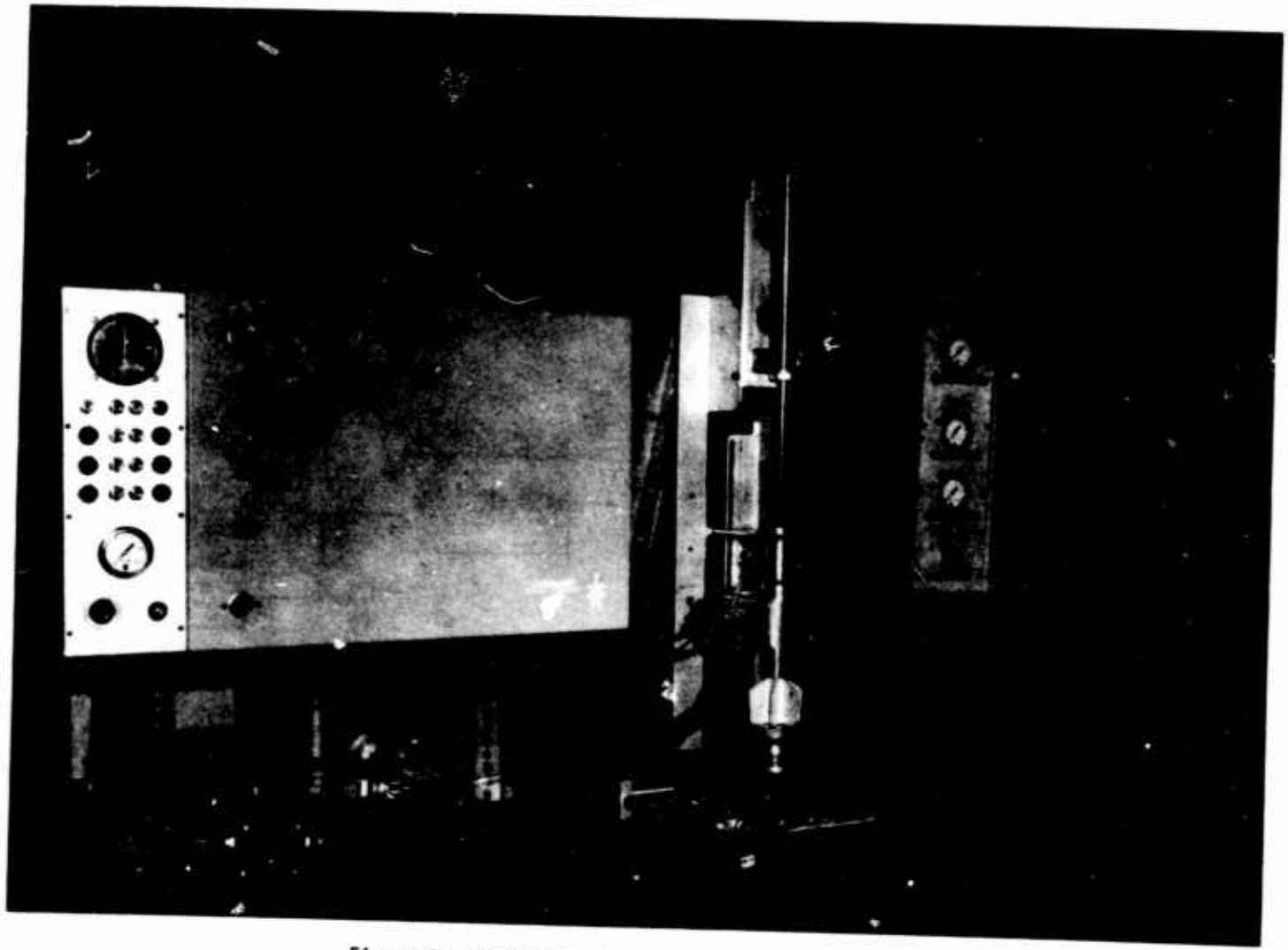


Figure 9: Fluidic mortar tail cone sensing system.

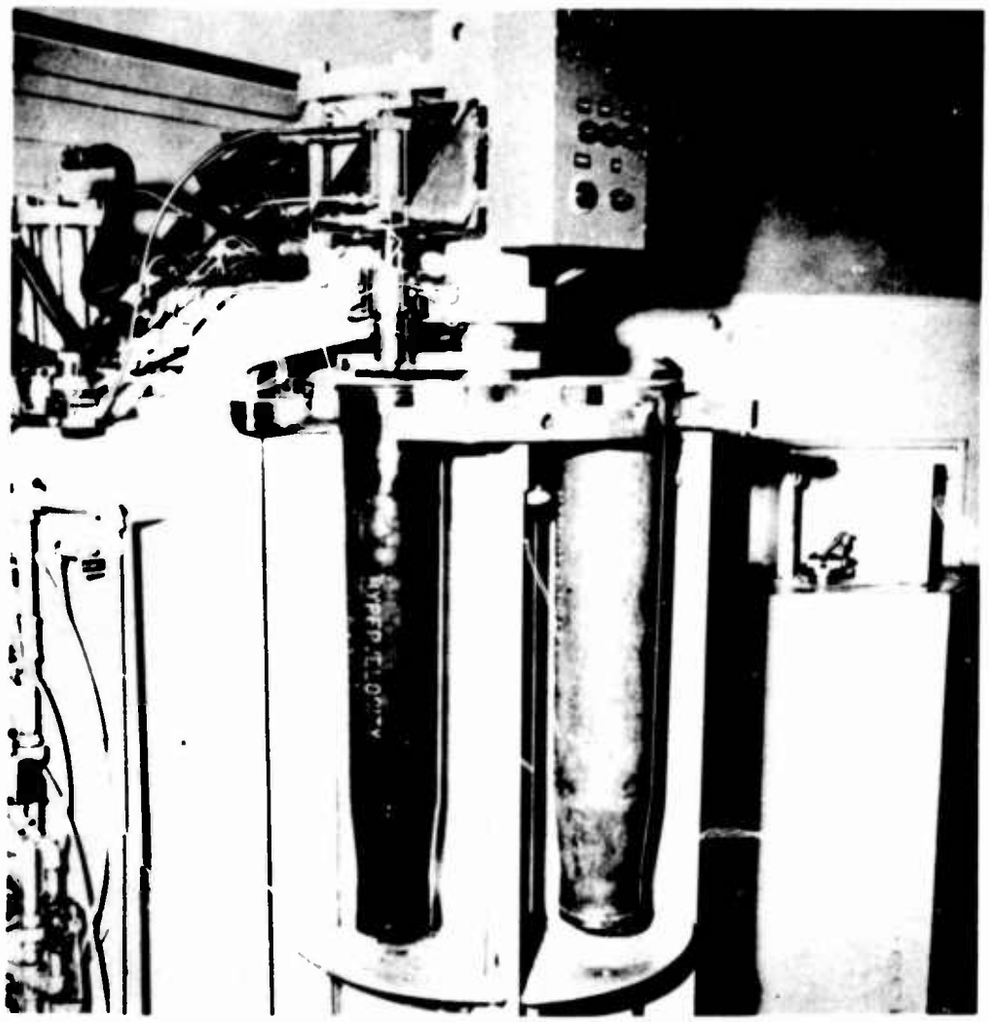


Figure 10. Fluidic primer remover and replacer

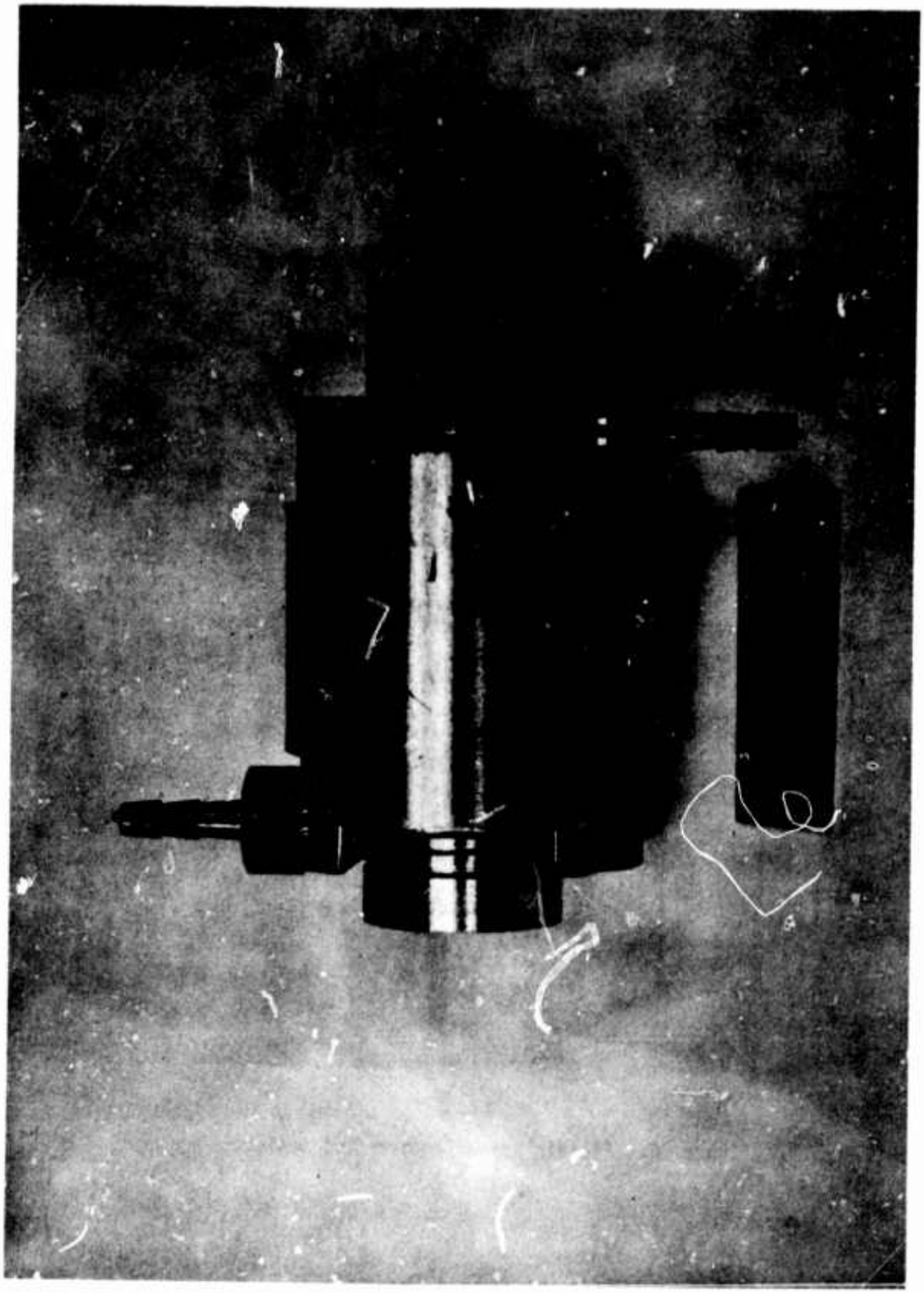


Figure 11. Fluidic strain gauge

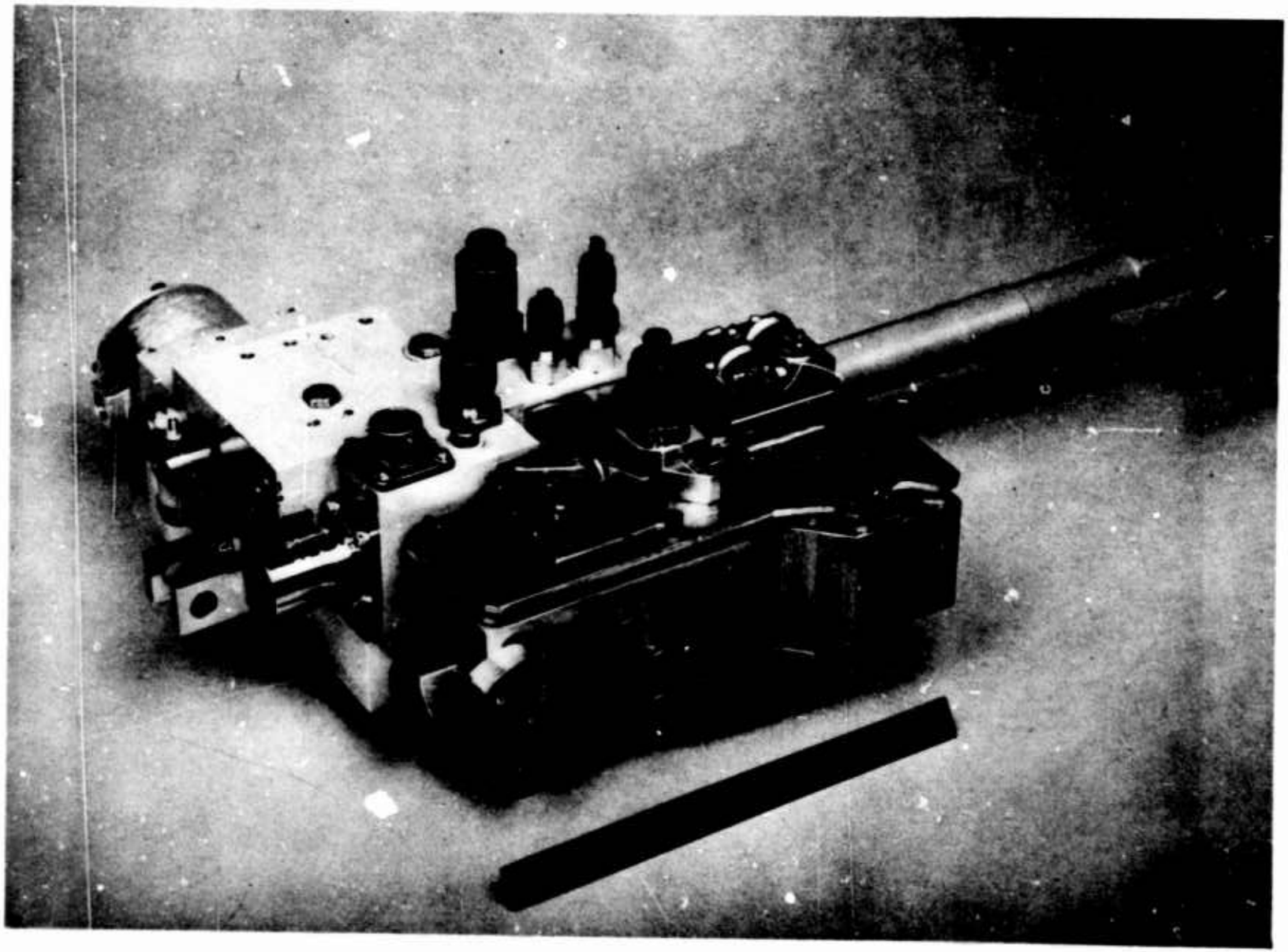


Figure 12: Single axis fluidic SAS for the OH-58

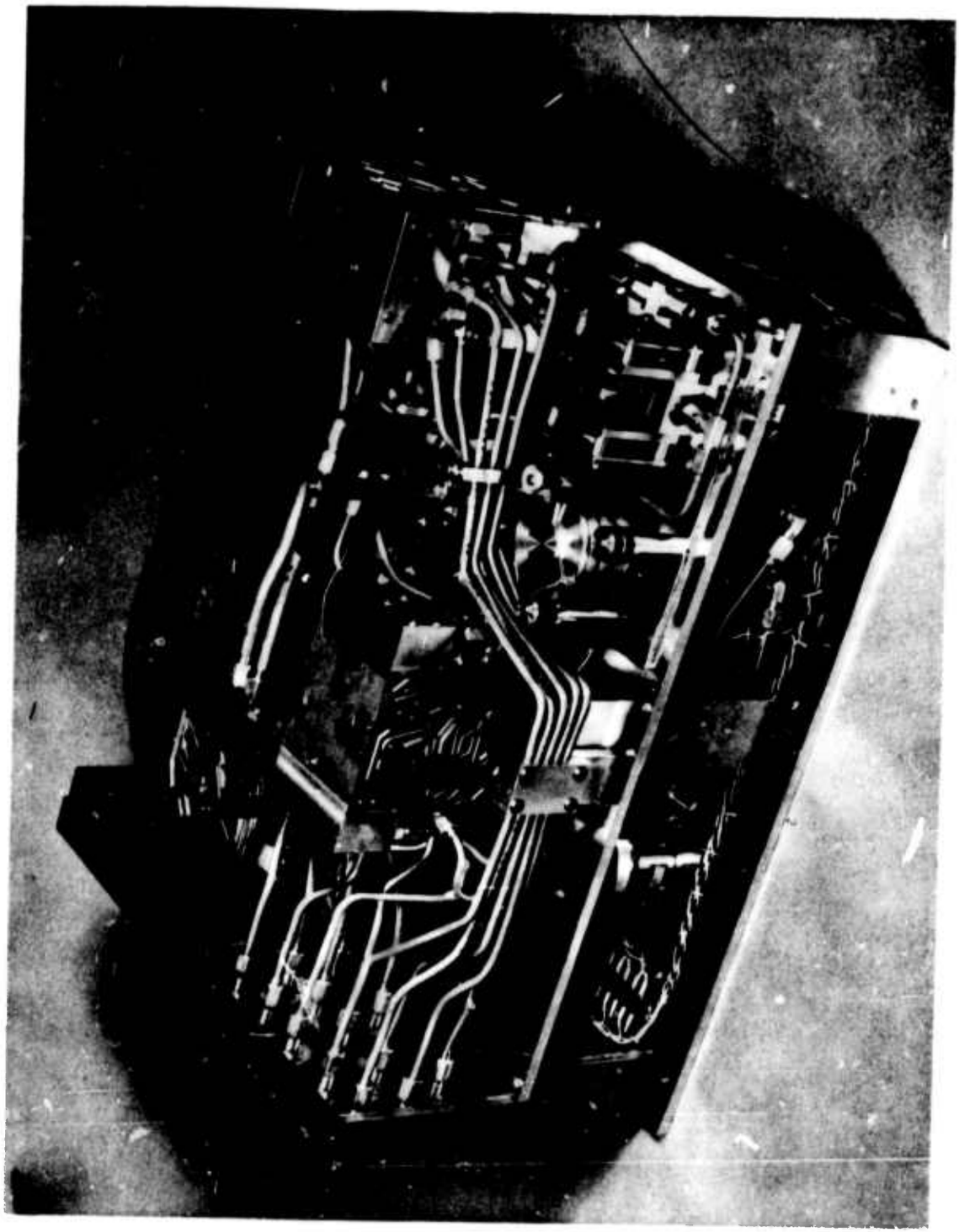


Figure 13: UH-1M Auto-pilot

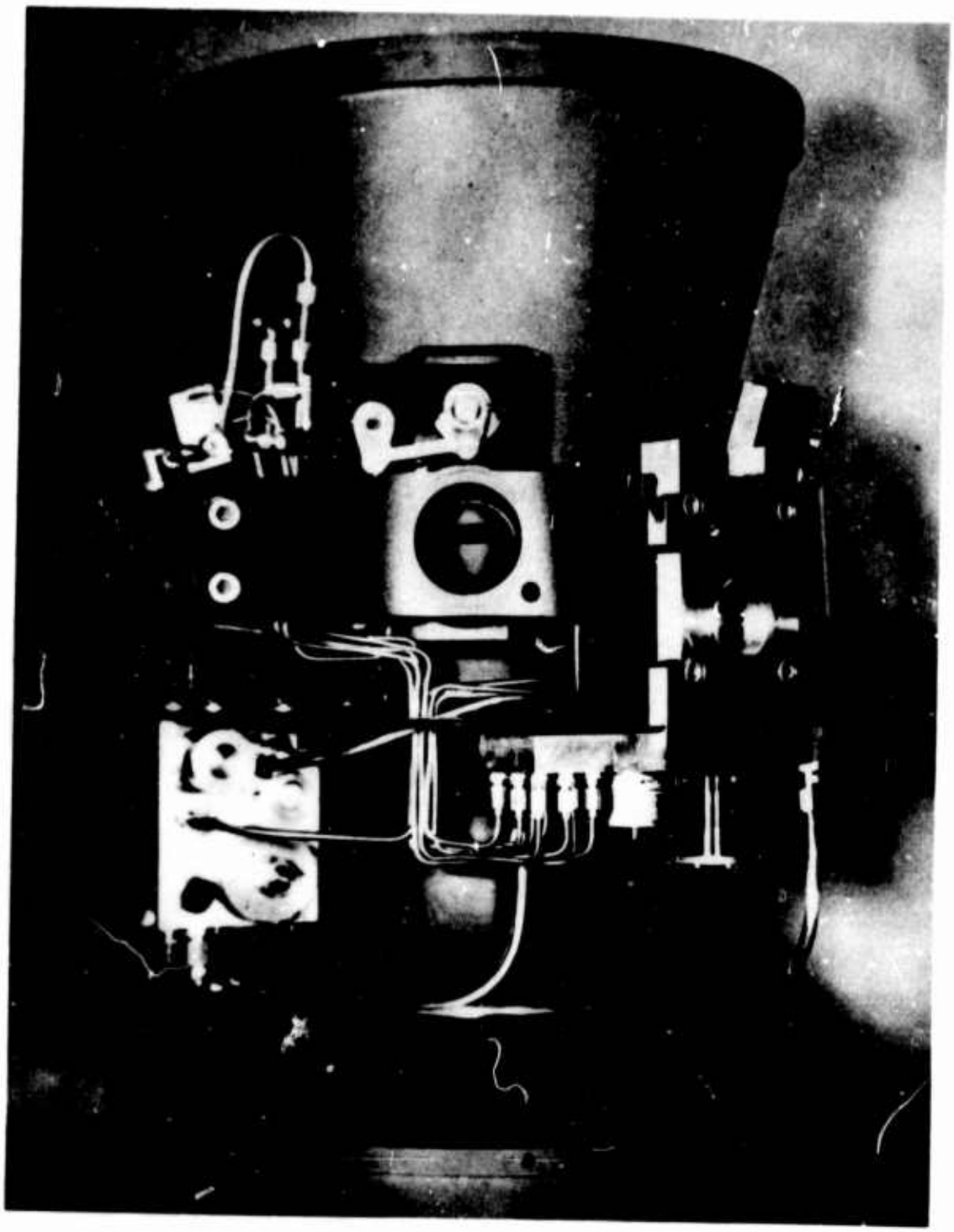


Figure 14. Fluidic directional control for Honest John

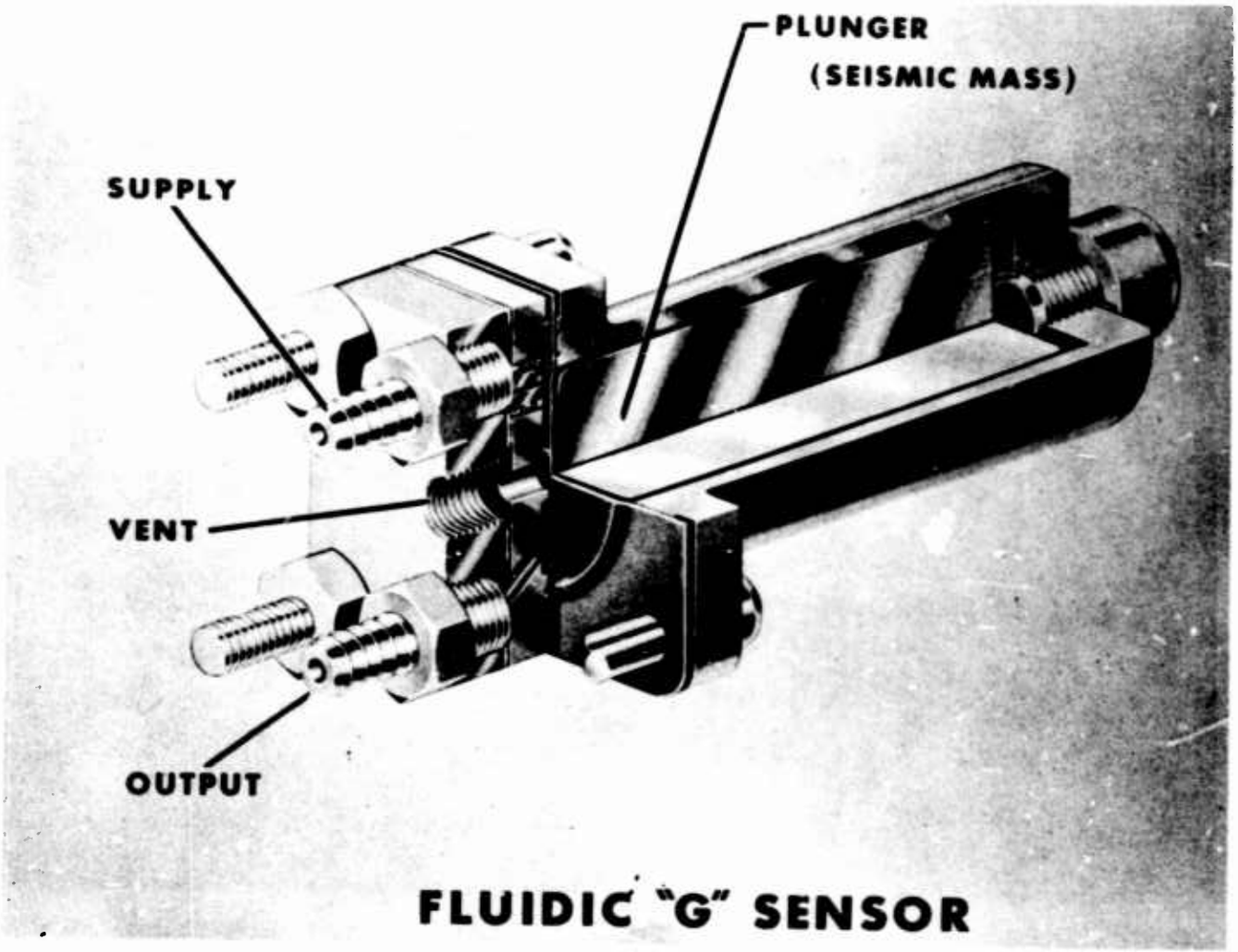


Figure 15

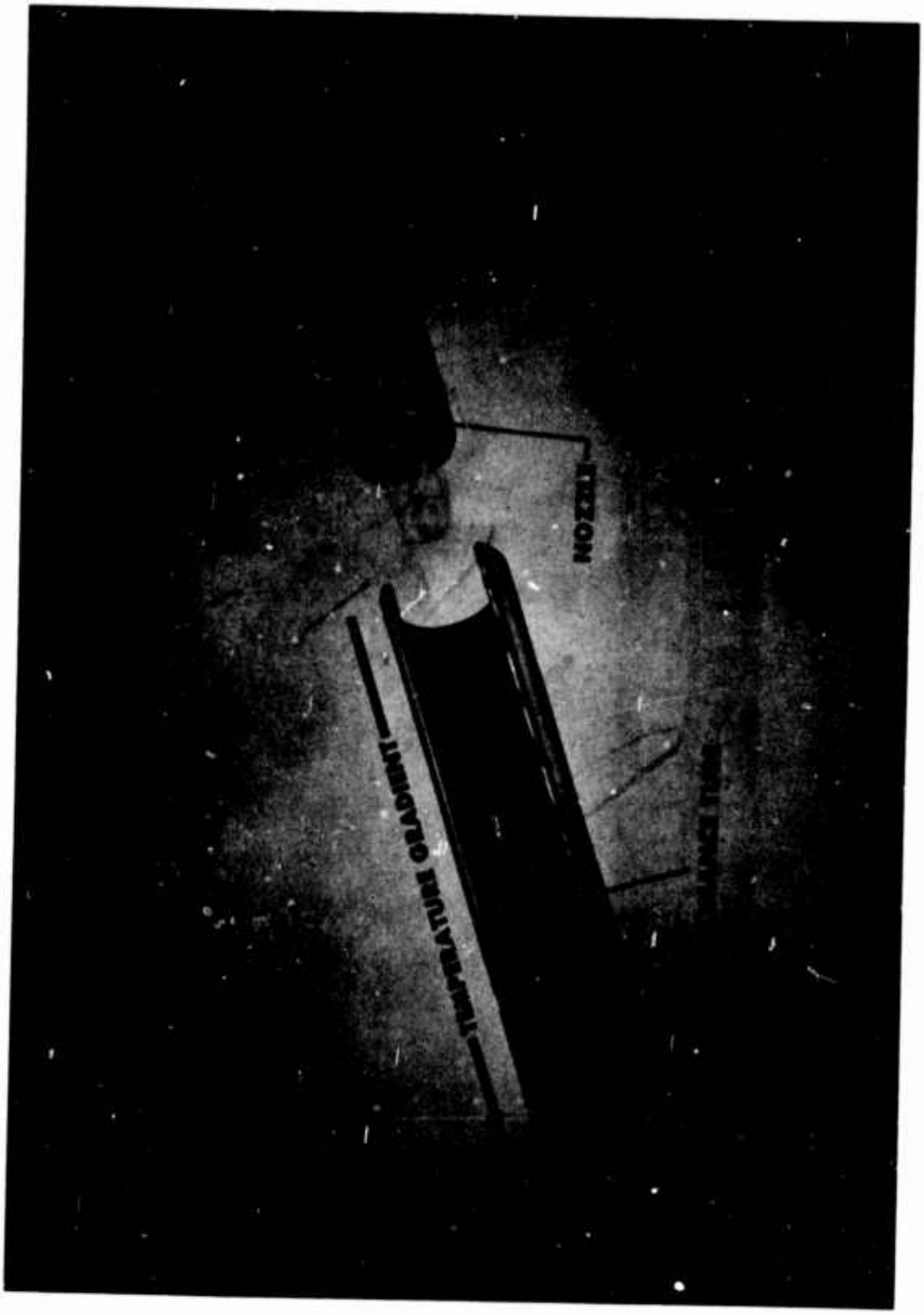


Figure 16

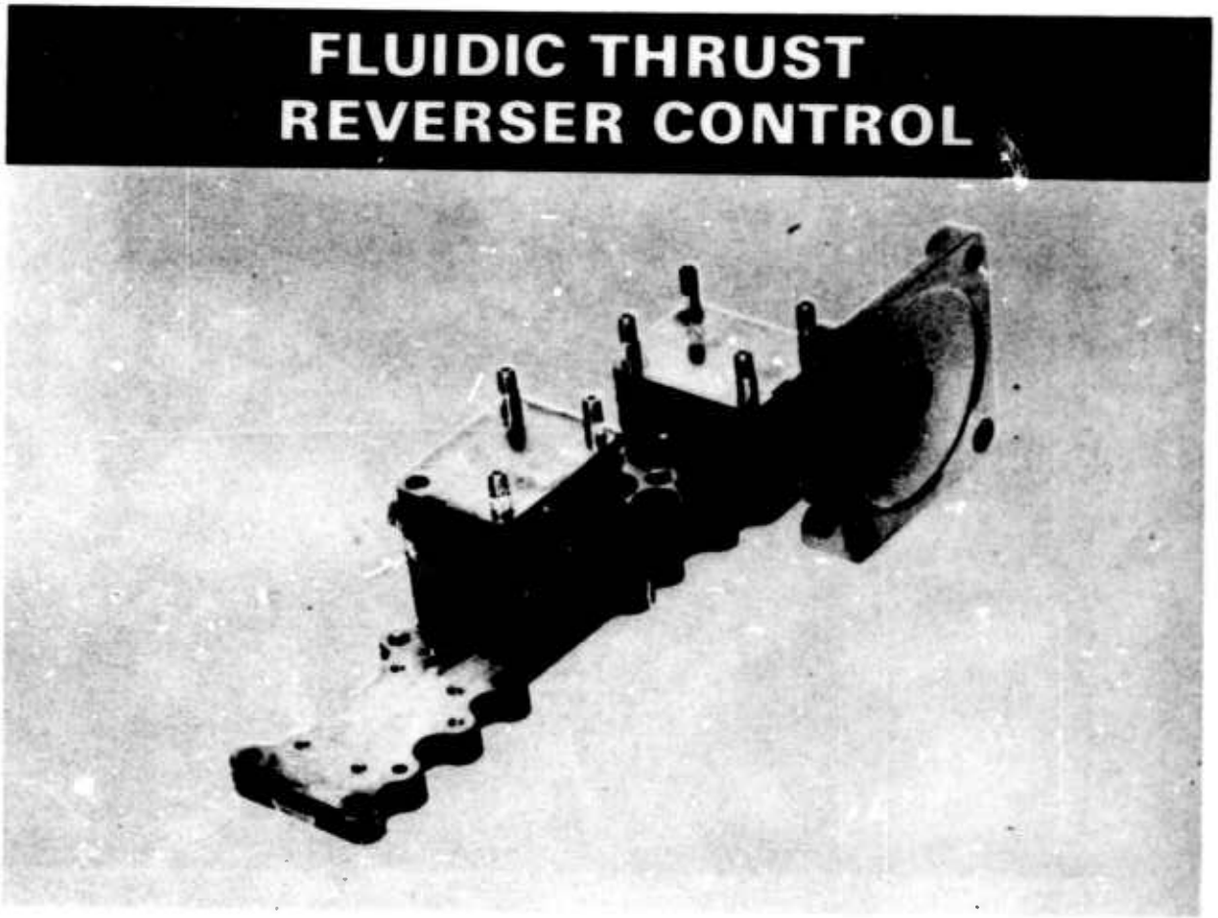


Figure. 17: Fluidic Thrust Reverser Control

A FLUIDIC OIL-WATER SEPARATOR

By

Dharam Pal
Research Mechanical Engineer
Civil Engineering Laboratory
Port Hueneme, California 93043

ABSTRACT

An experimental investigation establishing the feasibility of using the Coanda effect in developing an oil-water separator is described. Tests conducted on an experimental model with an oil-water mixture containing 6% oil showed that the oil content in the effluent can be reduced to less than 3%. A three-stage separator has produced effluent in the range of 1%. Conceptual designs of a practical separator are discussed. The space requirement for a Coanda effect separator when compared with typical parallel-plate type separators of the same capacity is considerably smaller. Analytical expressions useful in designing a Coanda effect separator of a given size are also given.

INTRODUCTION

Current methods of separating oil from oil-water mixtures are centrifugation, gravitation, coalesence, and ultrafiltration [1,2]. Centrifugation is an accepted method for separating water-oil dispersions or emulsions [2]. Commercial equipment is available for a wide range of applications. Despite their effectiveness, the power requirement, cost, and maintenance of such systems are relatively high. The gravitation method of separating oil from oily wastes relies upon differences in densities of the fluids being separated. Commercially available parallel separators are based upon the gravitation principle. Because of the laminar flow requirements for separation, such systems are normally bulky. Coalescence has been used quite extensively for removing finely dispersed water droplets from fuels. The basic mechanism behind this separation technique is the formation of larger oil drops on the coalescing material. The resulting larger drops are separated by gravity. The method, however, suffers from fouling of the coalescing element, and it requires frequent maintenance. Finally, ultrafiltration uses a filtering process to separate water from oil. This method, although very effective, suffers from fouling of the filter element; the system requires frequent cleaning.

A new method of separating free oil from oil-water mixtures [3] is under investigation at the Civil Engineering Laboratory (CEL). This technique uses the fluid dynamic phenomenon, called "wall attachment or Coanda effect," named after its discoverer, Henri Coanda.

A preliminary investigation was conducted to establish the feasibility of using the Coanda effect for separating two immiscible liquids. This paper describes in detail the feasibility program.

THEORY

Consider a thin jet sheet, quasi-two-dimensional, flowing into an unbounded region. The jet gets deflected towards an adjacent wall. When such a wall is relatively close to the jet axis, the jet gets attached to and flows along the wall enclosing a separation bubble as shown in Figure 1. As is evident, the jet undergoes considerable curving during its attachment, thus, generating a centrifugal force field on it. This results in a lower pressure within the separation bubble due to a recirculating vortex. The pressure, p_B, in the separation bubble, as derived in Appendix A, is given by

$$P_\infty - p_B = \frac{J}{b_o}\left[\frac{3\theta}{\sigma(1/t_1^2 - 1)}\right] \qquad (1)$$

where P_∞ = free stream pressure

J = jet momentum per unit span of the nozzle

b_o = nozzle width

θ = angular location of the reattachment point

σ = jet spread parameter

t_1 = $\tanh [\sigma y_1/(s_1 + s_o)]$

y_1 = half width of the jet at the reattachment point

s_1 = axial distance between the reattachment point and the nozzle

s_o = $\sigma b_o/3$ = distance of the nozzle exit from a hypothetical origin of the jet

Using the theory discussed in Appendix A, dimensionless pressure $(P_\infty - p_B)\, b_o/J$ was plotted against the plate offset, D/b_o, for values of 7.7, 10, and 12 for the jet spread parameter, σ. Figure 2 shows the pressure difference between the separation bubble and the ambient as a function of D/b_o.

For a jet composed of a mixture of two fluids which do not mix, such as oil and water, the lighter fluid flowing along the plate side of the jet seeks the separation bubble and gets trapped by it. If an outlet is provided at the center of the bubble, the accumulated oil can be tapped out while the water and rest of the oil flows out of the device. This is the principle of operation of the Coanda effect oil-water separator.

EXPERIMENTAL PROGRAM

A test program was designed to determine the feasibility of using the wall-attachment effect in separating two liquids. Two experimental elements with different flow parameters were built and tested. The experiments were conducted in the Mechanical Systems Laboratory at CEL using a mixture of regular tap water and hydraulic oil as the test fluid.

The Wall Attachment Elements

Based upon the theory developed in Appendix A, two experimental elements were designed. The 12-inch-long attachment wall of each element has an offset of 4 inches. The nozzles on Elements No. 1 and No. 2 are 1/4 and 3/8 inch wide, respectively. The depth of flow passages on both elements is 1/4 inch. Element No. 1 was designed to carry 0.8 gpm of water flow, whereas Element No. 2 was to have a flow-carrying capacity of 1.5 gpm. The jet flow parameters, such as reattaching distance x_R, jet center line radius r, and its half width y_1 at the reattachment point, were determined from Figures A-2 through A-5 given in Appendix A. The jet spread parameter, σ, for the above calculations was chosen to be 12. The dimensions of the elements are listed in Table 1.

Each element consisted of three major components: top and bottom cover plates, and the middle plate with the flow passages machined in it. For ease of fabrication and to facilitate flow visualization during tests, each component plate of the elements was made of a transparent plexi-glass sheet. Further, to extract the accumulated oil in the separation bubble, a 1/4-inch-diameter outlet was provided in the top cover plate of each element. The general layout showing major dimensions of the elements is given in Figure 3. The elements were assembled by gluing the two cover plates to the middle plate.

Feasibility Tests

The experiments were performed using the test setup shown in Figure 4. The adjustment of the supply water flow is possible by hand-controlled valves provided on the flow line. A mixture of red hydraulic oil (Appendix B) and water was used as the test fluid. The mixture was formed by injecting the oil into the water stream before it entered the element. To form a homogeneous mixture, the oil was released at the center of and parallel to the water flow in the pipe. The oil to the mixing junction was supplied by a variable flow pump. The element was immersed in water throughout the test series. The supply water flow was measured by a rotameter, and the static pressure in the water line was measured by conventional pressure gauges. The use of red oil in the test mixture allowed flow visualization through the elements. The photographs of flow patterns were taken by mounting a camera directly above the elements.

The feasibility tests were conducted by running the oil-water mixture containing 6 to 8% oil by volume through the elements. The optimum water flow rates were 0.8 gpm through Element No. 2 and 1.5 gpm through Element No. 2, respectively. The mixture jet reattachment distances from the corners were measured for both elements. They were found to be 7 inches for Element No. 1 and 7.5 inches for No. 2. These values are very close to the theoretically computed values listed in Table 1. The test results indicated that a portion of the oil in the mixture jet did accumulate in the separation bubble zone

of the flow. A photograph of the flow pattern (Figure 5) through Element No. 2 at its optimum flow rate clearly shows the accumulation of oil in the separation bubble. This oil when extracted contained about 50% water. Consequently, improved designs for collecting the oil transferred into the separation bubble were sought. One such design is that of providing a chamber at the top of the separation bubble. This chamber is connected to the separation bubble by means of holes in the top cover plate of the element (Figure 6). Under optimum conditions, the oil captured by the separation bubble flows into the collecting chamber through the connecting holes. Next, the oil collected in the chamber is transferred by siphoning to an oil storage tank. Two different designs of the collecting chambers were tested. These are shown in Figures 7 and 8. Due to its shape and its greater depth, the collecting chamber design shown in Figure 8 is more efficient in collecting the oil. Tests conducted on the elements with the modified design show that about 50% of the oil in the input flow can be extracted in this manner, whereas the remaining oil flows out with the attached water jet. Furthermore, the oil being extracted contained about 5% water. Thus, a separating device based upon this concept appears to be capable of gross separation only. However, tests on elements with modified designs must be conducted before deriving final conclusions about the degree of separation obtainable. A photograph of the flow pattern through Element No. 1 taken at its optimum flow rate is included as Figure 9. The accumulation of oil in the collecting chamber is clearly visible in this record.

Tests On A Multi-Stage Element

It was realized during the feasibility tests on the single-stage elements that to make the Coanda-effect separator suitable for practical applications, staging was necessary. The number of stages for the separator, however, depended upon the type of oily wastes to be handled together with the quality of effluent desired.

During the course of this study a three-stage test element was designed and built to evaluate the effect of staging. Figure 10 shows the sketch of the element's middle plate with flow passages cut in it. Each stage of the element has a 1/4-inch-wide nozzle. The depth of the element's flow passage was kept at 1/4 inch. The mixture jet in each stage is directed by a curved wall conforming to the curvature of a reattaching jet issuing parallel to a flat plate with an offset of 4 inches. This boundary was determined from the flow-governing equations given in Appendix A. It should be mentioned here that the flow configuration in the element is no longer a Coanda flow; instead it is flow over a cavity. Since the jet is held to the wall by centrifugal force, the pressure at the wall is greater than the ambient. Further, because of the swirling flow in the cavity, there is a gradual pressure gradient towards its center. Due to the imposed pressure gradient, the oil in the mixture jet seeks the center of the cavity. The element was designed to handle 0.8 gpm of water flow through each stage. Each stage was provided with oil collecting chambers

located directly on its separation bubble zone. The oil outlet line on each oil chamber was provided with a hand-controlled valve for outgoing oil flow adjustment.

The element was tested using the setup shown in Figure 4. The tests were conducted by varying the oil in the mixture from 6 to 8%. The test results indicate that each stage separated about 50% of the oil from its input flow. The effluent at the third stage outlet contained about 1% oil. The oil being extracted had about 3 to 5% water. Figure 11 shows the element undergoing tests. The flow pattern through the element is shown in Figure 12. The accumulation of oil in the collecting chambers and the separated oil flowing through the outflow lines are shown in the flow record.

DISCUSSION

Jet Velocity Distribution

As mentioned earlier, the mixture jet during its attachment develops a centrifugal acceleration. It was assumed prior to conducting the tests that the lateral acceleration so induced would force most of the oil in the jet into the separation bubble zone of the flow. The observed flow patterns through the experimental models, on the other hand, revealed that the oil particles were distributed uniformly over the entire cross section of the jet. This important observation can be explained from theoretical considerations discussed in Appendix A.

Consider the reattaching jet velocity profile described by Equation 2:

$$u(s,y) = \left[\frac{3J\sigma}{4\rho(s + s_o)}\right]^{1/2} \operatorname{sech}^2\left(\frac{\sigma y}{s + s_o}\right) \qquad (2)$$

where the various symbols are defined in Appendix A. The width of a two-dimensional jet expanding into a similar fluid at any axial location can be derived easily from a linear relationship given in References 4 and 5. The half width, y_1, of the jet is given by

$$y_1 = \left(\frac{s + s_o}{s_o}\right) b_o/2 \qquad (3)$$

It can be seen from Equation 2 that the jet velocity, u(s,y), is maximum at its center line and is

$$u_{max} = \left[\frac{3J\sigma}{4\rho(s + s_o)}\right]^{1/2} \quad (4)$$

Next, it can be deduced from Equations 2 and 3 that the jet velocity, $\ddot{u}(s,y)$, drops to 0.1814 $\ddot{u}_{max}$ at a distance equal to the half width of the jet from its center line. The centrifugal acceleration distribution in the jet can be derived from Equation 2 and is given by

$$\ddot{u}(s,y) = \frac{3J\sigma}{4\rho(s + s_o)(r \pm y)} \operatorname{sech}^4\left(\frac{\sigma y}{s + s_o}\right) \quad (5)$$

Again it is evident from Equation 4 that the centrifugal acceleration, $\ddot{u}(s,y)$ is maximum at the jet center line and is

$$\ddot{u}_{max} = \frac{3J\sigma}{4\rho(s + s_o)r} \quad (6)$$

The acceleration drops sharply to approximately 0.0327 $\ddot{u}_{max}$ at the jet half width points.

The typical velocity and acceleration for the reattaching jets are shown in Figure 13. Because of the nature of lateral acceleration on the jet, the oil particles are distributed over the entire cross section. Such a distribution of centrifugal acceleration affects the separating capability of a separator with this configuration.

The mixture jet velocity and, hence, its centrifugal acceleration distribution can be improved by modified designs. One such design is shown in Figure 14. The device uses a splitter located at the nozzle center line to divide the mixture jet into two sub-jets which flow along the curved walls as shown. The mixture jets flowing through the device will have a velocity distribution as shown in the figure, i.e., from a maximum near the curved walls monotonically decreasing to zero at the separation bubble center. Such a velocity distribution will induce a monotonically decreasing centrifugal acceleration on the jet with a maximum near the wall. This configuration will force most of the oil into the separation bubble. The effluent flows out through the two outlets provided on the device. Such a design should improve the separating capabilities of the separator markedly. An experimental investigation is under way to evaluate this concept.

Another possible improvement in the oil separation capability of the device can be accomplished by decreasing the static pressure within the separation bubble of the flow. This can be achieved by increasing the centrifugal force on the mixture jet which in turn can be increased by decreasing the radius of the jet center line. The separation bubble pressure can also be decreased by increasing jet efflux momentum.

An Automated Oil Extraction System

It was observed during the feasibility tests that the rate of oil extraction from the oil collecting chambers of the elements appreciably affected the quality of oil being extracted. Too high an extraction rate disturbed the oil-water interface in the collecting chamber, with the oil being extracted containing up to 50% water. A low oil extraction rate, on the other hand, reduced the rate of oil captured by the separation bubble. This resulted in more oil in the effluents, thereby deteriorating the performance of the device. A system to control the oil extraction rate is, therefore, required for proper functioning of the separator. Such a system can be either a proportional one or an on-off type. Because of the simplicity of their design and their lower costs, systems of the on-off type are considered for this application.

One such system, shown in Figure 15, uses the difference in electrical conductance of water and that of the oil. Practically all oils are electrical insulators. Water (excluding pure water) is capable of conducting electricity. The system of Figure 15 uses this property to sense the oil-water interface in the collecting chamber by providing two electrodes at different heights in it. For sensing, the electrodes are connected to a 10-volt AC supply through a 1000-ohm resistor. The solenoid valve on the outgoing oil line is operated by the output of the amplifier, which receives its input from a rectified voltage signal across the resistor in the sensing circuit. The AC supply in the sensing circuit minimizes the electrolysis in the collecting chamber. When the oil-water interface is below the bottom electrode, the resistance in the sensing circuit is very high and practically no current flows through it. This configuration leads to the opening of the solenoid valve provided on the oil outlet line. As the oil is extracted, the oil-water interface in the chamber eventually rises above the bottom electrode, thereby decreasing the resistance in the sensing circuit. This results in a voltage across the resistor, which, when amplified, closes the solenoid valve and, thus, stops the oil extraction.

Alternative means of sensing the oil-water interface may be employed in the foregoing control system. An ultrasonic transducer, although expensive, can sense the oil-water interface precisely. Another means of sensing is based upon the photo-electric principle. Irrespective of the type of sensing used, the basic design of the control system remains unchanged.

COMPARISON WITH THE TYPICAL PARALLEL-PLATE SEPARATORS

It was learned from the feasibility tests that a separating device based upon the Coanda-effect principle is capable of gross separation only. Therefore, for an evaluation the separator should be compared with typical, laminar-flow, parallel-plate separators.

Because of its design configuration and the flow velocities through it, the Coanda-effect separator will have a considerably smaller physical size. For instance, a separator to treat 20 gpm of oil-water flow can be 1.5 feet long by 1 foot wide by 1.5 feet high; a typical parallel-plate separator [1] of the same flow capacity occupies 3 feet 3-1/2 inches by 3 feet 6 inches by 1 foot 7 inches of space. The physical size comparison of the Coanda-effect separators with typical parallel-plate separators for handling 20 and 100 gpm of mixture flow is given in Table 2. Because of its smaller size, for a given flow rate, the equipment cost of the Coanda-effect separator will be lower.

Presently, the Coanda-effect separator is in its early stages of development and, thus, many design modifications are required; therefore, a comparison of its oil-separating capabilities with that of the fully developed parallel-plate separator is not possible. More work is required before such a comparison can be made. Finally, because of the simplicity of its design, the maintenance of the separator promises to be easier.

CONCLUSIONS

The investigation conducted to date establishes the feasibility of using the Coanda-effect principle in developing an oil-water separator. A separator based upon this concept will be considerably smaller than a laminar-flow separator of comparable capacity. Feasibility tests conducted on an experimental model of the separator, with an oil-water mixture containing 6% oil (mixture flow rate of 1.5 gpm), show that the oil content can be reduced to less than 3%. The extracted oil contains only 5% water. To make the separator practical, staging is necessary. Further, to improve the quality of extracted oil, an automated system is required to control the oil extraction rate. A concept of one such system given should be investigated by testing it on the experimental separator. Improvements in the effectiveness of the separator can be accomplished by modifying the velocity distribution of the mixture jet to alter the centrifugal acceleration on it.

REFERENCES

1. Naval Civil Engineering Laboratory. Mechanical and electrical engineering department, letter report, YF38.554.001.01.001: Program plan for oily waste handling at navy shore establishment, by E.L. Ghormley, PH.D., Port Hueneme, California, June 1972.

2. S.M. Finger and R.B. Tabakin. Development of shipboard oil/water separation systems, ASME paper 73-ENAS-38, presented at the Intersociety Conference on Environmental Systems, San Diego, California, July 16-19, 1973.

3. U.S. Navy Case 56,734: Patent application on coanda effect oil-water separator, by A.J. Paszyc, Ph.D., D. Pal, and J.B. Curry, 15 June 1973.

4. C. Bourque and B.G. Newman. Reattachment of a two-dimensional incompressible jet to an adjacent flat pole, the Aeronautical Quarterly, Vol XI, Aug. 1960, pp. 201-232.

5. R.A. Sawyer. The flow due to a two dimensional jet issuing parallel to a flat plate, J. Fluid Mech, Vol. 9, 1960, pp. 534-60.

6. Naval Civil Engineering Laboratory. Contract Report CR-73.015: Test and Evaluation of oil water separation systems, by the Ben Holt Co. of Pasadena, California. Port Hueneme, California, 8 Nov. 1972.

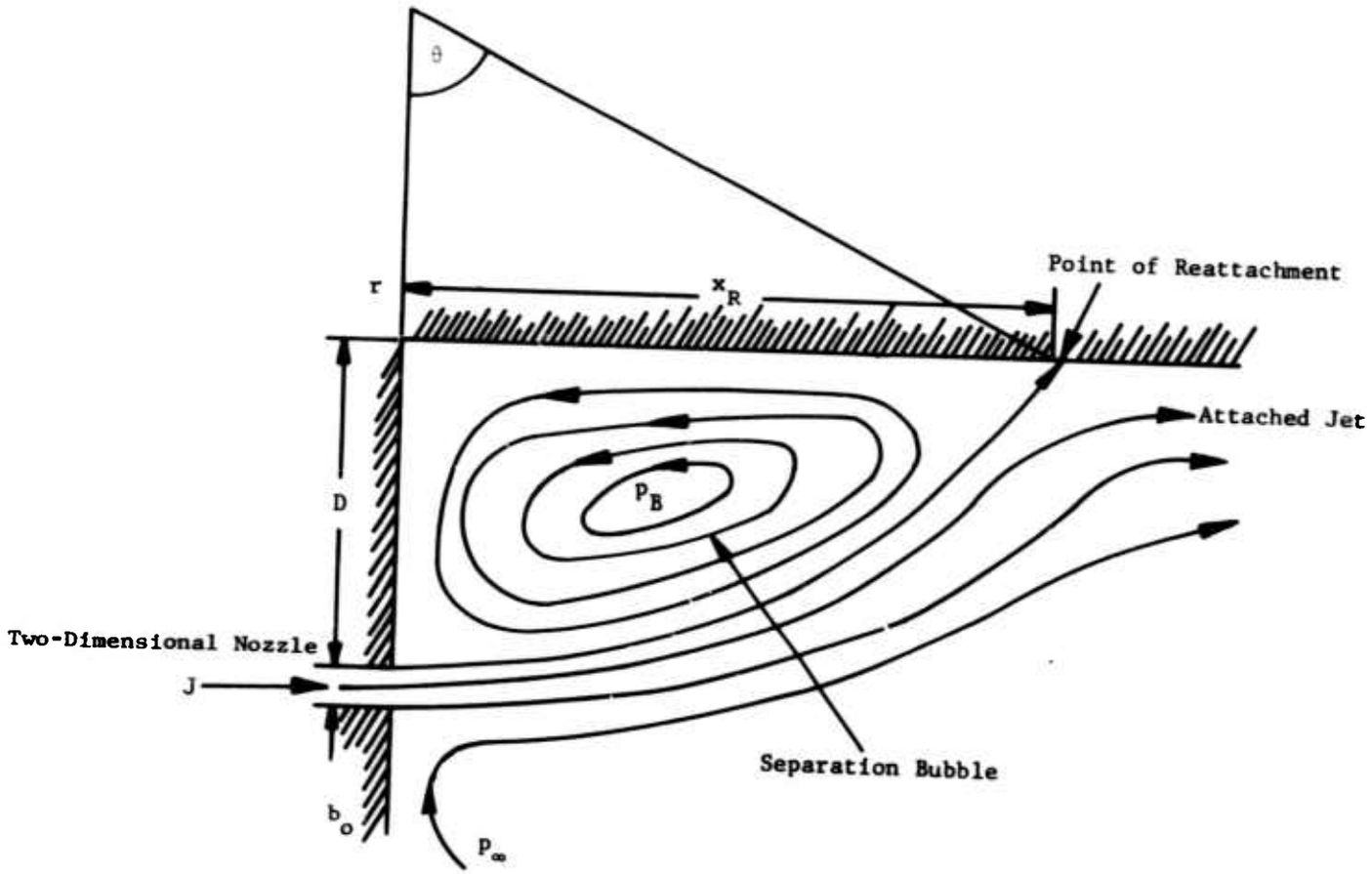


Figure 1. Two-Dimensional Jet Attaching to an Offset Parallel Plate

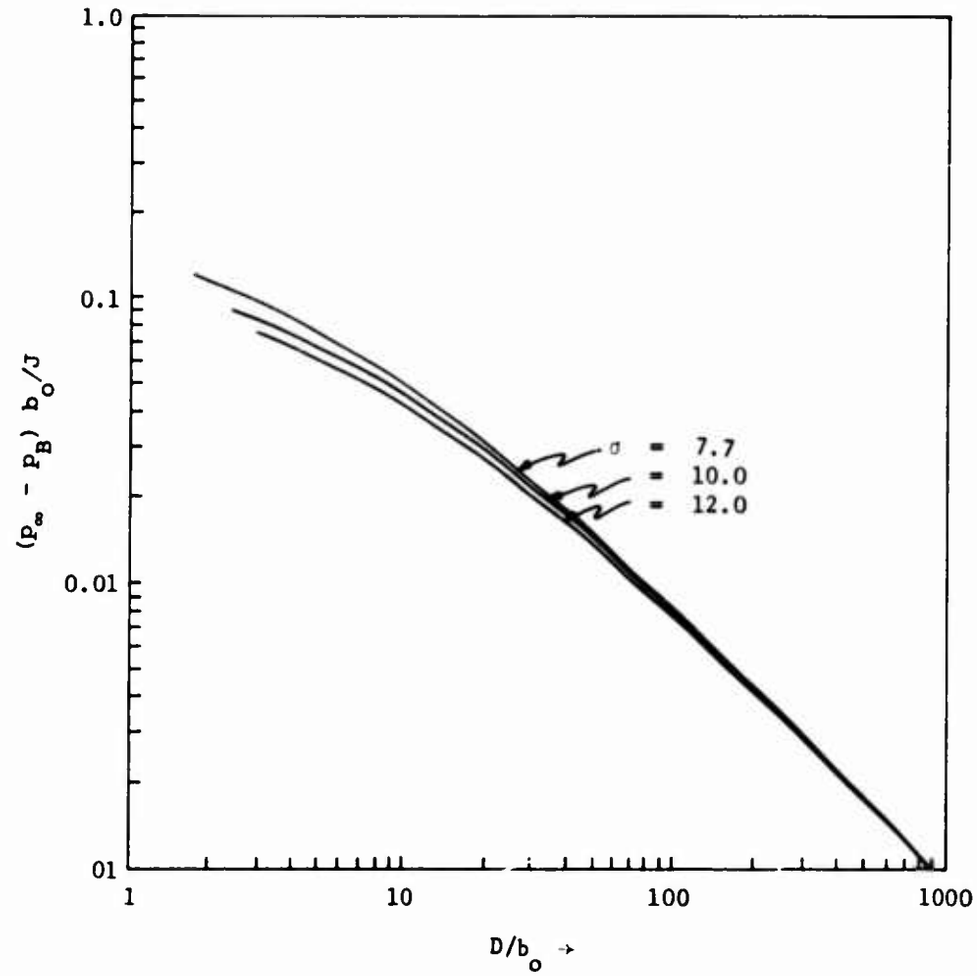
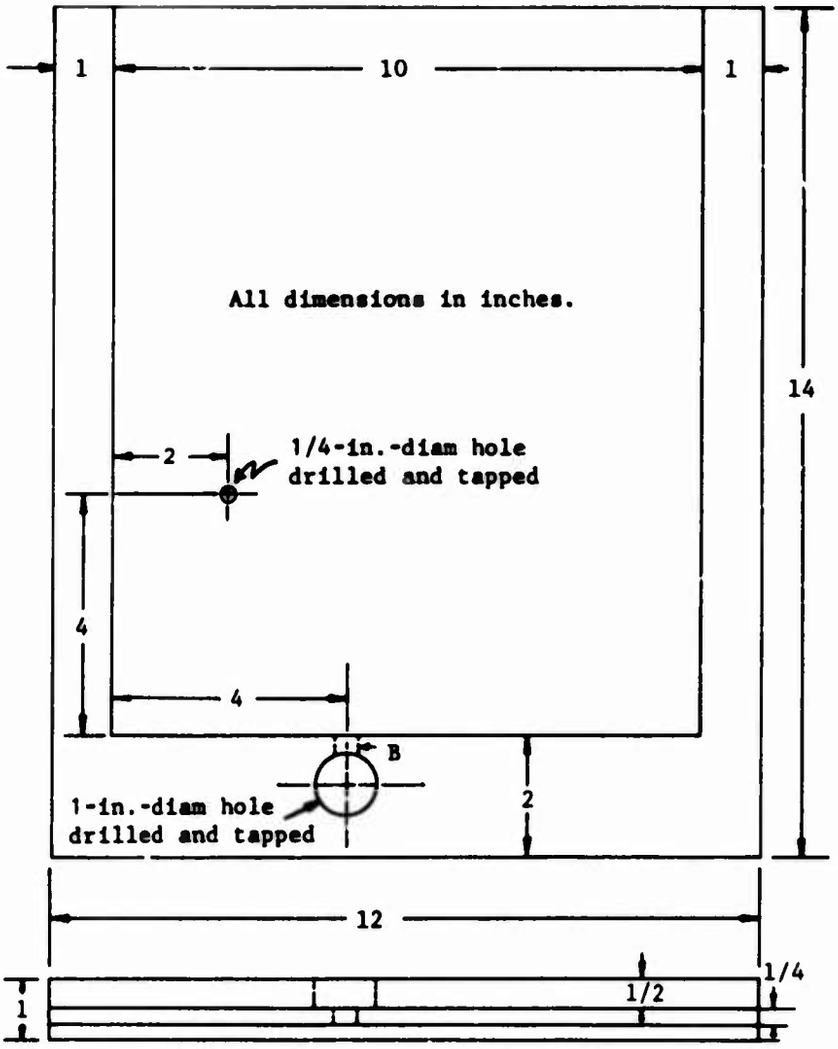


Figure 2. Dimensionless Pressure $(p_\infty - p_B)b_o/J$ Plotted Against Plate Offset Parameter, D/b_o, for Various Values of σ.



B is 1/4 in. for Element No. 1, 3/8 in. for Element No. 2.

Figure 3. Sketch of the Test Element.

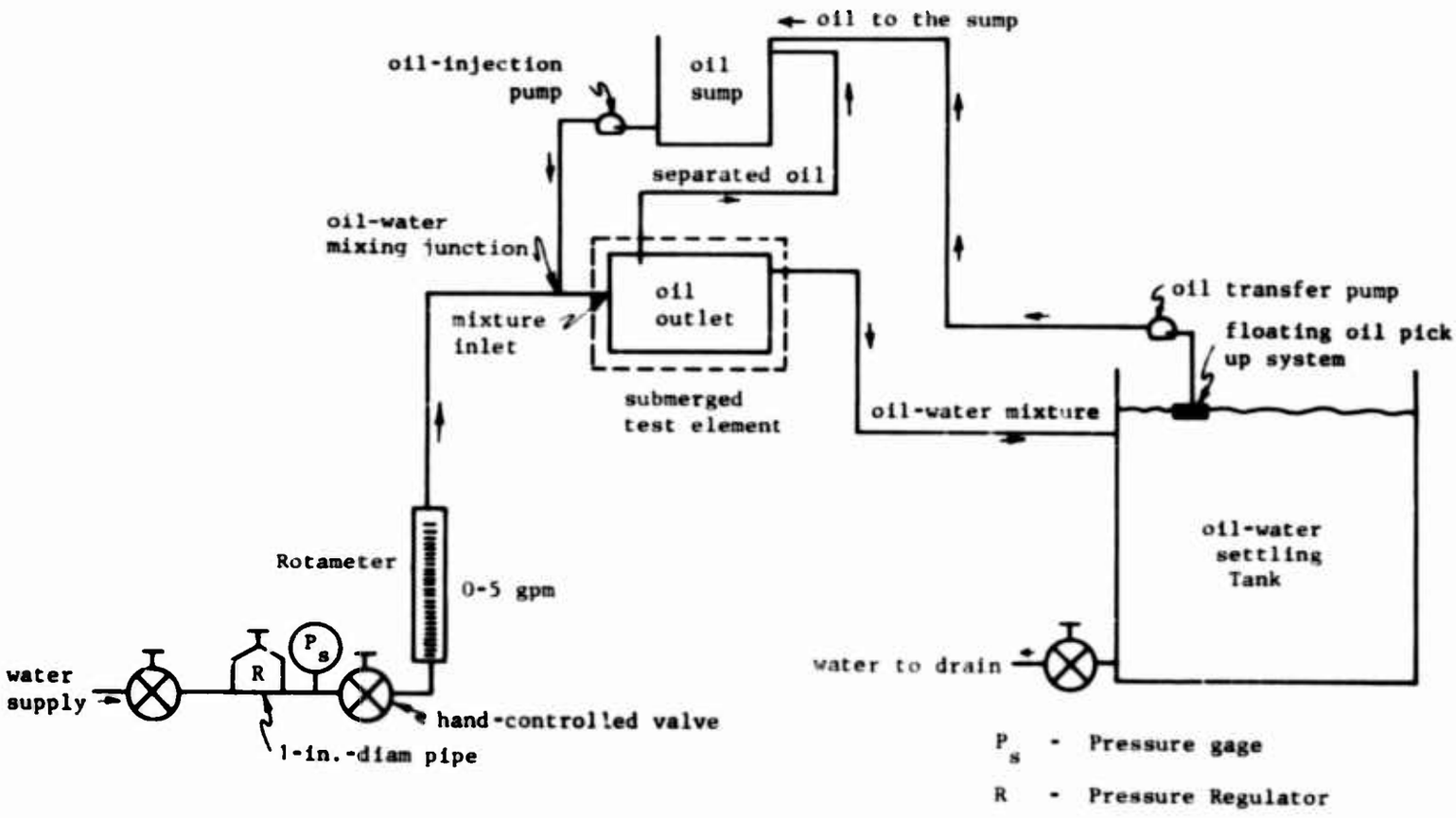


Figure 4. Schematic of the Test Setup.

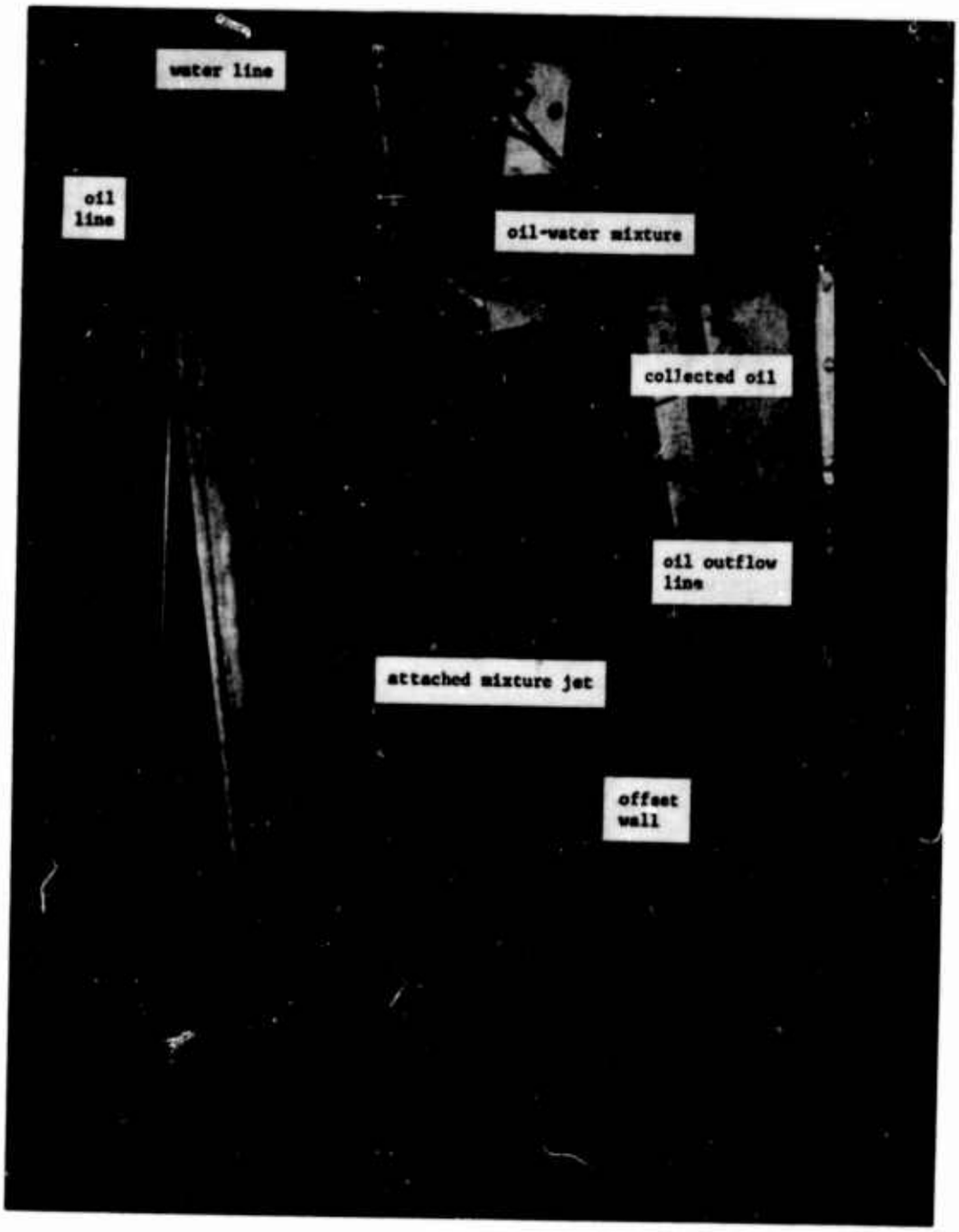


Figure 5. Flow Pattern Through Element No. 2 at a Mixture Flow Rate of 1.5 gpm Water With 7% Oil.

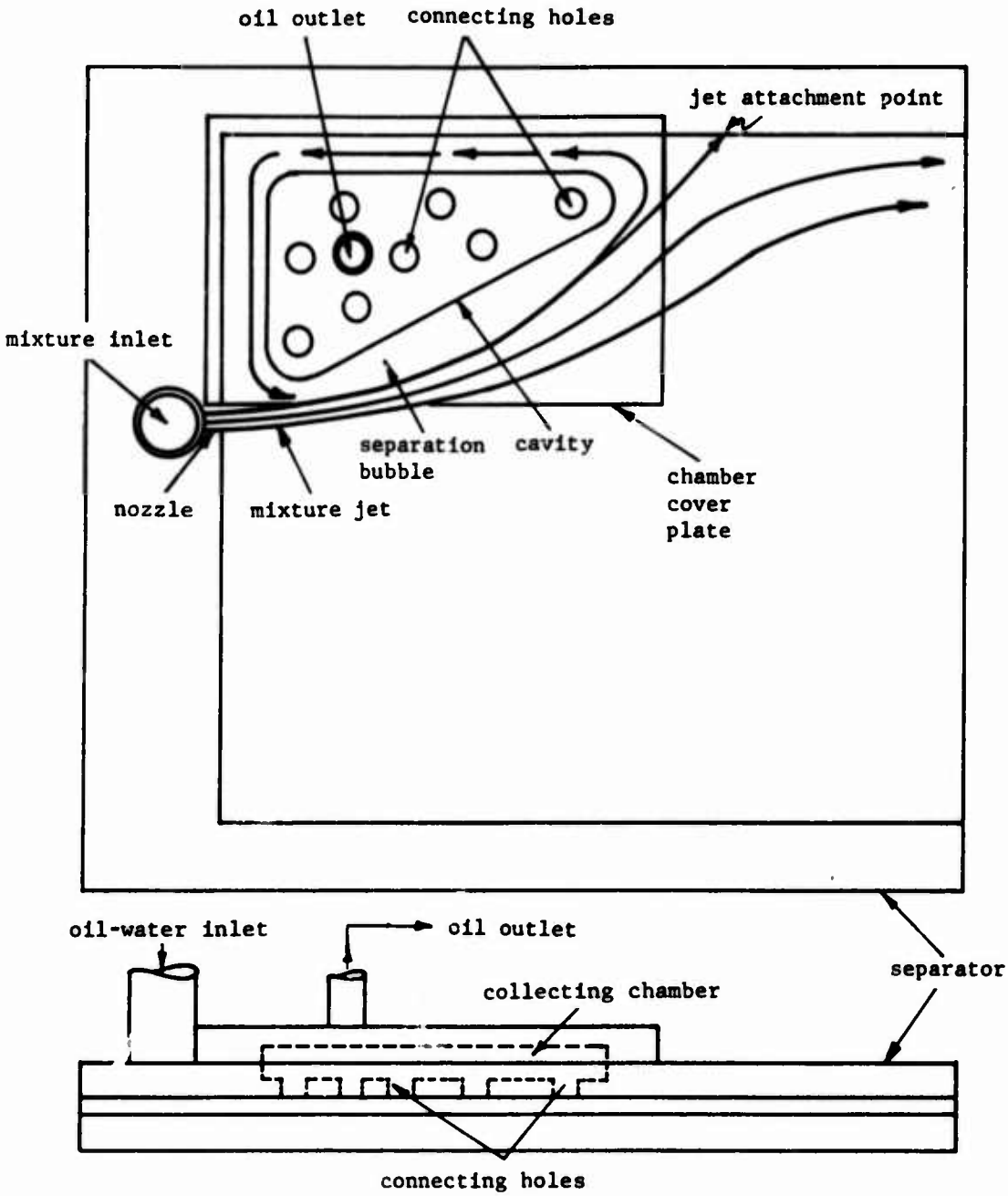


Figure 6. Test Model of Single-Stage, Coanda-Effect, Oil-Water Separator.

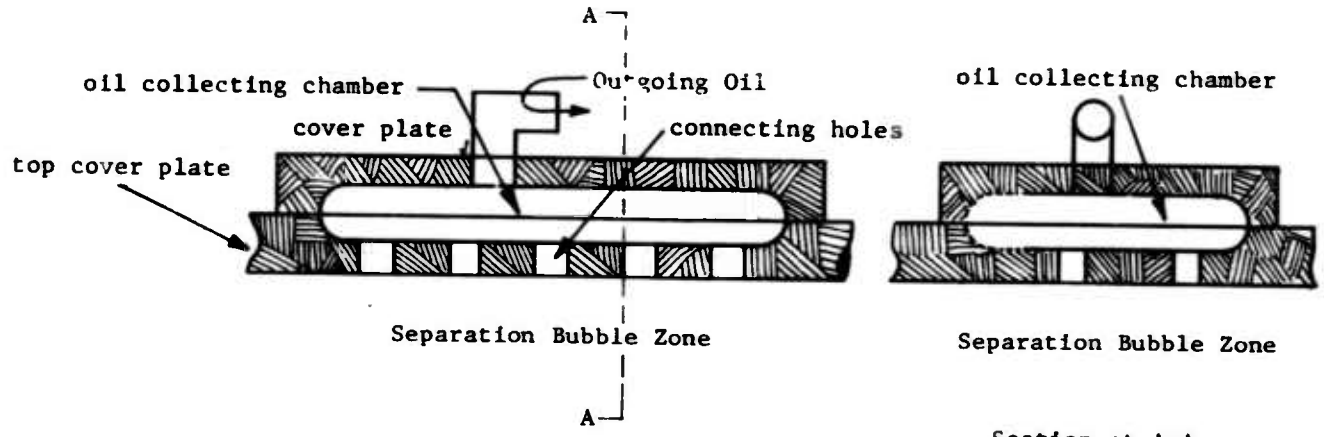


Figure 7. Design Features of the Oil Collecting Chamber.

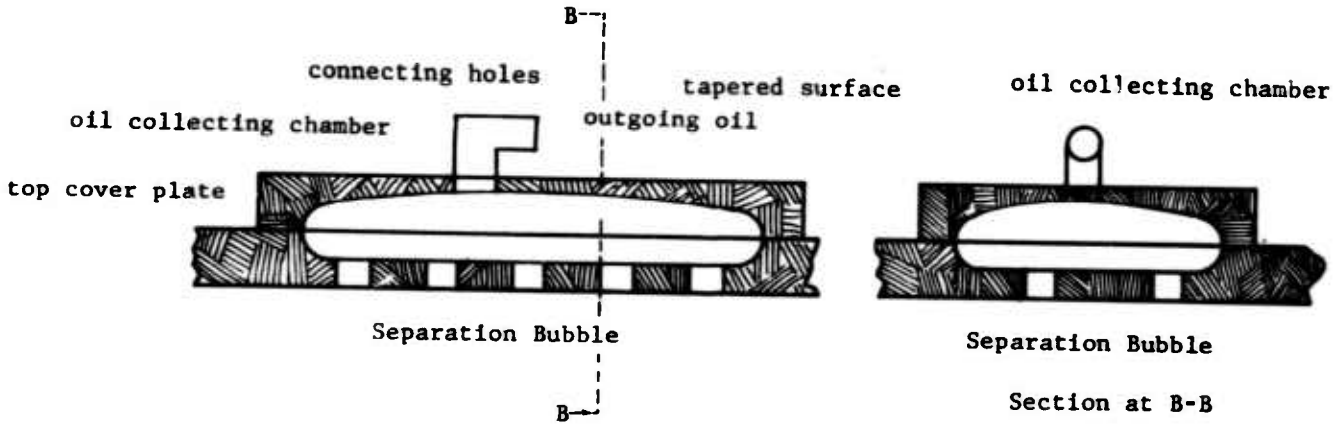


Figure 8. Modified Design of the Oil Collecting Chamber.

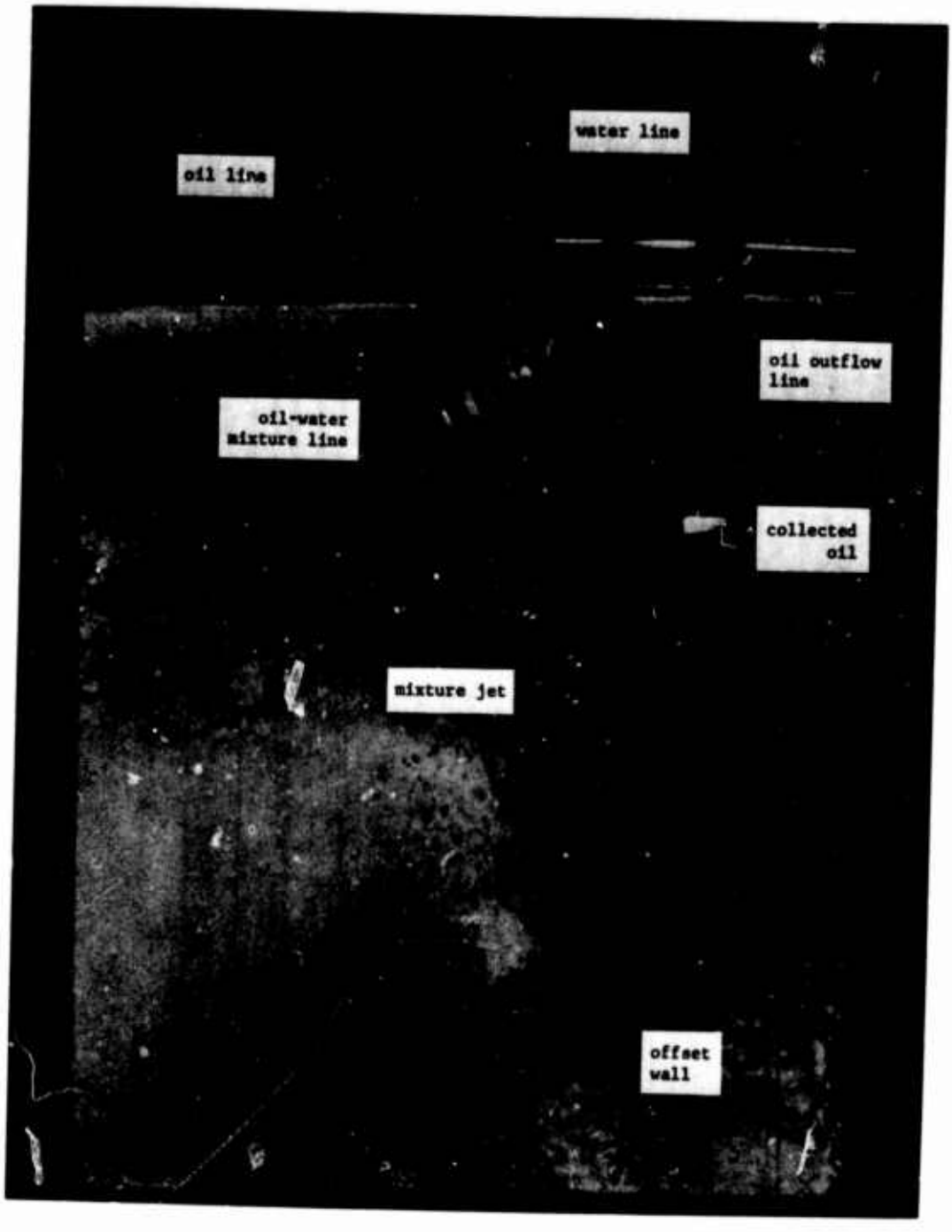
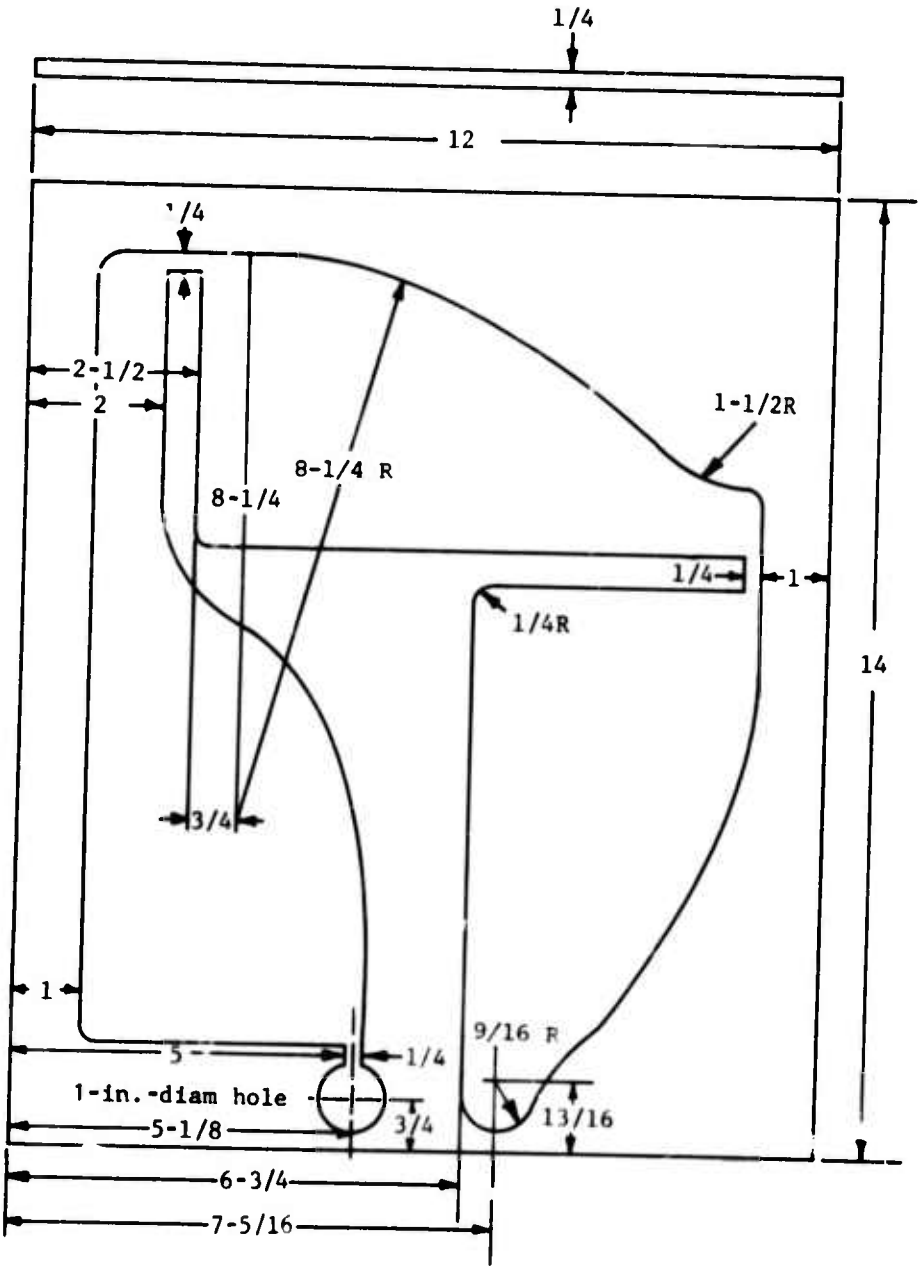


Figure 9. Flow Pattern Through the Modified Element No. 1 at 0.8 gpm Water Flow Rate With 6% Oil.



All dimensions in inches.

Figure 10. The Sketch of Experimental Three-Stage Element.

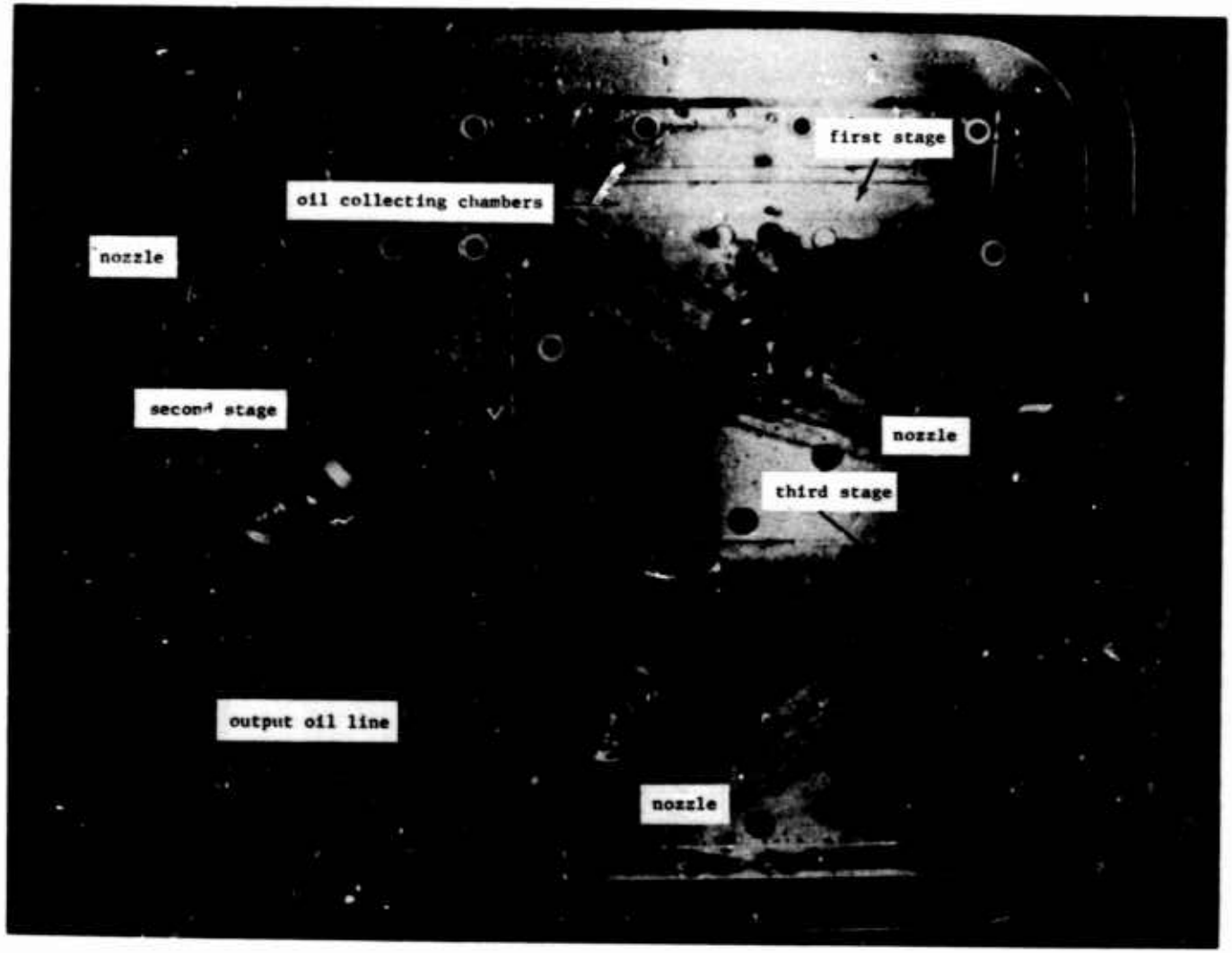


Figure 11. The Three-Stage Test Element With Water Flow Only. The Flow Through Device is 0.9 gpm. (The oil droplets in the collecting chambers is the residual oil from the previous tests.)

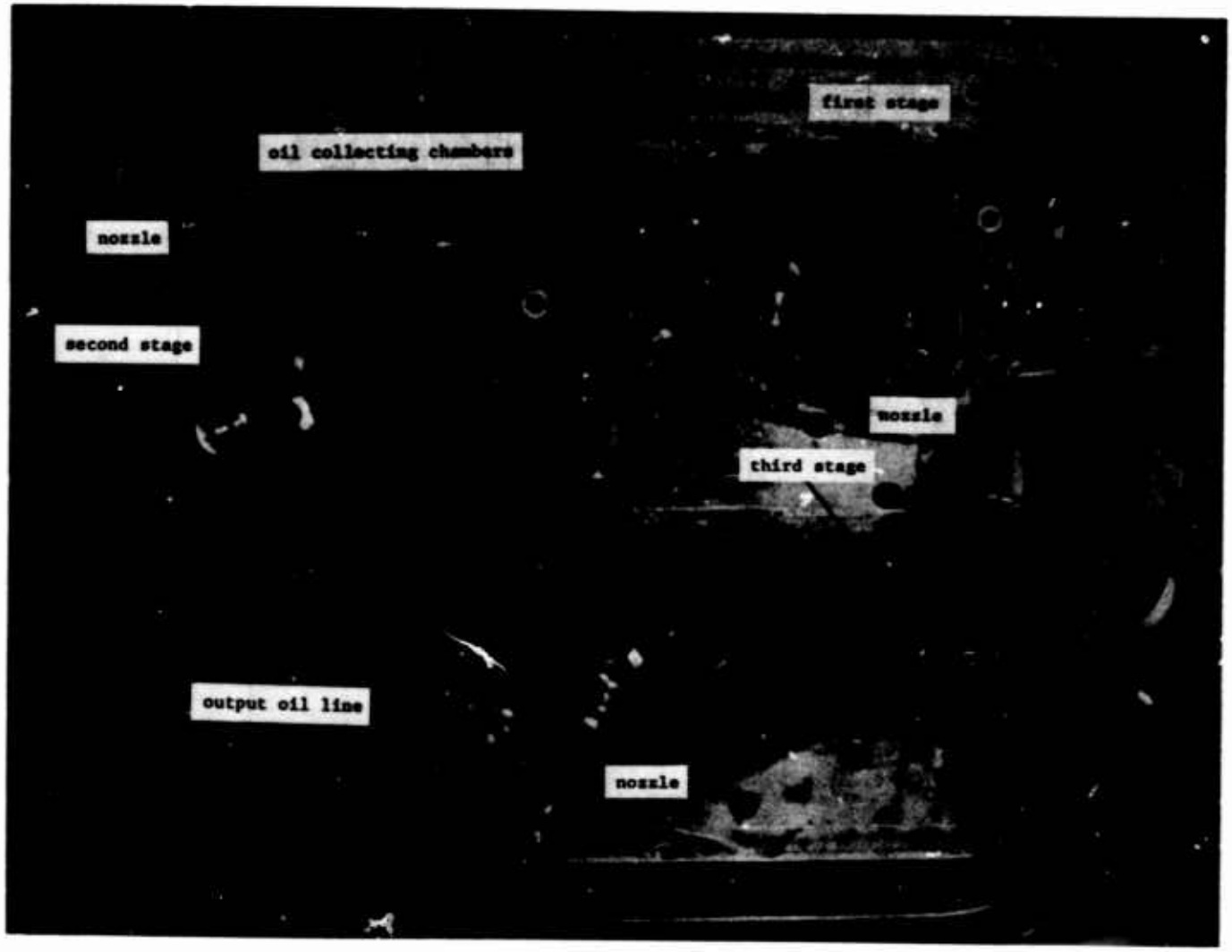
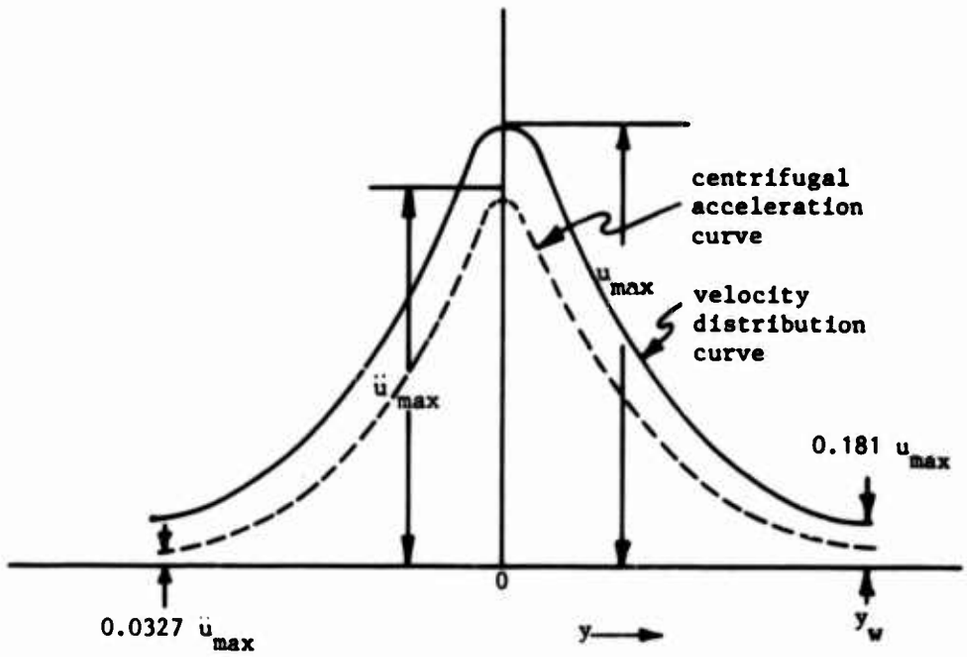


Figure 12. Flow Pattern Through the Three-Stage Repainting Device at 0.9 gpm Water Flow With 6% Oil.

$$u_{max} = \left(\frac{3J\sigma}{4\rho(s + s_o)}\right)^{1/2} \qquad \ddot{u}_{max} = \frac{3J\sigma}{4\rho(s + s_o)r}$$



Distance Perpendicular
to the Jet Center Line

Figure 13. Reattaching Jet Axial Velocity and Centrifugal Acceleration Distributions

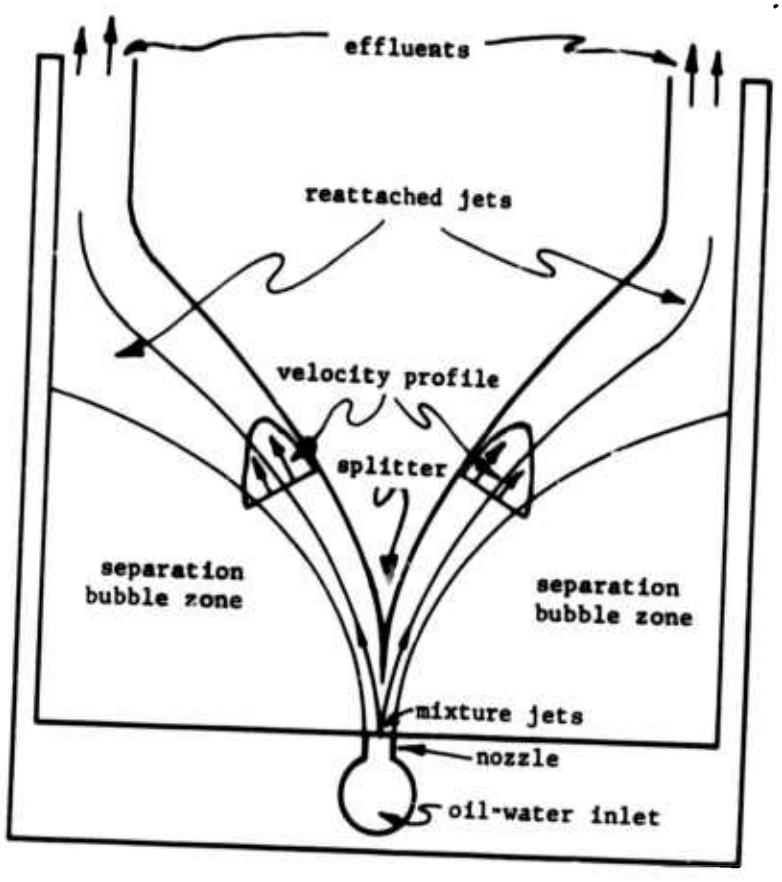


Figure 14. Conceptual Design of a Modified Separator With Improved Jet Velocity Profiles.

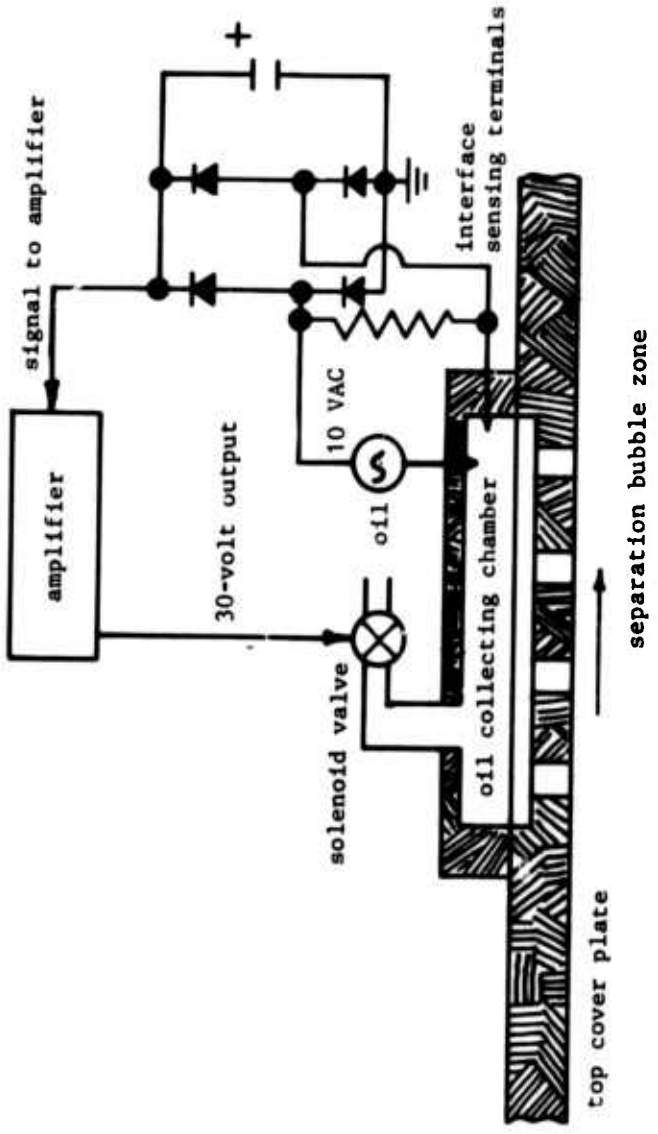


Figure 15. Schematic of an Oil Extraction System

Appendix A

A TWO-DIMENSIONAL INCOMPRESSIBLE JET ISSUING PARALLEL TO AN OFFSET FLAT PLATE

This appendix lists the equations and data describing the flow resulting from a two-dimensional incompressible jet issuing parallel to an offset flat plate.

Wall Attachment Flow Analysis

This problem has been treated in depth by Bourque and Newman [4], and by Sawyer [5] independently. The analysis conducted by Bourque and Newman is easy to understand and covers a wide range of flow parameters. In this study, therefore, only the results of Reference 4 were used.

The analysis can be described by considering the flow of a two-dimensional jet issuing from a nozzle in a wall adjacent to a parallel plate with an offset D as shown in Figure A-1. The jet during its expansion entrains fluid from its surroundings by turbulent action. The entrainment of fluid from the plate side causes a pressure difference across the jet, thus curving it toward the plate. If the plate is sufficiently long, the jet will strike it and reattach. The jet divides on striking the plate, sending part of the flow into the separation bubble. The flow equilibrium is reached when the flow entrained by the plate side of the jet is equal to that into the separation bubble from the jet at the point of striking. This is the model used in the analysis of Reference 4. Further, the analysis is based upon the following assumptions:

(1) The flow is incompressible and two-dimensional, i.e., only thin jet sheets are considered.

(2) The jet efflux velocity is uniform, i.e., the increase in its velocity with the reduced pressure in the separation bubble is neglected. The jet is submerged in a similar fluid, and its velocity distribution is that of a free jet.

(3) The jet entrains the same amount of fluid from each boundary.

(4) Pressure within the separation bubble is constant, and the jet center line is a circular arc up to the point of attachment.

(5) The force on the plate due to skin friction forces is small and is neglected.

The axial component of jet velocity used is

$$u(s,y) = \left[\frac{3J\sigma}{4\rho(s + s_o)}\right]^{1/2} \operatorname{sech}^2 \left(\frac{\sigma y}{s + s_o}\right) \qquad (2)$$

where s = axial distance from the nozzle

b_o = nozzle width

s_o = distance of the nozzle from a hypothetical origin of the jet where the flow originates = $\sigma b_o/3$

y = coordinate normal to the jet center line

σ = jet spread parameter, to be determined experimentally; it has a value of 7.7 for a turbulent free jet

Before going any further some quantities must be defined as follows:

P_∞ = free stream pressure

P_B = static pressure within the separation bubble

r = radius of the center line of the reattached jet

ρ = density of the fluid

θ = angular location of the point of reattachment from the nozzle

D = distance of the plate from the nozzle axis

x_R = distance of the point of attachment from the corner

P = length of the plate

J = jet momentum per unit span of the nozzle

The equation of the reattaching streamline is given by

$$\frac{3s}{\sigma b_o} = \left(\frac{1}{t^2}\right) - 1 \qquad (A\text{-}1)$$

where $$t = \tanh\left(\frac{\sigma y}{s + s_o}\right) \tag{A-2}$$

If $$t = t_1 \tag{A-3}$$

where $$t_1 = \tanh\left(\frac{\sigma y_1}{s_1 + s_o}\right) \tag{A-4}$$

and is the value of t at the point of reattachment, then the radius of the jet center line is derived from

$$\frac{r}{b_o} = \frac{\sigma(1/t_1^2 - 1)}{3\theta} \tag{A-5}$$

where t_1 and θ are determined from the following equations:

$$\frac{D}{b_o} = \frac{\sigma(1/t_1^2 - 1)\ (1 - \cos\theta)}{3\theta} - \frac{1}{2} \tag{A-6}$$

and $$\cos\theta = \frac{3}{2}t_1 - \frac{1}{2}t_1^3 \tag{A-7}$$

The half width of the jet at the reattachment point, i.e., y_1, can be derived easily from Equation A-5 and is

$$\frac{y_1}{b_o} = \frac{1}{3}t_1^2 \tanh^{-1} t_1 \tag{A-8}$$

Further, the distance of the reattachment point from the plane of the nozzle is

$$\frac{x_R}{b_o} = \frac{\sigma(1/t_1^2 - 1 - \sin\theta)}{3\theta} - \frac{\tanh^{-1}t_1}{3t_1^2 \sin\theta} \tag{A-9}$$

Finally, the mean pressure within the separation bubble is computed by

$$P_\infty - P_B = \frac{J}{b_o}\left[\frac{3\theta}{\sigma(1/t_1^2 - 1)}\right] \qquad \text{(A-10)}$$

A wall attachment element can be designed using Equations A-1 through A-9.

However, to use these equations conveniently, it is required that the flow parameters x_R/b_o, r/b_o, y_1/b_o, and θ be known as functions of the pre-determined parameter D/b_o. These equations are complex and can not be expressed explicitly in terms of D/b_o alone.

A numerical scheme was devised to compute x_R/b_o, r/b_o, y_1/b_o for known values of D/b_o. The numerical method runs as follows. By inspection of Equation A-7, maximum and minimum values of t_1 which render θ between 90 degrees and 30 degrees were determined. Since y_1 is positive, only positive values of t_1 must be considered. Further, it was determined from Equation A-7 that for θ to lie between 90 degrees and 30 degrees, t_1 must range between 0 and 0.50. A known value of t_1 yields θ from Equation A-7. For a selected value σ with known t_1 and θ, parameters D/b_o, r/b_o, y_1/b_o, and x_R/b_o can be determined from Equations A-6, A-5, A-8, and A-9, respectively. Thus, a set of values for x_R/b_o, r/b_o, and y_1/b_o for a known D/b_o can be computed. A series of similar sets were computed by increasing t_1 by 0.05 each time up to a final value of 0.50. Three series of sets were computed for a different σ of 12, 10, and 7.7, respectively.

For easy usage the parameters θ, y_1/b_o, r/b_o, and x_R/b_o were plotted against D/b_o for values of D/b_o ranging from 1 to 1000. These plots are shown in Figures A-2 through A-5. It should be added here that flow parameters become independent of the parameter D/b_o for D/b_o greater than 35. Also the analysis becomes inaccurate for a D/b_o less than 3. Further, the value of σ, the spread parameter, chosen can affect the flow parameters appreciably.

One last remark of interest is regarding the value of σ, the spread parameter to be used while using these curves. Because of the curvature effect a σ of 7.7 does not apply. It is reported in Reference 1 that a value of 12 for σ gives flow parameter values that are in fair agreement with the experimental data.

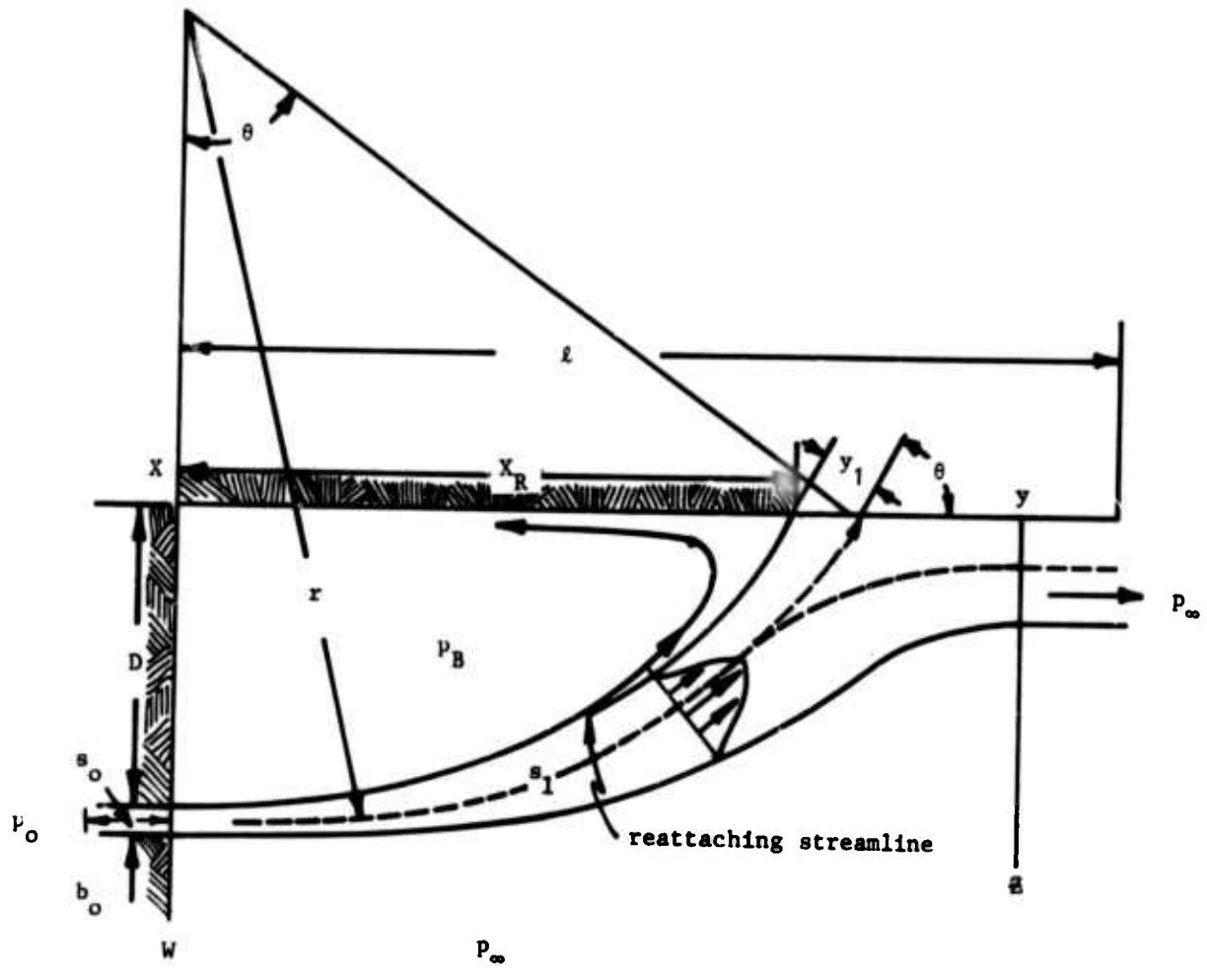


Figure A-1. A Two-Dimensional Jet Reattached to an Offset Parallel Plate.

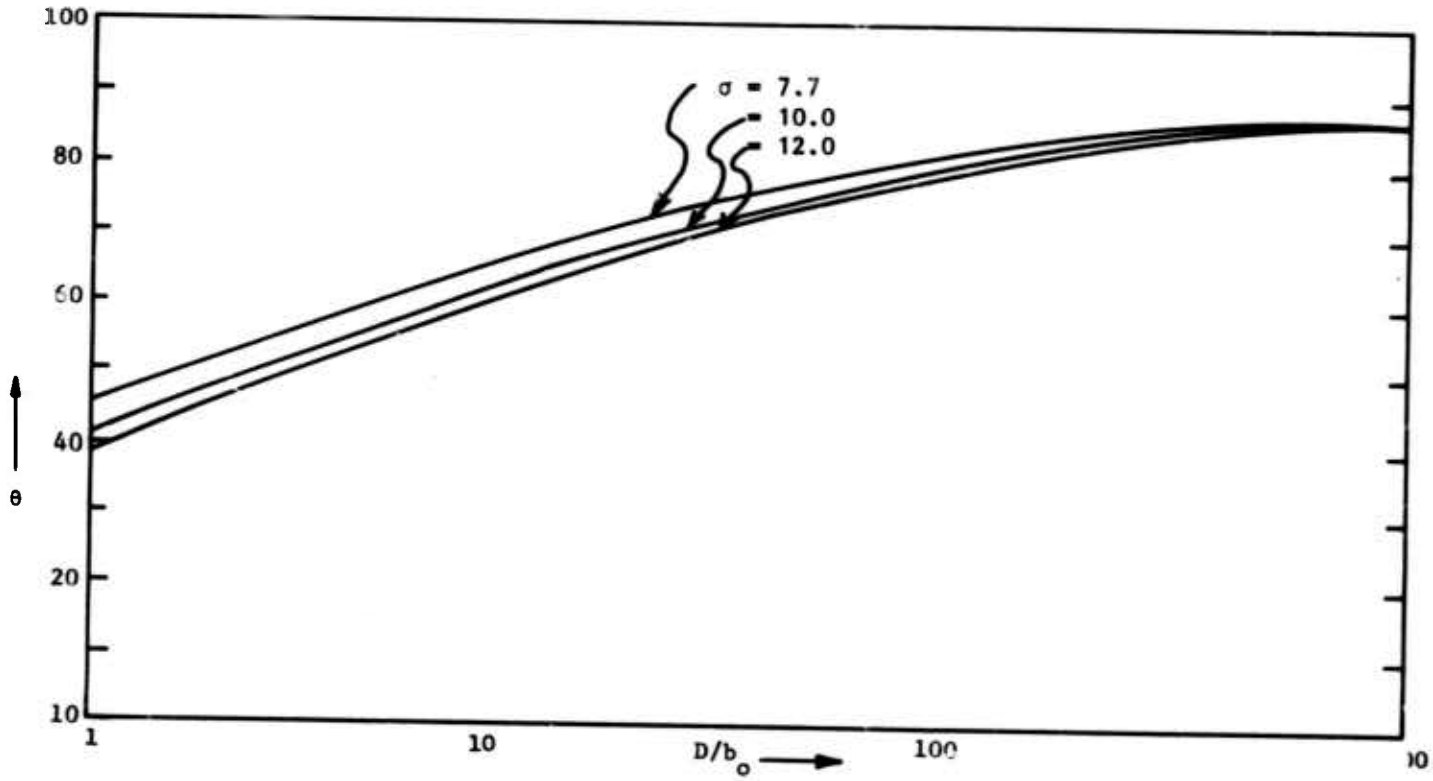


Figure A-2. Angular Location (θ) of the Jet Reattachment Point Plotted Against Plate Offset Parameter, D/b_o, for Various Values of σ.

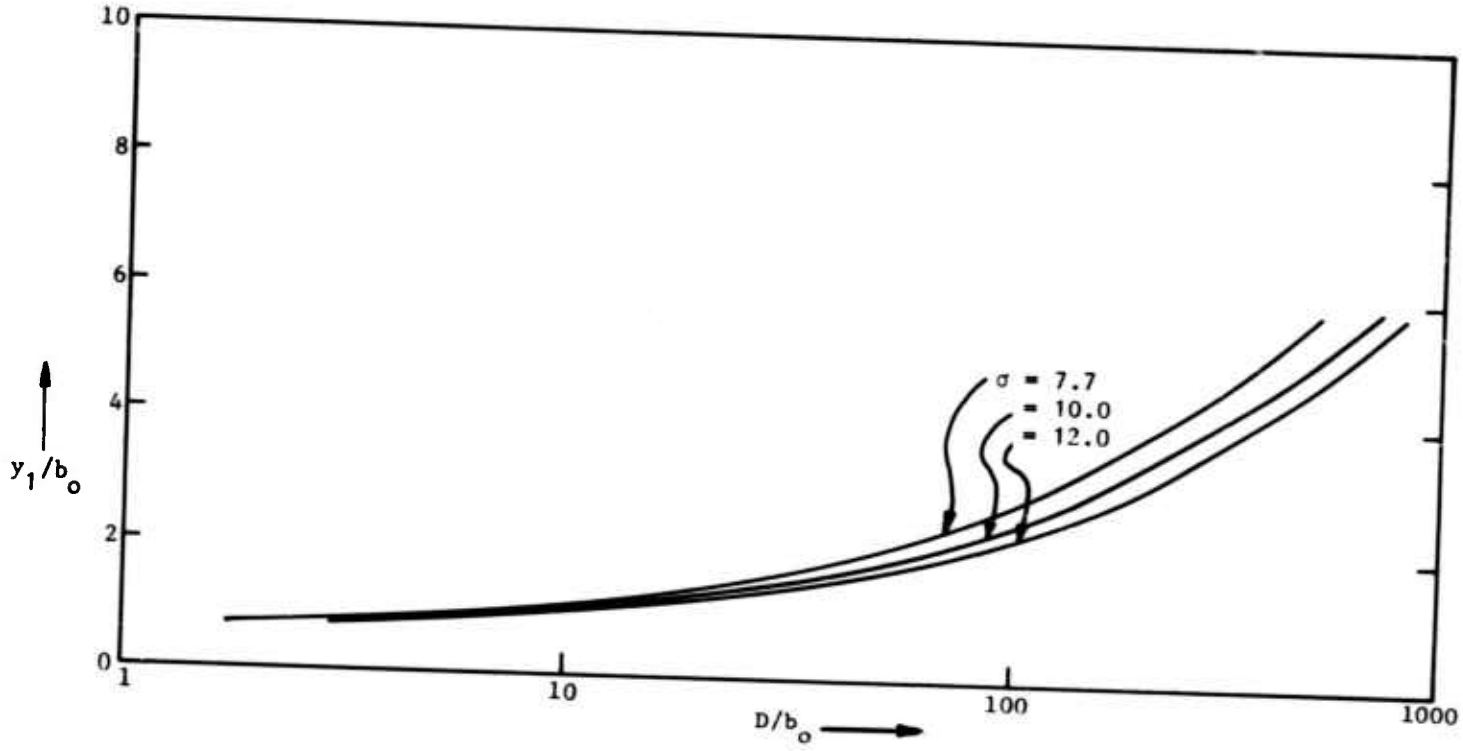


Figure A-3. Half Width (y_1/b_o) of the Jet at the Reattachment Point Plotted Against Plate Offset Parameter, D/b_o, for Various Values of σ.

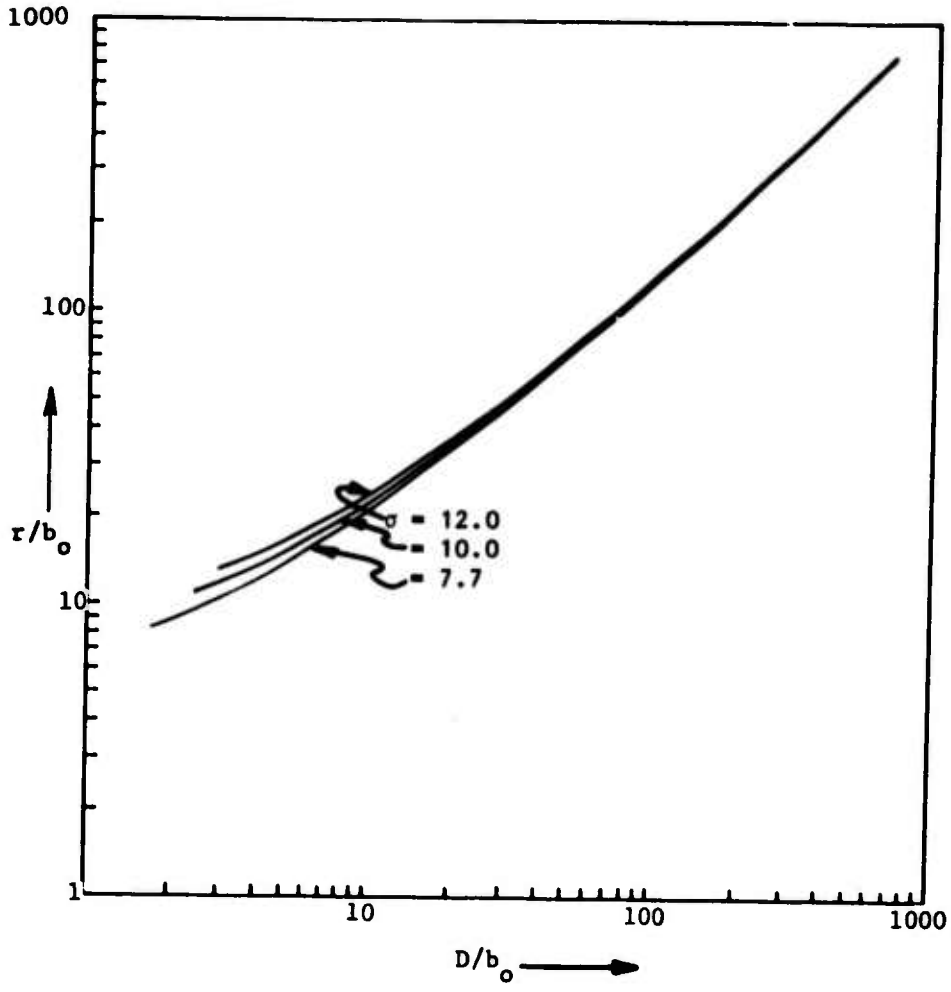


Figure A-4. Jet Center Line Radius, r/b_o, Plotted Against Plate Offset, D/b_o, for Various Values of σ.

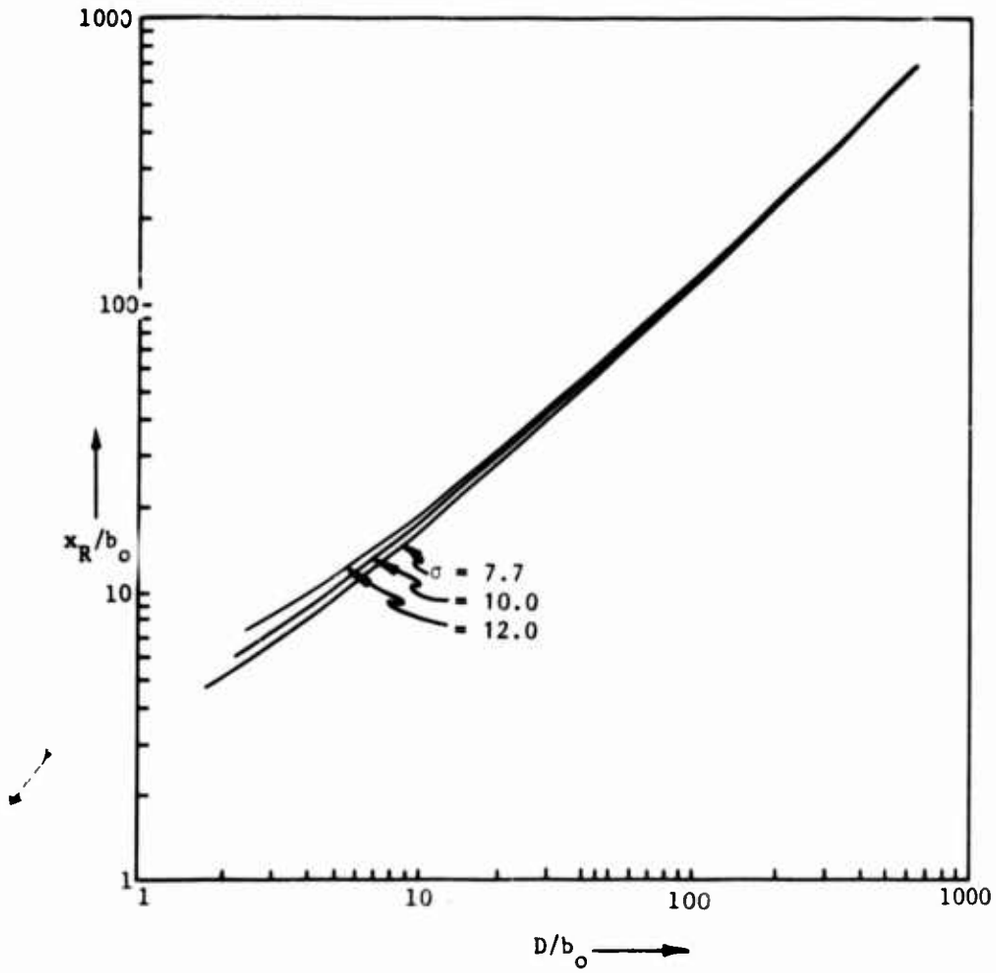


Figure A-5. Reattachment Distance, x_R/b_o, Plotted Against Plate Offset for Various Values of σ.

Appendix B

SPECIFICATIONS OF OIL USED IN THE TEST MIXTURE

Hydraulic fluid - Petroleum Base

Mil. spec.: MIL-H-5606C

Fed. Stock No.: FSN 9150-223-4134

Specific gravity: 0.88 to 0.90

Color: red

Kinematic viscosity: 8.0 stokes at 40°F to 0.10 stoke at 130°F

Table 1. Parameters of the Test Elements

Parameter	Element No. 1	Element No. 2
Nozzle width, b_o (inches)	1/4	3/8
Wall offset, D (inches)	4.0	4.0
Attachment wall length, ℓ (inches)	12.0	12.0
Offset parameter, D/b_o	16.000	10.67
Flow passage depth, h (inches)	1/4	1/4
Designed water flow (gpm)	0.80	1.50
Velocity at the nozzle at designed flow (ft/sec)	4.10	5.13
Reynold's number* at the nozzle, at designed flow	7119.7	13354.7
Jet momentum at the nozzle, J (lb/ft)	0.6794	1.595
Predicted pressure, p_B, within the separation bubble, from Figure 2 (inches of H_2O)	0.1978	0.3935
Predicted attachment distance, x_R, from Figure A-5 (inches)	6.6	7.2
Predicted jet centerline radius, r, from Figure A-4 (inches)	7.75	9.0
Predicted half width of the jet, y_1, from Figure A-3 (inches)	0.251	0.345

* Kinematic viscosity of water at 60^oF taken as 1.2×10^{-5} ft^2/sec.

Table 2. Physical Size Comparison of the Coanda-Effect and Typical Parallel-Plate Separators

Maximum Designed Mixture Flow Through The Separator (gpm)	Dimension	Coanda-Effect Separator	Parallel-Plate Separator
20	length	1 ft 6 in.	3 ft 3-1/2 in.
	width	1 ft	3 ft 6 in.
	height	1 ft 6 in.	1 ft 7 in.
100	length	3 ft	5 ft 9 in.
	width	2 ft	3 ft 6 in.
	height	1 ft 6 in.	3 ft 2 in.

DESIGN AND DEVELOPMENT

OF

A FLUIDIC BISTABLE ACTUATOR

J. C. DUNAWAY

GUIDANCE AND CONTROL DIRECTORATE
US ARMY MISSILE RESEARCH, DEVELOPMENT & ENGINEERING LABORATORY
US ARMY MISSILE COMMAND
REDSTONE ARSENAL, ALABAMA 35809

ABSTRACT

DESIGN AND DEVELOPMENT OF A FLUIDIC BISTABLE ACTUATOR

This paper describes the design and development of a fluidic bistable missile control actuator. The control system mechanization permitted the use of a simple open loop bistable actuator. The input was a ±10 psid, 11.5 Hz square wave from a fluidic pulse duration modulator. The output was a torque of 250 in-lb with a rotational limit of ±8 degrees when a nitrogen supply pressure of 1000 psig is used.

NOMENCLATURE

A - Orifice Area

A_{12} - Upstream Orifice Area

A_{23} - Downstream Orifice Area

A_p - Piston Area

D - Ball Diameter

d - Seat Diameter

P_c - Pressure, Control Differential

P_{dp} - Pressure, Piston Differential

P_d - Pressure Downstream

P_p - Pressure, Piston

P_s - Pressure, Supply

P_u - Pressure, Upstream

T - Torque Output

X_p - Bellcrank Lever Arm

X_b - Ball Poppet Opening

INTRODUCTION:

Artillery missile control systems are required to be low cost, reliable, and simple to operate in the field. Large missile errors are caused by surface winds during the propulsion booster phase. Directional control is a simple control scheme that reduces the surface wind errors, by using a loose attitude control system to control the weathercocking of a stable missile to make the wind forces on the missile body and the windward component of the boost thrust equal, which results in a cross range velocity of near zero at boost termination.

The directional control concept was further simplified by implementing fluidic control components. System analysis showed that one particular implementation would simplify the actuation system. A block diagram of this scheme is shown in figure 1, and makes use of a quasi-linear fluidic pulse duration modulator input to a bistable actuator. System simulation showed that the actuator must operate from stop to stop over the required linear range of ±70% modulation, where percent modulation is defined as:

$$\frac{\text{Time on - Time off}}{\text{Time on + Time off}} \times 100\% = \text{Percent modulation}$$

Figure 2 shows the pulse shape at 0% modulation and at the extreme required range of ±70%. At 70% modulation the shortest pulse width is 12 milliseconds.

Since the shortest pulse width is 12 milliseconds the period of a full cycle of minimum pulse width would be 24 milliseconds or a frequency of 41.6 Hz which is the minimum frequency response required of the actuator.

The actuator designed was a push-push piston actuator which operated on a bellcrank to give a rotary output. The pistons were driven by two three-way valves operated in a push-push mode to act as a four-way valve. The three-way valves consist of fixed upstream orifices and variable downstream orifices, in the form of a spherical poppet valve. Two spherical poppet valves are driven by low pressure pistons which operate against a flapper in a push-push mode. The pistons are driven by a bistable fluidic amplifier. Figure 3 is a schematic of the actuator.

ACTUATOR DESIGN

Following are the actuator design parameters:

Power Source - Stored GN_2

Gas Pressure - 250 - 2000 psig

Flow Rate - As low as possible

Input Differential Pressure - ±10 psid

Output Torque - 250 in/lb

Output Rotary Displacement - ±8 deg.

Frequency - Greater than 40.6 Hz

Moment of Inertia Load - 0.0118 in-lb-sec^2

HIGH PRESSURE PISTON DESIGN

A nominal piston diameter of 0.75 inches was chosen as a design starting point. A layout of the pistons and bellcrank showed that the minimum lever arm for this size pistons was 0.625 inches.

The piston seals were split teflon rings over o'ring expanders. Two rings were used on each piston. The friction force for each piston ring was estimated to be ten pounds which reduces the useable torque by 25 in/lb. Therefore the design torque was increased to 275 in/lb.

From the above design parameter the differential piston pressure P_{dp} was calculated to be 995 psid.

BALL POPPET DESIGN

A poppet design which used a .093" diameter ball (D) and a .067" diameter seat (d) was used with a .022" diameter upstream orifice. Figure 4 shows a schematic of the relationship between the fixed upstream orifice (A_{12}), the variable area ball poppet (A_{23}), and the piston actuation pressure (P_2). Figure 5 shows the ball poppet geometry and a plot of the geometrical area (A_{23}) vs. stroke (X_b) of the ball. This curve was generated by solving the equation given by Anderson (1).

$$A_{23} = \frac{\pi d^2}{4}\left(\frac{\left[2X_b/d + \sqrt{D^2/d^2 - 1}\right]^2 + 1 - D^2/d^2}{\sqrt{(2X_b/d + \sqrt{D^2/d^2 - 1})^2 + 1}}\right) \quad (1)$$

This area is the minimum area until it reaches the area of the poppet seat which is 3.52×10^{-3} square inches and corresponds to a poppet opening (X_b) of .025 inches.

The piston pressures for various poppet areas are plotted in figure 6. This curve was generated by solving the compressible flow equation:

$$W = g\,A\sqrt{\frac{2K}{R(K-1)}}\,\frac{Pu}{\sqrt{Tu}}\left(\frac{Pd}{Pu}\right)^{1/K}\sqrt{1-\left(\frac{Pd}{Pu}\right)^{\frac{K-1}{K}}} \quad (2)$$

This equation was programmed on a Hewlett-Packard 9820A calculator. This program calculates the flow through the upstream and downstream orifices and the pressure P_p that makes the flow through the orifices equal.

Since the actuator operates in the bistable mode the piston pressures of interest are the pressures when the poppets are completely closed or completely open. The curve in figure 6 shows that the differential pressure between the completely open and completely closed poppet is approximately 915 psid.

The force on the ball poppet is a maximum when the poppet is closed, and is simply the product of the seat area times the piston pressure. For the ball poppet designed this force was 3.53 pounds.

A control piston .75 inches in diameter will produce the required force at a pressure of 8 psi. The 10 psi control pressure will be adequate.

MECHANICAL DESIGN

The actuator was designed mechanically to operate with a supply pressure of 0 to 2000 psig. The actuator housing was made of 6061-T6 aluminum hard anodized over-all with both low and high pressure cylinder walls lapped to their final dimensions.

The high pressure pistons were also made of 6061-T6 aluminum and hard anodized. Two teflon piston rings with rubber o'ring expander rings were used for seals and wear rings.

The low pressure pistons are made of nylon and have a large clearance and no seals.

The bellcrank is a high stressed member and is made from 17-4 PH stainless steel in H900 condition.

Figure 7 shows a cross section through the actuator. Figure 8 is a photograph of the actuator.

TEST AND EVALUATION

Static Test

Static tests were conducted to determine the differential piston pressure for different supply pressures. Figure 9 is a schematic of the test setup for this test. Figure 10 is a plot of supply pressure vs. piston pressure differential with P_c set at 10 psig.

Frequency Response

A test setup as shown in Figure 11 was made to run frequency response data on the actuator. The actuator was loaded with a torsion bar load and an inertial load equivalent to the expected load in the missile system application. A peak to peak simulated fluidic sine wave of 7.5 psid was the input to the system and was held constant as the frequency was varied from 1 to 74 Hz. The actuator supply pressure for this test was set at 1000 psig. The input pressure differential and the rotary output position was recorded on a varian recorder. The results of this test are shown on the log magnitude plot in figure 11.

CONCLUSION

The fluidic bistable actuator was designed using standard pneumatic component design procedures for the ball poppet design and for determining the piston pressures between the fixed upstream orifices and the variable downstream poppet valves. Static and dynamic tests were conducted which verified the design procedure. Ten flight tests have been conducted using four actuators per test. All of the actuators have performed reliably.

REFERENCES

1. Anderson, Blaine W., The Analysis and Design of Pneumatic Systems. John Wiley & Son, New York, 1967, p 81.

2. Blackburn, John F., Reethof, Gerhard, and Shearer, J. Lowen, Fluid Power Control. John Wiley & Son, New York, 1960, p 67.

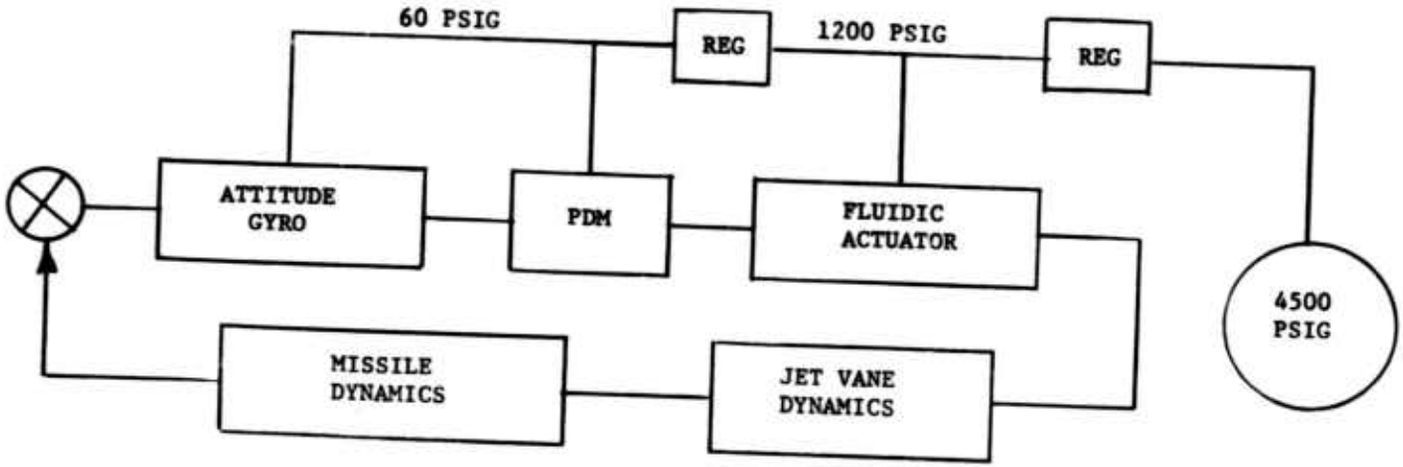


FIGURE 1 CONTROL SYSTEM BLOCK DIAGRAM

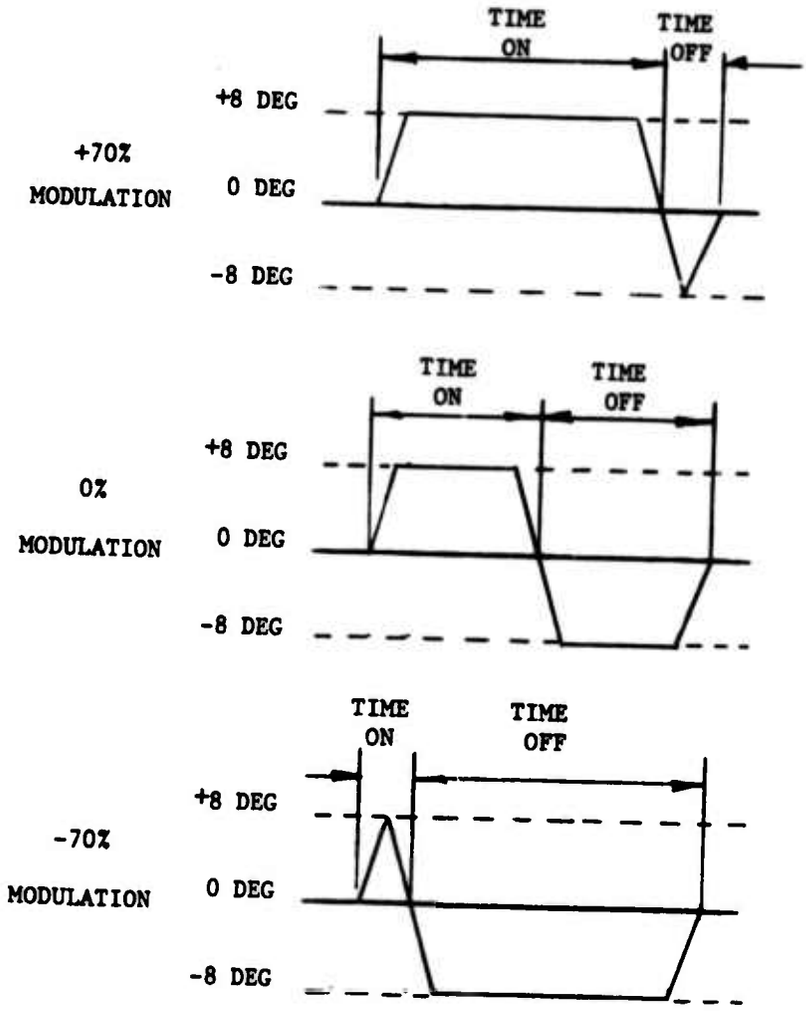


FIGURE 2 MODULATION RANGE

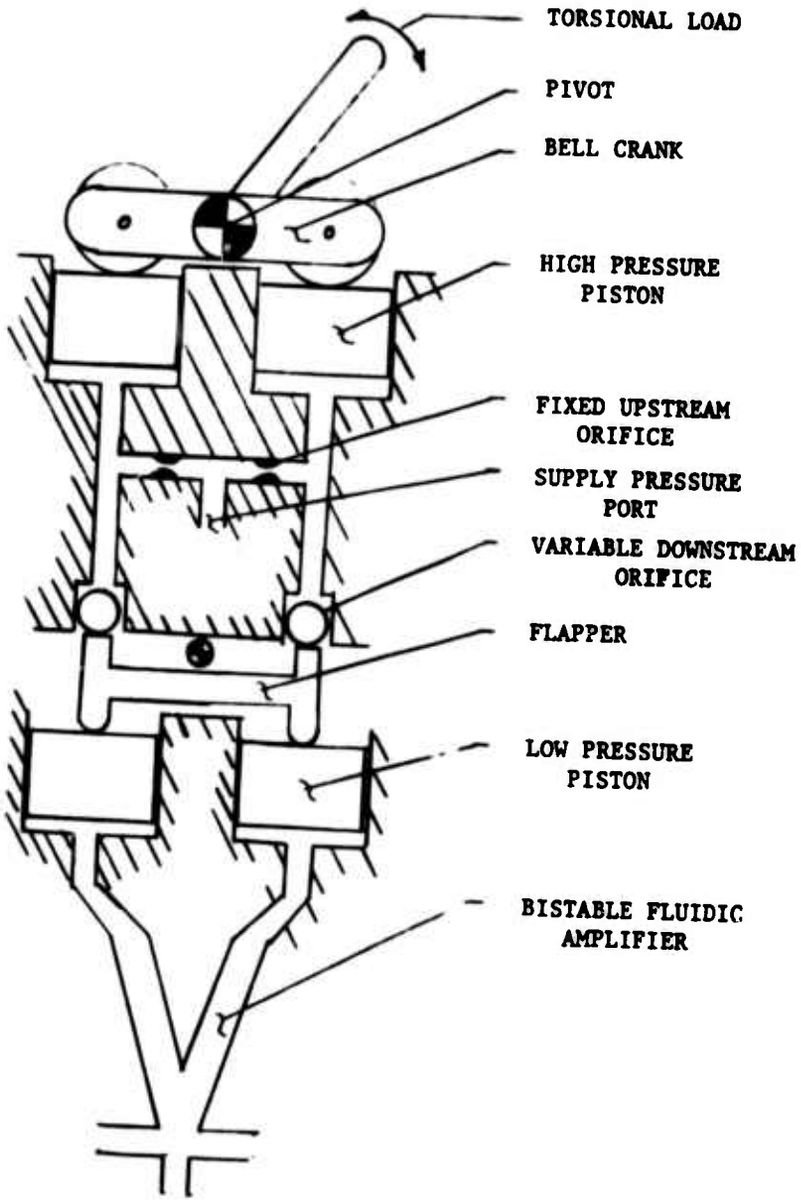


FIGURE 3 ACTUATOR SCHEMATIC

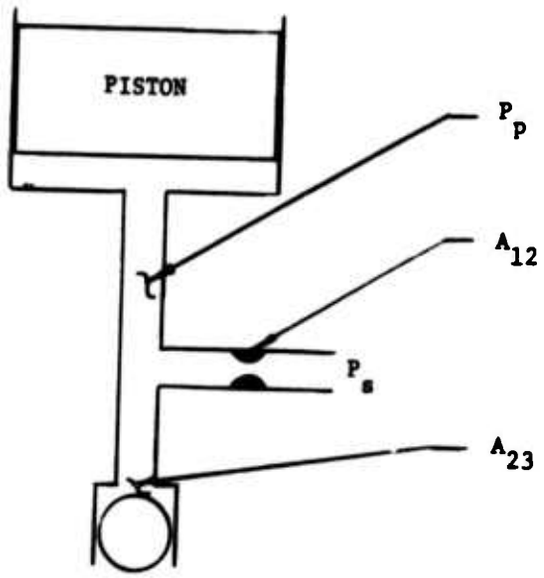


FIGURE 4 BALL POPPET SCHEMATIC

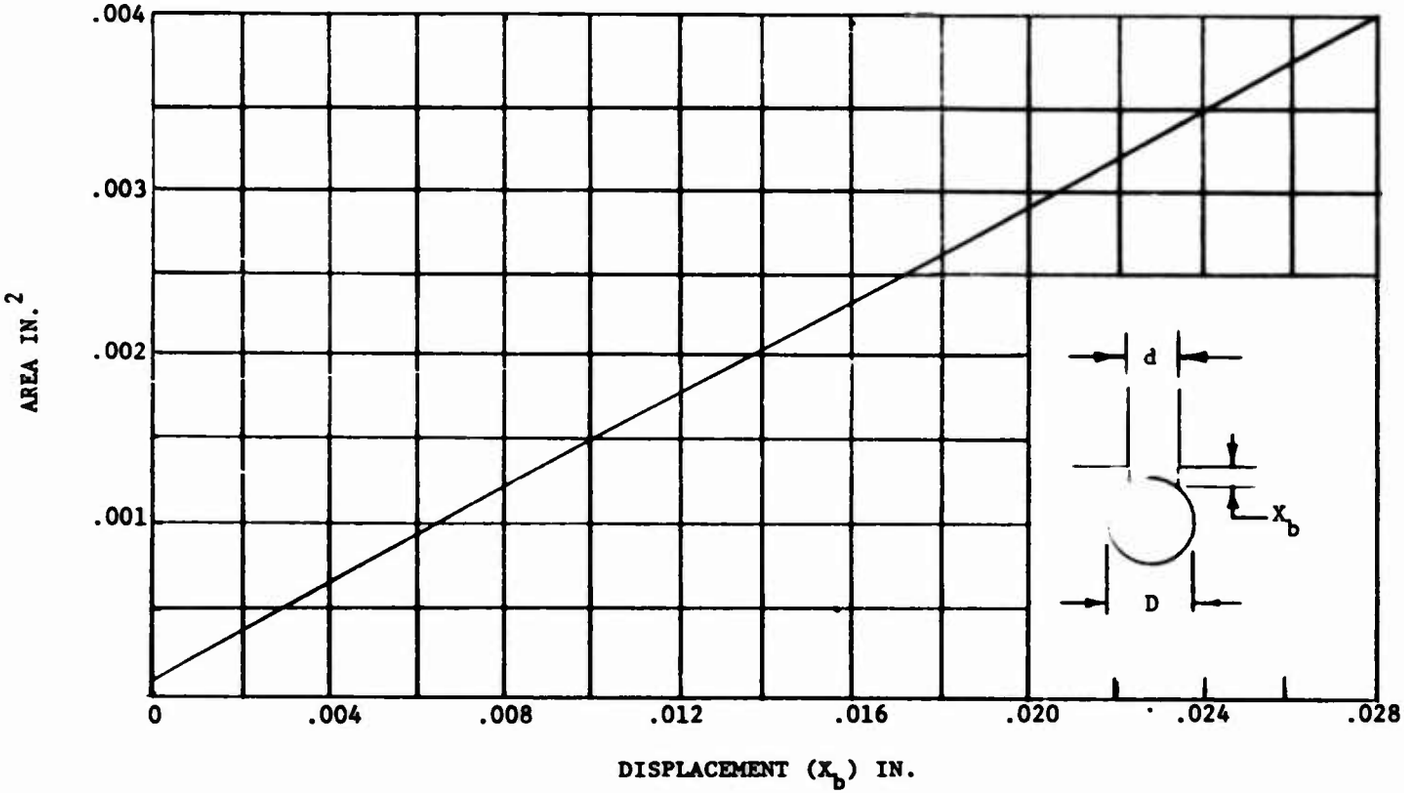


FIGURE 5 BALL POPPET AREA VS. DISPLACEMENT
SEAT DIA. - .067 IN. BALL DIA. .093 IN.

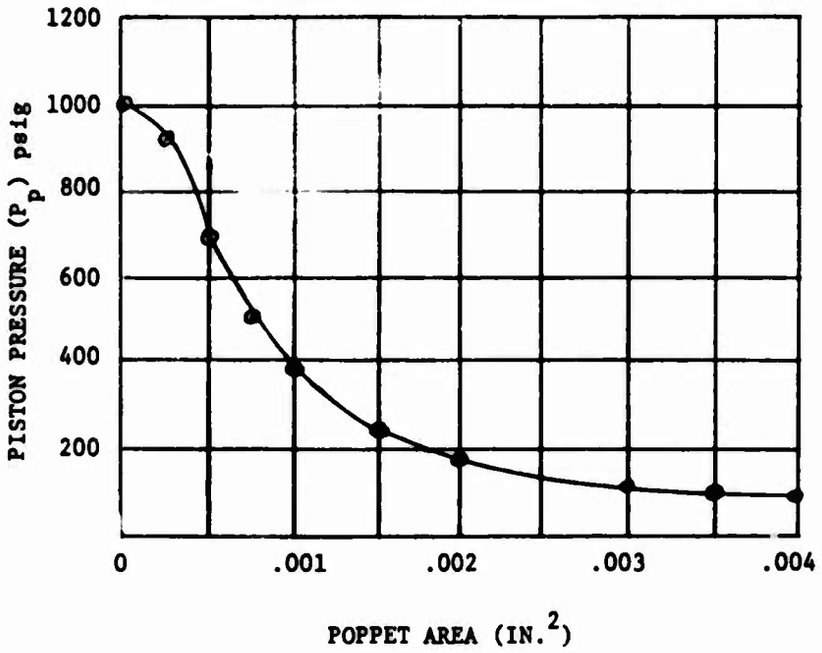


FIGURE 6 PISTON PRESSURE - POPPET AREA

UPSTREAM FIXED ORIFICE AREA = 3.8×10^{-4}

P_u = 1000 psig

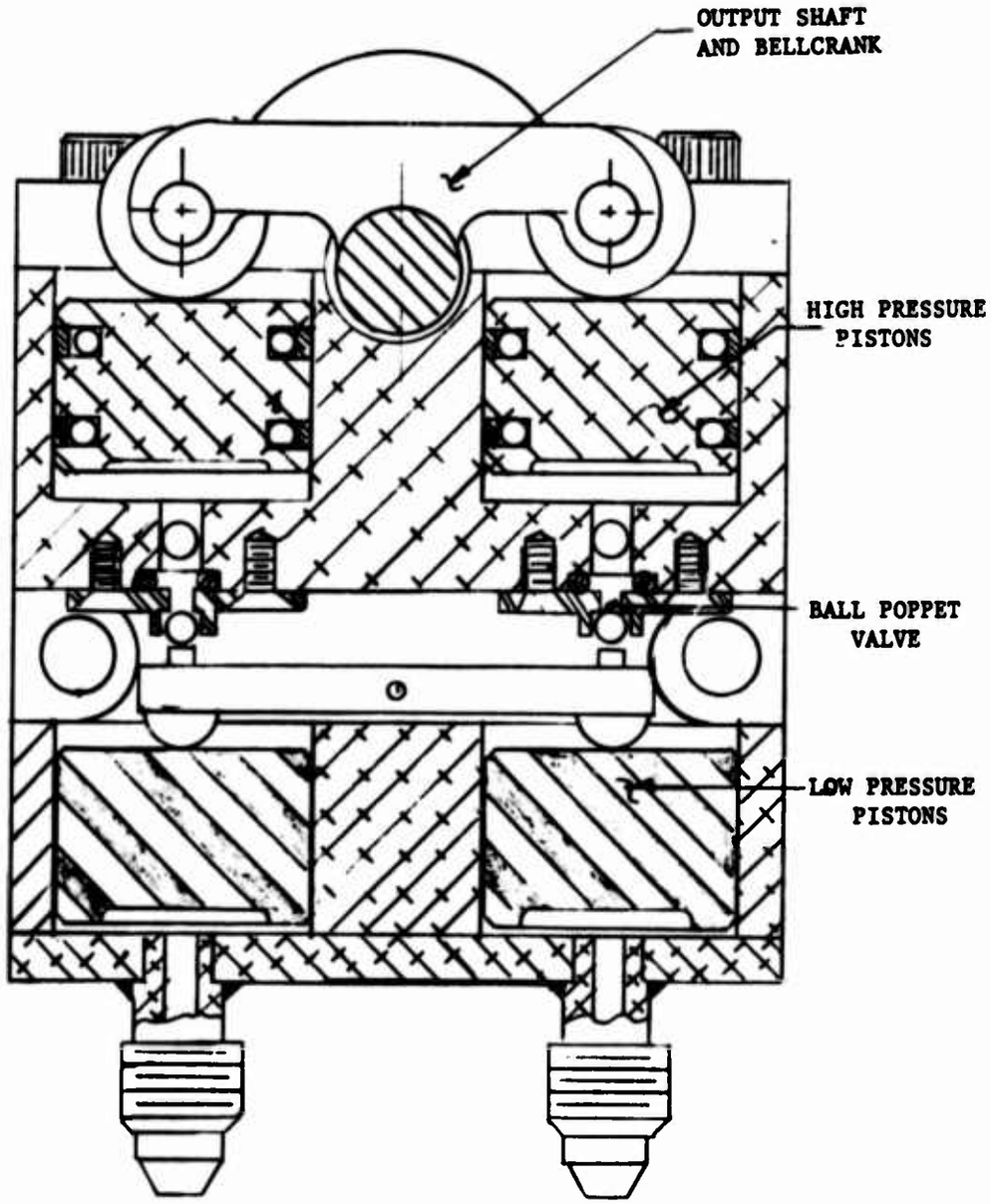
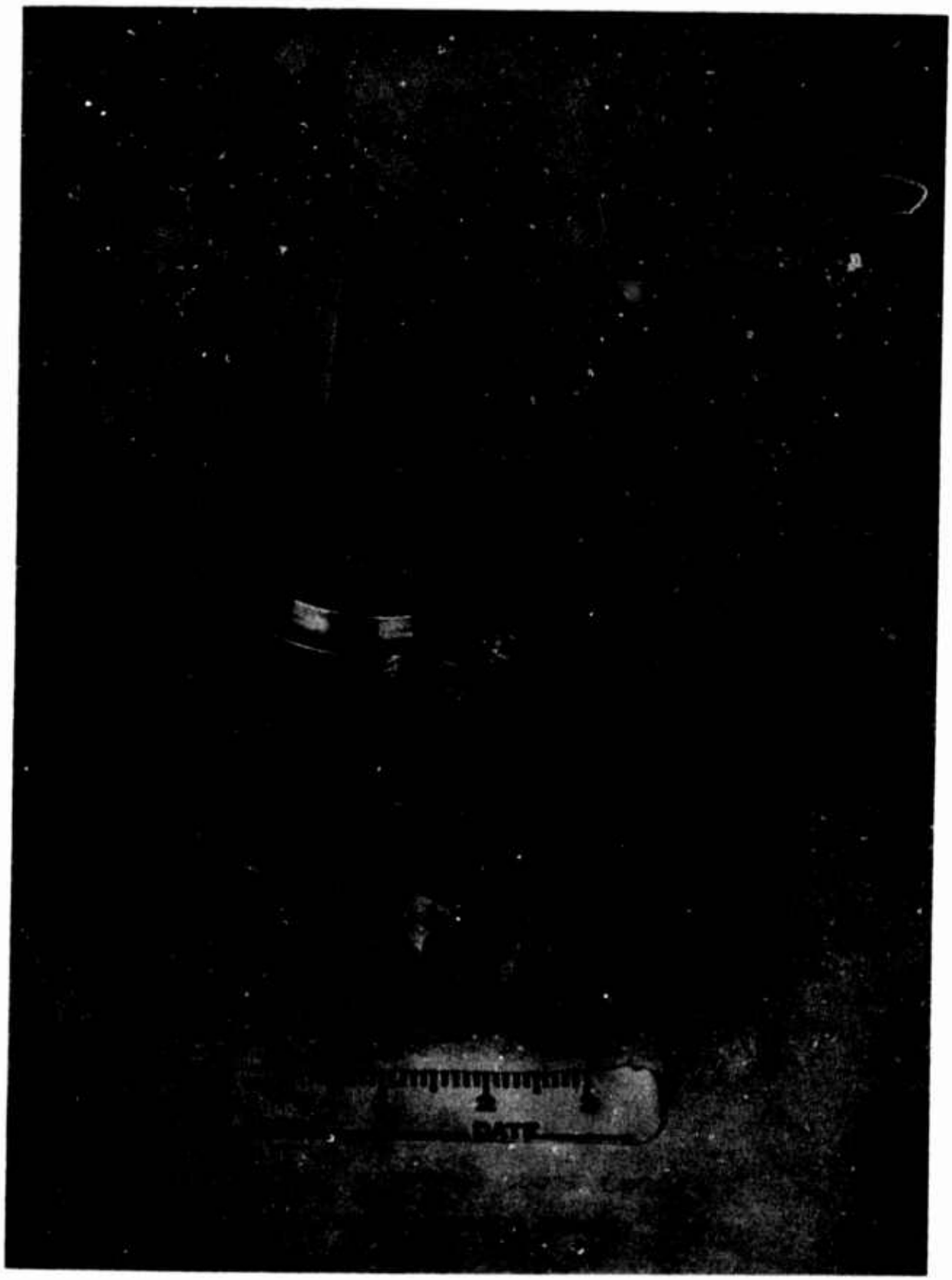


FIGURE 7 ACTUATOR CROSS SECTION


DATE

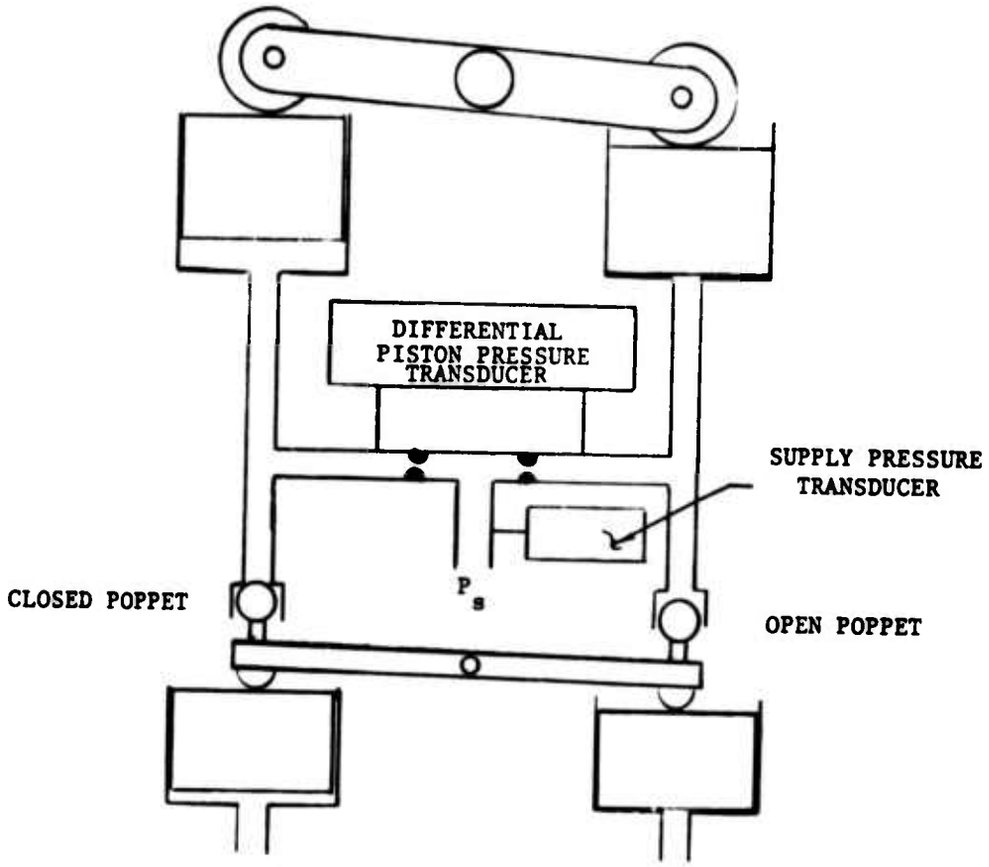


FIGURE 9 STATIC TEST SETUP

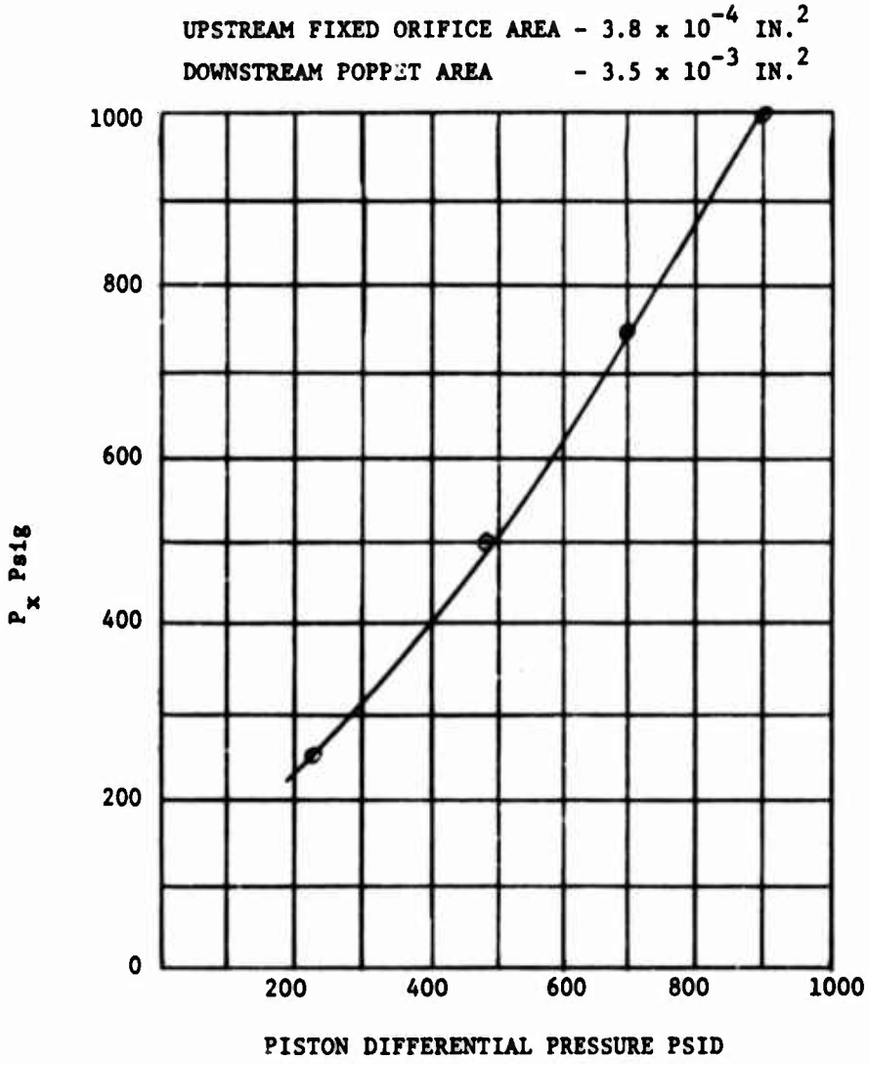


FIGURE 10 SUPPLY PRESSURE VS. PISTON PRESSURE DIFFERENTIAL

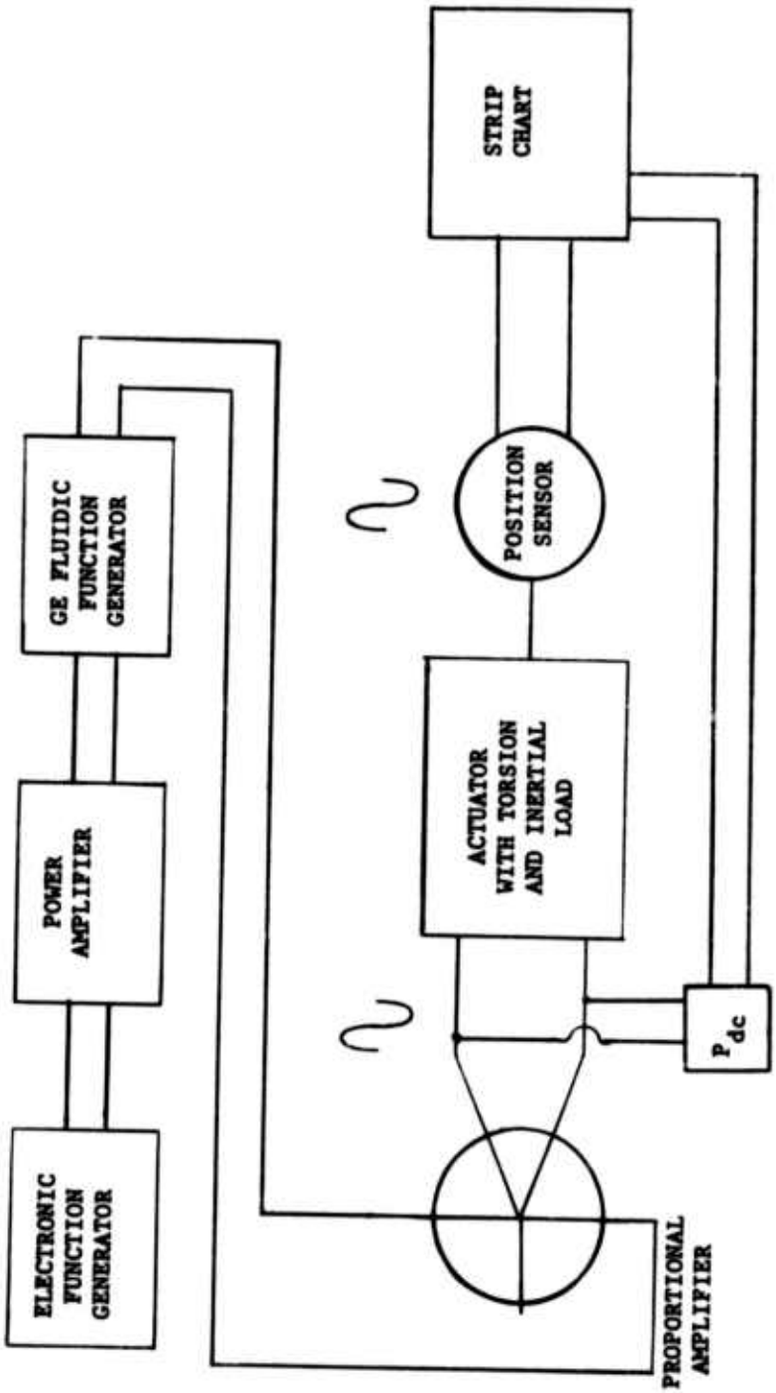


FIGURE 11 SETUP FOR FREQUENCY RESPONSE TEST

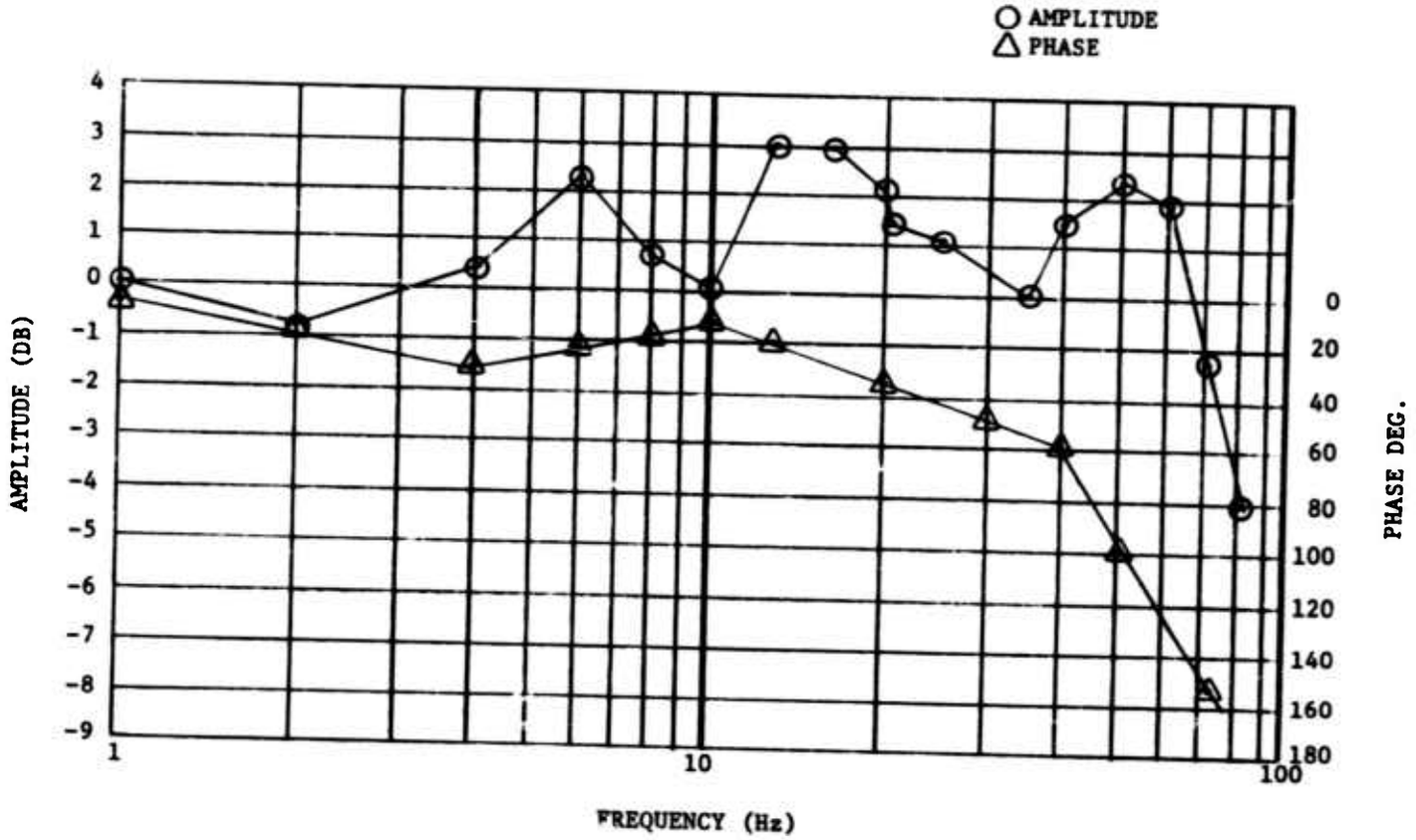


FIGURE 12 LOG MAGNITUDE PLOT

DEVELOPMENT OF A FLUIDIC MISSILE CONTROL VALVE

JOE L. BYRD

February 1974

Approved for public release; distribution unlimited.

GUIDANCE AND CONTROL DIRECTORATE
US ARMY MISSILE RESEARCH, DEVELOPMENT AND ENGINEERING LABORATORY
US ARMY MISSILE COMMAND
REDSTONE ARSENAL, ALABAMA 35809

SYMBOLS

A_e = Nozzle exit area, in^2

A_* = Nozzle throat area, in^2

C_f = Valve nozzle thrust coefficient

C_F = Valve thrust coefficient

F_s = Side force, lb

I_{sp} = Specific impulse, sec

k = Ratio of specific heats

$\dot{m}$ = Mass flow rate, lb/sec

N = Complete valve efficiency factor

P_o = Supply pressure, psia

P_e = Isentropic exit pressure, psia

P_∞ = Ambient pressure, psia or in. Hg

T_o = Gas stagnation temperature (°R)

t_1 = Time in State 1, sec

t_2 = Time in State 2, sec

t_{tot} = Total time, sec

t_{1-2} = Switching time, State 1 to State 2, sec

t_{2-1} = Switching time, State 2 to State 1, sec

DEVELOPMENT OF A FLUIDIC MISSILE CONTROL VALVE

INTRODUCTION

The experience obtained from MICOM valve department programs [1,2] has been applied to the Directional Control Antitank (DCAT) control valve requirement. A single stage, hot gas, direct bleed, jet reaction, control valve with an electrical/fluidic interface device (E/F) has been developed (Fig. 1). Since the basic design parameters for the supersonic valve had been established in other MICOM programs, the main development objectives were:

1. Develop a fast response electromechanical actuator for switching hot gas valves with ambient air.

2. Determine if the known design parameters for hot gas valves were applicable to valves with thrust levels as low as 1.5 pounds.

3. Evaluate direct motor bleed as a source of hot gases for use in hot gas jet reaction valves.

The present DCAT control valve with E/F device meets the objectives and is the result of several years of effort to apply fluidic controls to small antitank missiles. The efforts have been primarily directed at the development of a small actuator to be used for switching jet reaction valves. Due to the large control flow required, ambient air was used. For use with a conventional gyro with electrical output, an E/F device is required.

Certain bistable fluid amplifiers may be switched by closing or opening the control ports, thus permitting or retarding the inflow of ambient air. The hot gas, bistable MICOM valves may be switched in this manner. When using a mechanical flapper or armature to open and close the control ports, the problem is to generate enough force to overcome the differential pressure force created on the flapper by the low pressure in the closed control port.

Dunaway [2] has investigated several methods to reduce the pressure forces on the flapper or armature, including a leaf spring and sliding plate actuators.

In the leaf spring actuator, shown schematically in Figure 2, the leaf spring was used to overcome the vacuum force holding the spring over the closed control port. The force on the spring due to the spring deflection was larger than the vacuum force. When the "ON" solenoid was deenergized, the spring force alone would cause the spring (flapper) to break away from the control port. In this case the solenoids served a holding function, as the stored energy in the deflected spring produced the initial acceleration on the spring.

The leaf spring actuator was tested on a supersonic valve at frequencies up to 200 Hz. The spring and solenoids operated at full amplitude up to 200 Hz. However, the valve switching was only partial and spill-over was observed at frequencies above 5 Hz.

The poor valve performance was attributed to an excess pressure drop in the control port passage caused by the three 90° turns as shown in Fig. 2.

Dunaway used a two-slot and three-slot sliding plate actuator on two different supersonic valves. The actuators used a sliding plate, moving perpendicular to the control port vacuum force, to open and close a series of holes which emitted control air to switch the valve. The two-slot actuator is shown in Fig. 3.

The two-slot actuator operated to approximately 150 Hz at 0% modulation.

The three-slot actuator operated to slightly over 100 Hz and had a maximum modulation of 65% at a carrier frequency of 46 Hz. Dunaway concluded that the three-slot actuator had a high pressure drop across the open control port which reduced flow rate and switching frequency.

Dunaway has also patented a pressure balanced piston actuator illustrated in Fig. 4. This device uses pressure feedback to greatly reduce the amount of external power required to operate the armature. This method was evaluated on a 16-pound thrust valve and would operate to 50 Hz. The disadvantage of the device was the difficulty of assembly, as the pistons required a good fit in the cylinders. Also, the response was not quite good enough as the DCAT vehicle requires a carrier frequency of 80 Hz.

The present DCAT control valve (Fig. 1) uses an E/F device similar to the pressure balanced piston method shown in Fig. 4. The control ports and the actuator are contained in the top valve cover plate. The valve nozzle is an integral part of the main motor nozzle. This control valve meets the performance, weight, and packaging requirements for the various vehicles used in the DCAT development program.

SUPERSONIC VALVE NOZZLES

The DCAT control valve is a bistable fluidic device which may be switched by closing the appropriate control port. This type of hot gas supersonic valve has been developed by MICOM to withstand thrust levels up to 100 pounds. The ones used in the DCAT program represent the low end of the thrust range. These valves may also be staged as required. Several three-stage valves have been developed and are described in other MICOM reports [1].

Fig. 5 illustrates the primary dimensions on the 3-pound and 1.5-pound DCAT valves. The dimensions are based on previous experience with these types of valves. The calculations for the nozzle are based on one-dimensional, perfect gas, isentropic flow. No corrections are made for three-dimensional effects. In the thrust calculations, an over-all efficiency of 65% was used. This efficiency has been determined experimentally and compensates for nozzle, receiver section, and exit duct friction losses. Street [3] has measured the efficiency of a 12-pound valve which substantiates the 65%, as shown in Fig. 6. The different configurations refer to various reductions in exit channel width.

As shown in Fig. 5, the DCAT nozzle is converging, diverging with a short, straight throat section. The control valve nozzles are machined separately and pressed into the main motor nozzle and are not shown in the photographs of the valves.

The control valve side force is calculated in a very simple manner using the ideal thrust equation for the nozzle modified by the valve body efficiency:

$$F_s = N C_f A_* P_o$$

F_s = Valve side force, pounds

N = 0.65, valve body efficiency factor

C_f = Valve nozzle thrust coefficient

A_* = Nozzle throat area, square inches

P_o = Supply pressure, psia

Because the product of NC_f is very nearly equal to 1.0 for the DCAT valve, the valve side force can be estimated within ±5% by multiplying P_o by A_*:

$$F_s \approx A_* P_o$$

The product of NC_f can also be defined as the thrust coefficient for the complete valve.

$$\text{Valve thrust coefficient} = C_F = \frac{F_s}{A_* P_o}$$

A C_F = 1.046 has been measured on the DCAT valve using side force measurement on 16 valve outputs on cold gas (N_2) at supply pressures from 850 to 1500 psig. Note that for nozzles with area ratios different from 18.2, the nozzle C_f will be different. The C_f for the nozzle was calculated using the isentropic pressure at the nozzle exit and the design supply pressure.

k	P (psia)	P (psia)	$\frac{Ae}{A_*}$	Nozzle C_f	$NC_f = C_F$	Valve C_F
1.2	1264.5	7.25	18.2	1.602	1.041	1.0 (estimated)
1.4	1264.5	3.8	18.2	1.476	0.959	1.046 (measured)

The DCAT valve will switch on entrained air over a pressure range from approximately 700 to 1400 psig (cold gas) without spillover to the "off" side. When measuring side force, the supply pressure may be increased to 1700 psig before the spillover to the off side is detectable on the measured F_s curve. The switching range on hot gas with ambient air control flow has not been accurately determined. However, the low end of the switching range is approximately 600 psig as observed on several hot gas tests. The highest pressure attained with the DCAT propellant has been approximately 1700 psig and the valves will switch at that pressure.

Previous experience with supersonic valves had established the center of the cold gas switching range at the supply pressure which gives an isentropic exit pressure equal to 35% of ambient pressure. The low end of the switching range was at P_e equal to approximately 25% of P_∞ and the high end was at P_e equal to approximately 45% of P_∞. The DCAT valve switches at lower pressures as shown in the following chart:

P_o (psia)	Isentropic P_e (psia)	P_e/P_∞	
714	2.15	14.8%	Low range
1414	4.26	29.4%	High range

$\frac{A_e}{A_*} = 18.2 \qquad \frac{P}{P_o} = 0.003015 \qquad P_\infty = 14.5 \qquad k = 1.4$

The nozzle and valve mass flow rates are calculated by Fliegner's Formula. For cold gas using nitrogen:

$$\dot{m} = \frac{0.523\, P_o A_*}{\sqrt{T_o}} \quad \text{and} \quad A_* = \frac{F_s}{C_F P_o}$$

$$\dot{m}_{cold} = \frac{0.523 \frac{F_s}{C_F}}{\sqrt{T_o}} = \frac{0.523\ (3/1.046)}{\sqrt{530}} = 0.065 \text{ lb/sec}$$

For hot gas, Fliegner's Formula becomes:

$$\dot{m} = \frac{0.496\, P_o A_*}{\sqrt{T_o}} = \frac{0.496 \frac{F_s}{C_F}}{\sqrt{T_o}}$$

For the DCAT propellant, T_o approximates 5460° R, and C_F is estimated to equal 1.0, then:

$$\dot{m}_{hot} = \frac{0.496\ (3/1.0)}{\sqrt{5460}} = 0.020 \text{ lb/sec}$$

The DCAT control valve specific impulse I_{sp} is calculated from the measured side force and calculated flow rates on cold and hot gas.

$$I_{sp} = \frac{3.0}{0.065} = 46.2 \text{ sec (cold)}$$

$$I_{sp} = \frac{3.0}{0.020} = 150 \text{ sec (hot)}$$

These values agree closely with 65% of the specific impulse for nitrogen and the DCAT flight motor propellant:

(N_2)	$N\ I_{sp} = 0.65(70) = 45.5$ sec
(DCAT motor)	$N\ I_{sp} = 0.65(225) = 146.2$ sec

It is interesting to note that the cold gas flow rate is about three times the hot gas rate, which is a useful "rule of thumb."

The primary dimensions for the 1.5-pound valve nozzle are also shown in Fig. 5. Eight 1.5-pound valves were made for the DCAT program. They had the same over-all dimensions as the 3.0-pound valves. They were used in the first two controlled flights to reduce the over-all system gain. The 1.5-pound valve was the same as the 3.0-pound valve, except for the internal dimensions, and the operation was the same.

The 1.5-pound thrust valve required a 0.040-inch diameter nozzle throat. To evaluate clogging on that size nozzle throat, five hot gas tests were made using the DCAT motor. Each motor nozzle had four different sized bleed nozzles as shown in Fig. 7. A nozzle cap with a 0.085-inch diameter orifice was placed on each bleed nozzle. The pressure between the orifices was measured to determine if and when clogging occurred.

These tests gave the results of five separate motors on each of the 0.035, 0.040, 0.045 and 0.050 inch nozzles. None of the bleed nozzles were blocked during any of the firings. Some of the nozzle throats remained nearly perfectly round and some became slightly irregular. In general, the throats became slightly smaller in diameter.

The reduction in diameter, usually 0.001 to 0.004 inches, has been observed many times on the nominal 0.055-inch nozzle. However, it is not known when the build up occurs since the measured side force is always very close to the required value. This is illustrated in Fig. 8 which shows side force and motor chamber pressure versus time. Quite by accident, the deflections on the oscillograph were such that the side force (F_s) appears to be modulated by the P supply pressure (P_s). This

curve demonstrates that the side force is a function of supply pressure, that the valves switch on hot gas down to approximately 600 psig, and that the valve bleed nozzles did not clog up during the motor burn.

Three different materials have been used for the valve bleed nozzles:

1. Maraging steel
2. Copper-impregnated tungsten
3. Molybdenum

The molybdenum nozzles are best suited for the +5000°F temperatures and 3% aluminum content.

SUPERSONIC VALVE RECEIVER SECTIONS

Experience has shown that the following rules can be used to determine the receiver section dimensions [2]:

1. The exit area of the receiver section at the splitter should be four times the area of the nozzle exit.

2. The control channels should be equal in area to the nozzle exit area.

3. The maximum wall half angle should be 15°.

Until 1969, most of the MICOM supersonic valves had receiver sections made of stainless steel, with a few made of aluminum. Dunaway [4] investigated reinforced plastics for hot gas valves and found a high-temperature phenolic resin reinforced with a fiber material to be best suited for our applications. The fibers considered were asbestos, carbon, and silica. Asbestos was selected because it was relatively cheap, easy to fabricate, and it was already on hand. The asbestos phenolic used was Style 41-RPD made by Raybestos-Manhattan, Inc.

The valve bodies, Fig. 9, are machined on a line trace milling machine from a master drawing, ten times actual size. The valve passages are generally rectangular in cross section. The depth of the valve is equal to the nozzle exit diameter, 0.235 inches for the 3-pound valve.

The valve body is a slight press fit onto the bleed nozzle.

The aluminum top cover plate seals off the valve body and contains the E/F device. The valve body is not highly loaded by the pressure of the expanded gases due to the large area ratio in the nozzle. The DCAT valve has been pressure tested to 3200 psig on the nozzle. The output flow was evenly divided between the output channel at P_s greater than 2100 psig.

Street [3] goes into some detail on the output flow characteristics of MICOM valves. In general, the output flow is mixed (subsonic and supersonic) and non-uniform. Fig. 10 from reference [3] shows that most

of the flow comes out from the last 30% of the downstream edge of the channel exit. However, the output channel exit may not be significantly reduced in area.

Street also determined that there is definitely an influence on valve performance as a result of valve arrangement. This was not expected, but early in the DCAT program the valves were staggered so that the output jets would not be in the same transverse plane (Fig. 11). The DCAT valve has been tested with slightly different over-all widths as the missile diameter has increased. The slight increase in width did not affect the performance. The output exits are scarfed to conform to the missile skin curvature.

The output jet has no tendency to attach to the missile skin. The output jet also develops a slight force in the axial (longitudinal) direction of about 4% of F_s since the jet is not exactly perpendicular to the valve output. That corresponds to an exit angle of approximately 2%.

The scarfed ends of the flight valves have no apparent effect on the valve output jets. On nine hot gas tests on 30 valves, with and without scarfed ends, the output jets were always very distinct in the high speed movies. The jets were always observed coming straight out of the valve output within the 2° tolerance mentioned above (Fig. 12).

ELECTRICAL/FLUIDIC INTERFACE

The E/F interface device is a compact electromechanical actuator (Fig. 13). A subtle design feature of the E/F device is the unique spool and guide rod arrangement. The guide rod aligns the spool in the exact center of the control ports. The spool is a slight press fit through the control ports at assembly. This allows the spool ends to be INSIDE the control volumes, which means the differential pressure acts on the spool in a direction to open the closed control port. With supply pressure on the valve, the device will oscillate at approximately 200 Hz without any electrical power.

The pressure feedback acting on the spool, when the magnetic circuit is developing a weak force on the armature, allows the E/F device to operate at high frequencies. For example, as soon as coils 2 and 4 are turned off, the differential pressure across the spool starts to accelerate the spool away from the control port even though the armature is farthest away from the energized coils 1 and 3.

The spool does not have to move into the control port to cause switching as a complete seal is not required. The armature stroke is variable and is adjusted so that the spool ends come just to the edge of the control port and still allow clearance between the armature and the pole faces.

The magnetic circuit of the E/F device consists of four coils, two "C" cores, and one frame with pivoting armature. Laminated cores were used first, but during machining, the laminates tended to separate. Now the cores are machined from pure iron (Swedish iron). The laminated cores seemed to operate slightly better than the solid ones.

Experience has shown that there is a preferred polarity, or choice of magnetic flux paths, which will produce the highest response. That occurs when the flux changes are confined to the smallest piece of iron in the circuit, the armature.

The E/F device uses diodes to cut down on the inductive spikes. The E/F interface device operates in a pulse duration modulation (PDM) mode. The percent of modulation is defined as

$$\% \text{ Modulation} = \frac{t_{on} - t_{off}}{t_{total}} \times 100$$

The natural frequency of the DCAT vehicle is approximately 8 Hz so a carrier frequency of 80 Hz is used for the valves. The period, or total time per pulse, is 12.5 ms. A high percentage of modulation at 80 Hz requires the valve to pass a very short pulse. A short pulse is the equivalent of a higher frequency as shown below:

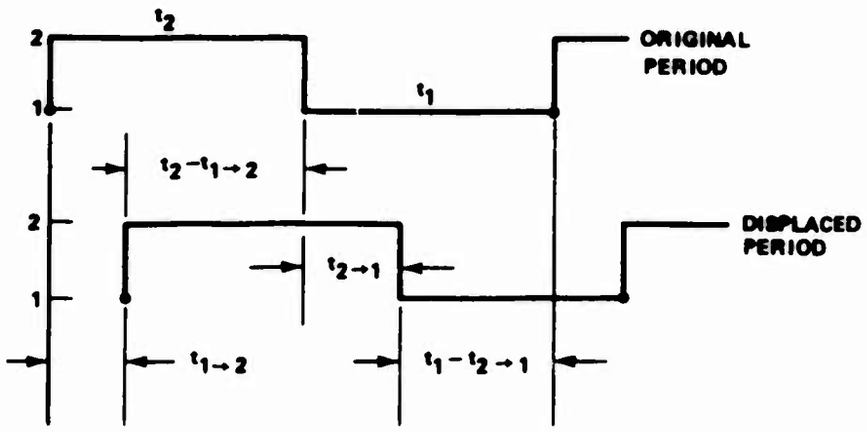
50% @ 80 Hz = 160 Hz @ 0%

60% @ 80 Hz = 200 Hz @ 0%

70% @ 80 Hz = 267 Hz @ 0%

The DCAT valve operates quite well up to ±60% modulation as shown in Fig. 14. At higher percentages of modulation, the valve will start missing the short pulses and the output modulation will approach ±100% (continuous flow out one exit). That explains the nonlinear spacing between the 60% and 100% curves of Fig. 14.

It has been observed that the output modulation is slightly higher than the input modulation on the DCAT valve. The apparent reason for this is a difference in switching times. If the time required to switch from state 1 (left) to state 2 (right) is different from that required to switch from state 2 to 1, there will be a drastic difference between the input and output modulations as shown below:



$$\% \text{ Modulation for Displaced Period} = \frac{\left[\left(t_2 - t_{1\to2}\right) + t_{2\to1}\right] - \left[\left(t_1 - t_{2\to1}\right) + t_{1\to2}\right]}{t_{tot}} \times 100$$

$$\% = \frac{t_2 - t_1 - 2t_{1\to2} + 2t_{2\to1}}{t_{tot}} \times 100$$

$$\% = \frac{t_2 - t_1}{t_{tot}} \times 100 + \frac{2t_{2\to1} - 2t_{2\to1}}{t_{tot}} \times 100$$

$$\% = \% \text{ input} + \frac{2t_{2\to1} - 2t_{2\to1}}{t_{tot}} \times 100$$

The above equation is based on sharp leading and trailing edges and not ramps as are found in an actual case. This formula has been used to correct some valve data where there was no apparent correlation between input and output modulation as shown in the following table.

Pulse Number	Input Modulation %	Measured Output Modulation %	Corrected Output Modulation %
1	+c	+38	+32
2	+3	+43	+29
3	-1	+39	+18
4	0	+38	+20
5	+2	+40	+41

While the amount of error between the input and output modulation is great, the switching time correction tends to bring the measured values into agreement considering the measured switching times. These data were taken from Fig. 16, reference [2], a three-slot sliding-plate actuator at 0% modulation (nominal) at 147 Hz carrier frequency.

The E/T device has not been optimized. The device will work on supply voltages as low as 15 volts, which indicates that the magnetic circuit is overdesigned.

VALVE PERFORMANCE

The important valve characteristic is gain, or side force versus percent modulation input signal as shown in Fig. 14. The side force is difficult to measure due to the 80 Hz carrier frequency. The ideal measurement would be to look at each individual output force pulse. However, it appears that it is not possible to build a test stand with

a natural frequency high enough to measure each individual pulse. The side force stands built by the Guidance and Control Directorate, MICOM, have had natural frequencies from 17 to 44 Hz.

In lieu of measuring each force pulse, the pulse pressures in the output channels may be monitored. However, due to noise it is difficult to measure percent modulation from the output pressure pulses.

The test stand effectively integrates the 80 Hz pulses. However, a much cleaner signal can be measured by passing the load cell signal through an active filter. In general, we use a low pass filter with a cutoff frequency of 7 Hz to simulate the missile dynamics.

During a test, the input modulation is varied between plus and minus 60% modulation, sine wave fashion, at a frequency of 2 or 3 Hz, as desired. Fig. 15 is a measured curve of side force and input percent modulation, corrected for phase lag in the filter and zero shifts due to thrust misalignment, for a pair of DCAT control valves.

Fig. 15 demonstrates a capability to follow a 3-Hz signal between peak modulation demands of ±65 percent. The following table compares the input signal to the valves, based on an average supply pressure, and the measured valve output force. The average corrected supply pressure between 0.4 and 0.9 seconds was 1443 psig. The design conditions are 6 pounds per axis (2 valves) at 1250 psig at 100% modulation. The forces are corrected by multiplying by the ratio of the supply pressures, with percent expressed as a decimal:

$$\text{Input } F_s = \% \times 6 \times \frac{1443}{1250} \text{ (lbs)}$$

t(sec)	P_o (AVG)	% INPUT	INPUT F_s (LBS)	MEASURED F_s (LBS)	% ERROR
0.38	1443 psig	+64	+4.43	+4.3	-2.9
0.54	1443 psig	-69	-4.78	-4.4	-7.9
0.71	1443 psig	+65	+4.50	+4.38	-2.7

On this particular hot gas test, the divergent section of the main motor nozzle separated at t = 1.14 seconds. The control valves operated properly for most of the test and operated very well for 0.8 seconds as shown in Fig. 15.

The Aeroballistics Directorate at MICOM has investigated the control jet-air stream-fin interaction problem of the DCAT vehicle [5] in several wind tunnel tests. The valves developed 3.75 pounds of thrust and operated at a scaled frequency of 68 Hz.

During the wind tunnel tests, it was found that the approximate center of the switching range was 750 psig rather than the desired 1250 psig. These valves used compressed air for switching, which was supplied to the control ports through copper tubing about 10 feet long.

The wind tunnel tests put some unusual hardships on the DCAT valves. The most difficult problem is the wide variation in the tunnel ambient pressure, which varies from 2 psia to 19 psia. Another problem is the long time required to make the wind tunnel runs. It is not unusual for the valves to operate for 16 hours per day for several days, which causes some wear on the spool.

It was proposed that altitude tests be made on some spare DCAT valves to determine the switching range at various ambient pressures to see how they would operate in the wind tunnel. Seven different valves were tested in an altitude chamber with an internal volume of approximately 8 cubic feet.

The wind tunnel data is scaled by the ratio of supply pressure to ambient pressure:

$$\frac{P_o}{P_\infty} = \frac{1250 \text{ psia}}{14.5 \text{ psia}} = 86.2$$

Therefore, as the tunnel ambient pressure is decreased, the valve supply pressure is also decreased to keep the ratio equal to 86.2. This was an advantage when testing in the small chamber as the lower supply pressures and flow rates caused slow changes in the chamber ambient pressure.

The test method was simple. The chamber was evacuated to approximately 2 psia. The valve was switched at 68 Hz generally to 40 or 50% modulation. When the valve supply pressure was turned on, the valve output flow would cause the chamber ambient pressure to slowly increase. The valve output was monitored (with pressure transducers) on an oscilloscope. When output pulses were first observed on the scope, the chamber pressure was recorded. The output pulses were monitored until they disappeared or the modulation changed. The chamber pressure was then recorded to establish the upper edge of the switching range.

The resulting data on the switching range for five valves is shown in Fig. 16. This curve illustrates that the switching range is evenly spaced about the $P_o/P_\infty = 86.2$ line. The conclusions from these tests were that the DCAT valve has clearly defined upper and lower switching boundaries when the supply to ambient pressure ratio is maintained at 86.2 on nitrogen. Also the valves switch down to ambient pressures of approximately 2 inches Hg and supply pressures of 150 psia.

VALVE SELECTION PROGRAM

Sixty-five DCAT control valves were fabricated for use in flight testing. A curve of side force versus supply pressure at different input modulations was measured on each valve using nitrogen (Fig. 14). Each valve was adjusted to get the best performance. The side force data was punched onto data cards.

The valve selection program was used to select the ten best sets of control valves for use in flight testing. Ten of the wors: valves were

deleted due to noisy, nonlinear, or bad zero offset traces. The ten sets (40 valves) were selected from the remaining 55 valves.

The selection criteria were side force at 1200, 1250, and 1300 psig; side force tolerance; gain tolerance, and roll torque due to null offsets. The tolerances were reduced until only ten valve sets were selected. The final side force tolerance was ±7%. The final gain tolerance was ±15% at 1200 psig and 1300 psig, and ±7% at 1250 psig. The average value gain was 4.1#/50% per axis. Fig. 17 is the gain curve of valves 110 and 138 as matched by the computer.

None of the valves selected by the computer program have been hot gas tested. However, 12 of the valves not meeting the selection criteria have been hot gas tested (Fig. 8 and 15) with good performance, which gives confidence to the valve selection program.

CONCLUSIONS

A single stage, hot gas, direct bleed, jet reaction control valve with a high speed pressure feedback E/F device has been developed for the DCAT experimental missile. Many cold gas, several hot gas, and two flight tests have been made to evaluate valve operation. The operation at low ambient pressures was determined.

The nominal side force is 3.0 pounds at 1250 psig. Smaller (1.5 pounds) versions have also been evaluated. Pulse duration modulation was used at 80 Hz carrier frequency. Good operation was obtained at ±60% modulation.

The concept of using direct motor bleed as a gas source for small control valves has been demonstrated.

NOMINAL SPECIFICATIONS, DCAT VALVE

Thrust - 3.0 pounds @ 1250 psig

Weight - 0.205 pounds with test nozzle

0.15 pounds without nozzle

Burn Time - 1.8 seconds

Gas Source - Solid, composite grain, 3% aluminum

Gas Pressure - 1250 psig ±300 psig

Gas Temperature - 5460°R

Specific Heat Ratio - 1.197

Material - Nozzle: Molybdenum

Body: 41-RPD asbestos phenolic

Cover: Aluminum

Design Flow - 0.020 lb/sec

Nozzle Throat - 0.055 inches diameter

Nozzle Exit - 0.235 inches diameter

Nozzle Area Ratio - 18.26

Nozzle Thrust Coefficient - 1.602 @ k = 1.2

1.476 @ k = 1.4

Valve Efficiency - 0.65

Valve Thrust Coefficient - 1.046 @ k = 1.4

Switching Range - P_o ≈ 700 psia to P_o ≈ 1750 psia

Input Signal - Pulse duration modulated 28V

Carrier Frequency - 80 Hz

Modulation Range - ±60%

Nominal Resistance - 70 ohms

Nominal Inductance - 11 mh

Nominal Current - 400 ma @ 28V

Coil Winding - 800 turns #38 awg, 50 ohms

1000 turns #39 awg, 80 ohms

Control Port Diameter - 0.25 inches

E/F Armature Stroke - 0.062 inches

REFERENCES

1. "Fluidic, Hot Gas, Valve Development Progress Report, FY 1966," Ayre and Dunaway, Report No. RG-TR-67-17, August 1967.

2. "The Development of a Hot Gas Reaction Control Valve for an Antitank Missile," Dunaway, Report No. RG-TR-65-23, September 1965.

3. "Static Test Performance Characteristics of Several Fluidic Control Valve Configurations," Street, Killough, and Becht, Report No. RD-73-29, 14 September 1973.

4. "The Application and Evaluation of Reinforced Plastic Materials to Flueric Hot Gas Valves," Dunaway, Report No. RG-TR-69-7, April 1969.

5. "Experimental Aerodynamic Characteristics of a Fluidic-Controlled, Antitank Missile with Wraparound Fins at Mach Numbers from 0.2 to 3.0," Street and Killough, MICOM Report No. RD-TR-71-27, Vols. I, II and III, December 1971.

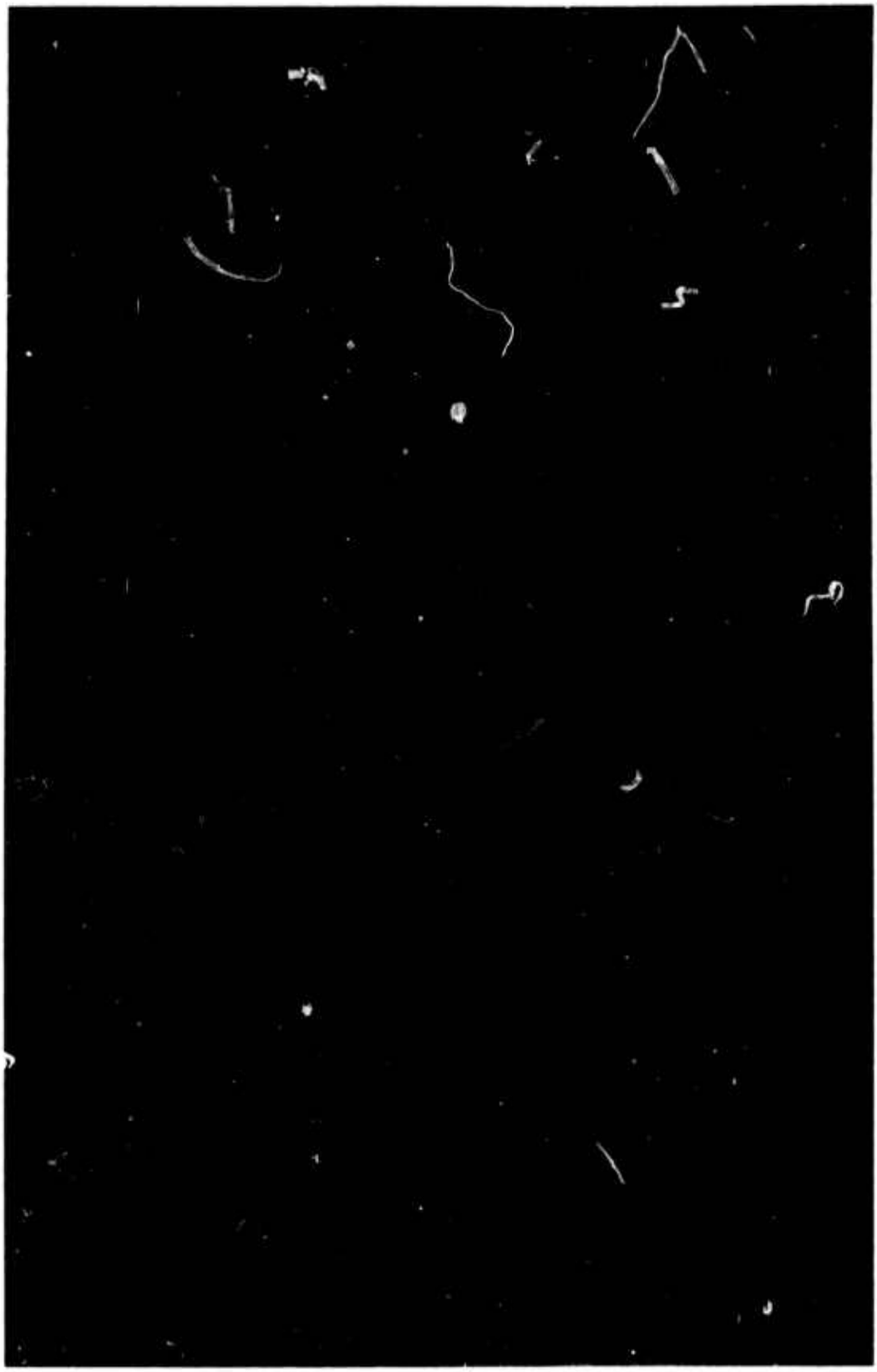


Figure 1. DCAT Direct Bleed Control Valve

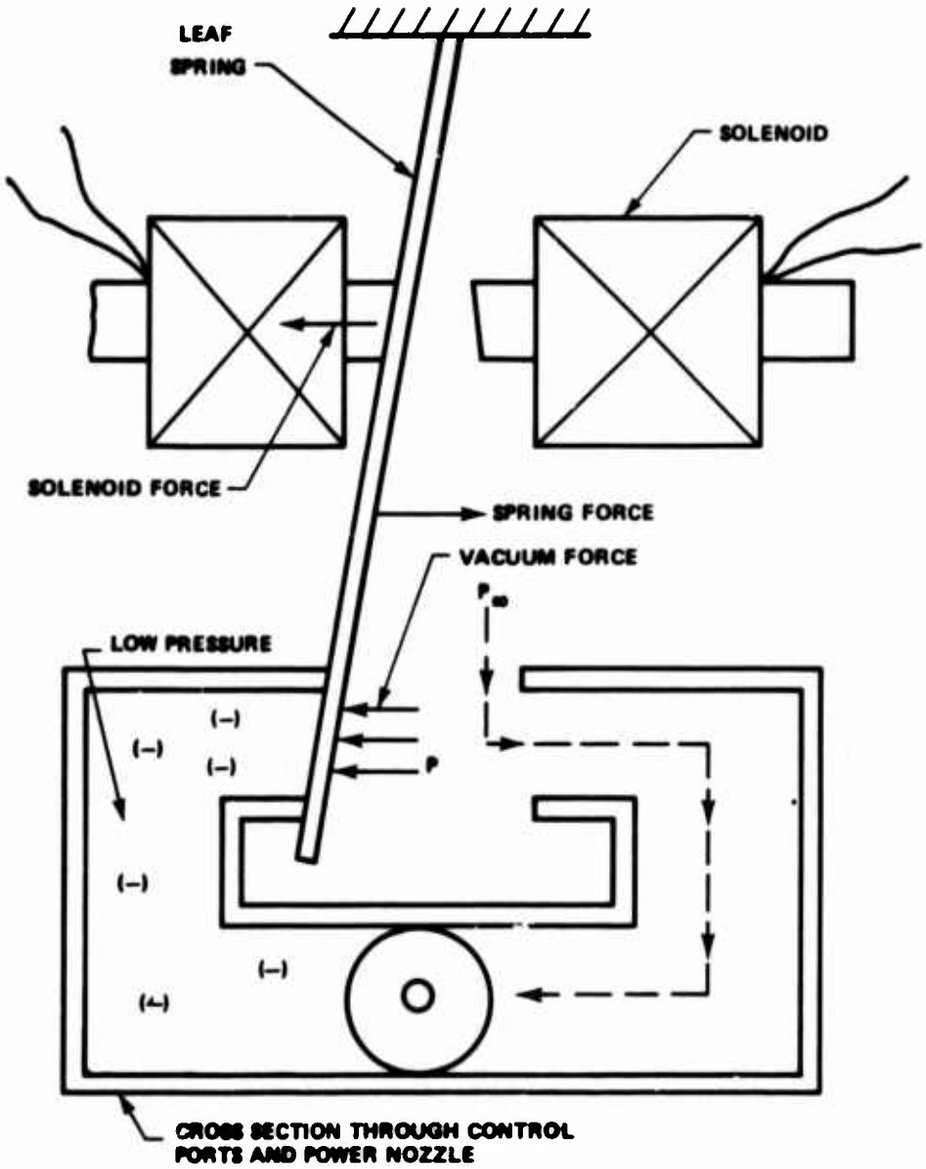
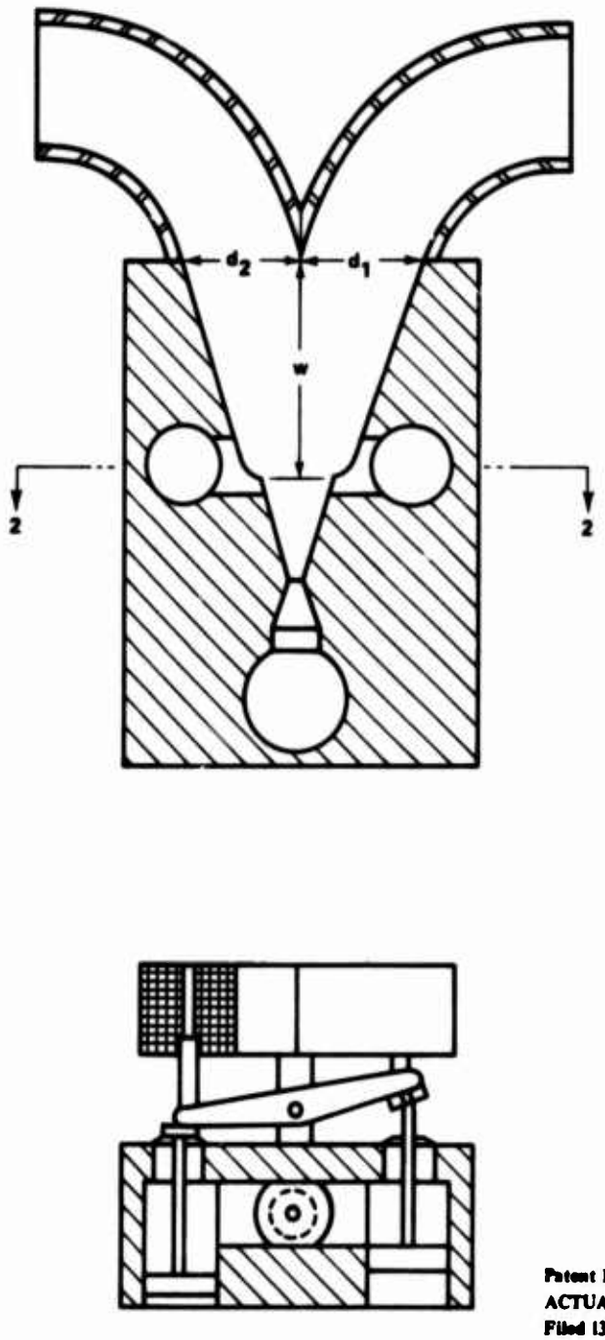


Figure 2. Leaf Spring Actuator

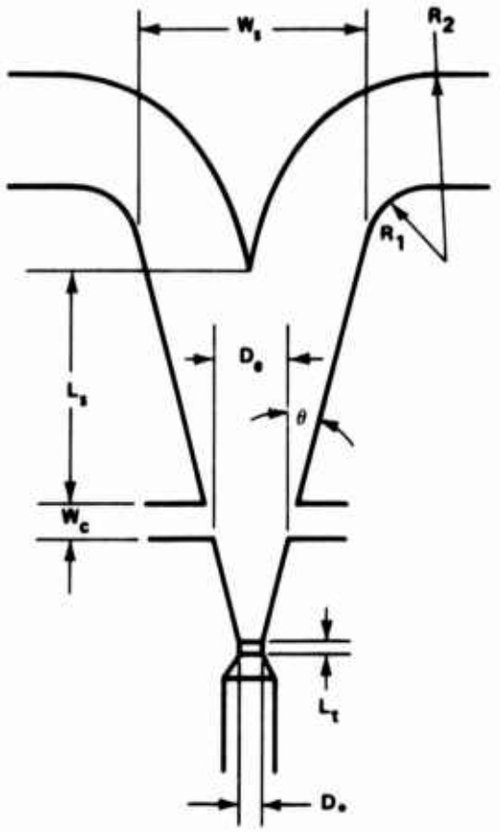


Figure 3. Sliding Plate Actuator



Patent No. 3,289,687 - J. C. Dunaway
ACTUATOR FOR PURE FLUID AMPLIFIER
Filed 13 Feb 64.

Figure 4. Pressure Balanced Piston Actuator



	D_o	L_t	W_c	L_s	W_s	D_e	θ	R_1	R_2
3 lb	0.055	0.025	0.25	0.973	0.756	0.236	15 deg	0.19	0.55
1.5 lb	0.040	0.020	0.174	0.696	0.546	0.174	15 deg	0.19	0.45

Figure 5. Three-Pound and 1.5-Pound DCAT Valve Dimensions

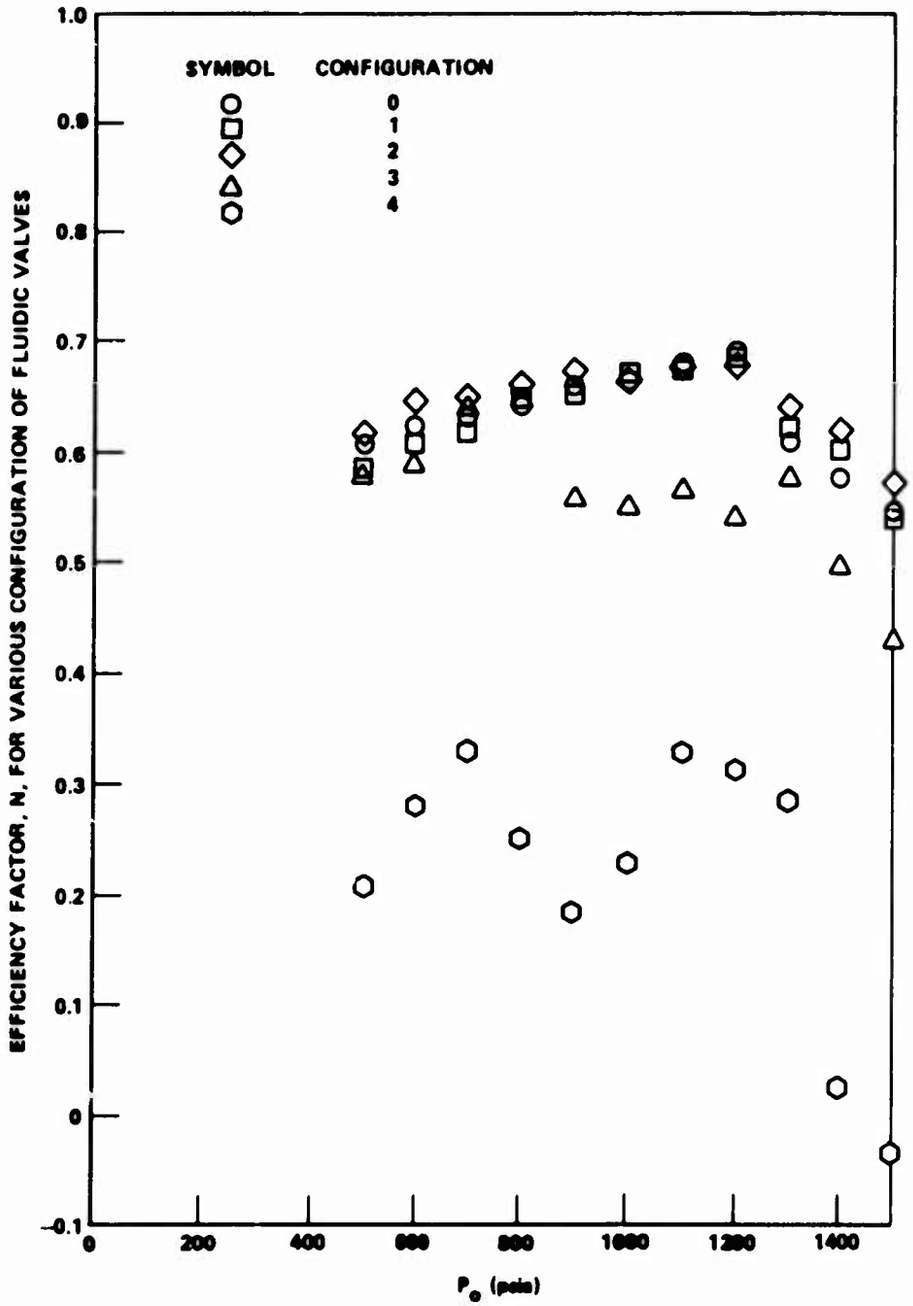


Figure 6. Efficiency of the 12-Pound Valve Configurations as a Function of Total Pressure

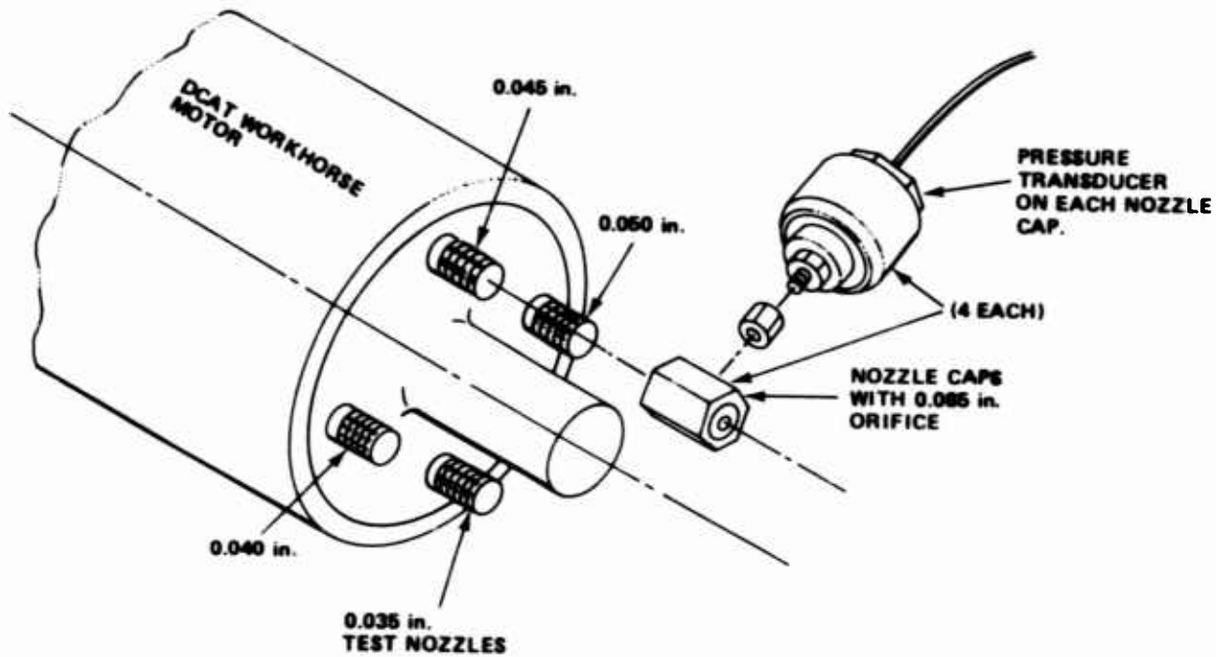
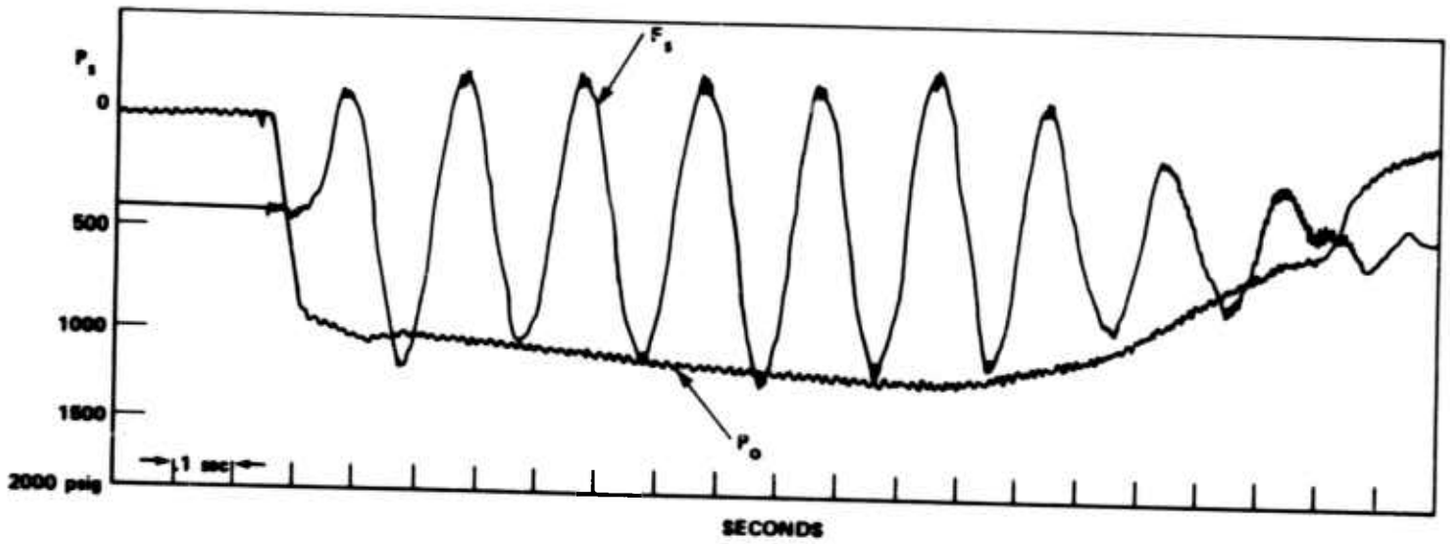


Figure 7. Bleed Nozzle Clogging Test



DCAT – VALVES 139 AND 117 ON LONG
NOZZLES – 31 OCT 73

Figure 8. Curve of F_s Modulated by P_s

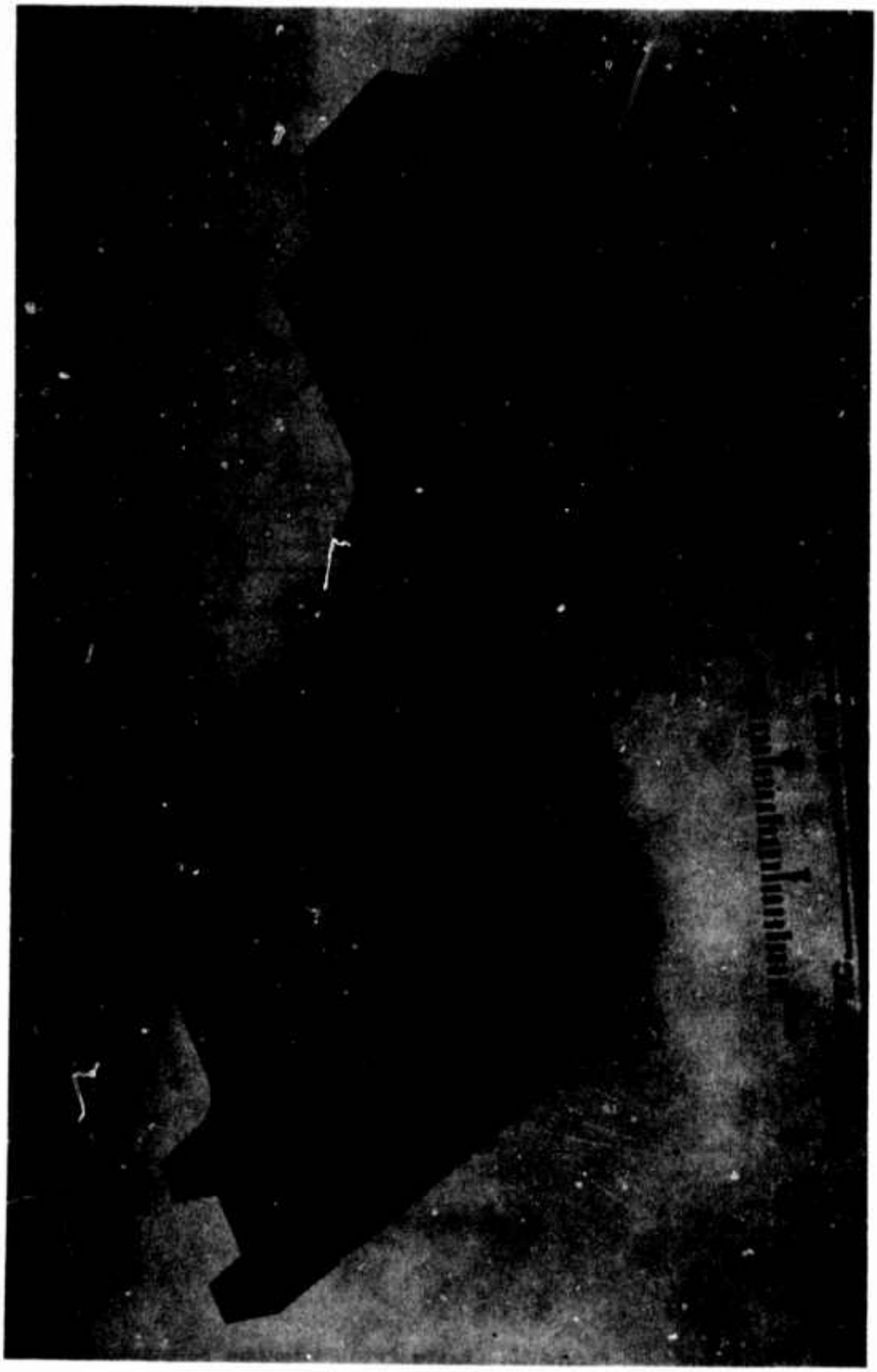


Figure 9. Asbestor-Phenolic Valve Bodies, DCAT

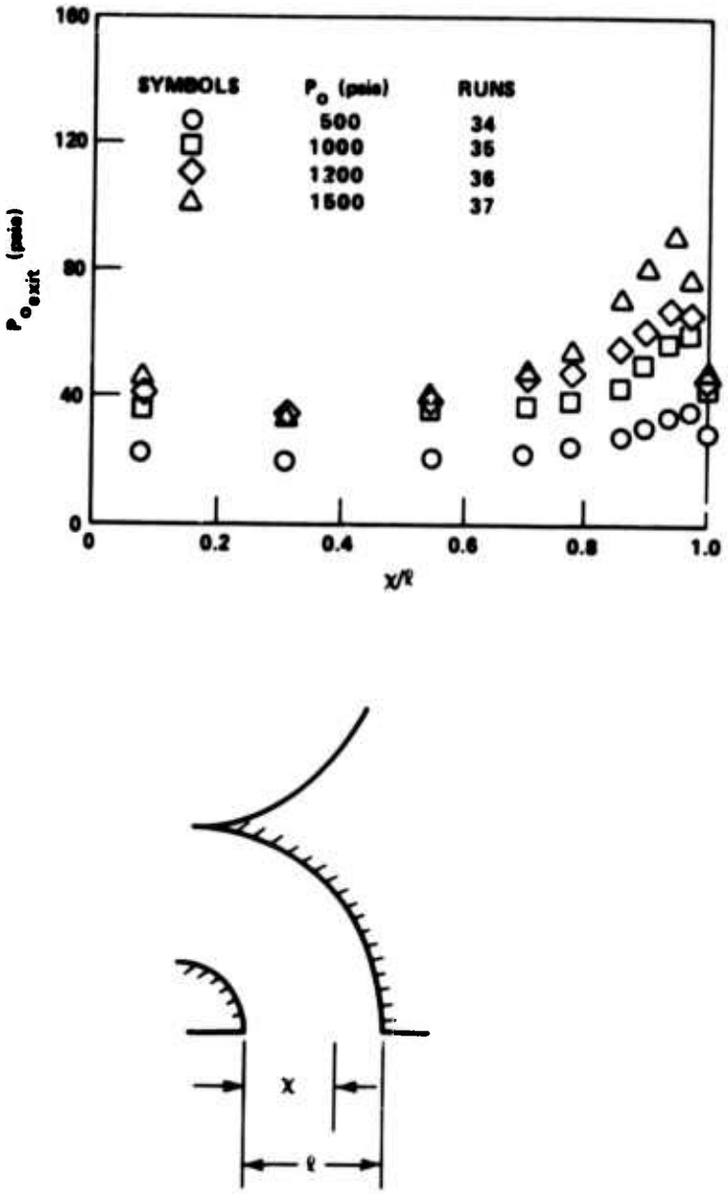


Figure 10. Valve Exit Centerline Survey

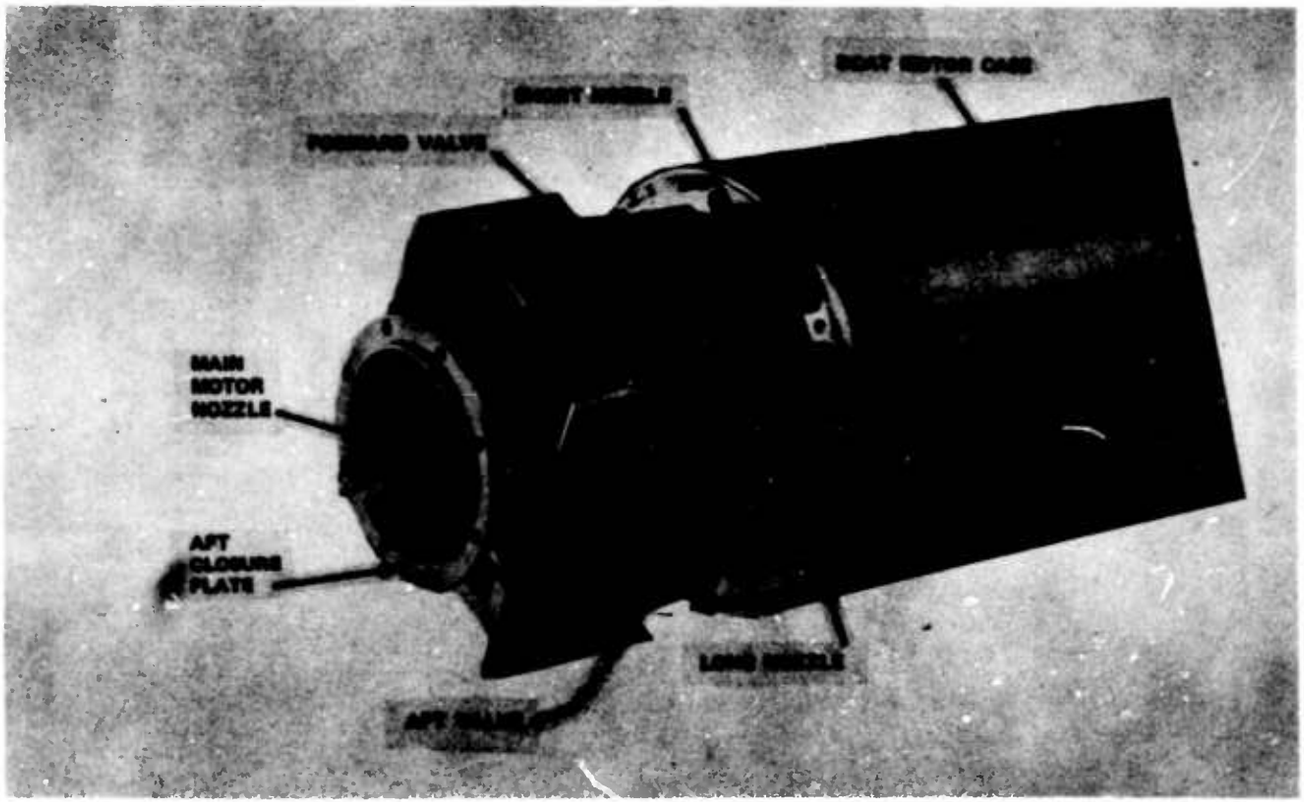


Figure 11. General Arrangement, DCAT Control Valves

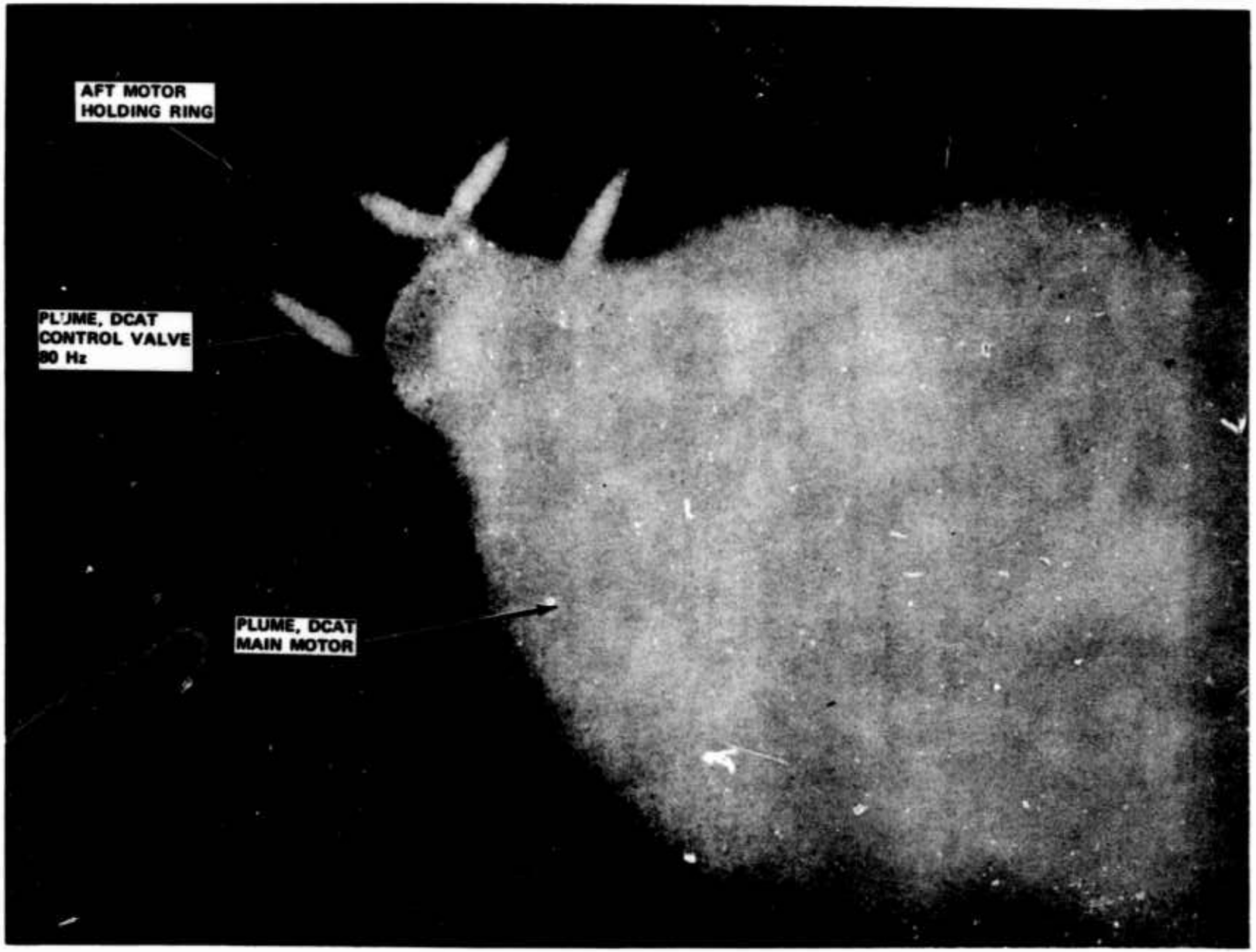


Figure 12. Three-Pound DCAT Valve Operation, Hot Gas

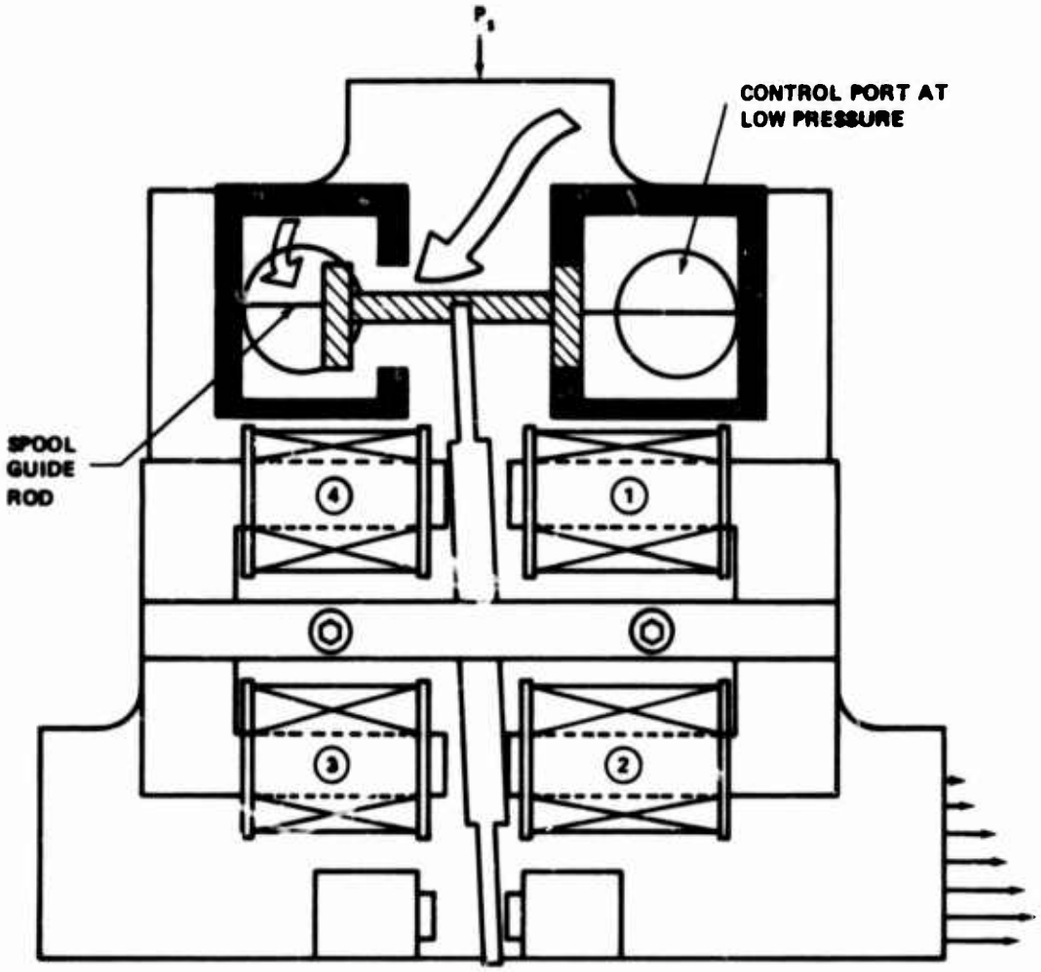


Figure 13. Electrical/Fluidic Interface Device

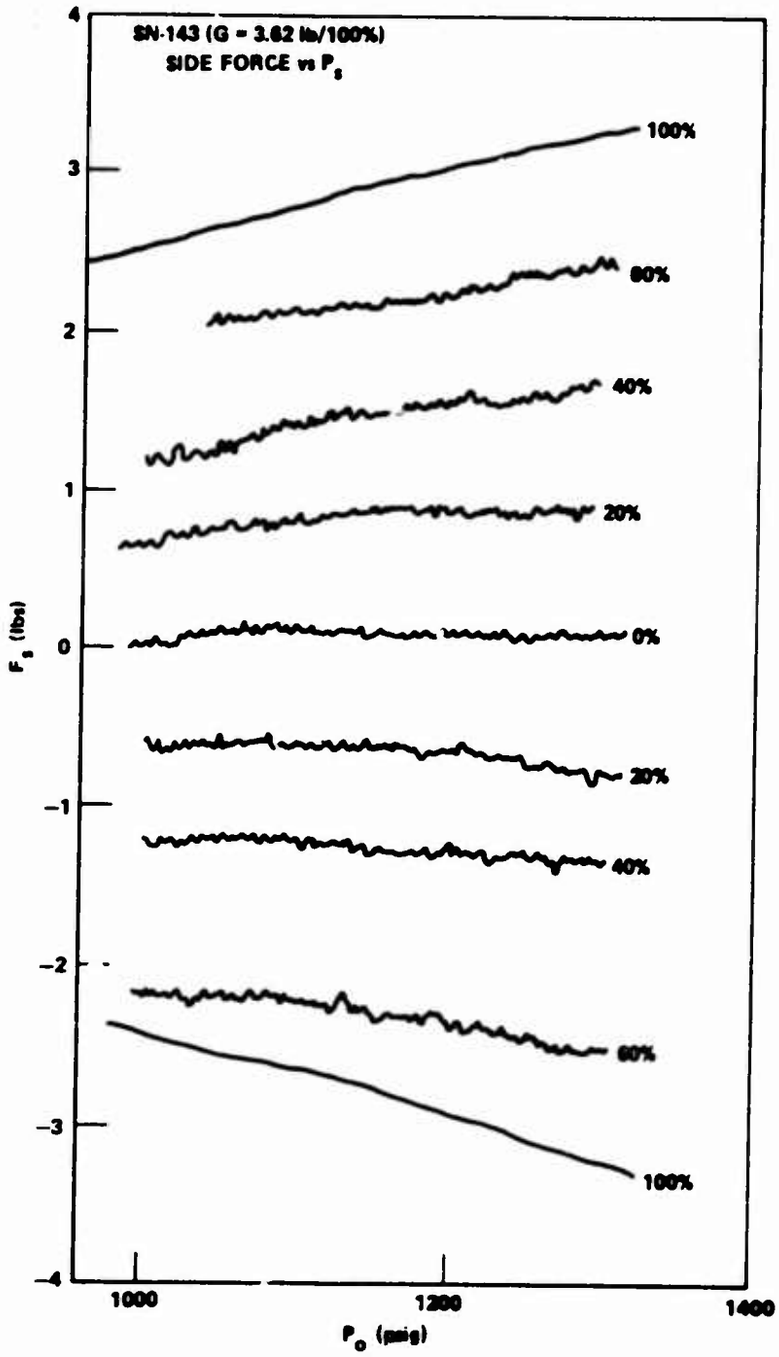


Figure 14. Typical Performance, DCAT 3-Pound Valve F_S vs. P_S at Various Percents of Modulation at 80 Hz

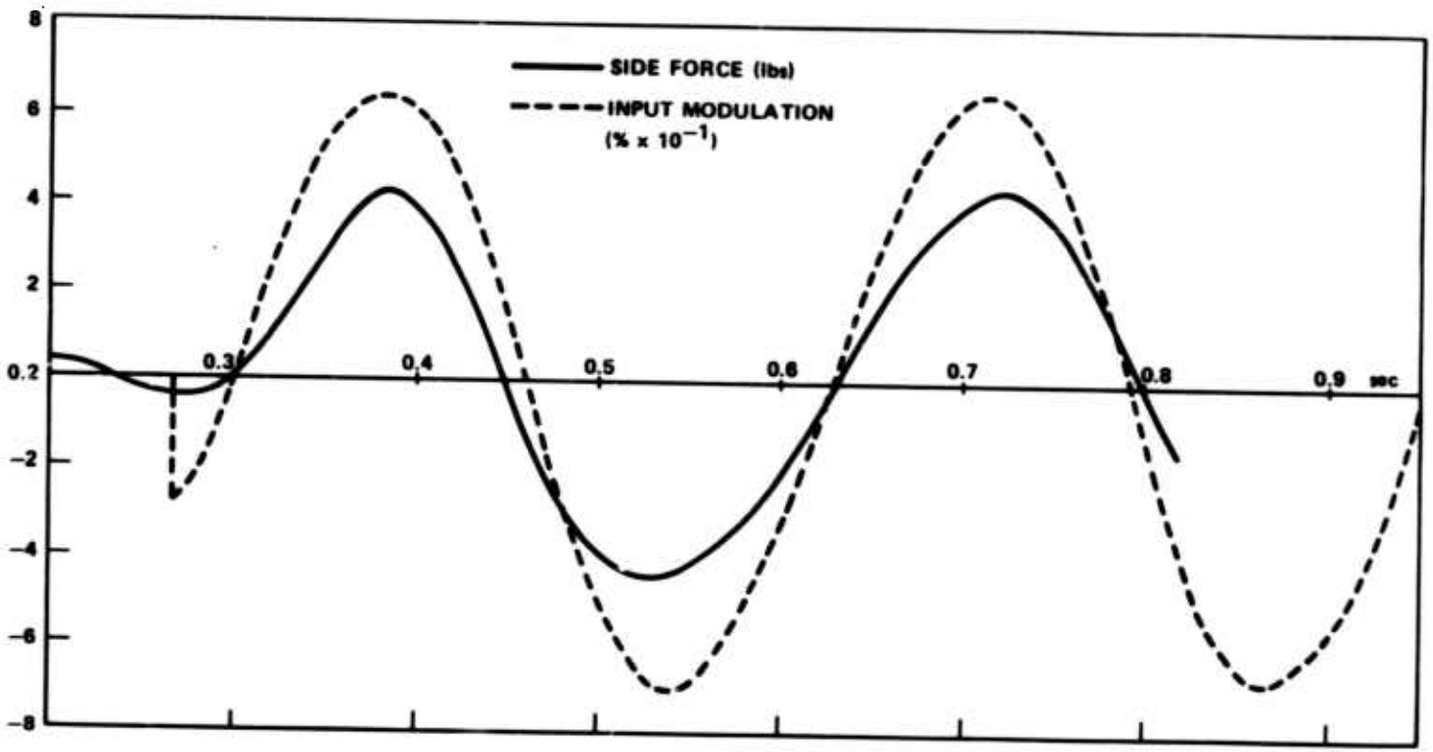


Figure 15. Side Force and Input Percent Modulation vs. Time, Corrected for Phase Lag and Zero Shifts

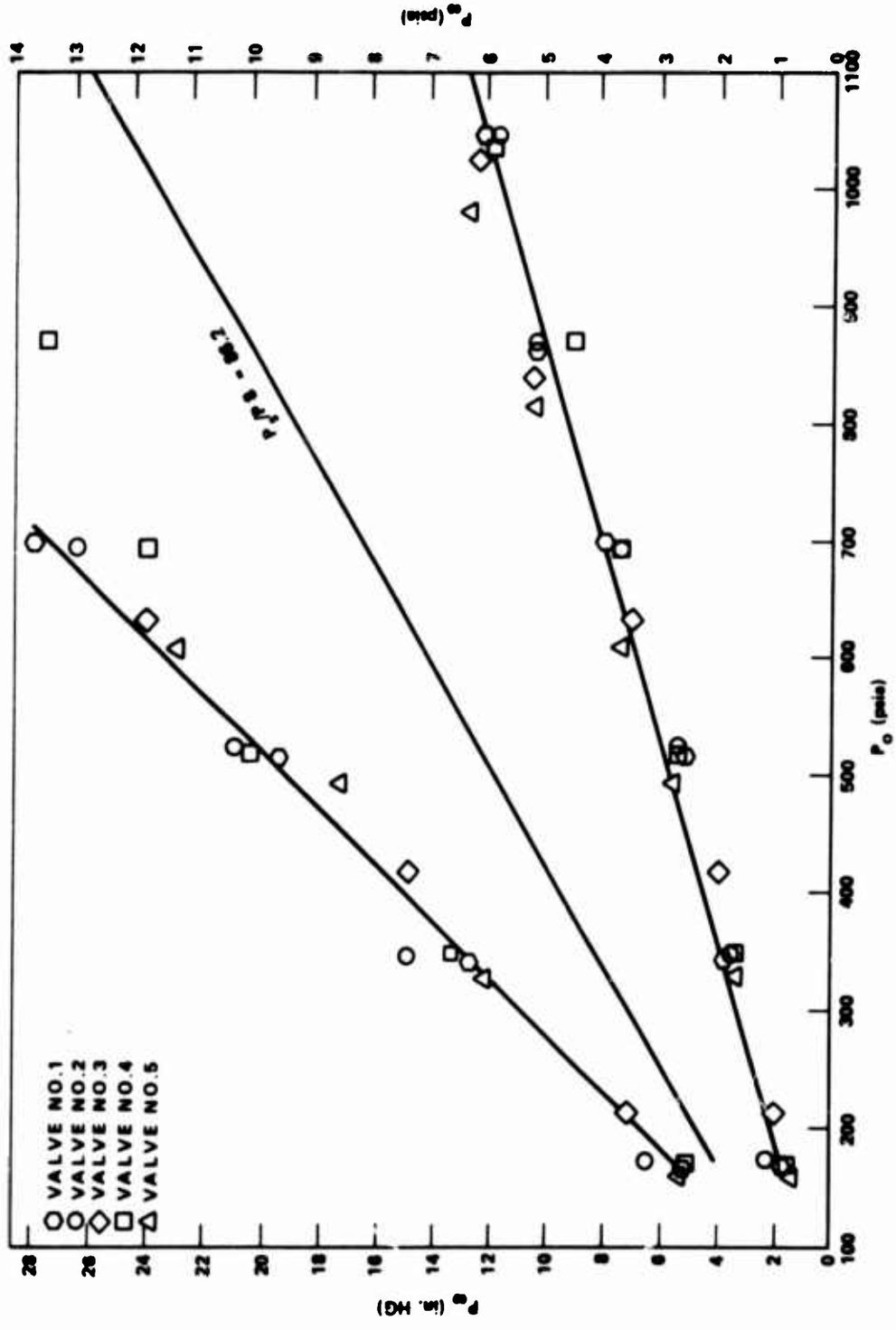


Figure 16. Switching Range, DCAT Wind Tunnel Valves

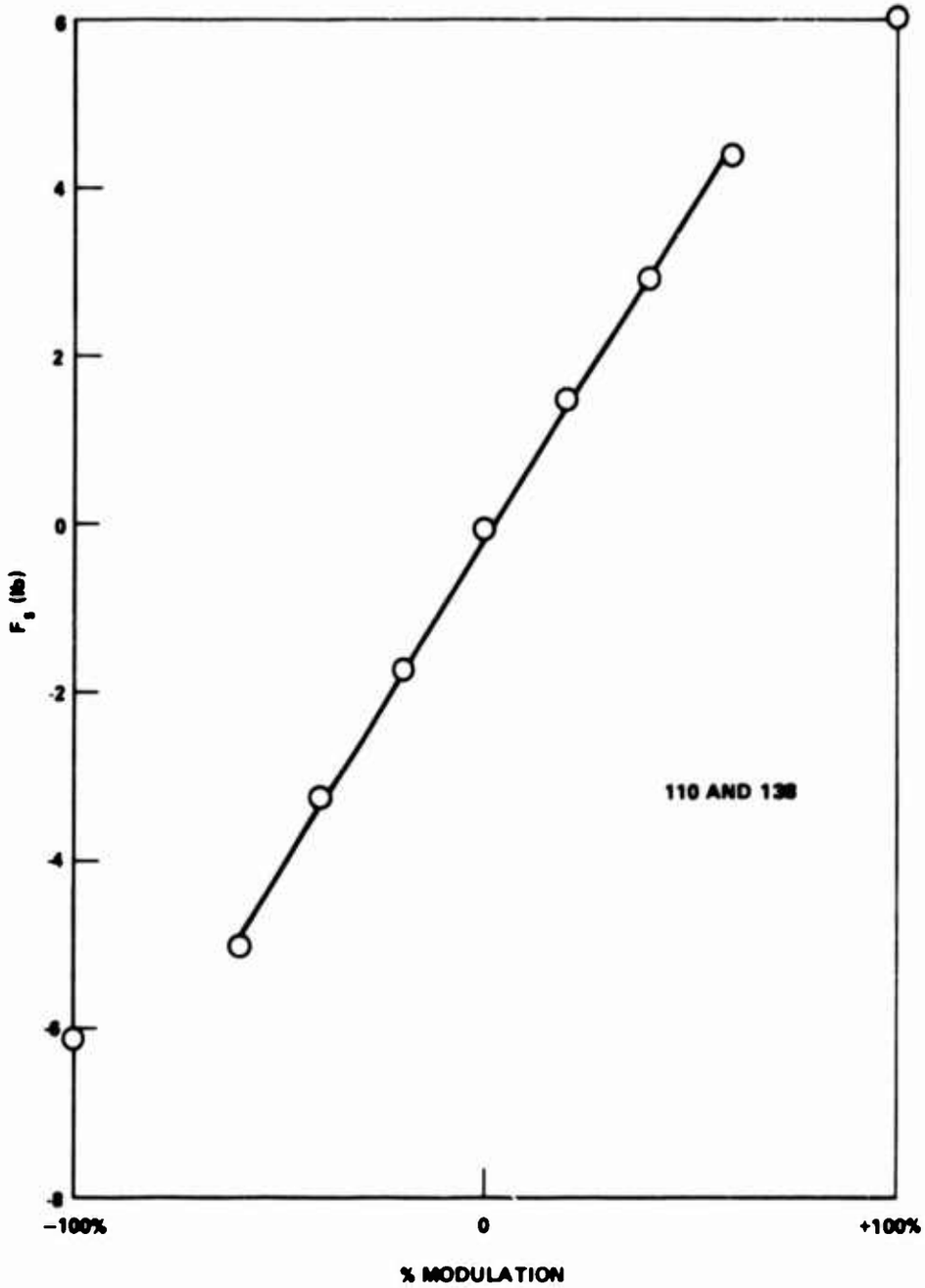


Figure 17. Valves 110 and 138, Gain as Matched by the Computer Selection Program

LIST OF FIGURES

1. DCAT Direct Bleed Control Valve
2. Leaf Spring Actuator
3. Sliding Plate Actuator
4. Pressure Balanced Piston Actuator
5. Three Pound and 1.5 pound DCAT Valve Dimensions
6. Efficiency of the 12 Pound Valve Configurations
7. Bleed Nozzle Clogging Test
8. Curve of F_s Modulated by P_s
9. Asbestos - Phenolic Valve Bodies, DCAT
10. Valve Exit Centerline Survey
11. General Arrangement, DCAT Control Valves
12. Three Pound DCAT Valve Operation, Hot Gas
13. Electrical/Fluidic Interface Device
14. Typical Performance, DCAT 3 Pound Valve F_s vs. P_s at Various Percents of Modulation at 80 Hz.
15. Side Force and Input Percent Modulation vs. Time, Corrected for Phase Lag and Zero Shifts
16. Switching Range, DCAT Wind Tunnel Valves
17. Valves 110 and 138, GAIN as Matched by the Computer Selection Program

FLOW CONTROL CIRCUITS FOR TOXIC FLUIDS

J.R. TIPPETTS*, N. SYRED*, J. GRANT+ and R.E. STRONG ≠
*Department of Chemical Engineering and Fuel Technology, University of Sheffield. +Reactor Group, U.K.A.E.A., Risley, ≠ Technical Services Department, British Nuclear Fuels, Windscale.

ABSTRACT

"Classical" and newly-developed fluidic devices are being used to control active fluids in a nuclear fuel processing plant.

Glove Box Systems (Operational since 1972)

A glove box permits hand access via gloves to active material. Sub-atmospheric air pressure at a pre-set level is maintained by a vortex amplifier (VA) connected in the suction supply line. It effectively lowers the suction source impedance and is able to compensate for accidental in-leaks of air. Here a single device replaces a complex electro-pheumatic system. The rational design of this simple circuit involves principles applicable to networks of any 3-terminal fluidic devices.

Multistage VA systems are described.

Filter-Compensator Circuit (Model tested May 1973).

The circuit includes a "Turn-up Vortex Amplifier" (TuVa) to compensate for the changing resistance of a filter. (Control flow in the TuVa destroys a vortex). The circuit is algebraically related to the previous circuit.

Parallel Source Circuits (Devices all existing, Design Studies)

Waste liquor entering a pipe from several sources involves some basic "parallel source" problems; here a device called the "Flow Junction" is uniquely useful. Some of its properties can be synthesised by using other devices called Reverse-Flow Vortex Amplifiers (RFVAs: 3-terminal active diodes) or sometimes using VAs and TuVAs. Also it is shown how pumps can be manifolded by simple circuits which prevent catastrophic pressure loss when one pump fails.

Pumping Circuits (Some have operated since 1972)

Circuits involving vortex-diodes, RFVAs, and special-purpose 3-terminal devices called "Jet-pump-diodes" enable alternating gas pressure to pump liquids. The Fluidic Hydraulic Ram is also described.

Emphasis on System Design

The important operational characteristics of the circuits are predicted from well-defined experimentally determined device characteristics.

NOMENCLATURE

Ae	Outlet cross-sectional area of a VA.
AT	Tangential control-port cross-sectional area of a VA.
e	Pressure difference.
E	Ratio of pressure differences.
F_c & F_s	Characterizing functions of a VA.
G^c	Control pressure ratio for a VA in the vortex state.
k	Resistance coefficient, of the form: pressure drop/flow^2.
K	Ratio of resistance coefficients.
n & v	Denote normal and vortex states in the figures.
q	Volume flow.
Q	Ratio of flows.
T	Turndown ratio.
X	Control pressure ratio for the TuVA in the vortex state.
η	Efficiency.
μ	Multiplier, defined as a flow ratio.

1st Subscripts

1 & 2	1st and 2nd stage values.
a,b,c,o,s	terminals of devices.
f	filter (pressure drop).
r	resistance (pressure drop).
y	circuit (pressure drop).

2nd Subscripts

f & r	forward and reverse state values (for the JPD).
n & v	normal and vortex state values.
1 & 2	specified states; also 1st and 2nd state values.

Abbreviations

BA	Bistable Amplifier.
CSV	Coanda-switched-vortex-device (BA connected to a VA).
FJ	Flow-junction, (a specially designed Y-joint).
JPD	Jet-pump-diode.
RFVA	Reverse flow vortex amplifier (A VA designed to facilitate flow in the wrong direction).
R-RFD	Reverse flow diverter.
TuVA	Turn-up vortex amplifier (control flow decreases its resistance).
VA	Vortex amplifier.

Also

iwg	inches water gauge pressure.
$\xrightarrow{e}$	pressure difference, arrow goes from high to low.

Introduction

When fluidics as a distinct technology was first conceived it was quickly realized that therein lay the capability to construct reliable flow switching systems that would yield great advantages in nuclear plants. The opportunities for such applications in the U.K.A.E.A. were identified by Grant and others, Refs. 1, 2, 3 and 4 and numerous ambitious schemes were envisaged. A particular one concerned the extraction of sample-fluid from many points within a reactor and the feasibility of this was shown by a prototype fluidic multiplexor (uni-selector or sampling circuit) Ref. 5. This showed in principle (using 8 devices) how 2n bistable amplifiers could form a synchronous, n-1 stage, shift-register which could be set into any of its 2^{n-1} states by a 3-level control signal conveyed by a single pipe.

Initially, progress was slow in the field of flow control because available device-designs were intended for information - switching (logic) so devices and circuits had to be constructed ab initio. Gradually a range of good fluidic flow control devices has been developed and simultaneously, simple but effective design methods.

Recently, with the cooperation of Strong and others at British Nuclear Fuels Limited these fluidic innovations have been successfully applied to cope with the stringent requirements associated with nuclear fuel re-processing. Furthermore, many other applications for fluidic techniques have been identified and studied. Some of these applications and design studies are described in the following.

Glove Box Pressure Regulator Circuit

An application which has shown the value of power fluidics compared with conventional moving-part valves is in the pressure-control and protection of glove boxes. These are transparent plastic boxes which allow hand-access, via sealed rubber gloves, to toxic materials and equipment in the box. Its interior is maintained at a sub-atmospheric pressure of 1.5 inches of water (iwg) so that no vapours or dust will leak out.

Such glove boxes and similar structures are used in great numbers and they are "supplied with suction" by purge-ducts which ultimately connect to a central filtration and pumping unit. The sub-atmospheric pressure in the purge-ducts, typically 6 iwg, is generally much greater than that required in the glove-boxes so pressure regulators are necessary.

Conventionally, a system shown in Fig. 1a. regulates the box pressure. An orifice A allows a small flow of air into the box and into the purge-duct through a second orifice B which is adjusted so that their combined action is to maintain

the 1.5 iwg depression. The gloves and working port hoods can by their nature have only fragile connections to the chamber, and there is a high risk that they will be pulled off, leaving a wide aperture which would allow toxic particles and gases to diffuse out to the operator. To guard against this solenoid valve is provided to connect the chamber directly to the low pressure purge line and gives a high velocity flow across the aperture preventing backward diffusion. The solenoid is operated from a pressure switch in the glove box which is actuated by the increase in box pressure after the containment is broken. The plant operators wished to improve both performance and safety. The major uncertainty is the reliability of the solenoid valve and pressure switch. Also the small apertures A and B might be blocked. Blocking A reduces the box pressure to -6 iwg and so could cause the walls to collapse. Blocking B prevents purging allowing toxic diffusion through the leaks.

Fig. 1b. shows the glove box protected by a vortex amplifier. The amplifier is connected in an unusual mode, analogous to an earthed grid triode valve. The radial inlet is connected to the box, the outlet to the purge duct, and the tangential control ports are at atmospheric pressure. Referring to the control pressure/flow characteristic (Fig. 2.) the amplifier normally operates near point v where it is at its maximum turndown. Control pressure is constant at atmospheric pressure, but an aperture in the glove box allows the radial inlet pressure to rise relative to control pressure, bringing the amplifier towards point n, the turned on condition. This increases flow across the glove or equipment aperture to the amount required by the "Sealed Sources Act". For smaller apertures, flow increases rapidly with box leakage, keeping the box near its design pressure.

Comparing the two glove box designs, the primary requirement of improving reliability is clearly met. The failure mechanisms of the mechanical valve and switch are removed, and because the vortex amplifier has no small apertures and four inlet and control ports it cannot be blocked by small particles. Several other advantages arise. The ability to maintain box depression even for moderately large leakages, and the general ability to control pressures due to rapid glove withdrawal and insertion are important advantages not shared by the mechanical valve. Reponse is much quicker, and the danger of collapse by blocking aperture A is removed, because in this case air will be drawn from the control ports to compensate. These control ports are not easily blocked because they are fairly large, and it would be necessary to block four simultaneously to cause the box to collapse.

The rational design of this circuit, is now described in detail because it involves procedures and concepts which

are useful in many other circuits.

Operational Characteristics of the Vortex Amplifier

Under the conditions prevailing in the circuit the VA can be described by the four flow (q) and pressure-difference (e) variables as indicated in Fig. 2. Pressure difference is represented by an arrow pointing from high to low. "Pressure" is ideally the total pressure when the dynamic pressure is small compared with important pressure differences in the system. Hence, e represents potential difference and the VA can be treated as a Kirchhoffian 3-terminal non-linear resistor. It, therefore, has much in common with electrical devices of this type such as transistors. But it is also essentially a fluid dynamic element and is subject to Eulerian Similarity in the same way that pumps or aerofoils are. These topics are described in general terms in Refs. 6 and specific features are applied in the following analysis.

The non-dimensional characteristics of a VA, designed by Syred specially for glove box use, are shown in Fig. 2. These characteristics are the result of testing the VA with air, holding e_s constant, varying e_c and measuring the remaining two dependent variables q_s and q_c. The results are plotted in terms of the non-dimensional variables denoted by capitals and defined by

$$E_c = \frac{e_c}{e_s} \qquad Q_c = \frac{q_c}{q_{sn}} \qquad Q_s = \frac{q_s}{q_{sn}}$$

q_{sn} is the value of q_s in a conveniently chosen "reference state" defined as occurring when $e_s = e_c$. This is purely for convenience in this application. The state is referred to as the "normal state" denoted by n in Fig.2. (Frequently, the normal state is defined when $q_c = 0$, in fact q_c is almost zero in the above definition of the normal state.)

The characteristics can be regarded algebraically as two non-dimensional functions of the single variable E_c.

$$Q_c = F_c(E_c)$$

$$Q_s = F_s(E_c)$$

but these apply for all values of e_s and furthermore q_{sn} is related to e_s by

$$k\, q_{sn}^2 = e_s$$

so the state of the device can be given explicitly in terms of the characterizing variables (in the form of driving-point

and transfer characteristics) by

$$q_c = (k\ e_s)^{-\frac{1}{2}} F_c(E_c)$$

$$q_s = (k\ e_s)^{-\frac{1}{2}} F_s(E_c)$$

Because the dependent variables are flows and the independent variables are pressures, this may be described as an "admittance format".

The characteristics are distinctive of fluidic elements because they are functions essentially of a single non-dimensional variable E_c and a magnitude e_s, the effect of the magnitude is simply a square-law scaling operation, but the effect of E_c varying is a unique characteristic of the VA.

Small-Signal Parameters

It is useful to write down the local linearization of the characteristics in terms of the four necessary partial differentials. These, in this format will be admittance parameters:

$$\frac{\partial q_c}{\partial e_c} \quad \frac{\partial q_c}{\partial e_s} \quad \frac{\partial q_s}{\partial e_c} \quad \frac{\partial q_s}{\partial e_s}$$

by partial differentiation, the first two of these are given by:

$$\frac{\partial q_c}{\partial e_c} = (k\ e_s)^{-\frac{1}{2}}\ F_c'(E_c)$$

and:

$$\frac{\partial q_c}{\partial e_s} = (k\ e_s)^{-\frac{1}{2}} \left\{ \tfrac{1}{2} Q_c - E_c\ F_c'(E_c) \right\}$$

where F_c' is the gradient of F_c.

the other two are formed in the same way.

Therefore as we would expect, the locally linearized parameters (admittances, gains, etc.) depend basically only on the gradients of the two non-dimensional functions (F_s and F_c) of a single variable E_c.

Having identified these parameters it is easy enough to put them into any other form: impedance or hybrid, by using standard matrix methods such as those described by Shekel, Ref.7.

Large-Signal Parameters

Because the VA is subject to similarity, intrinsic performance parameters can be defined which describe its large-signal operation concisely. These are T, the turndown ratio

and G, the pressure ratio, defined in terms of the normal and "vortex" states (when $q_s = 0$, indicated by v in Fig.2.) by

$$T = \frac{q_{sn}}{q_{cv}} \qquad G = \frac{e_{cv}}{e_s} \quad \text{when } e_s \text{ is constant}$$

For this particular VA $T = 14.2$ and $G = 1.43$

For reasons which will be shown the VA must have a specific value of G with the highest possible value of T and a smoothly declining characteristic as E_c increases.

Circuit Design

When the VA is connected into the circuit it is subject to different constraints from those used in its characterization. Hence its characteristics as represented by Fig.2 are not in a convenient form for the design of the circuit. They can be altered algebraically into a convenient form by a "data transformation" which, in its most general form can be regarded as operating on a series of listed operating points in a computer. These have been described in Refs. 6 and 8; they can be regarded as analogous to operations which convert an impedance matrix into an admittance (or hybrid) matrix in linear systems analysis.

By considering the circuit in Fig. 1b, it can be seen that the constrained variable is the control pressure e_c because the control port is open to atmosphere, and the VA outlet is connected to the suction source pressure (assumed constant at this stage). Therefore a simple form of data transformation is needed to convert the original characteristic from the e_s = constant form to the e_c = constant form.

Data Transformation

The desired data transformation is described here by considering how three points on the "original" characteristic are converted into the "new" characteristic (with e_c = const). The three points include the normal and vortex (n and v) states and an intermediate point.

Since the constraint is being changed, it is necessary to specify that the reference pressure is the value of e_s in the normal state e_{sn}; again, chosen for convenience. Also as a consequence, the non-dimensional pressures are now defined in terms of this specific value so the fourth variable E_s can be defined as

$$E_s = \frac{e_s}{e_{sn}}$$

In terms of these variables the data transformation is as follows:

State	E_s	E_c	Q_s	Q_c	
Normal	1	1	1	≐ 0	) original
	1	1.23	.64	.055	) values
Vortex	1	1.43	0	.070	)
					μ
Normal	1	1	1	≐ 0	1
	.813	1	.577	.049	.905
Vortex	.70	1	0	.059	.836

In each row, the pressures in the original characteristics have been multiplied so that in the new characteristics $E_c = 1$.

The flows have been multiplified by the square root of this factor, and this flow multiplying factor μ is listed in the fifth column; it is an indication of the extrapolation from the original data caused by the data transformation. Over the small range used here the similarity assumption is certainly justified.

By applying this method to all points on the characterics they become altered to the form shown in Fig.3. The states n and v are marked.

In these characteristics, $E_c = 1$ so the point 1 on the pressure axis represents atmospheric pressure and the point 0, the origin, represents the suction source pressure (a negative pressure). The flow being sucked out of the glove box is Q_s, the supply flow into the VA; this "Q_s characteristic" intersects the pressure axis at the vortex-state-value of .7 (in fact, $1 - \frac{1}{G}$) meaning that the suction applied to the glove box is never greater than the factor $(1 - \frac{1}{G})$ times the maximum suction source pressure. So, in this respect, the circuit has achieved the prime objective.

The Q_s curve in fact acts as a new source characteristic which "supplies" the glove box and it can be seen that the slope of this characteristic is typical of a low impedance source: a large amount of flow can be extracted without a large pressure loss. If the characteristics are turned through 90° so that the E_s axis is on the left hand side and vertical, the Q_s characteristic is seen to be like the output characteristic of a pump (drawn in the usual way with output pressure vertical) and an arbitrary parabolic line in Fig.3. represents a "load" in this case one of the possible "states" of the glove box (say: with one glove off). The

"operating point" of the circuit is represented by the intersection point of the two characteristics; as the state of the glove box varies so the intersection point "slides" along the characteristics.

The suction source characteristic has thus been converted from one with a high value (for example - 6 inches water) to another one with a lower, safe value (equal to - 1.8 inches water). But the "cost" of this is a small bypass flow, Q_c, which is maximum when the glove box flow is zero and minimum, virtually zero, when the glove box flow is maximum. Now, it can be noted that the intersection point of the Q_s curve with the atmospheric pressure line, $E_s = 1$, represents the maximum flow that can be extracted from the glove box and this can be increased almost arbitrarily by increasing the size of the VA; however, the value of Q_c will also rise in proportion. This is one obvious, but small, limitation on size. The main limitation can be understood in relation to certain practical details as described next.

The effect of parasitic resistances

Inevitably, in practice, resistances become added to the VA, in the form of: filters put on the control port, pipe connections between glove box and VA, and pipes connecting the outlet of the VA to the suction source, in principle, including all of the intervening pipe work. These effects can most clearly be seen by using another data transformation designated "STAR" which, in effect,regenerates characteristics of a "new device" consisting of the original device plus square-law (orifice type) resistances in series with its terminals as shown in Fig. 4.

STAR Transformation

The resistances are characterized by relative resistance coefficients denoted by capital K.s. For example K_s is defined by

$$K_s = k_s/k$$

where k_s = pressure drop/flow squared in resistance, and k is the VA resistance (i.e. e_{sn}/q_{sn}^2).

The STAR transformation can be described algebraically as follows in terms of operation on one state of a device:

$$E_s(\text{new}) = E_s + Q_s^2 K_s + (Q_s + Q_c)^2 K_o$$

$$E_c(\text{new}) = E_c + Q_x^2 K_s + (Q_s + Q_c)^2 K_o$$

$$\left.\begin{aligned} Q_s(\text{new}) &= Q_s \\ Q_c(\text{new}) &= Q_c \end{aligned}\right\} \text{ unchanged.}$$

The resulting characteristics no longer have the E_c = constant format but re-application of the previous data transformation will re-impose that constraint. (This is necessary because this is a series circuit and the characteristics are in an admittance format).

The effects of these parasitic resistances are shown in Fig. 4. The normal state is represented by the end point of the curves and this also represents what would have to be the atmospheric-line-intersection if the state n were to be reached. However, the atmospheric line is in fact at $E_s = 1$ and so the effect of resistance in all cases is to reduce the effective range of operation of the VA. In all cases, parasitic resistance is detrimental but it has the strongest effect on the supply port i.e. in between the glove box and the VA.

From this we can deduce why the VA cannot be arbitrarily increased in size. The parasitic resistances have fixed values and so their relative magnitudes K_s, K_o and K_c will increase as the size of the VA is increased (since k for the VA will decrease). Eventually the performance of the VA will be swamped by the effective series resistances.

There is obviously scope for optimization of the size of the VA but this is achieved adequately at the moment by commonsense. However, all of the equations are available in the foregoing analysis to carry this out if necessary.

Design of VAs for glove box applications

The foregoing analysis highlights the main features of design however some other details are worth noting and these have an effect on the design of the VA.

It is only recently that much information has become available concerning high performance vortex amplifiers (Refs. 9-16). In the following table the main characteristics of these devices are summarized. One common feature of all the vortex amplifiers is the use of conical outlet diffusers (typically 5° - 7° total angle). The reverse flow vortex amplifiers do not use conical outlet diffusers, but use the vortex chamber as a diffuser.

All these devices have a flat (or nearly flat) vortex chamber profile, except for the devices of Al-Shamma (14) and Syred (15) in which the vortex chamber is in the form ofacone. The linearity of the operating characteristics of the vortex amplifier may be improved slightly by preswirling the main inlet fluid through an angle of between 5 and 10°, (Refs. 9, 13, 14). More compact devices are produced with single outlet VAs, the only sacrifice being some loss of smoothness of the operating characteristic. A comparison between the characteristics produced by single and double outlet VAs (Fig. 5(a) and 5(b) respectively) is shown in Fig. 5(c). An even more compact

References.	No. of Outlets.	Performance.	*Inlet Configuration.	$H/_{De}$	Comments.
Keorper (9)	Two	T≈11	Annular	0.625	Noisy and characteristic contains much hysteresis.
Syred (10)(11) (12)	Two	T≈17 for G≈1.5 T≈20 for G≈3	4xRadial	0.665	Characteristic noisy & hysteric for G≈3. Characteristic very smooth and much less noisy for G≈1.5.
Saunders (13)	One	T≈20 for G≈2	4xRadial	0.125	Some noise and hysteresis in characteristic. Chamber profile very complex to obtain high T.
Al-Shamma (14)	One	T≈12 for G≈3 T≈9 for G≈1.5	Annular	Not known	Vortex chamber in form of 60° cone. Noise & hysteresis increase as G≈3.
Syred (15)	One	T≈12 for G≈4	Annular	0.475	Vortex chamber in form of 45° cone. Reverse flow vortex amplifier - similar to vortex amplifier and results comparable.
Syred (16)	One	T≈12 for G≈3.6 T≈11 for G≈1.5	Annular	0.16	Vortex chamber profile complex to obtain high T. Reverse flow Vortex Amplifier similar to vortex amplifier and results comparable.

*This refers to the main fluid inlet configuration.

device may be produced by using an annular main fluid inlet. However, these seem to produce an undesirable irregularity in the operating characteristic near to the high impedance operating position (Refs. 14,16) and some development is required to eliminate it.

The turndown ratio T, may be increased for a given device by reducing the AT/A_e ratio, but at the expense of increased control pressure ratio G, Fig.6. In fact there is usually little point in increasing G beyond 3 as there is little further increase in T. For $G > 2$ a substantial increase in noise and hysteresis of the operating characteristics usually occurs.

Despite the success of this glove box arrangement, several design points need to be very carefully considered to extrapolate these results as follows:-

(1) The signal to switch the VA from high to low impedance is provided by the change in control flow. In the high impedance state about 6 - 8 SCFM of air is being sucked into the tangential control inlets as opposed to about 1 - 2 SCFM for the mechanical valve system. When one is considering many glove boxes connected to a common ducting system care must be taken to ensure that the system is adequate to cope with this increased continuous air throughput. When the purge duct is at a greater level of suction the value of G must be less. For example, if the purge duct is at a pressure of - 12 iwg:

$$e_c = 12, \quad e_s = 10.5 \quad \text{so} \quad G = 1.14$$

VAs with very wide control ports have been designed to have these low values of G. This is achieved merely by substantially increasing the area of the tangential inlets. However, the flow being sucked into the tangential control inlets was approximately increased by 60% (and T reduced by about 60%), thus increasing the continuous load on the pump considerably.

(2) Operators of the glove boxes with VAs installed complained that they could not adjust the pressure level in the glove box as they could with the original mechanical system. Adjustment of the pressure level inside the glove box is sometimes necessary to facilitate removal of large objects such as contaminated filters or vessels. The first solution is to connect the four tangential control inlets of the VA in two opposite pairs, each pair of tangential inlets being of different cross-sectional area. Only one pair of inlets needs to be used for normal operation, the other pair being blocked off. When it is desired to adjust the pressure level in the glove box the other pair of tangential inlets can be exposed to atmosphere, and it must be emphasized the

important switching function of the VA is still retained.

Alternatively VA's with adjustable area tangential inlets can be constructed so as to alter G through the range of approximately $1.1 \rightarrow 3$. A simple way of achieving this is to use circular tangential inlets and a conical centre body which is adjustable axially in the inlet.

Vortex Amplifiers and Power Fluidics

The widespread use of vortex amplifiers in substituting for mechanical control valves has been hampered by several aspects of performance and configuration. Of the problems which arise, probably the need to provide a tangential control flow at a pressure greater than that of the main flow is the most daunting to the engineer. However, under certain circumstances this need can be met and in many fluid circuits there is an easily available source of high pressure fluid. This is particularly true when fluid circuits are operated, if only in part, under suction conditions. The control source may then be taken from the high pressure side of a pump, as shown in Fig.16, or simply from the ambient atmosphere.

It is often argued that inserting a vortex amplifier into a given circuit often merely moves the mechanical valve. Whilst this is sometimes true, valves in control lines are always much smaller than the main valve and hence

(a) Are much cheaper to replace.
(b) Overall reliability of the system can be increased by duplication of these small control lines.
(c) Often the control fluid may be less toxic and more innocuous than the main flow, thus making the task of control valve replacement much easier.

General Characteristics of the Glove-Box Circuit

The glove box circuit has interesting general characteristics which can be deduced by considering the circuit redrawn as in Fig.7. These variables may be defined:

e_r pressure across resistance (previously the glove box)

e_c pressure across the circuit

The circuit acts as a differential pressure amplifier; a small change in e_r causes a large change in e_c. The <u>important feature</u> of the circuit is that this amplification prevails over a usefully large range. This can be quantitatively and concisely described in terms of the end-points of its operating range using the parameters G and T as shown schematically in Fig.7. Averaged over the normal-to-vortex-state range, the differential pressure gain is $(G-T^{-2})/(G-1)$ and a measure of the range is GT^2.

Application as an Electromagnetic Brake Amplifier

The circuit is ideally suited for amplifying the effect of an electromagnetic brake. These are used in liquid-metal flow control circuits as no-moving-part valves. The size and cost of the E.M. brake depends largely on the fluid power that it must dissipate so, by using the EM brake to create the pressure e_r a significant gain can be achieved.

The expressions for gain and range show that with available VAs a range of circuits could be constructed. For example virtually infinite gain can be achieved by using VAs with an effective G value of unity, such as used by Brombach Ref.17; the operation of the circuit then corresponds to that of a Coanda-switched-vortex device ((CSV) originated by Adams and Moore, Ref.18) and the range factor would be about 25 for designs given in Ref.19. For the glove box amplifier, the gain is 3.3 and the range 290. Finally, for a VA described by Saunders Ref.13, the gain would be about 2 with a range of 800.

Staged Circuits

The foregoing discussion shows that gain and range are constrained but this constraint can be modified, and in some cases relaxed, by using multistage circuits. A two-stage circuit is shown in Fig.8. and is formed by replacing the variable resistance by a circuit identical to the original circuit. Its operation can be described approximately in terms of the two limiting states of stage 1.

(1) In the vortex state

$$\frac{e_{c1}}{e_{r1}} = \frac{G_1}{G_1 - 1}$$

now, suppose the flow emerging from stage 1 is small in comparison with the normal-state supply flow to stage 2 so that stage 2 is effectively in the vortex state also. The overall pressure ratio is

$$\frac{e_{c2}}{e_{r1}} = \left(\frac{G_2}{G_2 - 1}\right)\left(\frac{G_1}{G_1 - 1}\right)$$

(2) With stage 1 in the normal state the resistance of stage 1 is not zero and it acts as a parasitic resistance in the worst possible position for VA_2 which is supposed to operate in the normal state also.

As a result, VA_2 is subject to the conflicting requirements of small relative parasitic resistance and small relative outflow from VA_1 in the vortex state. Therefore, the multistage circuit is subject to constraints but within these there is a wider range of gains and range-factors than for single stage circuits.

Biasing with Active 3-terminal Elements

The initial normal-state parasitic pressure drop can be eliminated by replacing the tee-joint by a jet-pump with unit area-ratio as shown in Fig.7. The initial resistance of the EM brake, or any other element, can therefore be cancelled out by the active property of the jet-pump. The pressure drop is not removed from the circuit but it is no longer amplified by the VA.

It can be seen that n-stage VA-jet-pump circuits provide a wide scope for meeting various gain and range requirements.

In the consideration of these circuits it is interesting to note that in the CSV, the bistable amplifier can be regarded as a switchable jet-pump and according to its state the CSV has a high or low resistance.

Filter Compensator Circuits

A typical problem in some dust filtration systems results from the gradual blocking of the filter and the consequent changing source pressure experienced by equipment connected to the system. Without adding power to the circuit, the increased pressure drop cannot be diminished but simple fluidic circuits can add resistance when the filter is unblocked so that the system always provides a constant source pressure regardless of the filter state. Logically, resistance can only be added over a certain range to act as compensation; it would be useless to attempt to add resistance to cope with an end point at which the filter was completely blocked.

The Turn-Up Vortex Amplifier (Tu VA)

In the context of this circuit it becomes apparent that a special form of VA called here a "Tu VA" has unique properties. In the Tu VA shown in Fig.9, the addition of control flow diminishes the strength of a vortex which the supply flow creates and so the resistance of the device is reduced.

This basic type of device was identified early-on in fluidics and certain workers have investigated various applications. For example, Bell, Ref.20,and Sarpkaya et al, Ref. 21, as a negative resistance oscillator: more recently, Boucher et al, Ref.22, have drawn attention to a specially interesting parallel connection of two Tu VAs.

Many of the devices considered were symmetrical, in that the two ports entering the vortex chamber were equal in size, however, by contemplating the requirements of flow control, these attributes are found to be important:
(Variables are defined in Fig.9.)

When q_c is zero the resistance to q_s caused by the vortex should be large.

When q_c is increased to a small value the vortex should be cancelled out and there should be a very low resistance to through-flow.

Some non-dimensional large-signal parameters can be defined by this table:

State	Q_c	Q_s	E_c	E_s
Vortex	O	1	X	1
Normal	Q	T	G	1

The entries in the table represent values of variables non dimensionalised in terms of q_s and e_s in the vortex state. The capital letters denote parameters that must be measured and G and T have a similar significance to G and T for the VA. However, in the normal state Q the control flow is also to be determined, so only one independent terminal variable is listed for that state. This is insufficient to define the state. In fact, the second necessary independent state-defining criterion is: "No-vortex" in fact, an angular momentum constraint which implies that Q, T and G are inter-dependent. This, however, is a practical definition since the normal state can generally be recognised (thereby obviating the need for an instrument to measure angular momentum).

Obviously, Q and G should be small and T should be large and a range of Tu VAs with various values of these would be useful. For the prototype compensator circuit, the requirements were easily met by a very simple design of Tu VA but this design was guided by factors which are important to all such devices:

The dimensions of the tangential supply port and the outlet of the vortex chamber were consistent with the requirement that, in the vortex state, the major pressure drop must be only due to the vortex. This is similar to the requirement of vortex chambers for vortex diodes and CSVs and is consistent with VAs with very small values of G.

Also, it is important to have smooth characteristic curves without inessential hysteresis.

The prototype used a single control port and a single conical diffusing outlet. Its characteristics are shown in Fig.9. non-dimensionally in terms of independent flow variables defined as follows with the vortex-state ($q_c = 0$) values of q_s and e_s as denominators:

$$E_s = \frac{e_s}{e_{sv}} \qquad E_c = \frac{e_c}{e_{sv}} \qquad Q_c = \frac{q_c}{q_{sv}}$$

In the characteristics, q_s was held constant (i.e. = q_{sv}). The characteristics are very distinctive: as q_c increases, first the vortex diminishes and e_s and e_c decrease to a minimum, which is clearly apparent both in the characteristics and during tests; this is the normal state. Further increase in q_c creates a vortex in the opposite sense and the pressures increase again. In badly designed Tu VAs the characteristics are multivated in pressures and flows and the state of the device jumps unpredictably from one state to another. The characteristics shown in Fig.9. are not like that.

The values of the parameters of this device are

X = .97 Q = .76 T = 3.42 G = 5.2

Application of the Tu VA

The basic circuit is shown in Fig.10; it includes a variable resistance r which represents the filter, a jet-pump, and an adjustable control resistance e.g. a needle-valve n. Under correct design conditions, the jet-pump, filter and Tu VA are matched in size so that,

(1) When the filter is unblocked, the Tu VA operates in the vortex state so that it generates the highest resistance.

(2) When the filter becomes progressively blocked a point is reached where the Tu VA is in the normal state and imposes least resistance.

(3) Between states 1 and 2, the circuit resistance must be constant.

The effectiveness of the circuit can be characterized by a plot of the circuit pressure drop e_y against filter pressure drop e_f for a constant through-flow q_o as shown in Fig. 11. Three curves are shown corresponding to different settings of the needle-valve. For one particular setting (curve 3), the compensation is virtually perfect.

Two criteria of merit for this type of circuit may be defined in terms of the end-points of the nominally horizontal part of the characteristics. First, defining e_{f_1} = initial filter pressure drop, e_{f_2} = final maximum pressure drop and e_y = circuit constant pressure drop, the criteria are:

(1) $(e_y - e_{f_1})/e_{f_2}$: a measure of the pressure loss incurred by the circuit, equal to 1.08 for the test circuit.

(2) e_{f_2}/e_{f_1} the range factor. (equal to 12).

This performance met the initial feasibility requirements.

In practice, the needle-valve in the control by-pass would be a filter and there are many refinements that can be made to the circuit. The Tu VA could be greatly improved so that the control flow becomes much smaller. Also in certain applications, where the filter system is supplied by suction, the control source can be the atmosphere, resulting in the simplest compensator circuit as shown in Fig. 10.

It is now obvious that the compensators and the glove-box circuits have an interesting relationship. In the glove-box circuits the circuit amplifies the pressure changes across one of its branches whereas the compensator circuit applies amplification in the reverse sense which, under correctly matched conditions, can exactly compensate for the changing resistance of the controlling branch element.

These two contrasting characteristics are shown in Fig. 12.

Multistage Circuits

When multistage compensator circuits are considered, it is found that no satisfactory circuit can be made using ordinary VAs. Always there is a need to use a device which, in effect, has the negative driving point impedance characteristic of the Tu VA. It is, however, useful to consider the use of VAs since their controlling ability is very great and some multistage circuits using VAs, Tu VAs and jet-pumps are shown in Fig. 10; in some cases extra filters would be needed.

Parallel Source Circuits

Some general problems arise when pressure or flow scurces (pumps reservoirs etc.) are connected in parallel. A typical problem concerns the emptying of waste liquor from various reservoirs out through a single vaste pipe to single dump reservoir. The system is shown in Fig. 13 with three supply reservoirs and three pumps. In operation, reservoirs are occasionally emptied and it is desirable that no fluid from one reservoir should accidentally be transferred to another.

Flow Junction Circuits

A simple way of obviating this possibility is by using two flow junctions (FJs) which are specially designed Y joints described in Ref. 6. The FJ is specially designed to operate so that when flow enters one of the upstream ports a and it all emerges from the central outlet O, the ratio of pressures e_o/e_a (Fig. 13) is as large as possible. This factor is called efficiency E and the best value proven so far is .67.

Consider the circuit with pump A only operating and FJ_1 correctly designed so that no flow leaks out of port b to the other pumps or reservoirs. Consider that the reservoirs are all at the same levels. The pressure drop e_a and e_o associated with the FJ are equal to the pump delivery pressure and the pipe line pressure drop respectively so it is easy to see that the use of FJ_1 demands that the pump output pressure is $\frac{1}{E}$ times greater than the pressure drop created by the liquor flow through the waste pipe. Hence the FJ has cost a certain quantifiable pressure loss.

By similar arguments the excess pressure factors incurred by the liquor flows coming (always one at a time) from reservoirs B or C are $(\frac{1}{E})^2$ since the liquor must pass through two FJs.

Here there is a choice if power losses are important. The above allocation of reservoirs to FJ_1 and FJ_2 is best if most flow is abstracted from reservoir A since this only has to pass through one JF. Otherwise the reservoirs should be re-allocated to be consistent with the above criterion.

When more sources are involved, the choice becomes wider, for example, with 4 sources there are two types of circuit as shown in Fig. 14. As the number increases the optimum allocation of sources becomes an easily formulated combinatorial problem. In the simplest case, when all sources have equal value, and using a parameter n to describe the degree of complexity of the circuit, the number of sources is given by 2^n, the excess pressure factor by E^{-n} and the number of FJs by 2^n-1. So, generally speaking, the larger the number of sources the larger are the pressure losses, but leakage can always be designed to be zero.

No Leakage Design

The FJ must be correctly sized in relation to the rest of the system in order that "no-leakage" operation should ensue. In terms of the waste pipe and FJ_1 this procedure can be described by

$$a = \frac{Aw^2}{\sqrt{E\ C_p}}$$

where a represents the effective resistance of the pipe in terms of the cross-sectional area of a flow nozzle with unit discharge coefficient whose resistance is equivalent to the pipe. Aw^2 is a characteristic cross sectional area in the FJ and C_p is its characteristic Euler number.

If the pipe is rough, and these factors are determined under conditions similar to those prevailing in the real system (similar Reynolds numbers) then the above formula will give the correct size of FJ to ensure no-leakage operation

for a range of flow rates (e.g. a 2:1 range). To be on the safe side, the FJ could be made slightly smaller and, in the system shown in Fig. 13 a slight negative pressure would occur at the other pumps. Liquid would then be drawn up the pump inlet pipes to a height at which an equilibrium was reached, the small hydrostatic head adjusting exactly to the no-leakage pressure state in the FJ.

Duality of Flow Junction and Bistable Amplifiers

The FJ and the Bistable Amplifier (BA) have an interesting dual relationship, as described in Ref. 6. The BA can divert flow along different paths without leakage and the FJ can accept flow from different paths and direct it along a single path. For example, "trees" of three BAs could be connected to correspond with the FJ circuits shown in Fig. 14. These would be able to direct flow along any one of four paths.

A simple circuit in Fig. 15, enables flow to be directed along one of two pipes so that a low pressure could exist in the pipe with no flow while the pressure downstream is relatively high. Thus one pipe could be brought to atmospheric pressure for maintenance or modification while the circuit and circuit flow were maintained.

The pressure loss incurred by the circuit, expressed by the ratio: circuit pressure loss/gauge-pressure of downstream terminal, would be about 2.3 with current devices.

Vortex-type Devices in Parallel-Source Circuits

The properties of FJs can be synthesised in varying degrees by a range of circuits consisting of diodes, VAs, Reverse Flow VAs (i.e. RFVAs described in Refs. 15, 16, 19) and Tu VAs. One circuit which involves some important factors uses two VAs upstream of a single pump to select flow from reservoir A or B as shown in Fig. 16. Control flow for the VAs is piped from downstream of the pump; to select flow from reservoir A, as shown in Fig. 16, control flow is admitted to VA(B) thus cutting off flow from reservoir B. The two VAs operate in the normal and vortex states and so it is easy to write the circuit efficiency under no-leakage conditions:

$$\eta = \frac{G-1}{G} \quad \frac{T}{T+1}$$

where η = power supplied to waste pipe/pump power.

This expression shows an unfamiliar relationship between η and G and T; for example G should be <u>increased</u> to increase η. There are various other implications, but they all result from the basic fact that the simple selection of flows from the reservoirs is an easily-met demand for a circuit <u>upstream</u> of the pump. The waste pipe pressure loss is not imposed on

the VAs.

As a result, the circuit is potentially very efficient, but numerous other factors determine its utility in practice. Examples are: sensitivity to changes in the waste-pipe resistance, parasitic pressure loss upstream of the pump, cavitation, and the desirability of the control mode (using valves in the control pipes).

Another type of circuit using two pumps and two RFVAs is shown in Fig. 17. The RFVAs are connected in parallel and constitute a synthetic flow junction since the combined pair of devices has three terminals and it has some properties in common with an FJ. The interconnected control pipes mean that there is always some leakage; this can be obviated by further elaboration of the circuit but, basically, its best operating condition is not the "no-leakage" point.

Parallel pumping protection circuits

The parallel RFVA circuit just described may be useful in another distinct role associated with parallel sources. If two (or more) pumps operate simultaneously in parallel supplying a single load such as the waste pipe or a pressure vessel, it may be important to provide protection against catastrophic pressure loss if one pump fails. Various fluidic circuits may be considered and they all have a common feature. The degree of protection against reverse flow leakage out of the failed pump can be increased by increasing the normal operating pressure loss. Some circuits will offer different relative rates of increase of these two effects and in general a specific degree of protection may be optimally matched by a specific circuit.

Obviously the simplest circuit consists of the FJ and this could meet a "no-reverse leakage" demand when one source failed in a two-source circuit supplying a single waste pipe. Quantitatively this would mean, with current designs of FJ, and assuming:

1) two constant pressure sources (idealized "pumps")

2) waste pipe with square-law resistance

3) no reverse leakage into source which fails.

Then with both sources operating: each supplies one unit of flow into the waste pipe and the circuit efficiency is 81%. When one source fails, the other source supplies 1.78 units of flow and the circuit efficiency is 67%.

The type of operation just described depends on the large-signal parameters of the FJ and, for this catastrophically-imposed wide range of flow states, the FJ has desirable characteristics. It is interesting, however, to note that

the FJ also has useful differential properties at the equal-flow operating point. These can be stated as follows:

Suppose two nominally-equal flows are supplied to the FJ, if one flow increases by a small amount it experiences an increase of pressure of one unit; simultaneously the other source is subject to a decrease of pressure of .35 units. Hence the FJ tends to equalize the flows supplied to it both in a differential manner and when there are very great differences in the flow rates.

Many other circuits can be devised which have these properties and they may have useful applications in combining flows from pumps prone to surging.

Pumping Circuits

Fluidic pumping circuits enable pumping energy to be transmitted from a "clean" easily pumped fluid to a "difficult" toxic or abrasive fluid. Where there are no "practical" constraints on circuit design the mechanical efficiency of the fluidic system is a direct measure of its merit; however, when the design is constrained by such factors as: uncertainty of driving pressures or load resistances, or priming facilities, many more factors are involved and so a range of circuits can be considered. The important factors can be understood by considering first a "two-diode pump" as shown in Fig. 18.

The 2-Diode Pump

The pump transfers liquid from reservoir 1 to a higher reservoir (2). Alternating high and low air pressure is applied to the liquid in a "gas-piston" and the consequent alternating liquid flow at port a is rectified by the two diodes so that liquid is delivered intermittently to reservoir 2. A simple method of generating the alternating air pressure is by the use of a shut-off valve downstream of an air-ejector as shown in Fig.18.

A prototype portable pump of this type has been tested using various toxic and abrasive liquids. The air supply may be drawn from the plant circuit. The shut-off valve is electrically operated by probes inside the gas piston vessel and special u-bends in the piping ensure that the pump is self priming. A fortuitous feature of its operation is that there is an intermittent strongly swirling outflow from the diode in reservoir 1; when pumping a heavy slurry the outflow agitates the slurry and keeps it in suspension.

In general, the output head increases with available air pressure and prototypes have pumped 2½ gallons/minute up 40 feet. By combining two 2-diode pumps operating in antiphase the

delivery flow is no longer intermittent. Such a circuit would in fact be a 4-diode full-wave bridge rectifier, and the necessary air switching circuit would constitute an "alternator" or inverter circuit. These two combined circuits have been studied intensively in connection with regenerative systems Ref.6 and many of the results of this work are relevant to pumping circuits. When quasi-steady, incompressible non-cavitating conditions prevail certain aspects of design can be stated as follows:

For example, the optimum design of a 4-diode bridge requires that all diodes are the same size and tha ratio of driving pressure to load pressure-drop should have a specific value. The same optimality criteria apply, suitable translated, to the "half-bridge", i.e. the 2-diode pump: the two diodes should be equal and the pressures should be the same as if the two diodes were working in the optimal 4-diode bridge with equal "suck" and "delivery" times. Using practical diodes in a 4-diode bridge, more-or-less under these conditions of operation, McGuigan and Boucher Ref.23, measured an efficiency of 30%. Feasible maximum efficiencies of about 40% should be possible with these circuits however, there are much simpler, efficient rectifiers (see Ref.6.).

In the prototype 2-diode pump the foregoing design criteria serve only as a rough fuide since cavitation and low Reynolds number effects occur which detract from performance. But also the delivery pipe can drop the liquid into the upper reservoir so it is not subject to the reservoir pressure for the full suction stroke; this is a beneficial effect.

Other intermittent Pumping Systems

Contemplation of the general regenerative circuits described in Ref.6. shows that there are a large number of steady-flow pumping systems. By "cutting these circuits in half" an equally large number of intermittent pumping systems can be constructed. The optimised designs of symmetrical continuous circuits apply to intermittent ones when the such and delivery times are equal; when they are unequal, the optimum design of an intermittent circuit can be related to that of an unsymmetrical continuous one, these have not been studied in detail but the methods described in Refs.6, enable such optimization to be carried out. Very elaborate but efficient and versatile circuits result from using combinations of RFVAs, temporary capacitive control flow storage and specially designed vents on the RFVAs. A very simple but less efficient circuit consists only of a Rectifier-type-Reverse Flow Diverter (R-RFD) (described in Ref.6.) used as in Fig.18. An intermediate system which is simple and effective uses the Jet-pump-diode

(JPD) which is described next.

The Jet-pump-diode (JPD)

The JPD shown in Fig.19 is the result of merging a jet-pump (designed like an R-RFD, with a slowly converging drive nozzle) with a vortex diode. Used in an intermittent pump it would act as follows.

1. Suction Phase

Fluid is sucked from reservoir 1 into port c and into the cylinder of the gas piston via port a. The diffuser between port a and port c facilitates flow into the cylinder; the gap between the diffuser nozzle and the vortex diode (constituting port c) is made large enough (approximately $3d_1$) to prevent the suction being transmitted to the vortex diode. Simultaneously flow leaks from reservoir 2 through port b and out of port c into reservoir 1. The object of the diode section of the JPD is to minimize this leakage flow by creating a strong vortex as in a conventional vortex diode.

2. Delivery Phase

Fluid is driven out of the cylinder into port a and it flows as a jet from the diffuser nozzle into the diode section and out of port b into reservoir 2. In general, some fluid from reservoir 1 will be entrained by the jet at port c and so more fluid will emerge from port b than enters at port a, however, this entrained additional flow is not a necessary feature of the JPD's operation.

The JPD would work satisfactorily with no entrainment. The amount of entrained flow depends on the relative sizes of the two opposed nozzles at port c; by making the diffuser-nozzle (connected to the cylinder) small, the entrained flow is increased but at the expense of overall efficiency. The optimum design for the JPD is therefore dependent on the relative importante of volume pumped per cycle and overall efficiency.

Characteristics of a JPD

The main characteristics of a simple form of JPD are shown in Fig.20; they are the results of tests using air at low pressure. The variables are denoted in Fig.19 and the subscript f or r indicates delivery (forward:- f) or suction (reverse:- r) operation. In the forward states the driving jet flow q_a was held constant at 260 litres/min. air and the output characteristic e_{bf} against q_{bf} is the most important curve, e_{af} hardly changes.

In the reverse state there is virtually no interaction between the diode sectionand the driving nozzle so the

pressure-flow relationship for each one is sufficient to characterize the reverse-state operation. These pressure drops are e_{pr} and e_{ar}. The details of JPD systems have been described in Ref.24.

Improved designs can be expected but even in its present form the JPD offers an effective and simpler alternative to the 2-Diode Pump.

Fluidic Hydraulic Ram

Not all pumps derive from bridge circuits. Such a pump is the "fluidic hydraulic ram", described by Tippetts in Refs. 25,26,19 and which could be used in extracting an intermittent high-pressure sample from a flow without needing an external power source. The ram depends on the unique two-valued resistance characteristic of the CSV. This is connected downstream of a ram-pipe; when the CSV switches to its high resistance state, the fluid in the ram-pipe is retarded thereby generating a high pressure upstream of the CSV.

The CSV can be switched in many ways; the simplest results from joining the two control ports so that it oscillates continuously in the same way as the oscillating fluidic flowmeter (Ref.27). A regular sequence of pressure pulses is generated with an amplitude much higher (up to 20 times) than the average pressure drop across the system; their frequency is also a measure of flow and it was for flow measuring that the system was originally devised. Used as a pump, the output can be taken in many ways, the simplest being in the form of a free jet from point X in Fig.21.

Some typical signals are shown which were derived from a small demonstration fluidic hydraulic ram operating with water under low supply pressure conditions.

Conclusions

Application trials of power fluidics in the UKAEA and BNFL have shown that the technology is now at a stage where it can make an important contribution to the safe and reliable control of active fluids in nuclear plant. In the process industry there would appear to be even wider scope of application particularly in those cases where: corrosive or abrasive fluids reduce component life, the returns from automatic control are diminshed by poor actuator reliability, or if large, fast-acting and ultra-reliable valves are needed for protecting costly installations.

Design methods have been described that make the maximum possible use of the similarity property of fluid dynamic systems. This yields large-signal performance parameters,

which are unique to fluid systems, and computer implemented "data transformations" which are not the numerical extravaganzas which are usually associated with non-linear analysis but simple, easily accessible, algebraic routines.

In general, we conclude that the hardware and design studies described here show that fluidics can indeed provide the unique advantages that were envisaged 15 years ago.

References

1. Grant,J, and Fisher, M.Brit. Pat. 1,199,938 Fluid Flow arrangements using fluidic switches in cascades.
2. Grant,J and Wright,J. Potential Applications of fluidics in Nuclear Plant, Proc. 2nd. CFC, BHRA, Dec. 1966.
3. Grant, J. and Golder, J.A., Brit. Pat. 1,300,401, Method and Apparatus for pumping.
4. Grant, J. and Strong, R.E.: The Application of Power Fluidics, Proc. Symp. Power Fluidics For Process Control, Inst. Measurement and Control. April, 1973.
5. Tippetts, J.R. and Royle, J.K.: Synchronous Circuits using Bistable Fluid Amplifiers, Proc. 3rd. CFC. BHRA, May, 1968.
6. Tippetts, J.R.: Process Fluid Switching in Regenerative Circuits. Proc. HDL Symp. State of the Art, Washington, Oct. 1974.
7. Shekel, J.: Matrix Representation of Transistor Circuits, Proc. IRE, 40, 1492-1497, November, 1952.
8. Tippetts, J.R.: General Design Methods Applied to Circuits Associated with Regenerative Systems. Proc. 6th. CFC, BHRA, March, 1974.
9. Koerper, P.E.: Design of an Optimized Vortex Amplifier, EDC report 7 - 65 -, Case Inst. Tech. 1965.
10. Syred, N.: Ph.D. Thesis, University of Sheffield, 1969.
11. Syred, N., Royle, J.K. and Tippetts, J.R.: Optimization of High Gain Vortex Amplifiers, Paper J3, Proc. 3rd. Cranfield Fluidics Conference, Brit. Hydromechanics Res. Ass. 1968.
12. Syred, N., Royle, J.K.: Operating Characteristics of High Performance Vortex Amplifiers, Fluidics Quarterly, Vol.4. No.1. pp. 56-73, January, 1972.
13. Saunders, D.H.: The Development of a Vortex Valve for use as a Flow Control Valve. Proc. Symposium on Power Fluidincs for Process Control, Inst. Measurement and Control, April, 1973.

14. Al-Shamma, K.A.A., Vortex Amplifiers for Flow Control, Ph.D. Thesis, University of Sheffield. 1971.

15. Syred, N. and Tippetts, J.R.: The Coupling of a Fluid Amplifier and a Naturally Aspirated Pulsating Combustor. Proc. Symposium on Power Fluidics for Process Control, p.141-148, Inst. Measurement and Control, April, 1973.

16. Syred, N. and Tippetts, J.R.: A High Gain Active Diode - The Reverse Flow Vortex Amplifier, to be published 6th. Cranfield Fluidics Conference, BHRA, March, 1974.

17. Brombach, H.: Vortex Devices in Hydraulic Engineering, Paper B1, Proc. 5th. Cranfield Fluidics Conference, BHRA, 1972.

18. Adams, R.B. and Moore, C.B., Flow Control Apparatus, US. Pat. No. 3267946, Aug. 1966.

19. Tippetts, J.R.: A Survey of Fluidic Flow Control Devices, Proc. Symposium on Power Fluidics for Process Control, Inst. Measurement and Control, April, 1973.

20. Bell, A.C. The Dual Inlet Vortex Valve. Paper presented at a special summer course on fluid power control, M.I.T. Cambridge Mass. July, 1966.

21. Sarpkaya, T., Pavlin, C., and Sompong Phasook.: A Theoretical and Experimental Investigation of a Confined Vortex Oscillator, ASME J. Basic Eng., p.750-754, December, 1969.

22. Boucher, R.F. Asquith, R.W. and Royle, J.K. Vortex Flow Controllers: Design Stability and Applications. Proc. Symposium on Power Fluidics for Process Control, Inst. Measurement and Control, April, 1973.

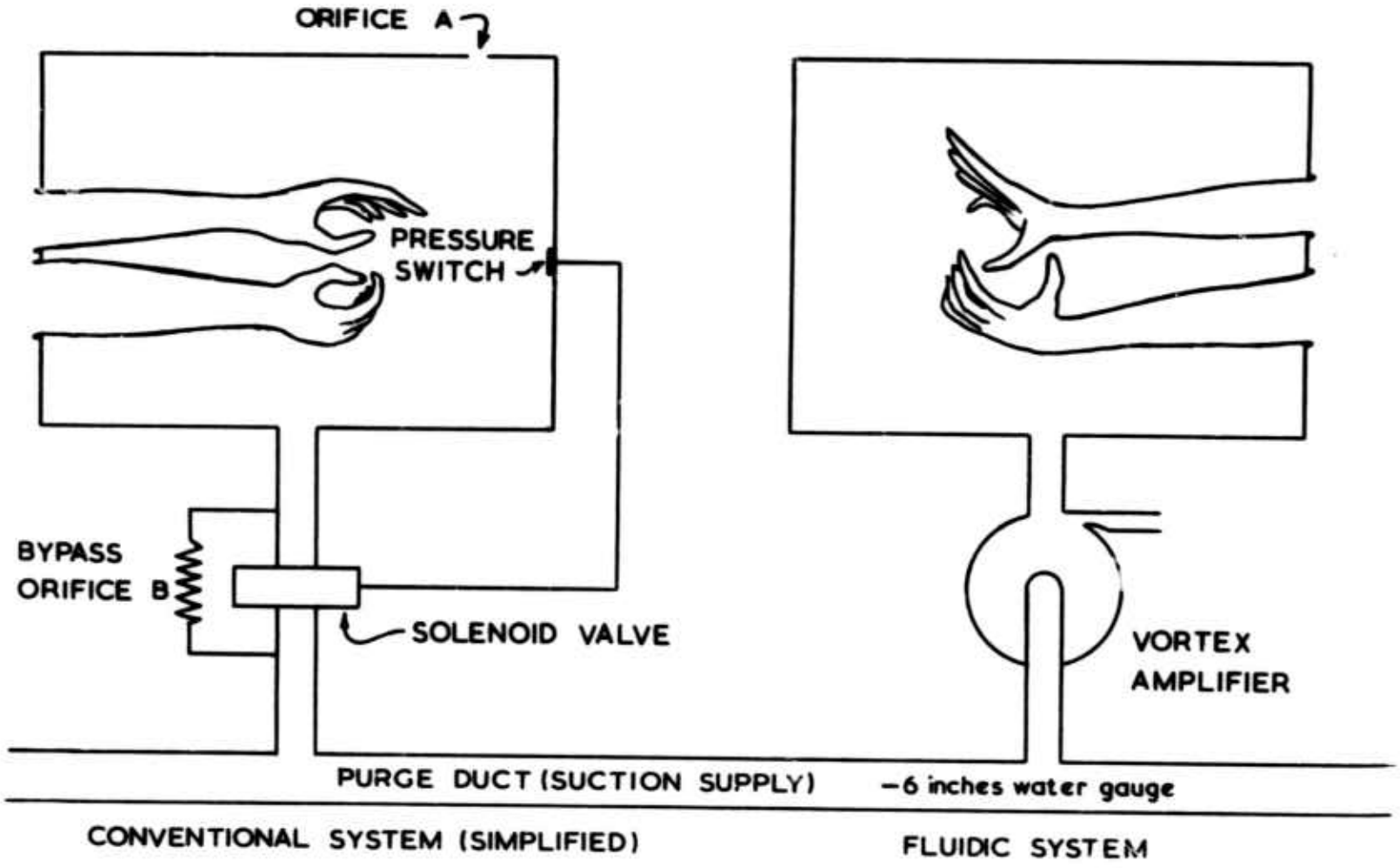
23. McGuigan, J.A.K. and Boucher, R.F.: A Fluidic Rectifier for Pumping, Proc. Symposium on Power Fluidics for Process Control, Inst.Measurement and Control, April,1973.

24. Tippetts, J.R.: The Jet-pump-diode (A no-moving-parts pump) Unpublished report, Department of Chem.Eng. and Fuel Technology, FTCE/72/JRT/73, University of Sheffield, March, 1973.

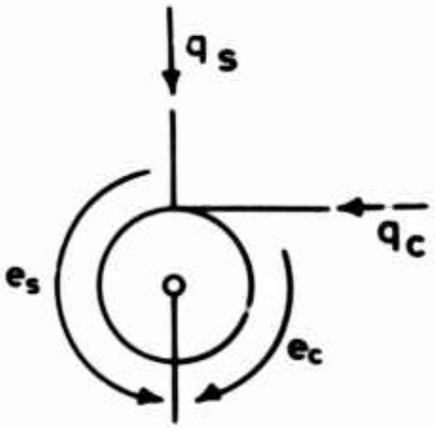
25. Tippetts, J.R.: Unpublished communications to UKAEA Risley, 1971.

26. Tippetts, J.R.: The Fluidic Hydraulic Ram and a Conjectured Pressure Amplifier, to be published in Fluidics Quarterly Ann Arbor.

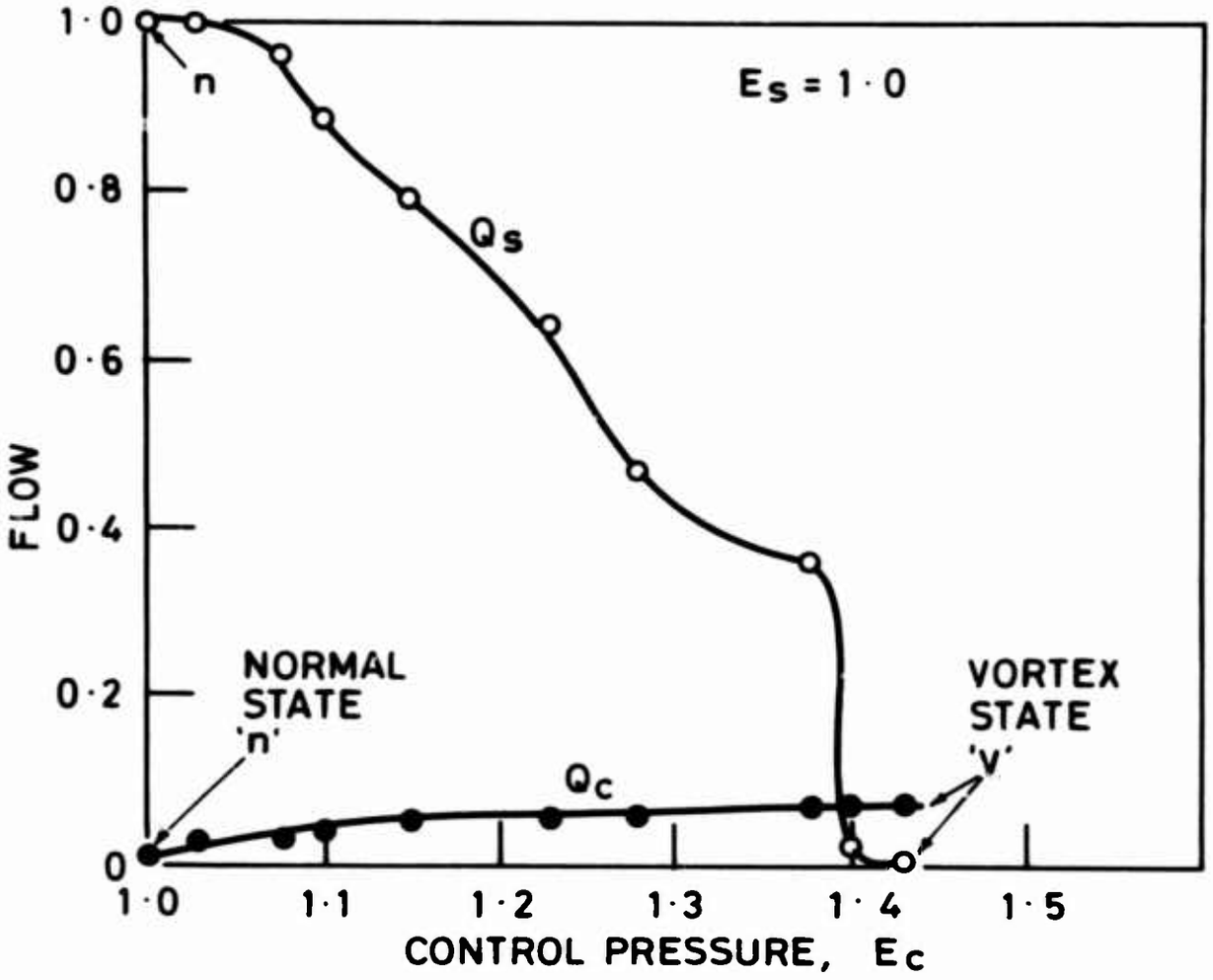
27. Tippetts, J.R., Ng, H.K. and Royle, J.K.: A Fluidic Flowmeter, Automatica, Vol.9, pp. 35-45, Pergamon, Jan. 1973.



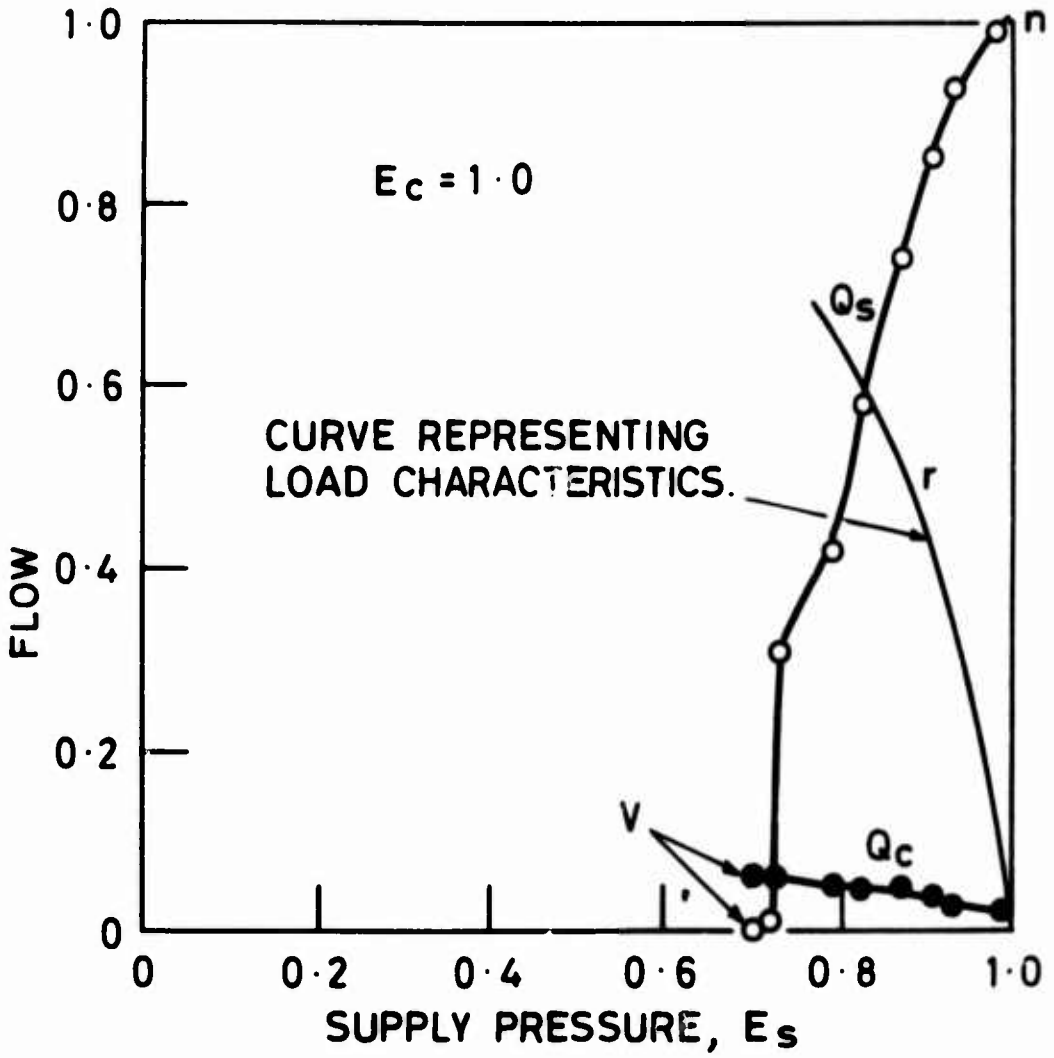
1 GLOVE BOX CONTROL AND PROTECTION



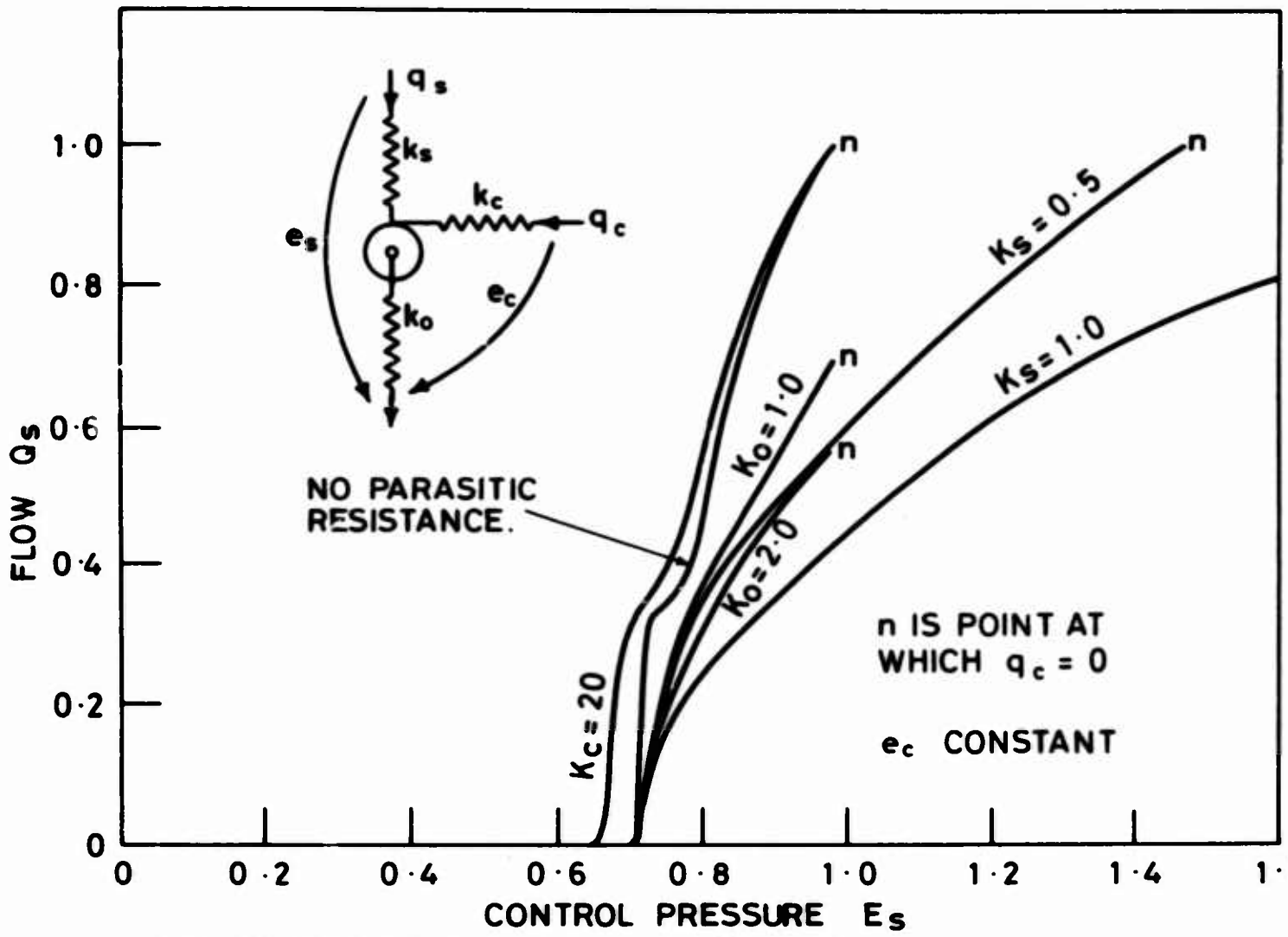
CHARACTERIZING VARIABLES CONSTRAINT:
e_s = CONSTANT



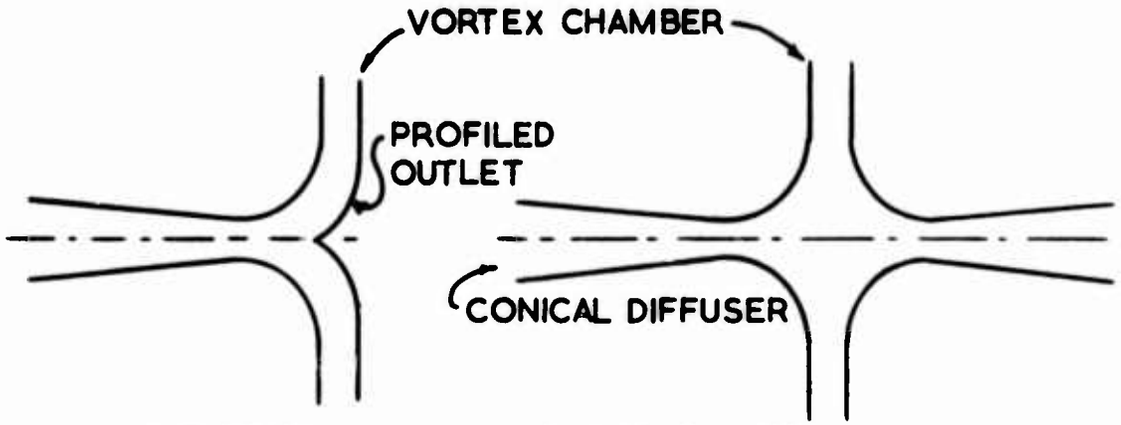
2 NON - DIMENSIONAL CHARACTERISTICS OF VORTEX AMPLIFIER.



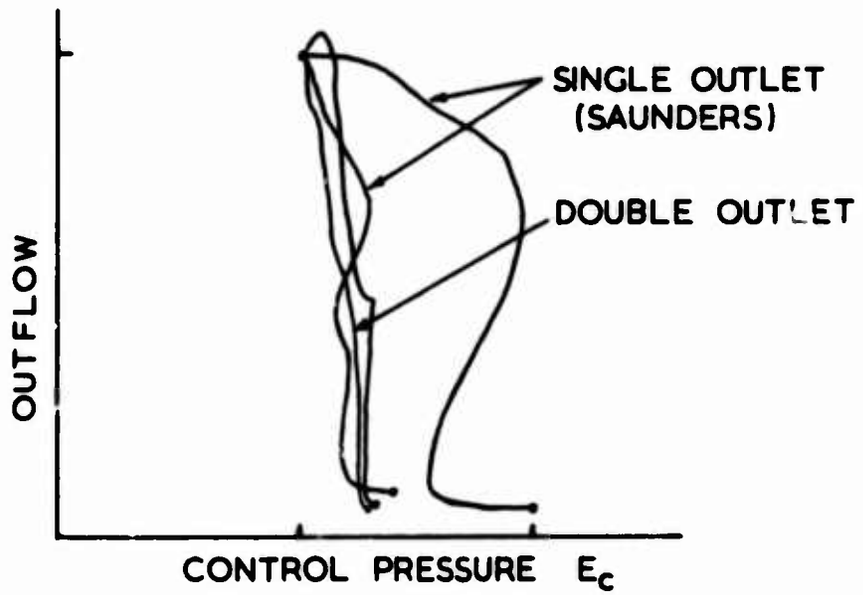
3 RESULT OF DATA TRANSFORMATION CHANGING CONSTRAINT TO e_c = CONSTANT.



4 THE EFFECT OF PARASITIC RESISTANCE.

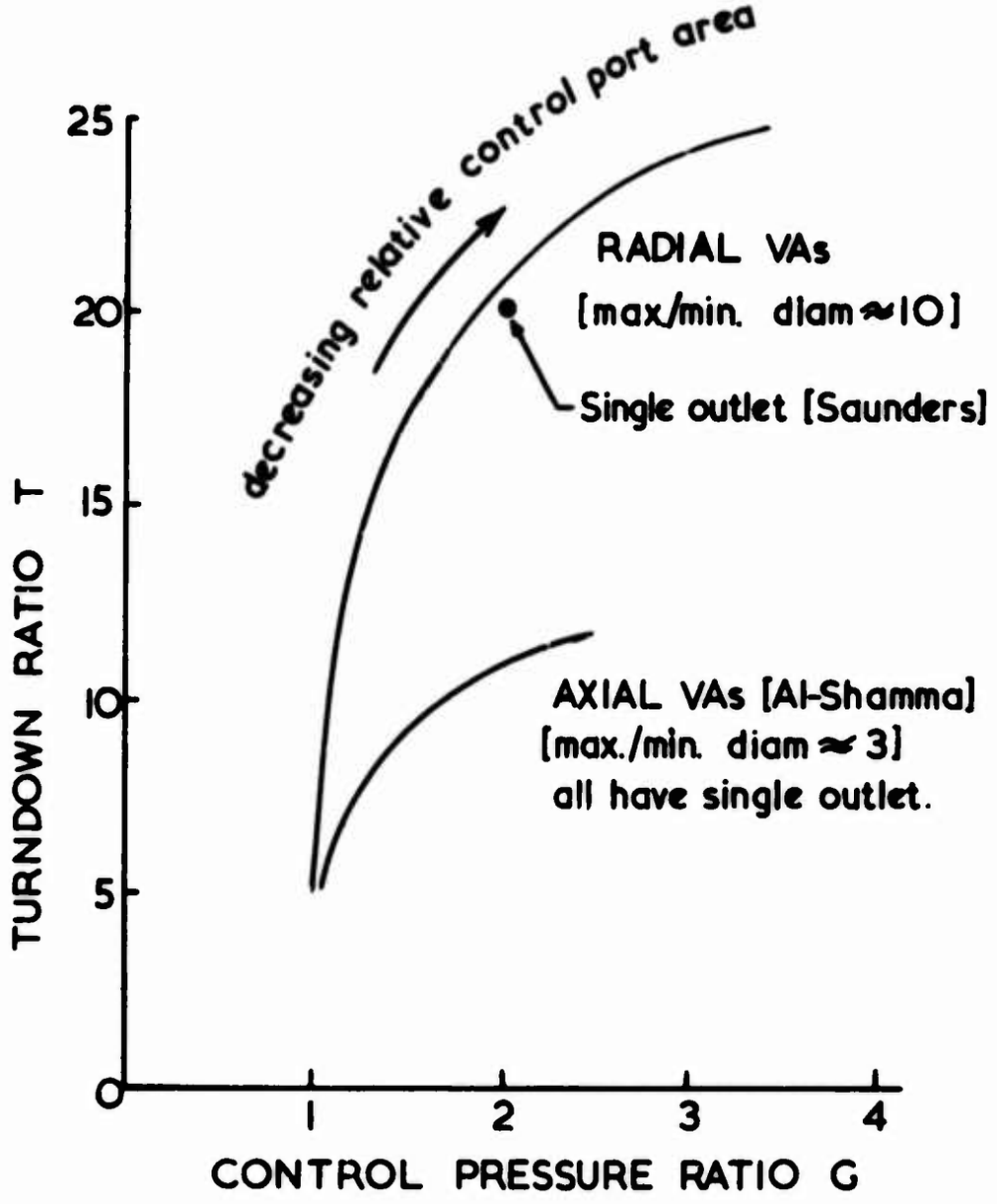


a SINGLE OUTLET b DOUBLE OUTLET

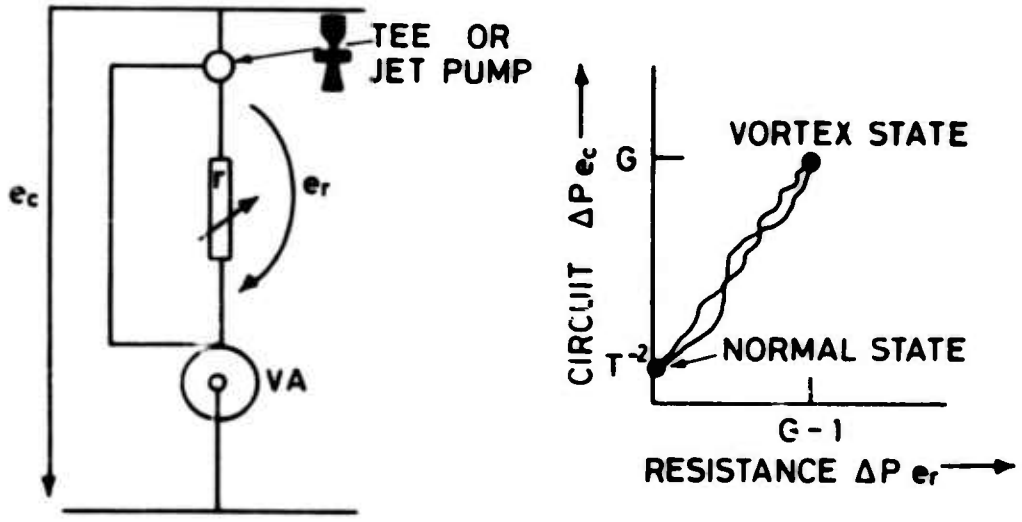


c COMPARATIVE CHARACTERISTICS

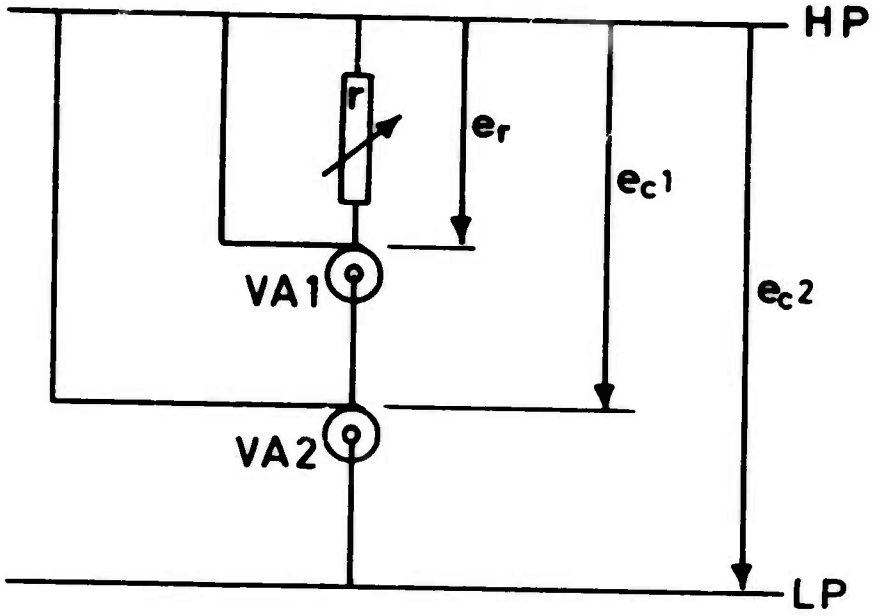
5 **EFFECT OF OUTLET CONFIGURATION ON VA CHARACTERISTICS**



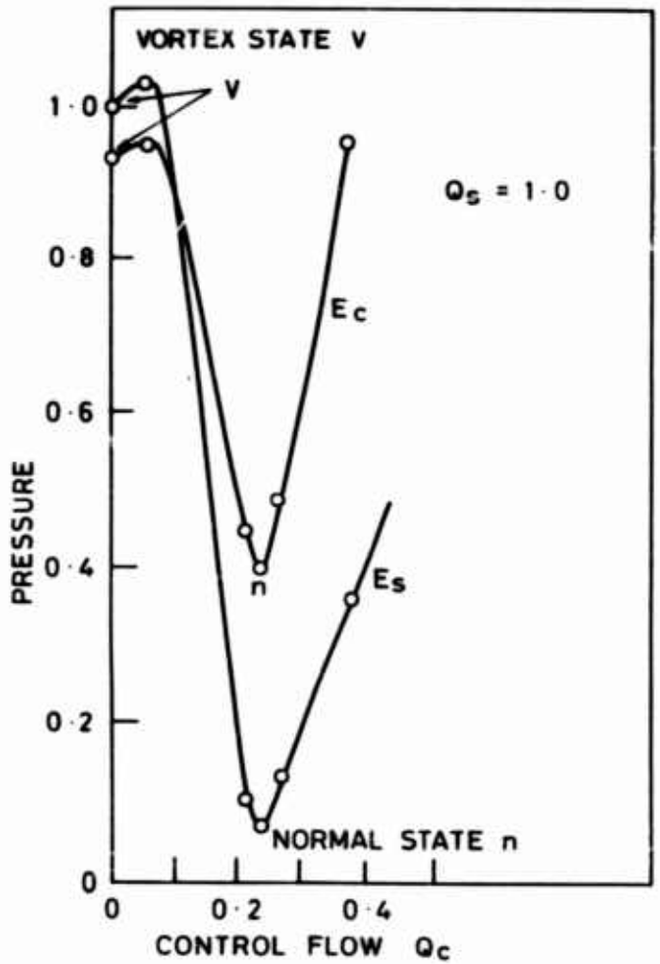
6 AVAILABLE RANGE OF LARGE-SIGNAL PERFORMANCE PARAMETERS FOR VORTEX AMPLIFIERS (SCHEMATIC FOR CURRENT GOOD DESIGNS). MOST SIGNIFICANT DESIGN VARIABLE IS RELATIVE CONTROL PORT AREA.

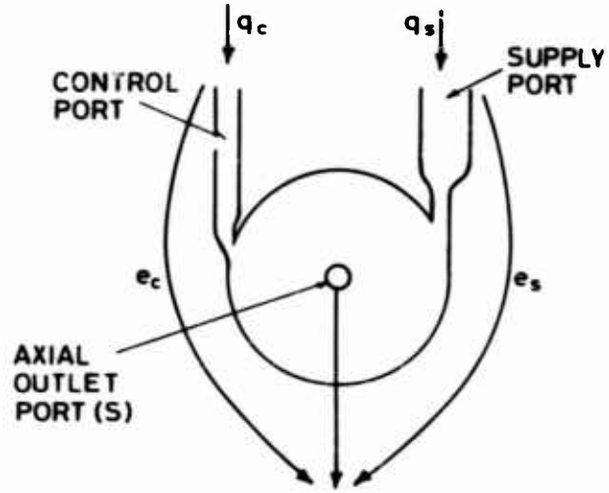


7 DIFFERENTIAL PRESSURE AMPLIFIER.



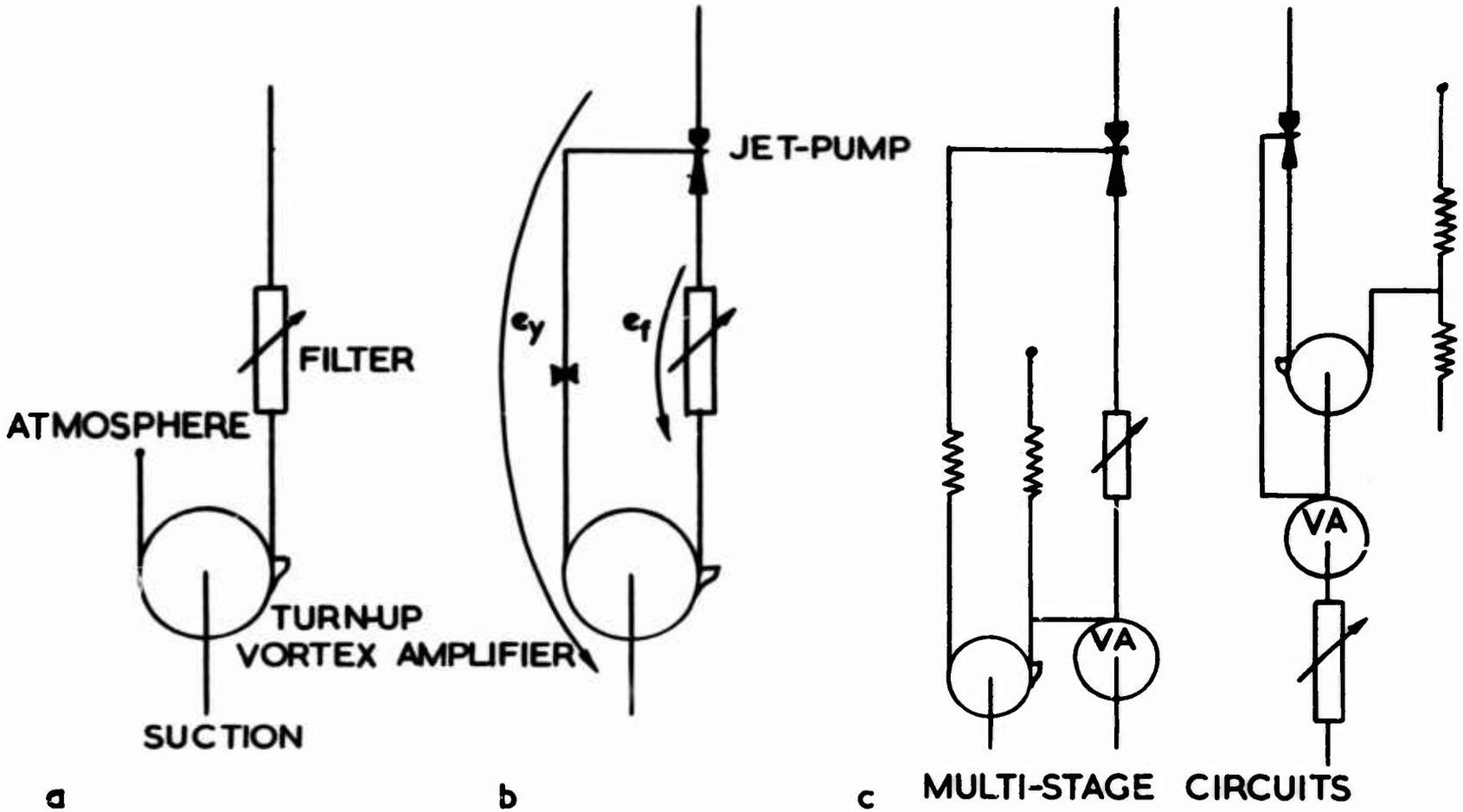
8 2-STAGE DIFFERENTIAL PRESSURE AMPLIFIER.



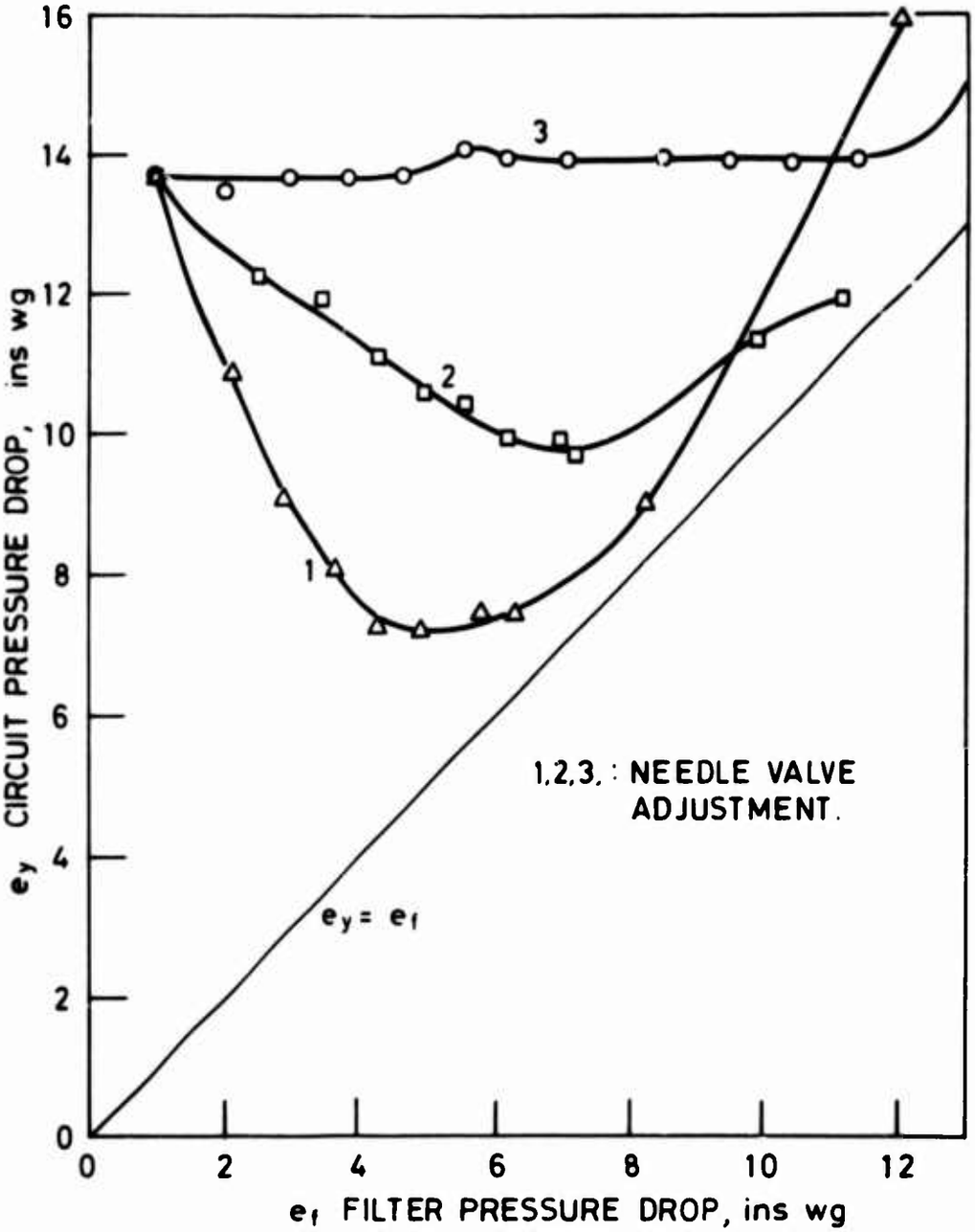


TURN-UP VORTEX AMPLIFIER (TuVA)

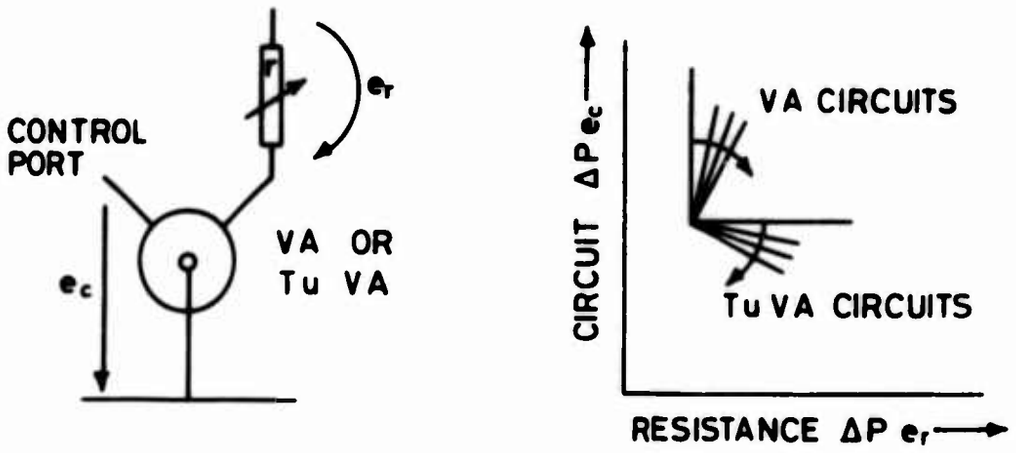
9 NON-DIMENSIONAL CHARACTERISTICS OF A TuVA.



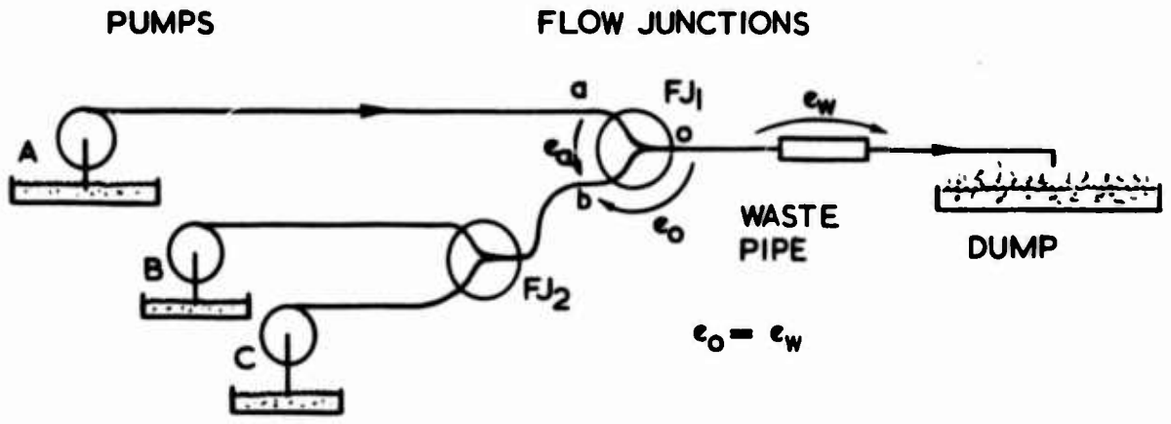
10 FILTER COMPENSATOR CIRCUITS



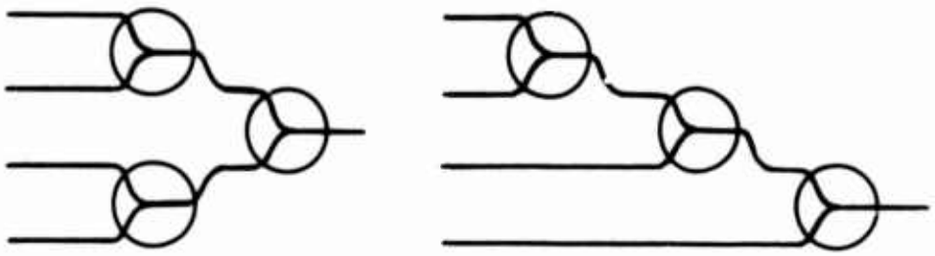
II CHARACTERISTICS OF PROTOTYPE FILTER COMPENSATOR.



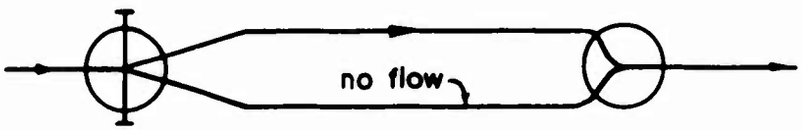
12 COMPLEMENTARY DIFFERENTIAL PRESSURE AMPLIFIERS.



13 WASTE LIQUOR DUMPING CIRCUIT USING FLOW JUNCTIONS

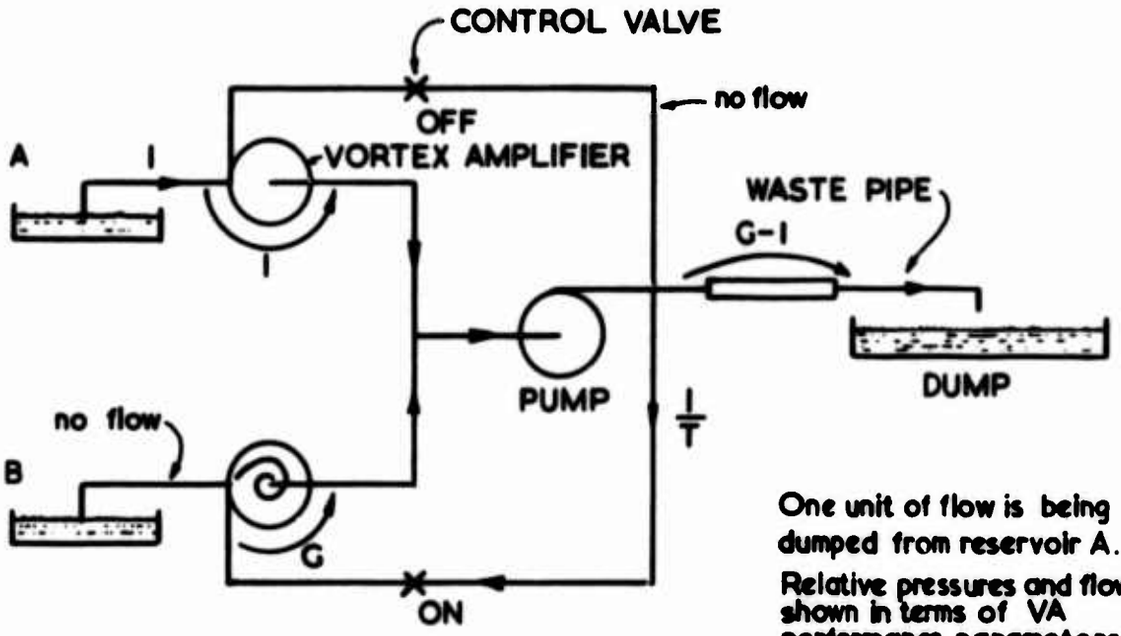


14 4-INPUT FLOW JUNCTION TREES



BISTABLE AMPLIFIER FLOW JUNCTION

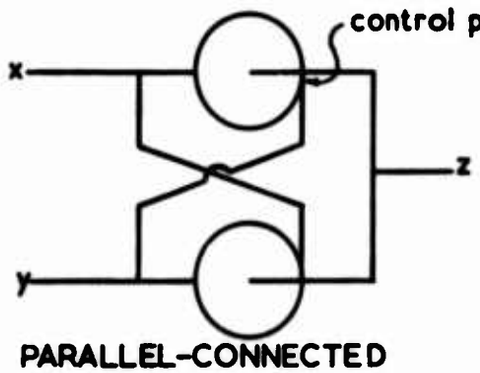
15 INTERCONNECTION OF MATCHED DUAL DEVICES



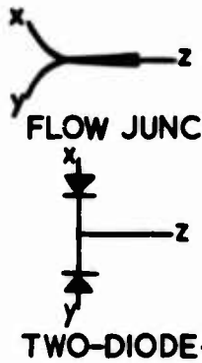
One unit of flow is being dumped from reservoir A.

Relative pressures and flows shown in terms of VA performance parameters G and T.

16 WASTE LIQUOR DUMPING CIRCUIT USING VAs UPSTREAM OF PUMP

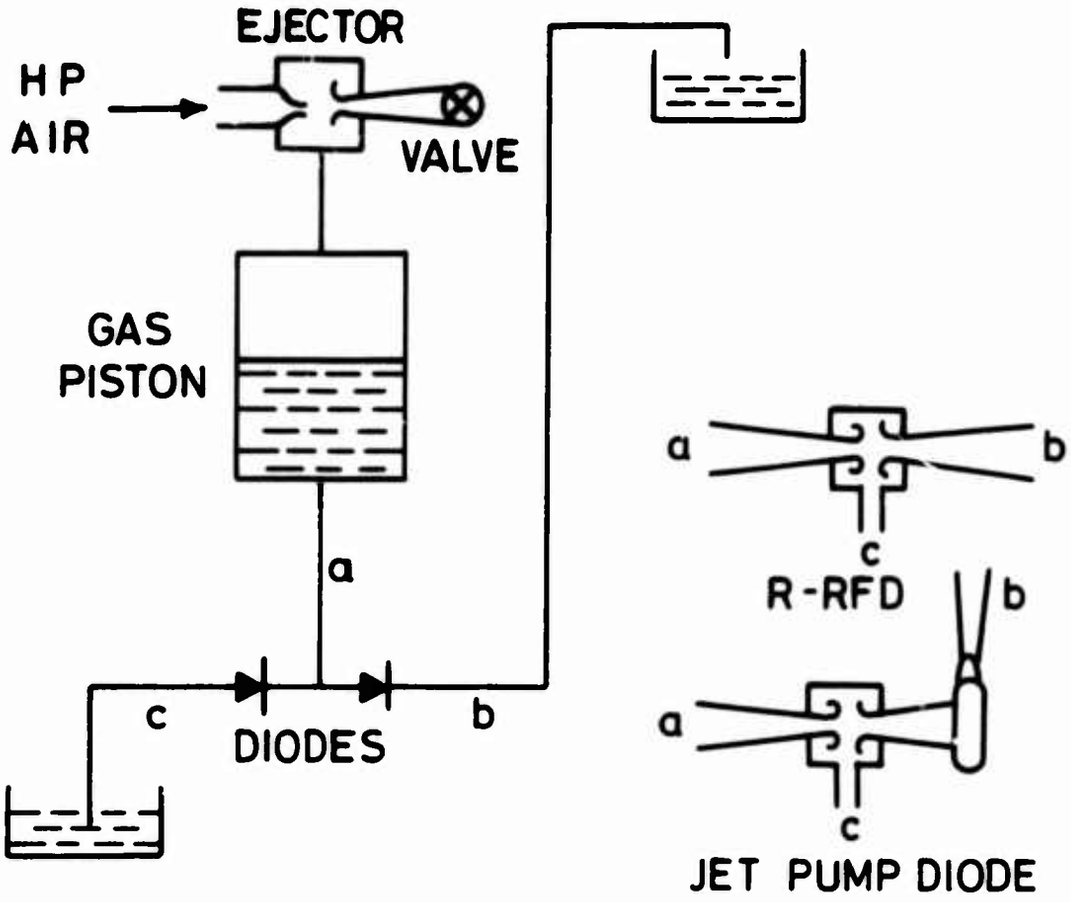


PARALLEL-CONNECTED REVERSE FLOW VORTEX AMPLIFIERS

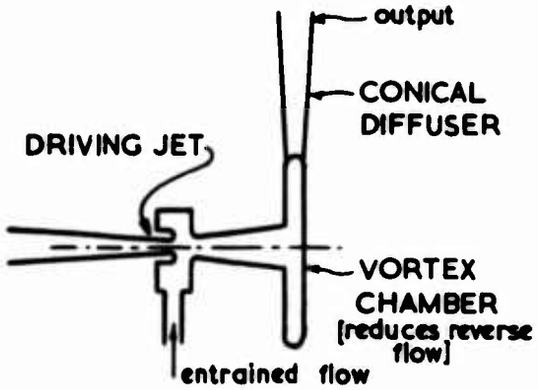


COMPARABLE DEVICES

17 PARALLEL SOURCE CIRCUITS



18 AIR DRIVEN LIQUID PUMP WITH THREE ALTERNATIVE FLUIDIC VALVE UNITS.



19 JET-PUMP-DIODE

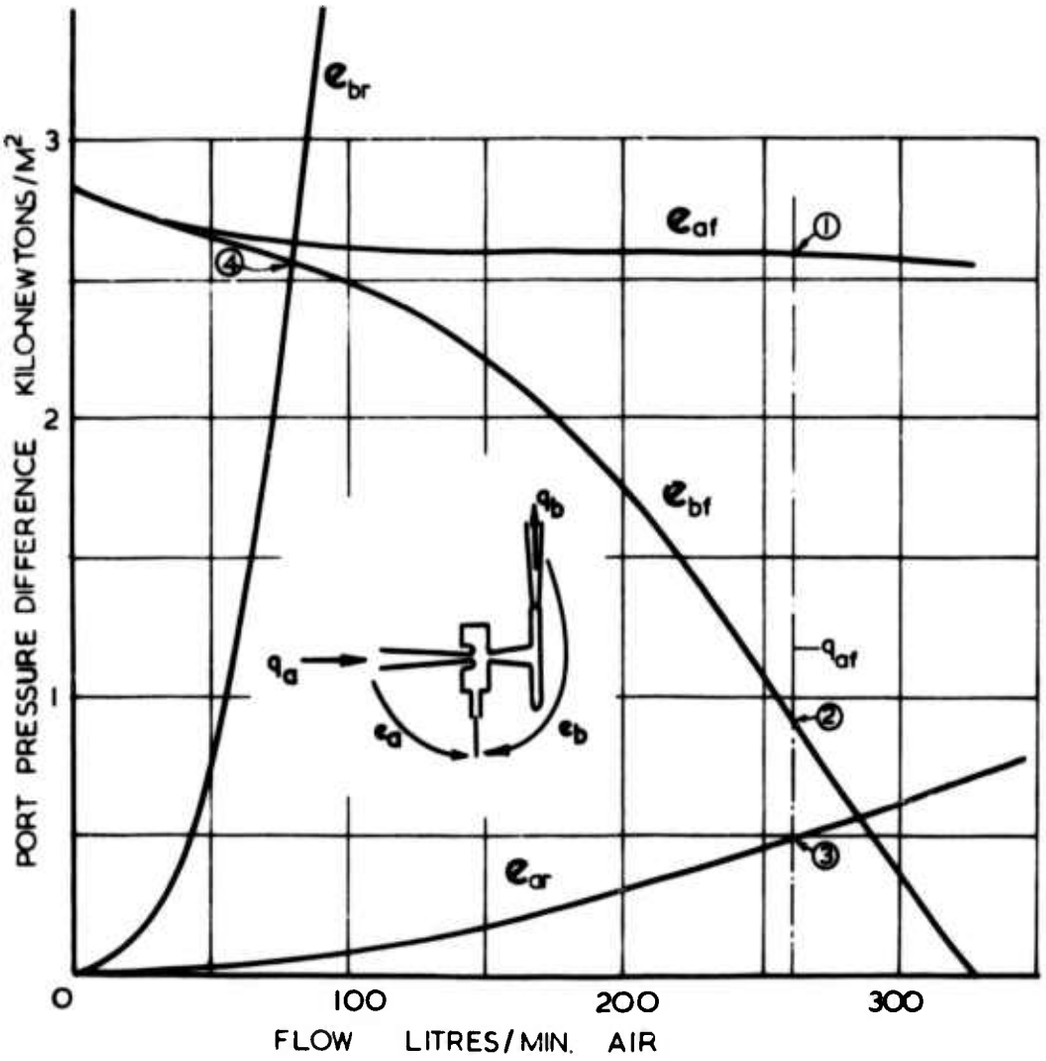
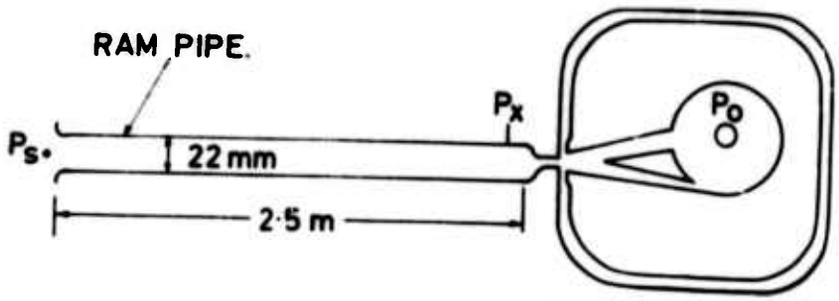
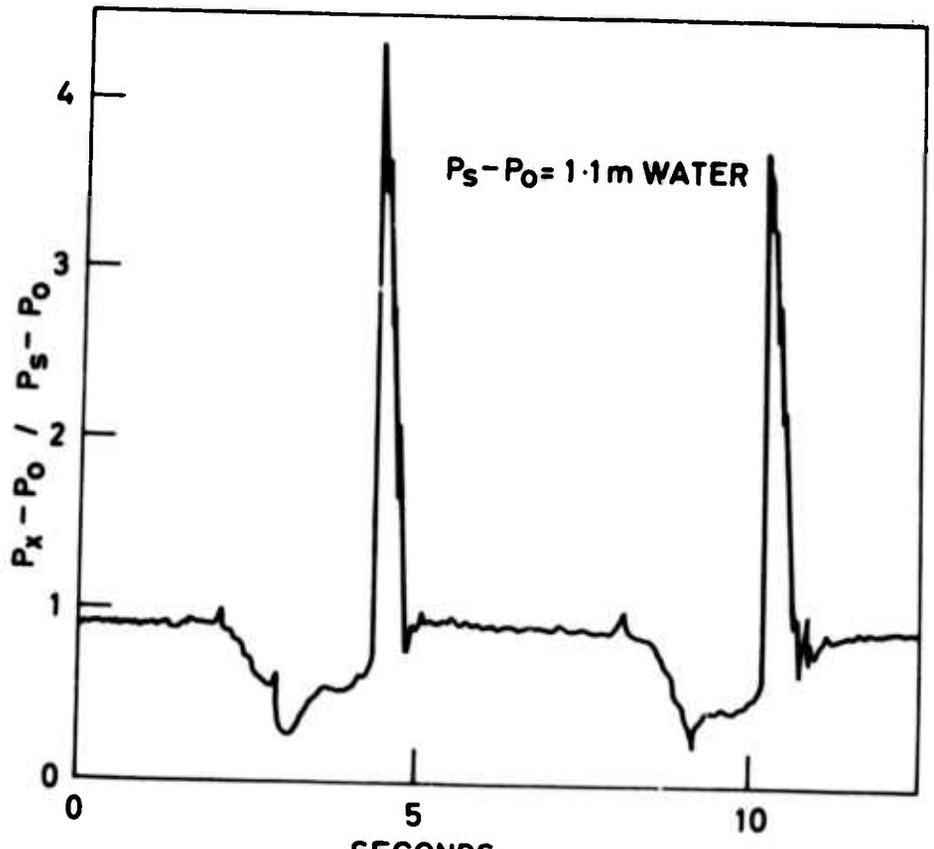


FIG 20 CHARACTERISTICS OF A JET-PUMP-DIODE



FLUIDIC HYDRAULIC RAM.

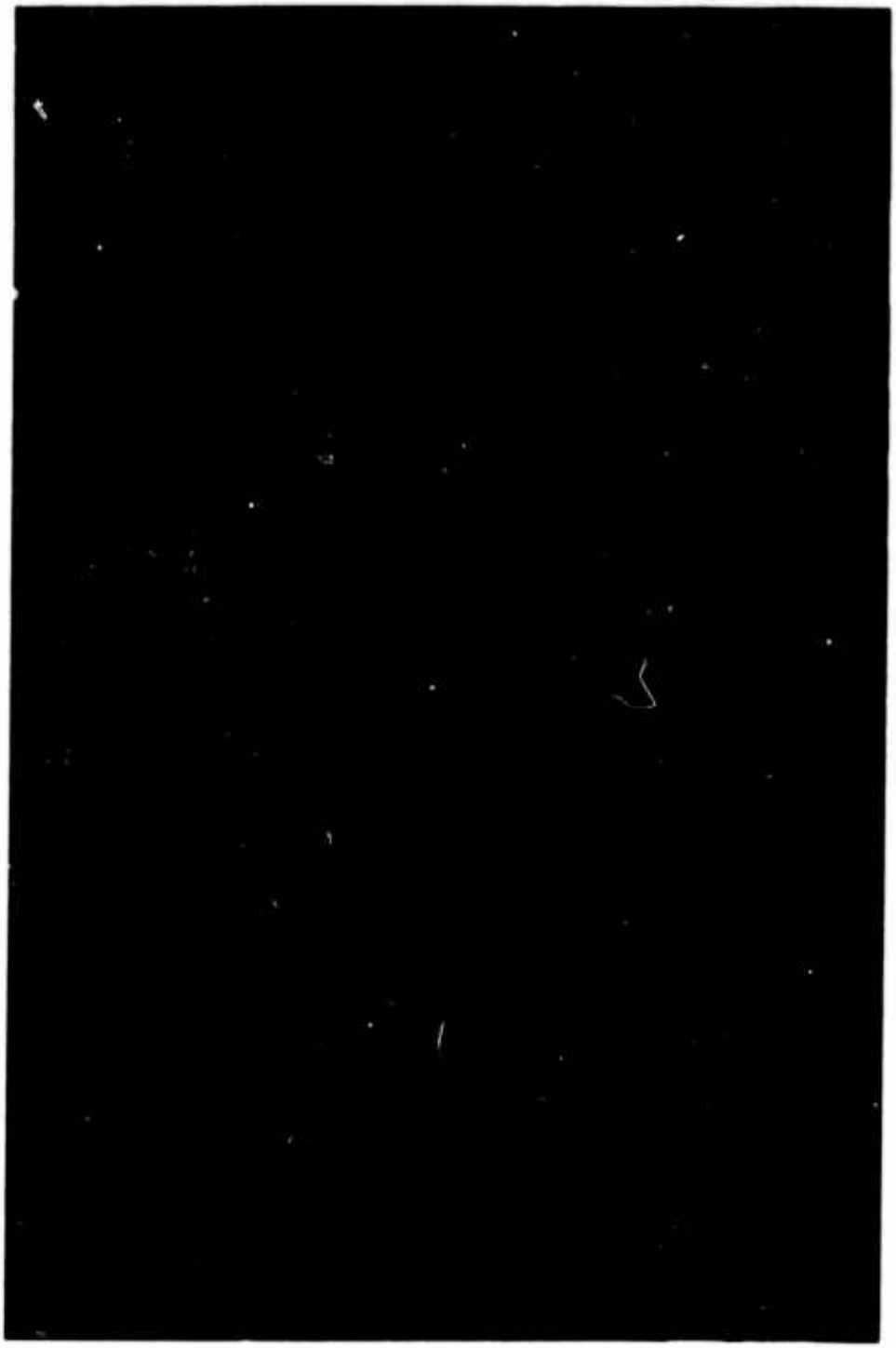


PRESSURE PULSES (FLUID WATER)

21 FLUIDIC HYDRAULIC RAM



22 **VORTEX-AMPLIFIER-CONTROLLED GLOVE BOX (DEMONSTRATION UNIT)**



23 **AIR-DRIVEN PUMP FOR TOXIC FLUIDS INCORPORATING TWO VORTEX DIODES (DEMONSTRATION UNIT)**

DEVELOPMENT OF A MINIATURE FLUIDIC DUAL CHANNEL FLUIDIC PROGRAMMER

by

T. S. Honda
General Electric Co.
Specialty Fluidics Operation
Schenectady, N.Y.

INTRODUCTION

Fluidic systems offer opportunities to perform control and computational functions in environments that have eluded exploitation by electronic and mechanical means. The minimum use of moving parts yields a rugged device capable of withstanding high temperature, shock, vibration, and radiation. Of the many fluidic devices that have been developed in recent years for application in hostile environments, the fluidic programmer has received extensive development. The results have been the fluidic implementation of relatively complex functions in a compact package meeting demonstrated capability of defined performance specifications.

This paper discusses the development and test results of the dual channel fluidic programmer for advanced ordnance applications. The programmer provides multiple time outputs which are used to schedule a predetermined sequence of events. The dual-channel configuration designed for fail-safe programming consists of dual torsional reed reference oscillators, a dual-channel binary counter, and ANDING logic and output amplifier circuits. The programmer circuit design, the hardware configuration and performance test results are presented.

The more pertinent design specifications imposed by the application were an overall package size not to exceed 3 in^3, consume less than 4 SCFM of air, and maintain ±0.1% timing accuracy over a temperature range of -65 F to 165 F and a supply pressure range from 10 to 20 psig. The practical achievement of the accuracy proved to be a significant development effort. Since the inherent accuracy of the programmer is derived from the oscillator performance, particular attention is devoted to the discussion of the balanced torsional reed oscillator development.

PROGRAMMER FUNCTION

The basic function of the programmer is to provide five time outputs. These are one settable and four fixed with respect to the settable

Preceding page blank

time as follows:

$T_1 = T_0 + T_S$ where T_S is any time to 256 seconds settable in increments of 0.1 second and T_0 is the start time of the programmer

$T_2 = T_1 + 2$ seconds

$T_3 = T_1 + 4$ seconds

$T_4 = T_1 + 8$ seconds

$T_5 = T_1 + 10$ seconds.

The basic operational concept is to accumulate the pulses from an oscillator in a binary counter and produce an output pulse when the counter has received a predetermined number of input pulses. Variable time durations are achieved by presetting the counter. By setting the counter to a predetermined number, the timed interval is determined by the number of input pulses required to fill the counter. The fixed times are derived by summing the set time with the cyclic time outputs of intermediate stages in the counter.

The programmer is configured with two parallel channels of oscillators and counters to provide fail-safe operation. This mode of operation results when the five outputs of each channel are combined in a fluidic AND logic circuit to produce a single set of time outputs from the programmer. If either channel malfunctions, no programmer output can be produced.

The programming function was implemented by an integrated assembly of four functional modular subassemblies as identified in Fig. 1. The modules are:

1. Dual oscillator module
2. Dual counter module
3. Logic module
4. Amplifier module.

A functional schematic diagram of the programmer is shown in Fig. 2.

HIGH ACCURACY FLUIDIC OSCILLATOR

A fluidic oscillator utilizing a balanced torsional reed reference was developed to provide the reference frequency of 256 Hz with

accuracy of ±0.1% over a temperature range of -65 F to 165 F and a supply pressure range of 10 to 20 psig. The accuracy achieved is at least an order of magnitude better than that possible with the flueric feedback oscillators. This development provides the basic accuracy required to apply fluidics to timed event programming in such precision applications as advanced munitions systems.

DESCRIPTION OF OSCILLATOR

The basic elements comprising the balanced torsional reed reference fluidic oscillator are shown in the isometric sketch in Fig. 3. The details of the fluidic circuit are shown in the diagram in Fig. 4. The oscillator consists of a torsional reed reference driven fluidic proportional amplifier, a flip-flop, and an output digital amplifier. The flip-flop output is fed back to drive the reference reed. As pressure is supplied to the fluidic circuit, the flow latches to one wall of the flip-flop and drives the reed. The opposite end of the reed has an orifice that directs fluid to the control ports of the fluidic proportional amplifier to switch the flip-flop output. By properly shaping the fluidic phase shift characteristics, the frequency of oscillation is made equal to the resonant frequency of the reed.

By making the fluidic circuit oscillation coincident with the natural resonant frequency of the reed, ability to maintain an accurate frequency reference is achieved.

The entire oscillator assembly is constructed from Ni-Span-C to minimize the variation in frequency with temperature. The fluidic elements and reference reed are chemically etched in Ni-Span-C laminations. The oscillator assembly is then assembled by the stack-up of laminations.

The design of the balanced torsional reed is shown in Fig. 5.

OSCILLATOR OPERATION

The ideal oscillator is one where the frequency of oscillation is controlled entirely by the mass and mechanical spring gradient of the reference. In practice, the ideal can be approached to within a predictable tolerance band providing the extraneous torques acting on the reed reference can be maintained below certain limits. In addition, the reference Quality Factor (Q) must be maintained above an established minimum to negate uncontrollable phase shifts associated with the feedback oscillator.

Referring to Figs. 6 and 7, it is apparent that the criteria for approaching the ideal oscillator can be met only by decreasing the

supply flow levels of the signal pickoff configuration. The data presented shows the influence of signal nozzle supply pressure on the reference frequency. This data was obtained by mounting the reed in an external mount and monitoring reed displacement with an electrical reluctance type displacement gage. The signal nozzle was then directed at the reed tab and the supply pressure varied. The reed was excited by plucking, hence, the measured frequency is the true resonant frequency of the reference. The rate of change of frequency vs supply pressure is 0.2%/psi. If ±0.1% accuracy is required over a 10 to 20 psig supply range to the oscillator, then the signal nozzle must be operated at a level where the 2:1 supply range reflects only a 1 psi change in signal nozzle pressure. This corresponds to 1-2 psig range on the nozzle, which can be achieved by a simple pressure dropping resistor.

Figure 7 shows the effect of signal nozzle supply on the reed Q. It is apparent that generally the maximum pressure should not exceed 1 psig. The Q degrades rapidly with pressure, making the oscillator frequency more dependent on feedback amplifier phase shifts.

Reducing the signal pickoff levels to a compatible range requires additional stages in the oscillator feedback loop with the oscillator operating over a range of 1-2 psig on the signal nozzle (with a 10 to 20 psig programmer input supply range).

In addition to the reduction in signal pressure levels, the reed configuration affects accuracy. The reed was designed to eliminate the influence of the normal force component produced by the signal nozzle on reference frequency and Q. The influence of non-uniform flow through the signal orifice is not eliminated. However, because of the square law relationship, this component is relatively small (compared to normal force component) and can be further reduced if required by increasing the area of the signal nozzle.

OSCILLATOR TEST PERFORMANCE

An oscillator designed to the recommended criteria was operated over a temperature range of -65 F to 165 F with the supply pressure held constant. The data obtained is shown in Fig. 8. The results show that at low supply pressures to the oscillator, the frequency drift with temperature is negligible. The test data indicates the temperature sensitivity increases as the supply pressure is increased. It is, therefore, concluded that an oscillator designed for negligible pressure sensitivity will also provide the desired accuracy over the specified temperature range.

The actual pressure sensitivity achieved is shown in Fig. 9. Over a supply pressure change of 2:1, less than 0.1% change in oscillator frequency was demonstrated.

In addition to the requirements for accuracy over the specified range of temperature and supply pressure, the oscillator is also designed to be insensitive to an operational vibration environment up to 2000 Hz in all three mutually perpendicular axes. The oscillator is also capable of withstanding a non-operating mechanical shock of 50 g's in all three mutually perpendicular axes. Insensitivity to a vibration environment below 2000 Hz is achieved by designing the spring-mass resonance of the torsion member and reed in all axes to exceed 2000 Hz. Sensitivity to vibration in the axis perpendicular to the reference reed in the plane of reed rotation was a problem with flat reeds. The problem was solved by special forming of the reed. The critically loaded member under mechanical shock is the reed torsion spring. This is designed to provide a factor of safety greater than three in the worst loading axes under 50 g's loading.

DUAL CHANNEL BINARY COUNTER

The binary counter circuit shown in Fig. 10 was used in the counter design. Seventeen of these counters cascaded in series establishes the time period of the last bit to be the maximum desired timing interval of 256 seconds for an input frequency of 256 Hz. The basic counter design was established previously. In the programmer development, the counter was designed for dual channel configuration as shown in Fig. 11. The power nozzles for the flueric elements were limited to 1×10^{-4} in^2 to conserve gas consumption.

In order to provide capability for simultaneous setting of "zeros" and "ones" into the counters, an "AND" gate was also incorporated in each counter stage as shown in Fig. 12.

During counter presetting and prior to programmer initiation, the oscillator outputs are blocked at the oscillator-counter interface. This function is accomplished as shown in Fig. 13 by inserting a flip-flop at the interface. This flip-flop is powered by a "positive" pressure input of approximately 20% of the programmer supply pressure. The oscillator outputs are the control inputs to the blockage amplifier. When the counter start signal is not present, the blockage element output is attenuated below the counter first stage flip-flop hysteresis so that the counter first stage is inhibited from switching.

The dual channel counter was assembled by stacking 0.003 inch titanium laminations. The simultaneous setting of "zeros" and "ones" was demonstrated. Setting of the counter stages through the AND gates simplifies the setting procedure, but it increases the set flow requirements by a factor of three.

"AND" LOGIC MODULE

The logic circuitry functions to inhibit the fixed cyclic time outputs from the intermediate stages of the counter until the present time has elapsed and a change in state occurs at the counter output stage. It also prevents the time outputs from appearing unless coincident outputs from both counters are present. The desired time outputs T_1 + 2 seconds, T_1 + 4 seconds, and T_1 + 8 seconds are obtained for each channel by ANDING the settable output with each of the fixed outputs. A special flueric "AND" element that is compatible with the memory flow in the binary counter circuit was developed to perform the time programming, i.e., the T_1 not present inhibit function. The corresponding time outputs from the two counters are then "ANDED" by means of passive "AND" elements to derive the desired programmed time outputs. Since a fixed time of 10 seconds is not available from the counter, the T_1 + 10 second output is derived by ANDING the T_1 + 2 second and T_1 + 8 second outputs. The "AND" logic circuit is shown schematically in Fig. 14.

The logic circuit was implemented with flueric elements using 1×10^{-4} in^2 power nozzle areas. The logic module is comprised of a stack of 0.003 inch thick titanium laminations.

OUTPUT AMPLIFIER MODULE

Output amplifiers are required to enable the five time outputs from the logic circuit to drive the load. The programmer output requirements are to provide dead ended output pressures of 50% of the programmer supply pressure. When the loads are passive AND gates with 0.010" x 0.010" nozzles, the output pressure is approximately 30% of the programmer supply pressure.

Two stages of amplification are utilized in the output amplifier module. Geometrically biased proportional amplifiers are used in the first stage to positively prevent the appearance of an output when no input is present. A digital amplifier comprises the second stage. Eight mil wide power nozzles are used in the amplifiers. The first stage has an aspect ratio of 1.0 and the second stage aspect ratio is 1.5.

PROGRAMMER ASSEMBLY

A dual channel fluidic programmer resulting from the development program is shown in the photograph in Fig. 15. All inputs to and outputs from the programmer are located at the base mounting surface. The integrated assembly of the four functional modules, previously

described, are arranged so that the supply pressure to each succeeding module is cascaded downward so that the oscillator and counter are operated at lower pressures. This design approach results in an improved oscillator accuracy and decreased counter preset pressure requirement.

The oscillator is comprised of 0.002" x 0.5" x 0.85" Ni-Span-C laminations stacked 0.265 inch high. The dual channel counter is assembled from 0.003" x 0.5" x 1.6" titanium laminations. The counter lamination stack height is 0.733 inch. The logic and amplifier modules are assembled from 0.003" x 1.0" x 1.6" titanium laminations. The AND logic lamination stack height is 0.132 in and that of the output amplifier is 0.142 inch.

PERFORMANCE

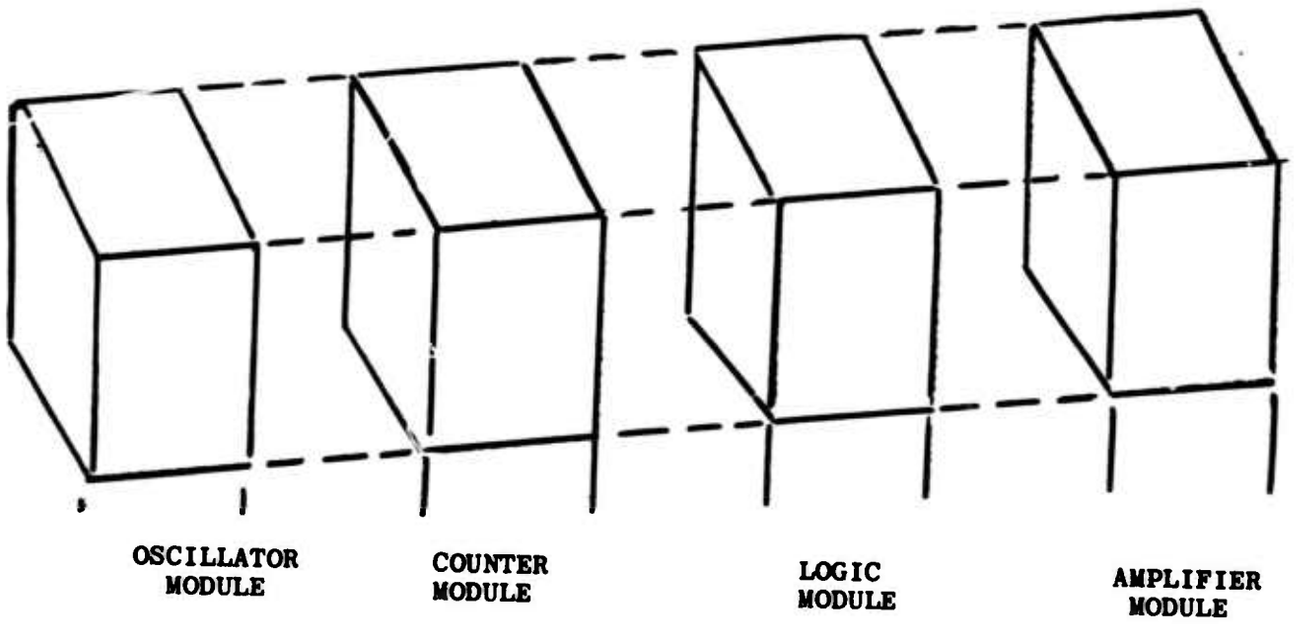
The timing accuracy of the programmer is established by the oscillator accuracy. It was previously noted that a timing accuracy of ± 0.1% over the temperature range of -65 F to 165 F with a programmer supply pressure variation from 10 to 20 psig was achieved. The pair of oscillators were readily trimmed to within 0.04% of the desired frequency of 256 Hz.

The programmer as developed meets the basic performance specified in for the intended application. Some of the basic performance data obtained are shown in Table I.

TABLE I

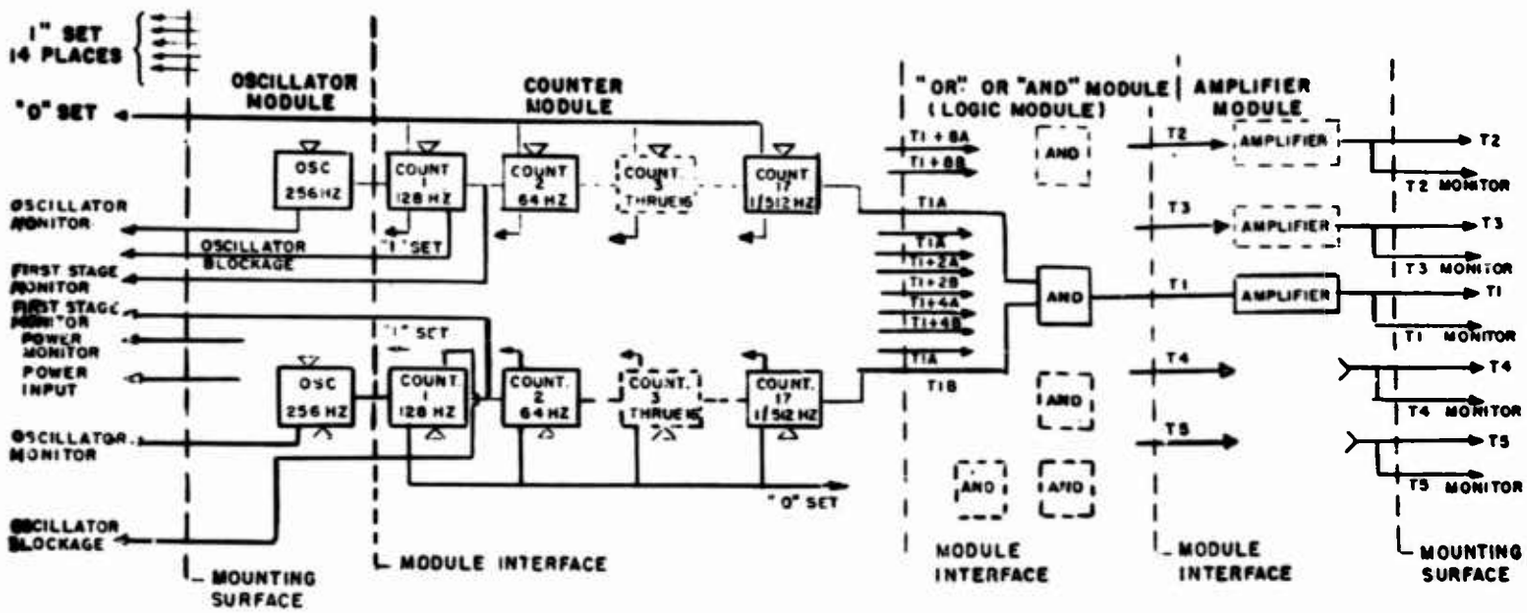
TITANIUM DUAL CHANNEL FLUIDIC PROGRAMMER
TEST DATA

Supply Pressure (psig)	10	20
Frequency (Hz)		
Oscillator A (left)	256.0	256.1
Oscillator B (right)	256.1	256.2
First Stage A	128.0	128.1
First Stage B	128.0	128.1
Time Outputs (set at 16 seconds)	(seconds)	
T_1	16.01	15.99
T_2	18.01	18.00
T_3	20.01	19.99
T_4	24.01	24.00
T_5	26.01	25.99
Pressure Outputs (blocked load)	(psig)	
T_1	6.0	12.3
T_2	6.1	12.3
T_3	5.2	10.7
T_4	5.0	10.3
T_5	5.0	10.8
Oscillator Initiate Pressure	1.4 - 2.6	2.5 - 6.8



MODULAR REPRESENTATION OF PROGRAMMER

Figure 1



FUNCTIONAL SCHEMATIC

Figure 2

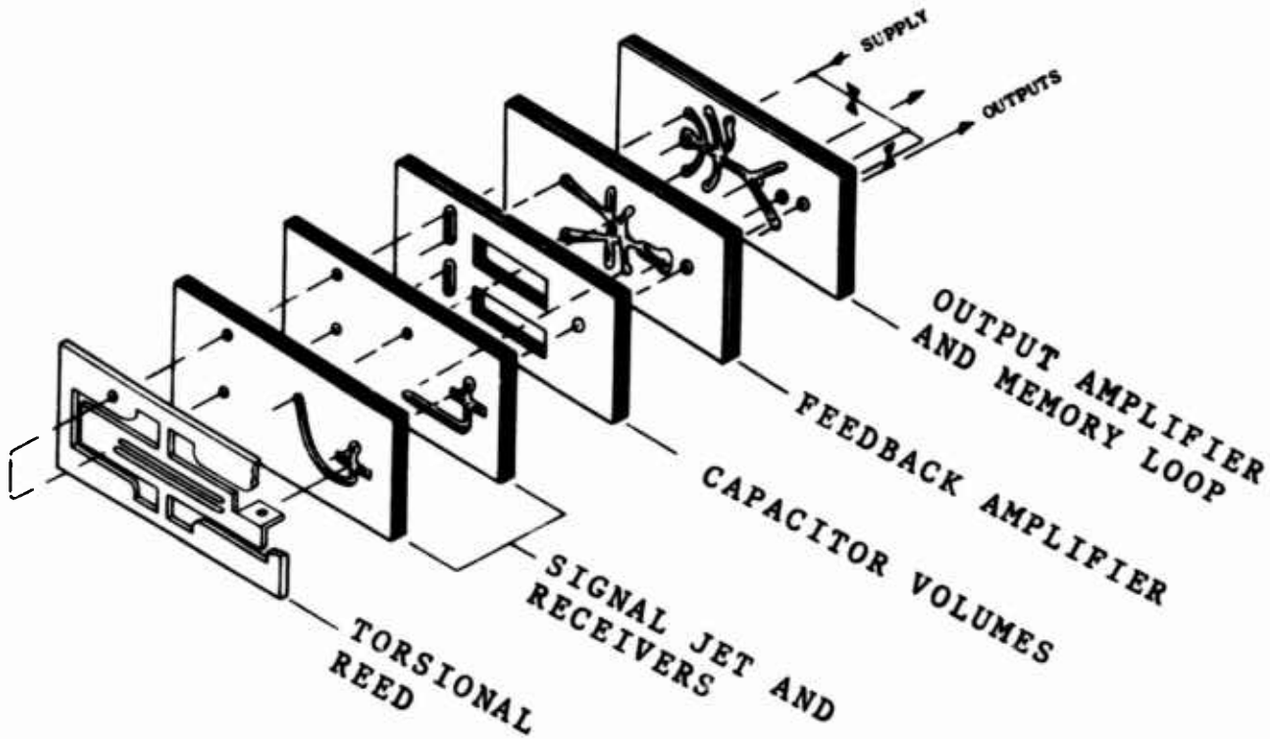
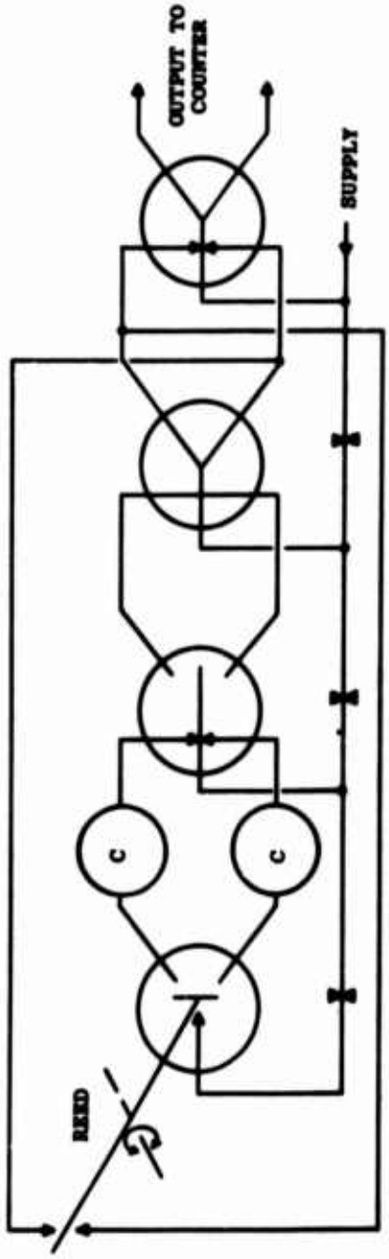


Figure 3 Torsional Reed Oscillator for Dual Channel Fluidic Programmer.



FLUIDIC CIRCUIT DIAGRAM
TORSIONAL REED OSCILLATOR

Figure 4

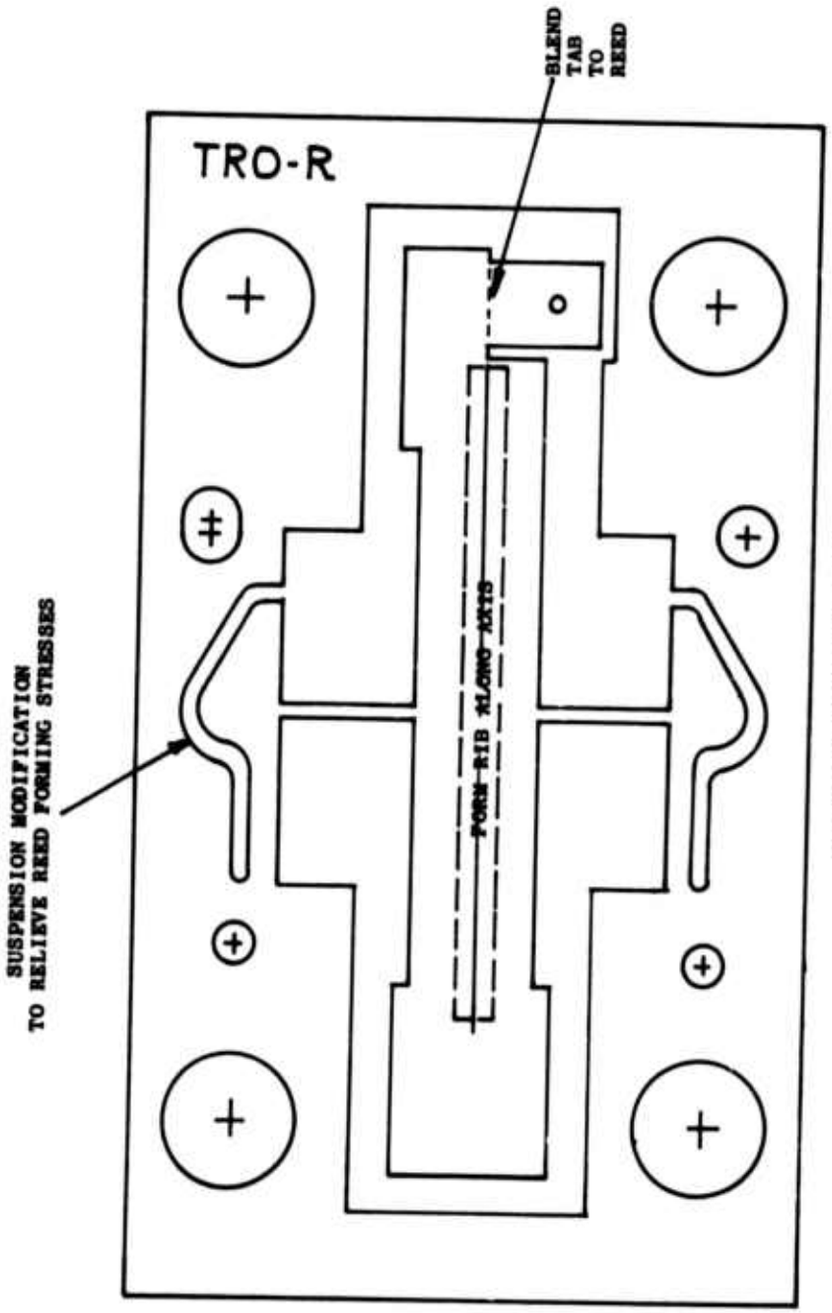
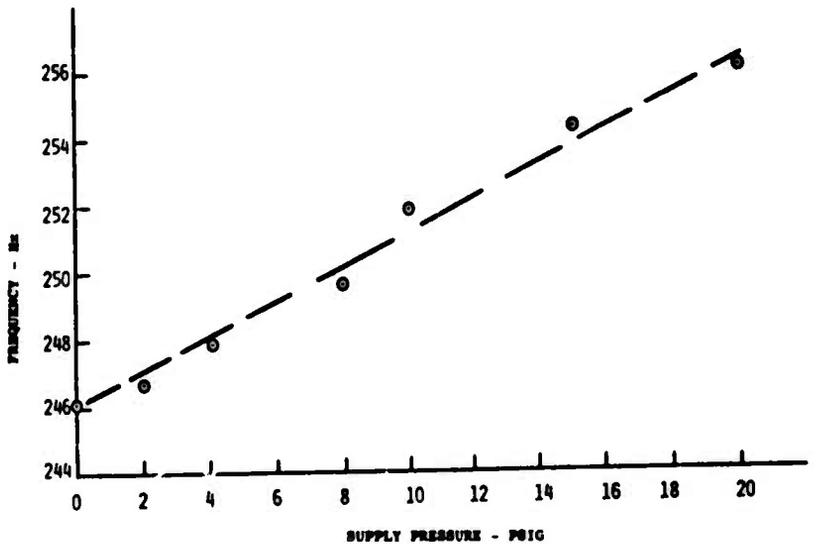
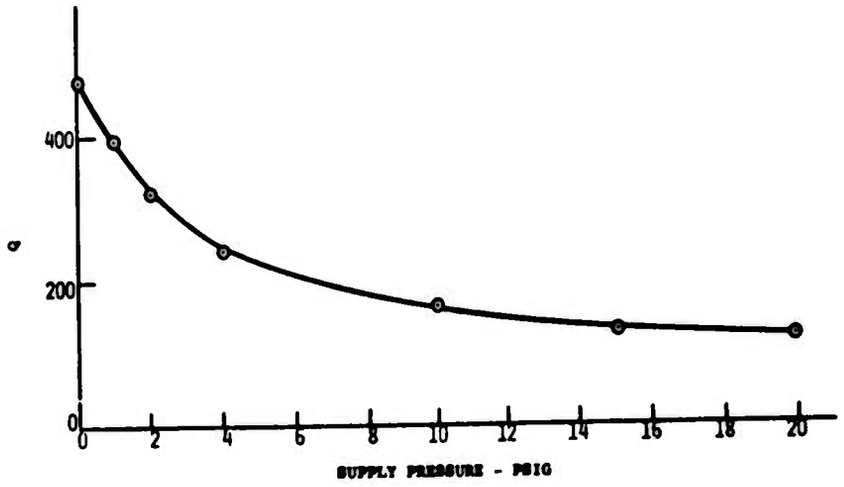

BLEND TAB TO REED
TRO-R
SUSPENSION MODIFICATION TO RELIEVE REED FORMING STRESSES
FORM RIB ALONG AXIS
BALANCED TORSIONAL REED

Figure 5



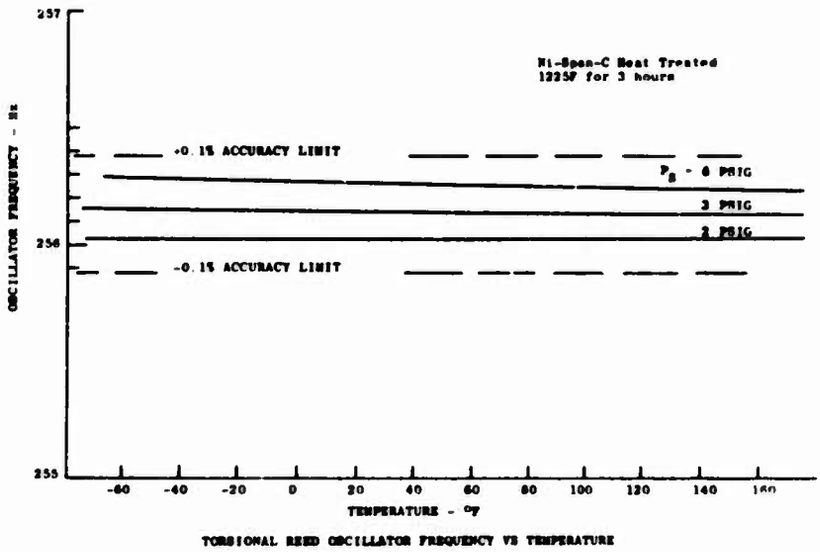
REED FREQUENCY VS SIGNAL NOZZLE SUPPLY

Figure 6



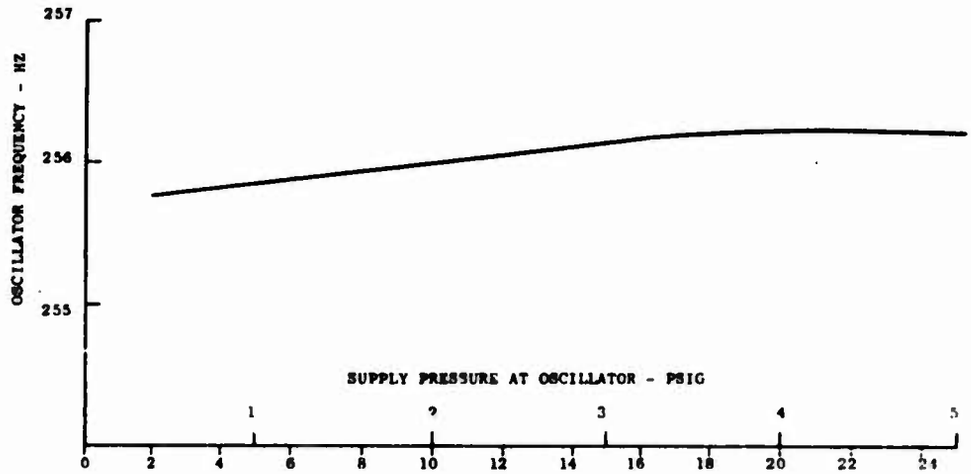
REED Q VS SIGNAL NOZZLE SUPPLY

Figure 7



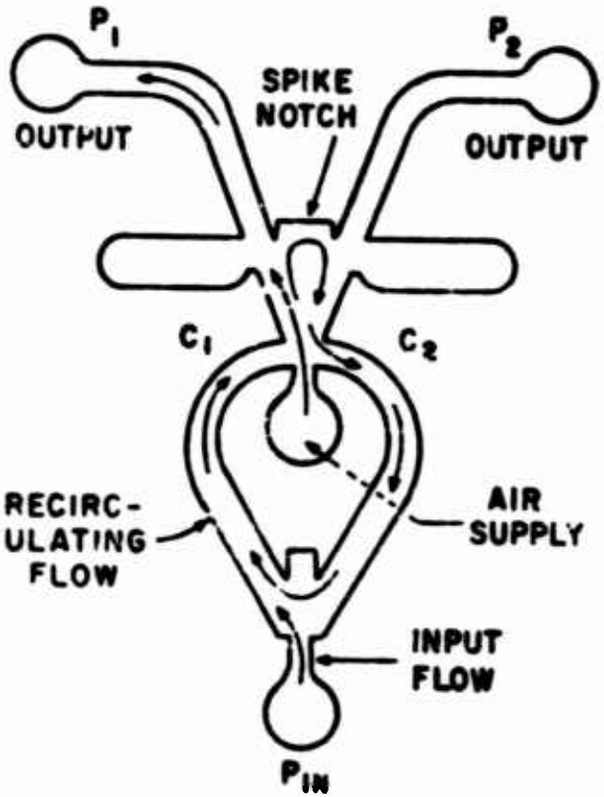
TORSIONAL REED OSCILLATOR FREQUENCY VS TEMPERATURE

Figure 8



TORSIONAL REED OSCILLATOR FREQUENCY VS SUPPLY PRESSURE

Figure 9



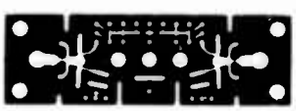
LOGIC

P_{IN}	C_1	C_2	P_1	P_2
0	0	0	X	0
X	X	0	0	X
0	0	0	0	X
X	0	X	X	0
0	0	0	X	0

Binary counter circuit.

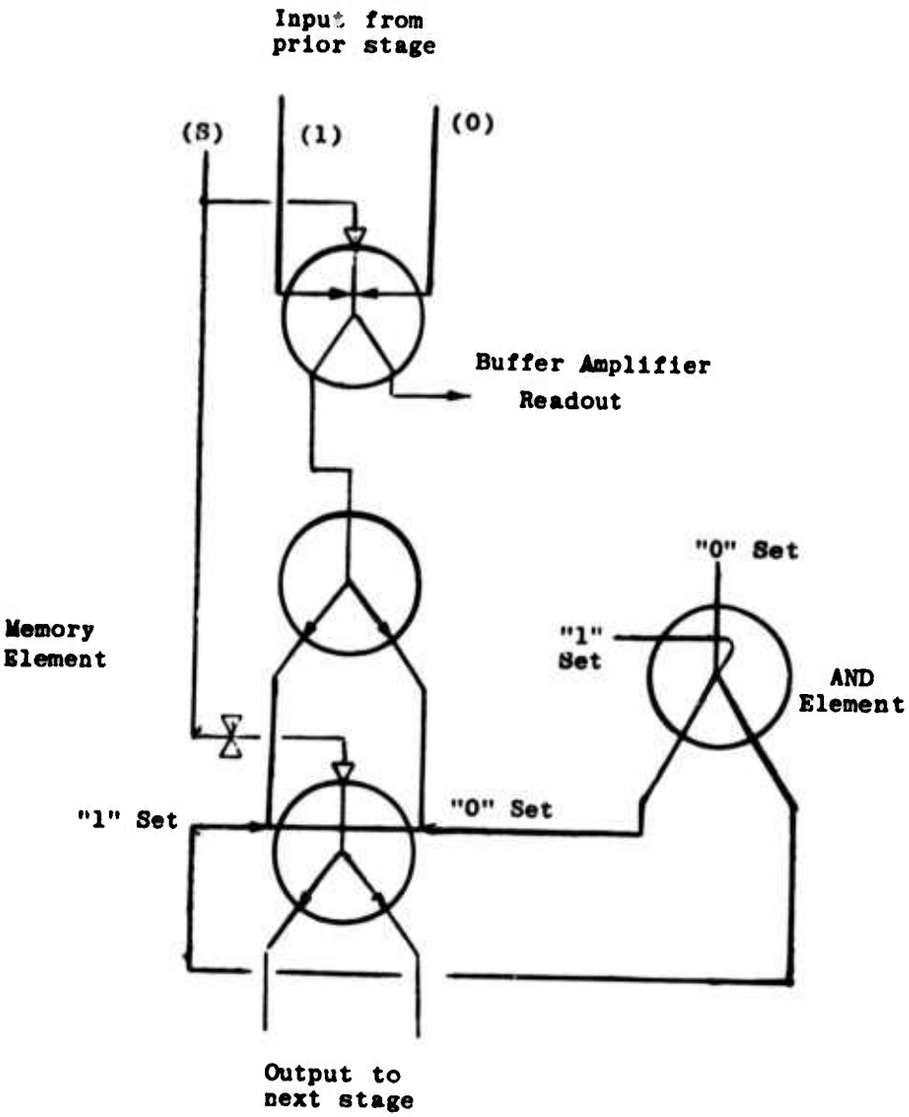
Figure 10





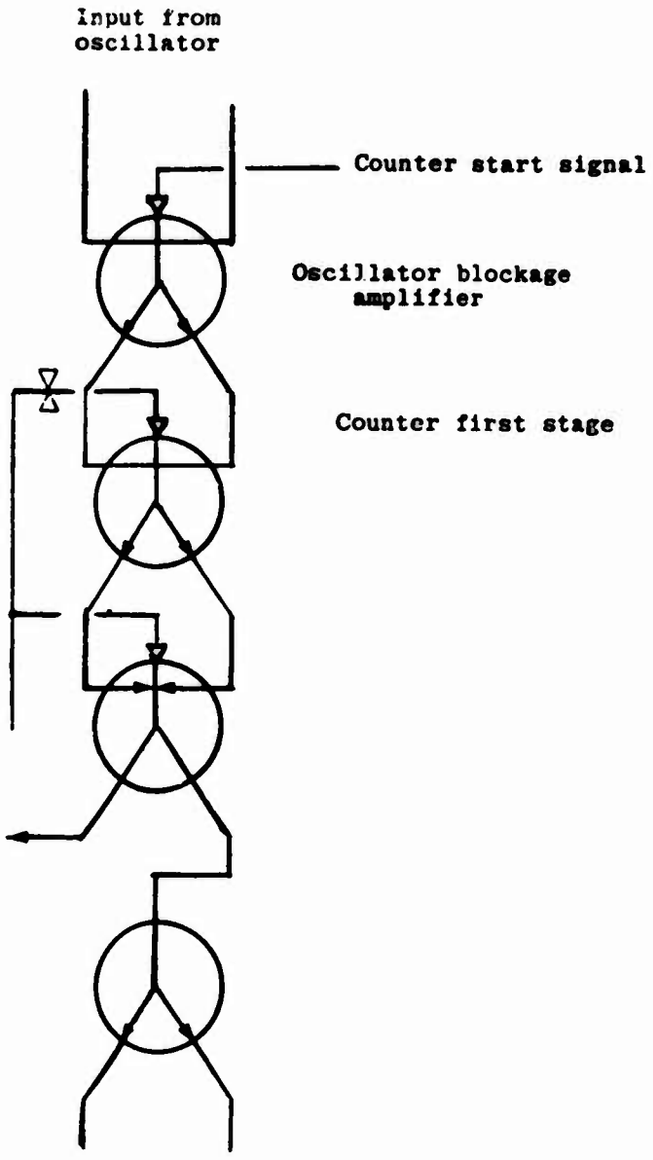
DUAL CHANNEL COUNTER LAMINATIONS

Figure 11



Typical Counter Stage Set Logic
Fluidic Circuit Diagram

Figure 12



Oscillator Blockage
Fluidic Circuit Diagram

Figure 13

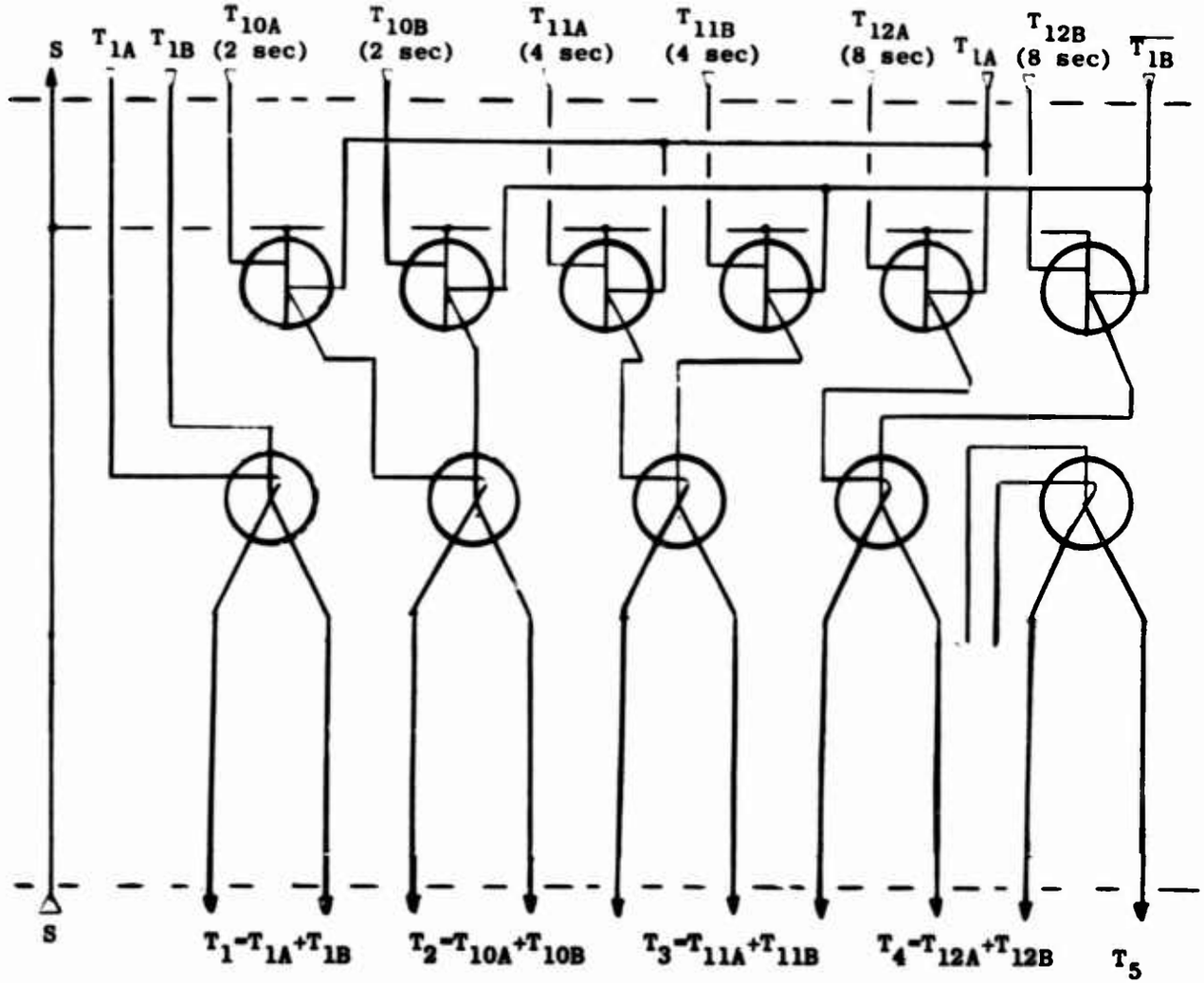
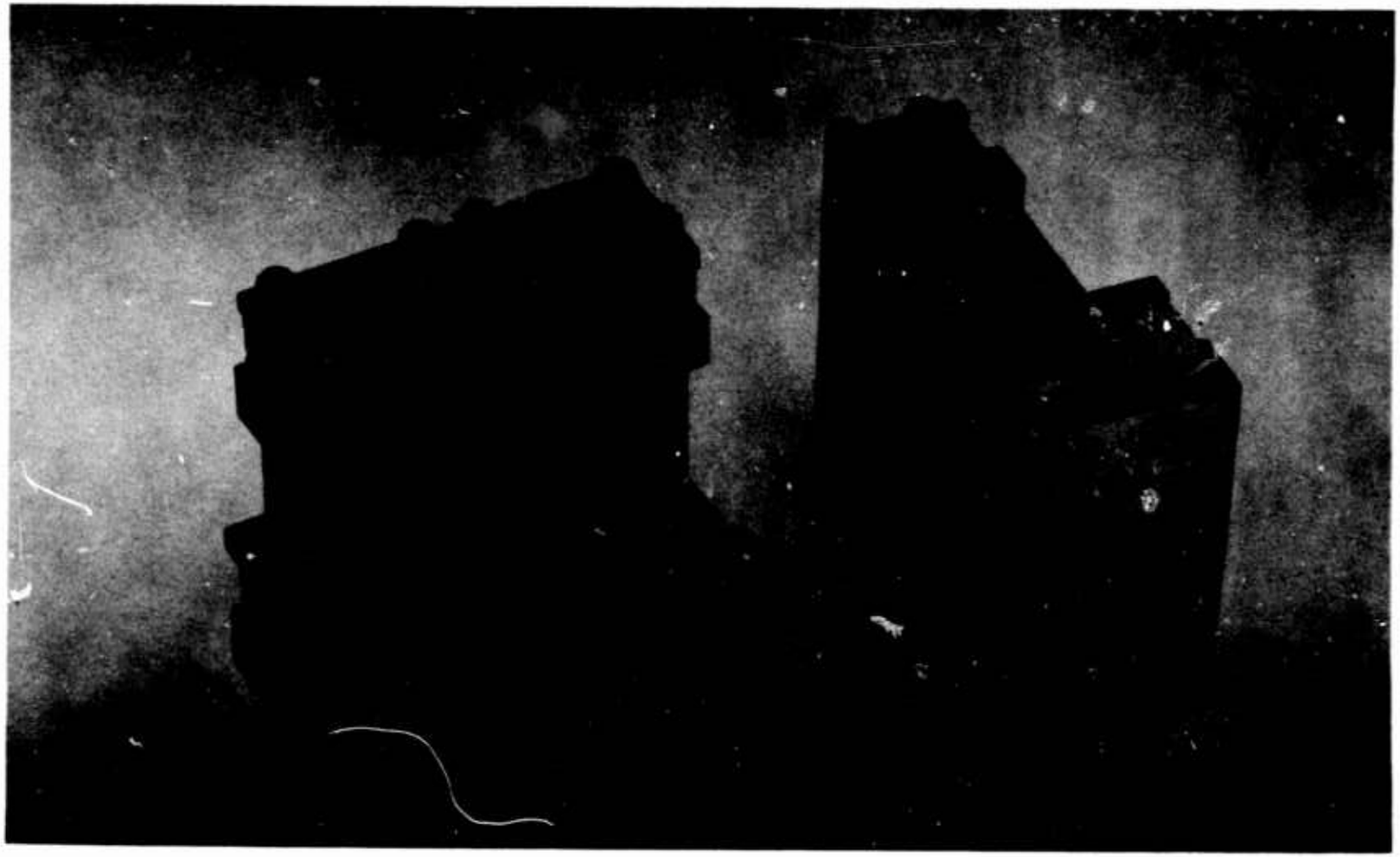


Figure 14

"AND" LOGIC MODULE CIRCUIT



DUAL CHANNEL FLUIDIC PROGRAMMER

Figure 15

ATTITUDE CONTROL SYSTEM OF AN UNDERWATER BODY USING LIQUID FLUIDIC ELEMENTS.

by Yoshiaki HARA, Toshinori OGAWA & Yoshiyuki SHIMAZAKI

Mechanical Engineering Laboratory of Japan

Abstract

This paper describes the theoretical and experimental analysis of an attitude control system of an underwater body using liquid fluidic elements. This paper consists of five parts: First a general survey is given, next the composition of the planned control system is introduced and then the construction and the theoretical and experimental analysis of the attitude angle sensor (pendulum type) are described. Then the characteristics of the summing amplifier and differential circuit are demonstrated. Finally, the tested results of the total system usdng a water tunnel and a model are demonstrated.

Preceding page blank

1. INTRODUCTION

The ocean is a very wide, deep and unknown space on the earth and Japan needs to develop the ocean's untouched respirces, because our country has no resources. But in the sea, there are many difficulties in developing control systems for machines or robots. One difficulty is the surrounding pressure rise according to the static water head. So the conventional control systems that have been developed are placed in an anti-pressure box. The second difficulty is the corrosive action of the sea water. So we must use anti-corrosive materials. Third is the microorganisms in the sea and so on.

Fortunately, fluidic elements can be operated by difference pressure only. Namely, the working principle of fluidic elements is based on the difference pressure between supply pressure and surrounding pressure. So if we use an underwater pump as the supply source to the fluidic elements, it is not necessary to place the control systems into an anti-pressure box. This fact means that the weight of the fluidic control systems is lighter than that of conventional systems. And also, reliability and durability of the fluidic elements in the sea will be superior to the other control elements.

Unfortunately, there are few papers reporting on liquid fluidic elements.[1] So, our study had to be started from basic research on the liquid fluidic elements, and we reached the conclusions that the pneumatic fluidic elements can be used with a water supply in water. It is necessary, of course, that the water supply pressure to the elements be adjusted to have same the Reynold's number as that when using the element with air. Our development of the attitude control system is based on this fact. The attitude angle sensor and the acceleration sensor, which operate with water, are newly created. Other parts of the control system are constructed with the fluidic elements on the market.

2. THE COMPOSITION OF THE CONTROL SYSTEM

The construction of the initially planned attitude control system is shown in Fig. 1. This system consists of an attitude angle sensor, two acceleration sensors, two summing fluidic amplifiers (G.E.'s element), two booster amplifiers and two actuator cylinders with position feedback. These elements are tested with water in the water.

Input ports of the summing amplifier 1 are connected to the output port of the attitude angle sensor and the acceleration sensor. In this amplifier, the difference output signal of these sensors are added. Input ports of the summing amplifier 2 are connected to the output ports of the amplifier 1, its differential signal and the position feedback signal from the actuator cylinder.

So in this amplifier, these three defference pressure signals are added.

In the next section, the characteristics of each element of the control circuit are given.

3. SENSOR

3.1. ATTITUDE ANGLE SENSOR

The construction of the attitude angle sensor is shown in Fig. 2. This sensor consists mainly of a pendulum supported by a gymbal mechanism and two pairs of the slide valve type nozzle flappers. If the sensor axis is inclined from the vertical axis, the difference output pressure of the nozzle-flapper is changed due to the inclined angle of the pitch or roll components.

The static difference output characteristic versus attitude angle of this sensor is shown in Fig. 3. This sensor is designed having a saturation characteristic at 5 deg. The static difference output is proportion to the attitude angle until the saturation point is reached. Thus the static characteristics of the sensor are very good, but the dynamic characteristics are unknown.

So, we try to analyze the dynamic characteristic of the sensor. The test set up and experimental apparatus are as follows. The sensor is attached on the rolling axis which can be inclined by the external rod. This rod is connected to an eccentric cam driven by a motor. These arrangements are shown in Fig. 4.

In this forced oscillation condition, we assume that the pendulum receives the direct effect of the external acceleration through the gymbal axis and thecontained water. A simplified analytical model of this system is shown in Fig. 5.

Then the horizontal displacement equation of the pendulum and cover box at the pendulum center of gravity is as follows:
External forced oscillation term:

$$\begin{aligned} x &= l_0 \sin \omega t \\ \dot{x} &= l_0 \omega \cos \omega t \\ \ddot{x} &= -l_0 \omega^2 \sin \omega t \end{aligned} \qquad (1)$$

Pendulum displacement with acceleration term:

$$\tan \alpha = \frac{\ddot{X}}{\left(1 - \frac{m'}{m}\right) g}$$

$$x_\alpha = l_0 \tan \alpha = \frac{-l_0 (l_0 \omega^2 \sin \omega t)}{\left(1 - \frac{m'}{m}\right) g} \qquad (2)$$

From equations (1) and (2),

$$x + x_{\alpha} = l_0 \sin\omega t \left\{1 - \frac{l_0 \omega^2}{(1 - \frac{m'}{m})g}\right\} \quad (3)$$

is obtained where, x is the horizontal displacement of the vessel at the pendulum center, x_{α} is the horizontal displacement of the pendulum by the external acceleration, g is the gravitational force, m is the mass of the pendulum, m' is the mass of the water, l_0 is the length from the gymbal axis to the pendulum gravitation center, ω is the forced oscillation frequency.

From equation (3), we can get the following equation.

$$\beta = \beta_0 \sin\omega t \left\{1 - \frac{l_0 \omega^2}{(1 - \frac{m'}{m})g}\right\} \quad (4)$$

From equation (3) or (4), we can get following condition.

$$1 - \frac{l_0 \omega^2}{(1 - \frac{m'}{m})g} = 0, \quad \therefore \omega = \sqrt{\frac{(1 - \frac{m'}{m})g}{l_0}} \quad (5)$$

Equation (5) shows the condition for tuned vibration of this sensor. At this condition, the relative displacement of the pendulum to the cover box converges to zero, and the difference output of this sensor is equal to zero. Hereafter the bracketed terms in equation (4) will be written as the correction factor.

Calculated values of the correction facter versus ω are shown in Fig. 6. (l_0 = 8 cm, m = 7.91, m' = 1.00, g = 980 cm/sec^2) The experimental data using experimental apparatus shown in Fig. 4 are shown in Figs.7 & 8. In this figure, the correction factor is also indicated. Data shows good agreement with the correction factor until the tuned vibration condition occurs.
The phase shift of the sensor is also shown in the figures, where the filled mark in the figure is from equation (4).

3.2. ACCELERATION SENSOR

Construction of this sensor is shown in Fig. 9. The inner seismic mass of the sensor is made from polypropylene and the specific gravity of it is about 0.9. The purpose of this sensor is to correct the decreasing difference output of the attitude sensor with the acceleration term. This idea is shown graphically in Fig. 10, and data of the sensor is shown in Fig. 11. The difference output pressure of the sensor was too low to correct the acceleration term, so the use of the sensor was abandoned in the final test.

4. CHARACTERISTICS OF THE SUMMING AMPLIFIER AND DIFFERENTIAL CIRCUIT

The characteristics of the summing amplifier using water as a working fluid are shown in Fig. 12. In this figure the supply pressure to the amplifier is fixed at 2.5 kg/cm^2. In the G.E.'s catalogue, 0.7 kg/cm^2 is recommended for the air supply pressure to the amplifier. But the amplifier is not stable at this water supply pressure. So we calculate Reynold's number at the recommended pressure based on the exit velocity of the main nozzle; then 2.5 kg/cm^2 is the value for the water supply pressure. From Fig. 12, we can determine the input signal level for the summing amplifier. This amplifier is saturated by the input pressure at 12 % of the supply pressure (P_s) when the three difference input pressures are present at the same time. It is also saturated at 24% of the supply pressure for the two difference input pressures.

Then we can get following matching conditions.

$$\sum \Delta P_{in} \leq 0.12\ P_s \qquad \text{(for three input)}$$

$$\sum \Delta P_{in} \leq 0.24\ P_s \qquad \text{(for two input)}$$

where $\sum \Delta P_{in} = \Delta P_{i1} + \Delta P_{i2} + \Delta P_{i3}$ (n = 1, 2, 3)

$$\sum \Delta P_{in} = \Delta P_{i1} + \Delta P_{i2} \qquad (n = 1, 2)$$

then $\Delta P_{i1} + \Delta P_{i2} + \Delta P_{i3} \leq 0.12\ P_s$ (for three input)

$\Delta P_{i1} + \Delta P_{i2} \leq 0.24\ P_s$ (for two input)

We assume that $\Delta P_{i1} = \Delta P_{i2} = \Delta P_{i3}$, then the matching condition

$\Delta P_{in} \leq 0.04\ P_s$ (for three input) $\Delta P_{in} \leq 0.12\ P_s$ (for two input)

is given.
If P_s is fixed at 2.5 kg/cm^2, ΔP_{in} = 0.1 kg/cm^2 (n=1,2,3), ΔP_{in} =0.3 kg/cm^2 (n=1,2) are given.
So, we adjust all signal pressure levels (such as sensor, output signal from differential circuit and position feedback signal) for those values.

The differential circuit is constructed as shown in Fig. 13. Fluid capacitance initially consisted of a cylinder, spring and ball as shown in the figure, but in the preliminary test, the time lag of this capacitance was too large. The final capacitance consisted of an air sealed bellows. The differential capability of this circuit is shown in Fig. 14.

5. TOTAL SYSTEM TEST

After the above mentioned study, the final attitude control system was as shown in Fig. 15. Then this system was mounted in a testing model which has four control wings at the tail end. The control wings are deflected by the actuator cylinders. (It has 40 mm stroke and 20 mm diameter)

The model is suspended in the water tunnel center by a gymbal mechanism and a strut with a hollow passage for the external water supply tubes. The final test set up is shown in Fig. 16. The water supply pressures to the control system are adjusted by an ordinary pressure regulator at the roof of the water tunnel. So the tested model is controlled by the control wire deflection in the pitch and roll direction.

The results of the water tunnel test is shown in Fig. 17. In this figure, the top and bottom photos show that the model is inclined forcibly by the external control signal. The middle photo shows that the model is controlled automatically by the installed control system. The water speed is about 1.2 m/s, flowing from right to left. Three to five seconds are required for the model to attain a level attitude from maximum inclined attitude (about 20 degrees) and the control system can control the model attitude to 3 degrees. This result is not satisfactory, but for the first step of our experiment, it is not so poor.

6. CONCLUSION

From above mentioned analysis and experiments, the following conclusions are given.

a) The characteristics of the summing amplifier are very good, but some of them don't satisfy zero balance.

b) The characteristics of the attitude angle sensor are satisfactory, but those of the acceleration sensor should be improved to have higher gain.

c) From the total system test, the tested model can be controlled by the developed control system, but the response of the system should be improved.

d) In this paper, the fluid dynamic considerations of the model and control wings are not described and this problem requires further study.

e) The other remaining problem is the actual test of the control

system in the sea, surveying the effect of corrosiveness and the microorganisms in the sea.

Regardless of these conclusions. it is seen that the practical use of the fluidic control systems in the sea is very hopefull.

REFERENCE

1) M. Briscoe, Some applications for fluidics in oceanography., 4th Cranfield Fluidics Conference, paper K2, 1970.

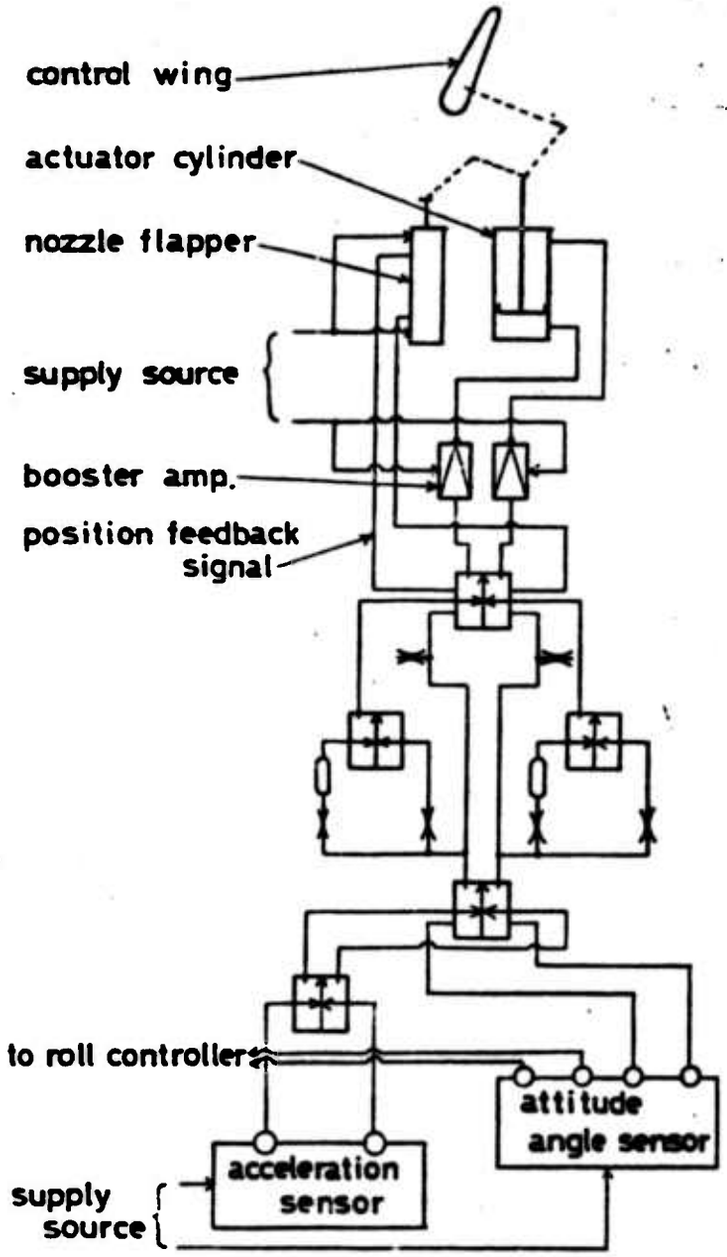


FIG.1 The construction of the attitude control system(pitch control only)

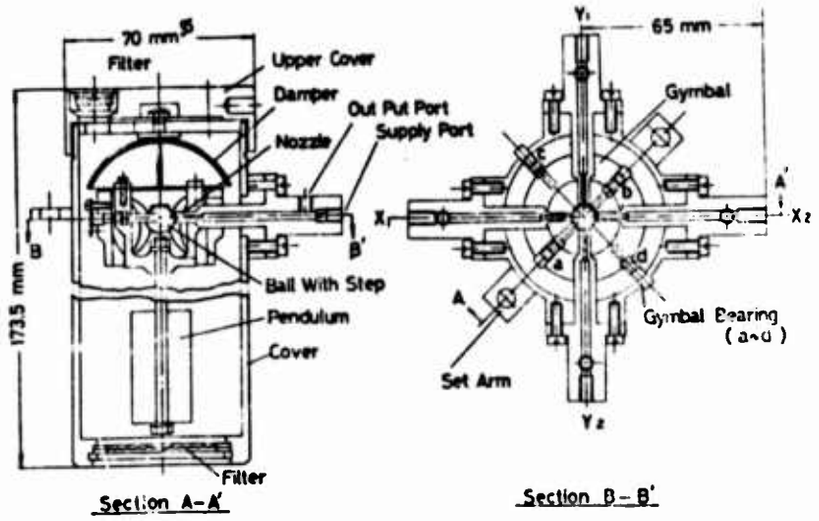


FIG.2 Construction of the attitude angle sensor

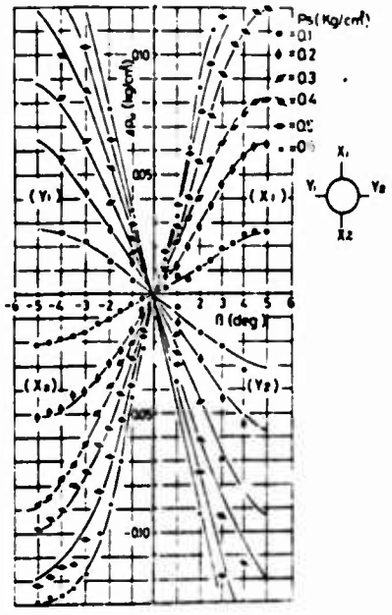


FIG.3 Input and output characteristics of the attitude sensor

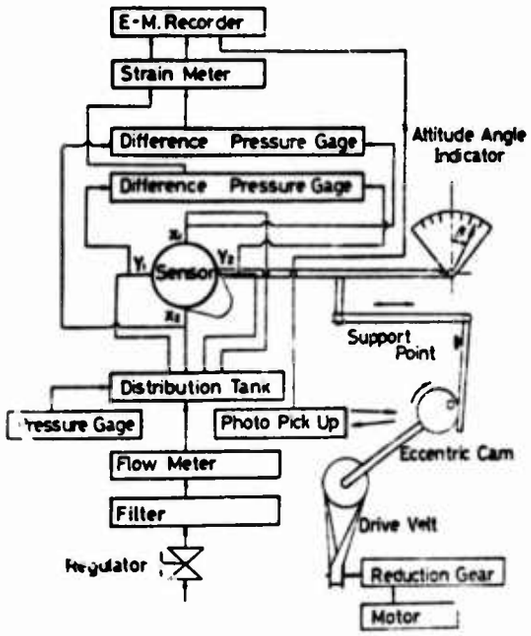


FIG.4 Arrangement of the experimental apparatus of the attitude sensor

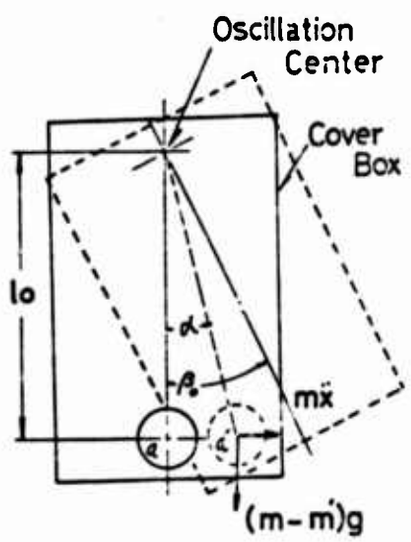


FIG.5 Analytical model of forced vibration system

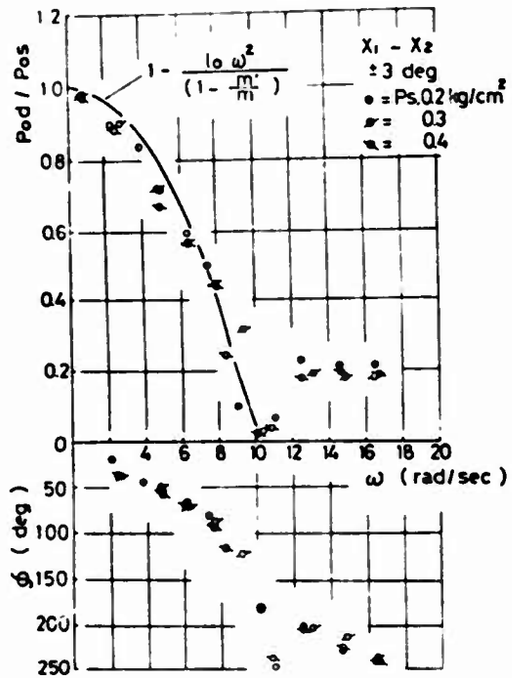


FIG.7 Output characteristics and phase shift of the attitude sensor (roll angle)

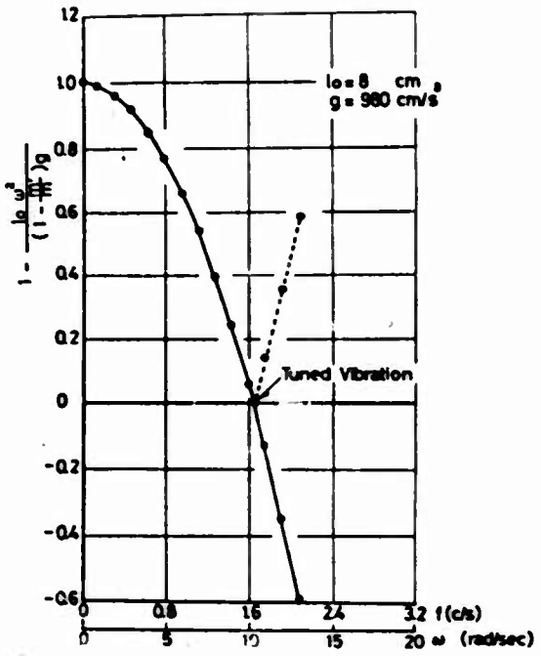


FIG.6 Correction factor versus ω

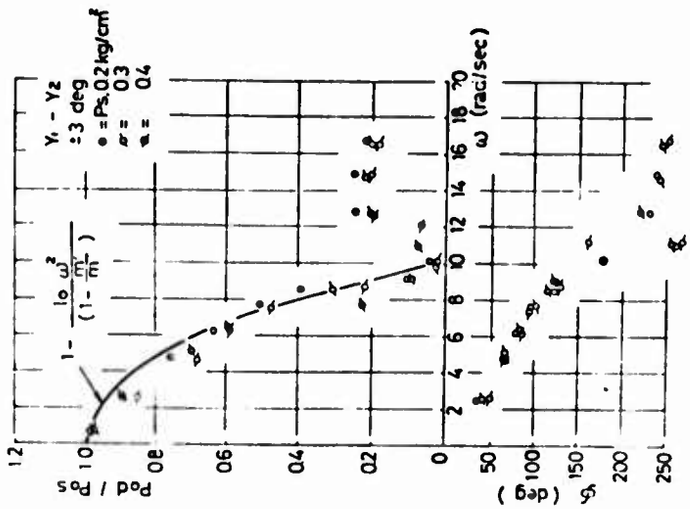


FIG.8 Output characteristics and phase shift of the attitude sensor (pitch angle)

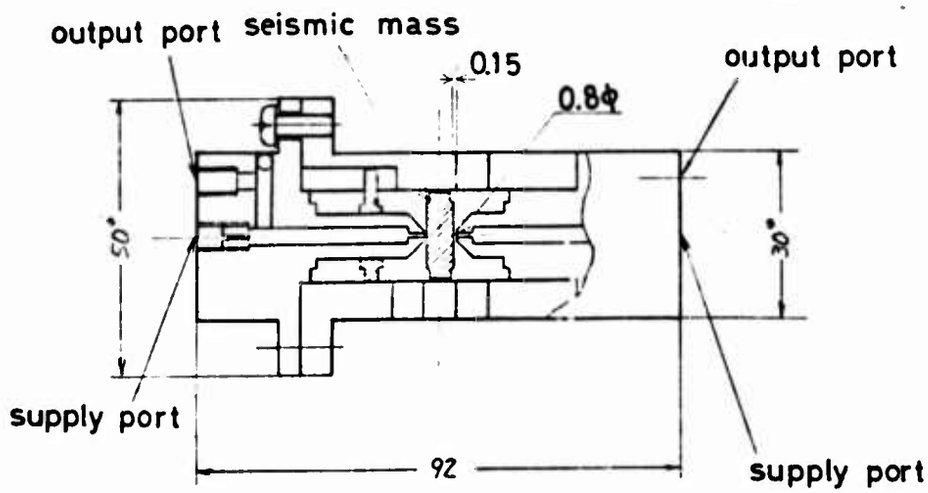


FIG.9 Construction of the acceleration sensor

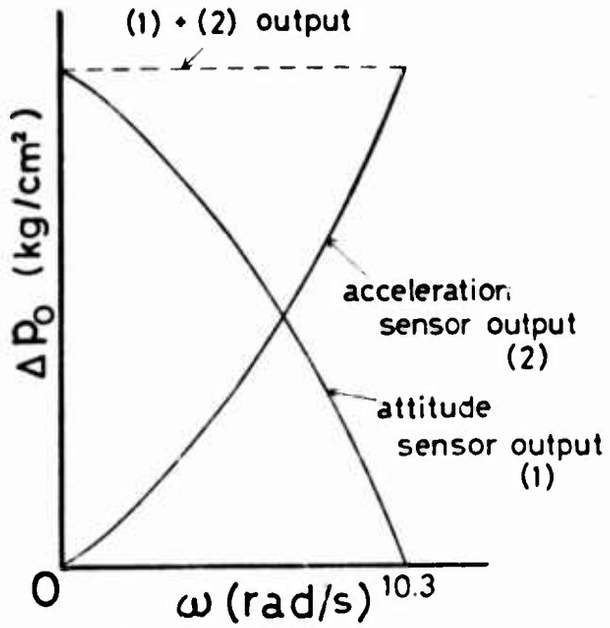


FIG.10 Conception of compensation with acceleration sensor

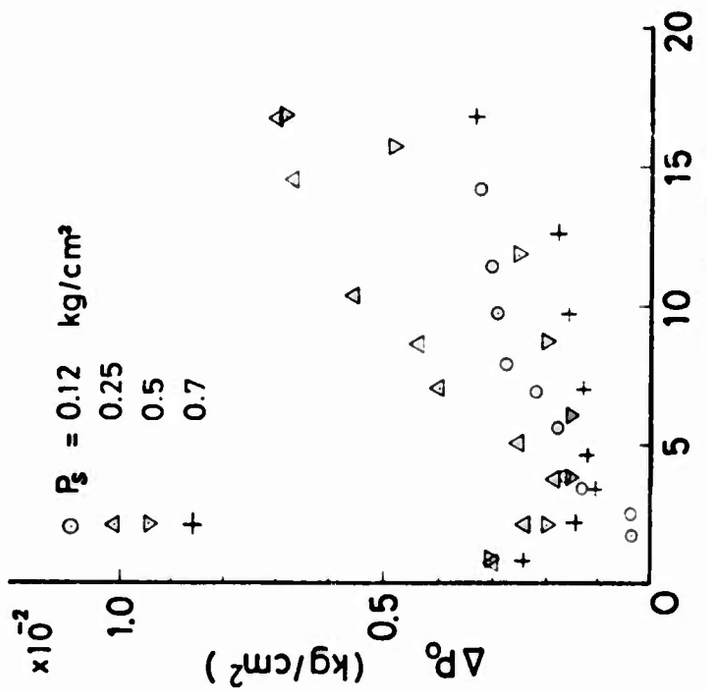


FIG.11 Output characteristics of the acceleration sensor

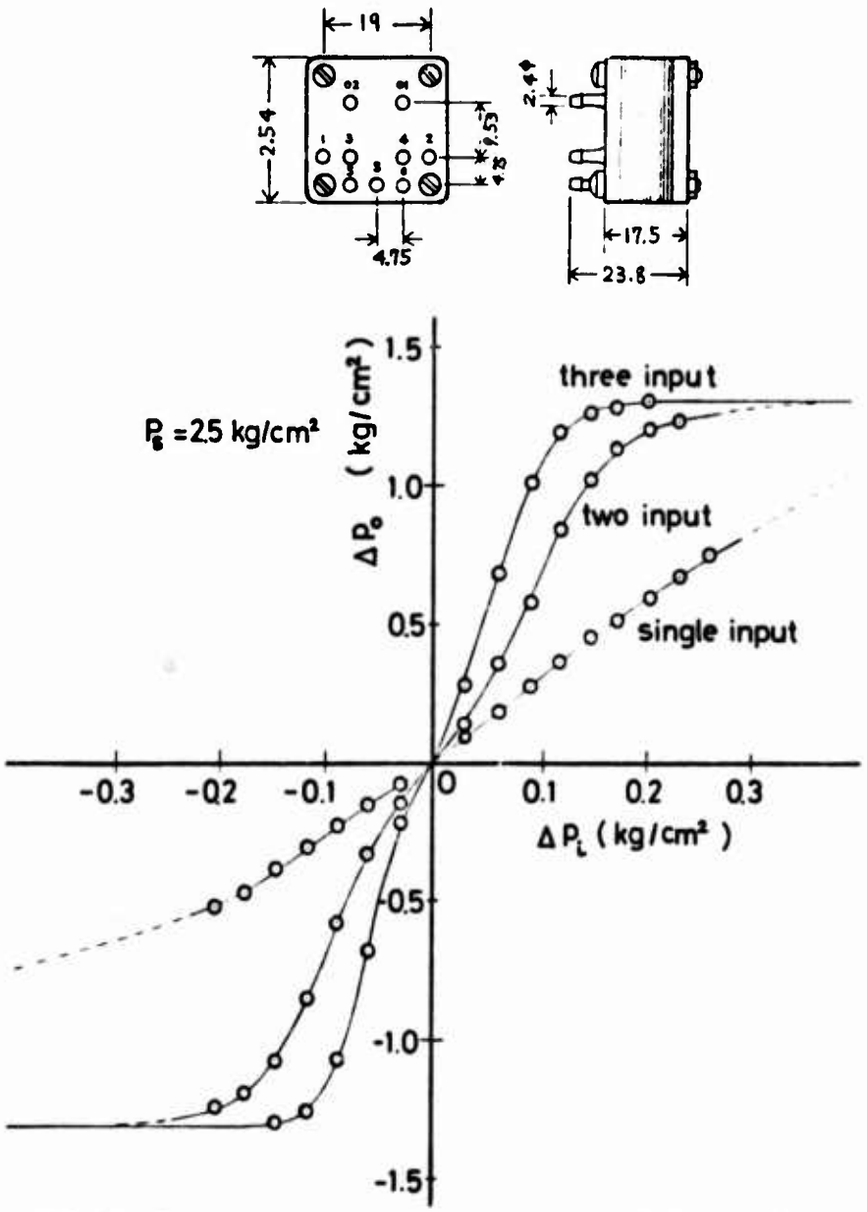


FIG.12 The input-output characteristics of the summing amplifier

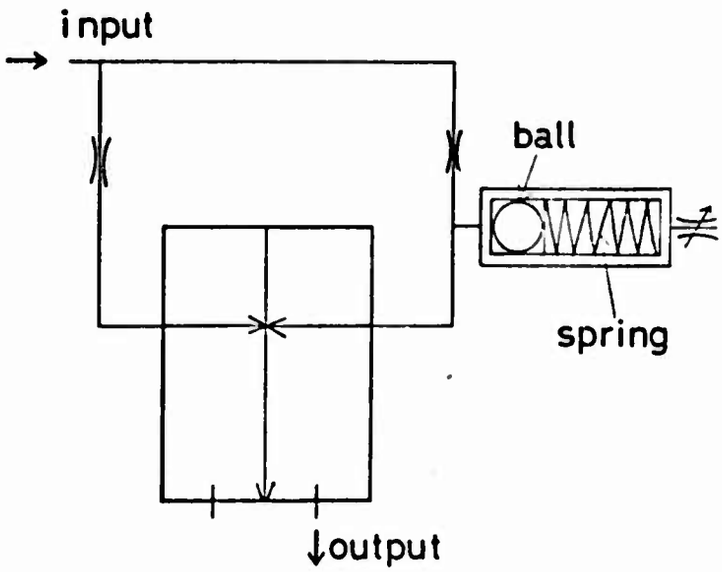


FIG.13 The construction of the differential circuit

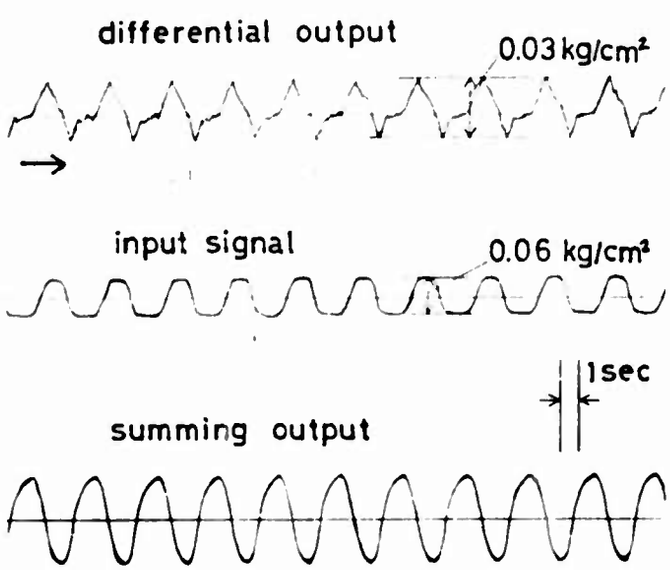


FIG.14 Output from differential circuits

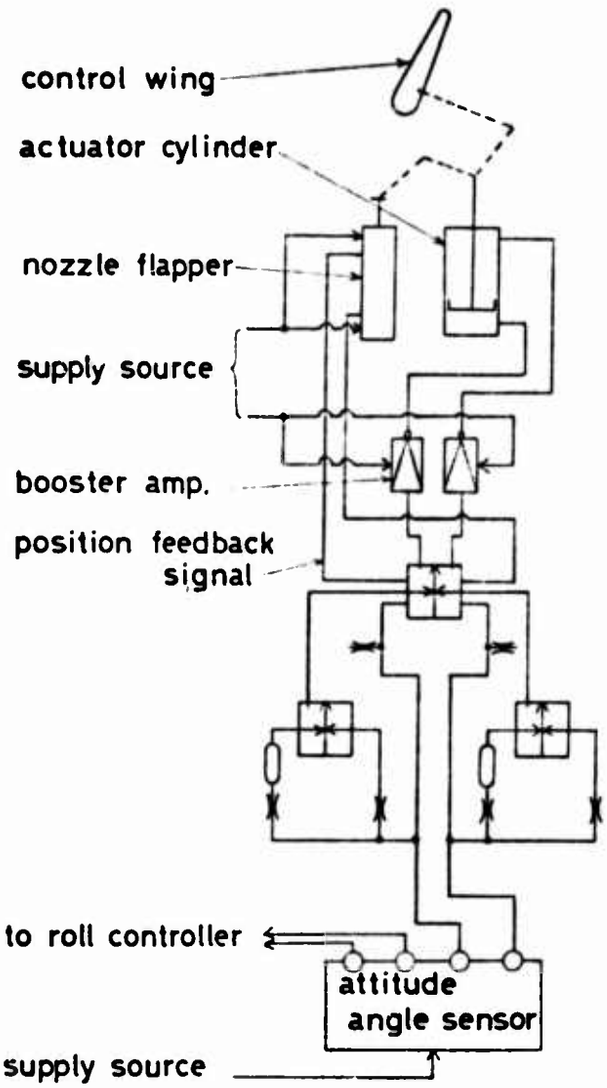


FIG 15 The diagram of the attitude control system in the final test (pitch control only)

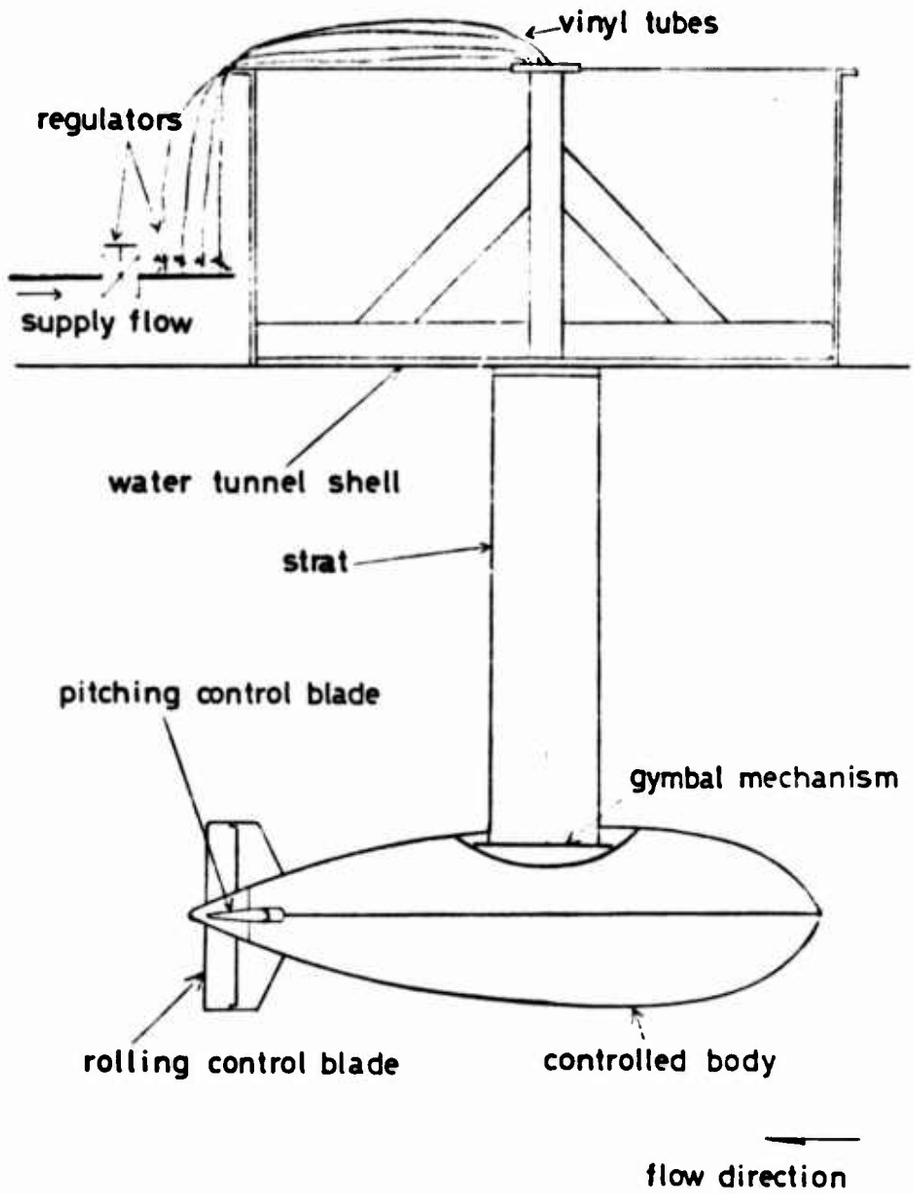
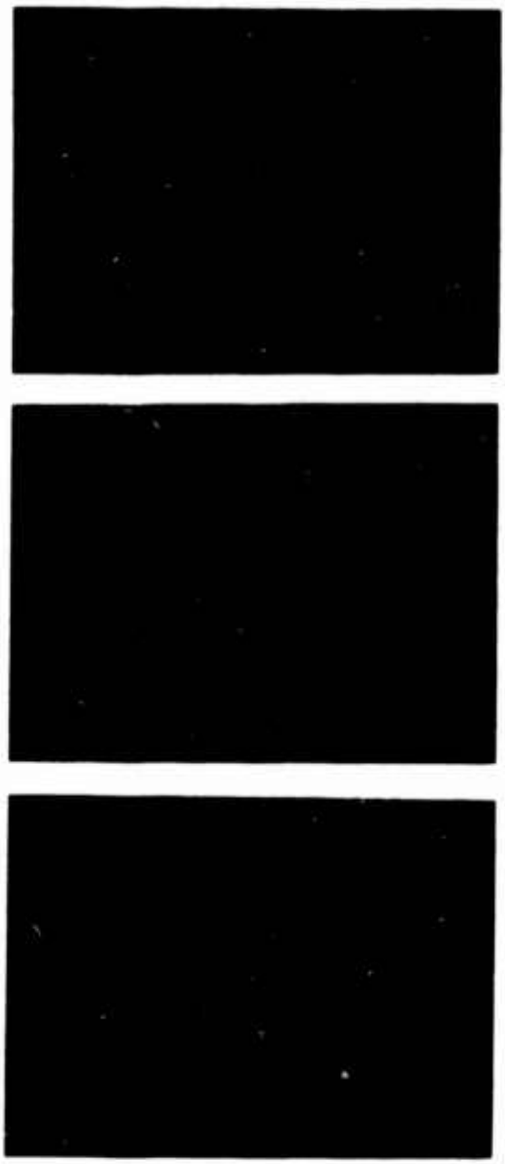


FIG.16 Outline of final test set up



← flow direction

FIG 17 Experiment in water tunnel

SYSTEM DESIGN FOR FLUIDIC MORTAR REPOSITIONING CONTROL WITH MULTIPLE NONLINEARITIES

C. N. Shen
Benet Weapons Laboratories
Watervliet Arsenal
Watervliet, New York 12189

ABSTRACT

The Mortar Control System employs fluidic components for its sensing elements and pneumatic devices for its controls. The following nonlinear behaviors exist in the system: The fluidic back-pressure switch is an on-off device with hysteresis. The pneumatic angular sensor can be adjusted to provide deadzone. The dry friction occurs at the piston walls.

This paper investigates the role of these physical parameters on the nonlinear system design. Dynamics of the mortar are modeled. Stability and limit cycle sustained oscillation are investigated. The performance of the fluidic mortar control system is also discussed.

STATEMENT OF THE PROBLEM

In this paper we discuss the application of fluidic components to an all-pneumatic mortar reposition system.

When a mortar is fired, the base plate turns backward, downward and perhaps sideway, which changes both the mortar elevation angle and the azimuth angle. To aim again at the same target, it is desirable to automatically reposition the elevation and azimuth angles back to the original values so that the range of the trajectory is approximately the same.

The mortar control system consists of a pneumatic angular sensing device and fluidic components such as a back-pressure switch, power amplifier, pneumatic piston-cylinder arrangement and a number of other mechanisms. The description of these devices is given in Reference [1].

---

[1] WOODS, G. W. and ZIEGLER, W. H., "Design of an Automatic Repositioning Mortar System", Watervliet Arsenal Technical Report WVT-7235, July 1972.

The purpose of this paper is to integrate these various elements into a complete system and to investigate the physical parameters of the elements in the nonlinear system design.

FLUIDIC COMPONENTS

Back pressure switches are used to indicate the mortar angular position. There are also two orifices, either or both of which can be blocked by the rotation of a cam which turns as the mortar changes its angular position. A back pressure switch is connected to each of these orifices. Blocking the orifices creates a back pressure in the switch as an input signal, designated S in Figure 1. There are also two outputs. If S is blocked the output O_1 is on. If S is open then output O_2 is on.

Experiments show that hysteresis exists for all these back pressure switches. As the input at S increases above a threshold the output O_1 starts going up until another input threshold is reached after which the output O_1 will remain constant as shown in Figure 2. There are two different input thresholds as the input decreases and the output is turned off. Figure 2 shows the hysteresis characteristics of the back pressure switch.

THE NONLINEAR ELEMENTS

A sensor is used to measure the relative angular position ε of the mortar barrel with reference to the axis of a cylinder which is mounted on the tripod of the mortar. The sensor rotates with trunions for supporting the tube, which changes its elevation angle as the mortar baseplate is displaced. The outside ring of the sensor has two orifices which are connected to two back pressure switches as shown in Figure 3. When the cam rotates, these orifices can be either open or closed depending on the design of the position of the flat surface of the cam in relation to the orifices location. Thus, the two orifices can be arranged so that they are either normally blocked (Figure 3) or normally open. In either case a deadzone can be created by adjusting the angular position of flat surfaces of the cam in relation to the two orifices.

The back pressure switch exhibits the characteristic of hysteresis. The output of the switch turns on at a high input threshold and off at a low input threshold. The output of the back pressure switch is connected to an on-off fluidic amplifier which has practically no hysteresis. The compressed air from the power amplifier pushes the piston of the cylinder which controls the angular position of the mortar.

For each input angle of rotation ε of the mortar barrel two pressure outputs can be obtained, one on each side of the piston inside the cylinder. This is a push-pull arrangement for an on-off fluidic system. The output-input relationship indicates that a combined hysteresis and deadzone exist as shown in Figure 4.

Figure 4 plots m, the net output force on piston by gas pressure versus ε, the relative angle of rotation of the input. The total hysteresis is h and the total deadzone is Δ. At point "a" where ε is $\frac{1}{2}(\Delta+h)$ output jumps from zero to M. As the input ε increases to point "b" the output is kept at the same amplitude M until the input drops to point "c". The input ε at point "c" is $(1/2)(\Delta-h)$ and the output drops to zero again. As the input further decreases to point "d" at the amount $-(1/2)(\Delta+h)$, the output becomes -M. The second half cycle repeats the same scheme. These are shown as points "d,e,f, and a".

In order to facilitate analysis the phase plane drawing of ε and $\dot{\varepsilon}$ is desirable. This can be achieved by transforming Figure 4 into Figure 5. There are four threshold values of ε in Figure 4. These values are $1/2(\Delta+h)$, $1/2(\Delta-h)$, $-1/2(\Delta-h)$, and $-1/2(\Delta+h)$, corresponding to four points in Figure 4 and four vertical lines in Figure 5. The output m = M for points "a,b and c" in Figure 4 is the shaped region which is marked m = M in Figure 5. The output m is zero for points "c and d" and is so indicated in an unshaded region in Figure 5. Thus Figure 5 gives the output at any region in the phase plane for a nonlinear element with both hysteresis and deadzone.

THE VELOCITIES AND EQUIVALENT MASS OF THE MORTAR

Figure 6 shows the initial, intermediate and final position of a mortar barrel under repositioning while the base plate is moving backward and a tripod supporting the cylinder stands still. A sleeve-hinge mechanism connects the piston to the mortar barrel. The motion of the barrel and that of the piston in the direction perpendicular to the axis of the sleeve should be equal, thus

$$R\dot{\theta} = \dot{c}\cos[90^\circ - (\theta+\phi)]$$

or

$$\dot{\theta} = \frac{1}{R}\dot{c}\sin(\theta+\phi) \qquad (1)$$

where

$\dot{\theta}$ = the angular velocity of the mortar barrel
$\dot{c}$ = linear velocity of the piston
θ = elevation angle of the barrel
ϕ = elevation angle of the cylinder
R = the distance between the sleeve and the baseplate
θ_f = reference elevation angle of the barrel, assumed to be constant.

The relative angular rotation of the mortar ε can be expressed as

$$\varepsilon = \theta_f - \theta \qquad (2)$$

Thus the derivative of the above gives

$$\frac{d\epsilon}{dt} = -\rho \frac{dc}{dt}$$

where

$$\rho = \frac{1}{R} \sin(\theta+\phi) \tag{3}$$

or $$\frac{dc}{dt} = -\frac{1}{\rho} \frac{d\epsilon}{dt} \tag{4}$$

The above equations relate the piston velocity in terms of the relative angular velocity of the mortar barrel.

The kinetic energy of the mortar and piston assembly can be written as

$$E = \frac{1}{2} I \dot{\theta}^2 + \frac{1}{2} m \dot{c}^2 \tag{5}$$

where I is the moment of inertia of the mortar about the ball at the baseplate and m is the mass of the piston assembly.

Substituting Equation (1) into Equation (5) we have

$$E = \frac{1}{2} m_e \dot{c}^2 \tag{6}$$

where the equivalent mass m_e is

$$m_e \cong m + \frac{I}{R^2} \sin^2(\theta+\phi)$$

This equivalent mass will be used to formulate the dynamics of the system.

THE DYNAMICS AND DRY FRICTION

The mortar barrel is rotating while the piston is set in motion by the pressure on one or both sides of the piston as shown in Figure 7. Let the equivalent mass of the piston and its connected part be m_e, the coefficient of viscous damping be μ, the displacement of the piston be c, the net pneumatic pressure on the piston be p, the area of the piston be A and the dry friction be G. The equation of motion becomes for net pneumatic pressure p on the left of the piston

$$m_e \frac{d^2c}{dt^2} = -\mu \frac{dc}{dt} + pA - G \qquad \text{if } \frac{dc}{dt} > 0 \tag{8}$$

$$m_e \frac{d^2c}{dt^2} = -\mu \frac{dc}{dt} + pA + G \qquad \text{if } \frac{dc}{dt} < 0 \tag{9}$$

For zero net pressure on the piston

$$m_e \frac{d^2c}{dt^2} = -\mu \frac{dc}{dt} - G \qquad \text{if } \frac{dc}{dt} > 0 \tag{10}$$

$$m_e \frac{d^2c}{dt^2} = -\mu \frac{dc}{dt} + G \qquad \text{if } \frac{dc}{dt} < 0 \tag{11}$$

For net pneumatic pressure p on the right of the piston

$$m_e \frac{d^2c}{dt^2} = -\mu \frac{dc}{dt} - pA - G \qquad \text{if } \frac{dc}{dt} > 0 \tag{12}$$

$$m_e \frac{d^2c}{dt^2} = -\mu \frac{dc}{dt} - pA + G \qquad \text{if } \frac{dc}{dt} < 0 \tag{13}$$

where the quantities m_e, μ, p, A and G are all positive real parameters. The above equations indicate that the pneumatic force pA depends on which side of the piston is pressurized and that the dry friction is a function of the direction of the velocity of the piston.

Substituting Equation (4) into Equation (8) one obtains

$$-\frac{m_e}{\rho} \frac{d^2\epsilon}{dt^2} = \frac{\mu}{\rho} \frac{d\epsilon}{dt} + pA - G \tag{14}$$

which is equivalent to

$$\tau \frac{d^2\epsilon}{dt^2} + \frac{d\epsilon}{dt} + q = 0 \tag{15}$$

where

$$q = Km_s - f \tag{16}$$

$$K = \rho/\mu, \tag{17}$$

$$\tau = m_e/\mu \tag{18}$$

$$m_s = M = pA \qquad \text{if pressure applies on the left} \tag{19}$$

$$m_s = 0 \qquad \text{if net pressure on the piston is zero} \tag{20}$$

$$m_s = -M = -pA \qquad \text{if pressure applies on the right} \tag{21}$$

$$f = F = \frac{\rho G}{\mu} \qquad \text{if } \frac{d\epsilon}{dt} < 0 \tag{22}$$

$$f = -F = -\frac{\rho G}{\mu} \qquad \text{if } \frac{d\epsilon}{dt} > 0 \tag{23}$$

Equations (19) to (23) are derived based on Equations (8) to (11).

To summarize the above formulations there are six regions in the

phase plane plot in Figure 8. The force function q in Equation (15) takes the following values:

Value of $q = Km_s - f$	net pressure on piston	relative mortar velocity	Equation number
$KM + F$	on left	$\dot{\varepsilon} > 0$	(24)
$KM - F$	on left	$\dot{\varepsilon} < 0$	(25)
$0 - F$	none	$\dot{\varepsilon} < 0$	(26)
$-KM - F$	on right	$\dot{\varepsilon} < 0$	(27)
$-KM + F$	on right	$\dot{\varepsilon} > 0$	(28)
$0 + F$	none	$\dot{\varepsilon} > 0$	(29)

THE FEEDBACK SYSTEM

It has been shown that the quantity $q = Km_s - f$ is a function of both the force on the piston and the dry friction. Thus this quantity q can be considered as the input of the linear element. However the force Km_s on the piston depends on the hysteresis and the deadzone of the nonlinear element, while the dry friction f relies on the velocity of the output of the linear element. Equation (16) gives the junction point between the nonlinear and linear elements in Figure 9.

In Figure 9 a feedback system is shown where the output mortar angle θ is subtracted from a reference setting r to obtain the error signal ε, which is the relative angular motion of the mortar and serves as the input to the nonlinear element.

THE NON-DIMENSIONIZED SYSTEM

The key equation in our analysis is Equation (15) where $\dot{\varepsilon}$ is related to θ by Equations (1) - (4), τ is given in Equation (18) and q is shown in Equations (16) - (29) for the nonlinear elements. This equation can be further simplified by multiplying through by τ and using the following transformation:

$$P = K M \tau \tag{30}$$

$$x = \frac{\varepsilon}{P} = \frac{\varepsilon}{KM\tau} \tag{31}$$

$$\sigma = t/\tau \tag{32}$$

Thus Equation (15) becomes

$$\frac{d^2x}{d\sigma^2} + \frac{dx}{d\sigma} + \frac{q}{KM} = 0 \tag{33}$$

or

$$x'' + x' + \frac{q}{KM} = 0 \tag{34}$$

Where

$$x' = \frac{dx}{d\sigma} \tag{35}$$

with the initial conditions

$$x_o = \frac{\varepsilon_o}{KM\tau} = \frac{\varepsilon_o}{P} \tag{36}$$

and

$$x_o' = \left(\frac{dx}{d\sigma}\right) = \frac{\tau}{P}\left(\frac{d\varepsilon}{dt}\right)_o = \frac{\tau}{P}\dot{\varepsilon}_o = \frac{\dot{\varepsilon}_o}{KM} \tag{37}$$

The values of q/KM in Equation (33) and its regions in the phase plane are given as follows:

q/KM	Region number	Region of x in phase plane	Region of x' in phase plane	Time Non-dimensional	Equation Number
$\frac{q_1}{KM} = 1 + \frac{F}{KM}$	(1)	$\frac{\Delta+h}{2P} < x$	$0 < x'$	$0 \leq \sigma \leq \sigma_1$	(38)
$\frac{q_2}{KM} = 1 - \frac{F}{KM}$	(2)	$\frac{\Delta-h}{2P} < x$	$x' < 0$	$\sigma_1 \leq \sigma \leq \sigma_a$	(39)
$\frac{q_3}{KM} = 0 - \frac{F}{KM}$	(3)	$\frac{-\Delta-h}{2P} < x < \frac{\Delta-h}{2P}$	$x' < 0$	$\sigma_a \leq \sigma \leq \sigma_b$	(40)
$\frac{q_4}{KM} = -1 - \frac{F}{KM}$	(4)	$x < \frac{-\Delta-h}{2P}$	$x' < 0$	-	(41)
$\frac{q_5}{KM} = -1 + \frac{F}{KM}$	(5)	$x < \frac{-\Delta+h}{2P}$	$0 < x'$	-	(42)
$\frac{q_6}{KM} = 0 + \frac{F}{KM}$	(6)	$\frac{-\Delta+h}{2P} < x < \frac{\Delta+h}{2P}$	$0 < x'$	-	(43)

The above relationship is shown by the phase plane in Figure 10. Note that Equation (33) is non-dimensionized and the values of q/KM become either 1 or -1 if there is no dry friction (F = 0) in Equations (38) - (43).

THE ANALYTIC SOLUTION FOR TRAJECTORIES IN PHASE-PLANE

For any starting conditions x_0 and x_0' in region (1) of Figure 10 when $0 \leq \sigma \leq \sigma_1$ the analytic solution for Equation (33) is

$$x' = x_0' e^{-\sigma} + \frac{q_1}{KM} (e^{-\sigma} - 1) \tag{44}$$

$$x = x_0 - \frac{q_1}{KM} \sigma + (x_0' + \frac{q_1}{KM}) (1 - e^{-\sigma}) \tag{45}$$

When $\sigma = \sigma_1$ the region ends at

$$x = x_1' = 0 \tag{46}$$

Thus

$$0 = x_0' e^{-\sigma_1} + \frac{q_1}{KM} (e^{-\sigma_1} - 1) \tag{47}$$

from which one obtains

$$\sigma_1 = \ln[(x_0' + \frac{q_1}{KM}) / (\frac{q_1}{KM})] \tag{48}$$

From Equation (45) we have

$$x_1 = x_0 - (\frac{q_1}{KM}) \sigma_1 + x_0' \tag{49}$$

where q_1/KM is given in Equation (38).

The end conditions (46) and (49) for region (1) become the initial conditions of Equation (33) in region (2) when $\sigma_1 \leq \sigma \leq \sigma_a$. Thus

$$x' = x_1' e^{-(\sigma-\sigma_1)} + \frac{q_2}{KM} [e^{-(\sigma-\sigma_1)} - 1] \tag{50}$$

$$x = x_1 - \frac{q_2}{KM} (\sigma - \sigma_1) + (x_1' + \frac{q_2}{KM}) [1 - e^{-(\sigma-\sigma_1)}] \tag{51}$$

When $\sigma = \sigma_a$ the region ends at

$$x_a = (\Delta-h)/(2P) \tag{52}$$

Let the initial condition of x at region (1) be

$$x_0 = (\Delta+h)/(2P) \tag{53}$$

By using Equations (51) - (53) we can determine $\sigma_a - \sigma_1$ by

$$-\frac{h}{P} = (x_1 - x_o) - \frac{q_2}{KM}(\sigma_a - \sigma_1) + (\frac{q_2}{KM})[1 - e^{-(\sigma_a - \sigma_1)}] \quad (54)$$

where $x_1 - x_o$ is given in Equation (49).

From Equations (46) and (50) the final condition of x_a' becomes

$$x_a' = \frac{q_2}{KM}[e^{-(\sigma_a - \sigma_1)} - 1] \quad (55)$$

where q_2/KM is given in Equation (39).

The end conditions (52) and (55) for region (2) become the initial conditions of Equation (33) in region (3) when $\sigma_a \leq \sigma \leq \sigma_b$. Thus

$$x' = x_a' e^{-(\sigma-\sigma_a)} + \frac{q_3}{KM}[e^{-(\sigma-\sigma_a)} - 1] \quad (56)$$

$$x = x_a - \frac{q_3}{KM}(\sigma-\sigma_a) + (x_a' + \frac{q_3}{KM})[1 - e^{-(\sigma-\sigma_a)}] \quad (57)$$

When $\sigma = \sigma_b$ the region ends at

$$x_b = (-\Delta-h)/(2P) \quad (58)$$

From Equations (52), (57) and (58) we can determine $\sigma_b - \sigma_a$ by

$$-\frac{\Delta}{P} = -\frac{q_3}{KM}(\sigma_b - \sigma_a) + (x_a' + \frac{q_3}{KM})[1 - e^{-(\sigma_b - \sigma_a)}] \quad (59)$$

after which the final condition of x_b' becomes

$$x_b' = x_a' e^{-(\sigma_b - \sigma_a)} + \frac{q_3}{KM}[e^{-(\sigma_b - \sigma_a)} - 1] \quad (60)$$

where q_3/KM is given in Equation (40).

Equations (58) and (60) are the final conditions of region (3).

Since the system is symmetric about the origin in Figure 10, the analytic solution for regions (4), (5) and (6) is similar to the regions (1), (2) and (3). One can derive these equations without difficulty.

SUSTAIN OSCILLATION FOR SYSTEM WITH NO DRY FRICTION

In the case where f = 0 in Equations (38) - (43) there is no dry friction in the system. The analytical solution for this special case is given in Appendix A with the following final conditions:

$$x_b' = x_o' e^{-\sigma_a} + (e^{-\sigma_a} - 1) + \Delta/P \tag{61}$$

$$x_b = x_o - \sigma_a + (x_o' + 1)(1 - e^{-\sigma_a}) - \Delta/P \tag{62}$$

The above formulae relate the final conditions x_b, x_b' in terms of the initial conditions x_o, x_o' in half a cycle. Under the conditions of sustained oscillation the final state remains the same value as the original initial state in one cycle. Since the system is symmetric with respect to the origin, the magnitude of the final state x_b, x_b' in half a cycle is the same as the magnitude of the initial state x_o, x_o', but opposite in sign. Thus from Equations (61) and (62)

$$x_b' = -x_o' = x_o' e^{-\sigma_a} + (e^{-\sigma_a} - 1) + \Delta/P \tag{63}$$

$$x_b = -x_o = x_o - \sigma_a + (x_o' + 1)(1 - e^{-\sigma_a}) - \Delta/P \tag{64}$$

We can solve Equation (63) for $-x_o'$ to give

$$x_b' = -x_o' = \left(\frac{\Delta}{2P}\right) \frac{2}{1+e^{-\sigma_a}} - \frac{1-e^{-\sigma_a}}{1+e^{-\sigma_a}} \tag{65}$$

and

$$x_o' + 1 = \left(2 - \frac{\Delta}{P}\right) \frac{1}{1+e^{-\sigma_a}} \tag{66}$$

Substituting Equation (66) into Equation (64) and solving for $-x_o$ we have

$$x_b = -x_o = -\frac{\Delta}{2P} - \frac{\sigma_a}{2} + \left(1 - \frac{\Delta}{2P}\right) \frac{1-e^{-\sigma_a}}{1+e^{-\sigma_a}} \tag{67}$$

Equations (65) and (67) are the final state in terms of the parameters σ_a and $\Delta/(2P)$. This is called the Hamal locus of the system if x_b and x_b' are plotted in the phase plane with the parameters σ_a and $\Delta/2P$. Sustained oscillation will occur if this Hamal locus [2] is intersected by the line

$$x_b^* = (-\Delta - h)/(2P) \tag{68}$$

in the third quadrant.

---

[2] GILLE, J. C., PELEGRIN, M. J. and DECAULNE, P., "Feedback Control Systems," McGraw-Hill Book Company, 1959.

Since the value of x_o and x_o' are positive and located in the first quadrant in the phase plane, the value of x_b and x_b' should be located in the third quadrant. There will be no sustained oscillation if the Hamal locus given by Equations (65) and (67) is not intersected in the third quadrant.

For example if $\Delta/(2P) = 1$ in Equations (65) and (67) we obtain

$$x_b' = 1 \tag{69}$$

$$x_b = -1 - \sigma_a/2 \tag{70}$$

which is in the second quadrant for any positive value of σ_a. We can thus conclude that there is no sustained oscillation for any arbitrary positive value of hysteresis $h/(2P)$ if $\Delta/(2P) = 1$ is chosen for the deadzone.

One can evaluate the final state for $\sigma_a = 0$ in Equations (67) and (65) as

$$x_b(\sigma_a = 0) = -\Delta/(2P) \tag{71}$$

$$x_b'(\sigma_a = 0) = \Delta/(2P) \tag{72}$$

which lie on the second quadrant.

Let us increase the value of σ_a from zero to some positive values. The value of x_b' will decrease from $\Delta/(2P)$. The Hamal locus moves toward the third quadrant from the second quadrant when x_b' becomes zero in Equation (65), i.e.,

$$x_b' = -x_o' = 0 \tag{73}$$

thus,

$$1 - e^{-\sigma_a} = 2\left(\frac{\Delta}{2P}\right) \tag{74a}$$

or

$$-\frac{\sigma_a}{2} = \frac{1}{2} \ln\left[1 - 2\left(\frac{\Delta}{2P}\right)\right] \tag{74b}$$

If Equations (74a) and (74b) are substituted into Equation (67) we have

$$x = \frac{1}{2} \ln\left[1 - 2\left(\frac{\Delta}{2P}\right)\right], \quad 0 \leq \Delta/(2P) \leq \frac{1}{2} \tag{75}$$

Let us compare x_b approaching third quadrant in Equation (75) and x_b^* in Equation (68). If x_b lies on the right of x_b^* sustained oscillation will occur. To avoid sustained oscillation x_b will be on the left of x_b^*, i.e.,

$$\frac{1}{2} \ell n[1 - 2(\frac{\Delta}{2P})] < (-\Delta - h)/(2P) \tag{76}$$

or

$$h/(2P) < - \Delta/(2P) - 0.5 \ell n[1 - 2\Delta/(2P)] \tag{77}$$

The above equation indicates that the hysteresis should be kept smaller than a certain value if the deadzone is given.

For the marginal case of stability the critical value of the hysteresis $h^*/(2P)$ is related to the deadzone $\Delta/(2P)$ by the following equation:

$$h^*/(2P) = - \Delta/(2P) - 0.5 \ell n[1 - 2\Delta/(2P)] \tag{78}$$

The following table gives the relationship of $h^*/(2P)$ vs $\Delta/(2P)$ at the margin of sustained oscillation (or stability):

Table 1. Critical Value of Hysteresis vs Deadzone at the Margin of Sustained Oscillation

$\Delta/(2P)$	0.5	0.45	0.40	0.35	0.30	0.25
$h^*/(2P)$	∞	0.700	0.405	0.252	0.158	0.097
$\Delta/(2P)$	0.20	0.15	0.10	0.05	0	
$h^*/(2P)$	0.055	0.028	0.0115	0.0025	0	

For any given $\Delta/(2P)$ sustained oscillation will not occur if the value of $h/(2P)$ is less than the above critical value of hysteresis $h^*/(2P)$.

The implication from Equation (73) is that the initial condition of x_o' is

$$x_o' = 0 \tag{79}$$

Similarly the implication from Equation (68) is that the initial condition x_o^* is at the threshold of switching line

$$x_o = x_o^* = (\Delta + h)/(2P) \tag{80}$$

The above implies that Equations (79) and (80) give the initial conditions

for systems having marginal stability.

MARGINAL STABILITY WITH DRY FRICTION

First it is desired to express the hysteresis $h/(2P)$ and the dead-zone $\Delta/(2P)$ in terms of certain known parameters of q/KM and x_0' and x_a'.

From Equation (48) we have

$$x_1 - x_0 = x_0' - \left(\frac{q_1}{KM}\right) \ln \left(\frac{x_0' + q_1/KM}{q_1/KM}\right) \tag{81}$$

From Equation (55) one obtains

$$\sigma_a - \sigma_1 = -\ln\left[\frac{x_a' + q_2/KM}{q_2/KM}\right] \tag{82}$$

It is noted here that the initial condition for x_0 is given in Equation (53). Adding Equations (54) and (55) yields

$$-\frac{h}{P} = (x_1 - x_0) - x_a' - \frac{q_2}{KM}(\sigma_a - \sigma_1) \tag{83}$$

Substituting Equations (81) and (82) into (83) gives

$$\frac{h}{2P} = -\frac{1}{2}\left[x_0' - \left(\frac{q_1}{KM}\right)\ln\left(\frac{x_0' + q_1/KM}{q_1/KM}\right)\right] + \frac{1}{2}\left[x_a' - \left(\frac{q_2}{KM}\right)\ln\left(\frac{x_a' + q_2/KM}{q_2/KM}\right)\right] \tag{84}$$

Thus the hysteresis is given as a function of the parameters x_0' and x_a' besides the fixed constants q_1/KM and q_2/KM.

From Equation (60) one obtains

$$e^{-(\sigma_b - \sigma_a)} = \frac{x_b' + q_3/KM}{x_a' + q_3/KM} \tag{85}$$

Thus

$$\sigma_b - \sigma_a = -\ln\left(\frac{x_b' + q_3/KM}{x_a' + q_3/KM}\right) \tag{86}$$

Adding Equations (59)and (60) yields

$$-\frac{\Delta}{P} = -\frac{q_3}{KM}(\sigma_b - \sigma_a) + x'_a - x'_b \tag{87}$$

Substituting Equation (86) into (87) gives

$$-\frac{\Delta}{2P} = \frac{1}{2}(x'_a - x'_b) - \frac{1}{2}\frac{q_3}{KM}\ln\left(\frac{x'_a + q_3/KM}{x'_b + q_3/KM}\right) \tag{88}$$

For the condition of sustained oscillation

$$x'_b = -x'_o \tag{89}$$

Thus Equation (88) becomes

$$\frac{\Delta}{2P} = -\frac{1}{2}(x'_a + x'_o) + \frac{1}{2}\frac{q_3}{KM}\ln\left(\frac{x'_a + q_3/KM}{-x'_o + q_3/KM}\right) \tag{90}$$

It is noted here that the dead zone is also expressed as a function of the parameters x'_o and x'_a, besides the fixed constant q_3/KM.

The physical constant q/KM is given in Equations (38) - (43). If these values are substituted into Equations (84) and (90) we have

$$\frac{h}{2P} = -\frac{1}{2}\left[x'_o - \left(1 + \frac{F}{KM}\right)\ln\left(\frac{x'_o + 1 + F/KM}{1 + F/KM}\right)\right] +$$

$$+\frac{1}{2}\left[x'_a - \left(1 - \frac{F}{KM}\right)\ln\left(\frac{x'_a + 1 - F/KM}{1 - F/KM}\right)\right] \tag{91}$$

and

$$\frac{\Delta}{2P} = -\frac{1}{2}(x'_a + x'_o) - \frac{1}{2}\frac{F}{KM}\ln\left(\frac{x'_a - F/KM}{-x'_o - F/KM}\right) \tag{92}$$

In the case where the dry friction is absent, F = 0, Equations (91) and (92) become

$$h/(2P) = -\frac{1}{2}[x_o' - \ell n\,(x_o' + 1)] + \frac{1}{2}\,[x_a' - \ell n(x_a' + 1)] \quad (93)$$

$$\Delta/(2P) = -\frac{1}{2}\,(x_a' + x_o') \quad (94)$$

In the case where $x_o' = 0$ for the marginal stability the above equations give

$$h/(2P) = 0.5[x_a' - \ell n(x_a' + 1)] \quad (95)$$

and

$$\Delta/(2P) = -0.5\,x_a' \quad (96)$$

One may obtain the following relationship from the above equations

$$h/(2P) = -\Delta/(2P) - 0.5\,\ell n[1 - 2\Delta/(2P)] \quad (97)$$

which is given previously in Equation (78) derived by a different method.

In determining the marginal case of stability we notice that x_o' is zero in Equation (79) from previous derivations where dry friction is assumed to be zero. This is also true if dry friction does occur. Under these conditions we have from Equations (91) and (92)

$$\frac{h}{2P} = \frac{1}{2}\left[x_a' - \left(1 - \frac{F}{KM}\right)\ell n\left(\frac{x_a' + 1 - F/KM}{1 - F/KM}\right)\right] \quad (98)$$

$$\frac{\Delta}{2P} = -\frac{1}{2}\,x_a' - \frac{1}{2}\,\frac{F}{KM}\,\ell n\left(\frac{x_a' - F/KM}{-F/KM}\right) \quad (99)$$

Equations (98) and (99) are in terms of the parameter x_a' for any given dry friction F/KM. Table 2 shows the choice of x_a' to give a set of values for h/(2P) to be in the neighborhood of 0.027 and 0.099 for different values of F/KM. For the same hysteresis h/(2P) the higher the dry friction F/KM the lower will be the critical value of dead zone $\Delta/(2P)$. That is, with h/(2P) remaining to be 0.027, $\Delta/(2P)$ is 0.150 if F/KM is zero, $\Delta/(2P)$ is 0.038 if F/KM is 0.25, $\Delta/(2P)$ is 0.016 if F/KM is 0.50 and $\Delta/(2P)$ is 0.0055 if F/KM is 0.75. Thus dry friction does help to stabilize the system.

Equation (77) gives the maximum allowable hysteresis for a given dead zone. The converse is also true. For a given set of parameters for dry friction F/KM and hysteresis h/(2P) one can determine the minimum amount of dead zone $\Delta/(2P)$ required to stabilize the nonlinear system. This can be achieved by using Equations (98) and (99) or

examining a table similar to Table 2.

Table 2. Marginal Stability for Systems with Dead Zone and Dry Friction, While Hysteresis Is Small.

F/KM	0		0.25		0.50		0.75	
F/KM		0		0.25		0.50		0.75
h/(2P)	0.027		0.027		0.028		0.027	
h/(2P)		0.097		0.098		0.100		0.101
x'_a	-0.29		-0.25		-0.20		-0.13	
x'_a		-0.50		-0.42		-0.325		-0.20
Δ/(2P)	0.150		0.038		0.016		0.0055	
Δ/(2P)		0.250		0.087		0.038		0.0105
(Δ+h)/P	0.354		0.130		0.088		0.065	
(Δ+h)/P		0.694		0.370		0.276		0.223

Table 3. Marginal Stability for Systems with Dead Zone And Dry Friction, While Hysteresis Is Large.

F/KM	0		0.25		0.50		0.75	
F/KM		0		0.25		0.50		0.75
h/(2P)	1.025		.997		1.032		1.00	
h/(2P)		∞		∞		∞		∞
x'_a	-0.95		-0.73		-0.497		- .24997	
x'_a		-1.0		-0.75		-0.50		-0.25
Δ/(2P)	0.475		0.193		0.075		0.017	
Δ/(2P)		0.500		0.202		0.077		0.017
(Δ+h)/(2P)	1.500		1.190		1.107		1.017	
(Δ+h)/(2P)		∞		∞		∞		∞

PERFORMANCE-RESOLUTION IN THE FINAL ELEVATION ANGLE

It is inherent for a nonlinear system with hysteresis and dead zone that the final state can rest at a wide range of values. This is to say that the final elevation angle of the mortar has a range of uncertainty.

Let us reexamine Figure 4 where the error ε starts at point b with the output M driving the error ε back to point c. At point c the output m drops to zero. If the error ε of the system cannot reach point d then there is no chance for the output to go to -M. Thus the error will stay between point c and d. Similarly if the error ε starts at point e there is a possibility that the error ε will remain between point f and a. Combining the above two cases the error ε can stop at any value between point d and a, which is a distance of $(\Delta+h)$. This is the resolution of the system, i.e. a range of uncertainty where the final elevation angle of the mortar stops. The non-dimensionized resolution $(\Delta+h)/P$ is shown in the last rows of Tables 2 and 3.

For best performance in resolution these numbers might be made as small as possible for any given constant hysteresis $h/(2P)$, by choosing the smallest $\Delta/(2P)$ in Table 2 or 3. However this will increase the value of F/KM to approach unity which makes the system response very sluggish and undesirable. This will be shown in the next section.

PERFORMANCE-SLUGGISHNESS IN RESPONSE TIME

As an indication of the sluggishness of the system we take region 2 in Figure 10 where the final state x_a' is in terms of the response time $\sigma_a - \sigma_1$ in Equation (55). Solving for the response time with the aid of Equation (39),

one obtains

$$\sigma_a - \sigma_1 = \ln\left(\frac{1 - F/KM}{x_a' + 1 - F/KM}\right) \tag{100}$$

Similarly one solves for the response time in Equation (86) with the aid of Equation (40)

$$\sigma_b - \sigma_a = -\ln\left(\frac{F/KM}{-x_a' + F/KM}\right) \tag{101}$$

Adding the above two equations we have

$$\sigma_b - \sigma_1 = \ln\left[\left(\frac{-x_a' + F/KM}{F/KM}\right)\left(\frac{1 - F/KM}{x_a' + 1 - F/KM}\right)\right] \tag{102}$$

In order that the system response time be reasonably fast we put an upper bound T for the actual response time $\sigma_b - \sigma_1$

$$\sigma_b - \sigma_1 \leq T \tag{103}$$

or

$$e^{(\sigma_b - \sigma_1)} \leq e^T \tag{104}$$

Taking the exponential of Equation (102) and comparing with Equation (104) we have

$$\left(\frac{-x'_a + F/KM}{F/KM}\right)\left(\frac{1 - F/KM}{x'_a + 1 - F/KM}\right) \leq e^T \tag{105}$$

It is noted that

$$0 < F/KM \leq 1 \tag{106}$$

and

$$x'_a + 1 - F/KM > 0 \tag{107}$$

Thus

$$(-x'_a + F/KM)(1 - F/KM) \leq e^T [x'_a + (1 - F/KM)](F/KM) \tag{108}$$

or

$$x'_a \geq \frac{-(e^T - 1)(F/KM)(1 - F/KM)}{(e^T - 1)(F/KM) + 1} \tag{109}$$

where x'_a is less than zero in region 2. The critical value of x'_a is shown in Table 4 for given dry friction F/KM and allowable response time T.

Table 4. Critical Value of x'_a for given F/KM and T.

e^T =	F/KM=0	0.10	.25	0.5	0.75	1.0
1	0	0	0	0	0	0
1.25	0	-0.0220	-0.044	-0.0555	-0.0394	0
1.67	0	-0.0561	-0.107	-0.125	-0.083	0
2.50	0	-0.117	-0.205	-0.214	-0.1322	0
5.00	0	-0.257	-0.375	-0.333	-0.1875	0
11	0	-0.450	-0.536	-0.417	-0.221	0
101	0	-0.817	-0.722	-0.490	-0.247	0
∞	0	-0.900	-0.750	-0.500	-0.250	0

It is shown in Table 3 and Equation(109)that the critical x'_a is a function of (F/KM) if a response time T is assigned. For example, let us choose $e^T = 5.00$, then Equation(109)gives

$$x'_a \geq \frac{-(4)\ (F/KM)\ (1 - F/KM)}{4(F/KM) + 1} \tag{110}$$

If a value of F/KM = 0.50 is used then

$$x'_a \geq -0.333 \tag{111}$$

The above suggest x' can be -0.332 but not -0.334 due to the negative polarity of x'_a.

SYSTEM DESIGN

Here we employ the results from previous sections on stability, response time and resolution for system design. The margin of stability can be evaluated from Equations (98) and (99) or Table 2. This is plotted with $h/(2P) = 0.100$ in Figure 11 as a solid line under which is the shaded stable region. The values of $(\Delta+h)/P$ are marked on the curve having F/KM as abscissa and x'_a as ordinate. The response time can be determined from Equation (109) or Table 4. This is shown with $e^T = 5.00$ in Figure 11 as a chain-dotted line above which is the shaded good response.

It is seen that there is a feasible region where both stability and good response can be achieved. This triangular region is located where $0.32 \leq F/KM \leq 0.59$. On the other hand where $F/KM \leq 0.32$ or $0.59 \leq F/KM$ there is no feasible region.

In order to obtain best resolution or lowest uncertainty we choose the lowest $(\Delta+h)/P$ in the triangular shade region. This locates at $F/KM = 0.59$, $x'_a = -0.28$, and $(\Delta+h)/P = 0.26$. We can conclude that the dry friction of $F/KM = 0.59$ and the dead zone of $\Delta/(2P) = 0.03$ are our choices in optimizing our system design, which gives us the minimum amount of uncertainty satisfying our required response time and stability.

However, we may use $F/KM = 0.32$ at $x'_a = -.39$ if the dead zone is not critical as the ratio Δ/h is small in this case. The feasible region for all system designs is shown as a shaded area in Figure 11.

CONCLUSION

A method is devised for the system design of fluidic mortar repositional control. The system has nonlinear on-off fluidic elements, which give hysteresis and dead zone. The mortar has dry friction which contributes further nonlinearity. By choosing the proper dead zone, the nonlinear system can be compensated such that the stability and performance are within the design criterion.

CAPTION

Fig. 1 Fluidic Back Pressure Switch
Fig. 2 Hysteresis Characteristics of the Back Pressure Switch
Fig. 3 Schematic Diagram for sensor system with Back Pressure Switch
Fig. 4 Hysteresis and Dead Zone for Piston Force as Output vs. Mortar Angle as Input

Fig. 5 Phase Plane Diagram Without Dry Friction.
Fig. 6 Mortar Barrel Angular Positions
Fig. 7 Dry Friction on Piston
Fig. 8 Phase Plane Diagram with Dry Friction
Fig. 9 The Feedback System
Fig. 10 Phase Plane Diagram with Non-dimensional Variables and Parameters
Fig. 11 Feasible Region for System Design

APPENDIX A

ANALYTIC SOLUTION FOR SYSTEM WITH NO DRY FRICTION

For a special case where no dry friction occurs in the system the forcing function q becomes very simple and is derived from Equations (38) - (43) as

$$q_1/KM = q_2/KM = 1 \tag{A1}$$

$$q_3/KM = q_6/KM = 0 \tag{A2}$$

$$q_4/KM = q_5/KM = -1 \tag{A3}$$

Let the system start at $\sigma = 0$ with

$$x_o = (\Delta+h)/(2P) \tag{A4}$$

and

$$x_o' = \text{arbitrary} \tag{A5}$$

For regions (1) and (2) where $q_1/KM = q_2/KM = 1$ during $0 \leq \sigma \leq \sigma_a$

one obtains from Equations (44) and (45) the following

$$x' = x'_o e^{-\sigma} + (e^{-\sigma} - 1) \tag{A6}$$

$$x = x_o - \sigma + (x'_o + 1)(1 - e^{-\sigma}) \tag{A7}$$

When $\sigma = \sigma_a$ the region ends at

$$x_a = (\Delta - h)/2P) \tag{A8}$$

By using Equations (A4), (A7) and (A8) we can determine σ_a by

$$-\frac{h}{P} = -\sigma_a + (x'_o + 1)(1 - e^{-\sigma_a}) \tag{A9}$$

From Equation (A6) the final condition of x'_a is

$$x'_a = x'_o e^{-\sigma_a} + (e^{-\sigma_a} - 1) \tag{A10}$$

Equation (A7) can thus be written as

$$x_a = x_o - \sigma_a + (x'_o + 1)(1 - e^{-\sigma_a}) \tag{A11}$$

For region (3) where $q_3 = 0$ during $\sigma_a \leq \sigma \leq \sigma_b$ we have from Equations (56) and (57) the following

$$x' = x'_a e^{-(\sigma - \sigma_a)} \tag{A12}$$

$$x = x_a + x'_a[1 - e^{-(\sigma - \sigma_a)}] \tag{A13}$$

When $\sigma = \sigma_b$ the region ends at

$$x_b = (-\Delta - h)/(2P) \tag{A14}$$

From Equations (A8) and (A14) one obtains

$$x_b - x_a = -\Delta/P \tag{A15}$$

At $\sigma = \sigma_b$ Equations (A12) and (A13) are

$$x'_b = x'_a e^{-(\sigma_b - \sigma_a)} \tag{A16}$$

$$x_b = x_a + x'_a - x'_a e^{-(\sigma_b - \sigma_a)} \tag{A17}$$

Adding the above two equations we have

$$x'_b = x'_a - (x_b - x_a)$$

$$x'_b = x'_a + \Delta/P \tag{A18}$$

by virtue of Equation (A15).

To express the final conditions x'_b and x_b in terms of initial conditions Equation (A10) is substituted into Equation (A18) and Equation (A11) is substituted into Equation (A17) to give

$$x'_b = x'_o e^{-\sigma_a} + (e^{-\sigma_a} - 1) + \Delta/P \tag{A19}$$

$$x_b = x_o - \sigma_a + (x'_o + 1)(1 - e^{-\sigma_a}) - \Delta/P \tag{A20}$$

which are Equations (61) and (62) in the text.

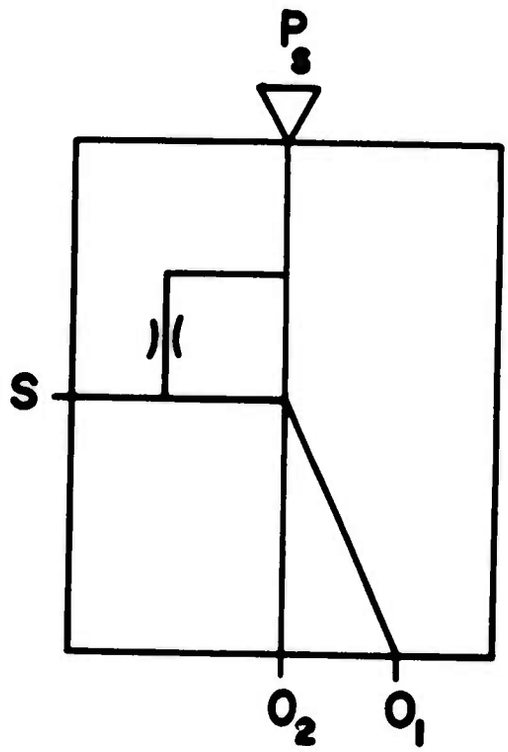


Figure 1 Fluidic Back Pressure Switch

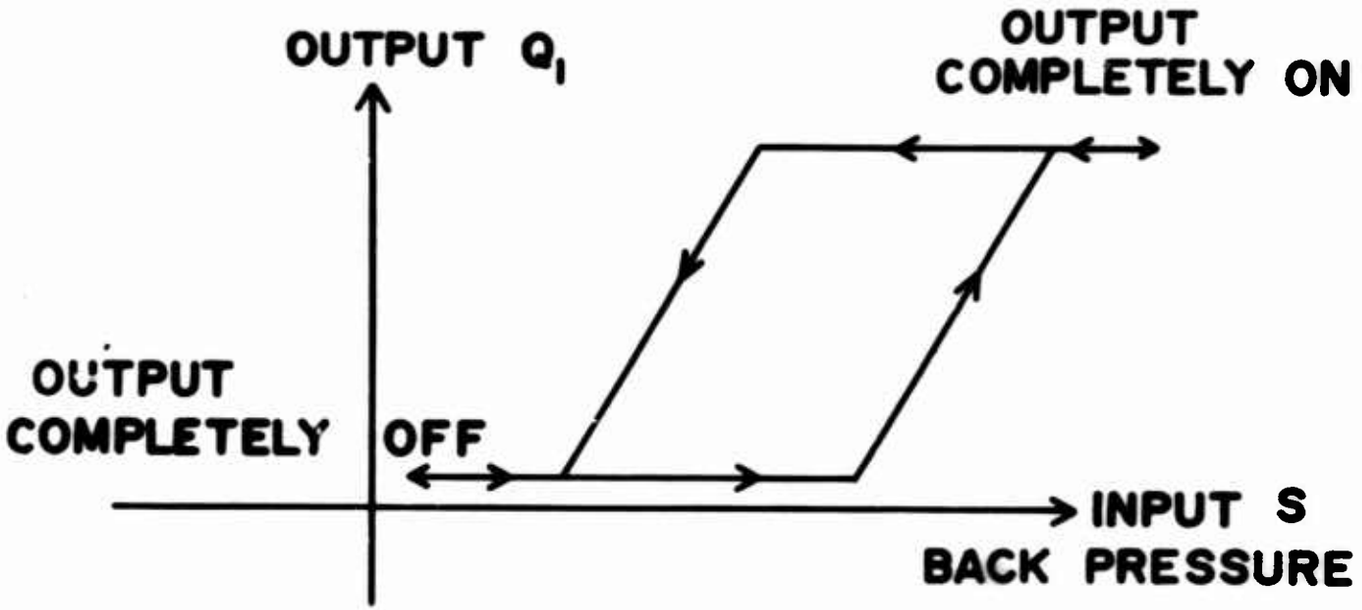


Figure 2 Hysteresis Characteristics of the Back Pressure Switch

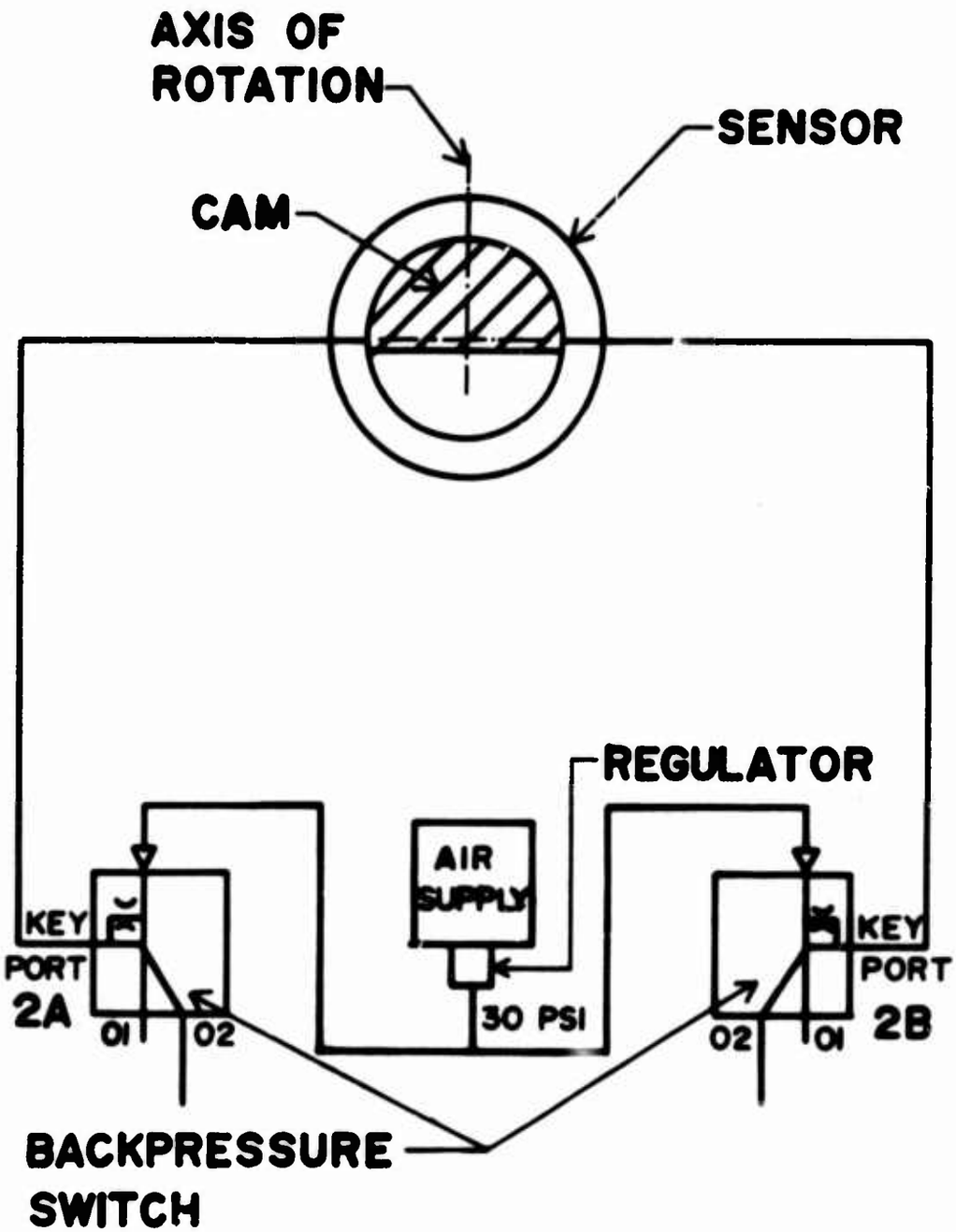


Figure 3 Schematic Diagram for Sensor System with Back Pressure Switch

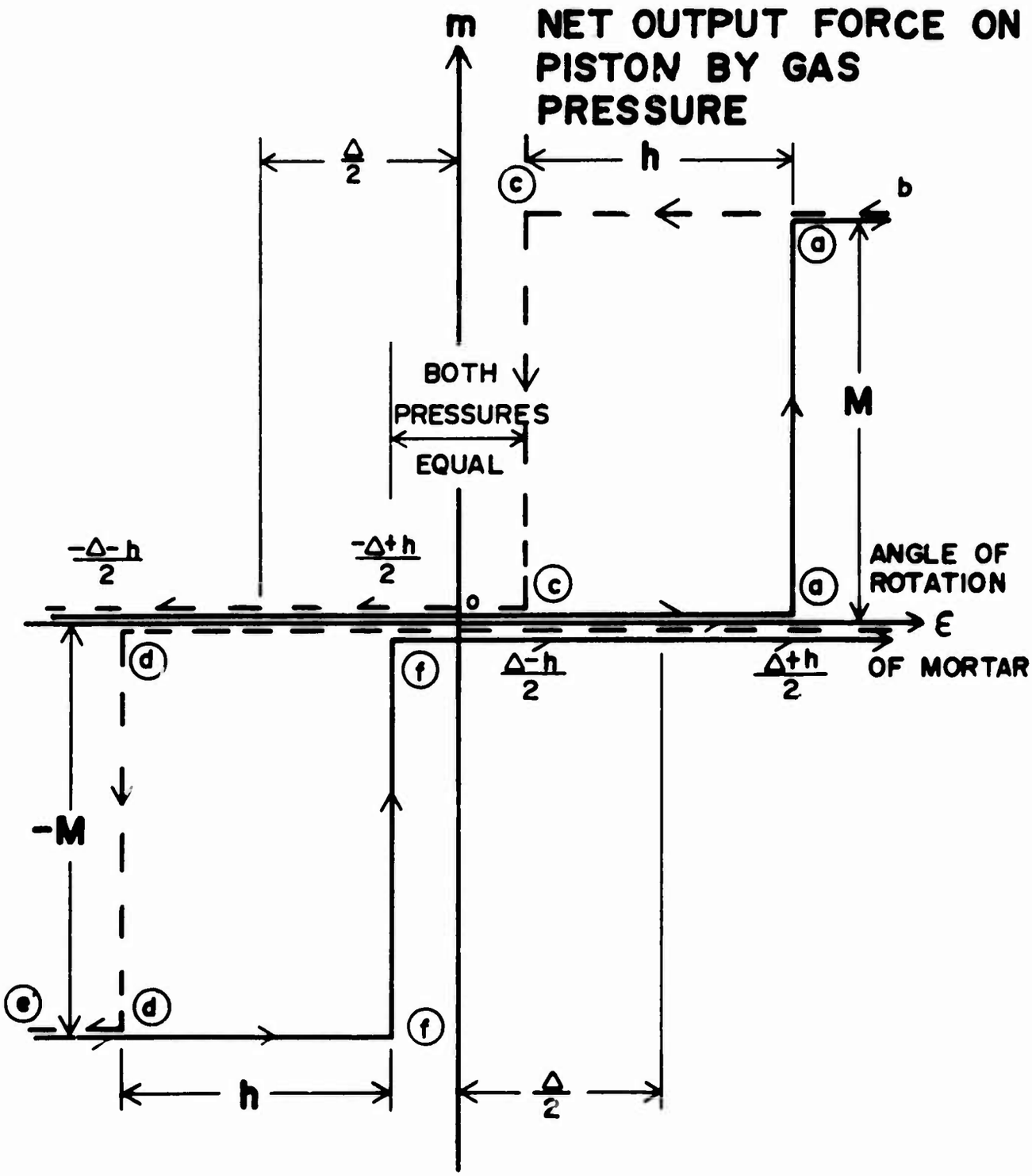


Figure 4 Hysteresis and Dead Zone for Piston Force as Output vs. Mortar Angle as Input

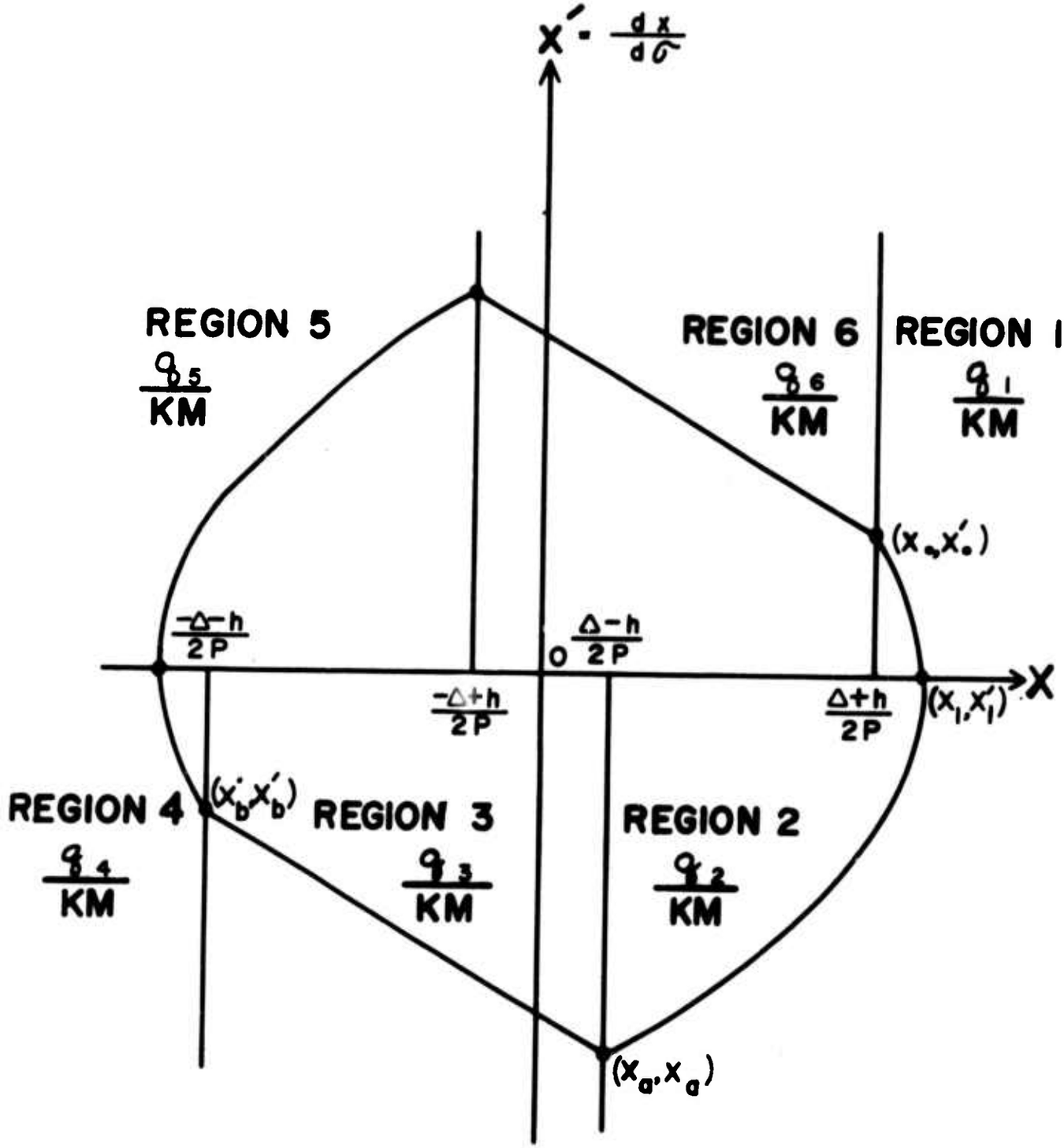


Figure 5 Phase Plane Diagram Without Dry Friction

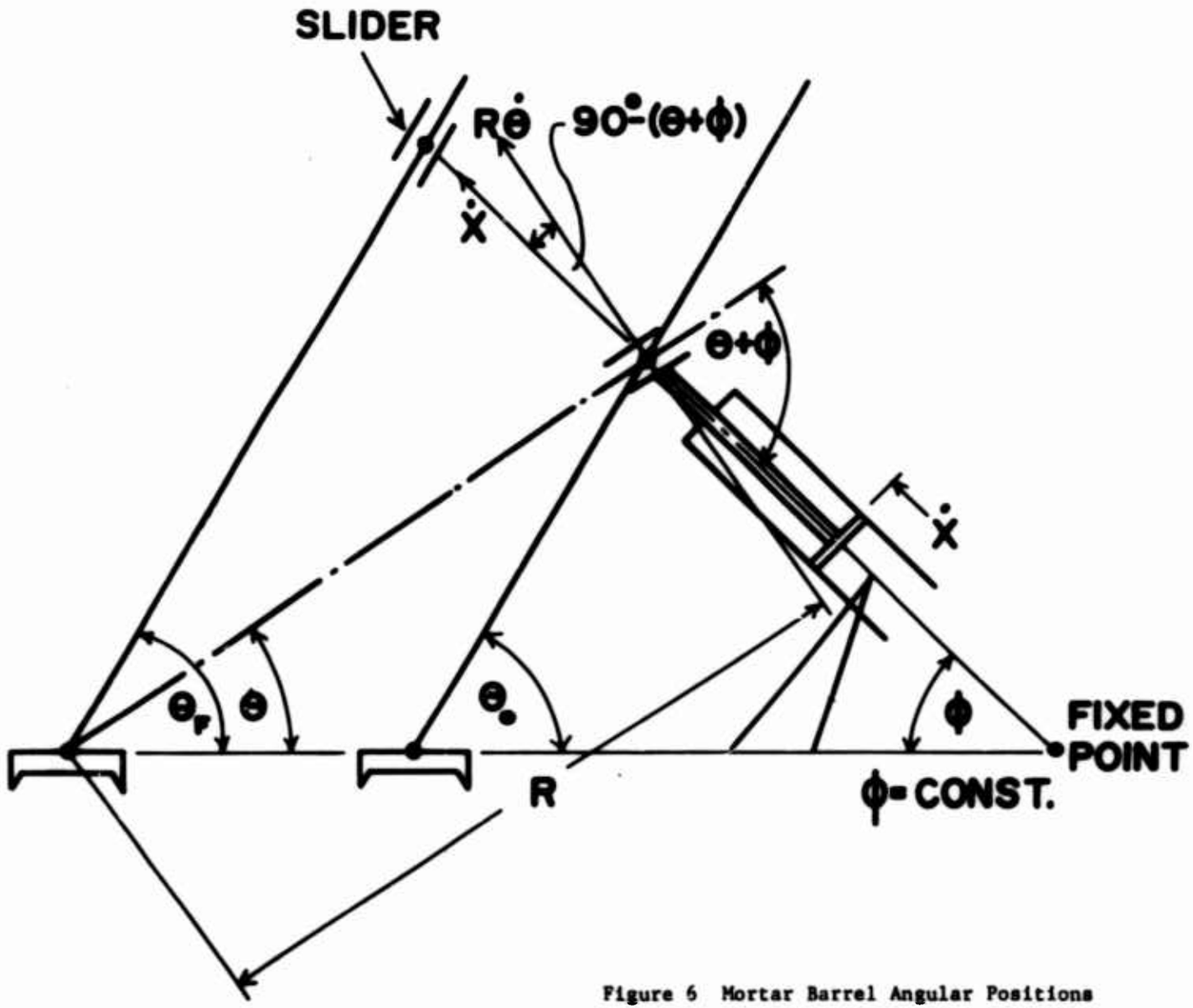


Figure 6 Mortar Barrel Angular Positions

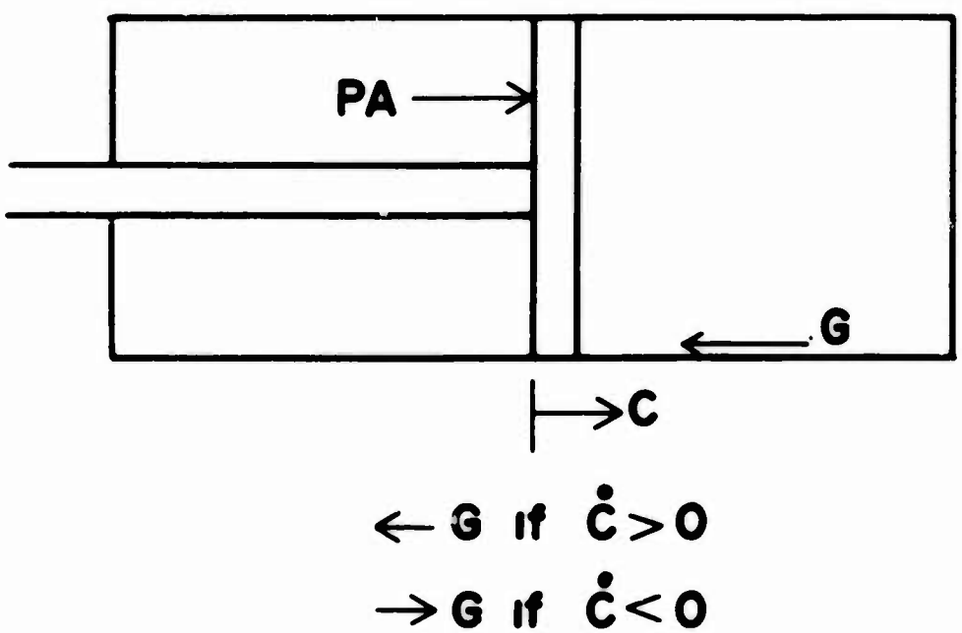


Figure 7 Dry Friction on Piston

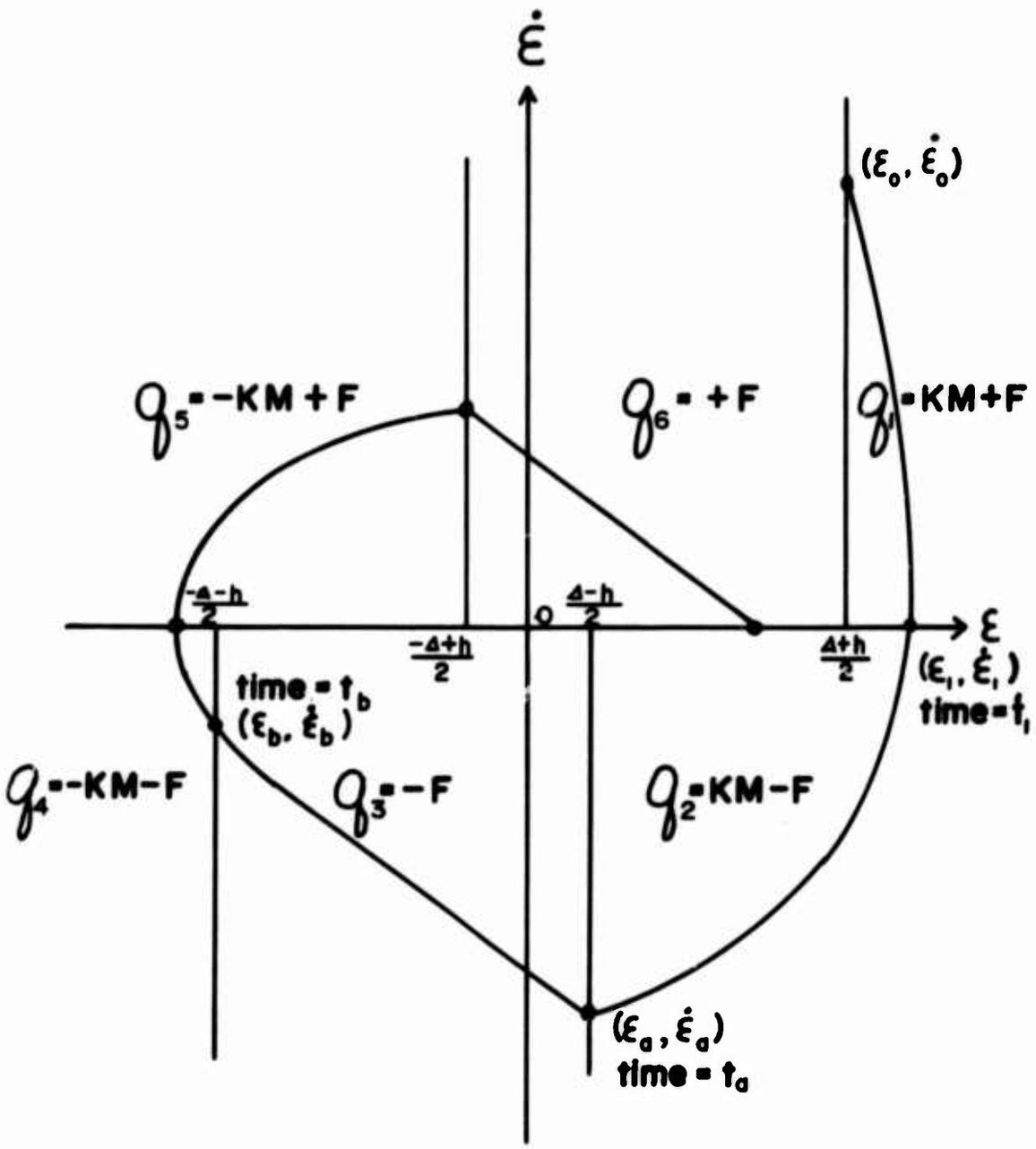


Figure 8 Phase Plane Diagram with Dry Friction

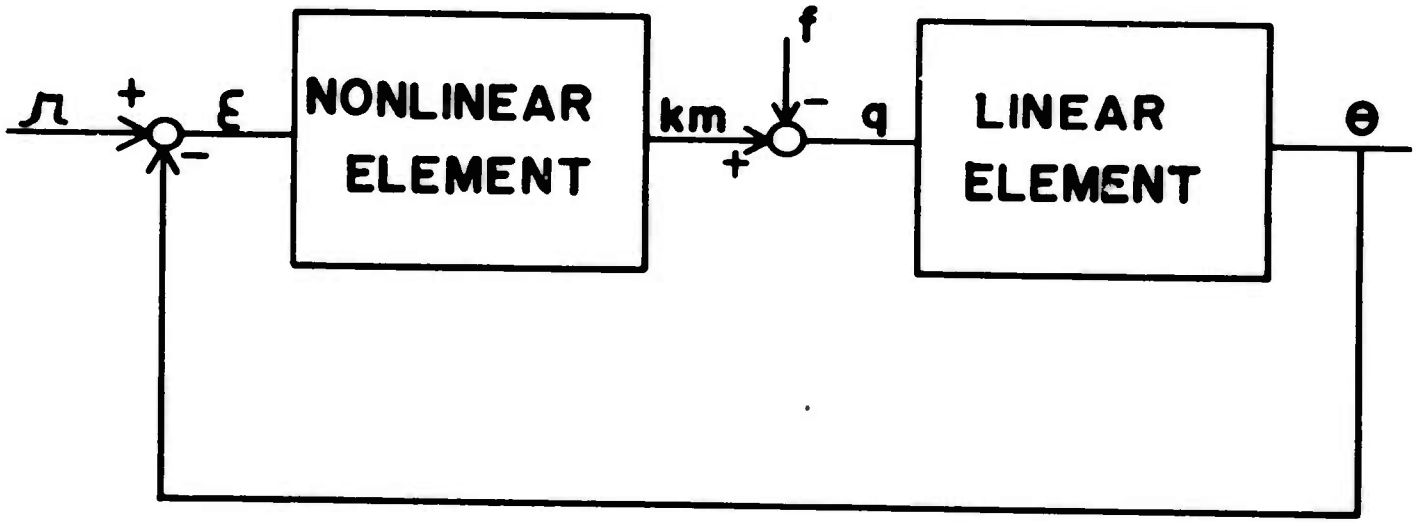


Figure 9 The Feedback System

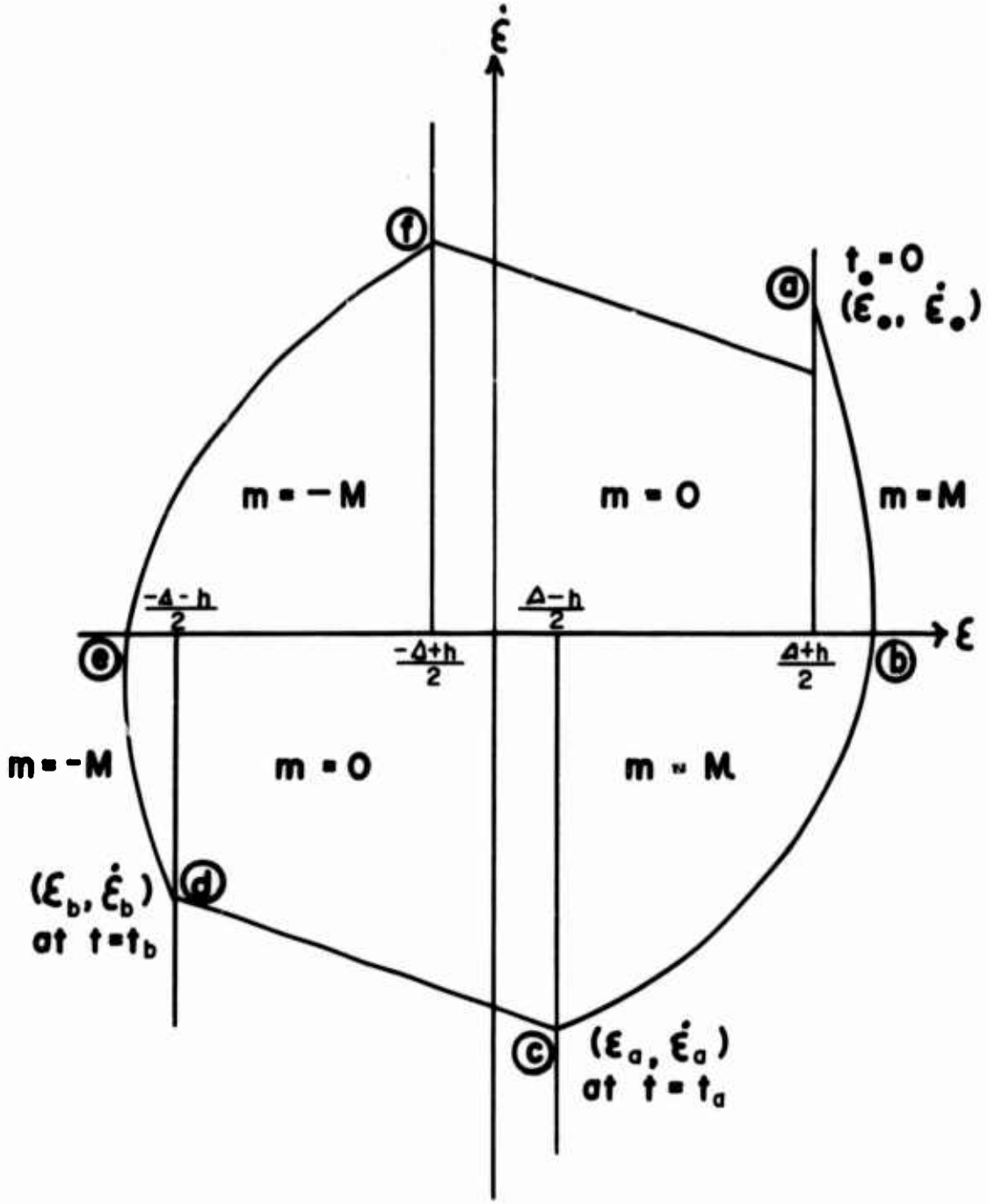


Figure 10 Phase Plane Diagram with Non-dimensional Variables and Parameters

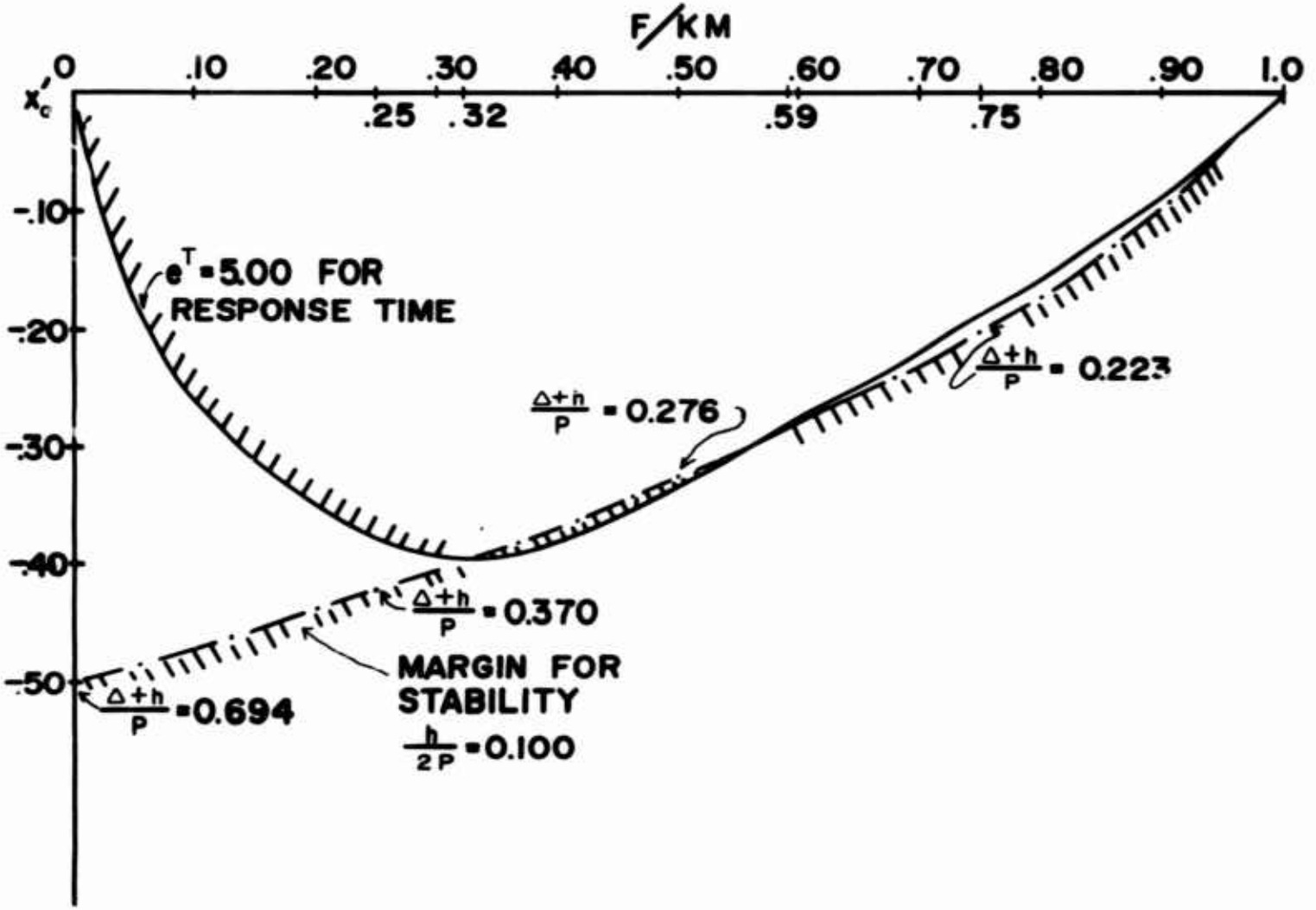


Figure 11 Feasible Region for System Design

FLUIDIC EMERGENCY ROLL CONTROL

K. Haefner and T. S. Honda
General Electric Company
Specialty Fluidics Operation
Schenectady, New York

INTRODUCTION

This paper summarizes the work performed under Task III of Contract NAS 2-5467. The program included the design, development, fabrication, and test evaluation of a prototype emergency roll control (ERC) for aircraft stabilization. The fluidic control units were designed to provide, between two diametrically opposed nozzles, a thrust differential proportional to an input voltage signal. The emergency roll control requirements of the X-14 VTOL research aircraft were defined as typical design goals. Two control units, one on each wing tip, were intended to provide a maximum thrust of 224 pounds per unit. The units were designed to operate with 2500 psig, 2000 F gas from a solid propellant gas generator. The emergency system including the gas generator was designed to add less than 11 pounds per wing tip. The operating time under emergency conditions was specified as five seconds. The fluidic emergency thruster is similar in concept to a JATO system but has the added feature of controllable thrust.

The emergency roll control system developed in the program is shown in a typical conceptual package installation in Fig. 1. The control package consists of:

- solid propellant gas generator
- two diametrically opposed vortex valve modulated thrust nozzles with an electro-magnetic torque motor
- electronic controlled logic.

The gas generator is ignited on an emergency command signal from the flight control logic and the control modulates differential thrust output proportionately from an electrical signal to the torque motor generated by the flight control computer.

The specific program objectives were to design, fabricate and test three fluidic emergency thruster units for hot gas evaluation.

Orderly accomplishment of the program goals was achieved by pursuing the following program plan.

Fluidic emergency thruster design analysis and system study including the specification of performance requirements for the thruster and the gas generator.

Design, fabrication and test evaluation of breadboard components. To obtain design data and to demonstrate compliance with the design requirements.

Fabrication of three prototype control units for hot gas evaluation.

Hot gas test evaluation at NASA/ARC with hydrazine.

Hot gas evaluation with prototype hot gas generator.

CONTROL SYSTEM CONCEPT

The requirements of a specific VTOL aircraft were selected as typical design goals in this development program. The pertinent characteristics of a typical vehicle (based on the X-14 research aircraft) are:

Roll inertia - 2340 ft-lb sec^2

Roll radius - 16.7 ft.

The functional requirements of the emergency roll control system were based on a probable worst case roll control maneuver for a VTOL. The emergency roll control is activated by the flight control computer when the sum of the roll angle and angular rate exceed a predetermined value. The regime in which the emergency condition is assumed to exist is denoted by "fire" in phase plane plot, Fig. 2. The control "activate" signal is given based on a simple computation of rate and attitude, which if allowed to persist would permit the aircraft to fall into an unsafe flight regime.

The control maneuver is comprised of three phases as shown in Fig. 3. During Phase I a hardover thrust command reduces the aircraft roll rate to zero at a wing attitude angle no greater than 30 degrees. During the second control phase the aircraft is torqued back to an approximate wings level, zero rate condition. Phases I and II are assumed to be preprogrammed into the flight control computer such that no action is required by the pilot. During Phase III the pilot controls the aircraft and trims the wings to the desired level attitude. The emergency roll control is assumed to be active for five seconds after initiation. The selection of each control phase is accomplished by electronic logic with suitable rate and attitude control input sensors. The electronic logic was designed by NASA/ARC. An extensive analog simulation of the ERC was also conducted by NASA/ARC in order to determine the most optimum system gains and time duration of Phase I, II, III control modes.

GAS GENERATOR DESIGN STUDY

The maximum available thrust vs time schedule delineated in Fig. 3 was preprogrammed into the hot gas generator design. The gas generator design was investigated by Thiokol Chemical Corporation to provide a three-step pressure profile over a burn time of 5 seconds by proper shaping of the propellant charge. The calculated weight of the propellant is 3.1 lbs., with an inert generator weight of 6.2 lbs. The gas generator weight estimates are compatible with the overall system design goals.

FLUIDIC EMERGENCY THRUSTER DEVELOPMENT

The fluidic emergency thruster hardware developed by General Electric is shown in Fig. 4. The package consists of an electromagnetic torque motor driven flapper nozzle first stage, controlling two vortex valves in push-pull. The primary development effort was directed toward the achievement of a vortex valve turndown ratio of at least 5.0. This turndown ratio was determined by system analysis as being essential in keeping the hot gas propellant weight within design goals. Compactness and light-weight packaging of the control unit were major design objectives, which resulted in a fluidic thruster weight of 4.7 lbs.

VTOL EMERGENCY ROLL CONTROL REQUIREMENTS

The control system in which the fluidic emergency thrusters are to operate is depicted in the block diagram representation of Fig. 5. The fluidic thruster is driven by a hot gas source and electrically commanded to provide the roll torques. Roll rate and attitude gyro signals are compared in an electronic logic circuit and ignition of a solid propellant in the gas generator is initiated when the rate and attitude signals exceed the limits (i.e. ±30 degree roll attitude at zero roll rate) set in the logic. These limits correspond to the approximate θ vs $\dot{\theta}$ defined in Fig. 2. The firing values of rate and attitude are obtained by summing the aircraft attitude and rate gyros. A control law is preprogrammed into the automatic control system which brings the aircraft to a wings level zero rate condition and the system operates in an automatic mode without benefit of pilot interaction in the loop.

Two separate gas generator thruster packages are used to provide redundancy. If one of the gas generators fails to fire, a couple is still achieved; but the control torque is at one-half the normal level. The use of solid propellant gas generators in conjunction with fluidic control components provide a reliability level approaching that of JATO systems.

GAS GENERATOR IMPULSE

The total impulse required for the three control phases is shown in Fig. 6. The total impulse is the value required at each wing tip and this total is plotted as a function of the acceleration level α_1. On the average, 21% of the total impulse is required in Phase I, 30% in Phase II, and 49% is required for Phase III maneuver. The three thrust levels were preprogrammed on an open loop basis by proper design of the burning surfaces in the gas generator grain. The emergency system is assumed to supply all of the impulse required for vehicle stabilization and that no torque is available from the normal reaction control system. To obtain a weight estimate, it was assumed that twice the normal roll torque to inertia ratio, α_1=3.2 rad/sec^2 is utilized under emergency conditions; thus, requiring a total impulse (Fig. 6) of 430 lb-sec. A thrust during control Phase I of 224 lbs (shown on Fig. 3) is required at each wing tip for the typical aircraft inertia of 2340 slug-ft^2 and lever arm of 16.7 ft. For a representative gas generator propellant, an average delivered specific impulse of 139 seconds is available with the fluidic system dictating a total propellant load of 3.1 lbs.

GAS GENERATOR DESIGN

A Thiokol Q-series propellant is the basis for the gas generator design. This propellant is based on an oxygenated polyester binder cured with an epoxide. The oxidizer is ammonium perchlorate which is used with a unique coolant, Thiokol LL-521. The propellant exhibits low flame temperature, clean exhaust products and a wide range of burning rate characteristics. This type of propellant also has excellent mechanical properties, is resistant to moisture and has excellent aging capability. It has no phase changes, has a high cure density, and is easily ignited. The specific designation of the propellant is TP-Q-3074A-01.

A preliminary gas generator design for the fluidic emergency thruster indicated a design which is 4.5 inches in diameter (maximum) and 9.9 inches long from the initiator interface to the thruster interface. The nominal calculated weight to provide the specified impulse requirements is 7.2 pounds, of which the estimated propellant weight is 3.6 pounds. The generator meets the three step pressure profile specified by system requirements. The maximum operating pressure at 70 F is 2500 psia and the burn time is 5 seconds. The gas generator design is based on an effective throat area of 0.0765 in^2 and an assumed discharge coefficient of 1.0.

FLUIDIC EMERGENCY THRUSTER DESIGN (FET)

The final thruster design selected is shown schematically in Fig. 7. It consists of two vortex valves controlled differentially by an electromagnetic torque motor driven flapper nozzle. The inputs to the

thruster are the high pressure supply gas from the generator and an electrical command signal from the flight control computer. The output is a differential thrust proportional to the voltage input to the torque motor. The vortex valves act as flow modulators for the thrusters.

The performance data obtained for a typical radial in-flow vortex valve developed on this program is shown in the non-dimensionalized characteristic turndown curve in Fig. 8. The valve turndown refers to the reduction in flow which can be achieved by introducing a control flow to the vortex valve. The control flow is modulated with an inverted flapper which operates at a pressure in excess of the vortex valve supply pressure. Both the first stage flapper and the vortex valve operate with the hot gas generator supply.

The sizing of the flow controlling orifices and passages is based upon providing 224 pounds differential thrust with a gas supply pressure of 2500 psig, and vortex valve turndown ratio (TDR) of 5.0. Since half of the supply pressure will be available up-stream of the thrust nozzles, which are the outlets of the vortex valves, the nozzle throat on the vortex outlet diameter required is 0.4 inch for an optimum nozzle expansion ratio of 10. The calculated thrust vs supply pressure is shown in Fig. 9.

A single outlet radial-in-flow vortex valve with the outlet configured as a divergent thrust nozzle was selected and developed as the primary thrust controller. The pertinent dimensions of the vortex valve and thrust nozzle are:

Outlet (nozzle throat) diameter (D_o) = 0.4 in.

Nozzle expansion ratio = 10

Spin chamber diameter (D_s) = 2.0 in.

Control nozzle area (A_c) = 0.031 in^2

Spin chamber height (h) = 0.30 in.

The torque motor and flapper nozzle design were finalized to conform to the vortex valve control requirements. The flapper nozzle requirements, based on providing a maximum ratio of control to vortex valve supply pressure of 1.4 are:

Flapper nozzle diameter (D_N) = 0.186 in.

Flapper travel (X) = ±0.015 in.

A wet coil torque motor was selected to provide the required flapper stroke and force. Some of the significant torque motor characteristics specified are:

Stroke	±0.20 in.
Mid-Position Force at Rated Current and Stroking Position	20 lb.
Resonant Frequency	Greater than 250 Hz
Maximum Operation Temperature - at Flapper for 5 seconds	2000°F
Weight	24 oz.

Heat transfer and stress analysis were performed to determine the most suitable material for the control fabrication. Strength and weight were the criteria for selection. The short time (five seconds) during which the control is exposed to 2000 F and the fact that the highest pressures are experienced when the unit is cool alleviates the material high temperature strength problem so that super alloys are not required. The material selected is A. I. S. I. Type 347 stainless steel to be compatible with the welded assembly design.

ERC PERFORMANCE TESTS

In order to provide an effective demonstration of the ERC performance, a test plan was defined to furnish data on the static as well as the dynamic ERC characteristics. The tests were divided into two categories:

1. Static and Dynamic Cold gas tests.

2. Static and Dynamic Hot gas tests.

The static cold gas tests were conducted to provide data with respect to static gain, hysteresis, and change in performance parameters under different operating conditions. The dynamic cold gas tests were performed using an analog simulation of the aircraft and an attitude control simulator in conjunction with the FET hardware. These tests were conducted operating the FET as a closed loop system at various operating pressures up to 2500 psi in order to ascertain the response characteristics of the ERC control, and determine possible problem areas prior to hot gas firing.

Static hot gas tests of the fluidic Emergency thruster (FET) were conducted by NASA/ARC using a hydrazine generated 1000 F warm gas as the operating medium. These tests were performed to yield a preliminary evaluation of the thruster performance. Preliminary results indicated that the thrust levels were below the desired design levels. As a result of these tests, the FET was modified with larger orifices and a higher force torque motor in order to increase the thrust levels of the initial design.

The dynamic hot gas tests were carried out at Thiokol with a hot gas generator furnishing power to the FET. The hot gas tests were performed in a manner similar to the cold gas dynamic tests in that the ERC was evaluated closed loop, using an electronic breadboard for the control logic and an aircraft simulation.

A photograph of the dynamic hot gas test hardware mounted in the test bay is presented in Fig. 10.

The dynamic hot gas tests were completely successful as demonstrated in the phase plane plot (Fig. 11). The hot gas generator was fired automatically at an angle of 37° and accelerated in a direction to reduce the error. When the rate attitude errors reached a ratio of 3 to 1, the thrust was reversed to reduce the rate and attitude error to zero. At the completion of the automatic control, the simulation was also manually controlled by means of a mechanically driven potentiometer, attached to a "Joy" stick as an input. Instrumentation was also provided during the hot gas tests to monitor the performance of the gas generator and the temperatures of various points on the F.E.T. Figure 12 is a trace of the gas generator pressure-time profile. The time sequence of the pressure levels was in close correspondence with the design objectives. Pressure levels were in excess of the desired levels which was attributable to a lower flow demand from the F.E.T. The temperature test data verified the thermal analysis in that the torque motor temperatures did not exceed 400 F and the vortex valve case reached a level of 1200 F during the five second control period.

CONCLUSIONS

The major goal of fabricating vortex valves for modulating the flow of hot gases was achieved.

A hot gas generator was successfully developed and tested by Thiokol. When mated to an equivalent orifice of 0.350 inches diameter the gas generator met all the performance specifications with respect to pressure profile, initial transient and burn time.

The method of machining the solid propellant grain as a means of preprogramming the three supply pressures vs. a time schedule has definitely been proven feasible. The shaped grain provides adequate timing accuracy for generating the different pressure levels required in the mechanization of the ERC.

On the basis of the hot gas test firing, the ERC control concept, employing non-moving part vortex valves and a preprogrammed hot gas generator is a feasible approach for controlling VTOL aircraft in an emergency situation.

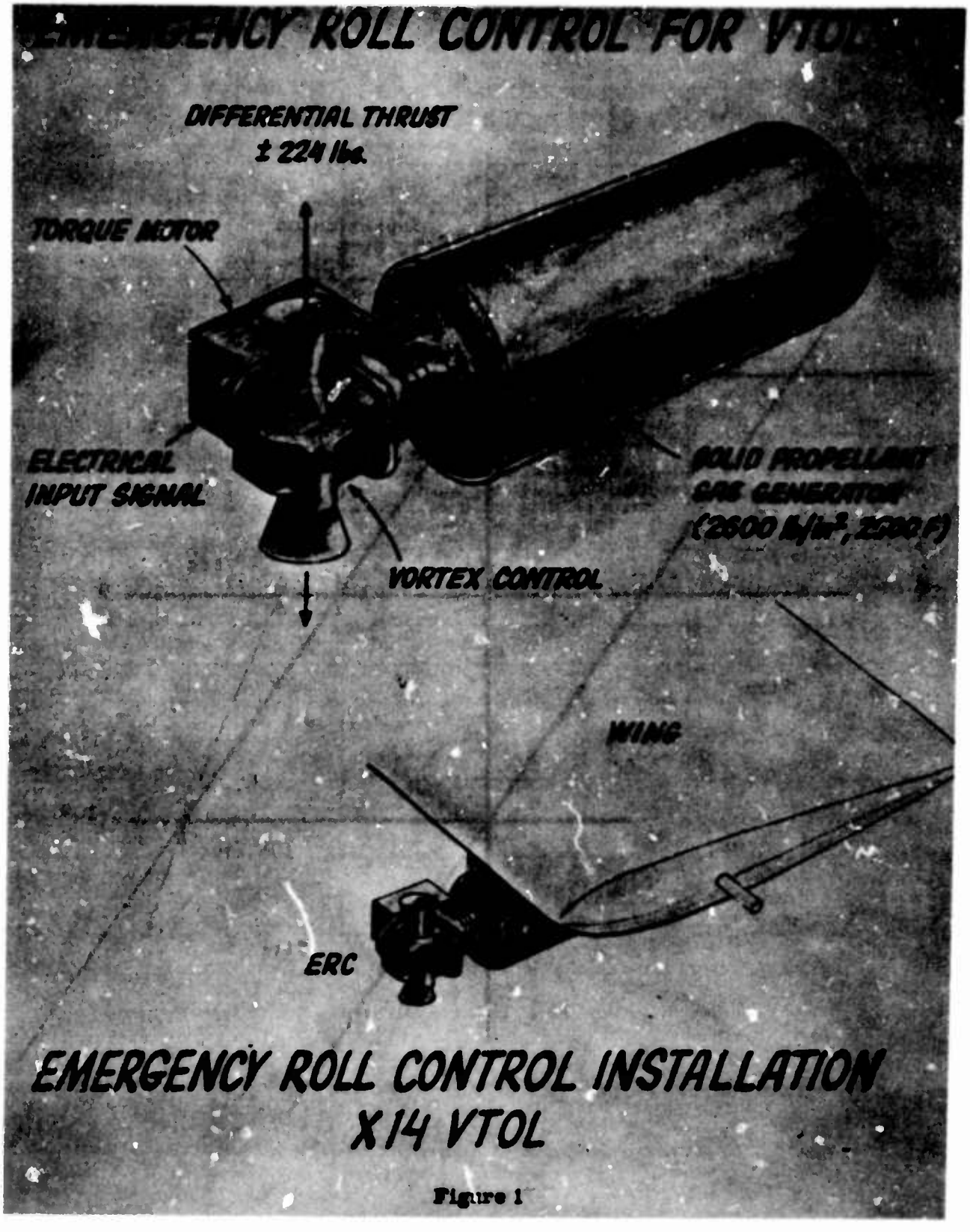

EMERGENCY ROLL CONTROL FOR VTOL
DIFFERENTIAL THRUST
± 224 lbs.
TORQUE MOTOR
ELECTRICAL
INPUT SIGNAL
SOLID PROPELLANT
GAS GENERATOR
(2600 lb/in², 2500 F)
VORTEX CONTROL
WING
ERC
EMERGENCY ROLL CONTROL INSTALLATION
X14 VTOL

Figure 1

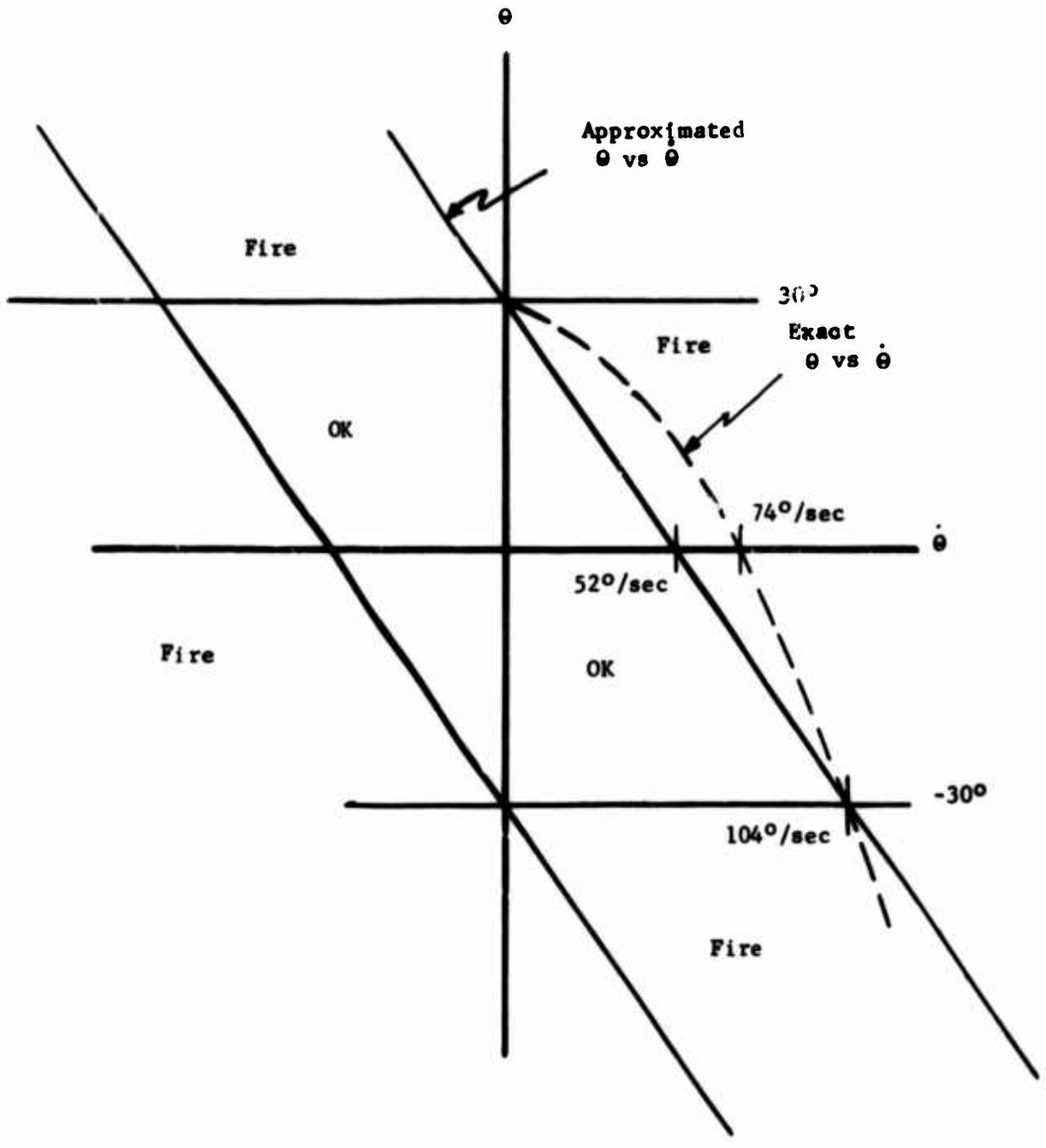


Figure 2

VTOL Emergency Flight Conditions

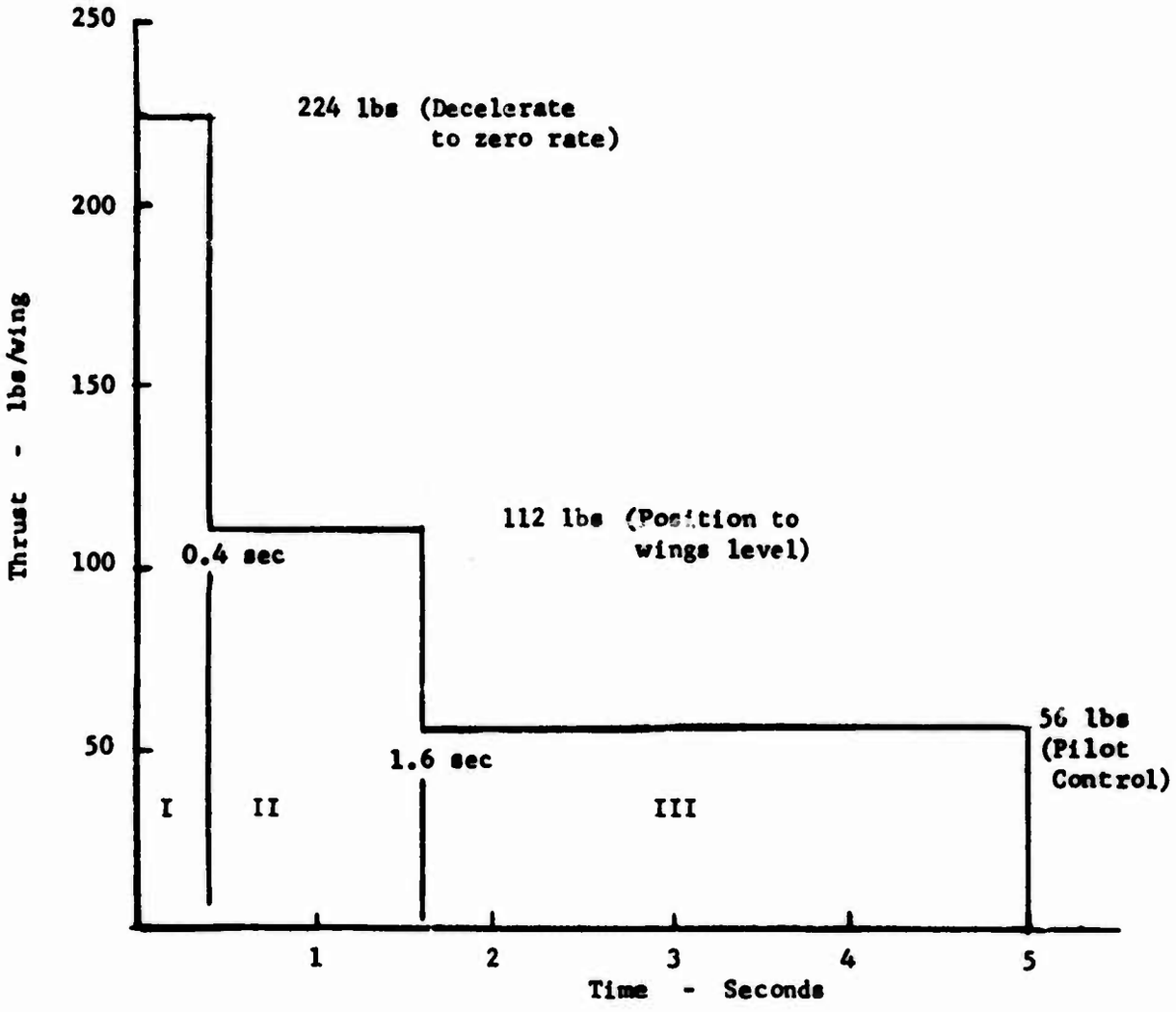
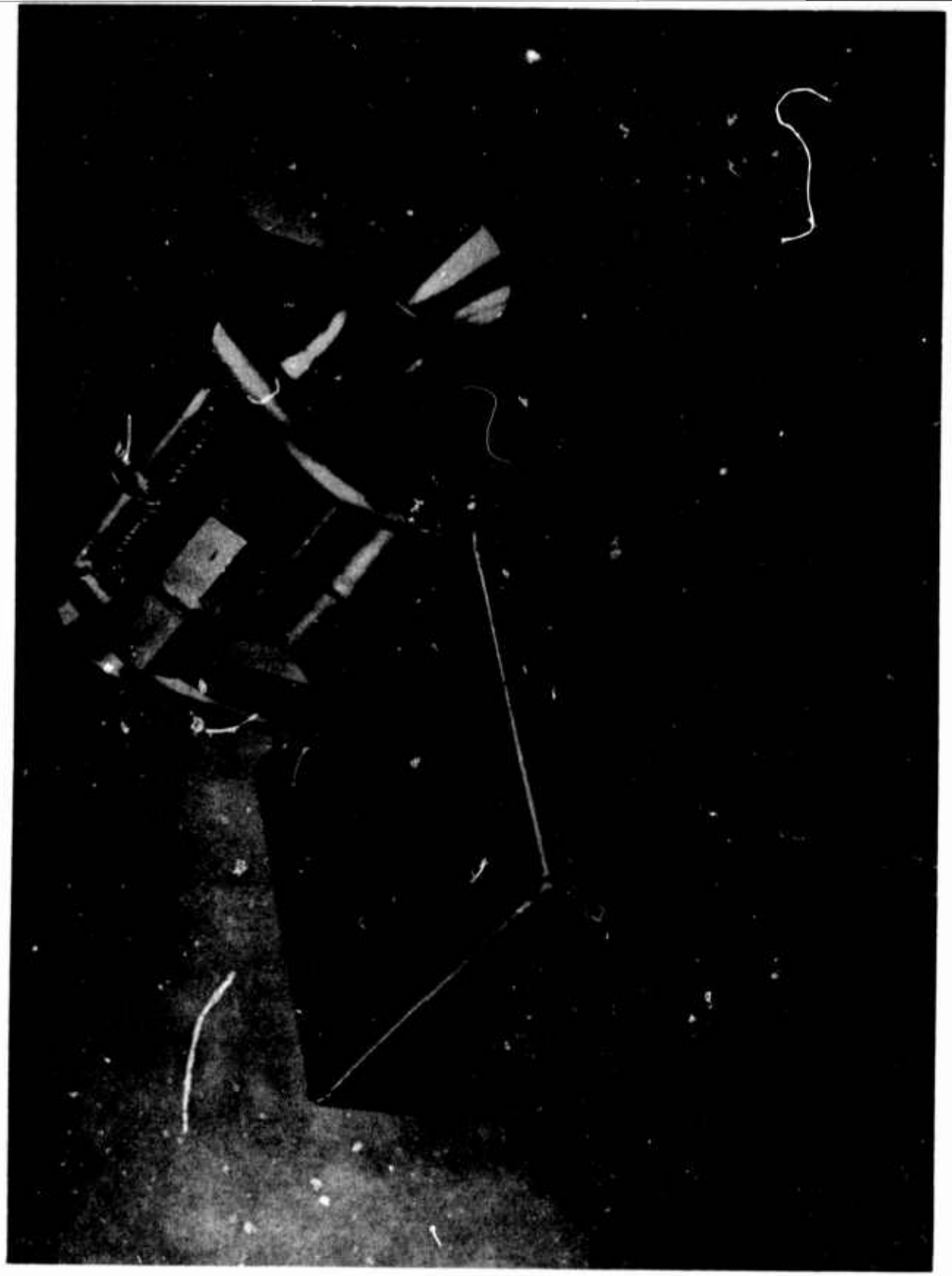


Figure 3

VTOL Emergency Thrust Schedule



Fluidic Emergency Thruster

Figure 4

$.2 < K_3/K_4 < 5$

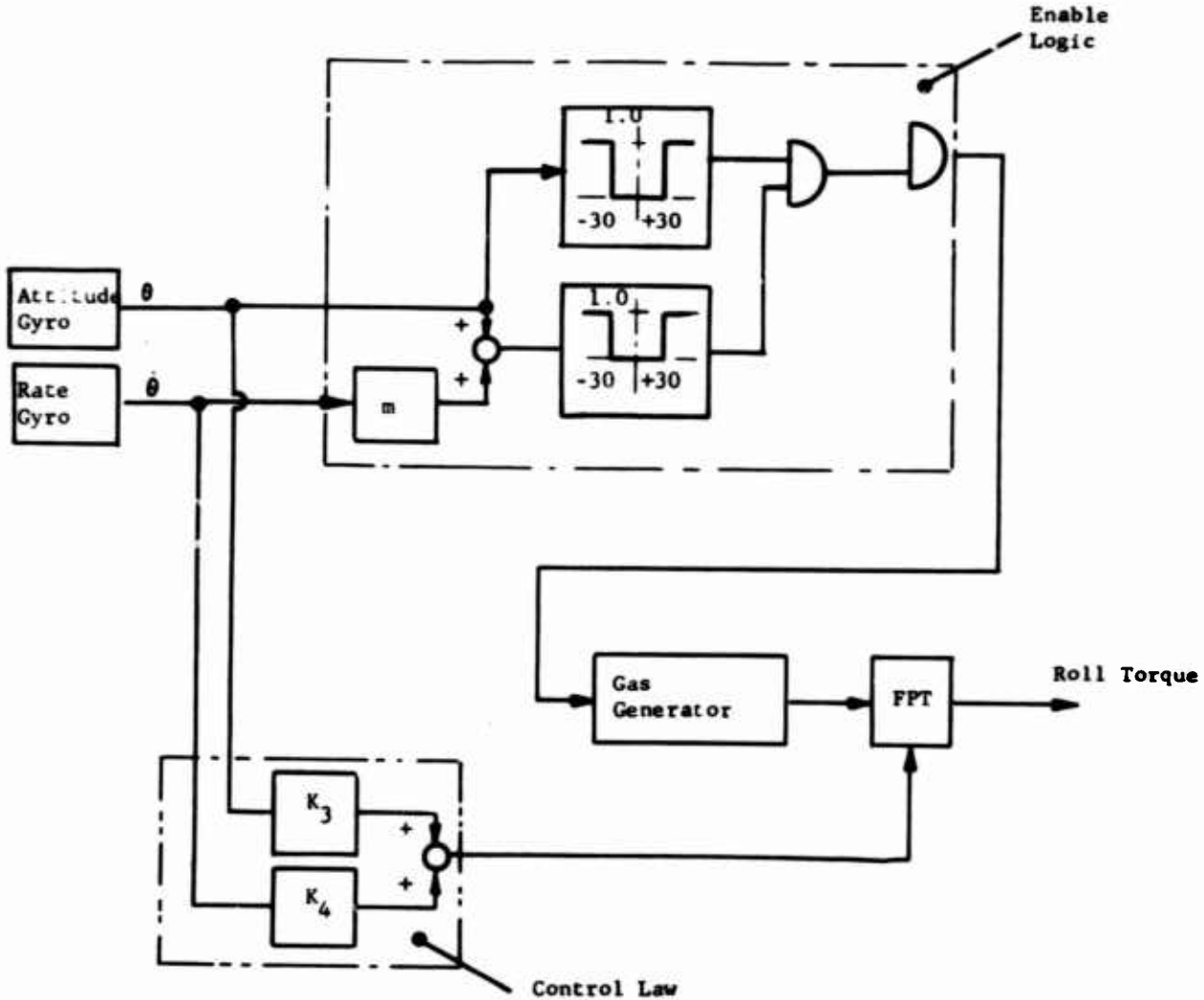


Figure 5
Emergency Roll Control System Block Diagram

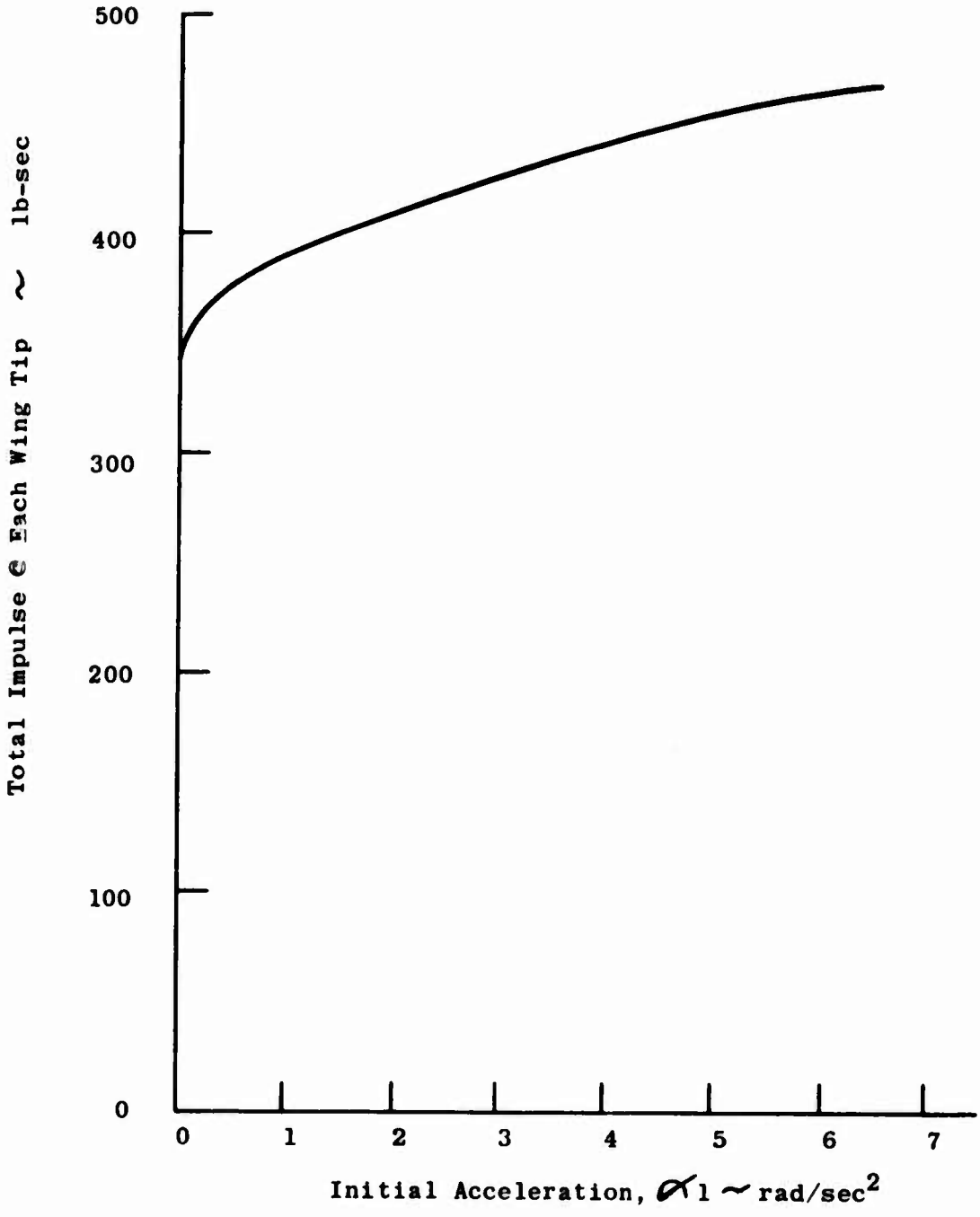


Figure 6
Total Impulse vs Acceleration

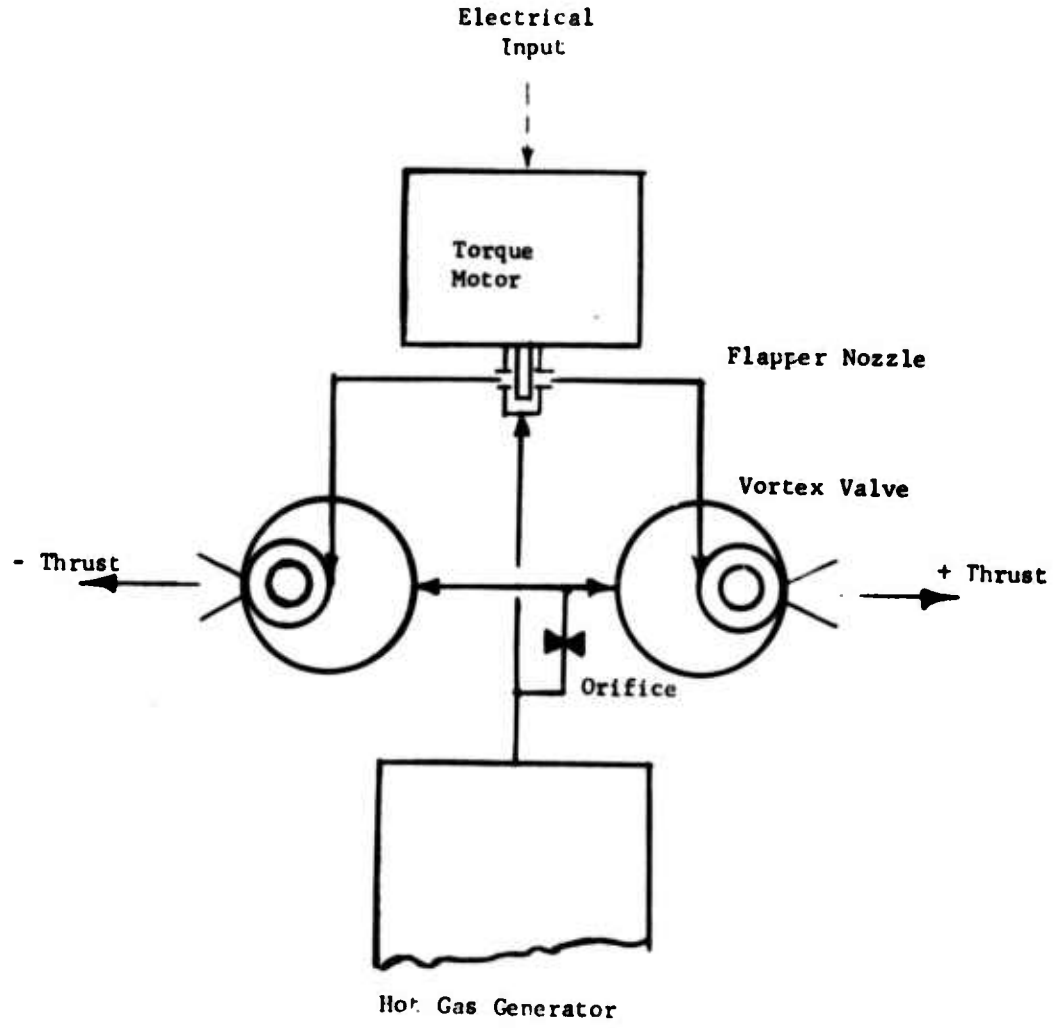


Figure 7
Fluidic Emergency Thruster Schematic

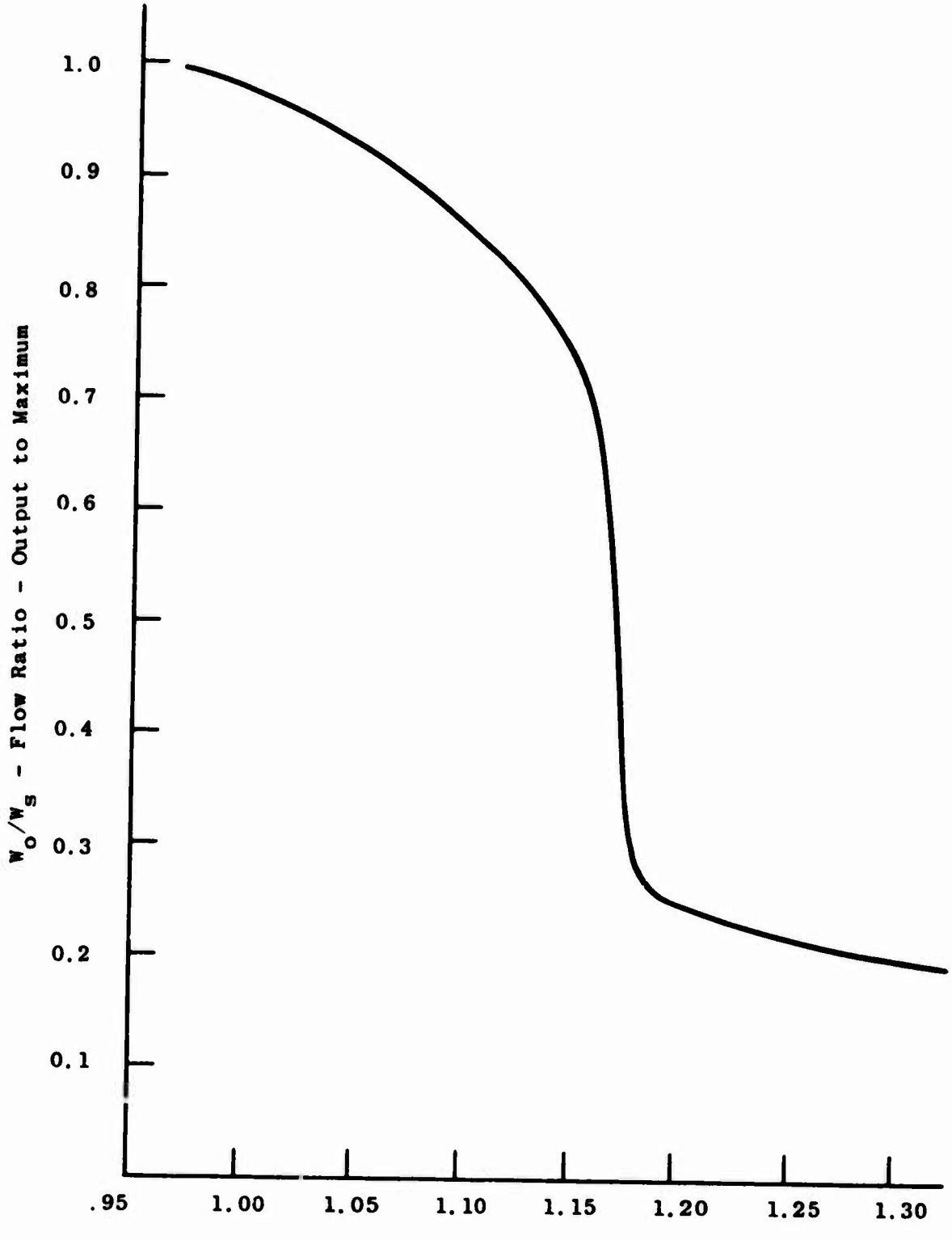


Figure 8
Vortex Valve Turndown Characteristic with Air

Figure 9

Fluidic Emergency Thruster
Theoretical Characteristics

Thrust Area (A_T) = 0.127 in^2

Expansion Ratio $\frac{A_E}{A_T}$ = 10

Ambient Pressure (P_a) = 14.7 psia

Turndown Ratio (TDR) = 5.0

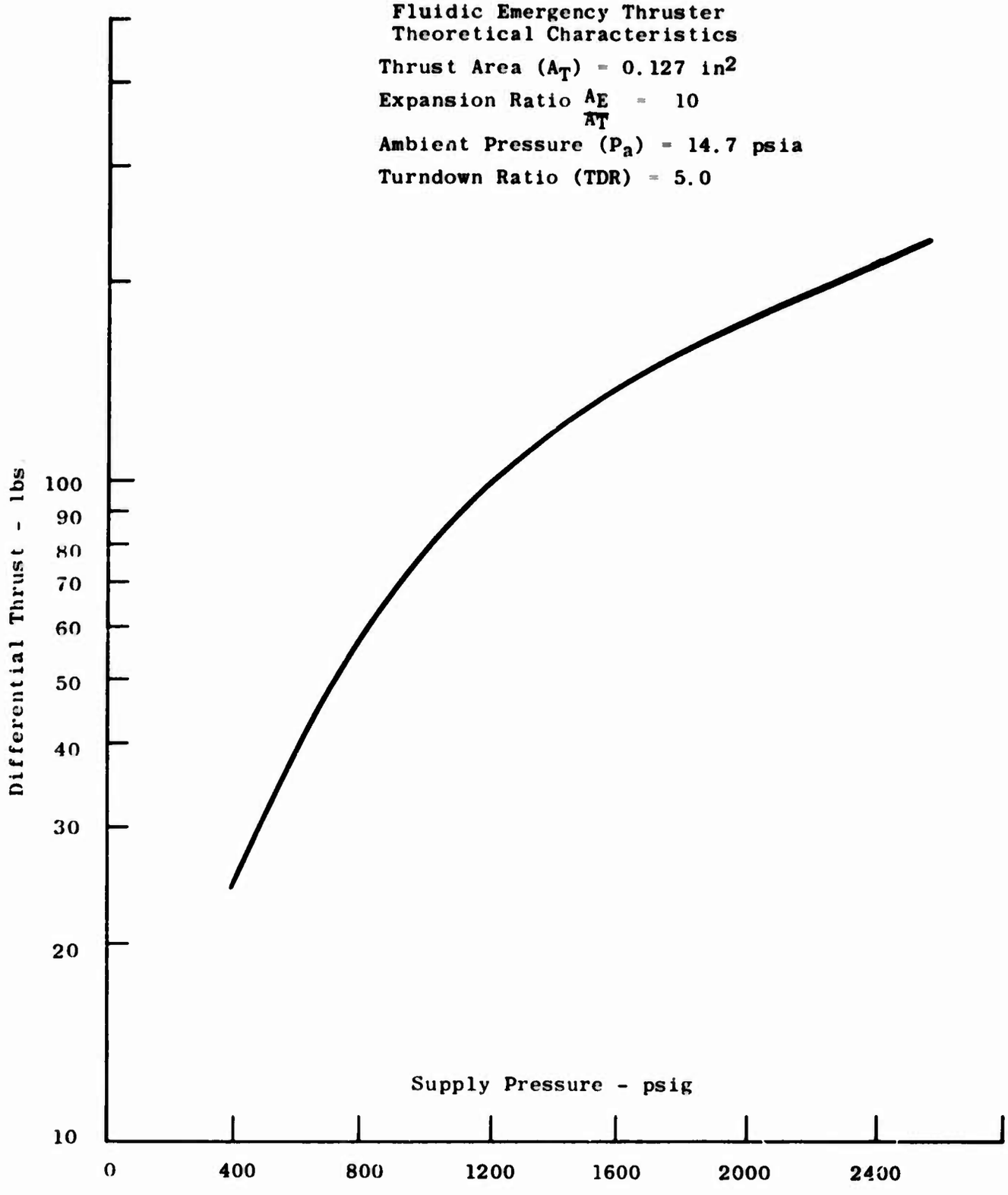
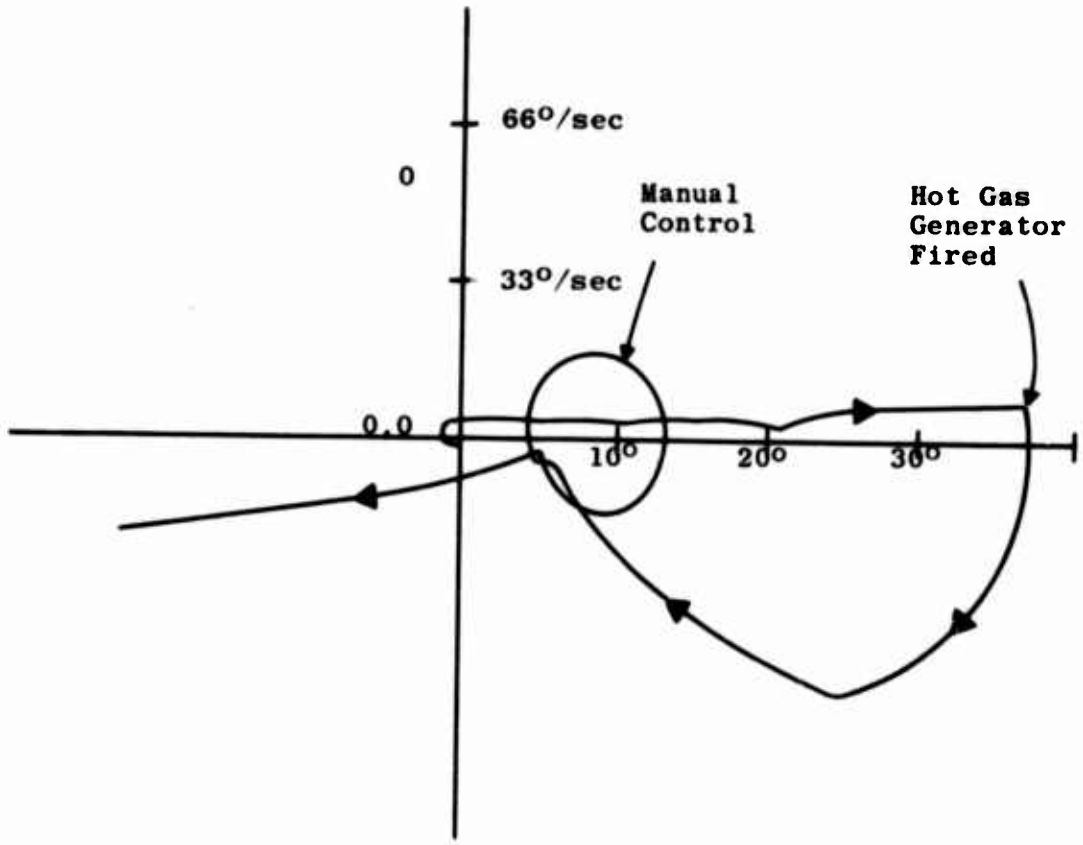




Figure 10 Photograph of Post Firing Unit #2



HOT GAS TEST #2

FET - JULY 18, 1972

Figure 11

HOT GAS TEST #2

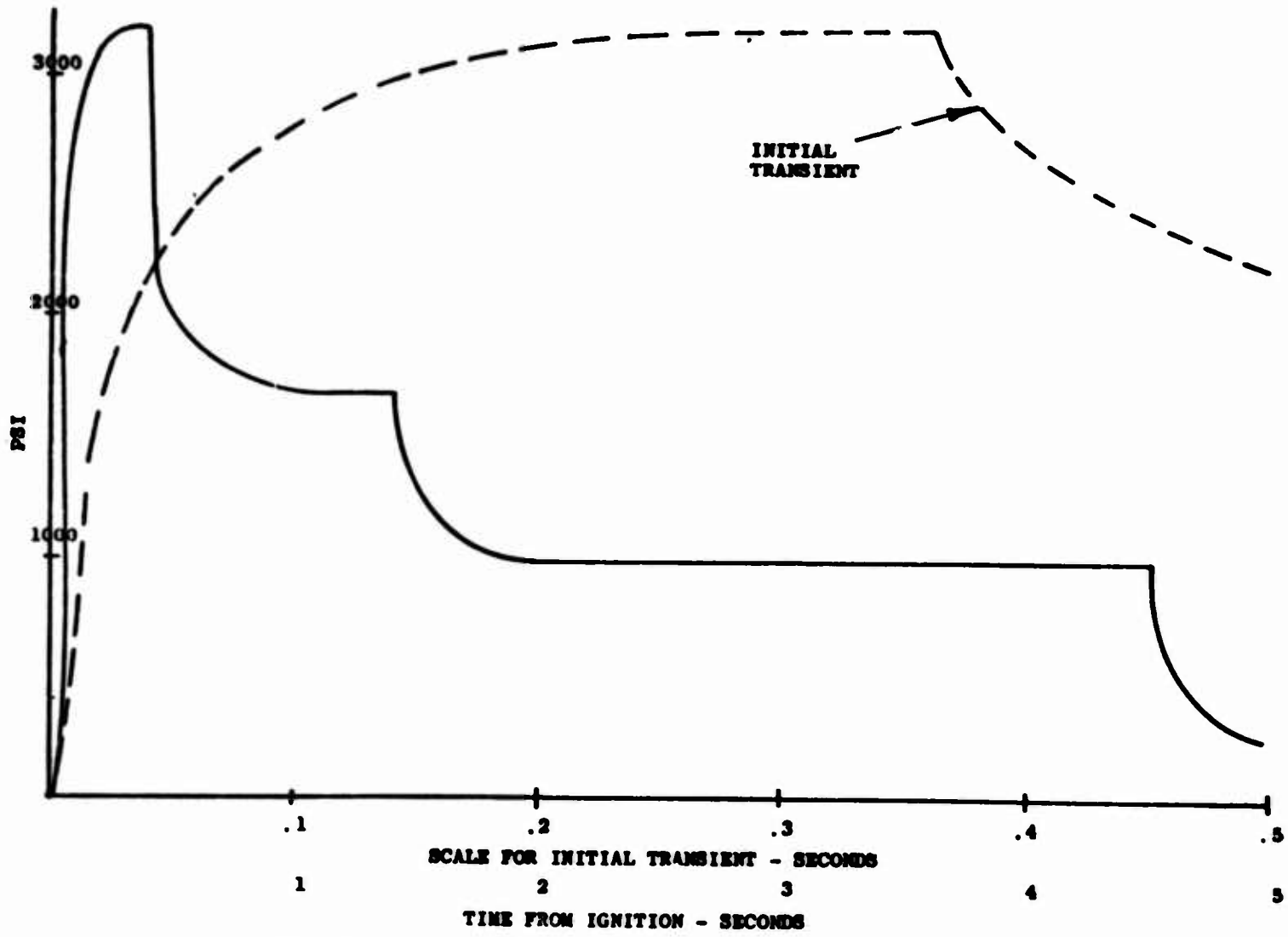


FIGURE 12 HOT GAS TEST #2 PRESSURE VS TIME